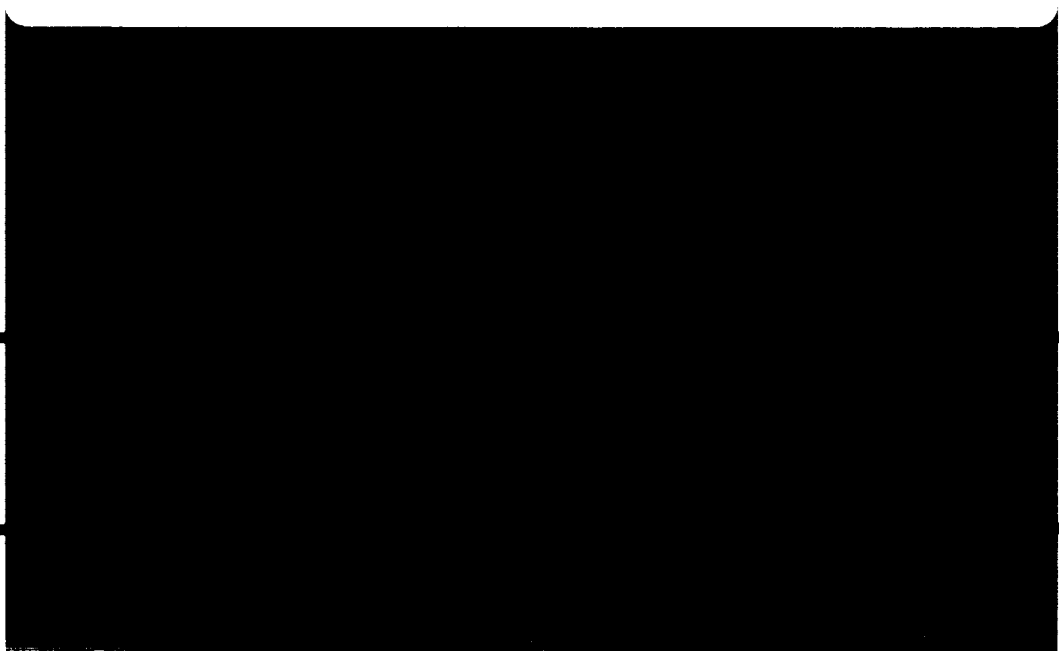


# 17th Space Simulation Conference *Terrestrial Test for Space Success*

CONFERENCE ON SPACE SIMULATION  
17th SPACE SIMULATION CONFERENCE  
17th SPACE SIMULATION CONFERENCE  
(NASA) 3181-1

CONFERENCE  
17th SPACE SIMULATION  
CONFERENCE

01/12 0120-12





*NASA Conference Publication 3181*  
*PREPRINT*

# **17th Space Simulation Conference *Terrestrial Test for Space Success***

*Compiled by*  
Joseph L. Stecher  
*Goddard Space Flight Center*  
*Greenbelt, Maryland*

Sponsored by  
National Aeronautics and Space Administration  
Institute of Environmental Sciences  
American Institute for Aeronautics and Astronautics  
American Society for Testing and Materials  
Canadian Space Agency



National Aeronautics  
and Space Administration

**Goddard Space Flight Center**  
Greenbelt, Maryland 20771

**1992**





## FOREWORD

The Seventeenth Space Simulation Conference, held at the Omni Inner Harbor Hotel in Baltimore, Maryland from November 9th through 12th, 1992, was hosted by the Institute of Environmental Sciences (IES) and was supported by the American Institute of Aeronautics and Astronautics (AIAA), the American Society for Testing and Materials (ASTM), the National Aeronautics and Space Administration (NASA), and the Canadian Space Agency.

The fine technical papers in these proceedings evidence the quality of the contributed presentations. In addition, three speakers were invited to address issues of technical, economic, and political importance in the rapidly changing global political and financial environment in which the world currently finds itself. First, Roald Sagdeev, Distinguished Professor of Physics at the University of Maryland and formerly Head of the Theory Division, Institute of Space Research, USSR, spoke on "International Space Efforts: Past and Future" at the opening plenary session. Frank Cepollina, our luncheon speaker, Project Manager for the Hubble Space Telescope Flight Systems Servicing Project, spoke on the repair mission--the most difficult NASA has ever undertaken. Finally, Jack Mannix, Assistant Administrator for Commercial Programs at NASA, spoke on "Space Commerce--A Long-Term Project for People with Long-Term Vision" at the second plenary session. The conference was also preceded by a tutorial on selected space simulation technical disciplines on Monday, November 9.

I would like to thank the conference technical chairman, Dr. Rolf Mamen, of the Canadian Space Agency, and his capable committee for a job very well done. I would also like to thank Russell T. Hollingsworth, facilities chair, for arranging the logistics with the hotel, John Campbell, Meeting Manager, for planning the operation of the conference, and Joseph L. Stecher, III, without whom these proceedings would not have been published. Our host society, the IES, provided program coordination by Vinette N. Kopetz, and contributed support from Executive Director Janet A. Ehmann; I extend my appreciation to both of them.

These proceedings constitute a milestone as the technical/scientific community associated with the space industry grapples with changing times, and will be beneficial from that standpoint to all who read them.

Raymond D. Rempt  
General Chairman



**COMMITTEES FOR  
17TH SPACE SIMULATION CONFERENCE**

**MEETING MANAGEMENT COMMITTEE**

General Chairman:	Dr. Raymond D. Rempt, Boeing Defense & Space Group
Technical Program:	Dr. Rolf Mamen, Canadian Space Agency
IES Meeting Manager:	John D. Campbell, Consultant
Publication Chairman:	Joseph L. Stecher, NASA Goddard Space Flight Center
Publication Co-chairman:	Alda Simpson, NASA Goddard Space Flight Center
IES Executive Director:	Janet A. Ehmann, Institute of Environmental Sciences
IES Program Coordinator:	Vinette N. Kopetz, Institute of Environmental Sciences

**TECHNICAL PROGRAM COMMITTEE**

Greg Proulx, Hughes Aircraft Company  
John W. Harrell, Jet Propulsion Laboratory  
Albert R. Lunde, Boeing Aerospace  
Robert P. Parrish, Jr., Martin Marietta Corporation  
Piero Messidoro, Alenia Spazio, S.p.A.  
Patric F. Neary, TRW  
Alda Simpson, NASA Goddard Space Flight Center

**JOINT POLICY COMMITTEE**

**IES**

John D. Campbell, Consultant  
Joseph L. Stecher, NASA Goddard Space Flight Center

**ASTM**

Albert R. Lunde, Boeing Defense & Space Group  
George F. Wright, Jr., Sandia National Laboratories

**AIAA**

John W. Harrell, Jet Propulsion Laboratory  
Robert P. Parrish, Jr., Martin Marietta Corporation



# CONTENTS

## SESSION A: ATOMIC OXYGEN

Low Earth Orbit Atomic Oxygen Simulation for Durability Evaluation of Solar Reflector Surfaces .....	1
<i>Kim K. de Groh, Bruce A. Banks</i>	
Simulation of the Synergistic Low Earth Orbit Effects of Vacuum Thermal Cycling, Vacuum UV Radiation and Atomic Oxygen .....	19
<i>Joyce A. Dever, Kim K. de Groh, Curtis R. Stidham, Thomas J. Stueber, Therese M. Dever, Elvin Rodriguez, and Judith A. Terlep</i>	
The Use of Plasma Ashers and Monte Carlo Modeling for the Projection of Atomic Oxygen Durability of Protected Polymers in Low Earth Orbit .....	37
<i>Bruce A. Banks, Bruce M. Auer, Sharon K. Rutledge, Kim K. de Groh, and Linda Gebauer</i>	
Leveling Coatings for Reducing the Atomic Oxygen Defect Density in Protected Graphite Fiber Epoxy Composites .....	49
<i>D. A. Jaworske, K. K. de Groh, G. Podojil, T. McCollum, and J. Anzic</i>	

## SESSION B: DYNAMICS TESTING

Multi-Axis Transient Vibration Testing of Space Objects-- Test Philosophy, Test Facility and Control Strategy .....	59
<i>G. Lachenmayr</i>	
Vibration and Acoustic Testing of TOPEX/Poseidon Spacecraft .....	75
<i>Dave Boatman, Terry Scharton, Donald Hershfeld, and Paul Larkin</i>	
The Design Concept of the 6-Degree-of-Freedom Hydraulic Shaker at ESTEC .....	85
<i>P. W. Brinkmann and D. Kretz</i>	

## SESSION C: SPECIAL TOPICS

An Environmental Testing Facility for Space Station Freedom Power Management and Distribution Hardware .....	109
<i>Arthur S. Jackola and Gary L. Hartjen</i>	
Manned Testing in a Simulated Space Environment .....	111
<i>Donna L. Fender</i>	

### SESSION C (cont.)

On-Orbit Deployment Anomalies: What Can be Done? .....	113
<i>Michael T. Freeman</i>	
Hypervelocity Impact Simulations of Whipple Shields .....	137
<i>Steven B. Segletes and Jonas Zukas</i>	
Offloading Techniques for Large Deployable Space Structures .....	151
<i>Levino Caravaggio and Alex Golob</i>	

### SESSION D: THERMAL VACUUM TESTING I

A New Approach for Data Acquisition at the JPL Space Simulators .....	153
<i>Terry C. Fisher</i>	
A New Thermal Vacuum Facility at the Martin Marietta Waterton Plant .....	165
<i>Robert N. Watson and John W. Bonn</i>	
Application of Programmable Logic Controllers to Space Simulation .....	183
<i>Janet Sushon</i>	
An Alternate Method for Achieving Temperature Control in the -130 °C to 75 °C Range .....	197
<i>Kenneth R. Johnson, Mark R. Anderson, Robert W. Lane, and Maximo G. Cortez</i>	

### SESSION E: THERMAL VACUUM TESTING II

The Evolution of Space Simulation .....	207
<i>Arthur A. Edwards</i>	
From Diffusion Pumps to Cryopumps: The Conversion of GSFC's Space Environment Simulator .....	221
<i>Ron Cary</i>	
Cleaning of a Thermal Vacuum Chamber With Shrouds in Place .....	229
<i>William R. Bond</i>	
Intespace's New Thermal-Vacuum Test Facility: SIMMER .....	239
<i>Raymond Duprat and André Mouton</i>	

## SESSION F: MATERIALS/CONTAMINATION I

Operational Strategies for Contamination Control of Composite Materials .....	251
<i>Patricia A. Hansen</i>	
Accelerated Simulation of Near-Earth-Orbit Polymer Degradation .....	253
<i>Eric Laue</i>	

## SESSION G: MATERIALS/CONTAMINATION II

Degradation of Radiator Performance on Mars Due to Dust .....	275
<i>James R. Gaier, Marla E. Perez-Davis, Sharon K. Rutledge, and Mark Forkapa</i>	
Control of On-Orbit Contamination for the ARGOS (P91-1) Satellite .....	289
<i>Joseph G. Kelley</i>	
A New Approach for Performing Contamination Control Bakeouts in JPL Thermal Vacuum Test Chambers .....	303
<i>Kenneth R. Johnson, Daniel M. Taylor, Robert W. Lane, Maximo G. Cortez, and Mark R. Anderson</i>	
Mass Spectrometer Use in a Large Chamber .....	313
<i>Tom Chuvala</i>	

## SESSION H: PROGRAM/SYSTEMS TESTING

TQM in a Test Environment .....	315
<i>Gary D. Chambers, Elizabeth A. King, and Keith Oleson</i>	
Acoustic and Thermal Testing of the Titan/Centaur Upper Stage .....	327
<i>Mark Gehringer, Chris Gibson, and Ron Janes</i>	
System Test Approach for the SAX Satellite .....	329
<i>Pietro Giordano, Giacomo Raimondo, and Piero Messidoro</i>	

## AUXILIARY SESSION

Overview of the Environmental Test Plans for Space Station Freedom Work Package 4 .....	343
<i>Tom J. Peterson</i>	





## LOW EARTH ORBIT ATOMIC OXYGEN SIMULATION FOR DURABILITY EVALUATION OF SOLAR REFLECTOR SURFACES

Kim K. de Groh  
Bruce A. Banks  
NASA Lewis Research Center

### ABSTRACT

To evaluate the performance and durability of solar reflector surfaces in the atomic oxygen environment typical of low Earth orbit (LEO) one must expose the reflector surface either directly to LEO or to ground-laboratory atomic oxygen environments. Although actual LEO exposures are most desired, such opportunities are typically scarce, expensive, and of limited duration. As a result, ground-laboratory exposures must be relied upon as the most practical long-term durability evaluation technique. Plasma ashers are widely used as LEO simulation facilities by producing atomic oxygen environments for durability evaluation of potential spacecraft materials. Atomic oxygen arrival differs between ground and space exposure in that plasma asher exposure produces isotropic arrival and space solar tracking produces sweeping arrival. Differences in initial impact reaction probability occur, dependent upon the energy and species existing in these environments. Due to the variations in ground-laboratory and space atomic oxygen, quantification of in-space performance based on plasma asher testing is not straightforward. This paper addresses the various atomic oxygen interactions that can occur with reflector surfaces, such as undercutting in organic substrates at protective coating defect sites, ground-laboratory techniques recommended for evaluating the atomic oxygen durability of reflectors based on asher exposures, and computational techniques which make use of ground-laboratory atomic oxygen exposure to predict in-space LEO durability.

### INTRODUCTION

Long term space exposure on the Long Duration Exposure Facility (LDEF), which orbited in the low Earth orbit environment for 5.8 years, provided evidence of environmental degradation of many potential spacecraft materials. Organic materials are particularly susceptible to erosive degradation in LEO. A number of polymer films up to 0.076 mm (0.003") thick located on the leading edge of LDEF were completely eroded, and approximately 1 ply (0.127 mm) of graphite epoxy composite was eroded (ref. 1). The ram atomic oxygen fluence for the leading edge of LDEF (8° yaw off-set) was  $8.72 \times 10^{21}$  atoms/cm<sup>2</sup> (ref. 2). Figure 1 shows the erosion morphology of a fluoro-polymer (polychlorotrifluoroethylene) which was located on the leading edge of LDEF (row 9). This cone-like morphology is typical of direct ram impact erosion of organic materials.

Atomic oxygen, formed through photodissociation of molecular oxygen by ultraviolet (UV) radiation having wavelengths less than 240 nm, is the predominant species in LEO (ref. 3). Spacecraft orbiting at altitudes of  $\approx 400$  km ram into these oxygen atoms with velocities on the order of  $\approx 7,000$  m/sec. At ram velocities the oxygen atoms have an average impact energy of 4.5 eV (ref. 4). These oxygen atoms have sufficient energy to break chemical bonds and oxidize many materials. In the case of organic materials, the oxidation product is often a volatile species (ref. 5). The use of thin film inorganic protective coatings has been found to protect underlying organic materials from atomic oxygen erosion. In general, metal oxides (i.e. SiO<sub>2</sub>) and metals which form inherent protective oxide layers (i.e. Al) provide protection from atomic oxygen interaction.

To evaluate the performance and durability of potential spacecraft materials in the LEO atomic oxygen environment one must expose the material either directly to LEO (such as on LDEF or on the shuttle) or to ground-laboratory atomic oxygen environments. Although actual LEO exposures are most desired, such opportunities are typically scarce, expensive, and of limited duration (i.e. typical shuttle exposure duration is 40-80 hours, with atomic oxygen fluences generally  $\leq 4 \times 10^{20}$  atoms/cm<sup>2</sup>). As a result, ground-laboratory exposures must be relied upon as the most practical evaluation technique.

This paper discusses various atomic oxygen interactions that can occur with solar reflector materials, ground-laboratory techniques recommended for evaluating atomic oxygen durability of solar reflectors using plasma ashers, and computational techniques which make use of ground-laboratory atomic oxygen exposure to predict in-space LEO durability.

## ATOMIC OXYGEN UNDERCUTTING ON LDEF

Materials shielded from atomic oxygen by means of protective coatings are still vulnerable to atomic oxygen degradation due to undercutting oxidation (oxidation below the defect site that can exceed the original defect area) at protective coating defect sites. Undercutting can occur from sweeping ram atomic oxygen exposure if a spacecraft rotates with respect to its direction of travel. Undercutting can also occur if the spacecraft is oriented with a fixed direction of travel. There are three contributions to direct ram atomic oxygen undercutting: scattering of unreacted atomic oxygen (both from scattered energetic as well as thermally accommodated), angular distribution of incoming atomic oxygen flux due to thermal velocity contributions, and spacecraft orbital inclination with respect to the Earth's velocity vector (ref. 6). Scanning electron micrographs in figures 2 and 3 show atomic oxygen undercutting of a protected (400 Å Al/800 Å Cr) graphite epoxy composite coupon which was located on the leading edge of LDEF. A crack in the protective coating next to a larger circular defect is shown before and after removal of the protective coating in figures 2a and 2b. Figure 2c shows the profile of the undercut cavity at the crack site. This profile was obtained by tilting the sample at 45° and viewing through the large defect cavity. Figure 3a is an image of what appears to be a micrometeoroid or debris impact site that resulted in damage to the protective coating. Figure 3b shows the amount of undercut damage below the protective coating at this impact area. The integrity of the protective coating is important for providing protection. Figure 4 provides a view of a protective coating which did not remain intact on the leading edge of LDEF. Energy dispersive x-ray analysis indicates that the coating is Al<sub>2</sub>O<sub>3</sub>. The original film thickness is not known but it appears that the film was < 1000 Å. Significant undercutting may have contributed to the failure of this coating. Although atomic oxygen undercutting is expected to occur in LEO, direct ram atomic oxygen undercutting has not been documented prior to LDEF retrieval.

## SOLAR REFLECTOR DURABILITY ISSUES

Solar reflector concentrators have been designed for use on Solar Dynamic Power Modules (SDPM) for delivery of additional electrical power for Space Station Freedom (SSF). In a SDPM, the solar concentrator reflects and focuses solar energy into the receiver of a heat engine. Various types of reflector compositions have been considered for solar concentrators for SSF and for advanced solar dynamic concepts. The solar concentrator designed and LEO durability tested for SSF was composed of a sandwich type structure with graphite epoxy face and back sheets bonded to an Al honey-comb core. A multi-layer reflective/protective system was designed for LEO durability. Silver was chosen as the reflective material. Silver will oxidize in the presence of atomic oxygen, therefore two atomic oxygen protective layers were deposited on top of the Ag, Al<sub>2</sub>O<sub>3</sub> (also an adhesion promoting layer), followed by an outer coating of SiO<sub>2</sub>. Figure 5 shows a sketch of a SDPM with a section view of the concentrator. For efficient operation of the SDPM, the solar concentrator must have and maintain a high solar specular reflectance in LEO. Maintaining a high solar specular reflectance is the critical atomic oxygen durability issue.

Other concentrator concepts have been considered either for SSF SDPM or for advanced solar dynamic systems with a variety of substrates including stainless steel, aluminum and glass. If an inorganic substrate such as Al or SiO<sub>2</sub> is used with a Ag reflective coating, Ag-oxide can expand out of the protective coating defect sites and a Ag-oxide "fluff" can develop (see figure 6)(ref. 7). Although undercutting is prevented in this case, the Ag-oxide can cause a decrease in the solar specular reflectance (ref. 7). If an organic material is used, such as graphite epoxy as the substrate for SDPM concentrators, then atomic oxygen undercutting can occur at protective coating defect sites. Decreases in solar specular reflectance due to atomic oxygen interactions with oxidizable reflectors result from oxidation of the reflecting material at defect sites, and undercutting and subsequent reflective material oxidation at defect sites. If the protective film tears when undercut, curling of the protective/reflective film will allow more atomic oxygen to enter the defect area and a catastrophic undercutting-tearing propagation process can occur. Figure 7 shows atomic oxygen undercutting, and tearing of the reflective and protective films in a graphite epoxy concentrator coupon after a Kapton based effective fluence of  $3 \times 10^{21}$  atoms/cm<sup>2</sup>. The extent of the undercutting is visible as a

bright area around the defect sites. In this case the undercut regions of several defects have propagated into each other. Figure 8 is a micrograph of the adjoining undercut cavities of several defect sites where the reflective and protective films have flaked off due to lack of support from the volatilized substrate.

The use of a leveling layer on rough graphite epoxy substrates has been found to significantly reduce the number of protective coating defect sites. In the case of line of site deposition, if a rough substrate is being coated, areas in the shadow will not be coated. These sites are then vulnerable to atomic oxygen erosion. If a surface tension leveling layer is first applied to the graphite epoxy followed by reflective and protective coatings, the number of atomic oxygen defect sites has been found to be reduced by up to 2 orders of magnitude (ref. 8). In addition to decreased defect density, the specular reflectance may also be improved through the use of a leveling coating.

## GROUND-LABORATORY ATOMIC OXYGEN

Radio frequency generated plasma ashers are widely used for LEO durability evaluation by producing an inexpensive, high flux atomic oxygen environment. The environment that plasma ashers produce when operated on air contains oxygen and nitrogen ions, atoms and molecules (ref. 10). Studies on Kapton have found that the nitrogen species have a negligible effect on the erosion processes (ref. 11). Ashers typically provide accelerated exposures with atomic oxygen effective fluxes (based on Kapton erosion) on the order of  $10^{15}$  atoms/cm<sup>2</sup> sec as opposed to  $10^{14}$  atoms/cm<sup>2</sup> sec at 400 km in LEO (ref. 9). The arrival of oxygen atoms on a surface differs between asher and space exposure in that plasma asher exposure produces isotropic arrival and space produces either direct ram arrival or sweeping arrival on solar tracking surfaces. In addition, differences in the initial impact reaction probability occur which are dependent upon the energy and species existing in these environments. The erosion yield of organic materials has been found to be dependent on the impact energy of the incident atomic oxygen. The erosion yield of Kapton was found to be proportional to the 0.68 power of the impact energy by Ferguson (ref. 12), and proportional to  $e^{-0.38}/\text{Energy}$  by Koontz (ref. 13).

The average reaction probability upon first impact (at normal incidence) for direct space ram or sweeping space ram with Kapton is approximately 0.138 (ref. 4). The majority of unreacted atomic oxygen is believed to thermally accommodate and leave the surface with a cosine distribution. For plasma ashers, the reaction probability on first impact is thought not to be greater than 0.0054 (ref. 13). In both space and plasma environments the reaction probability for the second and subsequent impacts is approximately 0.00134 because the atoms have thermal energies (0.04 eV for 300 K) (ref. 13). Because of the higher initial impact reaction probability, direct ram exposure will produce a deeper undercut cavity than would be produced by the same actual fluence in an asher. In the asher, the cavity beneath a pin window defect will be shallower but wider. This is due to the high absolute fluences needed to produce effective fluences simulating space because of the low thermal energies. For solar facing systems which are exposed to sweeping ram arrival, the undercut cavity will be shallower and wider than direct ram impact, but not as shallow and wide as asher exposures. Because the atomic oxygen impact energies, reaction probabilities, and direction of arrival are different between plasma asher atomic oxygen exposure and space atomic oxygen exposure, one cannot directly extrapolate space predictions based on asher exposures. A Monte Carlo model is currently being developed at Lewis for predicting undercut profiles for ground-based and LEO atomic oxygen exposures (ref. 13). The model will be used to predict long term LEO atomic oxygen durability of Space Station Freedom (SSF) power system materials.

## GROUND-LABORATORY TECHNIQUES FOR ATOMIC OXYGEN DURABILITY EVALUATION

The following techniques are recommended for atomic oxygen durability evaluation of solar reflectors using a plasma asher. First, it is important to carefully document pristine samples. Detailed characterization prior to and after atomic oxygen exposure is critical for understanding any failure mechanisms involved and for projecting durability trends. For solar reflector surfaces, it is advised to document the pristine solar specular reflectance, solar absorptance, and the surface morphology. Optical microscopy is a technique which can provide non-destructive surface morphology characterization. Some surface features are only noticeable using polarized light, so both polarized and non-polarized images should be obtained when possible. Due to variations in surface morphology and reflectance of test coupons, care should be taken when obtaining reflectance values to measure exactly the same location(s) prior to and after atomic oxygen exposure. For large aperture specular reflectance measurements, (such as

with integrating spheres) it is advised to obtain at least two measurements (preferably at 90° rotation) and average the values. For small aperture reflectance measurements (such as D&S 15 R reflectometer), an average of 5 or more values should be made.

One should expose a witness coupon during plasma ashing simultaneously with the sample coupon in order to calculate the effective atomic oxygen fluence. It is recommended to use a coupon of the same material being evaluated if in-space erosion data exist. For example, if a solar reflector with a graphite epoxy substrate is being evaluated, an uncoated graphite epoxy witness coupon should be simultaneously ashed with the concentrator sample. For a material whose in-space erosion is not known, Kapton polyimide is frequently used as a witness coupon because the erosion yield of Kapton in LEO has been well characterized ( $3.0 \times 10^{-24} \text{ cm}^3/\text{atom}$ ) (ref. 14). A piece of 0.0127 cm Kapton can be used for continuous exposure for approximately 4 days, or an approximate effective fluence of  $1 \times 10^{21} \text{ atoms/cm}^2$ . Pyrolytic graphite can be used for long term exposures because samples are generally thicker and the erosion yield is less than half that of Kapton. Due to the hygroscopic nature of polymer materials it is best to dehydrate the witness coupons prior to measuring the mass. Kapton 0.0127 cm thick is completely dehydrated in 48 hours under vacuum. Thicker material may take longer to dehydrate. Because the flux can vary in the asher chamber, the witness coupon should be placed in close proximity to the sample being evaluated. It is recommended that the sample being evaluated should be placed in the center of the asher. Glass racks can be custom made with a variety of spacings (for exposure on all sides) to position samples. After atomic oxygen asher exposure, the effective fluence (F) can be calculated as shown in equation 1.

$$F = \frac{(M_o - M_a)}{A \rho E} \quad (1)$$

where:

$M_o$  = original dehydrated witness coupon mass, g

$M_a$  = ashed dehydrated witness coupon mass, g

$A$  = surface area of witness coupon,  $\text{cm}^2$

$\rho$  = density of witness coupon,  $\text{g/cm}^3$

$E$  = in-space erosion yield of witness coupon,  $\text{cm}^3/\text{atom}$

One of the common problems with atomic oxygen exposure in ground-laboratory facilities and in space, is the interaction with silicones and the resulting contamination. Silicone contamination was found on many samples on LDEF (ref. 15) and in some cases resided as a brown film (ref. 16). Silicone contamination as deposited in the asher (on samples, witness coupons, support racks and chamber walls) can range from a thin rainbow film, to a thick waffled deposit as shown in figure 9. Silicone contamination, once obtained inside an asher, will linger and be re-deposited on inside walls and on samples well after the original source of silicone is removed. To decrease the threat of silicone contamination on samples in plasma ashers one should not use the gaskets which contain silicone, such as those typically provided by the manufacture. Second, do not use any silicone-containing vacuum grease. Even brands which are quoted not to contain silicones, can show Si peaks with Energy Dispersive X-ray analysis. It is recommended to use a petroleum jelly as a vacuum grease. It is also important to keep the pressure above 60 mtorr to prevent back streaming of the pump oil which can contain silicone. Ashers can be partially cleaned of silicone contamination by running the ashers empty with cleaned microscope slides in them. It is believed that some of the silicone fragments will be deposited onto the slides, and so frequent replacement will reduce the contamination. If silicone contamination is severe, it is recommended to replace all removable parts (including the inner and outer chambers). If possible, it is advised to have two ashers, one for evaluating silicone-containing materials, and one for "clean" non-silicone containing samples.

Often during atomic oxygen exposure it is desirable to mask a section of the sample. For example, to determine the effect of atomic oxygen on the transmittance of a transparent sample generally only one side of the sample should be exposed to the plasma environment. In many cases samples have protective coatings deposited on one side only. For thin samples coated on one side it is necessary to mask the back-side of the sample so that only the protected side is exposed to the plasma for evaluation. Aluminum foil is a flexible, atomic oxygen durable material which can be considered, but it should be kept in mind that metals heat up in RF plasmas and may also cause local flux increases. The recommended material for masking samples is glass. The backside of a thin sample can be adequately protected

by sandwiching the sample between two glass slides, with the top slide containing holes for exposure. It is critical that there be intimate contact between the masking material and the sample, because a plasma can form inside an air pocket, and atomic oxygen scattering allows the oxygen atoms to travel along thin pathways.

When evaluating results from plasma asher exposures, it needs to be kept in mind that there is a high level of vacuum ultraviolet radiation (VUV) produced in the plasma environment. The exact level of VUV is not known, but is reported to have a flux of  $10^{12} - 10^{14}$  photons  $\text{cm}^{-2}\text{s}^{-1}$  at 130 nm, as compared to  $\approx 4 \times 10^{11}$  photons  $\text{cm}^{-2}\text{s}^{-1}$  at 121.6 nm in LEO (ref. 17). It is therefore difficult to determine if certain appearance changes, such as discoloration, are due to UV darkening, or atomic oxygen interactions, or both. Atomic oxygen durability evaluation of solar concentrator coupons for SSF indicated spectral changes and a corresponding surface yellowing with plasma asher exposure (ref. 18). Analytical analysis (secondary ion mass spectroscopy & Auger electron analysis) indicated the deposition of an oxide film which may have occurred during plasma ashing. Therefore the possibility of discoloration due to a variation in the oxide thickness or color center formation through stoichiometric changes due to interaction with atomic oxygen appears to be as likely a contributor to darkening as UV solarization (ref. 18). In an attempt to further understand the potential for film deposition during plasma ashing, a SDPM concentrator coupon, such as those described under Solar Reflector Durability Issues, was 1/3 covered with a fused silica slide and then exposed to atomic oxygen in a "clean" plasma asher. After an effective fluence of  $2.1 \times 10^{21}$  atoms/ $\text{cm}^2$  the exposed side of the coupon, particularly near the fused silica cover, was discolored (whitish) as seen in figure 10. This indicated that either a film had been deposited on the exposed side or color centers had developed. X-ray photoelectron spectroscopy analysis of the exposed and unexposed sides indicate the top oxide layer ( $\text{SiO}_x$ ) is 100 Å thicker on the atomic oxygen exposed side than the on masked side. A complication with this technique is that a very large area is scanned (1 mm) and probably contains undercut defect sites. The oxide film may appear thicker if the undercut film has curled down into the undercut cavity.

Another durability evaluation issue that one should recognize when using plasma ashers is the potential acceleration in atomic oxygen damage which can occur during iterative ashing. Often it is desirable to observe trends such as solar specular reflectance change versus effective fluence. Concentrator coupons durability tested for use on SSF have been found to undergo accelerated erosion damage when iteratively ashed, as opposed to continuously ashed to the same effective fluence (ref. 18). It is advised when ashing samples iteratively, to ash at least one similar sample continuously to the same effective fluence to check for accelerated damage due to repeated atmospheric exposures and pressure changes.

## EXTRAPOLATION OF IN-SPACE REFLECTANCE DEGRADATION BASED ON GROUND-LABORATORY TESTING

Although ground-laboratory plasma asher testing is highly valuable to discriminate relative solar specular reflectance performance of reflector surfaces in an atomic oxygen environment, quantification of in-space reflectance durability based on plasma asher testing is not obvious. A series of conversion factors does allow reasonable arguments to be made to perform this extrapolation. Based on the results of Banks, et.al. (ref. 19), if one assumes that the concentrator surface consists of an atomic oxygen protective coating over an oxidizable substrate with pin window defects, then the rate of change of solar specular reflectance  $\rho_{p,s}$  with atomic oxygen fluence in sweeping space ram,  $f_s$ , can be expressed as an identity of conversion terms shown in Equation 2:

$$\frac{d\rho_s}{dF_s} = \frac{d\rho_s}{dN_s} \frac{dN_s}{dV_s} \frac{dV_s}{dV_a} \frac{dV_a}{dN_a} \frac{dN_a}{d\rho_a} \frac{d\rho_a}{dF_e} \frac{dF_e}{dF_s} \quad (2)$$

where:

$\rho_s$  = solar specular reflectance for pin window defects in space

$\rho_a$  = solar specular reflectance for pin window defects in plasma ashers

$F_s$  = atomic oxygen fluence in sweeping space ram, atoms/ $\text{cm}^2$

$F_e$  = Kapton effective atomic oxygen fluence in plasma ashers, effective atoms/ $\text{cm}^2$

$N_s$  = non-reflecting undercut area below pin window defects in space,  $\text{cm}^2$

$N_a$  = non-reflecting undercut area below pin window defects in plasma ashers,  $\text{cm}^2$   
 $V_s$  = undercut cavity volume below pin window defects for in space,  $\text{cm}^3$   
 $V_a$  = undercut cavity volume below pin windows in plasma ashers,  $\text{cm}^3$

One can show that:

$$\frac{d\rho_s}{dN_s} = \left( \frac{dN_a}{d\rho_a} \right)^{-1} = -\rho_o n \quad (3)$$

where:

$\rho_o$  = unexposed solar specular reflectance  
 $n$  = number of pin window defects per  $\text{cm}^2$

Thus, the first and fifth factors in Equation 2 cancel. One can also show that:

$$\frac{dN_s}{dV_s} = \frac{1}{cV_s^{\frac{1}{3}}} \quad (4)$$

where:

$c$  = constant

and:

$$\frac{dV_a}{dN_a} = cV_a^{\frac{1}{3}} \quad (5)$$

Note that for Equations 4 and 5 the constant is the same in each equation because the geometry of the undercut cavities are assumed to be approximately the same for plasma ashers and sweeping space ram, that of a one-half prolate spheroid. One can also argue, based on reference (ref. 19), that:

$$\frac{dV_s}{dV_a} = \frac{P_i + \frac{(1-P_i) k P_t A_s}{k P_t A_s + \pi r_d^2}}{4P_t + \frac{(1-4P_t) k A_a}{k P_t A_a + \pi r_d^2}} \quad (6)$$

where:

$P_i$  = atomic oxygen initial impact reaction probability in space = 0.138  
 $A_a$  = surface area of undercut cavity in plasma asher,  $\text{cm}^2$   
 $P_t$  = reaction probability of thermally accommodated atomic oxygen  
 $A_s$  = surface area of undercut cavity in space,  $\text{cm}^2$   
 $r_d$  = pin window defect radius, cm  
 $k$  = 2/3

For the purposes of further quantification of Equation 6, the erosion yield of the undercut polymer material is assumed to be  $3 \times 10^{-24} \text{ cm}^3/\text{atom}$  for normal incident atoms. The value,  $k$ , is used to correct the reaction probabilities for averaging overall angle of incidence in a defect cavity, knowing that the erosion yields depend on  $(\cos$

$\Theta)^{1/2}$  where  $\Theta$  is the angle from normal incidence (see reference 19). Based on reference 13, the presence of more reaction-excited species in an asher causes the asher atomic oxygen initial reaction probability to be four times that of subsequent interactions. Although the erosion modeling is based on Kapton, the equation is valid for different erosion yield reflector substrates provided Kapton effective fluence  $F_e$  measurements are made. The reaction probability of normal incident thermally accommodated atomic oxygen,  $P_t$ , is 0.00134. Thus, equations 4, 5, and 6 are fluence-dependent, which implies that the conversion of plasma asher to in-space performance will be fluence-dependent. The term  $d\rho_a/df_e$  is the input change in solar specular reflectance with respect to effective atomic oxygen fluence. The last term can be quantified through Monte Carlo modeling measurements as shown in reference (ref. 19), and is given by:

$$\frac{dF_e}{dF_s} = \frac{dy_a}{dy_s} = 0.0483 \quad (\text{ref. 13}) \quad (7)$$

where:

$y_a$  = Monte Carlo predicted Kapton thickness loss for uncoated Kapton in a plasma asher, Monte Carlo cell length units

$y_s$  = Monte Carlo predicted Kapton thickness loss for uncoated Kapton in a sweeping space ram environment, Monte Carlo cell length units

The ratio  $dy_a/dy_s$  is not simply equal to  $4P_t/P_i$  because in an asher the reaction probability for scattered thermally accommodated atoms can contribute measurably to erosion of an unprotected rough material, whereas in space the higher reaction probability of energetic atoms dominates.

Thus, combining equations 2-7 results in a range of ground-laboratory to in-space projection coefficients depending on whether large undercut cavities exist ( $A_s > \pi r_d^2$ , high fluence) or undercut cavities on the same order of magnitude as the defect area ( $A_s \approx \pi r_d^2$ , low fluence) exist. Substituting quantities in the equations results in the following fluence-dependent relationships.

For small undercut cavities ( $A_s \approx \pi r_d^2$ ):

$$\frac{d\rho_s}{dF_s} = \frac{d\rho_a}{dF_e} \quad (8)$$

For large undercut cavities ( $A_s > \pi r_d^2$ ):

$$\frac{d\rho_s}{dF_s} = 0.05 \frac{d\rho_a}{dF_e} \quad (9)$$

Thus, as can be seen in Equation 8 and Equation 9, for low fluence exposure, the degradation of solar specular reflectance in space occurs at the same rate measured in plasma ashers, whereas for high fluence the rate of degradation of in-space reflectance is only 5% that which is observed in a plasma asher, with a range of degradation rates in between. The reason the plasma asher degradation rate is much higher than that which occurs in space for high fluences is related to the high degree of trapping (in the undercut cavity) of thermally accommodated atomic oxygen. Samples are exposed to very high quantities of thermally accommodated atomic oxygen in the asher, because a larger quantity of lower energy thermally accommodated oxygen atoms are needed to achieve an equivalent effective fluence based on high energy LEO ram atomic oxygen.

Two concentrator coupons continuously ashed to a Kapton based effective fluence of  $3.1 \times 10^{21}$  atom/cm<sup>2</sup> (1.08 years on SSF) were found to decrease in solar specular reflectance by 0.055 and 0.085, with resulting values of 0.806 and 0.775 (ref. 18). If this data were directly extrapolated to 15 years on SSF, it would be predicted that the remaining solar specular reflectance would be only 0.096 and 0.000. Based on the above calculated ground-laboratory

to in-space projection coefficient for large undercut cavities, and the plasma asher results, the predicted solar specular reflectance for 1.08 year in LEO would be 0.858 to 0.856. Figure 11 shows solar specular reflectance decrease versus atomic oxygen fluence for asher results and for the LEO predictions based on the asher results. The lines represent the average of two values (two LEO predicted solar specular reflectance values appear as one). The calculated prediction for in-space solar specular reflectance for 15 years, based on the asher results for 1.08 years, would be 0.819 to 0.804. This is the best case scenario because the smallest projection coefficient was used. For more accurate lifetime predictions, higher effective fluence exposures should be conducted.

## CONCLUSIONS

Materials shielded with an atomic oxygen protective coating are still vulnerable to LEO atomic oxygen degradation due to undercutting at defect sites. Protected organic materials located on the leading edge of LDEF provided evidence of atomic oxygen undercutting in direct ram exposure. To evaluate performance and durability of potential spacecraft materials, ground-laboratory exposures are relied upon as the most practical technique. Techniques have been recommended for durability testing of solar reflector coupons using a plasma asher. Although plasma ashers provide atomic oxygen environments which are quite different from LEO, these facilities provide an easy, inexpensive method to evaluate the atomic oxygen durability of potential spacecraft materials. Because of the variations in the arrival direction of oxygen atoms, reaction probability (based on impact energy), and species in plasma ashers as compared to space, direct extrapolation cannot be made from asher exposures. Correction calculations must be made in order to extrapolate in-space reflectance degradation based on plasma asher exposure. Based on calculation conversion, for low fluences, the solar specular reflectance degradation would be at the same rate in LEO as in ashers. For high fluences, the rate of solar specular reflectance degradation in space would be only 5% of that observed in an asher. This is a result of the high absolute atomic oxygen fluence in plasma ashers needed to produce reasonable effective fluences. The high absolute fluence of oxygen trapped in undercut cavities results in higher rates of undercutting in the asher as compared to space.

## REFERENCES

1. Stein, B. A. and Pippin, H. Gary: Preliminary Findings of the LDEF Materials Special Investigation Group. LDEF - 69 Months in Space, First Post-Retrieval Symposium, NASA CP 3134, Part 2, 1991, pp. 617-641.
2. Bourassa, R. J. and Gillis, J. R.: Atomic Oxygen Exposure of LDEF Experiment Trays. NASA CR 189627, 1992, pp. A-307.
3. U.S. Standard Atmosphere, 1976 (U.S. Government Printing Office, Washington DC, 1976), p. 30.
4. Banks, B. A.; Rutledge, S. K.; Auer, B. M. and DiFilippo, F.: Atomic Oxygen Undercutting of Defects on SiO<sub>2</sub> Protected Polyimide Solar Array Blankets. *Materials Degradation in Low Earth Orbit (LEO)*, The Minerals, Metals & Materials Society, 1990, pp. 15-33.
5. Dever, J. A.: Low Earth Orbital Atomic Oxygen and Ultraviolet Radiation Effects on Polymers. NASA TM 103722, 1991.
6. de Groh, K. K. and Banks, B. A.: Atomic Oxygen Undercutting of LDEF Aluminized-Kapton Multilayer Insulation. LDEF - 69 Months in Space, First Post-Retrieval Symposium, NASA CP 3134, Part 2, 1991, pp. 781-795.
7. Gulino, D. A.: Atomic Oxygen Durability of Impact Damaged Solar Reflectors. *J. of Spacecraft and Rockets*, Vol. 25, No. 2, Jan.-Feb. 1988, pp. 39-44 (also see NASA TM 88874).



8. Jaworske, D. A., de Groh, K. K., Podojil, G., McCollum, T. and Anzic, J.: Leveling Coatings for Reducing the Atomic Oxygen Defect Density in Protected Graphite Epoxy Composites. 17th Space Simulation Conference, NASA CP-3181, 1992. (Paper 4 of this compilation.)
9. Bourassa, R. J. and Gillis, J. R.: Atomic Oxygen Flux and Fluence Calculation for LDEF. Boeing Defense and Space Group, 1991. LDEF document available from LDEF Science Office, NASA Langley Research Center.
10. Rutledge, S. K. and Mihelcic, J. A.: Undercutting of Defects in Thin Film Protective Coatings on Polymer Surfaces Exposed to Atomic Oxygen. NASA TM 101986, 1989.
11. Rutledge, S. K.; Banks, B. A.; DiFilippo, F.; Brady, J. A.; Dever, T. M. and Hotes, D.: An Evaluation of Candidate Oxidation Resistant Materials for Space Applications in LEO. NASA TM 100122, 1986.
12. Ferguson, D. C.: The Energy Dependence and Surface Morphology of Kapton Degradation Under Atomic Oxygen Bombardment. 13th Space Simulation Conference, The Payload - Testing for Success, NASA Conference Publication 2340, 1984, pp. 205-221.
13. Banks, B. A.; Auer, B. M.; Rutledge, S. K., de Groh, K. K. and Gebauer, L.: The Use of Plasma Ashers and Monte Carlo Modeling for the Projection of Atomic Oxygen Durability of Protected Polymers in Low Earth Orbit. 17th Space Simulation Conference, NASA CP-3181, 1992. (Paper 3 of this compilation.)
14. Leger, L. J. and Visentine, J. T.: A Consideration of Atomic Oxygen Interactions with the Space Station. Journal of Spacecraft and Rockets, Vol. 23, No. 5, 1986, pp. 505-511.
15. Crutcher, E. R. and Warner, K. J.: Molecular Films Associated With LDEF. LDEF - 69 Months in Space, First Post-Retrieval Symposium, NASA CP 3134, Part 1, 1991, pp. 155-177.
16. Banks, B.A.; Rutledge, S. K. and de Groh, K. K.: Low Earth Orbital Atomic Oxygen, Micrometeoroid, and Debris Interactions with Photovoltaic Arrays. Space Photovoltaic Research and Technology 1991, NASA CP 3121, 1991, pp. 45-1 - 45-10.
17. Koontz, S. L.; Albyn, K. and Leger, L. J.: Atomic Oxygen Testing with Thermal Atom Systems: A Critical Evaluation. J. Spacecraft, Vol. 28, No. 3, May-June 1991, pp. 315-323.
18. de Groh, K. K.; Dever, J. A.; McCollum, T. A.; Rodriguez, E.; Burke, C. A. and Terlep, J. A.: Low Earth Orbit Durability Evaluation of Solar Concentrator Materials. Solar Engineering 1992, Volume 2, The American Society of Mechanical Engineers, N.Y., 1992, pp. 775-782.
19. Banks, B. A.; Rutledge, S. K. Gebauer, L. and LaMoreaux, C.: SiO<sub>x</sub> Coatings for Atomic Oxygen Protection of Polyimide Kapton in Low Earth Orbit", AIAA Paper 92-2151, Proceedings of the Coatings Technology for Aerospace Systems Materials Specialists Conference, Dallas, Tx, April 16-17, 1992.

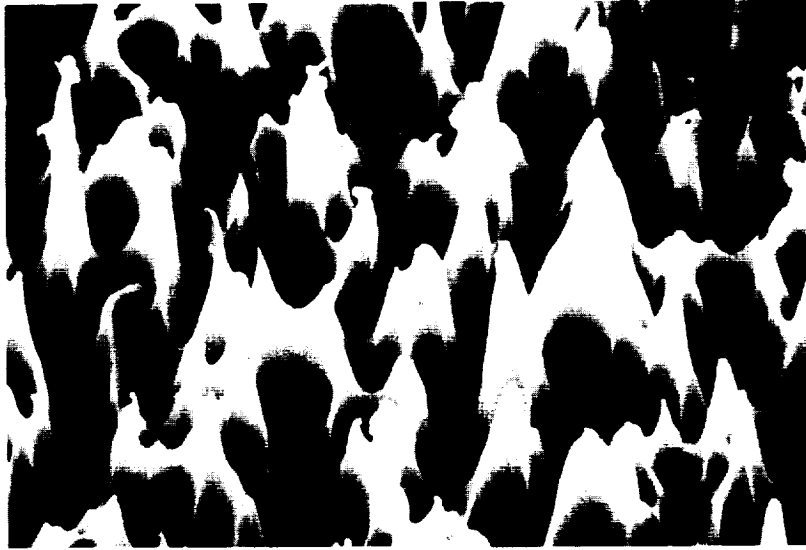


Figure 1. Polychlorotrifluoroethylene exposed to LEO atomic oxygen on the leading edge of LDEF. Typical erosion morphology of LEO direct ram atomic oxygen erosion of polymers.

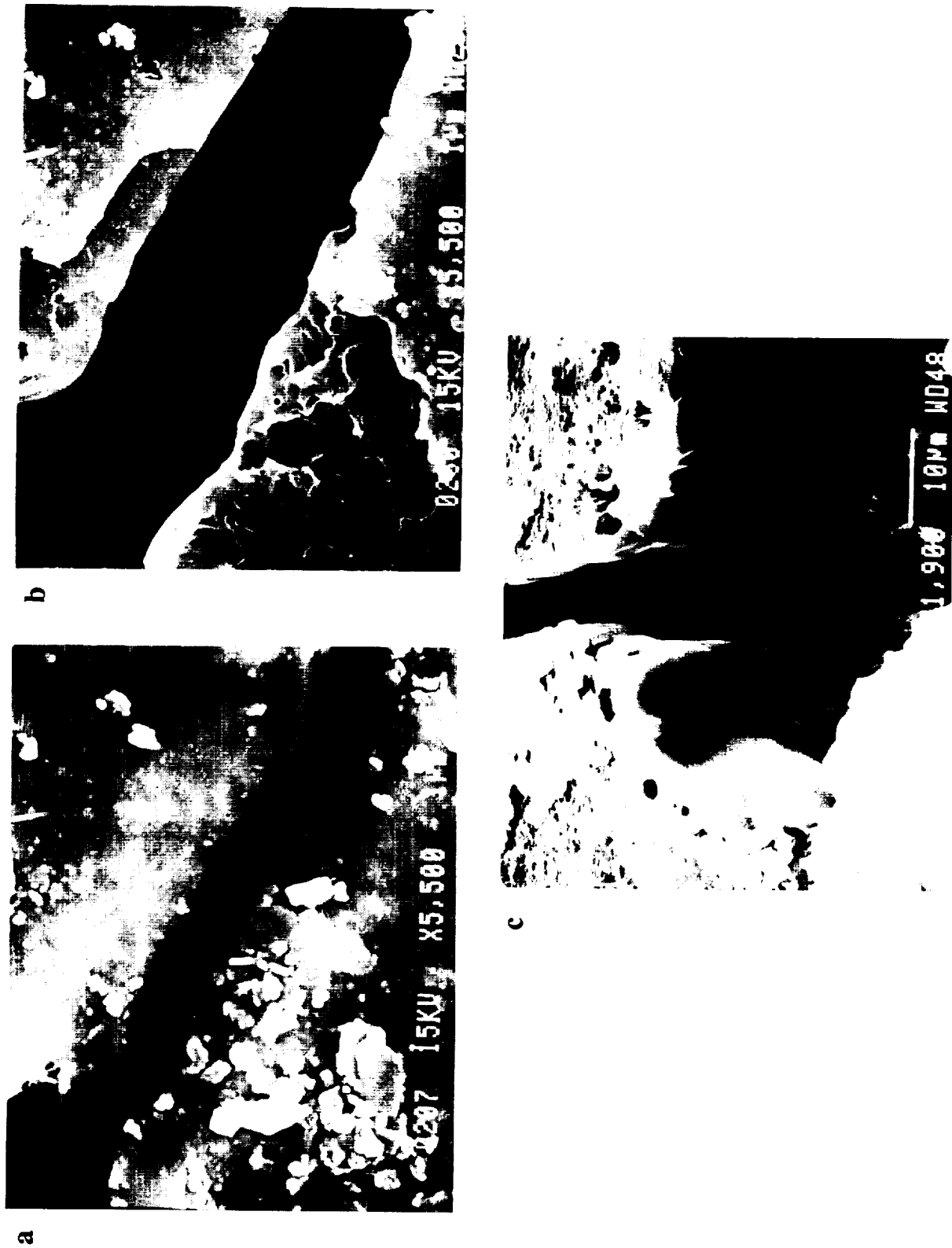
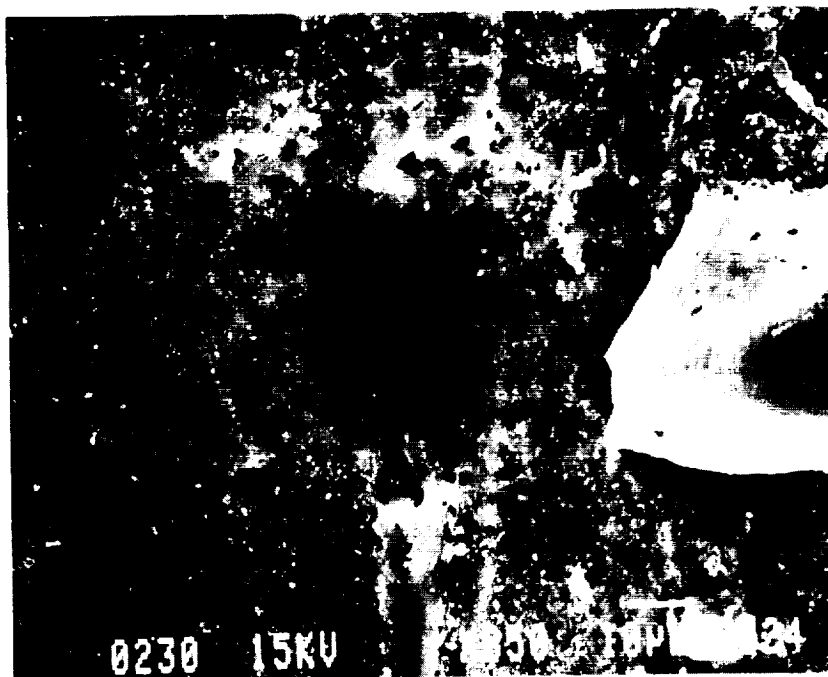


Figure 2. Protected (400Å Al/800Å Cr) graphite epoxy composite exposed to LEO atomic oxygen on the leading edge of LDEF: a. Crack site prior to removal of the protective coating, b. Undercut area at crack site after removal of protective coating, c. Undercut cavity profile at crack defect site (45° tilt).

a



b

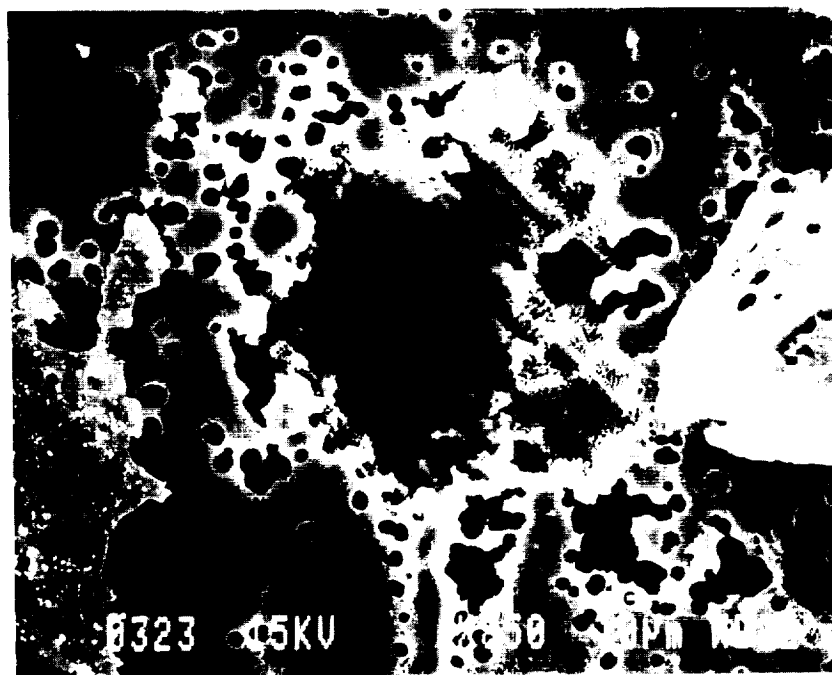


Figure 3. Protected ( $400\text{\AA}$  Al/ $800\text{\AA}$  Cr) graphite epoxy composite exposed to LEO atomic oxygen on the leading edge of LDEF: a. Damage in protective coating at possible impact site, b. Extent of undercut damage visible after removal of protective coating.

ORIGINAL PAGE  
BLACK AND WHITE PHOTOGRAPH

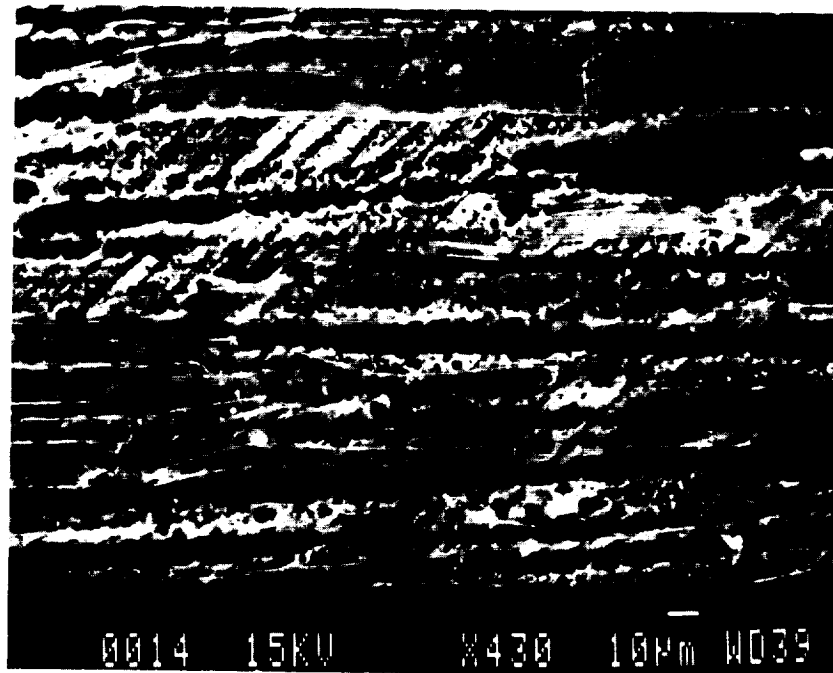


Figure 4. Failure of a protective coating exposed to LEO atomic oxygen on the leading edge of LDEF.

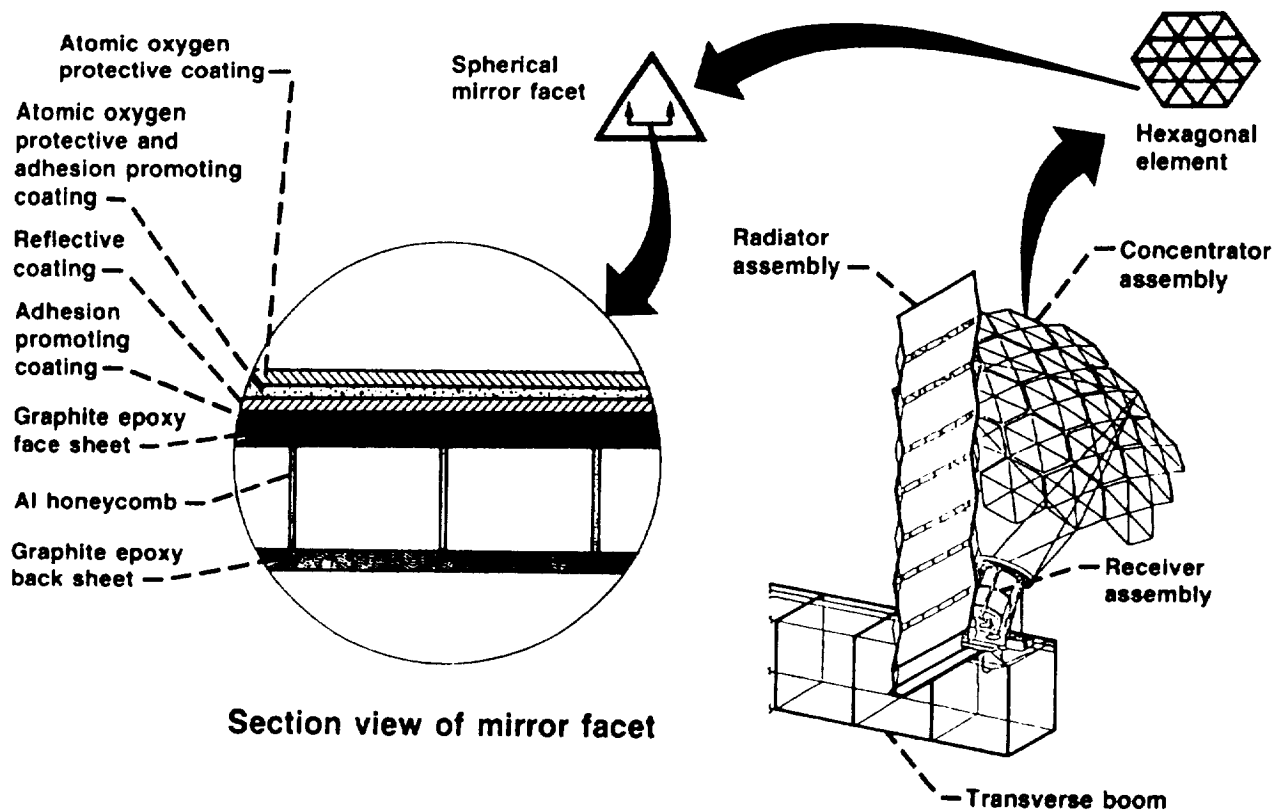


Figure 5. Solar concentrator for Space Station Freedom Solar Dynamic Power Module.

ORIGINAL PAGE  
BLACK AND WHITE PHOTOGRAPH

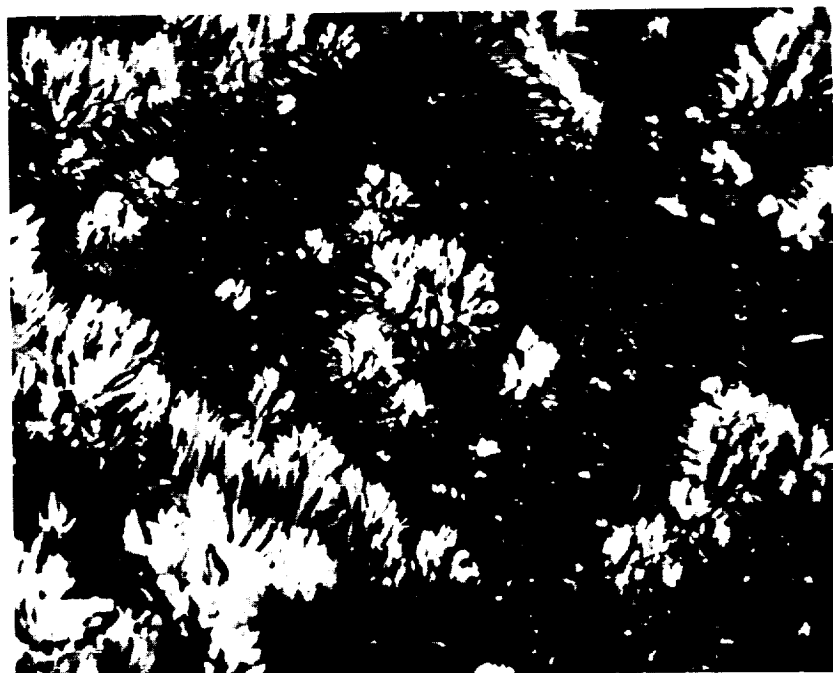


Figure 6. Silver-oxide "fluff" extending out of protective coating defect sites after atomic oxygen plasma exposure.



Figure 7. Atomic oxygen undercutting in a concentrator coupon. Protective coating film failure through an undercutting-tearing propagation process.

ORIGINAL PAGE  
BLACK AND WHITE PHOTOGRAPH

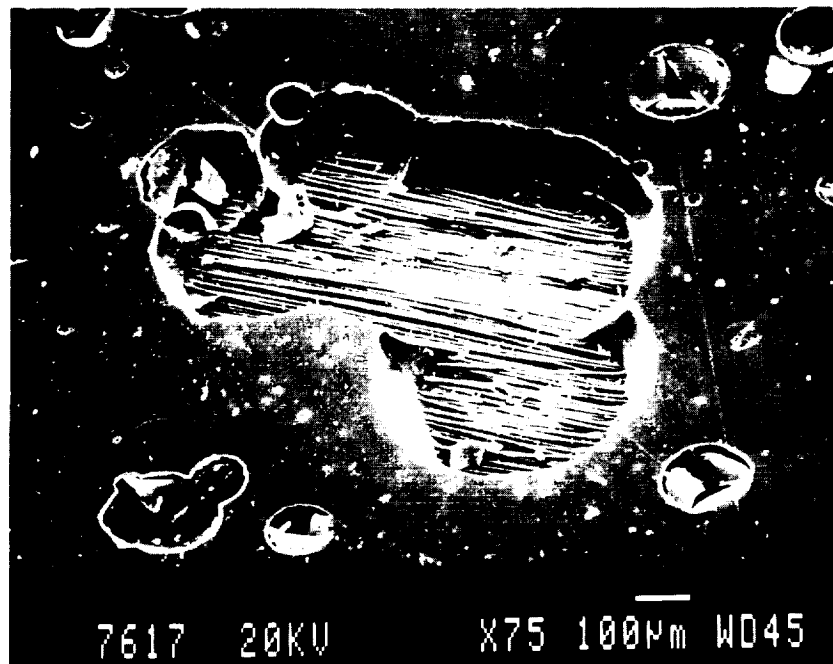
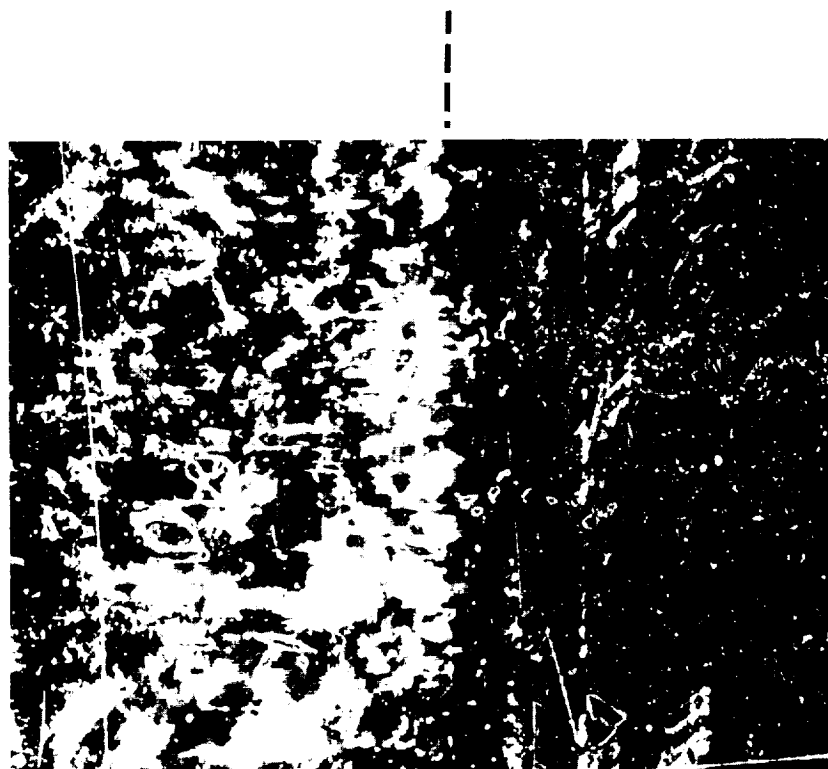


Figure 8. Atomic oxygen undercut cavities in a concentrator coupon exposed to a Kapton effective fluence of  $3 \times 10^{21}$  atoms/cm<sup>2</sup>.



Figure 9. Silicone contamination on a Kapton witness coupon deposited during plasma ashing.



Optical Macrograph

40X

**Atomic oxygen  
exposed side  
(F= 2.1 E 21)**

**Covered with  
fused silica**

Figure 10. Concentrator coupon partially masked during atomic oxygen plasma exposure. The exposed side appears discolored.



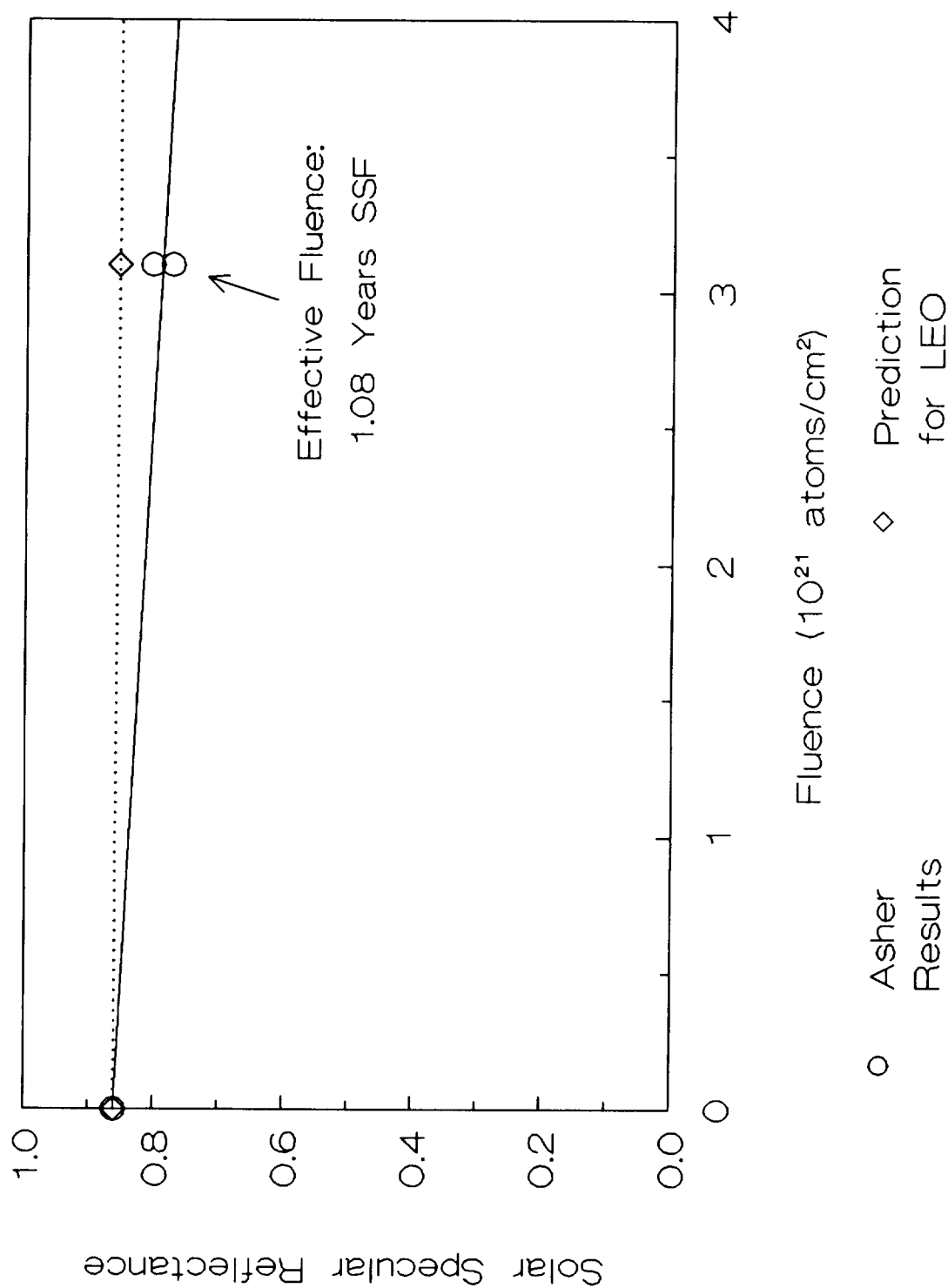


Figure 11. Ground-laboratory and in-space predictions of solar specular reflectance decrease with atomic oxygen exposure.



## **SIMULATION OF THE SYNERGISTIC LOW EARTH ORBIT EFFECTS OF VACUUM THERMAL CYCLING, VACUUM UV RADIATION AND ATOMIC OXYGEN**

Joyce A. Dever  
Kim K. de Groh  
NASA Lewis Research Center

Curtis R. Stidham  
Thomas J. Stueber  
Sverdrup Technology, Inc.

Therese M. Dever  
Elvin Rodriguez  
Cleveland State University

Judith A. Terlep  
Case Western Reserve University

### **ABSTRACT**

In order to assess the low Earth orbit (LEO) durability of candidate space materials, it is necessary to use ground laboratory facilities which provide LEO environmental effects. A facility combining vacuum thermal cycling and vacuum ultraviolet (VUV) radiation has been designed and constructed at NASA Lewis Research Center for this purpose. This facility can also be operated without the VUV lamps. An additional facility can be used to provide VUV exposure only. By utilizing these facilities, followed by atomic oxygen exposure in an RF plasma asher, the effects of the individual vacuum thermal cycling and VUV environments can be compared to the effect of the combined vacuum thermal cycling/VUV environment on the atomic oxygen durability of materials. The synergistic effects of simulated LEO environmental conditions on materials were evaluated by first exposing materials to vacuum thermal cycling, VUV, and vacuum thermal cycling/VUV environments followed by exposure to atomic oxygen in an RF plasma asher. Candidate space power materials such as atomic oxygen protected polyimides and solar concentrator mirrors were evaluated using these facilities. This paper will discuss characteristics of the Vacuum Thermal Cycling/VUV Exposure Facility which simulates the temperature sequences and solar ultraviolet radiation exposure that would be experienced by a spacecraft surface in LEO. Results of durability evaluations of some candidate space power materials to the simulated LEO environmental conditions will also be discussed. Such results have indicated that for some materials, atomic oxygen durability is affected by previous exposure to thermal cycling and/or VUV exposure.

### **INTRODUCTION**

Ground laboratory evaluation of candidate space materials can be used to supplement space flight data for predicting long-term LEO materials durability. Furthermore, because the environmental effects of LEO can act synergistically, it is important to use laboratory facilities which provide combined environmental effects. NASA Lewis Research Center has designed and constructed a facility to provide the combined effects of vacuum thermal cycling and VUV radiation for materials durability evaluation. In this system, heating and cooling are provided through radiative processes in a high vacuum environment. The cycling process simulates space orbital cycles with respect to heating, ultraviolet radiation, and cooling. The heating and ultraviolet radiation exposure occur simultaneously for the

first part of a cycle, then the samples are physically moved to a cooling environment which does not contain VUV. This facility can also be used for vacuum thermal cycling without ultraviolet radiation exposure. The flexible control system developed for this facility permits unattended tests to be safely conducted for long periods of time while preserving the research integrity of the test in the event of any of a variety of malfunctions.

Facilities at NASA Lewis have been used to determine the effects of vacuum thermal cycling (VTC), VUV and combined VTC/VUV on the atomic oxygen durability of materials. Exposure to VTC, VUV and/or combined VTC/VUV is followed by atomic oxygen exposure in an RF plasma asher for such studies. Although the most exhaustive testing would include simultaneous exposure to VTC, VUV and atomic oxygen, facility limitations prevented the inclusion of an atomic oxygen environment with the VTC/VUV combined environment. For this reason, samples are sequentially exposed first to VTC/VUV and then to atomic oxygen. Following this sequence of tests, samples can be analyzed for changes in mass loss rate, optical properties, surface morphology, etc. as compared to samples which were only exposed in the plasma asher. By analyzing results of such testing, it is possible to determine which environmental effects act synergistically on the material being studied. Results have revealed that some materials are synergistically affected by VUV, thermal cycling and atomic oxygen. These results illustrate the importance of utilizing laboratory durability evaluation procedures which permit determination of synergistic effects rather than simply analyzing damage from individual environmental effects.

## SPACE SIMULATION FACILITIES

### Vacuum Thermal Cycling/Vacuum Ultraviolet Radiation Exposure Facility

The VTC/VUV exposure system utilizes a diffusion pumped vacuum system which operates at a pressure of  $< 10^{-6}$  torr. An overall view of the hardware in the VTC/VUV facility is shown in figure 1. Samples are located in the sample holder, as shown, which is physically transported between an environment providing heating and ultraviolet radiation exposure and an environment which allows samples to radiatively cool. Therefore, this facility simulates the thermal cycling and UV exposure to which surfaces in space would be exposed, because heating and UV radiation exposure occur during the sunlit portion of an orbit, and on-orbit cooling occurs in the absence of solar UV radiation when surfaces are in the Earth's shadow. This facility uses two VUV lamps for accelerated VUV exposure in the wavelength range between 115 and 200 nm. A near ultraviolet (NUV) lamp is used to provide UV radiation between 200 and 400 nm; however, because of the long light path from the NUV source to the samples, the NUV intensity is less than one sun. Therefore, the facility is typically referred to as a vacuum thermal cycling/VUV exposure facility, because the shorter wavelength, higher energy VUV, which is most damaging to materials, is accelerated, and the NUV radiation is not accelerated.

#### UV Lamps

As shown in figure 1, two VUV lamps are located inside of the water-cooled shroud. These are 30 watt deuterium lamps with magnesium fluoride windows which provide radiation between 115 and 300 nm; however, the radiation above 200 nm is much less than that of the sun. Therefore these lamps are used for accelerated VUV exposure between 115 and 200 nm. The light path for these lamps is directed upward toward the samples. Also shown is a near ultraviolet (NUV) source which is located outside of the vacuum chamber. This is a 500 watt mercury-xenon short arc lamp which provides radiation of wavelengths between 200 and 400 nm. Light from this source is transmitted through a quartz feedthrough window and directed upward toward the samples using a 90° light bending mirror.

Lamps were individually calibrated using a radiometer/pyroelectric detector system and a series of narrow bandpass filters to obtain irradiance values in air at wavelengths ranging from 180 to 400 nm. Points on a manufacturer-supplied relative spectral irradiance curve (arbitrary units) were multiplied by an appropriate factor, determined from calibration data for the lamp, in order to generate an irradiance curve (in units of power/area x wavelength). Resulting spectral irradiance curves for the combination of VUV and NUV lamps used in this system are shown in figure 2 as compared to the air mass zero solar spectral irradiance. Because VUV wavelengths do not transmit in air, actual VUV irradiance calibrations could not be performed. Therefore, the entire manufacturer-provided VUV lamp irradiance curve between 115 and 300 nm was scaled to fit between the measured data points from 180 to 300 nm. Irradiance curves for the two lamps to be used in the system were summed. Then the integrated intensity between 115 and 200 nm was calculated and used to determine the number of VUV suns. The

ratio of lamp intensity to air mass zero solar intensity in the same wavelength range is referred to as the number of equivalent suns. For the VTC/VUV system, VUV lamps were typically distanced from the sample site such that samples were exposed to approximately 5 VUV suns between 115 and 200 nm. This distance is adjustable for the desired VUV intensity.

Figure 3 shows a plot of the relative intensity (arbitrary units) of a typical VUV lamp as a function of off-axis angle. This data was used to determine the optimum distance between two VUV lamps to minimize the intensity gradient across the 3"x3" sample area.

Because of the long light path to the sample site, the NUV intensity is approximately 0.5 suns. This was calculated by integrating the irradiance curve between 200 and 400 nm. Although 0.5 suns is not an accelerated intensity, the NUV range of wavelengths is represented during exposure.

### Infrared Heating Lamps

The infrared quartz tungsten halogen lamps are also located inside the water-cooled shroud in the VTC/VUV facility as shown in figure 1. These lamps are capable of producing 1000 watts. The actual power to these lamps during the thermal cycling process is controlled using a variable transformer. This is desirable for adjusting the heating rate so that the maximum temperature limit is reached in the same amount of time needed for exposure to a recommended VUV dose.

### Temperature Distribution Across Sample Area in Heating/VUV Environment

Figure 4 shows typical temperature distributions across the sample area for the VTC/VUV system with UV lamps (figure 4a) and without UV lamps (figure 4b). For these experiments, exposed junction thermocouples were located at sites on the sample holder as shown and the lamps were turned on with typical settings and allowed to come to an equilibrium condition. Then readings for the thermocouples were recorded. This experiment was repeated with the NUV and VUV lamps off, because the system is also operated without these lamps. The maximum temperature change between sites was determined to be approximately 22% when operating with the IR, NUV and VUV lamps on and 17% when operating with only the IR lamps. Such temperature variations may result in slightly different levels of damage across a sample surface.

### Cooling Chamber

The liquid nitrogen (LN<sub>2</sub>) cooled copper chamber (see figure 1) provides the surface to which samples radiatively cool during the cooling portion of the cycle. Plumbing for the liquid nitrogen is brazed to the top of the chamber. Insulating composite mica flake sheets were inserted between the bottom of the chamber and the base plate, and "washers" of this same material were used with the mounting screws so that conductive losses to the base plate are minimized.

### Sample Transport Mechanism

The sample holder transport mechanism (see figure 1) provides positioning of the samples between the LN<sub>2</sub> cooled chamber and the heating/VUV exposure section of the facility. The mechanism is a four bar linkage that consists of the drive bar linkage, connecting linkage, swing arm, and the staging platform (ground). Electrical solenoids provide the force input into the system via the drive bar linkage. The drive bar linkage provides the rotation of the connecting linkage which, in turn, drives the swing arm. Test specimens are mounted in a sample holder mounted off the end of the swing arm.

The speed of the transport mechanism is controlled by a variable transformer that provides electrical power to the solenoids. The linkage system is designed such that sudden changes in acceleration (jerk) and deceleration are minimized on the samples as they are moved between the heating/VUV and cooling positions, and mechanical advantage is maximized when needed. The angle between the connecting linkage and the swing arm is 45 degrees when the samples are both in the cooled chamber and the VUV exposure/heating section. This angle results in an initial slip at the pin-slot interface when the solenoids are energized. The linkage design, along with controlled minimal power to the solenoids, results in a smooth transport of the test samples in the cycle process.

### Thermocouple Temperature Monitors

To provide the most realistic temperature response for the particular material being tested, exposed junction thermocouples are attached to a surface or embedded in a film material simulating the material being thermal cycled. A thermocouple is used to obtain a strip chart readout of the temperature as a function of test time. Thermocouples can also be utilized for controlling the thermal cycling process as described in the following section.

### VTC/VUV Control System

A programmable logic controller (PLC) is utilized for monitoring and controlling the VTC/VUV process permitting safe operation for long-term unattended tests. The controller actuates the solenoids of the sample transport mechanism to move a sample from the heated/VUV environment to the cooling chamber and then returns the samples to the heated/VUV environment to complete the cycle. With the PLC, the user can select from three methods of VTC/VUV control: manual control, temperature control or timer control.

Using manual control, the operator observes the temperature on a thermocouple readout, and, when the desired temperature is reached, actuates the sample transporter to move between the heating/VUV and cooling environments.

With temperature control, the PLC monitors the temperature from a thermocouple and automatically moves the samples between the heating/VUV and cooling environments at the appropriate temperature limits. Two thermocouples are monitored by individual meter/relays with dual manually adjustable set points. These meter/relays monitor and display sample temperature. One of these signals the controller to move the samples between environments at the appropriate programmed temperatures. The other is programmed with set-points slightly beyond the thermal cycling temperature limits. In the event that its temperature limits are exceeded due to failure of a solenoid or failure of the first thermocouple, this meter/relay signals the PLC. If this occurs, the test is automatically discontinued, and an error indicator is energized. The number of completed cycles is saved in the PLC memory, and samples remain under vacuum.

Using timer control, the operator can program the PLC to expose samples in each environment for predetermined amounts of time. Due to the flexibility of the control system and the repeatable nature of the thermal cycling process, the user can operate the system manually to determine the amount of time needed in each of the heating/VUV and cooling environments, program the PLC with these time durations, and complete the test using timer control. This is the method typically used, because of its convenience in only using one thermocouple, for the chart recorder, and because it is reliable.

For the most precise control of the sample cycling temperatures without concern for sample overheating, the system can be operated in temperature limit mode coupled with timer mode. Using this method of operation, the timer mode takes over for the remainder of the test in the event of thermocouple system failure.

At any time during the process, the user has the option of manually moving a sample between environments or terminating the test. The user defines the end of the test by programming the PLC with the number of cycles required. The user can display the number of cycles completed on the PLC readout.

The PLC also monitors the cooling chamber temperature, water-cooled shroud temperature, VUV, NUV and IR lamp status (on or off), bell jar vacuum, cooling water flow switches and solenoid movement. Malfunctions result in process shutdown, energizing of the appropriate indicator light for the malfunction, and maintenance of vacuum (if possible) until the user can correct the condition.

### **Vacuum Ultraviolet Radiation Exposure Facility**

The VUV Exposure Facility contains three water cooled copper compartments each equipped with a 30 watt deuterium lamp with a magnesium fluoride window. These compartments are located inside of a diffusion pumped high vacuum system bell jar which operates at a pressure of approximately  $2 \times 10^{-6}$  torr. Samples are located on the floor of these compartments. The stainless steel base plate of each compartment is instrumented with a thermocouple. The distance between the lamp and the sample was adjusted for the desired VUV intensity.

### **RF Plasma Asher**

The atomic oxygen environment of LEO was simulated using an RF plasma asher which generates a 13.56 Mhz RF discharge of oxygen or air, depending on which feed gas is used. Samples were placed on a glass rack in the

center of the asher which can support a sample area of approximately 3 inches by 6 inches. Various species of oxygen (and nitrogen, if air is the feed gas) atoms, ions and molecules are contained in the plasma. This discharge results in random directional thermal energy atomic oxygen attack of samples. It is expected that the only reactive species are the oxygen species, because nitrogen species were not found to contribute to the erosion of a polyimide material [1]. Samples located in the plasma are also exposed to a high intensity of VUV radiation at the 130 nm oxygen resonance line [2]. Intense spectral lines from nitrogen species also occur in the VUV [3], and are present in the plasma when an air is used as a feed gas.

## DURABILITY EVALUATIONS USING SIMULATED SPACE ENVIRONMENTS

A variety of materials have been analyzed for their changes in atomic oxygen durability due to previous exposure to VTC, VUV and/or combined VTC/VUV. Experimental procedures and results of these studies are described in the following sections.

### Candidate Atomic Oxygen Protective Solar Array Blanket Materials

Solar array blankets are intended to provide structural support and the proper thermal environment for efficient performance of the Space Station Freedom Photovoltaic Power System. Candidate materials have been analyzed for their durability and performance upon exposure to simulated LEO environments. These candidate materials have included  $\text{SiO}_x$  (where  $x$  is approximately 2) coated Kapton<sup>®</sup> film (Kapton is a registered trademark of DuPont), manufactured by Sheldahl, and polysiloxane-polyimide film made from silicone and polyimide cast from a solution mixture which were manufactured by DuPont. Two types of this polysiloxane-polyimide material, 93-1 and AOR Kapton, were studied. The 93-1 is an earlier formulation of the AOR Kapton material. The polysiloxane-polyimide materials are atomic oxygen protective, because silicone surfaces are expected to form a skin of  $\text{SiO}_x$  upon exposure to atomic oxygen [4], and  $\text{SiO}_x$  has been found to be an effective barrier to atomic oxygen attack [1, 4-6].

Solar array blanket surfaces are expected to see temperature swings between  $+80^\circ\text{C}$  and  $-80^\circ\text{C}$  in Space Station Freedom orbit. During each orbit, surfaces will be exposed to sunlight for approximately 59 minutes. These specifications were used for materials testing in the VTC/VUV facility. The VUV lamps were arranged to provide 5 VUV suns, so the time needed for samples to receive the same amount of VUV that they would receive in an orbit was 11.8 minutes (59 minutes/5 suns). The heating rate was adjusted so that the temperature change from  $-80^\circ\text{C}$  to  $+80^\circ\text{C}$  was accomplished in the same amount of time. It is important to note that different materials will have different thresholds of ultraviolet intensity which can be tolerated and above which unrealistic damage will occur. Results of accelerated VUV exposure must, therefore, be interpreted with caution unless a comparison can be made between damage at a level of one sun and at the level desired to be used. If a material passes a highly accelerated test, then it is probable that it will survive in the real-time space environmental exposure. However, a material which fails due to overtesting may still perform well in the space environment. For this reason, accelerated tests yield very conservative results.

#### DuPont 93-1 and AOR Kapton

Figure 5 shows the fractional mass loss of samples of 93-1 upon exposure to the atomic oxygen environment of an RF air plasma asher [7]. The sample previously exposed to 1000 ESH VUV showed a fractional mass loss of approximately 1.5 times that of the sample not previously exposed; however, the data may be within experimental error of each other. The sample exposed to VTC/VUV showed a fractional mass loss per unit area of approximately 2 times that of the sample not previously exposed. Furthermore, the data does not appear to be within experimental error of the data from samples not exposed to VUV prior to atomic oxygen exposure. Figure 6 shows scanning electron micrographs of a sample which was only plasma ashed and a sample which was plasma ashed following VTC/VUV exposure. Note that the sample which was only ashed (figure 6a) showed undercutting due to atomic oxygen erosion primarily at linear defect areas on the sample. These linear defect areas were probably produced during processing of this material. The sample exposed to 700 VTC/VUV cycles then air plasma ashed (figure 6b) showed a significantly different type of atomic oxygen damage than the previously unexposed sample. Note the severe branching of cracks with atomic oxygen undercutting. It is possible that the VTC/VUV exposure resulted in cracking at the silicone enriched surface of the film which became visible as atomic oxygen undercutting took place.

As shown in figure 7 [8], exposure to VTC/VUV had a reversed effect on the AOR Kapton material as

compared to its effect on the 93-1 material. In fact, previous exposure to VUV or VTC/VUV resulted in significantly improved atomic oxygen resistance for AOR. The surface of the AOR Kapton material appeared to have "water spots" possibly due to a release agent used in the processing of the material which left a residue on the surface. This residue was not observed on the 93-1 material. This residue may affect the VTC, VUV and/or atomic oxygen reactions with the material. Other undisclosed processing changes between 93-1 and AOR Kapton may also have affected the materials' durability to these environmental effects which would explain the different behavior for these two materials.

#### SiO<sub>x</sub> Coated Kapton

Figure 8 [8] shows that there is little difference in the atomic oxygen susceptibilities of samples of pristine, VUV exposed and VTC/VUV exposed SiO<sub>x</sub>/Kapton. Although these samples were exposed to a fraction of the fluence that the 93-1 and AOR Kapton samples received, the trends in atomic oxygen degradation are obvious.

#### **Solar Concentrator Mirror Materials**

##### Candidate Space Station Freedom Solar Concentrator Materials

Solar concentrator coupons were composed of a sandwich type structure of two sheets of graphite epoxy bonded to an aluminum honeycomb core. Coupons of this type were fabricated at Hercules Aerospace and sent to 3M Corporation where copper (an adhesion promoting layer), silver (a reflecting layer), aluminum oxide and silicon dioxide (atomic oxygen protective layers) were deposited onto the face sheets of the coupons. These samples were exposed to VUV and to VTC/VUV followed by atomic oxygen exposure [9]. Coupons were exposed to thermal cycling between -17.8°C and +121°C, and a VUV intensity of 5 VUV suns was used. The heating rate was adjusted so that the temperature change from the minimum to the maximum temperature was accomplished in the amount of time necessary for exposure to a full orbital VUV dose, 11.8 minutes, equivalent to 59 minutes of exposure to sunlight in LEO. Figure 9a shows changes in spectral specular reflectance for a coupon exposed first to 1000 ESH VUV at an intensity of 3 equivalent suns, then to an atomic oxygen fluence of  $1.4 \times 10^{21}$  atoms/cm<sup>2</sup>. Exposure to VUV caused a significant decrease in the specular reflectance centered at a wavelength of approximately 375 nm, and the sample showed a yellow discoloration. This may be due to either VUV induced color center formation, referred to as solarization, in the SiO<sub>2</sub> and/or Al<sub>2</sub>O<sub>3</sub> layers or to a layer of contamination which may have settled on the surface due to volatilization of organics from adhesives upon heating by the VUV lamps. Subsequent exposure to atomic oxygen resulted in reversal of this damage which is thought to be due to either "bleaching," oxidation resulting in reversal of the chemical reactions which occurred upon VUV exposure, or a thermal effect due to heating of metals in the plasma asher. Solarization has been known to reverse in some cases with heat treatment [10]. Metals are known to heat up during plasma asher exposure as evidenced by an aluminum sample instrumented with a temperature strip which reached a temperature of approximately 104°C during exposure.

The sample exposed to 908 vacuum thermal cycles containing 893 ESH VUV experienced the same type of spectral changes in specular reflectance as the VUV exposed sample. However, the extent of this damage was less as shown in figure 9b. This may be due to a competition between VUV induced degradation and thermal "annealing" of this damage. As with the VUV exposed sample, the VTC/VUV damage is somewhat reversed by subsequent exposure to atomic oxygen.

Possible conclusions from this data are that VUV damage and atomic oxygen bleaching are competing processes which may occur upon exposure to these two environments simultaneously. If bleaching of color centers is the mechanism of atomic oxygen reaction with this coupon, then the damage observed due to VUV radiation alone may be more severe than the on-orbit behavior of a solar concentrator mirror, because atomic oxygen may be able to reverse this damage. Another possible conclusion is that heat treatment results in the reversal of the VUV damage. It is likely that this was the reason that the VTC/VUV exposed sample was less damaged than the VUV exposed sample. Furthermore, if extensive heating occurred upon plasma asher exposure, this may explain the reversal of damage for both samples. As mentioned previously, it is important to interpret results of accelerated testing with caution. It is not known whether the severity of damage would have been the same for samples exposed to less VUV intensity for the same number of equivalent sun hours. Therefore, it is expected that the results of this testing are conservative and are not likely to be representative of real-time exposure but, rather, they represent worst-case degradation.



## Sol-gel Planarized Mirrors

Sol-gel planarized mirrors, developed by Sandia National Laboratories, have been considered for advanced solar concentrator applications. The sol-gel mirrors described in this study consisted of a stainless steel foil substrate, a silicate sol smoothing layer, a silver reflecting layer, a silicon oxide layer and finally a silicate sol atomic oxygen protective layer. The surface layer on Sample A consisted of a silicate sol with a hydrolysis ratio of 1:10. Sample B contained a surface layer of silicate sol with a hydrolysis ratio of 1:5. These samples were incrementally atomic oxygen exposed in the plasma asher followed by exposure to vacuum thermal cycling between -18°C and +93°C without VUV exposure. Changes in solar specular reflectance of these samples as a function of atomic oxygen exposure and vacuum thermal cycling are shown in figure 10a-b. Sample A displayed a significant decrease in solar specular reflectance upon exposure to an atomic oxygen fluence of  $1.3 \times 10^{21}$  atoms/cm<sup>2</sup>. An air plasma ashed sample of exactly the same composition was analyzed using Auger Electron Spectroscopy and showed evidence of Ag and Fe in the silicate sol top layer. This may be due to thermally induced diffusion of silver and iron from underlying layers due to heating which accompanies plasma ashing and may be responsible for the reduced solar specular reflectance. Sample B, in contrast, showed a slight improvement in solar specular reflectance upon exposure to the same atomic oxygen fluence; however, this may have been within experimental error, because the exposed samples showed variations in appearance across their surface, and it was difficult to measure the sample in exactly the same location each time, it is expected that there was some error associated with each of these reflectance measurements. Both samples showed significant decreases in reflectance upon subsequent exposure to 10 vacuum thermal cycles. It is likely that heating during the thermal cycling resulted in further diffusion of metal species from underlying layers resulting in this specular decrease. Continued exposure to both ashing and thermal cycling led to smaller changes in specular reflectance for both samples. From this data, it is difficult to determine how, if at all, atomic oxygen affected these samples. However, because the temperature suspected in the asher, 104°C, was only slightly higher than the maximum temperature during thermal cycling, 93°C, it is likely that this thermally induced diffusion effect would occur on surfaces of this type exposed in space. Other information, such as combined effects of vacuum thermal cycling and VUV would be necessary in conducting a thorough LEO durability and performance evaluation of this material.

## CONCLUDING REMARKS

It is important to utilize ground laboratory facilities and procedures which provide the synergistic effects likely to occur in the LEO environment when conducting durability and performance evaluation of candidate space materials. Data obtained from exposure of materials to a combined environment containing both vacuum thermal cycling and VUV radiation followed by atomic oxygen exposure can be compared to data from exposure to the singular environments of VUV or vacuum thermal cycling prior to ashing. This type of test matrix can be used to determine whether these environments are expected to react synergistically with the material being tested. The VTC/VUV exposure facility designed and constructed at NASA Lewis provides the capability of evaluation of the synergistic effects of vacuum thermal cycling and VUV radiation and, along with other NASA Lewis facilities, can be used in such a test matrix. Candidate materials for use on space power system surfaces have been evaluated utilizing these facilities to determine potential LEO synergistic effects. Results indicated that for some materials, such as the solar concentrator mirrors, there is a competitive process between VUV or VTC/VUV induced damage and atomic oxygen reversal of this effect. This type of behavior should be considered when predicting the in-space performance of a concentrator mirror. For materials such as DuPont 93-1, cracking due to VTC/VUV exposure may result in degradation of the material which would not have been observed upon exposure to atomic oxygen alone. In the case of AOR Kapton, VUV and VTC/VUV exposure resulted in improved atomic oxygen durability. Materials such as the sol-gel mirrors appear to be sensitive to heating and it is unknown what affect, if any, atomic oxygen has on these surfaces.

Data from the tests summarized above show the wide range of synergistic reactions possible between vacuum thermal cycling, VUV and atomic oxygen on various types of materials and illustrate the importance of evaluating these synergistic effects when conducting durability and performance testing. Finally, caution must be used when interpreting the results of accelerated testing, because materials which fail due to overtesting may still adequately survive real-time space exposure.

## REFERENCES

1. Rutledge, S. K. et al.: "An Evaluation of Candidate Oxidation Resistant Materials for Space Applications in LEO." NASA Technical Memorandum No. 100122. Paper presented at the Workshop on Atomic Oxygen Effects, Pasadena, CA. 1986.
2. Koontz, S. L.; Albyn, K; and Leger, L. J.: "Atomic Oxygen Testing with Thermal Atom System: A Critical Evaluation." Journal of Spacecraft and Rockets. Vol. 28, No. 3, May-June 1991, pp. 315-323.
3. Zaidel, A. N.; and Shreider, E. Ya.: Vacuum Ultraviolet Spectroscopy. Ann Arbor-Humphrey Science Publishers, Ann Arbor, MI, 1970, p. 195.
4. Rutledge, S. K.; and Mihelcic, J. A.: "The Effect of Atomic Oxygen on Altered and Coated Kapton Surfaces for Spacecraft Applications in Low Earth Orbit." Materials Degradation in Low Earth Orbit, V. Srinivasin and B. A. Banks, eds. The Minerals, Metals and Materials Society, 1990, pp. 35-48.
5. Banks, B. A. et al: "Ion Beam Sputter-Deposited Thin Film Coatings for Protection of Spacecraft Polymers in Low Earth Orbit." NASA Technical Memorandum No. 87051, January 1985.
6. Banks, B. A. et al.: "Sputtered Coatings for Protection of Spacecraft Polymers." NASA Technical Memorandum 83706, April 1984.
7. Brady, J. A. and Banks, B. A.: "Vacuum Ultraviolet and Thermal Cycling Effects on Atomic Oxygen Protective Photovoltaic Array Blanket Materials." Materials Degradation in Low Earth Orbit, V. Srinivasin and B. A. Banks, eds. The Minerals, Metals and Materials Society, 1990, pp. 133-43.
8. Dever, J. A.; Bruckner, E. J. and Rodriguez, E.: "Synergistic Effects of Ultraviolet Radiation, Thermal Cycling and Atomic Oxygen on Altered and Coated Kapton Surfaces." American Institute of Aeronautics and Astronautics. Paper No. 992-0794. Presented at the AIAA 30th Aerospace Sciences Meeting and Exhibit, Reno, NV, January 1992.
9. de Groh, K. K. et al.: "Low Earth Orbit Durability Evaluation of Solar Concentrator Materials." Solar Engineering 1992, Vol. 2, William Stine et al., eds., The American Society of Mechanical Engineers, 1992.
10. Koller, L. R.: Ultraviolet Radiation. John Wiley & Sons, Inc., N.Y. 1965, p. 169.

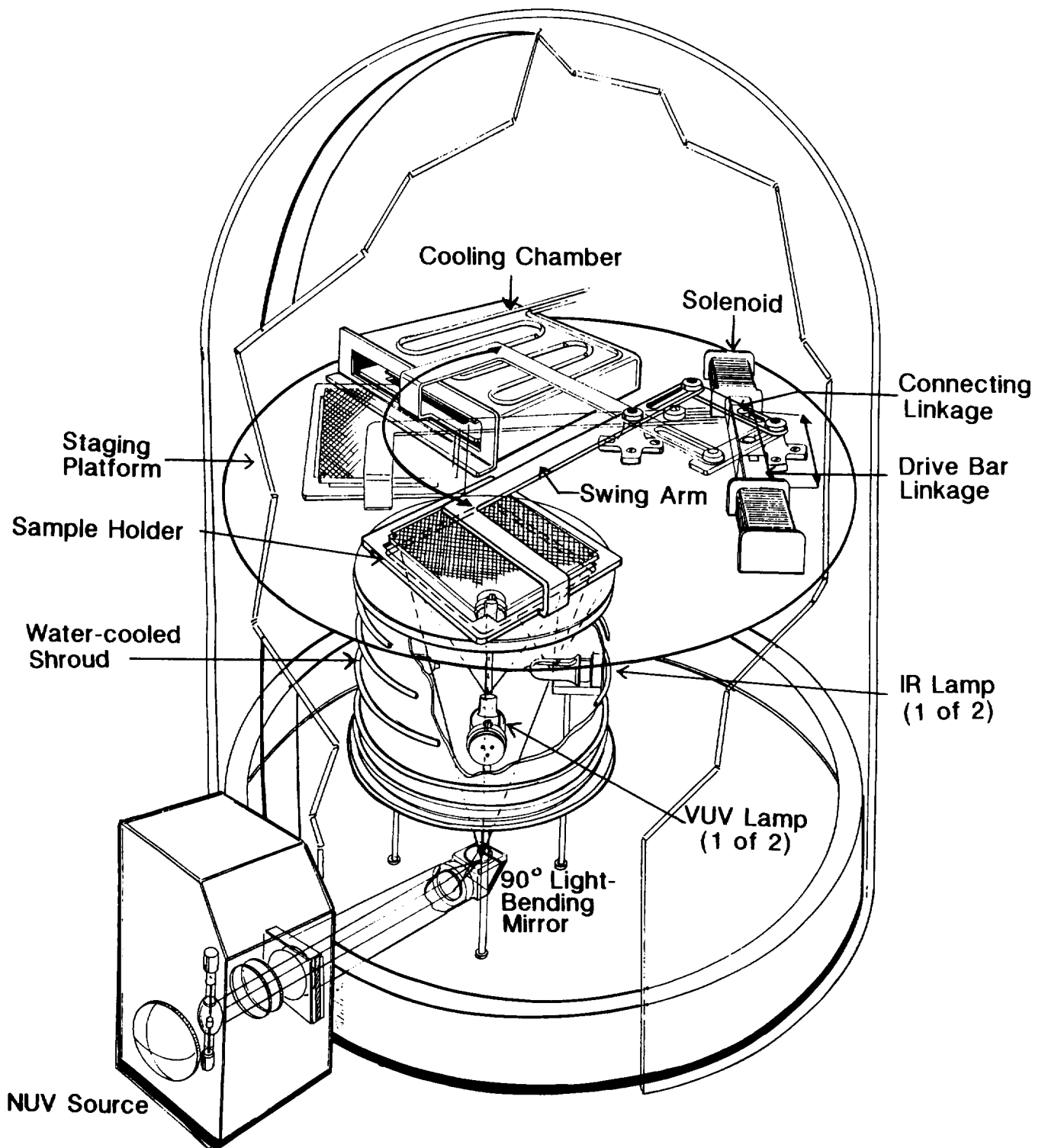
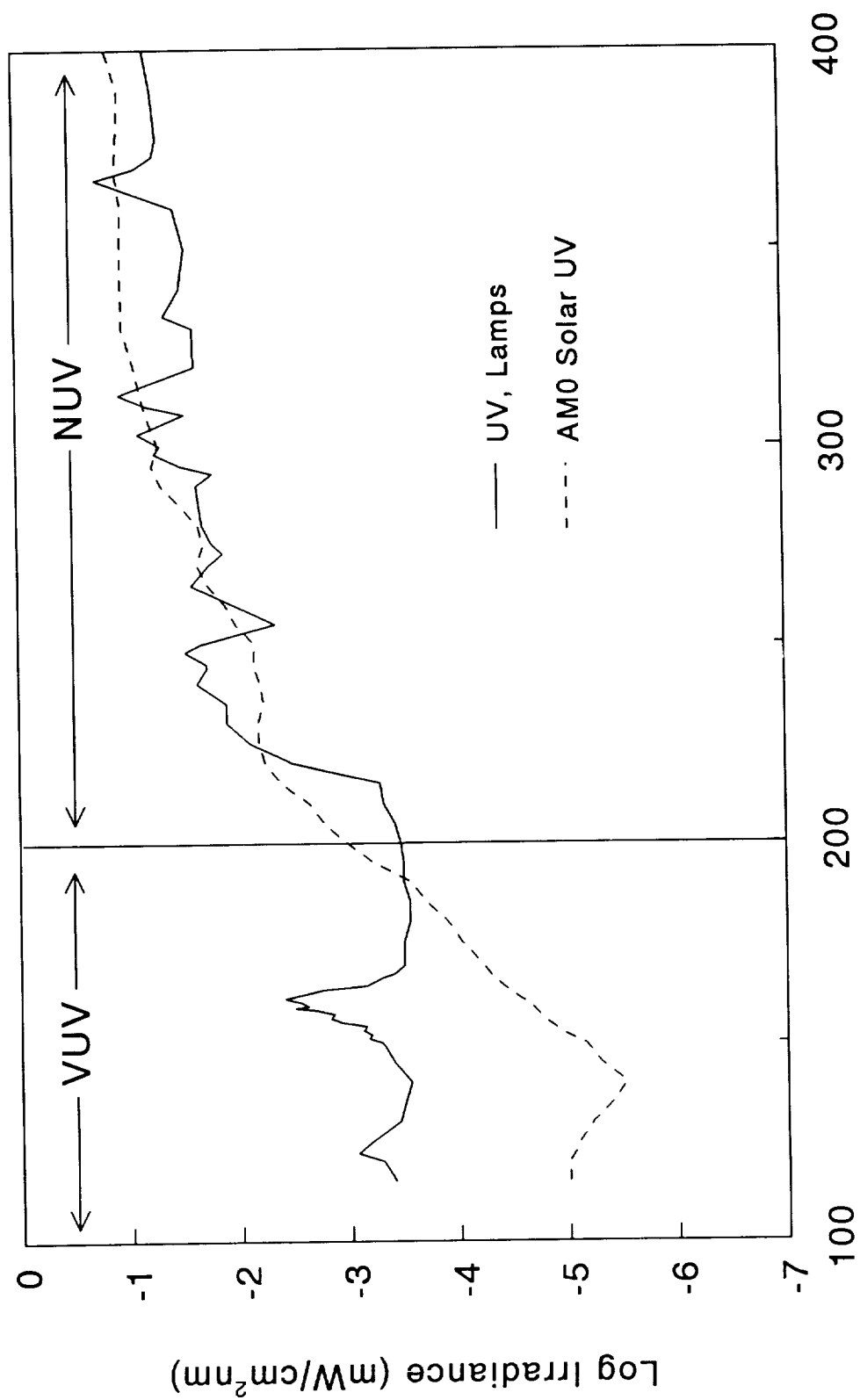


Figure 1: Vacuum Thermal Cycling/VUV Exposure System.



### Wavelength (nm)

Figure 2: Spectral irradiance measured in air for VUV and NUV lamps used in VTC/VUV system as compared to air mass zero solar irradiance.

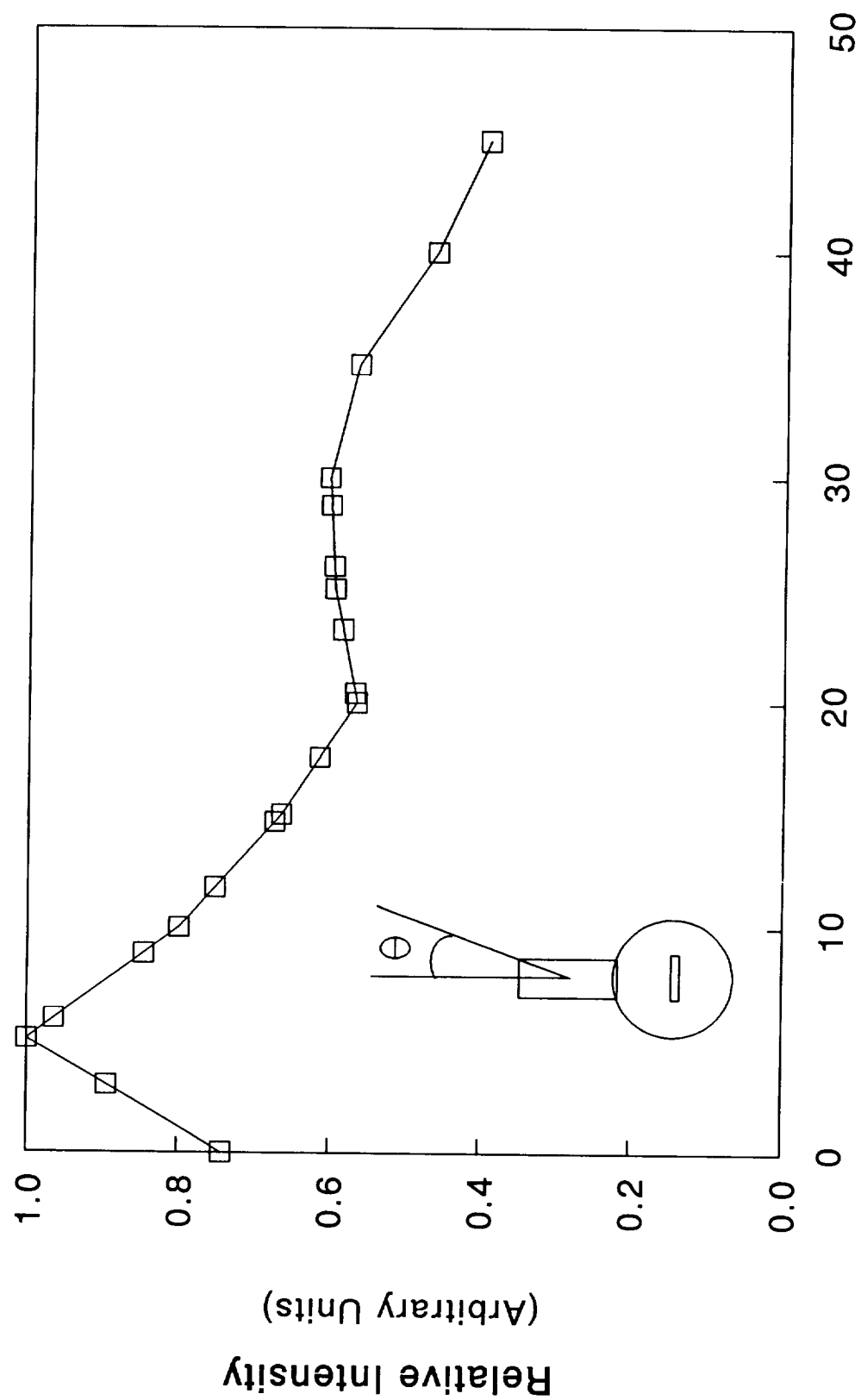
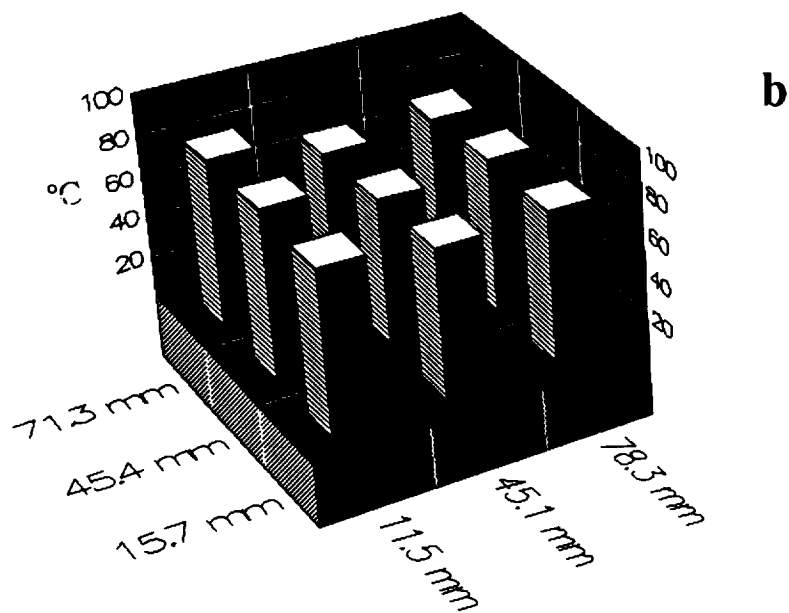
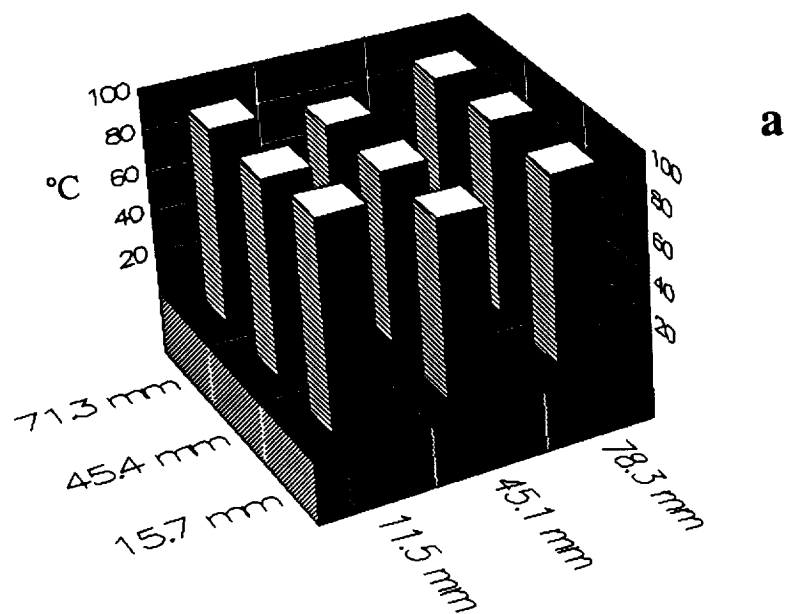


Figure 3: Relative intensity of a typical VUV lamp as a function of off-axis angle.



**Figure 4:** Typical temperature distributions across VTC/VUV system sample holder a) using VUV, NUV and IR lamps, and b) using only IR lamps.

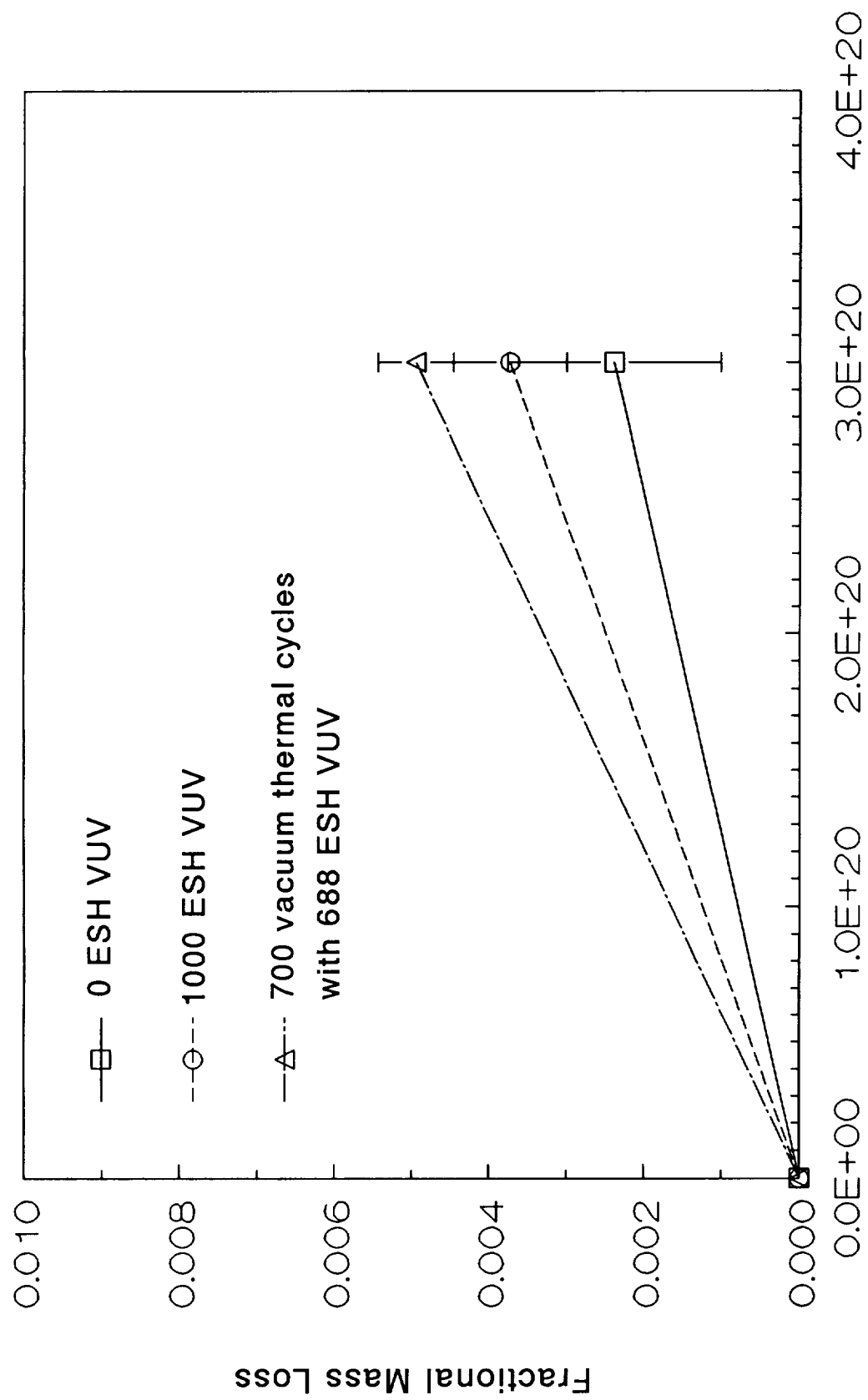


Figure 5: Atomic oxygen erosion of DuPont 93-1 exposed in a plasma asher.

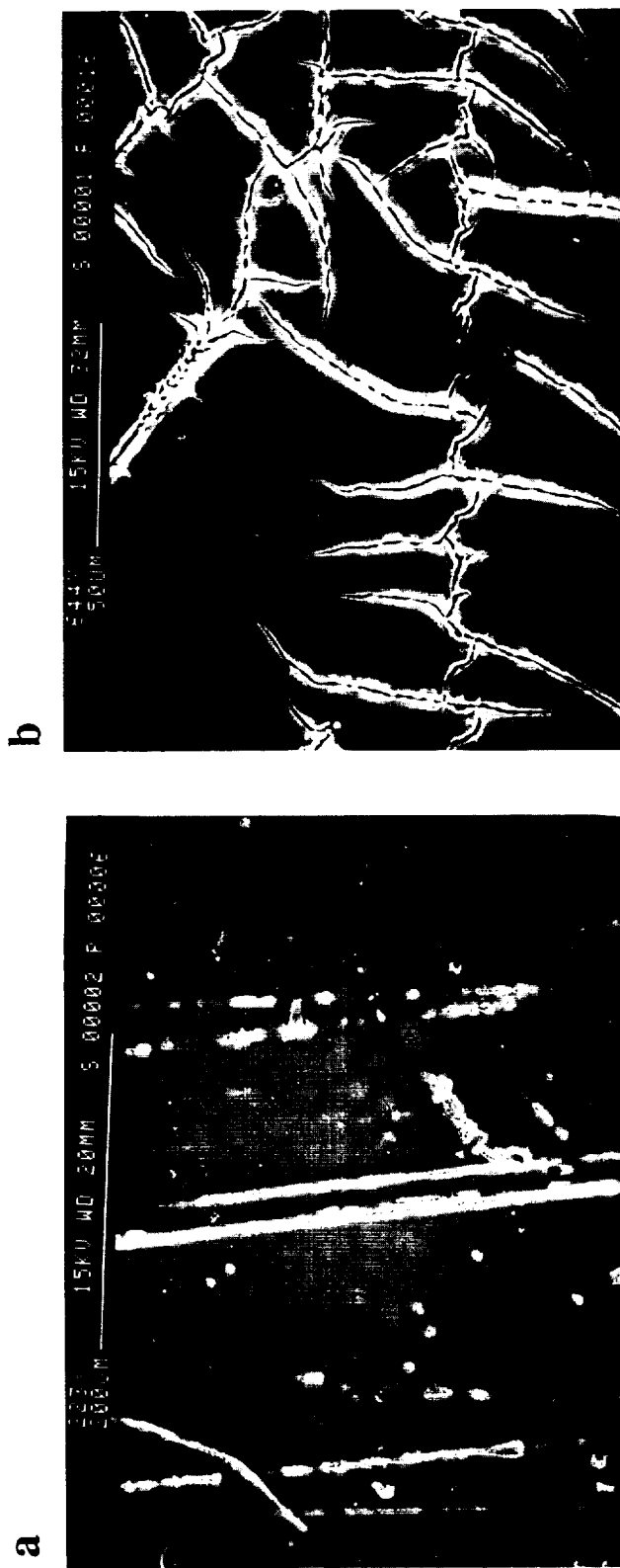


Figure 6: SEM photographs of DuPont 93-1 exposed to a) atomic oxygen (effective fluence =  $3 \times 10^{20}$  atoms/cm<sup>2</sup>) and b) 700 vacuum thermal cycles with 688 ESH VUV followed by exposure to atomic oxygen (effective fluence =  $3 \times 10^{20}$  atoms/cm<sup>2</sup>).



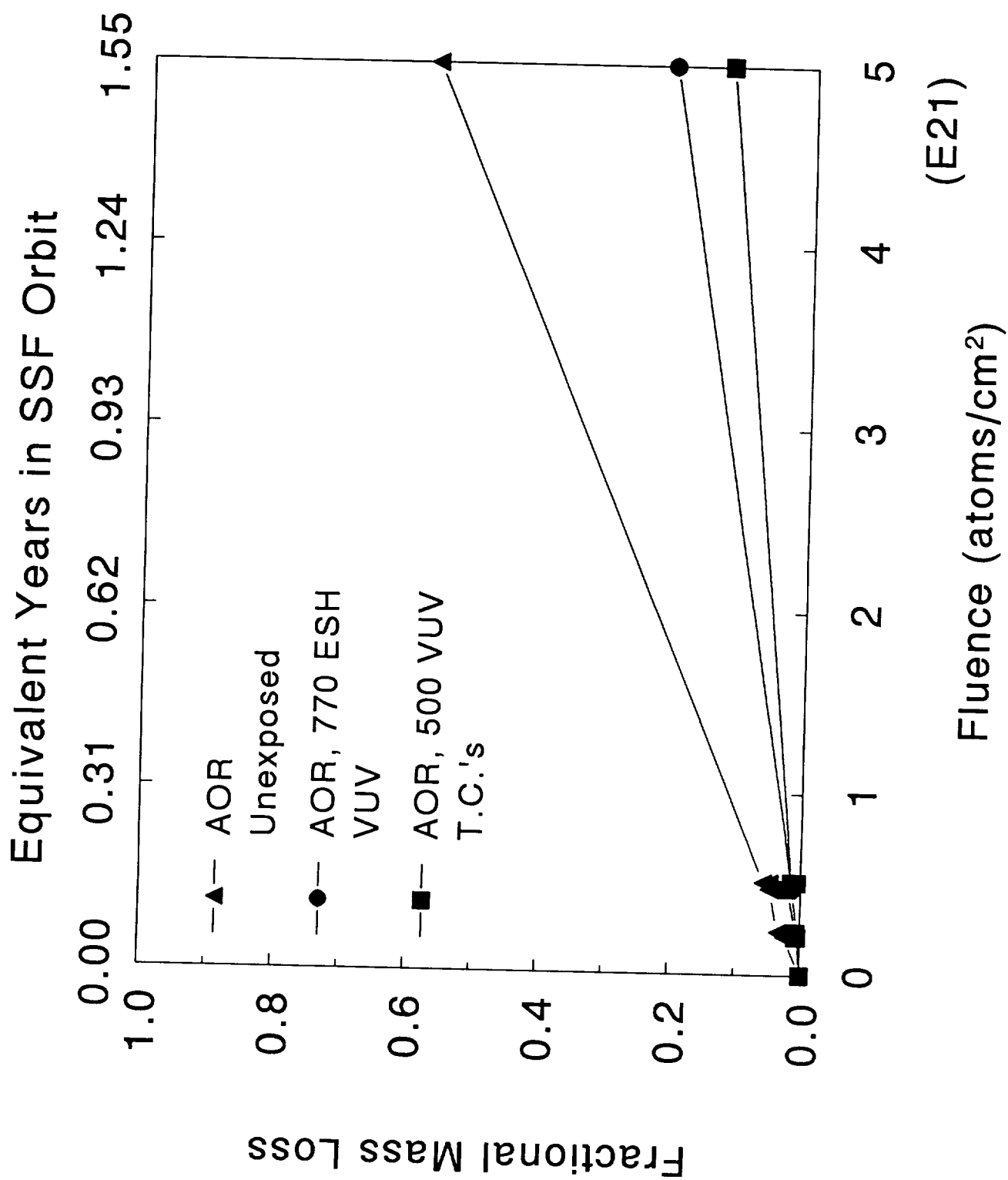
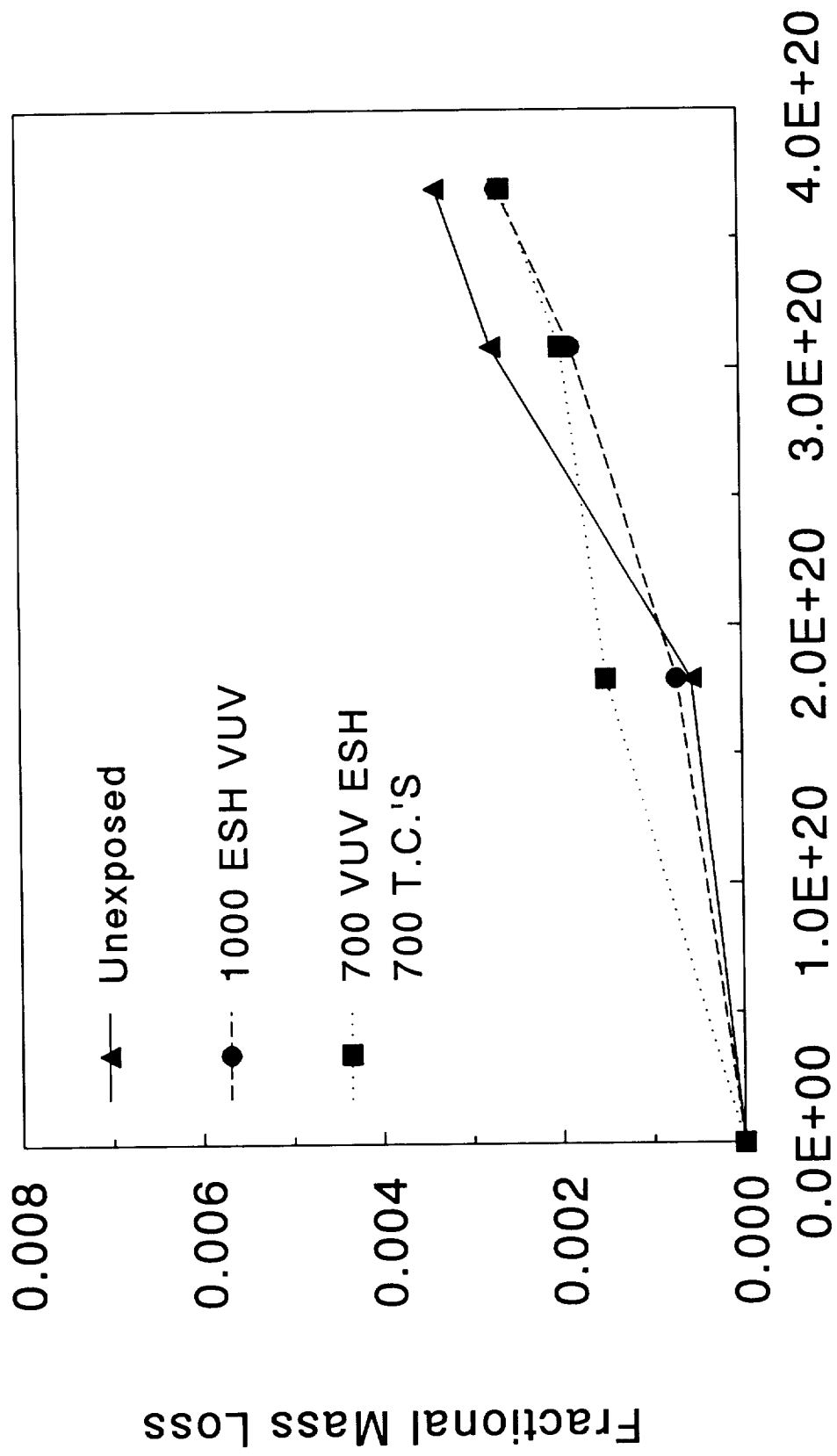
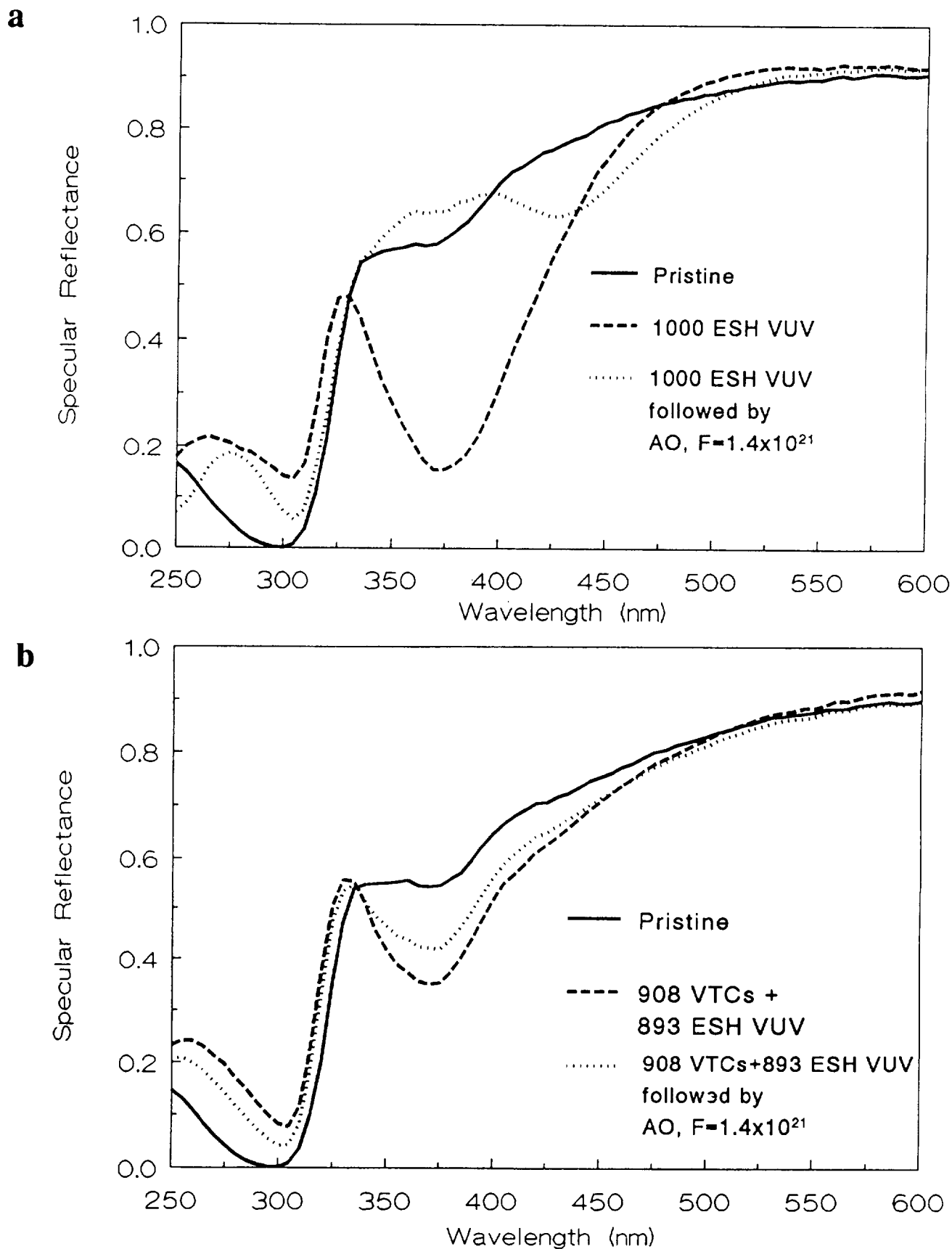


Figure 7: Atomic oxygen erosion of AOR Kapton exposed in a plasma asher.



Effective Fluence (atoms/cm²)

Figure 8: Atomic oxygen erosion of SiO<sub>x</sub> coated Kapton exposed in a plasma asher.



**Figure 9:** Changes in specular reflectance for solar concentrator coupons exposed to a) 1000 ESH VUV followed by atomic oxygen (effective fluence =  $1.4 \times 10^{21}$  atoms/cm<sup>2</sup>) and b) 908 vacuum thermal cycles combined with 893 ESH VUV followed by atomic oxygen (effective fluence =  $1.4 \times 10^{21}$  atoms/cm<sup>2</sup>).

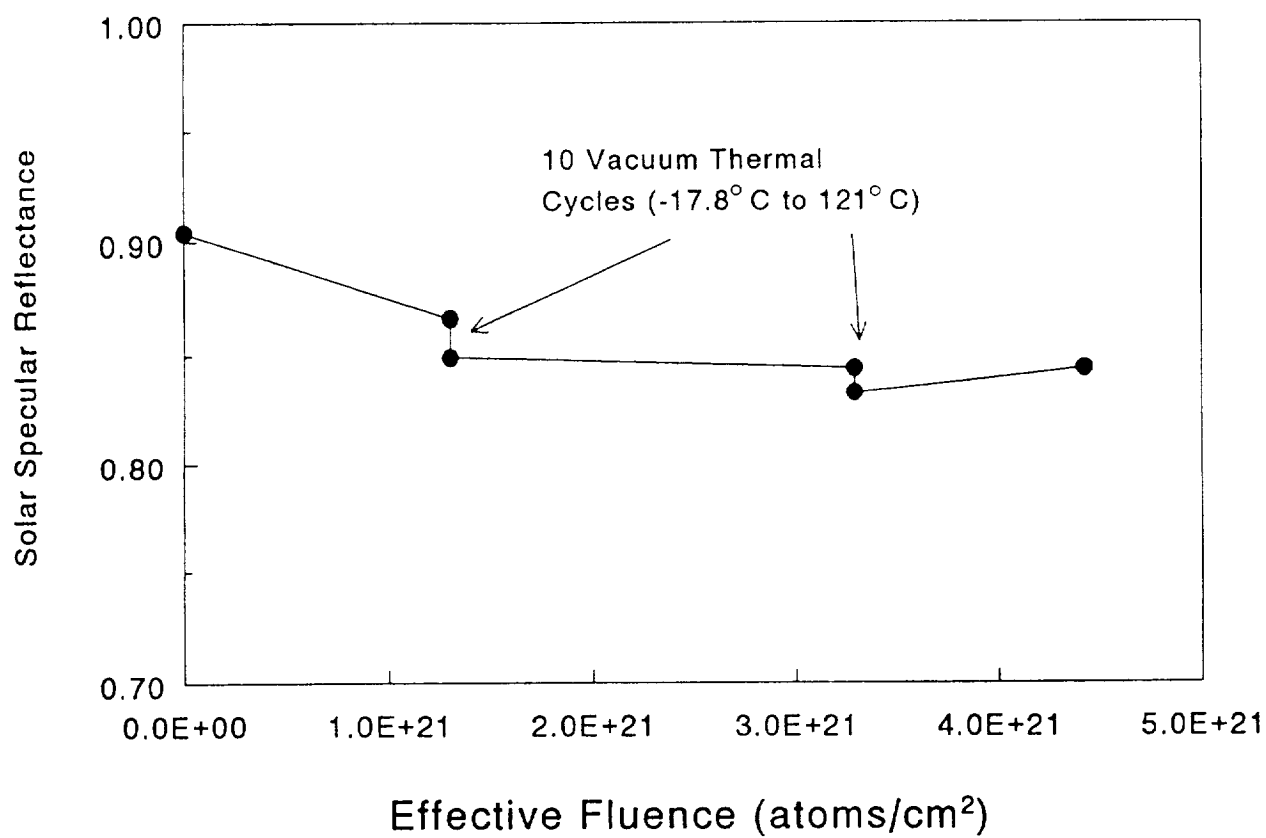
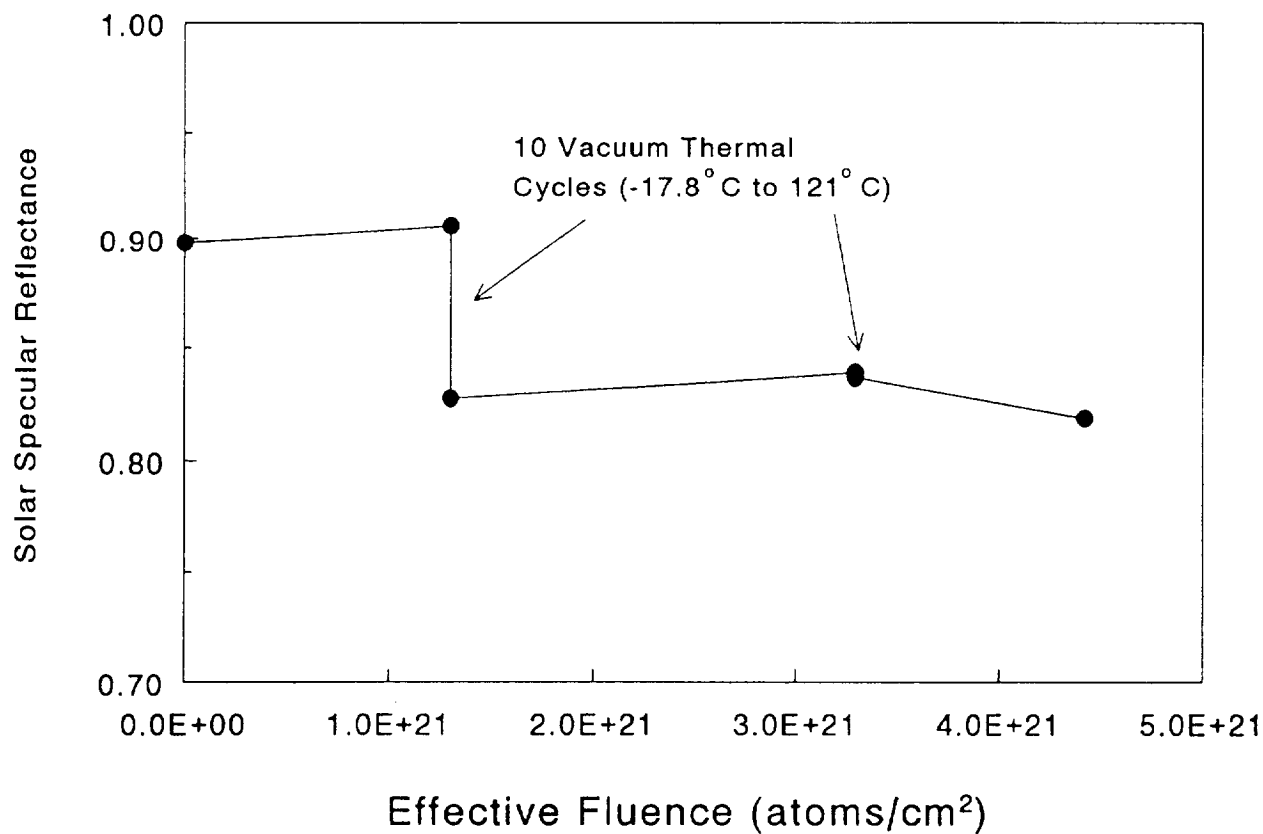
**a****b**

Figure 10: The effect of incremental air plasma ashing and thermal cycling on the solar specular reflectance of sol-gel mirrors for a) Sample A and b) Sample B.

**THE USE OF PLASMA ASHERS AND MONTE CARLO MODELING  
FOR THE PROJECTION OF ATOMIC OXYGEN DURABILITY  
OF PROTECTED POLYMERS IN LOW EARTH ORBIT**

Bruce A. Banks, Bruce M. Auer, Sharon K. Rutledge, and Kim K. de Groh  
NASA Lewis Research Center

Linda Gebauer  
Cleveland State University

**ABSTRACT**

The results of ground laboratory and in-space exposure of polymeric materials to atomic oxygen has enabled the development of a Monte Carlo computational model which simulates the oxidation processes of both environments. The cost effective projection of long-term low-Earth-orbital durability of protected polymeric materials such as SiO<sub>x</sub>-coated polyimide Kapton photovoltaic array blankets will require ground-based testing to assure power system reliability. Although silicon dioxide thin film protective coatings can greatly extend the useful life of polymeric materials in ground-based testing, the projection of in-space durability based on these results can be made more reliable through the use of modeling which simulates the mechanistic properties of atomic oxygen interaction, and replicates test results in both environments. Techniques to project long-term performance of protected materials, such as the Space Station Freedom solar array blankets, are developed based on ground laboratory experiments, in-space experiments, and computational modeling.

**INTRODUCTION**

Low-Earth-orbital (LEO) atomic oxygen interacts with exposed polymers, resulting in loss of material due to oxidation. Long-term LEO missions, such as Space Station Freedom, will require the use of materials which are inherently durable to atomic oxygen or are provided with protective coatings to prevent exposure of underlying materials which would be subject to oxidation. In-space evaluation of the durability of protected polymers is neither cost effective nor timely when considering requirements for high fluence atomic oxygen exposures such as required for Space Station Freedom. Evaluation of the atomic oxygen durability of protected polymers in LEO may be possible through a combination of ground laboratory experiments, in-space LEO exposure data, and computational modeling (ref. 1 and 2). Ground-based, accelerated atomic oxygen exposure of protected polymers in RF plasma ashers can provide valuable insight into the atomic oxygen undercutting processes and the ultimate fate of protected polymers such as those required for the Space Station Freedom photovoltaic array

blanket. The projection of in-space durability based on ground laboratory testing requires an understanding of the differences between the two exposure environments and quantified modeling to enable credible durability projections. Recent LDEF results (ref. 2), coupled with Monte Carlo modeling, have provided great assistance in quantifying durability projections for Space Station Freedom (SSF) solar array blanket materials based on ground-based plasma asher testing. Although previous in-space durability projections have been made using asher data from single sheets of protected Kapton and Monte Carlo modeling, new asher data with laminated solar array blanket materials in a more flight-like configuration and results of undercutting of protected polymers from LDEF allow a fresh perspective on durability projections.

## **APPARATUS AND PROCEDURE**

### **Experimental Data**

Samples of 1300Å-thick  $\text{SiO}_x$  ( $1.9 < X < 2.0$ ) protected Kapton H on both surfaces were laminated to an unprotected sheet of Kapton H by means of a silicone fiberglass scrimcloth. The  $\text{SiO}_x$  protective coatings were magnetron sputter deposited by Sheldahl, Inc. and laminated by McGhan-NuSil, Inc. Kapton polyimide was provided by DuPont De Nemours. Two identical pieces of the flexible laminant (each constitute the SSF solar array blanket) were then clad to each other by bonding with an acrylic adhesive, as shown in figure 1, to allow atomic oxygen durability evaluation of the protected side of the laminant in an RF plasma asher. The clad laminant sample was exposed to atomic oxygen by laying the sample on a glass rack in an SPI Plasma Prep II plasma asher, with air as the working gas. Periodic documentation of the mass of the test sample, as well as the Kapton HN witness coupon ashed with the sample, was made to calculate mass loss and Kapton atomic oxygen effective fluence. The assumed erosion yield for Kapton H and Kapton HN was  $3 \times 10^{-24} \text{ cm}^3/\text{atom}$  (ref. 3).

To assess the effects of atomic oxygen on the fiberglass scrim cloth in a silicone matrix, a sample of just this portion of the solar array laminant was also exposed in a plasma asher. This sample was exposed to atomic oxygen on both sides at the same time by also laying it on a glass rack in the plasma asher.

LDEF data from reference 2 were used to estimate atomic oxygen reaction probabilities for thermally accommodated atomic oxygen in undercut cavities beneath defects in protective coatings. The protected polymers exposed on LDEF consisted of a T-300 carbon fiber 934 epoxy composite sample, which was coated with 400Å of aluminum over 800Å of chromium. The sample was exposed to an atomic oxygen fluence of  $8.72 \times 10^{21} \text{ atoms/cm}^2$  on row 9 of the LDEF spacecraft (ref. 4).

### **Procedure**

Atomic oxygen erosion modeling relations derived from reference 2 were used as a basis to convert plasma asher mass loss data from solar array blanket laminant specimens (shown in figure 1), along with Monte Carlo modeling to predict in-space

mass loss. The Monte Carlo computational model is designed to replicate the atomic oxygen interaction with SiO<sub>x</sub>-protected polyimide Kapton at defect sites in the protective coating. Kapton is modeled as an array of square cells which can be removed (oxidized) by atomic oxygen which interacts in accordance with a prescribed series of assumptions listed below:

1. The model is two-dimensional with atomic oxygen trajectories confined to a plane which simulates a crack or scratch defect in the protective coating.
2. Reaction probability of atomic oxygen with Kapton is proportional to:
  - a.  $e^{[-0.38 \text{ eV/energy, eV}]}$  (from reference 5) or as determined by LDEF data (to be discussed).
  - b. the square root of the cosine of the angle between the surface normal and the arrival direction (ref. 2).
3. Reaction probability at normal incidence is equal to:
  - a. 0.1380 for space (first impact), (ref. 2).
  - b.  $7.7 \times 10^{-6}$  (based on thermal accommodation to 300K) or as determined by LDEF data (to be discussed) for space ( $\geq$  second impact).
  - c. Four times the second or later impact reaction probability for first impact in plasma ashers, (ref. 2).
  - d.  $7.7 \times 10^{-6}$  (based on thermal accommodation to 300K) or as determined by LDEF data (to be discussed) for plasma ashers ( $\geq$  second impact).
4. Atomic oxygen which thermally accommodates (i.e. leaves surfaces with a kinetic temperature equal to that of the surface) upon first impact with surfaces, results in a reduced reaction probability.
5. Atomic oxygen does not react with protective coatings, nor recombines and remains atomic after impacting protective coatings.
6. Unreacted atomic oxygen leaves surfaces in a cosine ejection distribution if it is thermally accommodated, and scatters off surfaces almost specularly if it is nonaccommodated (elastic scattering).
7. Arrival direction of space atomic oxygen is angularly distributed because of the high temperature Maxwellian distribution.
8. Arrival direction of ground laboratory plasma asher atomic oxygen is isotropically distributed.

The first step in the procedure is to establish the relationship and variables needing quantification to allow in-space performance to be predicted based on plasma asher testing.

The Kapton mass loss per unit area of protected Kapton in a plasma asher relationship to the mass loss per unit area in space as shown in equation 1, as derived in reference 1.

$$\frac{M_S}{F_S} = \frac{M_A}{F_E} \frac{Y_A}{Y_S} \quad (1)$$

where:

- $F_E$  = Effective atomic oxygen fluence in RF plasma asher based on Kapton erosion, atoms/cm<sup>2</sup>.
- $F_S$  = Atomic oxygen fluence in space, atoms/cm<sup>2</sup>.
- $M_A$  = Kapton mass loss per unit area under SiO<sub>x</sub> coating defects in RF plasma asher, gm/cm<sup>2</sup>.
- $M_S$  = Kapton mass loss per unit area under SiO<sub>x</sub> coating defects in sweeping space ram exposure, gm/cm<sup>2</sup>.
- $Y_A$  = Monte Carlo predicted Kapton thickness loss for uncoated Kapton in an asher environment after the same fluence used to measure both  $Y_A$  and  $Y_S$ , cell length units.
- $Y_S$  = Monte Carlo predicted Kapton thickness loss for uncoated Kapton in a sweeping space ram environment, cell length units.

The actual fluence in a plasma asher greatly exceeds the effective fluence,  $F_E$ , because of the low erosion yield of thermal (0.04 eV) atoms compared to LEO ram atoms (4.5 eV).

Equation (1) assumes well developed undercutting where the undercut area is much greater than the protective coating defect area. Thus, additional undercutting via oxidation which would occur in an asher is identical to that which would occur in space for the same fluence for both pin window and crack defects. This is thought to be true because undercutting should become dominated by the thermally accommodated reaction probabilities which are the same for ashers and in space. The values of  $Y_A$  and  $Y_S$  for Monte Carlo predicted Kapton thickness loss for uncoated Kapton in an asher and sweeping space ram environment respectively are highly dependent upon the modeling assumptions which were determined from LDEF results.

The atomic oxygen reaction probability of thermally accommodated atomic oxygen is needed to predict the ratio of surface recession in a plasma asher,  $Y_A$ , and that which would occur in-space,  $Y_S$ , sweeping ram for atomic oxygen attack for unprotected polyimide Kapton using Monte Carlo modeling techniques. The results of LDEF atomic oxygen undercutting data (ref. 2) and ground laboratory thermal energy atomic oxygen experiments (ref. 5) are used in conjunction with Monte Carlo modeling of atomic oxygen undercutting erosion to quantify these parameters.

## **RESULTS AND DISCUSSION**

The results of plasma ashing of the clad solar array blanket laminant indicated that atomic oxygen was able to attack, not only the most external Kapton layers, but the inner layers as well. The light areas on the sample shown in figure 2 are areas where no Kapton remains after ashing to an effective fluence of  $3.98 \times 10^{22}$  atoms/cm<sup>2</sup>. Although some oxidation from the edges of the sample can occur, it is doubtful that a degree of loss of Kapton in the inner layers could be attributed to this effect alone. It is more probable that the defects in both the top and the bottom surface SiO<sub>x</sub> layers, as well as



bubbles in the fiberglass scrim cloth silicone matrix material allowed oxidation of the innermost Kapton layers. Because the innermost Kapton layers were clad with acrylic adhesive, which is also subject to oxidation, it is probable that regions of the acrylic adhesive were also oxidized. Figure 3 is a plot of the mass of the sample which is shown in both figure 1 and figure 2 as a function of effective fluence in the plasma asher. The plot shown in figure 3 represents 29 weight measurements at approximately equal fluence intervals. Based on figure 3, the average mass loss per area per effective fluence is  $1.54 \times 10^{-25}$  grams/atom. It is this quantity that will be used in equation 1 for the  $M_A/F_E$  term. Because erosion of both Kapton and the acrylic adhesive was possible, correction of this  $M_A/F_E$  quantity is needed if the erosion yield and density of the acrylic adhesive are significantly different than that of Kapton. The erosion yield of acrylic (polymethylmethacrylate) has been measured to be  $3.1 \times 10^{-24}$  cm<sup>3</sup>/atom for LEO atomic oxygen (ref. 6), which is quite comparable to that of Kapton ( $3 \times 10^{-24}$  cm<sup>3</sup>/atom). The density of Kapton and acrylic adhesive are also sufficiently similar that one can consider erosion of the acrylic to be equivalent to erosion of the Kapton for the purposes of this paper. The largest uncertainty is the erosion yield of the acrylic at thermal energies compared to Kapton. Another consideration in the quantity  $M_A/F_E$  is the change in mass per unit area associated with the silicone matrix for the fiberglass scrim cloth in the solar array blanket laminant. As a result of defects in the SiO<sub>x</sub> protective coating, as well as bubbles in the silicone matrix, atomic oxygen was available to oxidize hydrocarbon pendant groups on the Si-O silicone polymer backbone. However, weight loss of the silicone due to oxidation of hydrocarbon pendant groups is counteracted by weight gain of the Si-O backbone through oxygen attachment, causing silicone-to-silicate transformations (refs. 7-8). The net result of the weight loss and weight gain processes is a very slight gain with effective fluence. Figure 4 is a plot of the mass per unit area of fiberglass scrim cloth in a silicone matrix as a function of effective atomic oxygen fluence in the plasma asher. As can be seen in figure 4, even though oxidation of the silicone is occurring, very little net mass change occurs. For simplicity of computation and because very little mass change of the silicone occurs, all mass loss from experimental data in this paper will be assumed to be Kapton mass loss.

As mentioned in the procedures section of this paper, Equation 1 assumes that for well-developed undercutting, additional undercutting oxidation occurs at the same rate for both ashers and sweeping space ram. Figure 5 tests these assumptions by comparing Monte Carlo predicted undercutting for scratch defects in a plasma asher and sweeping space ram environments where full thermal accommodation is assumed upon first atomic oxygen impact. As can be seen from figure 5, although the initial growth of the undercut cavities appear to be dominated by the initial impact reaction probability, the rates of growth of the cavities with atomic oxygen fluence quickly become identical and independent of initial impact reaction probability after the undercutting has exposed the bottom SiO<sub>x</sub> protective coating. Thus, except for small initial differences in the undercut cavity associated with the rapid development of undercutting in space due to its higher initial reaction probability, the rate of mature undercutting growth with atomic oxygen fluence does appear to be identical for sweeping space and plasma asher environments, as one would expect. A similar reasoning process can be made for pin window defects in both environments, thus Equation 1 should be valid for either or a mix of types of defects. The reaction probability for second or later impacts of 0.00134 shown in figure

5 is based on the results of interpolation of Monte Carlo predictions to match LDEF undercutting results based on reference 2. These results suggest thermally accommodated reaction probabilities based on LDEF results, which are lower by a factor of 7.3 than those previously predicted using reaction probabilities proportional to the 0.68 power of the oxygen kinetic energy.

The  $Y_A/Y_S$  term in Equation 1 is highly dependent upon the choice of initial atomic oxygen reaction probabilities because very few scattered atomic oxygen atoms have view factors to allow subsequent impacts with Kapton. Figure 6 compares the Monte Carlo predicted atomic oxygen undercutting of a wide defect to simulate the erosion that would occur for unprotected Kapton in both space and plasma asher environments for the same initial and subsequent impact reaction probabilities as were used in figure 5. Because  $Y_A/Y_S$  are the ratio of the Monte Carlo predicted recessions for the same actual fluence, the ratio of the recessions shown in figures 6a and 6b must be corrected to predict what they would be if they had the same fluence. The result of this correction to the profiles shown in figure 6a and 6b is  $Y_A/Y_S = 0.048$ . Thus, substituting the observed plasma asher mass loss data and the Monte Carlo modeling data in Equation 1 results in a projected Kapton mass loss per area per fluence in a sweeping space ram environment of  $7.4 \times 10^{-27}$  grams/atom as shown in Table 1. This result is based on full thermal accommodation of atomic oxygen upon its first impact with Kapton or  $\text{SiO}_x$ . In addition, a reaction probability of  $1.34 \times 10^{-3}$  is assumed for thermally accommodated atomic oxygen reacting with Kapton based on Monte Carlo modeling to match observed LDEF undercutting results (ref. 2). Thus, based on these assumptions, the projected Kapton mass loss per area per fluence in a sweeping space ram environment would be 0.048 of the amount which is measured in a plasma asher environment based on effective fluence. Based on the amount of Kapton initially in the Space Station Freedom photovoltaic array blanket laminant, as shown in figure 1, and a Kapton density of  $1.42 \text{ grams/cm}^3$ , the fraction of Kapton which would be remaining in an asher environment at the end of life ( $5.4 \times 10^{22} \text{ atoms/cm}^2$ ) would be -0.153. Thus, the rate of mass loss of Kapton in the blanket laminant in a plasma asher environment is more than sufficiently high to result in the complete oxidation of all the Kapton in the laminant as shown in Table 1. However, based on the conversion factors to project rates of loss in a sweeping space ram environment, 94% of the solar array blanket Kapton would be remaining, as shown in Table 1.

Observed LDEF undercutting results can be made to agree with Monte Carlo modeling of undercutting by assuming full thermal accommodation of atomic oxygen upon its first impact, and using the Monte Carlo model to fit the observed undercut cavity by adjustment of the reaction probability of thermally accommodated atomic oxygen, as was the case for the previously described projections. One can assume that the reaction probability of thermally accommodated atomic oxygen bears an Arrhenius relation with the atomic oxygen energy as described in reference 4 with an activation energy of 0.38 eV and solve for the accommodation fraction, again using Monte Carlo modeling to fit the LDEF undercut cavity profiles. Using an activation energy of 0.38 eV, and assuming 300 Kelvin atoms, a reaction probability for thermally accommodated atomic oxygen of  $7.7 \times 10^{-6}$  is predicted. Based on Monte Carlo modeling to fit the observed LDEF undercut profile (ref. 2), an accommodation fraction of 0.9 is predicted.

An accommodation fraction of 0.9 for the model used means that nine out of ten atoms fully thermally accommodate upon first impact with Kapton or  $\text{SiO}_x$ , and that one out of ten atoms leaves those surfaces with the same energy that they initially arrive at, and with a near specular ejection angle. This process would continue for additional impact until all the atomic oxygen has become fully thermally accommodated. Based on this set of assumptions, a projected Kapton mass loss per area per fluence of  $4.3 \times 10^{-29}$  grams/atom is predicted for a sweeping space ram environment (Table 1). Because the reaction probability for thermally accommodated atomic oxygen is much lower ( $7.7 \times 10^{-6}$  compared to  $1.34 \times 10^{-3}$ ) for this set of assumptions, the ratio of Monte Carlo predicted erosion rates of unprotected Kapton in plasma asher and space environments,  $Y_A/Y_S$ , is equal to  $2.8 \times 10^{-4}$ . Because of the lower reaction probability of thermally accommodated atomic oxygen which dominates the erosion processes, the relative Kapton mass loss per area per fluence in a sweeping space ram environment is only  $2.8 \times 10^{-4}$  of that which would be observed in a plasma asher environment as shown in Table 1. The fraction of initial Kapton remaining in the Space Station Freedom solar array blanket laminant at end of life would be 99.97% of the initial mass. Thus a negligible mass loss is predicted in spite of the fact that in the plasma asher more than all the Kapton would be lost for the same effective fluence. For both columns in Table 1, initial impact atomic oxygen reaction probabilities are assumed to be four times that of thermally accommodated reaction probabilities as a result of the presence of excited state species which are more reactive. The factor of four was determined by fitting Monte Carlo results to match observed plasma asher undercut profiles as described in reference 9. Although it is not clear what fraction of atomic oxygen thermally accommodates upon first impact, and what the reaction probability of thermally accommodated atomic oxygen actually is, one would be perhaps optimistic to choose the lowest thermally accommodated reaction probabilities without good cause. Based on the results shown in Table 1, it appears that observed Space Station Freedom photovoltaic array blanket laminant will lose mass at a very acceptable rate (only 4.83% that observed in plasma ashers) in a sweeping space ram environment. Clarification or verification of the previous or other durability projections would be greatly assisted through experiments which are able to quantify erosion yields and reaction probabilities of thermally accommodated atomic oxygen.

## **CONCLUSION**

The results of observed LDEF atomic oxygen undercutting of protected polymers are used in conjunction with Monte Carlo modeling of both plasma asher and sweeping space ram environments to project the relationship between Kapton mass loss in plasma ashers to Kapton mass loss in a sweeping space ram environment. Two models were analyzed which replicate observed LDEF undercutting geometries. The first model, based on 100% accommodation of atomic oxygen upon first impact required a reaction probability for thermally accommodated atomic oxygen of  $1.34 \times 10^{-3}$ . This model predicts Kapton mass loss per area per fluence in space equal to 0.0483 that observed in a plasma asher environment. This model also predicts that the Space Station Freedom photovoltaic blanket laminant at end of life will have 94.4% of its Kapton remaining ( $5.4 \times 10^{22}$  atoms/cm<sup>2</sup> fluence). A second model was based on selection of a thermally

accommodated atomic oxygen reaction probability of  $7.7 \times 10^{-6}$  based on an Arrhenius erosion yield relationship with an activation energy of 0.38 eV. This model required an accommodation fraction of 0.9 to replicate observed LDEF undercutting results. The projected sweeping space ram mass loss rates were two orders of magnitude lower than that for the first case, predicting more than 99% of the Kapton remaining in the Space Station Freedom photovoltaic array blanket at end of life.

Although the results are highly encouraging, they should be regarded with cautious optimism until more definitive measurement of atomic oxygen accommodation fraction and erosion yield of thermally accommodated atomic oxygen can be made.

## **REFERENCES**

1. B.A. Banks, S.K. Rutledge, and L. Gebauer, "SiO<sub>x</sub> Coatings for Atomic Oxygen Protection of Polyimide Kapton in Low Earth Orbit," AIAA Paper No. 92-2151, paper presented at the Coatings Technologies for Aerospace Systems Materials Specialist Conference, Dallas, Texas, April 16-17, 1992.
2. B.A. Banks, K.K. de Groh, B.M. Auer, L. Gebauer, and J.L. Edwards, "Monte Carlo Modeling of Atomic Oxygen Attack of Polymers with Protective Coatings on LDEF," paper presented at the 2nd LDEF Post-Retrieval Symposium (NASA Conference Publication in Press), San Diego, California, June 1-5, 1992.
3. B.A. Banks, S.K. Rutledge, and J.A. Brady, "The NASA Atomic Oxygen Effects Test Program," Proceedings of the 15th Space Simulation Conference, Williamsburg, Virginia, October 31-November 3, 1988.
4. R.J. Bourassa and J.R. Gillis, "Atomic Oxygen Exposure of LDEF Experiment Trays," NASA CR-189627, Boeing Defense and Space Group, May, 1992.
5. S.R. Koontz, K. Albyn, and L.J. Leger, "Atomic Oxygen Testing with Thermal Atom Systems: A Critical Evaluation," Journal of Spacecraft and Rockets, Vol. 28, No. 3, May-June, 1991.
6. B.A. Banks and S.K. Rutledge, "Low Earth Orbital Atomic Oxygen Simulation for Materials Durability Evaluation," Proceedings of the Fourth European Symposium on Spacecraft Materials in a Space Environment, CERT, Toulouse, France, September 6-9, 1988.
7. A.D. Butherus, T.W. Hou, C.J. Mogab, and H. Schonhorn, "O<sub>2</sub> Plasma-Converted Spin-On-Glass for Planarization," Journal of Vacuum Science and Technology, Vol. 3, No. 5, September-October, 1985.
8. B.G. Bagley, W.E. Quinn, C.J. Mogab, and M.J. Vasile, "The Effect of Reactor Configuration on the Oxygen Plasma Conversion of an Organosilicone to SiO<sub>2</sub>," Materials Letters, Vol. 4, No. 3, April, 1986.

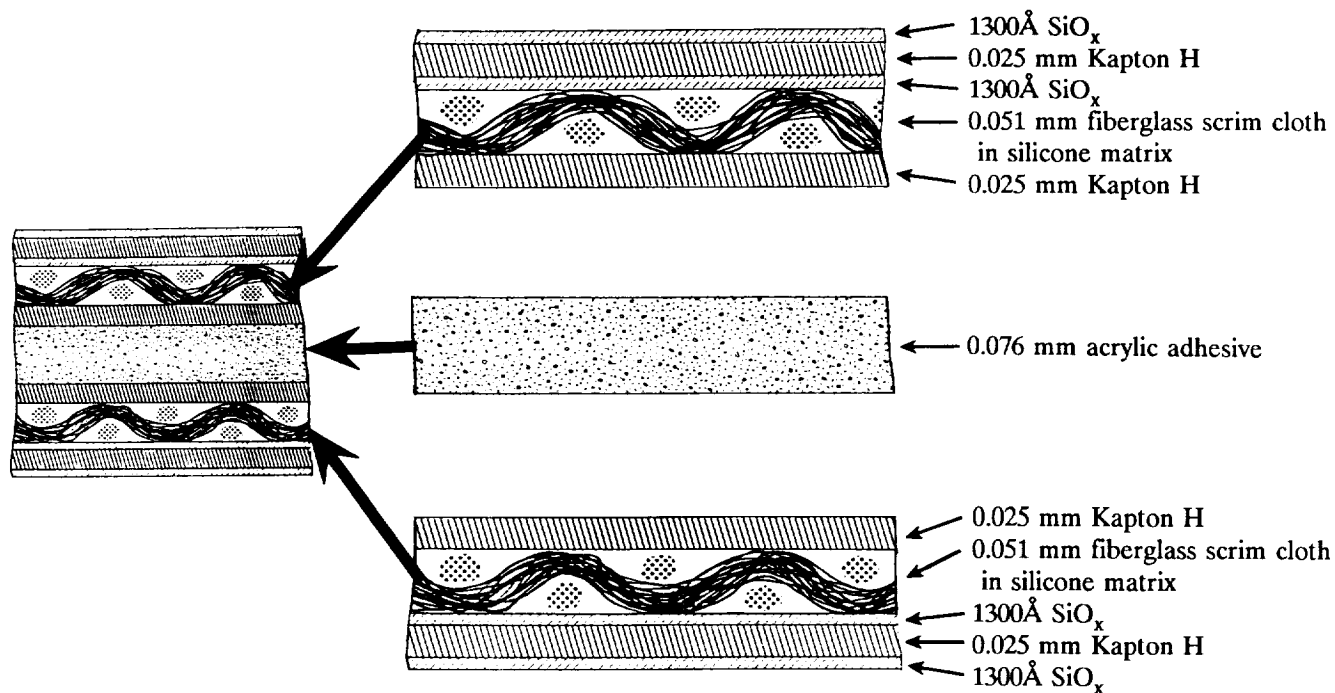
9. B.A. Banks, B.M. Auer, S.K. Rutledge, and C.M. Hill, "Atomic Oxygen Interaction with Solar Array Blankets at Protective Coating Defect Sites," Proceedings of The Fourth Annual Workshop on Space Operations, Automation, and Robotics (SOAR '90), sponsored by the U.S. Air Force, National Aeronautics and Space Administration, and Wright State University, Albuquerque, NM, June 26-29, 1990.

**TABLE I:** Projection of In-Space Durability of SSF Photovoltaic Blanket Laminate Based on Plasma Asher Testing

		Environment		
		Measured in Plasma Asher	Projected in Space Sweeping Ram Based on:	
			LDEF and full accommodation $P_R = 1.34 \times 10^{-3}$ $P_A = 1$	LDEF, Activation Energy = 0.38, and partial accommodation $P_R = 7.7 \times 10^{-6}$ $P_A = 0.9$
Mass Loss ----- (Area)(Fluence)	Relative Comparison	1	0.048	$2.8 \times 10^{-4}$
	grams/atom	$1.54 \times 10^{-25}$	$7.4 \times 10^{-27}$	$4.3 \times 10^{-29}$
Fraction of initial Kapton remaining in SSF photovoltaic blanket laminate at End-of-Life fluence ( $5.4 \times 10^{22}$ atoms/cm <sup>2</sup> )		-0.153	0.94	0.9997

$P_R$  = Probability of thermally accommodated atomic oxygen reacting with Kapton upon each impact.

$P_A$  = Probability of energetic atomic oxygen atoms thermally accommodating upon each impact.



Clad sample in configuration for plasma ashing

Two unclad laminate samples and acrylic adhesive

Figure 1. - Configuration of flexible solar array laminant used for atomic oxygen durability evaluation in an RF plasma asher.

ORIGINAL PAGE  
 BLACK AND WHITE PHOTOGRAPH

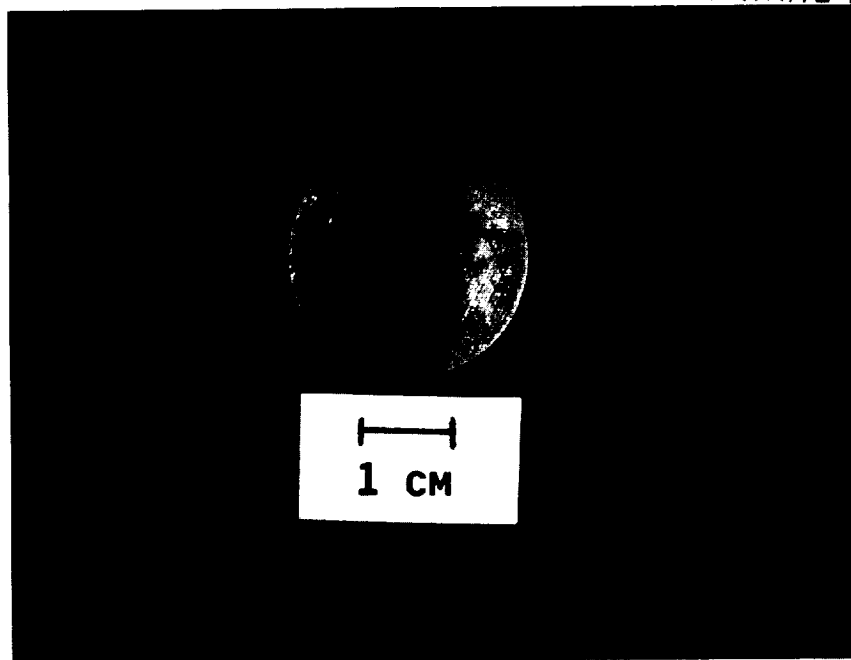


Figure 2. - Photograph of a clad flexible solar array laminant sample after atomic oxygen exposure in a plasma asher to an effective fluence of  $3.98 \times 10^{22}$  atoms/cm<sup>2</sup>.

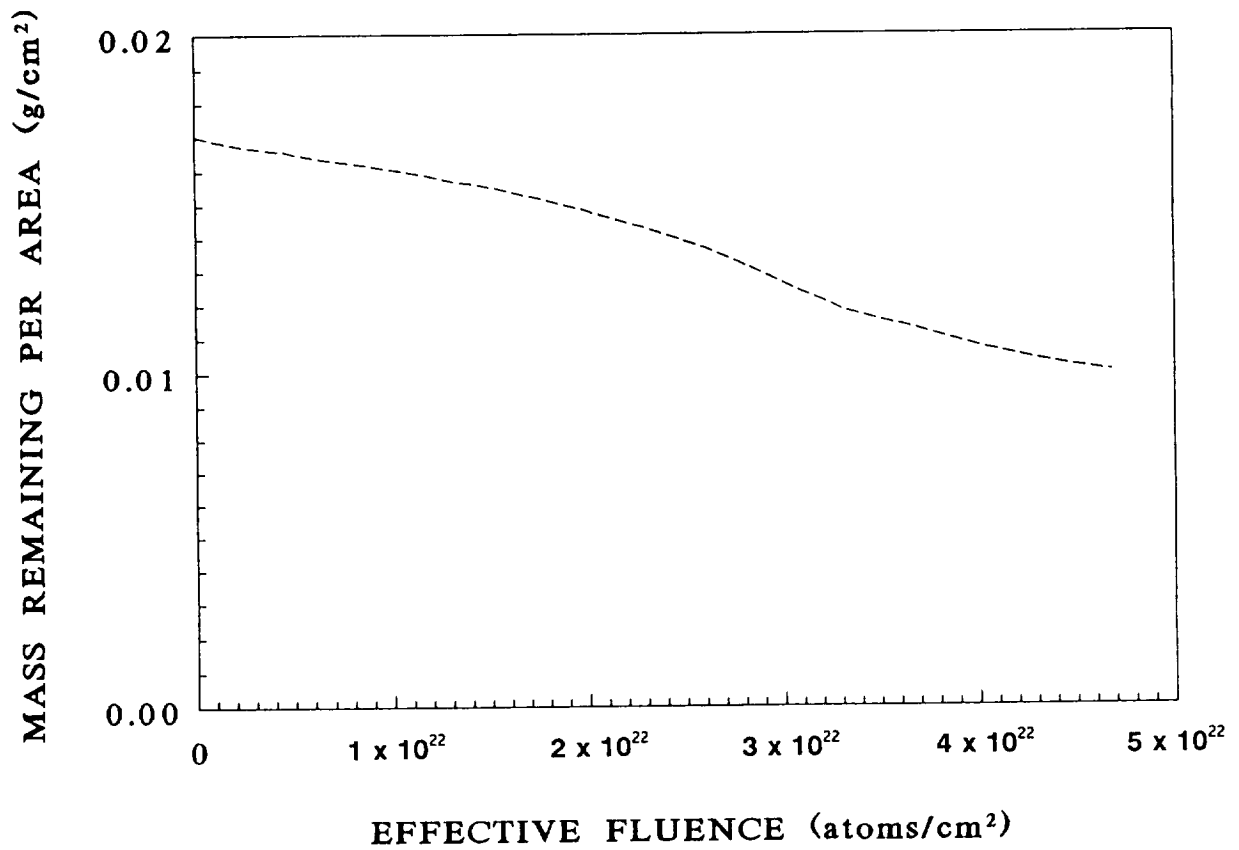


Figure 3. - Mass per unit area of clad, flexible laminant sample as a function of atomic oxygen effective fluence in a plasma asher. Based on figure 2, the average mass loss per unit area per effective fluence is  $1.54 \times 10^{-25}$  grams/atom.

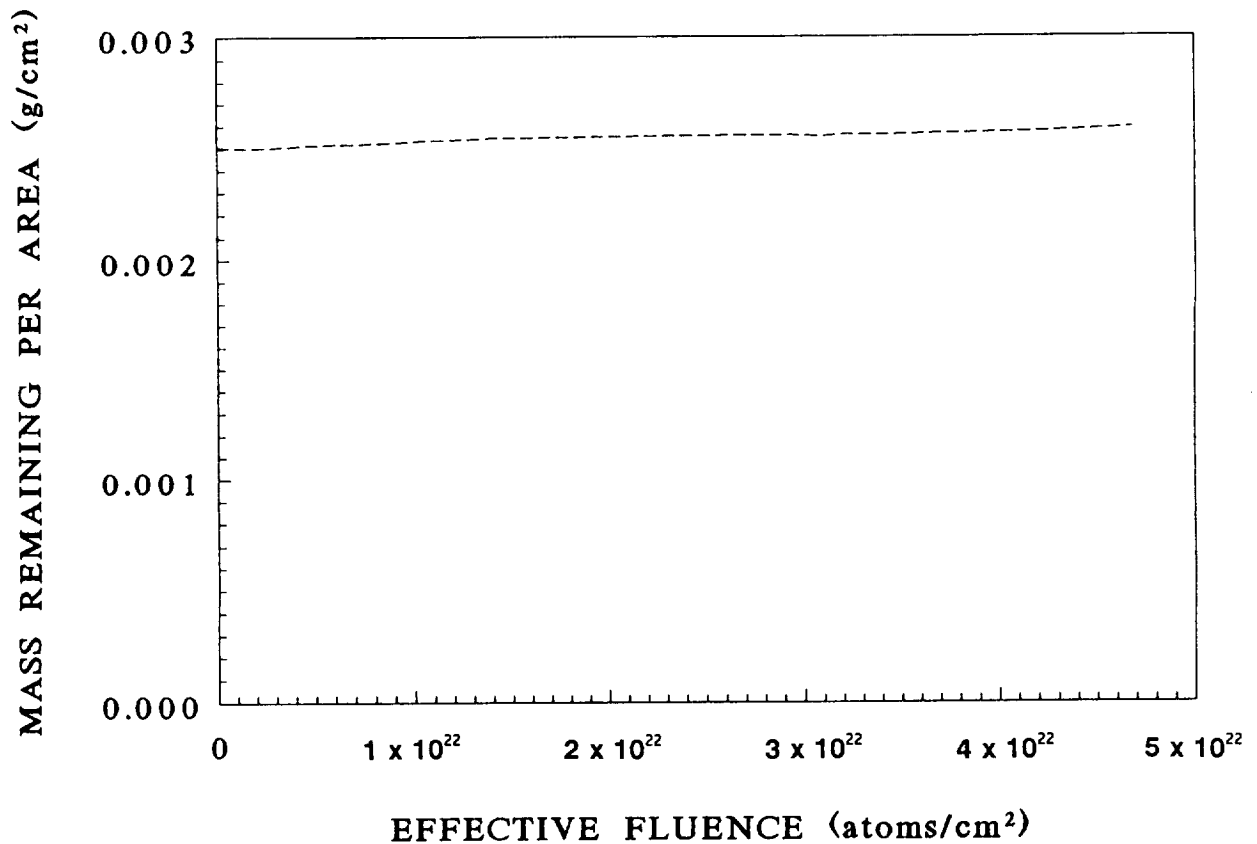


Figure 4. - Mass per unit area of fiberglass scrim cloth in a silicone matrix dependence upon effective atomic oxygen fluence.

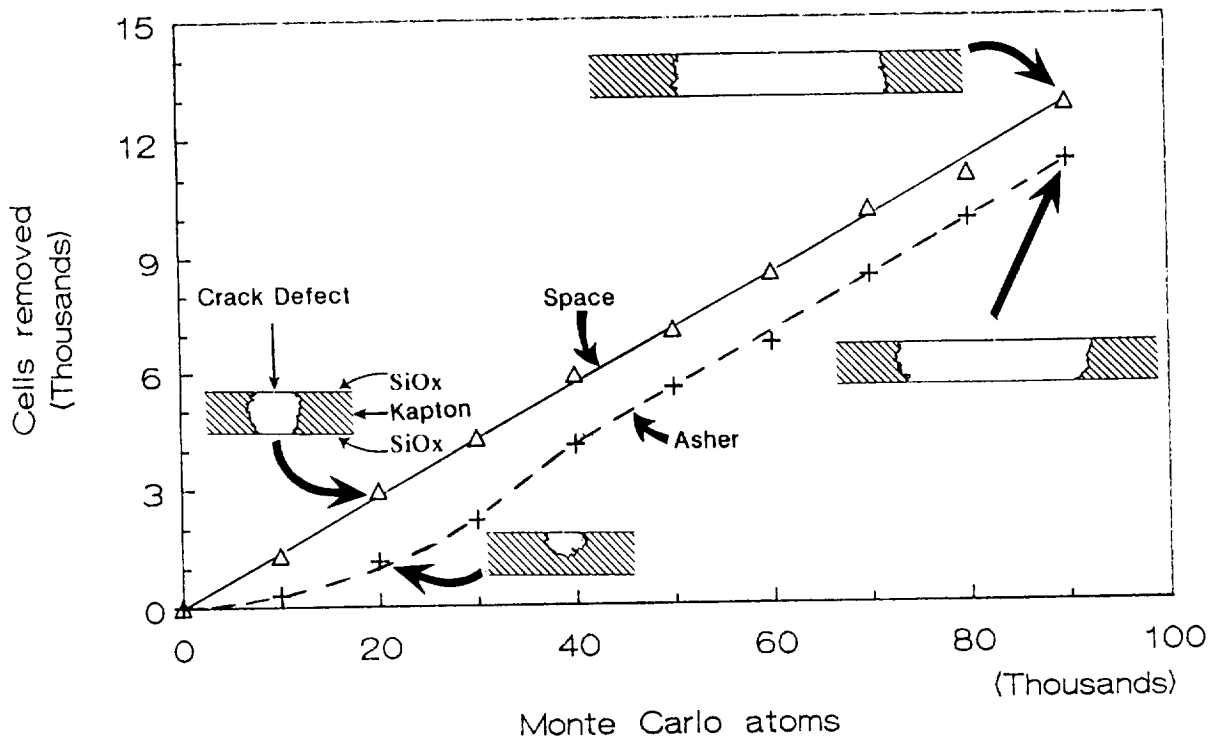
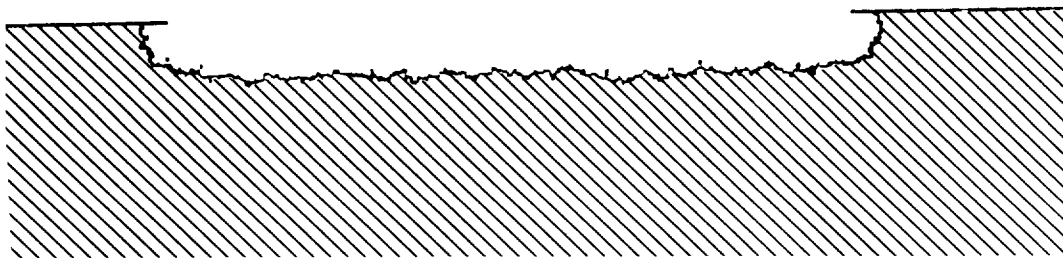
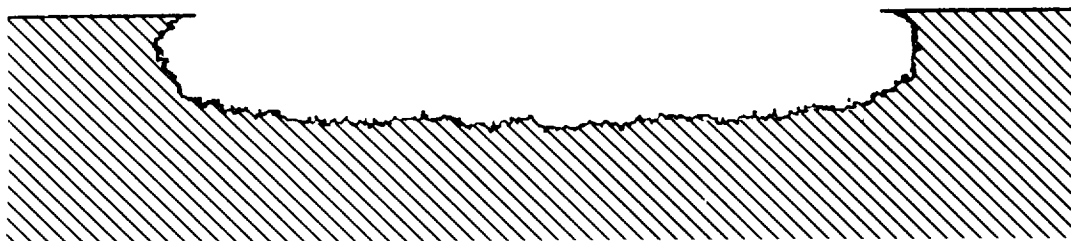


Figure 5. - Monte Carlo model predicted atomic oxygen undercutting at scratch defect sites in Kapton protected on both sides by  $\text{SiO}_x$  based on initial impact reaction probabilities of 0.138 in space, and 0.00536 in plasma ashers; and second or later impact reaction probabilities of 0.00134 for both environments.



6a. - In plasma asher environment after 2,200,000 atoms arrival.



6b. - In sweeping space ram environment after 200,000 atoms arrival.

Figure 6. - Monte Carlo model predicted atomic oxygen undercutting for wide defects in Kapton protected on its exposed surface using the identical assumptions as shown in figure 5. The defect shown is 400 Monte Carlo model cell units wide.



## LEVELING COATINGS FOR REDUCING THE ATOMIC OXYGEN DEFECT DENSITY IN PROTECTED GRAPHITE FIBER EPOXY COMPOSITES

D. A. Jaworske and K. K. de Groh  
NASA Lewis Research Center  
Cleveland, Ohio

G. Podojil, T. McCollum, and J. Anzic  
Cleveland State University  
Cleveland, Ohio

### ABSTRACT

Pinholes or other defect sites in a protective oxide coating provide pathways for atomic oxygen in low Earth orbit to reach underlying material. One concept for enhancing the lifetime of materials in low Earth orbit is to apply a leveling coating to the material prior to applying any reflective and protective coatings. Using a surface tension leveling coating concept, a low viscosity epoxy was applied to the surface of several composite coupons. A protective layer of 1000 Å of SiO<sub>2</sub> was deposited on top of the leveling coating, and the coupons were exposed to an atomic oxygen environment in a plasma asher. Pinhole populations per unit area were estimated by counting the number of undercut sites observed by scanning electron microscopy. Defect density values of 180,000 defects/cm<sup>2</sup> were reduced to about 1000 defects/cm<sup>2</sup> as a result of the applied leveling coating. These improvements occur at a mass penalty of about 2.5 mg/cm<sup>2</sup>.

### INTRODUCTION

Space power components made from graphite fiber-epoxy composites and exposed to the low Earth orbital environment are subject to degradation from atomic oxygen. Atomic oxygen attacks both the epoxy and the carbon fibers forming volatile oxides. Although there are several metal oxide coatings that can be deposited on top of the epoxy, thorough coverage is difficult because dust particles, scratches, and surface irregularities create defects in the protective coating (ref. 1). These pinhole and scratch defect sites are numerous, and provide a pathway for atomic oxygen undercutting (ref. 2-3). Once started, the undercutting may progress to the extent that the protective coating tears thus allowing more epoxy to be exposed to the atomic oxygen environment.

Lightweight solar mirrors made from graphite fiber-epoxy composite face sheets are particularly susceptible to this kind of erosion. The defect sites that are inevitably in the protective coating are often too small to see, until after atomic oxygen undercutting has begun. However, based on laboratory research with samples having a large pinhole population, catastrophic optical failure of composite mirror surfaces occurs at the fluences expected at Space Station Freedom altitude over a time of 15 years (ref. 4).

One technique proposed to diminish the pinhole population in the graphite fiber-epoxy composite face sheet of a solar mirror is to apply a surface tension driven leveling coating over the composite prior to applying the reflective and protective coatings. The purpose of the leveling coating is to cover the small projections and cracks where the pinholes originate, creating a smoother surface onto which the reflective and protective coatings may be deposited, as shown in figure 1. The smoother surface finish created by the leveling coating should also enhance the specular reflectance of the mirror. A previous study using epoxies that were poured onto the substrate surface has reported an order of magnitude decrease in defect density and an order of magnitude increase in specular reflectance (ref. 1). The present study compares leveling coatings that were produced by dipping the substrates into epoxies. Subsequent improvements were found in defect density population and specular reflectance.

## MATERIALS AND METHODS

The application of a surface tension driven leveling coating was accomplished by dipping the substrate into a container of low viscosity epoxy and withdrawing the sample slowly. All samples were pulled out of the epoxy vertically. Several different epoxies were considered initially, as shown in Table I. Aluminum substrates were used for the initial screening experiments, and profilometry was used to make surface roughness comparisons between the aluminum and the epoxy-covered aluminum. The numbers to the right of each sample represent average surface roughness, in angstroms, based on the method of standard deviation by successive differences (ref. 5). Only the aluminum substrates were cured vertically. All of the other substrates were cured horizontally.

The sample with the smoothest finish after dipping was Epotek 305, manufactured by Epoxy Technology, Inc. However, the Epotek 305 had a pot life of only 20 minutes. With such a short pot life, the viscosity of the epoxy increased substantially during the course of several dipping experiments, making it difficult to produce consistent coatings.

Due to the short pot life of the Epotek 305, it was decided to continue the leveling coating work with the next best performer, Epotek 301-2, also manufactured by Epoxy Technology, Inc. The pot life of the Epotek 301-2 was found to be much longer, allowing for several samples to be dipped (or one sample to be dipped several times) in one session. In subsequent experiments, an additive (FC-430 Flourad Brand Coating Additive, manufactured by 3M) was added to the Epotek 301-2 to enhance the wetting of the low viscosity epoxy to the T300/934 graphite fiber-epoxy composite substrates chosen for this study.

Dipping the 2.23 cm x 2.23 cm x 0.30 cm coupons was accomplished mechanically by an Oriel Miniature Motorized Translator. The dipping speed was on the order of 1 cm per minute. No time dependent studies were conducted. Each coupon was dipped half way into the Epotek 301-2 so that half of the sample was coated with a leveling coating and the other half with no leveling coating. Care was taken to mix the resin and hardener thoroughly without creating a lot of bubbles. The mixture was often allowed to settle for several minutes and a pipet was used to skim off any of the remaining bubbles from the surface. Figure 2 shows a photo of the dipping apparatus, with a sample installed.

Additional techniques for sample preparation were also considered. Some of the initial composite samples dipped in the Epotek 301-2 exhibited a tacky surface, attributed to humidity. Mixing of the epoxy, dipping, and curing were performed in a nitrogen-filled glove box to avoid the tacky surface. A simple tube furnace made from nichrome wire wound around a glass tube served as a means of curing the samples at 80°C. The temperature of the tube furnace was controlled manually, and heating was accomplished using a ramp-and-soak technique over about an hour. Samples were allowed to cure for at least another 1 1/2 hours. It was necessary to place the samples horizontally in the tube furnace during curing, which also seemed to minimize the formation of a small lip on the bottom of the composite where the epoxy would otherwise collect by gravity.

Those samples prepared for defect density counting were coated with about 1000 Å of SiO<sub>2</sub>. An SiO<sub>2</sub> coating was chosen over an aluminum reflective coating because the defects generated by undercutting are best seen by charging in a scanning electron microscope and an aluminum coating would diminish the charging. Samples were coated using an electron-beam (e-beam) evaporation technique. Atomic oxygen exposure followed, using a Structure Probe, Inc., Plasma Prep II plasma asher. The asher was operated on air at 50-100 mtorr, at a continuous RF power of 100 watts. Effective atomic oxygen fluence was determined by measuring mass loss in adjacent Kapton (a product of the E. I. du Pont de Nemours & Co., Inc.) witness coupons and calculating fluence based on the erosion yield of Kapton in low Earth orbit. This was necessary because of the lack of in-space erosion yield data for the specific epoxy materials used. An erosion yield of  $3 \times 10^{-24}$  cm<sup>2</sup>/atom was assumed such that the Kapton effective fluence is the epoxy effective fluence. Defect density measurements were made by obtaining several scanning electron micrographs of random leveling coated (and uncoated) regions and counting the number of defects that could be identified in the photo. Magnification was on the order of 150 to 500 times. Both secondary electron and back scattered electron images were used, but the back scattered images showed the undercutting more clearly. The area occupied by the photo was determined so that defect density could be cited as defects/cm<sup>2</sup>.

Samples for reflectance measurements were prepared differently. The as-received T300/934 composite coupons were first coated with 1000 Å of aluminum, again using e-beam evaporation. Electron-beam evaporation was chosen

over other deposition techniques because the reflective and protective coatings for Space Station Freedom solar dynamic concentrators were to be prepared using e-beam techniques (ref. 3). Total and diffuse reflectances were measured to an accuracy of  $\pm 2\%$  on a Perkin-Elmer Lambda-9 spectrophotometer equipped with a 60 mm diameter integrating sphere over the wavelength range of 250-2500 nm. Specular reflectance was determined by difference, and all three measurements were corrected to air mass zero and integrated to obtain solar integrated reflectance values. Then, the samples were dipped entirely in the Epotek 301-2, so that the whole mirror face was coated with epoxy. After curing at 80°C, 400 Å of gold were deposited via sputter deposition to inhibit curtaining (a roughening of the surface attributed to uneven heating) of the epoxy and another 1000 Å of aluminum were e-beam deposited on the surface. Total, diffuse, and specular reflectance were measured again, for comparison to the non-leveling coating values.

The reflectance samples were also subjected to atomic oxygen exposure in the plasma asher. Again, Kapton witness coupons were used to confirm the atomic oxygen fluence.

In addition to the graphite fiber-epoxy substrates used for the bulk of the study, a small fused quartz slide was used as a substrate in one part of the study to compare the atomic oxygen defect density of a leveling coating on a generically different substrate with that of the graphite fiber-epoxy substrate.

## RESULTS AND DISCUSSION

The leveling coatings described in this paper provide two benefits for low Earth orbital space systems. For satellites that will reside in low Earth orbit, the leveling coating provides a means to reduce atomic oxygen degradation by reducing the number of atomic oxygen susceptible defect sites. And for satellites using a solar mirror, the leveling coating also provides a means to increase the solar specular reflectance of a light-weight graphite fiber-epoxy substrate.

### Atomic Oxygen Durability

The degree of improvement in atomic oxygen durability was determined by comparing the defect density of the pristine graphite fiber-epoxy composite surface with the defect density of the surface after one application of the leveling coating. Figure 3a shows a scanning electron micrograph of one of the non-leveling coating surfaces coated with SiO<sub>2</sub> after ashing to a fluence of  $1.75 \times 10^{21}$  atoms/cm<sup>2</sup>. Figure 3b shows another scanning electron micrograph of the adjacent region coated with Epotek 301-2. Undercutting defects are best identified by the rings around each of the initial pinhole defects, produced by charging under the electron beam. Note the variety in the size and shape of the undercutting defects. The size and shape of the defects shown here are similar to the ones that have been characterized before (ref. 6). Given more time in the atomic oxygen environment, the undercut areas would grow together causing the coating to tear, making it impossible to count the number of defects sites. Having such a variety in defect size, shape, and extent, defect density counting remains somewhat inexact. However, with the selection of the proper fluence of atomic oxygen, the technique of counting defects on scanning electron micrographs can be useful for the purpose of sample comparison, at least to an order of magnitude.

Table II summarizes the non-leveling and single leveling coating data collected for both the graphite fiber-epoxy substrate samples and the fused quartz samples. Although there is some scatter in the data, the uncoated samples of graphite fiber-epoxy show a defect density on the order of  $10^5$  defects/cm<sup>2</sup> while the coated samples show a defect density on the order of  $10^3$  defects/cm<sup>2</sup>. Hence, for these graphite fiber-epoxy samples, the leveling coating provides a two order of magnitude improvement in the atomic oxygen defect density. Although there are no data for the fused quartz slide before dipping, the fused quartz slide with a leveling coating applied had a defect density on the order of  $2.4 \times 10^4$  defects/cm<sup>2</sup>, something of a surprising result.

The data from the quartz slide experiment is puzzling, in that the smoother quartz substrate gave a higher defect density after application of a leveling coating than the rougher graphite fiber-epoxy substrate. As there were several weeks between the time that the graphite fiber-epoxy composite data and the fused quartz data were collected, there may have been some aging of the epoxy resin or some increase in the amount of dust that accumulated in the glove box which gave these curious results.

Using the mass of one of the graphite fiber-epoxy samples before and after dipping and the geometry of the sample, this level of improvement is obtained at a weight penalty of  $2.5 \text{ mg/cm}^2$ . Using  $0.95 \text{ g/cm}^3$  as the density of the cured Epotek 302-1, this corresponds to a thickness of about  $26 \text{ }\mu\text{m}$ . Leveling coatings of this thickness are comparable to other spray-on leveling coatings reported previously (ref. 7).

Finally, the issue of having a second leveling coating was addressed, along with the added improvement that it provides. Another set of coupons were dipped in the Epotek 301-2. Each coupon was dipped halfway into the epoxy, cured, rotated  $90^\circ$ , dipped halfway into the epoxy again, cured, and coated with  $1000 \text{ }\text{\AA}$  of  $\text{SiO}_2$ . In this way, there were four quadrants on each coupon, one quadrant with no leveling coatings, two quadrants with one leveling coating, and one quadrant with two leveling coatings. The results from this series are summarized in table III. From this sample we conclude that the application of a second leveling coating provides no further improvement in defect density population, leaving the sample with about  $10^3 \text{ defects/cm}^2$ . This result is interesting, in that it may be pointing to a limiting value imposed by the leveling coating technique.

A certain amount of caution needs to be used during the interpretation of leveling coating atomic oxygen durability data. The glove box facility used here was admittedly not comparable to a Class-100 clean room. Dust particles residing in the glove box at the time of the dipping may well have populated the leveling coating, likewise, dust particles may have populated the surface while transporting the samples from the glove box to the e-beam deposition facility. Hence, the data presented here are meant to be used only as a guide. In subsequent work, emphasis ought to be placed on maintaining cleanroom conditions during the critical processing steps of preparing the leveling coating, and the reflective and protective coatings. With additional cleanroom practices, one should expect further improvements in atomic oxygen durability. Perhaps other techniques for applying leveling coatings will also yield a lower defect density population.

### Solar Specular Reflectance

The role of the leveling coating on improving the solar specular reflectance of graphite fiber epoxy composite coupons was also investigated. As mentioned previously, in order to get non-leveling coated and leveling coated solar specular reflectance values on the exact same coupon, it was necessary to first coat the bare graphite epoxy surface with aluminum. After obtaining the solar specular reflectance, the aluminum-coated samples were dipped entirely into the Epotek 301-2, sputter coated with  $400 \text{ }\text{\AA}$  of gold and coated with aluminum again. Subsequent solar specular reflectance values were obtained for comparison. The results from this set of experiments are shown in table IV.

Comparing the reflectance of the initial aluminum on the graphite epoxy coupon with the reflectance of the leveling coating, the leveling coating seems to improve the solar specular reflectance from an average value of 0.82 to a value of 0.86, at the expense of the diffuse portion of the reflectivity. Total reflectivity perhaps dropped slightly, from 0.89 to 0.88. These results are similar to those reported previously for Epotek 277 (ref. 1).

Next, aluminum covered samples with and without a leveling coating were exposed to an effective fluence of  $2.0 \times 10^{21} \text{ atoms/cm}^2$ , equivalent to about 0.7 years of solar facing surfaces (not direct ram) at Space Station Freedom altitude. Table V shows that the specular component for the non-leveling coating sample went down from a value of 0.83 to 0.76 while the specular component went down from a value of 0.86 to 0.81 for the leveling coating samples.

It is likely that the leveling coating samples would continue to degrade in solar specular reflectance as a result of atomic oxygen exposure, in a fashion similar to the uncoated samples. The main difference would be in the length of time required to reach the same magnitude of change. More experimentation will be needed to quantify the added performance factor over time.

The atomic oxygen defect density of the reflectance samples cannot be directly compared to those of the  $\text{SiO}_2$ -coated samples cited previously because of the presence of a sputter deposited layer of gold on the reflectance samples. Gold is a catalytic recombinant surface for atomic oxygen. The atomic oxygen recombines to form  $\text{O}_2$  so that less atomic oxygen is present in the vicinity of the undercut region. For example, Table VI summarizes the defect density of graphite fiber-epoxy samples (from ref. 1) that were aluminum-coated or gold-coated, then exposed to a fluence of  $8.32 \times 10^{20} \text{ atoms/cm}^2$  of atomic oxygen. Although sputter deposition provides a catalytic surface, it is not conducive to

the kind of large scale deposition needed for solar concentrators. Chemical vapor deposition techniques may provide a more thorough coverage resulting in lower defect density values.

## CONCLUSIONS

The use of Epotek 301-2 as a leveling coating provides the designer with essentially two advantages. First, the number of pinhole defect sites on graphite epoxy composite structures coated with an atomic oxygen resistant coating for use in low Earth orbit can be reduced by nearly two orders of magnitude. Additional leveling coatings provide little or no additional protection, suggesting that there is a limiting value to the pinhole population established by the use of leveling coats. It should be noted that the presence of defect sites in a protective coating means that the graphite fiber-epoxy structure will eventually succumb to atomic oxygen attack, however, reducing the number of defect sites will extend the performance lifetime of the graphite fiber-epoxy solar mirror. Perhaps there are other leveling coating application techniques or materials that will yield even lower defect density populations, and longer performance lifetimes.

The second advantage of using a leveling coating is that the leveling coating improves solar specular reflectance of initially rough graphite fiber-epoxy composite mirror surfaces to a value of 0.86. This improvement is consistent with previous studies. The durability of the solar specular reflectance of graphite fiber-epoxy composite mirror surfaces to simulated atomic oxygen attack is also improved, although further experimental work is needed to quantify the extended performance.

## REFERENCES

1. K. K. de Groh, T. M. Dever, and W. F. Quinn, "The Effect of Leveling Coatings on the Atomic Oxygen Durability of Solar Concentrator Surfaces." NASA TM 102557, April, 1990.
2. K. K. de Groh and B. A. Banks, "Atomic Oxygen Undercutting of LDEF Aluminized-Kapton Multilayer Insulation." NASA CP 3134, June 1991.
3. D. J. McClure, "Design and Demonstration of a System for the Deposition of Atomic Oxygen Durable Coatings for Reflective Solar Dynamic Power System Concentrators." NASA Contractor Report 4158, 1988.
4. K. K. de Groh, J. A. Dever, T. A. McCollum, E. Rodriguez, and C. A. Burke, and J. A. Terlep, "Low Earth Orbit Durability Evaluation of Solar Concentrator Materials." *Solar Engineering 1992*, W. Stine, J. Kreider, and K. Watunaba, eds., American Society of Materials Engineers, New York, pp 775-782, 1992.
5. D. A. Jaworske, T. T. Jeunnette, and J. M. Anzic, "Measurements of Print-Through in Graphite Fiber Epoxy Composites." 34th International SAMPE Symposium, Book 1, pp 780-789, Reno, Nevada, May 1989.
6. S. K. Rutledge and J. A. Mihelcic, "Undercutting of Defects in Thin Film Protective Coatings on Polymer Surfaces Exposed to Atomic Oxygen." NASA TM 101986, April, 1989.
7. S. W. Richter, "Technology Development of Fabrication Techniques for Advanced Solar Dynamic Concentrators." 26th Intersociety Energy Conversion Conference, Volume 1, pp 301-307, Boston, Massachusetts, August, 1991.

TABLE I. - COMPARISON OF SURFACE ROUGHNESS AFTER APPLYING A SINGLE LEVELING COATING OF VARIOUS EPOXIES.

Epoxy	Result	Average Roughness (Å)
Aluminum	n/a	1500
Epotek 301	Coating was very thin with a small lip on the end where epoxy had collected.	1000
Epotek 305	Coating was similar to 301, but smoother. Short pot life.	340
Epotek 301-2	Coating was similar to 305, but some holes were noted on the end where the epoxy had collected. Much longer pot life.	380
Epotek 377	The epoxy did not adhere well to the aluminum and had streaks.	1700
Epotek 314	Poor surface finish	3800
Epotek 360	Poor surface finish	1500

Table II. - DEFECT DENSITY POPULATION OF EPOTEK 301-2 GRAPHITE FIBER-EPOXY COUPONS AND KAPTON WITH NO LEVELING COATING AND ONE LEVELING COATING APPLIED.

Sample	Fluence	uncoated	coated
Graphite epoxy	$1.93 \times 10^{21}$	70000 defects/cm <sup>2</sup>	3800 defects/cm <sup>2</sup>
Graphite epoxy	$1.93 \times 10^{21}$	180000	1000
Graphite epoxy	$5.78 \times 10^{21}$	140000	700
Graphite epoxy	$5.78 \times 10^{21}$	140000	200
Quartz	$6.50 \times 10^{20}$	-----	25000

TABLE III. - DEFECT DENSITY POPULATION OF EPOTEK 301-2 GRAPHITE FIBER-EPOXY COUPONS WITH NO LEVELING COATING, ONE LEVELING COATING, AND TWO LEVELING COATINGS APPLIED, EXPOSED TO A FLUENCE OF  $2.3 \times 10^{21}$  ATOMS/CM<sup>2</sup>.

no coating	one coating	two coatings
210000	5700 4600	7600 defects/cm <sup>2</sup>

Table IV. - SOLAR SPECULAR REFLECTANCE VALUES OF ALUMINUM-COATED GRAPHITE EPOXY COUPONS BEFORE AND AFTER APPLICATION OF A SINGLE LEVELING COATING.

Aluminum on Pristine Epoxy			Aluminum on Leveling Coating		
Specular	Diffuse	Total	Specular	Diffuse	Total
0.808	0.085	0.893	0.859	0.020	0.879
0.830	0.059	0.889	0.862	0.013	0.875
0.806	0.081	0.887	0.861	0.015	0.876

Table V. - SOLAR SPECULAR REFLECTANCE VALUES OF ALUMINUM-COATED GRAPHITE EPOXY COUPONS BEFORE AND AFTER ASHING TO A FLUENCE OF  $2.0 \times 10^{21}$  ATOMS/CM<sup>2</sup>, ON SAMPLES WITH AND WITHOUT A SINGLE LEVELING COATING.

Aluminum on Pristine Epoxy					
Before ashing			After ashing		
Specular	Diffuse	Total	Specular	Diffuse	Total
0.837	0.060	0.897	0.763	0.094	0.857
0.840	0.054	0.894	0.752	0.090	0.842
0.827	0.064	0.891	-	-	-

Aluminum on Leveling Coating					
Before ashing			After ashing		
Specular	Diffuse	Total	Specular	Diffuse	Total
0.859	0.020	0.879	0.826	0.020	0.847
0.862	0.013	0.875	0.817	0.015	0.832
0.861	0.015	0.876	0.791	0.022	0.813

Table VI. - DIFFERENCE BETWEEN E-BEAM LINE-OF-SIGHT DEPOSITION AND SPUTTER DEPOSITION ON THE ATOMIC OXYGEN DEFECT DENSITY OF GRAPHITE EPOXY SUBSTRATES, AT AN ATOMIC OXYGEN FLUENCE OF  $8.32 \times 10^{20}$  ATOMS/CM<sup>2</sup>.

Graphite epoxy	260000 defects/cm <sup>2</sup>
Graphite epoxy + Al (e-beam)	22000 defects/cm <sup>2</sup>
Graphite epoxy + Au (sputter deposition)	15000 defects/cm <sup>2</sup>
graphite epoxy + leveling coat + Au	6000 defects/cm <sup>2</sup>

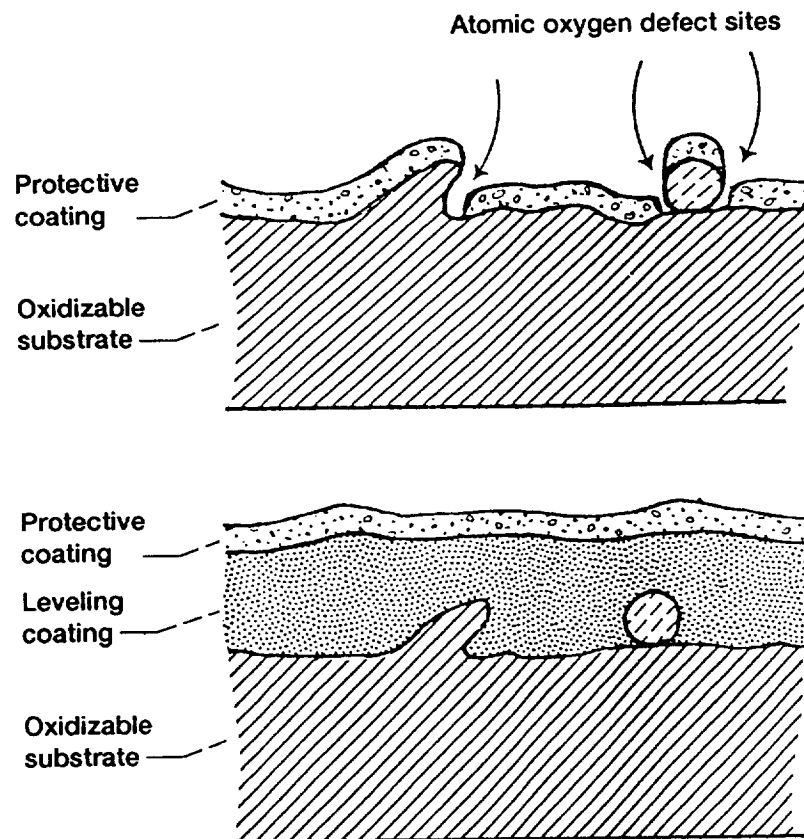
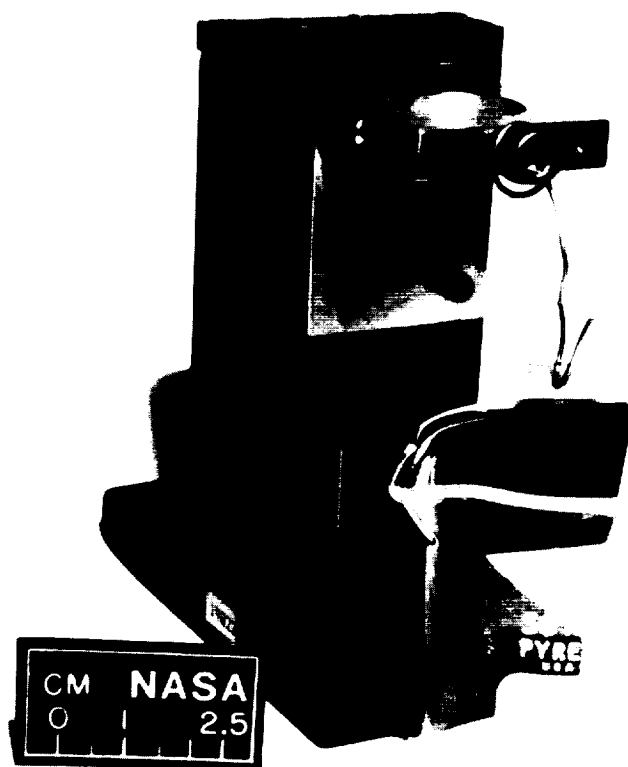


Figure 1.—Schematic diagram showing the role of a leveling coating in reducing atomic oxygen defect density.



ORIGINAL PAGE  
BLACK AND WHITE PHOTOGRAPH

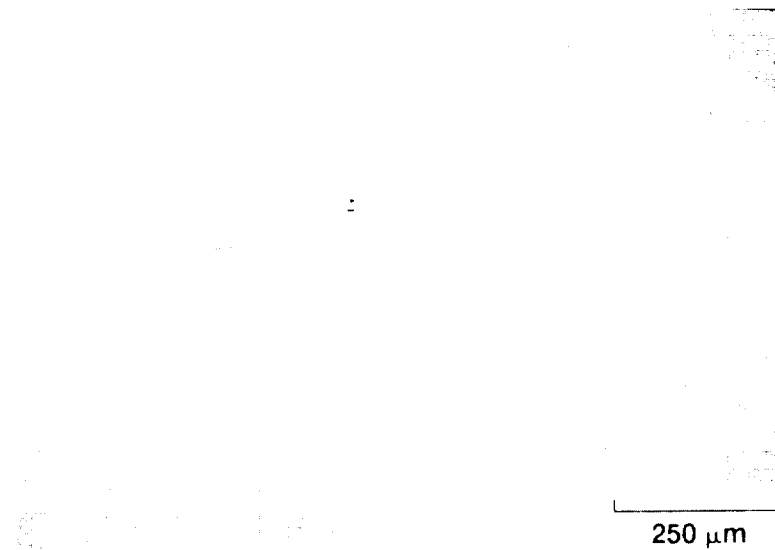


**Figure 2. Photograph of the dipping apparatus, showing a graphite epoxy composite coupon installed.**

ORIGINAL PAGE  
BLACK AND WHITE PHOTOGRAPH



(a) With no leveling coating applied.



(b) With a leveling coating applied.

**Figure 3. Scanning electron micrographs of  $\text{SiO}_2$  coated graphite epoxy composite coupons after exposure to atomic oxygen at a fluence of  $1.75 \times 10^{21}$  atoms  $\text{cm}^2$ .**

# Multi-axis Transient Vibration Testing of Space Objects — Test Philosophy, Test Facility and Control Strategy

Dr. Georg Lachenmayr  
Industrieanlagen-Betriebsgesellschaft mbH — Abt. TFM  
Einsteinstraße 20  
W-8012 Ottobrunn

## Abstract

IABG is using various servohydraulic test facilities since many years for the reproduction of service loads and environmental loads on all kinds of test objects. Since more than 15 years a multi-axis vibration test facility is under service, originally designed for earthquake simulation but in the meanwhile upgraded to the demands of space testing. First tests with the DFS/STM showed good reproduction accuracy and demonstrated the feasibility of transient vibration testing of space objects on a multi-axis hydraulic shaker. A novel approach to structural qualification is possible by using this test philosophy. It will be outlined and its obvious advantages over the state-of-the-art single-axis test will be demonstrated by example results. The new test technique has some special requirements to the test facility exceeding those of earthquake testing. Most important is the high reproduction accuracy demanding for a sophisticated control system. The state-of-the-art approach of analog closed-loop control circuits for each actuator combined with a static decoupling network and an off-line iterative waveform control is not able to meet all the demands. Therefore the future over-all control system is implemented as hierarchical full digital closed-loop system on a highly parallel transputer network. The innermost layer is the digital actuator controller, the second one is the MDOF-control of the table movement. The outermost layer would be the off-line iterative waveform control, which is dedicated only to deal with the interaction of test table and test object or non-linear effects. The outline of the system will be presented.

## 1 Introduction

Since the very beginning of structural testing the test engineers had the problem how to reproduce the real vibration environment, which very often is multi-axial. Due to the limitations of the available test hardware in most cases only a simplification to a single-axis test was possible. In the early 70's test laboratories in the whole world have started to develop methods and test facilities for the reproduction of multi-axial vibrations in structures. The first step was the simulation of random loads due to road roughness in automobile structures, see e.g. (ref. 1), afterwards it was achieved to simulate seismic loads due to earthquakes. The complexity of those test facilities reflects the technical problems associated with such tests. The now available multi-axis vibration test facilities can be divided into three groups:

1. **Multi-axis vibration tables:** Their purpose is the reproduction of seismic loads and similar transient events in 2-6 DOF<sup>1</sup> to all kinds of industrial components, as e.g. high-voltage switch gears, transformers or large control valves, see (ref. 2, 3, 4).
2. **Dynamic multi-actuator simulators:** They allow the reproduction of service loads in vehicle structures due to road roughness and maneuvers; the forces are usually introduced directly to the wheel suspension, see (ref. 5, 6, 7, 8, 9, 10). These test facilities have become an essential tool for the development and qualification of automobile structures.
3. **Dynamic roller test facilities:** On these facilities complete road or rail vehicles can be tested running on their wheels on the rollers which are moved due to the roughness profiles of road or rail, see (ref. 11, 12, 13).

---

<sup>1</sup> (mechanical) degree of freedom.

From these three types of multi-axis vibration test facilities a lot of installations exists all over the world. This paper *exclusively deals with the first group, the multi-axis vibration tables*, driven by electro-hydraulic servo actuators<sup>2</sup>. Their first application certainly was earthquake testing; the most demanding one will be the testing of complete satellites in near future.

The availability of appropriate test facilities is one aspect of the multi-axis transient testing — it will be discussed more in detail in section 3. At least of the same importance is the derivation of the test signals and the test philosophy standing behind; this will be the topic of section 2. Some example results from tests will be shown in section 4.

## 2 Multi-axis Transient Test Philosophy

The external loading to which structures are exposed in their environment is *nearly always multi-axial*. Nevertheless most of structural testing is done in single-axis tests up to now due to the less testing effort. In this section the problems of this approach will be reviewed and discussed what benefits are available with the multi-axis transient test. Afterwards the steps necessary to prepare a multi-axis transient test will be discussed, especially the process needed for the derivation of test transients.

### 2.1 Problems of Single-axis Testing

The single-axis vibration test on the electrodynamic shaker is state-of-the-art for the mechanical qualification of components and structures of all kind. The signals used are *constant or swept sine*, *random* (shaped to a given PSD<sup>3</sup>) *shock* (synthetic) or *time histories* in a frequency range from about 5 – 10 Hz up to the kHz-range. Single axis tests are also often performed with hydraulic shakers, especially for larger test items — the frequency range is from  $\approx 0$  up to about 50 Hz<sup>4</sup>.

Most of the test specifications and applicable standards can be covered by that performance data; indeed the standards seem to reflect more the limits of the test facilities than the requirements of the environment to be reproduced. With respect to the reliability of the qualification test and the relevance of the whole procedure of single-axis testing one has to be aware of the following problems:

- single-axis excitation is a *strong simplification* of the real environment, as all except one components of the external loading vectors are neglected,
- the *superposition* of local responses due to several single-axis tests in different directions may be *not valid* due to the neglected phase relations; this is especially true in the case of non-linear structural dynamics,
- the neglect of *small DOFs* of the excitation (e.g. the rotational DOFs) can change the *local responses* drastically, especially in complex structures,
- on the other hand electrodynamic shakers normally produce reasonable *crosstalk*, which is *not controllable* due to their construction; on a multi-axis test facility these components are under control,
- *quasistatic components* (0 – 5 Hz) cannot be reproduced on an electrodynamic shaker due to its stroke limitation; especially for non-linear dynamics and in large structures the quasi-static loads are essential for realistic test results, as they determine e.g. pre-stressing and working points,
- the replacement of real (transient) loading by sine, random or shock is at least *dubious*, as this excites the structural modes in quite a different way as the real environment,
- therefore usually complicated *notching procedures* are necessary in order to avoid overtesting of critical parts; this automatically implies undertesting of the rest of the structure.

This list of problems underlines that the single-axis vibration test needs careful adaptation to the special circumstances, which normally is a drastic simplification. This procedure may certainly be justified and appropriate in the case of

<sup>2</sup>Due to the limited stroke and other design problem it is difficult to build up multi-axis test facilities with electro-dynamic actuators, see e.g. (ref. 14, 15, 16).

<sup>3</sup>Power spectral density.

<sup>4</sup>With small hydraulic actuators or special equipment frequencies in the range of 100-300 Hz are possible.

*small components* which must work under quite different conditions (e.g. small electric parts); then also the test philosophy of *enveloping spectra* might be a good choice. But in order to cover the uncertainty of the simplification process usually a reasonable 'safety factor' must be chosen; this implies over-dimensioned design.

## 2.2 Advantages of Multi-axis Testing

The multi-axis vibration and transient testing technique has been developed due to the demand of the reproduction of service loads as exact as possible for a more reliable qualification. The reasons for it are :

- the excitation at the *interface*, the interface accelerations, between the test object (component, device, satellite) and its surrounding structure (vehicle, building, launcher) can be reproduced *completely* and in all DOFs *simultaneously* during test,
- the test signals are equivalent to *real loading functions* in amplitude, phase, and frequency contents,
- therefore all relevant structural modes are excited similar to reality and *all* parts of structure are loaded correctly,
- *quasistatic components* (0 – 5 Hz) can be simulated due to the much larger stroke of electro-hydraulic servo actuators,
- *no* manipulations during test like 'Notching' are necessary; more precisely: they are not allowed as the test signals represent the real loading, the test object has to withstand,
- the results of identification tests with multi-axis excitation yield *effective, dynamic characteristics* on the level of the real loading; this is a valuable feedback for the verification or updating of the computer models.

The above listed advantages of the multi-axis testing gain more importance, if the structures under consideration become large and more complex. This is especially the case with lightweight constructions; they are very sensitive to overtesting. The accurate reproduction of the real stresses on the other hand causes a reasonable effort both for the test facility and for the definition of the test signal.

## 2.3 Derivation of Test Transients

The important prerequisite for multi-axis testing is a thorough knowledge of the service loads the test item has to endure. Normally only a measurement campaign under real service conditions is able to acquire this knowledge. On this basis there exist three possibilities to derive the input for a multi-axis test:

1. Direct measurement and reproduction of the interface accelerations,
2. Specification of synthetic signals based on engineering knowledge, specifications, standards or similar measurements,
3. Computation of the interface accelerations from the external loading functions by 'coupled analysis'.

The first approach — direct reproduction of measured signals — certainly is the easiest way to define the test input; it is e.g. state-of-the-art for testing against seismic loads. The only thing what is to be done is some pre-processing (filtering, resampling) in order to adapt the signal to the test facility.

The second way to define the test input uses specifications for the different DOFs from which synthetic transient or random-like time histories are generated; also 2-DOF-swept sine or sine-beat is used. This approach is applied often in earthquake and transportation testing.

The third approach seems to be more complicated, as it requires the measurement of the *external*. This can be not so easy in reality. But it has the great advantage, that the characteristics of the individual combination of test object and structure during the service measurement are eliminated. Therefore the external loads obtained are applicable also to new constructions. They can be used in the design process and very early for the test of engineering models. The interface accelerations are calculated with a coupled model of the test object in its surrounding structure under the external excitation, see Figure 1. The individual characteristics of a new test object are reflected in its mathematical submodel.

Summarizing the requirements for this procedure are:

1. representative measurements of external loads under service,
2. computer model of the test object,
3. computer model of the surrounding structure, and
4. new test philosophy.

The first three items are realisable quite straightforward in aerospace applications and in the automotive industry; a lot of measurement work is done there as well as computations with sophisticated models. The most demanding step perhaps is the definition of a *New Test Philosophy*.

As the transient multi-axis vibration test reproduces the real service loads quite well the test philosophy must be changed in comparison to the single-axis test:

1. selection of relevant loadcases (transients, external events) out of the service measurements which are the design drivers,
2. no enveloping spectra and similar coarse specifications as each transient has its individual properties,
3. definition of a new 'Safety Factor', which can be smaller as it has to cover only the scattering of material properties a.s.o. and not the problems of the test procedure,
4. finally randomisation of relevant properties of the transients can be used in order to include the influence of parameter errors in the mathematical models or even the scattering of the external loading events.

The process for the last step is shown in Figure 2 and called 'mutation'. The original transient (which is the output of a coupled analysis, see Figure 1) is analysed with respect to its relevant components and is represented by some parametric approximation. Those parts which could change in amplitude, phase and frequency due e.g. model errors are marked to the mutation process; others which are well-known shall not be modified. The variation process, the 'mutation' generates a series of new transients similar to the original one but varied a little. So a statistical approach to the scattering of the model parameters is implemented. The prediction of local responses based on calculated or measured transfer functions (from the interface to relevant local responses) can be employed in order to reduce testing time.

This approach has been defined for testing large space structure (e.g. ARIANE 4/5 satellites) and is the very first step into this direction. IABG and DASA/ERNO (Bremen) have developed a software package for the 'mutation' process of Figure 2. In the very next future we will perform experiments with a test dummy structure for verification of the procedures<sup>5</sup>.

### 3 Test Facility for Multi-axis Transient Testing

In comparison with a single-axis shaker a servo-hydraulic multi-axis vibration test facility is a high complex dynamic system. A detailed presentation of how to design it certainly would be beyond the scope of this paper. Several subsystems are state-of-the-art. Therefore in this section first the existing test facility at IABG will be presented. Afterwards those subsystems will be discussed in more detail, which are critical with respect to the over-all performance, especially if test with space-objects are envisaged.

#### 3.1 The Multi-axis Vibrator HYMAS at IABG

IABG has built the first version of the HYMAS<sup>6</sup> test facility 1975, see (ref. 2); it was the first such facility in Europe. The configuration of the today existing facility which is shown in Figure 3 has been established during the last 5 years. IABG has performed over 650 qualification tests with both versions.

The table of the test facility is a welded steel construction with a mass of 4348 kg and the lowest structural resonance above 100 Hz. The outer dimensions of the table are 4.1 m × 3.2 m and the fixation area is 2.5 m × 2.0 m. The vertical actuators (z-direction) have a stroke of ±50 mm and a nominal force of 100 kN. In the horizontal plane three

<sup>5</sup> A detailed presentation of this new technique, would be beyond the scope of this paper and is devoted to another publication to follow; the method and software have been developed in the course of a study financed by DARA, the German Space Agency.

<sup>6</sup> HYdraulic Multi-Axis Shaker.

actuators with  $\pm 125$  mm stroke are attached, one in the x-direction with 250 kN force and in the y-direction two with 100 kN. All actuators are connected to the table and to the foundation by ball joints with PTFE coating. The whole facility is mounted on a seismic foundation with about 500 tons and a resonance at about 1 Hz. With the empty table vertical accelerations up to  $80 \text{ m/s}^2$  and up to  $40 \text{ m/s}^2$  in the horizontal directions can be reproduced depending on the frequency contents of the signal. The more mass the test object has, the lower the accelerations are, which can be applied to it; IABG has already tested objects with about 10 tons, the design payload is 4 tons. This test facility is presented in this paper as an example and had been used for obtaining the test results in section 4.

### 3.2 Mechanical and Hydraulic Equipment

With respect to the over-all performance of a multi-axis vibration test facility the following effects must be considered:

- **Dynamics of the table structure:** Usually the control concept to be discussed later assumes the table *rigid*, what means that the table has no eigen mode within the test frequency range. If this is not valid the modes of the table could be compensated by the design of the control system. The better solution certainly is to design the table structure properly.
- **Backlash and friction of the joints:** Both effects are strong non-linearities, which cannot be linearized (step functions). They cause non-linear dynamic behaviour of the control system e.g. limit cycles and instability. Therefore the choice of the controller parameters is restricted to a — often very small — stable region within the parameter space. Especially the over-all gain is limited strongly. The ideal joint would have no backlash, no friction and high stiffness; in reality a compromise must be found, which is quite difficult as all available variants — coated ball bearings, roller bearing and hydrostatic bearings — have their individual disadvantages. The higher the upper end of test frequency range is, the more this problem causes difficulties.
- **Friction of the actuators:** In principle here the same arguments as before are valid; but the today available actuators with hydrostatic bearings solve the problem sufficiently. For lower frequencies also actuators with sliding sealing (reduced friction) can be considered.
- **Signal distortions caused by the servo valves:** Due to the hydrodynamic processes in the different stages of the servo-valve and in the actuator the relation between servo valve input and the actuator acceleration is non-linear; this causes the well-known signal distortions as random-like noise and harmonics. This is especially true for three-stage servo valves with nozzle-flapper pilot stage, which often are used. Only careful design of the servo valve itself and optimization of the actuator control circuits can minimize this problem.

### 3.3 Control System

The automatic control system of a multi-axis test facility has several levels, see Figure 5, which are nested:

1. controllers for spools of the servo valves,
2. actuator controller,
3. the table controller,
4. off-line iteration<sup>7</sup>.

The first three layers establish the automatic control system, whereas the off-line iteration is a software to prepare the drive signals, see section 3.4.

#### 3.3.1 Spool controller

Three-stage servo valves and modern two-stage servo valves employ an inductive sensor to measure and a special controller to control the movement of the spool. These controllers have significant influence to the dynamics and linearity of the servo valve. Therefore they must be adapted very well to the individual valve on a special test

---

<sup>7</sup>This technique is in the American literature often called 'Digital Control' or 'Closed-Loop Control', which can be misunderstood, because the 'control' is done off-line and not in real-time.

facility of the valve manufacturer. Only small modifications of this 'optimal' adjustment are allowed in the application for stable operation. The control law itself is quite simple; often PD-control is used. Usually these controllers are implemented as analog circuits often integrated together with the power amplifier in the servo valve housing. So they can be considered as part of the servo valve.

### 3.3.2 Actuator controller

The next layer of the control system is the actuator controller, which has to ensure that the actuator displacement and acceleration follow the specified signals. The choice of the structure of this controller and the setting of the related parameters offers a lot of possibilities to influence the over-all dynamics of the test facility. In order to achieve the desired accuracy and bandwidth necessary for testing space objects the following properties should be implemented:

1. feed-back and/or feed-forward of a subvector of the state vector of the actuator rod, usually displacement velocity and acceleration; if not all these signals are available from the measurement system in the required accuracy they can be obtained from an observer,
2. compensation of poles of the actuator e.g. the oil-spring/mass resonance and those due to the elasticity of the actuator housing or the joints,
3. compensation of poles of the payload, especially if they are weakly damped.

This concept involves only linear control techniques, as for them a lot of powerful design tools are available. Experimental investigations and numerical simulations, see (ref. 17, chapter 3), have shown that for usual configurations of multi-axis test facilities these linear control concepts provide a sufficient performance if they are applied correctly; this is especially true, if the relevant parameters are well-adapted to the actual test object.

Especially the last item can be a very critical task, as this cannot be done for each actuator alone due to the cross-coupling of all actuators, and due to the sensitivity to parameter changes.

Certainly non-linear control techniques as gain scheduling or model following offer some possibilities to achieve better performance. But we think that the application of these much more complicated techniques should be reserved for future improvements.

### 3.3.3 Table controller

The most important — and most complicated — of the control system of a hydraulic multi-axis vibration table is the table controller. It is a multiple-input-multiple-output system, which has to perform the following tasks:

1. transformation of the command vector for the six rigid body degrees-of-freedom of the table to the individual command input for each of the  $n_a$  actuators. In the hypothetical case of an ideal actuator controller (which would ensure a very accurate reproduction of each actuator input) this transformation will be only a linear(ized) kinematic transformation, which is quite simple for  $n_a = 6$ . In the case of  $n_a > 6$  this transformation is not unique and therefore additional assumptions (e.g. "rigid table") or balancing techniques are necessary (force balancing),
2. compensation of the cross-coupling between the actuator due to the kinematics of the actuator arrangement,
3. compensation of the typical multi-axis dynamic effects known as "overturning moments" and "off-center load moments", which are due to the fact that the line of action of the actuators does not go through the over-all center of gravity of test facility and test object.

Our investigations, see (ref. 17, chapter 3), have shown, that here also linear approaches lead to a quite good performance. The kinematic transformation implements only linearized kinematics due to the very small possible angular displacement of the table. In the usual case of more than 6 actuators one has to use pseudo-inverse techniques, see e.g. (ref. 18) to get the transformation matrix. In order to compensate the dynamic effects (item 3) we have found out a reduced inverse model of the test facility to be sufficient, which includes only the linear dynamics of the rigid (loaded) table excited by the actuator forces. From this model and the desired table state the required force for each of the actuators can be calculated; they can be used for an additional feed-forward or feed-back loop which is superimposed to the position/acceleration control of the table.

Essential for good performance here is the adaptation of the control parameters to the individual test object.

The complexity of the over-all system to our opinion does not allow to merge the actuator controller and the table controller into one MIMO-control system due to the difficulty how to design such a system.



### 3.3.4 Implementation as digital system

In both preceeding sections parts of the control systems had to be adapted to the special test circumstances. With a control system implemented in analog electronic this adaptation is a very complicated task. With respect to the quality requirement applicable for space tests it is also a very critical task. Therefore best would be to implement both the actuator controller and the table controller as digital control system calculating the servo valve input in real-time. For a test frequency range of 100 Hz at least a sampling frequency of 2 kHz is necessary, which implies that all data acquisition, computation and data output within the control loops must be done within a frame time of 0.5 ms.

The recent development of computer hardware allows now the implementation of such a real-time system with acceptable costs. In principle several hardware approaches are possible: standard multi-processor systems (e.g. based on VME-bus), signal processors or transputer networks.

After some preliminary investigations IABG decided to implement the digital control system<sup>8</sup> on a transputer network containing 11 T 800 transputers (ref. 19) (for computational work) and 6 T 222 transputers (connected to D/A- and A/D-converters). The host system is a personal computer (industry standard) on which the user interface is implemented. The system has been built up and is now under test; finally it will replace all analog parts of the existing control system except the signal amplifiers and filters.

The control software includes all elements discussed in sections 3.3.2 and 3.3.3 and has been written in OCCAM 2 (ref. 20). The sampling rate is 2 kHz. The communication structure is shown in Figure 6. This structure has been chosen base on a detailed analysis of the times needed for computation and communication of the different processes working in parallel. Only a good balancing of both leads to acceptable performance.

## 3.4 Off-Line Iteration

The *off-line iteration* is a software which builds up some sort of *off-line 'outer control loop'*, see Figure 5. The approach is to modify the input signals to the MIMO-System by pre-filtering with the inverse dynamics of the loaded test facility and to minimize the errors between specified and measured signal iteratively.

Several software systems for off-line iteration are today available on the market, e.g. (ref. 21, 22, 23, 24). They all are based more or less on theoretical work done in USA (ref. 25, 26). Only few extensions of this primary approach have been discussed, see e.g. (ref. 27). Up to now a thorough theoretical investigation of the procedure and a proof of its convergence are not available. As an Example IABG's software system ISA, see (ref. 24), will be used; it consists of two independent steps:

1. Identification of the transfer function matrix  $H$  by means of dividing the cross power spectral densities between the components of the input vector (exciting signal) and the components of the output vector (measured signals) by the components of the auto power spectral densities of the input signals, see Figure 7; this yields under some additional assumptions a *linear approximation* in the frequency domain of the non-linear dynamics of the loaded test facility.
2. Iteration for a transient signals by using *Newton's* method with the transfer function matrix from the identification step as approximation for the Jacobian matrix of the iteration function at a set of discrete frequency points. This means that the Fourier transform of the error between the measured and the desired (transient) output vector is multiplied by the inverse  $I := H^{-1}$  of the transfer function matrix, the so called impedance function matrix, and added — multiplied by a factor  $0 < \alpha \leq 1$  — to the last iterated input vector, see Figure 8. This is done for all frequency points to get a Fourier transform of a new input vector. The corresponding input vector in the time domain yields a smaller error between the system response and the desired output — convergence presumed. Depending on the desired accuracy, the value of  $\alpha$  and test object dynamics 2 ... 10 iteration steps are necessary.

---

<sup>8</sup>This is one part of a current study financed by DARA, the German Space Agency.

This procedure is state-of-the-art in controlling complex test facilities and has turned out to be quite successful under certain circumstances. Although an elaborated automatic on-line control system (actuator controller and MIMO-system) will be able to minimise the differences between the desired and reproduced test signals, an off-line adaptation of the test signals to the specific characteristics of the test object (mass, moment of inertia, height of center of gravity, stiffness etc.) will be necessary — at least as supporting tool. This is especially true if the dynamic behaviour of the test object has an essential influence on the overall dynamic of the test arrangement as e.g. in the case of structural resonances or non-linear dynamic behaviour. Any on-line method, e.g. model following has to cope with exactly the same problems — and in addition with the stability problem.

In any case, the *main advantage* of the off-line iteration procedure is, that between the individual iteration steps the operator can have a look at intermediate results, judge about the convergence and the loading of the test object — and decide to go on or to modify the procedure in a suitable sense. This would not be possible in any on-line procedure; here all control is done by an automatic system and no operator interaction is possible to avoid overload of the test object or instability.

During a recent study with the DFS/STM (ref. 28) it was demonstrated that multi-axis transients can be reproduced with almost the accuracy required for the qualification of space objects by a multi-axis hydraulic vibration test facility using ISA. But some problems still exist and have to be solved by improvements of the iteration procedure. These are ensuring the convergence from one side (from below), reduction of iteration steps (acceleration of convergence) and optimization of preprocessing steps considering the transfer and impedance function.

## 4 Some Test Results

Figure 9a) shows the time history of a 6-DOF test transient derived from ARIANE-4 flight measurements. The physical event behind it is the unsymmetric burnout of the fluid boosters (PAL-D), which is a design load case for AR-4 payloads. Similar transients are caused during launch by burn-out of main motor, gusts, separation of stages and blast-off of fairings. The transient in Figure 9a) has been derived by the procedure from Figure 1 for the structural model of the german communication satellite DFS-Kopernikus. The DFS/STM was investigated by IABG during a study financed by BMFT<sup>9</sup>, see (ref. 28).

The transient LC2 has quite strong excitation in the first 2 DOF, which represent the horizontal translations, whereas in the other components only relatively small signals appear. This causes that the cross-talk of the strong DOF to the smaller ones is nearly in the same order of magnitude as the specified signal. This is a problem for the reproduction and can only be solved with the ISA-procedure in section 3.4. The result of the 9<sup>th</sup> Iteration is shown in Figure 9b). The coincidence is quite good. So it is demonstrated, that even difficult transient signals can be reproduced with a multi-axis vibration test facility. The results of measurements of local responses (e.g. antenna dummy) have also shown clearly, that all considerations discussed in section 2 are valid.

## References

- [1] C. J. Dodds und J. D. Robson. Road Simulation. *Journal of Automotive Engineering*, 3(4) 17–19, 1972.
- [2] W. Mercklinghaus et al. Computer Controlled Hydraulic Earthquake Simulation for Testing H.V. Switch Gear. *Siemens Review*, XLIV(9), 1977.
- [3] Multi-Axis Vibration Test. Technical Data Sheet IABG.
- [4] Vibration Test Facility Juelich — MAVIS 1. Technical Data Sheet DLR — Institut für Aeroelasticity.
- [5] C. J. Dodds. The Laboratory Simulation of Vehicle Service Stress. *ASME Journal of Engineering for Industry*, 391–398, 1974.
- [6] D. D. Styles und C. J. Dodds. Simulation of Random Environments for Structural Dynamics Testing. *Experimental Mechanics*, 16(11) 416–424, 1976.
- [7] B. W. Cryer, P. E. Nawrocki, und R. A. Lund. *A Road Simulation System for Heavy Duty Vehicles*. SAE Technical Paper 760361, Feb. 23 1976.

---

<sup>9</sup> German ministry for research and technology.

- [8] C. J. Dodds. Environmental Testing Under Random Loading. In: *Symposium on Service Fatigue Loads Monitoring, Simulation and Analysis*, MTS Systems Corporation, November 1977.
- [9] K.-H. Knoche und K.-P. Weibel. Mehrkomponenten-Karosserieprüfstand zur Simulation von Betriebsbeanspruchungen unter Berücksichtigung freier Massenkräfte. *ATZ Automobiltechnische Zeitschrift*, 82(6) 329–334, 1980.
- [10] G. Jacoby. *Mechanical Testing in the Automobile Industry*. Technical Report, Carl Schenck AG, Darmstadt, 1985.
- [11] W. Raasch. Rollprüfstand zur Verifizierung der Theorien. *ZEV-Glasers-Annalen*, 106, 1982.
- [12] Roller Test Facility Munich — Dynamic Drive Simulator for Rail Vehicles. Technical Data Sheet IABG/DB.
- [13] Richard C. Stroud und Hamma George A. Multiexciter and Multiaxis Vibration Exciter Control Systems. *Shock and Vibration*, 22(4) 18–28, April 1988.
- [14] W. Douglas Everett und Thomas M. Helfrich. Triaxial Vibration System. *Shock and Vibration Bulletin*, 55, Part 2(6) 1–15, June 1985.
- [15] George A. Hamma und Richard. C. Stroud. Closed-Loop Digital Control of Multiaxis Vibration Testing. In: *Proceedings of the Institute of Environmental Sciences, 31st Annual Technical Meeting, Las Vegas*, 29.4. – 2.5 1985.
- [16] S.A. Foster und Ceng Miere. Electro-Dynamic Multishaker System. In: *Proc. 34th Ann. Techn. Meeting*, S. 224–227, Inst. of Environmental Sciences, 1988.
- [17] G. Lachenmayr. *Investigations on Upgraded Offline Iteration, Improvement of Actuator Control, Safety Switch-Off Valves and Experimental Investigations with Hydraulic Components — Final Report*. Technical Report B-TF 2887, IABG, 1992.
- [18] T. N. E. Greville. Some Applications of the Pseudoinverse of a Matrix. *SIAM Review*, 2(1) 15–22, January 1960.
- [19] *IMS T800 Transputer – Data Sheet*. Inmos, 1989.
- [20] C. A. R. Hoare, Hrsg. *Occam 2 Reference Manual*. Prentice-Hall, (UK), 1988.
- [21] Performance Specification for Multiexciter Vibration Control Systems. Data Sheet Synergistic Technology Incorporated, Santa Clara CA.
- [22] RPC Remote Parameter Control. Firmenbroschüre MTS.
- [23] ITFC Ein Computersystem für die Simulationstechnik. Firmenbroschüre Carl Schenck AG, Darmstadt.
- [24] Seiler. *Iterative Steuersignalanpassung (ISA) — Programmdokumentation*. Bericht B-TF-V 222, IABG, 1985.
- [25] D. K. Fisher. Theoretical and Practical Aspects of Multiple-Actuator Shaker Control. *Shock and Vibration Bulletin*, 43(3) 153–174, Sept. 1973.
- [26] D. K. Fisher und Posohn M. R. Digital Control System for a Multiple-Actuator Shaker. *Shock and Vibration Bulletin*, 47(3) 77–96, Sept. 1977.
- [27] Volker Tews. Iterative Drive-Signal Determination for Nonlinear and Deadtime Plants. In: *Intern. Conf. on Control*, IEEE, Oxford, April 1988.
- [28] G. Lachenmayr, W. Raasch, und W. Saad. Multi-Axis Vibration Simulation in Space Structures — Experiments with DFS/STM. In: *International Symposium on Environmental Testing for Space Programmes, Noordwijk (ESA SP-304)*, ESA/ESTEC, September 1990.

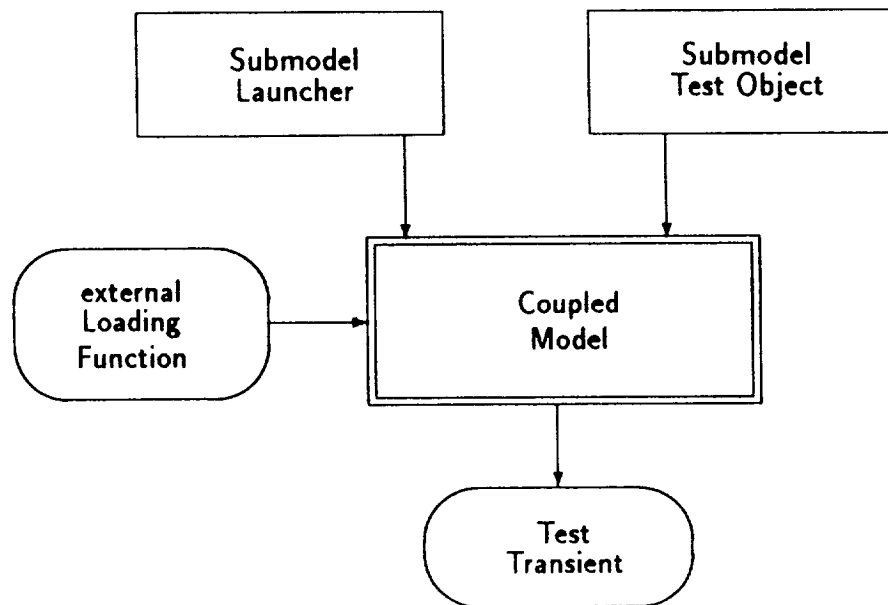


Figure 1: Derivation of test transients by 'coupled analysis'

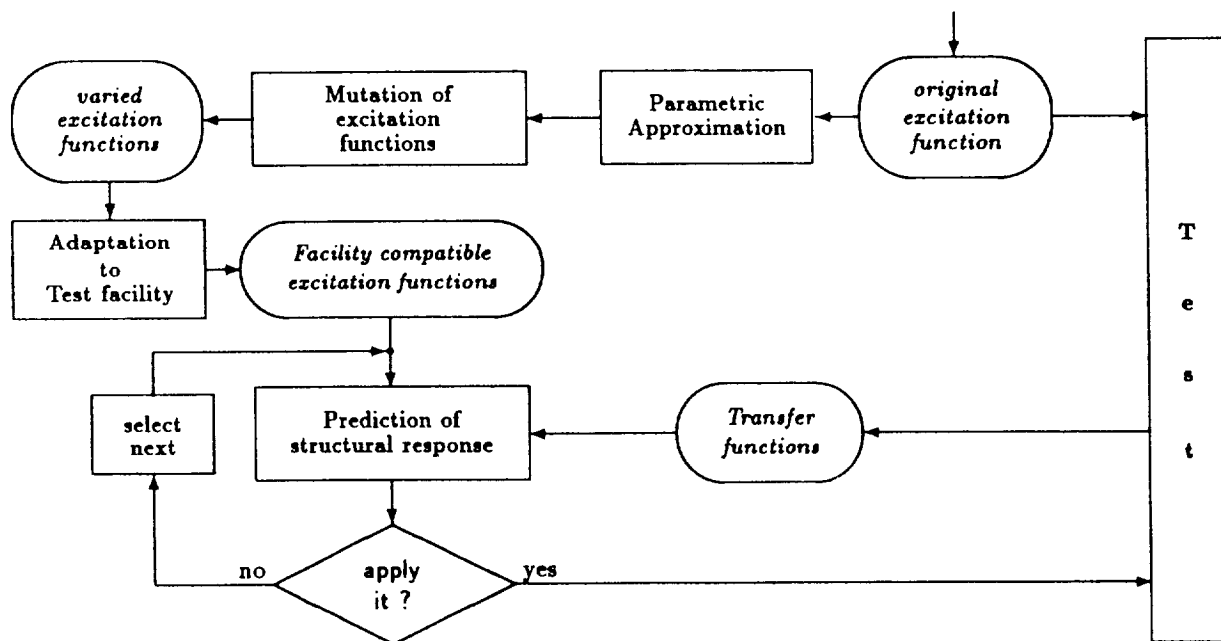


Figure 2: Randomization of test transients by mutation

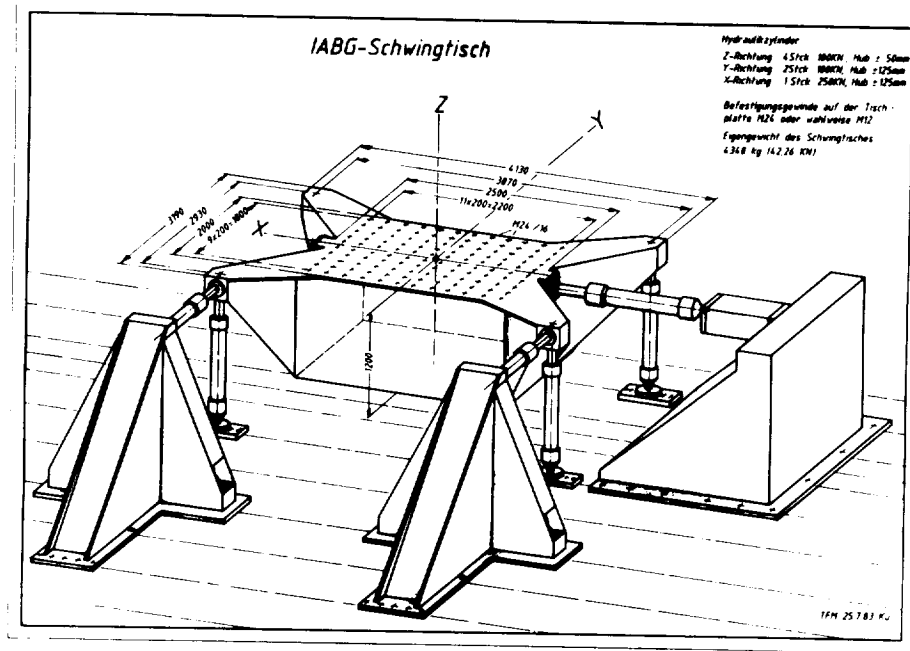


Figure 3: Schematic drawing of the IABG multi-axis test facility

ORIGINAL PAGE  
 BLACK AND WHITE PHOTOGRAPH



Figure 4: IABG multi-axis test facility with DFS/STM

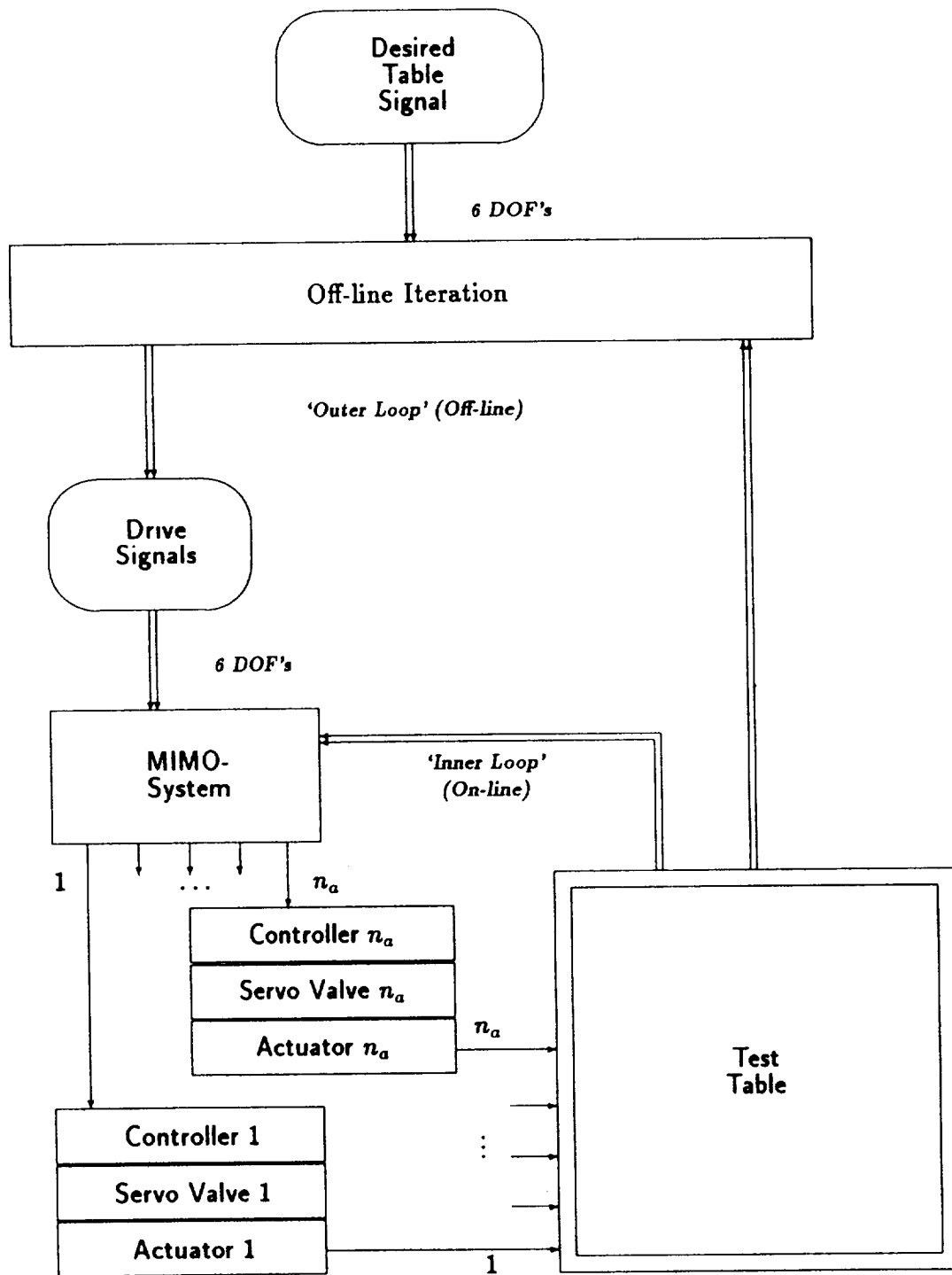


Figure 5: Block diagram of the Over-all Control system

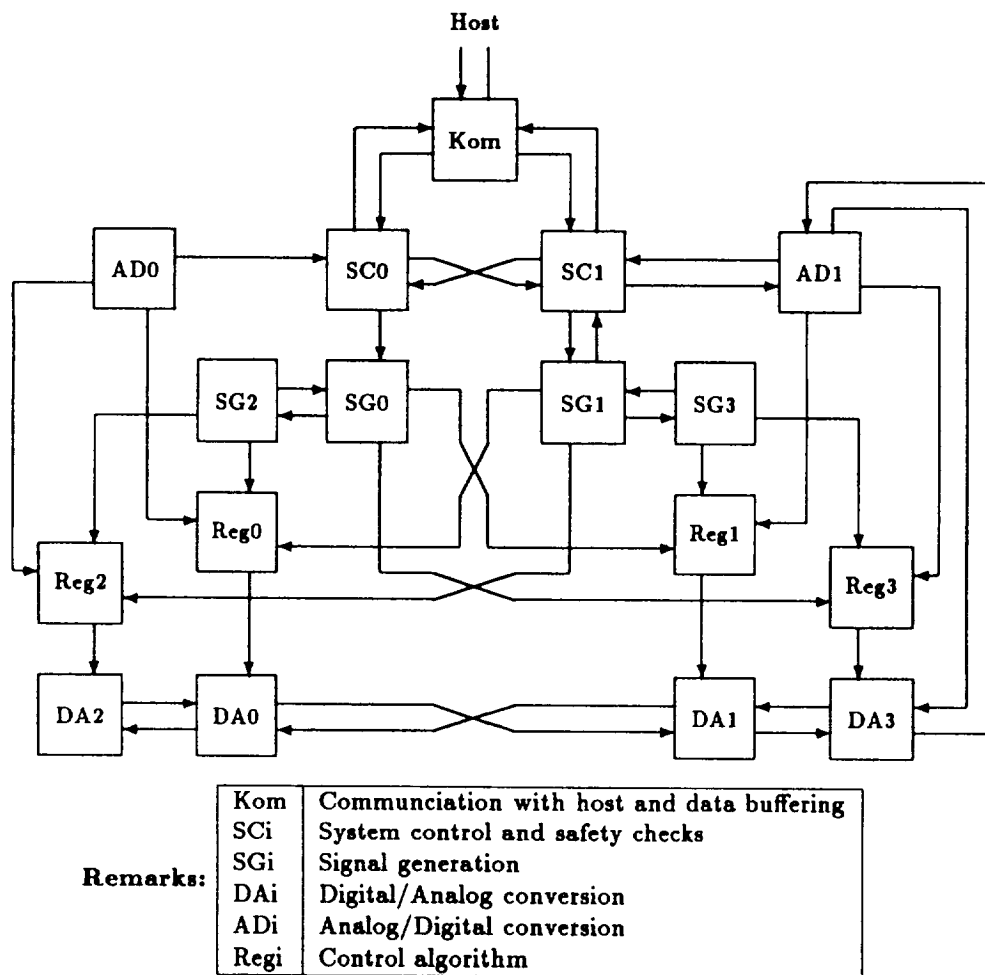
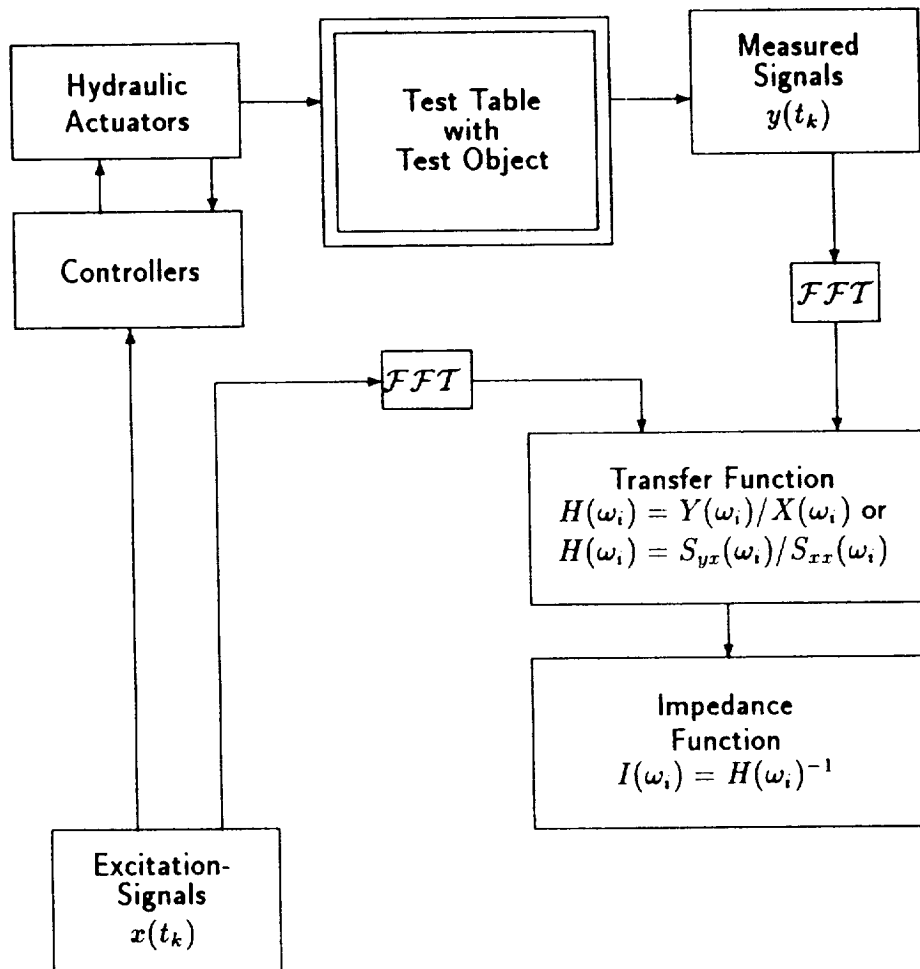


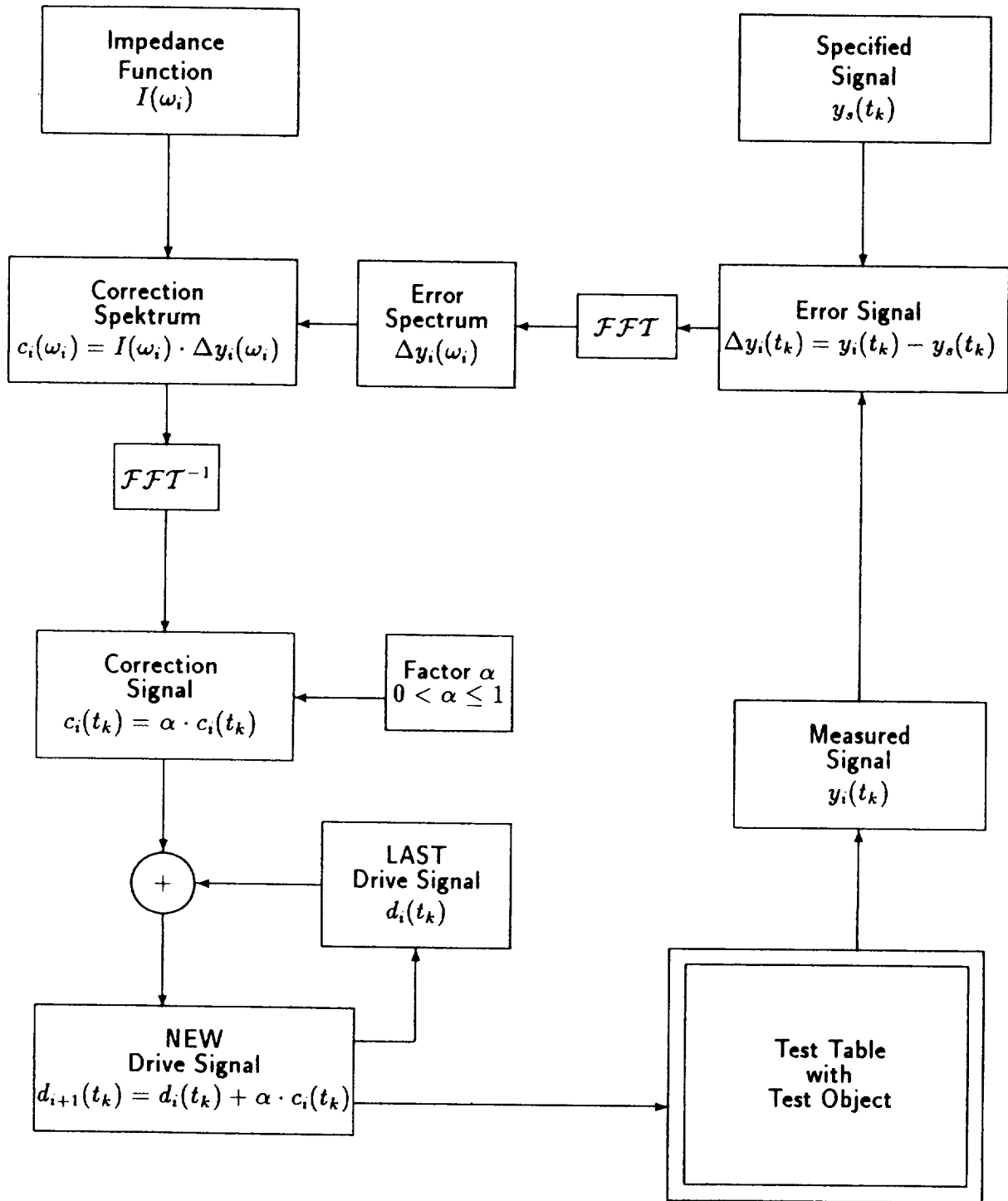
Figure 6: Communication structure of the transputer network used for the digital control system



<b>Remarks:</b>	$FFT$	Fast Fourier Transformation
	$Y(\omega)$	Fourier transform of $y(t_k)$
	$X(\omega)$	Fourier transform of $x(t_k)$
	$S_{yx}(\omega_i)$	cross spectral density
	$S_{xx}(\omega_i)$	power spectral density

Figure 7: Block diagram of the *Identification Step* of ISA





Remarks:  $FFT$  — Fast Fourier Transformation

Figure 8: Block diagram of the *Iteration Step* of ISA

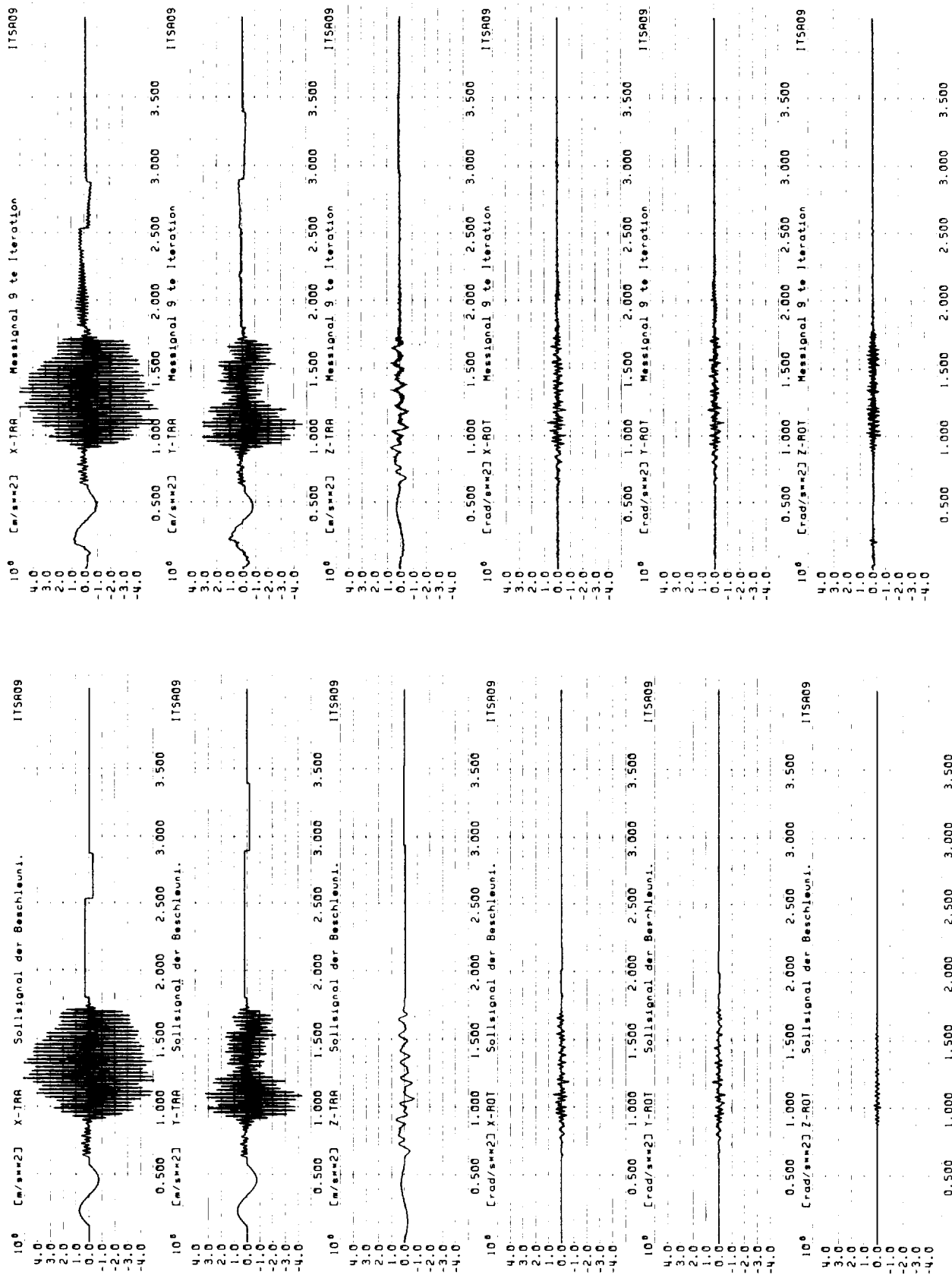


Figure 1: 6-DOF test transient LC2 of DFS/STM

VIBRATION AND ACOUSTIC TESTING OF TOPEX/POSEIDON SATELLITE<sup>1</sup>

Dave Boatman and Terry Scharton  
Jet Propulsion Laboratory  
California Institute of Technology

Donald Hershfeld  
NASA Goddard Space Flight Center

Paul Larkin  
Fairchild Space Company

ABSTRACT

The satellite was subjected to a 1.5G swept sine vibration test and a 146 dB overall level acoustic test, in accordance with Ariane launch vehicle requirements, at the NASA Goddard Space Flight Center. Extensive pretest analysis of the sine test was conducted to plan the input notching and to justify vibration testing the satellite only in the longitudinal axis. A unique measurement system was utilized to determine the six components of interface force between the shaker and the satellite in the sine vibration test. The satellite was heavily instrumented in both the sine vibration and acoustic test in order to insure that the launch loads were enveloped with appropriate margin and that satellite responses did not exceed the compatibilities of the structure and equipment. The test specification, objectives, instrumentation, and test results are described herein.

INTRODUCTION

TOPEX (Ocean TOPOgraphy EXperiment)/Poseidon is a collaborative mission between the United States and France. Its purpose is to obtain highly accurate measurements of global sea level to improve understanding of ocean circulation and its impact on the environment.

The satellite was developed by Fairchild Space Company and launched by an Ariane 42P rocket from Arianespace launch facilities at Kourou, French Guiana. The Jet Propulsion Laboratory has overall project management responsibility in addition to providing five payload sensors for the satellite.

---

<sup>1</sup>The work described in this paper was carried out at the Jet Propulsion Laboratory, California Institute of Technology, under a contract with the National Aeronautics and Space Administration.

The TOPEX/Poseidon flight satellite was subjected to sinusoidal vibration and acoustic noise as part of its system level qualification acceptance test program. The tests were conducted in the facilities of the Goddard Space Flight Center over the period of January 21 through February 5, 1992.

These sine and acoustics tests, run at protoflight levels, satisfy the respective JPL institutional requirements for a Class B mission as well as those of Arianespace - provider of the launch vehicle.

## **DESCRIPTION**

### **Sinusoidal Vibration**

The satellite, in its launch configuration, and with propellant tanks filled with water was subjected to a single, longitudinal axis, of swept sinusoidal vibration (Fig. 1). The inputs in the sine tests were notched to limit the responses at a number of critical positions to limits based primarily on structural capability. Three levels were performed in the sequence up to and including protoflight ( $1.5 g_{o-pk}$ ). The two preliminary levels were 0.25 g and 0.75g. For each sine level the frequency band was 5-100 Hz and the sweep rate was 4 octaves per minute going from the lower to the upper frequency only. The protoflight test provided a margin of 1.5 over previously measured payload/Ariane 4 interface flight levels.

Just prior to and again immediately following the sine vibration sequence the satellite was subjected to a very low level unnotched random vibration excitation. The purpose of these two runs was to provide a diagnostic comparison of pre- and post-sine satellite responses as a means of detecting any structural degradations. The applied levels were  $0.0002 g^2/Hz$  across the frequency band of 4-400 Hz which is an overall level of  $0.28g_{rms}$ .

### **Acoustics**

The satellite was in its launch configuration. Its LVA was mounted to the TOPEX/Galileo dolly through the vibration adapter ring. This entire assemblage was placed in the Goddard  $1100m^3$  reverberant acoustic chamber.

The acoustic 1/3 octave spectrum for this test was based on measurements taken during a recent flight of an Ariane-4. This spectrum is compared in Figure 2 with the original spectrum upon which TOPEX design was based, and with the data from the recent Ariane 4 flight. The protoflight test generally provided a 4 dB margin over the maximum expected flight levels.

The acoustics test was conducted in three incremental steps; -12dB, -6dB and finally, the full protoflight level. The two preliminary runs were with the PF acoustic levels reduced uniformly in each 1/3 octave band, i.e., each lowered 12dB or 6dB, respectively. Following each of these runs, all accelerometer data were analyzed; primarily to assess the potential for exceeding the random vibration input, at higher acoustic levels, to any assemblies above

that to which they had been qualified. The protoflight test duration was one minute.

## **OBJECTIVES**

### **Sine Vibration**

The stated objectives of the satellite system sine vibration test were:

- to verify that the flight satellite will withstand the low frequency, transient vibration environment associated with launch, and

- to verify workmanship of the fully assembled flight satellite.

A secondary "objective" of the system vibration test was to "qualify" those satellite integration elements and interconnections which cannot be dynamically tested at any lower level of assembly.

### **Acoustics**

The stated objectives of the satellite system acoustics test were:

- to verify that the flight satellite is able to withstand the launch vibroacoustic environment without physical or functional performance degradation,

- to verify workmanship of the fully assembled flight satellite, and

- to assess the adequacy of assembly random vibration criteria.

The secondary objective described above for the sine test also applies to acoustics

## **INSTRUMENTATION**

### **Sine Vibration**

For the sine vibration test the satellite was instrumented with 125 accelerometers in addition to 16 strain gages and four force washers on the solar array. The three primary control accelerometers were located on the fixture baseplate at the LVA interface.

A unique feature of this test setup was a force gage plate assembly which was installed between the C220 shaker and the vertical shaker head expander. These four gages allowed force in each orthogonal axis to be measured, and, from this, moments and torsion at the shaker head plane could also be derived. The need for these measurements came about as

a result of the project decision not to use a large existing JPL spacecraft longitudinal vibration fixture with lateral restraint system. Analysis had indicated (and was confirmed during this test) that the shaker manufacturer's published limits for armature lateral loading would be greatly exceeded unless the input to the test item was reduced at certain frequencies. The sine sweep input was also notched to limit the shaker lateral forces and moments to 1.5 times the manufacturer's limits.

## **Acoustics**

For the acoustics test, the satellite was instrumented with 108 accelerometers - the majority of which were common with the sine vibration locations. Several sine test accelerometers were not recorded for this acoustics test and a few new locations were added - primarily internal to the instrument module at inputs to the sensor electronics assemblies. No strain gages or force washers were recorded for the acoustics test.

## **RESULTS AND CONSTRAINTS**

### **Sine Vibration**

The initial very low level random and the 1/4g sine were performed with all 48 satellite response safety aborts set at their original 100% level. The principal objective of this was to obtain the data from a complete, unbroken sine input across the test frequency range of 5 to 100Hz.

For the intermediate (3/4g) level sine sweep, the 48 peak limit abort thresholds were set proportional to the full level limits (although not exactly 50%) and the first cut notching, scaled from the expected full level sine, was implemented. The intermediate level sine sweep had seven peak limit aborts. This necessitated the increase of abort limit levels and/or lowering of the limiter low pass filter settings on the affected locations from 200Hz to 100Hz. The input sine profile was not changed.

For the full, protoflight, level sine sweep, the 48 peak limit abort thresholds were set as previously described. These abort values were  $\approx 10\%$  above the desired limit levels to allow for overshoot, etc. All limit low pass filters were set at 100Hz. The sine profile for this run was modified slightly from the 3/4g level based on the data from that run. The profile is shown in Figure 3 along with the respective notch determining locations along the frequency band. The sine vibration input to the LVA satisfied an Arianespace request that it envelope 1.5 times the shock spectrum, divided by Q, of the predicted launch vehicle transient events. This is also shown in Figure 3. There were no peak limit aborts during the PF sine sweep.

The very low level random vibration was repeated immediately upon conclusion of the PF sine run for the purpose of comparing before and after sine response characteristics and assessing structural integrity. No significant changes were revealed.

## Acoustics

The revised, Ariane-4 acoustic noise spectrum was applied to the satellite in three steps up to and including full protoflight as previously described. A primary concern centered around predicted random vibration input levels to some assemblies that would exceed their qualification/acceptance test inputs at the frequencies where the new acoustic spec was increased - principally in the 100Hz to 250Hz range. This situation did, in fact, present itself based on the -12dB data for the input to the Global Positioning System receivers on the Instrument Module + Y access panel. Extrapolation of the -12dB data indicated that the PSD level at  $\approx 140\text{Hz}$  would reach  $0.8\text{g}^2/\text{Hz}$  at full level as compared to the assembly test level of  $0.2\text{g}^2/\text{Hz}$  at that frequency. Three additional accelerometers were added to the outside of this access panel before going to the -6dB level to confirm the reading and to determine whether or not the high response was the result of some localized effect.

The -6dB acoustic run data verified that the GPS receiver input reading was correct and not just a localized phenomenon. However, the increase in the vibration response was less than the 6dB increase in the acoustic level - actually closer to 4dB. Based on this result, anticipation of a similar increase at full level and consultation with the GPS cognizant engineers, it was decided to proceed with the full PF acoustic exposure without modification. A comparison of the responses at the GPS receiver and other electronic box locations on the spacecraft instrument module and bus with the  $0.2\text{g}^2/\text{Hz}$  random vibration test specification is shown in Figure 4.

The PF acoustic run (146dB overall) gave a reading of  $0.35\text{g}^2/\text{Hz}$  at the input to the GPS receivers. Again, this represented an increase of just over 4dB from the -6dB acoustic run. No other assembly level random vibration input levels were exceeded during this test. The only other area of minor concern was at the High Gain Antenna Subsystem mechanism. Even though the response level here was quite high ( $3\text{g}^2/\text{Hz}$  at 160Hz) it was nearly identical to that measured during its assembly random vibration qual. In the acoustics test, this mechanism response is believed to be predominantly driven by the HGAS dish motion, rather than the IM panel.

## SUMMARY AND CONCLUSIONS

The sine vibration and acoustics tests on the TOPEX/Poseidon flight satellite are considered to have been successfully accomplished. The formal, stated objectives of the sine test were met. The initial indications of an anomaly in an inertial reference unit were resolved.

The acoustics test was performed to the revised acoustics levels for Ariane-4 without the need to modify the spectrum. The generally lower than anticipated response throughout the satellite is at least partially attributable to its higher than assumed damping. This was initially observed during the sine vibration and resulted in some notching not having to be as deep as pre-test analysis predicted.

In conclusion, the TOPEX/Poseidon flight satellite is considered to have successfully met each of the principal objectives of both the sine vibration and the acoustics environmental tests and has therefore demonstrated, with margin, its ability to survive the Ariane-4 launch dynamics environments.



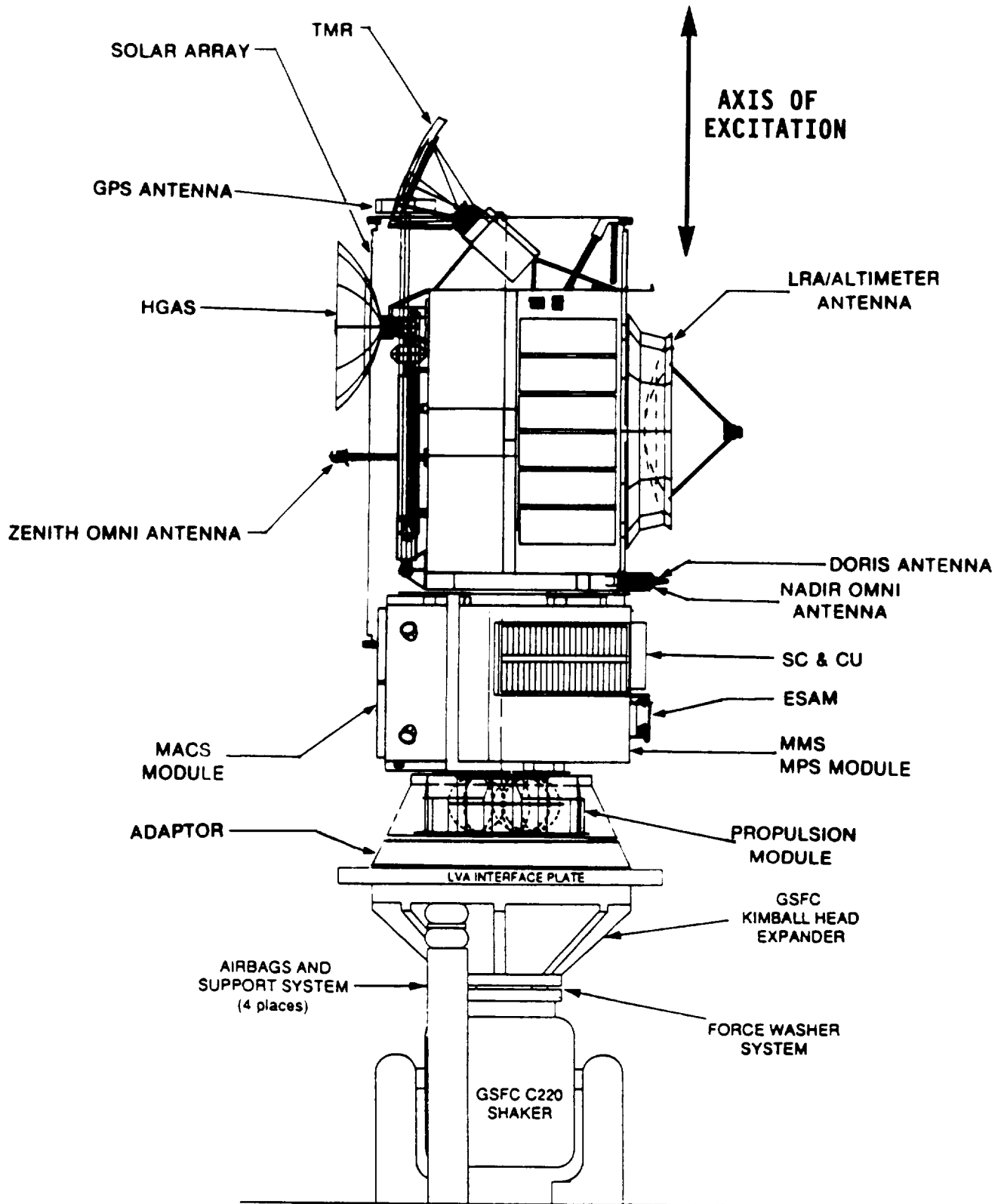


FIGURE 1. TOPEX/POSEIDON SATELLITE SINE TEST CONFIGURATION

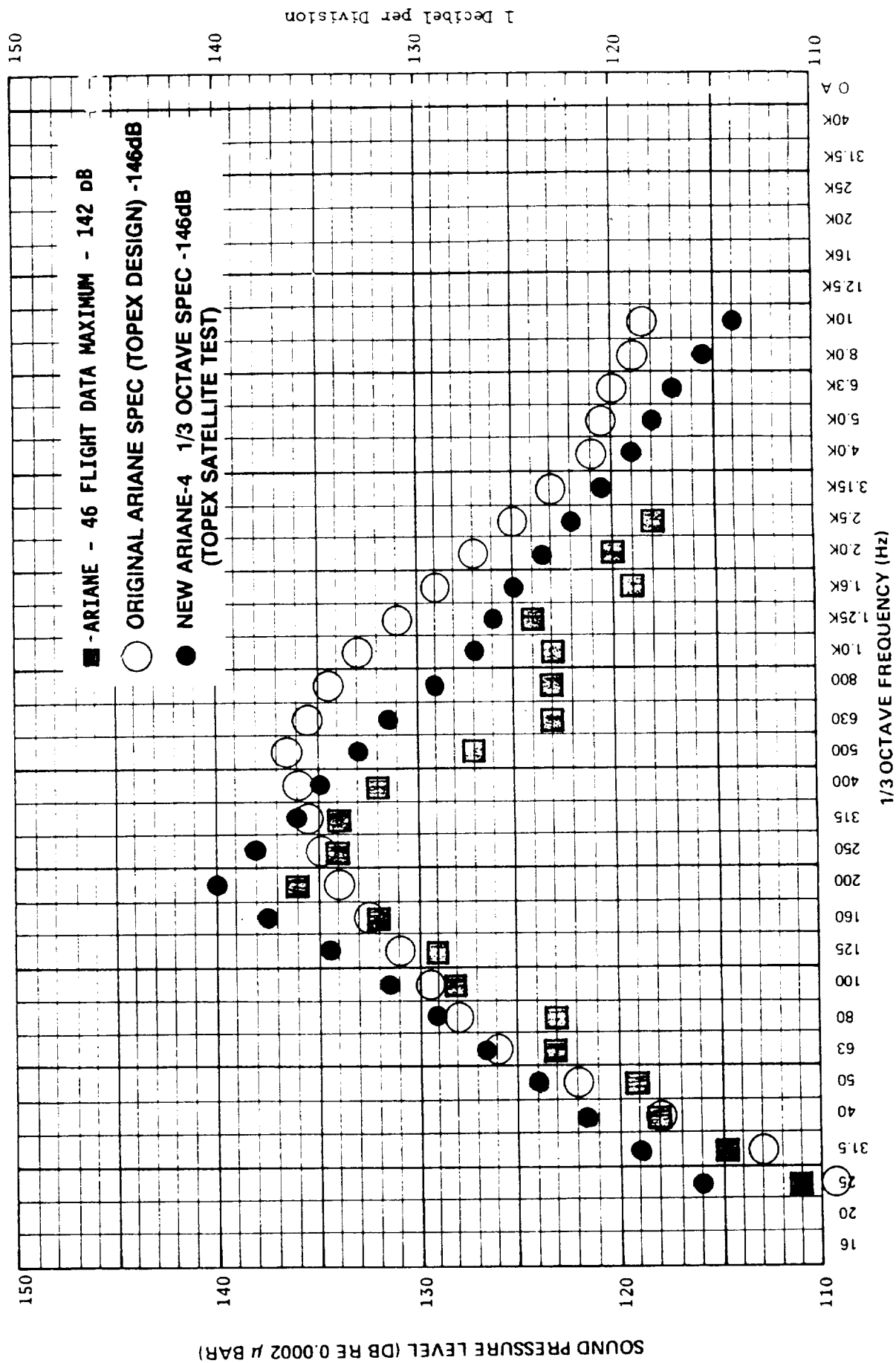
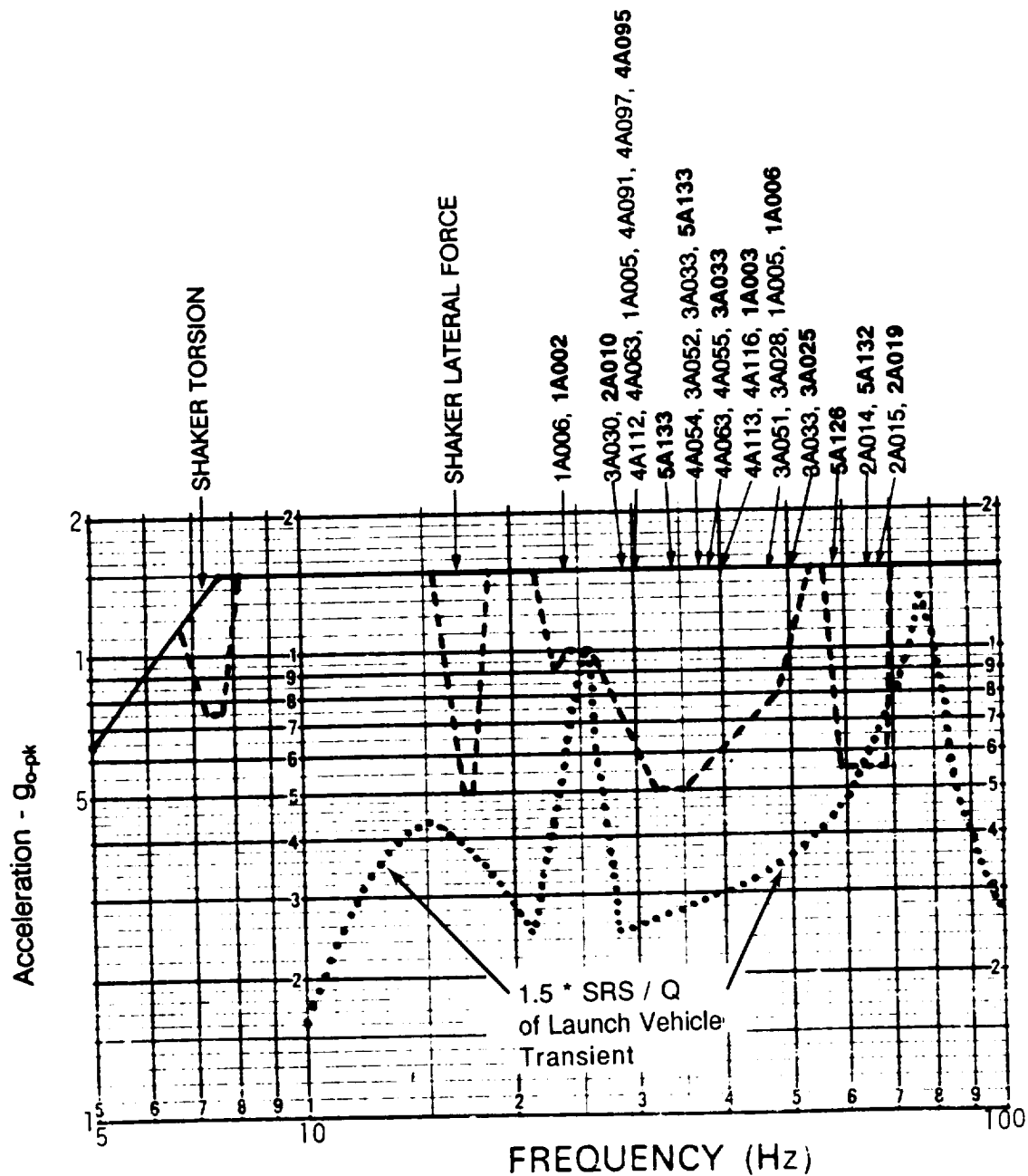


FIGURE 2. TOPEX/POSEIDON FLIGHT AND TEST ACOUSTIC SPECTRA



1A002 - LVA Leg #1; 'Y'  
 1A003 - LVA Leg #1; 'Z'  
 1A005 - LVA Leg #2; 'Y'  
 1A006 - LVA Leg #2; 'Z'  
 2A010 - Prop. Mod./PME; 'X'  
 2A014 - ATK Top; 'Y'  
 2A015 - ATK Top; 'Z'  
 2A019 - ATK Top; 'Z'  
 3A025 - C&DH B'plate center; 'W1'

3A028 - MACS Mod/RWA; 'W2'  
 3A030 - MACS Mod/Opt Bench; 'V2'  
 3A033 - MACS Mod/ B'plate; 'V2'  
 3A051 - SCCU/ESAM; 'Y'  
 3A052 - SCCU/ESAM; 'Z'  
 4A054 - IM +X, +Y, +Z Corner; 'Y'  
 4A055 - IM +X, +Y, +Z Corner; 'Z'  
 4A063 - IM +X, -Y, -Z Corner; 'Y'  
 4A091 - S/A panel 4 +X, -Z; 'X'

4A095 - S/A panel 4 -X, +Z; 'X'  
 4A097 - S/A panel 4 -X, +Z; 'Z'  
 4A112 - S/A truss leg -X, +Z; 'X'  
 4A113 - S/A truss leg -X, +Z; 'Y'  
 4A115 - S/A truss leg -X, -Z; 'X'  
 4A116 - S/A truss leg -X, -Z; 'Y'  
 5A126 - Alt. Feed Horn; 'X'  
 5A132 - TMR box; 'X'  
 5A133 - TMR box; 'Y'

FIGURE 3. NOTCHED INPUT IN SATELLITE SYSTEM SINE TEST

Project: TOPEX

Test Date: 05-FEB-1992

Power spectral density (PSD)

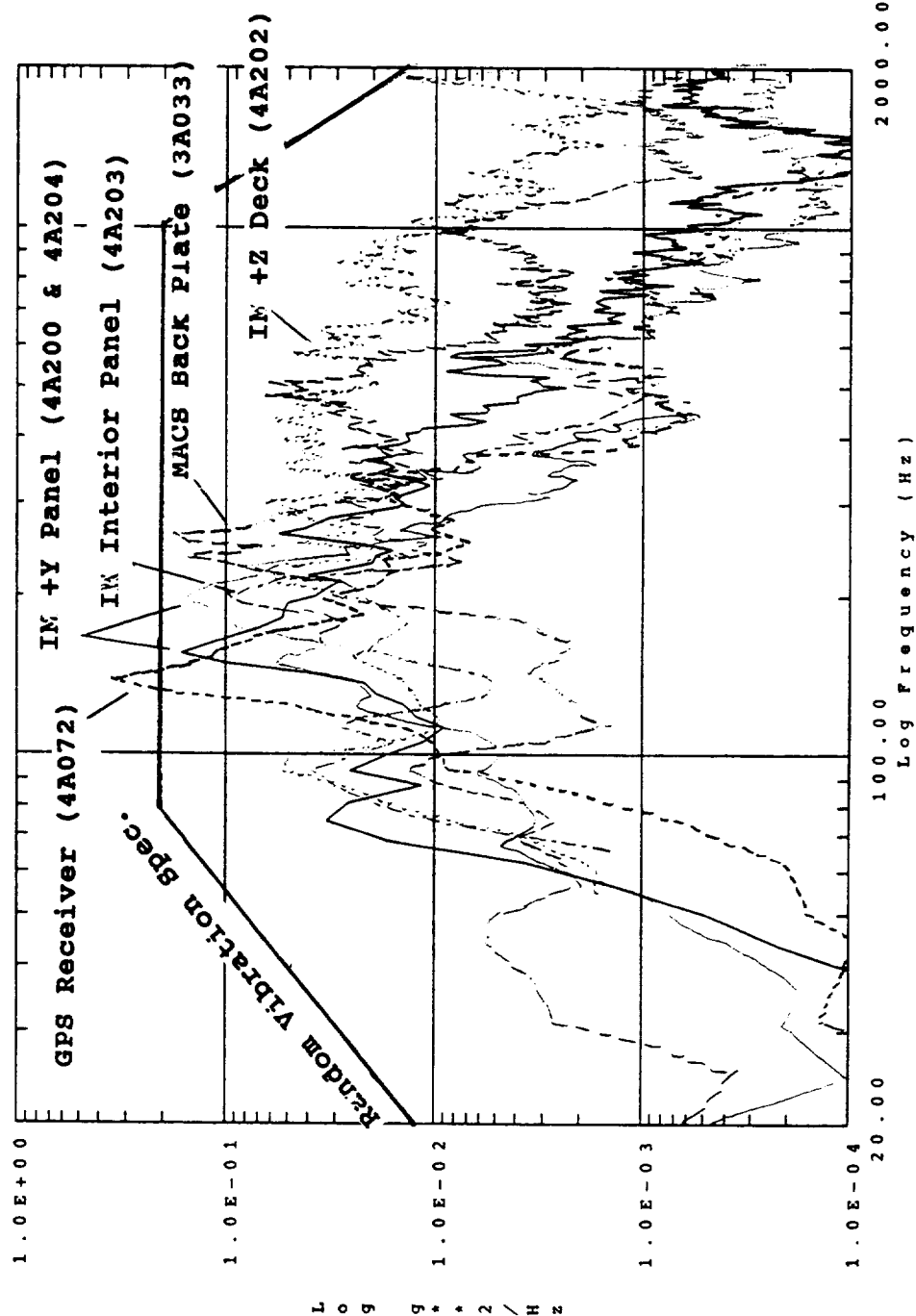


FIGURE 4. COMPARISON OF ELECTRONIC BOX INPUTS IN SYSTEM ACOUSTIC TEST WITH BOX RANDOM VIBRATION TEST SPECIFICATION

## THE DESIGN CONCEPT OF THE 6-DEGREE-OF-FREEDOM HYDRAULIC SHAKER AT ESTEC \*

P.W. Brinkmann  
ESA/ESTEC, Noordwijk, The Netherlands

D. Kretz  
Mannesmann-Rexroth, Lohr a/Main, Germany

**ABSTRACT**

The European Space Agency (ESA) has decided to extend its test facilities at the European Space and Technology Centre (ESTEC) at Noordwijk, The Netherlands, by implementing a 6-degree-of-freedom hydraulic shaker.

This shaker will permit vibration testing of large payloads in the frequency range from 0.1 Hz to 100 Hz. Conventional single axis sine and random vibration modes can be applied without the need for a configuration change of the test set-up for vertical and lateral excitations. Transients occurring during launch and/or landing of space vehicles can be accurately simulated in 6-degrees-of-freedom. The paper outlines the performance requirements of the shaker and provides the results of the various trade-offs, which are investigated during the initial phase of the design and engineering programme. Finally the paper presents the resulting baseline concept and the anticipated implementation plan of the new test facility.

**INTRODUCTION**

The European Space Agency (ESA) has developed and maintains major environmental test facilities, at its Technology Centre (ESTEC) at Noordwijk, the Netherlands. The facilities are at the disposal of industry, scientific institutes and projects to support space programmes, in particular those of ESA and its member states.

Performance characteristics of the test facilities are regularly reviewed and adapted to the needs of future Agency programmes. In this context the Agency is executing a design and engineering phase of a 6-degree-of-freedom hydraulic shaker ("HYDRA") and of the associated infrastructure. The addition of these facilities will make the ESTEC Test Centre fully compliant with potential payloads of Ariane IV and Ariane V. An illustration of the extended Test Centre is shown in Figure 1.

The main facilities co-located in one building complex are:

- Large Space Simulator (LSS)
- Electrodynamic Vibration Systems
- Compact Payload Test Range (CPTR)
- Acoustic Facility (LEAF)
- 6-DOF Hydraulic Shaker (HYDRA)
- Support Facilities for Integration, EGSE, etc.

\* Work supported by subcontracts from AGE-ELEKTRONIK gmbH (D), SEREME (F) and ASAP (D).

The co-location of facilities with transportation links within one building is a prerequisite for short system level test campaigns.

### **REASON FOR A HYDRAULIC SHAKER**

Considerable effort has been spent by ESA during the last decade in order to study the possibilities for dynamic structure qualification and system acceptance of Ariane IV and Ariane V payloads. Mass and size of these payloads demand an extension of shaker forces and shaker table sizes, as well as an extension of the lower frequency range below 5 Hz. Also the introduction of a test method, which reflects a more realistic representation of the actual flight environment, has been a major objective of these studies (Ref. 1). It has been concluded that the simulation of the transients in multi-direction at the interface of launcher and spacecraft produces the most realistic structural responses, unlike traditional sine- or random tests, which lead to unrealistic responses and therefore bear the risk of over- or under-testing. Figure 2 illustrates a transient at the payload interface during an Ariane IV launch. Based upon experiments with multi-degree-of-freedom hydraulic shakers designed for earthquake simulation and taking into consideration the vast improvements of control systems in recent years, it has now become feasible to apply this technology for spacecraft testing. Multi-degree-of-freedom vibrators at DLR and IABG (Germany) have successfully demonstrated the reproduction of transients representative of the Ariane and Space Shuttle environment on structure models of a telecommunication satellite and of the Spacelab Pallet (Ref. 2 and 3). The encouraging results of the studies and demonstrations have lead to the decision to build a 6-DOF Hydraulic Shaker ("HYDRA") at ESTEC, which shall be operational in 1996. The shaker will allow conventional sine and random testing as well as multi-axes transient testing. Sine and random tests can be performed without any re-configuration of the test set-up for tests in the longitudinal and lateral axes. This will contribute to shortening of test campaigns and it will reduce the risks of damage to the test article because of reduced handling operations. The existing facilities in Europe were designed primarily for earthquake simulation and do not meet with stringent safety and cleanliness requirements which, together with the technical requirements, are necessary for the test of spacecraft. Therefore, the design and engineering phase for the HYDRA Facility has started in February 1992. The baseline concept was confirmed in a preliminary design review; it is based upon the following requirements.

### **MAIN PERFORMANCE REQUIREMENTS**

- |   |                                    |                 |
|---|------------------------------------|-----------------|
| - | Span of test table                 | 5.5 m           |
| - | Eigenfrequency in loaded condition | > 100 Hz        |
| - | Frequency range                    | 0.1 Hz - 100 Hz |
| - | Displacement in x, y, z direction  |                 |
|   | a) baseline                        | ± 25 mm         |
|   | b) growth potential                | ± 50 mm         |
| - | Rotation around x, y, z            |                 |
|   | a) baseline                        | ± 0.5 degrees   |
|   | b) growth potential                | ± 1 degrees     |

- Dynamic performance see Figures 3 and 4
  - Control accuracy
    - o translation acceleration  $\pm 0.05 \text{ m/s}^2$  (rms)
    - displacement  $\pm 0.05 \text{ mm}$
    - o rotation acceleration  $\pm 0.02 \text{ rad/s}^2$  (rms)
    - displacement  $\pm 0.001^\circ$  degrees
    - or  $\pm 2,5 \%$  of the input signal, whichever is the larger.
  - Test modes
    - a) sine / sine sweep
    - b) random
    - c) transient
  - Test Article Mass 7000 kg <sup>\*)</sup>
  - Centre of gravity above table surface 5.0 m <sup>\*)</sup>
  - Offset of payload centre-line from table centre-line 0.5 m <sup>\*)</sup>
  - Moments of inertia related to centre of gravity
 
$$\begin{aligned} I_{xx}^* &= I_{yy}^* \leq 40.000 \text{ kg/m}^2 \\ I_{zz}^* &\leq 15.000 \text{ kg/m}^2 \end{aligned}$$
  - Moments of inertia related to test table surface
 
$$I_{xx}^* = I_{yy}^* \leq 215.000 \text{ kg/m}^2$$
  - The design must provide for on-line checks to protect the spacecraft against over-testing and for safe shut-down procedures in case of facility malfunctions.
- <sup>\*)</sup> These parameters are related to the maximum dynamic performance stipulated in Figures 3 and 4 and will increase if the acceleration requirements decrease.

### TEST TABLE / SYSTEM GEOMETRY

The test table is the mechanical interface between the test article and the hydraulic actuators. It must meet the following requirements:

- a) The lowest elastic natural frequency in loaded condition should be above 100 Hz, to reduce resonance problems in the operating frequency range of the facility.
- b) The location of the actuator attachment points should be optimized to minimize distortions, which could be induced by the basic elastic modes.
- c) The mass should be minimized in order to reduce the installed power.

The system geometry is a major element effecting the vibration modes of the table and therefore its natural frequency. Also the positioning of the actuators around the table has a large influence on the actuator forces and oil flow requirements. Therefore a compromise has to be found. The trade-off was

based upon finite element models for six different options (Figure 5). For each actuator arrangement, the rigid body modes and the first three elastic modes were calculated. The model took into account the stiffness, position, and mass of all actuators; the table was modelled as a simple box structure. The main conclusion of this study was that the interfaces of the horizontal servo actuators must be located as high as possible in order to minimise the coupling factor between translation modes along X and Y axes and rotation modes around X and Y axes. Horizontal and vertical actuators must be located as far as possible from the vertical centre-line of the table. For the elastic modes, the asymmetric arrangements of options 1 and 2 have low stiffness (compared with the other four options) and an uneven weight distribution. This would be more difficult to control and would also require a larger seismic foundation to absorb asymmetric forces. The finite element analysis on the square table showed clearly that the torsional resonance is in most cases much lower than that of the other modes (Figure 6). This was one of the main reasons why options 5 and 6 were rejected. If the X-Y actuators are positioned on the nodal lines of the torsional mode, the actuators will have no influence on the resonance frequency, whereas positioning the X-Y actuators on the table corners would considerably reduce the torsional frequency. Consequently, the best choices for the X-Y actuators are options 3 and 4. With respect to the Z-actuators, option 4 has the advantage that all actuators are positioned on the table-sides. In this configuration it is possible to cut the corners of the table (Figure 7), thereby forming an octagonal table and saving approximately 3000 kg on the overall table mass. As this corner mass has a large influence on the torsional mode of the table, it would also raise its first natural frequency. Option 4, however, leads to a mass and stress concentration at the co-located actuator/table interfaces. Option 3 was finally chosen as the optimum arrangement, because it allows to remove the corners, but also distributes the lumped masses of the actuators evenly around the table. The interface of the Z-actuators with the table is illustrated in Figure 8. It is located as far as possible from the table centre line to cope with the turning moments.

## **ACTUATOR FORCES**

The actuators dynamic force and flow requirements for various arrangements were computed with a specially developed computer program called 'MAP', which permits the input of table motions at different frequencies and amplitude levels in any of the six degrees of freedom. The program can calculate the maximum dynamic force and flow requirements for all of the system's eight actuators at any given point in time, or the dynamic force, flow, velocity, displacement and acceleration requirements of the actuators over the test period. With this tool, the optimum positions of the actuators can be determined for any given specification. Figure 9 shows the data supporting the selection of actuators. For commonality reasons, 630 kN (static force) standard actuators (type Mannesmann-Rexroth) were selected for X, Y and Z. These have a piston rod diameter of 160 mm and are equipped with hydrostatic pocket bearings. The analysis illustrated in Figure 10 shows that the maximum dynamic forces lie below 500 kN for all single translational or rotational motions. This is also the case with translational motions that do not lie on the systems main axis, but are arbitrary vectors in space. The largest dynamic force requirements (580 kN) were found in a combination of rotation about the X and Y axis simultaneously (rotation about a diagonal axis). As the dynamic force requirement of 580 kN arises during the part of the sine wave cycle where the



velocity is at its minimum (i.e. the acceleration is at its maximum), an actuator with a static force capacity of 630 kN is adequate.

### **TABLE DESIGN**

The design for the test table takes into account all the above conclusions, as well as the results of investigations with respect to materials and construction. The use of steel and aluminium was considered, and showed that the price disadvantage of an aluminium table can be justified with its high internal damping and the reduction in the overall mass. The high internal damping of aluminium can reduce some of the difficulties associated with multi-axes control systems and the reduction in the table mass reduces the demands on the power of the hydraulic system. Furthermore, a double layer box structure (Figure 11), manufactured from welded aluminium plates, was selected. The rectangular boxes of this structure have the dimensions 0.786 m x 0.786 m x 0.800 m and a plate thickness of 20mm. These dimensions were chosen as a compromise between the need for high web plate local modes and sufficient space to allow for good welding conditions. Plate resonance problems were experienced with other tables of this size, because the natural frequencies of the individual plates were very similar. Therefore, access holes of varying sizes will be cut into the plates to avoid these effects.

### **SUSPENSION OF SEISMIC FOUNDATION**

Air springs and steel springs (Figure 12) combined with viscose dampers were investigated. For both suspension systems the dynamic performances were very good and very similar. The highly damped steel springs were selected because they have the following advantages:

- Easy on-site implementation. They can be introduced into the form work of the seismic foundation before pouring the concrete by prestressing the steel spring boxes to their final working height.
- High damping ratio in each degree of freedom, which allows operations at very low frequencies.
- High reliability and no maintenance.

The configurations which were investigated are illustrated in Figure 13. In option 1 the seismic mass is suspended at the level of its centre-of-gravity. This provides de-coupling of lateral and the respective rotational rigid body modes. The second option with a base-suspension does not provide this de-coupling but leads to a simpler construction and a lower mass. A detailed analysis of the dynamic performance has shown no essential differences between the two options for this application. Therefore option 2 has been selected for cost reasons.

### **CARDANIC BEARINGS**

The table motions in six degrees of freedom (D.O.F.) are achieved with eight linear actuators, which will be connected between table and foundation by means of bearings having at least two rotational degrees of freedom.

The main technical requirements placed on these bearings are:

- low mass, due to the dynamic application [ $< 500$  kg];
- backlash free, as this will affect the mechanical noise;
- high stiffness, as this will affect the actuator's overall natural frequency [ $> 10^{10}$  N/m];
- low friction coefficient [ $< 0.005$ ];
- stiffness and friction should be as linear as possible (Figure 14);
- acceptable life rating even when subjected to unfavourable operating conditions, such as shock or high frequency loading with very small radial movements.

Figure 15 shows 3 groups of bearings, which were investigated. The first group relies on the use of dissimilar materials (Steel/ PTFE) sliding over each other (usually referred to as plain bearings). This type of bearing can meet the stiffness requirements. However, it is essential that the bearing is pre-loaded to prevent excessive wear, which leads to unacceptable friction levels. The second group uses the hydrostatic principle and assures no metal-to-metal contact and thereby leads to very low friction levels. Unfortunately the bearing has to be extremely large to achieve the required stiffness and would therefore lie outside the weight limit. The last and possibly the only acceptable solution for such an application is the pre-loaded cylindrical roller bearing, because it is most suited for taking large forces. With this type of assembly the bearing stiffness can be optimised by the use of two, three or even four row bearings, providing a very compact solution with friction levels very much lower than that of plain bearings. Interference fits are used to pre-load such a bearing without the possible risk of alignment errors. The pre-load can be very accurately controlled by preheating the bearing housings before assembly. The influence of high frequency vibration on fretting corrosion can to a certain extent be reduced by optimising the pre-load. Lower pre-loads increase the relative motion between the rolling elements and the raceways, while higher pre-loads increase the contact pressure. As the life of the bearing will be reduced by contamination or local heat build-up it is extremely important that a continuous supply of filtered oil to the bearings is guaranteed. The oil also functions as a coolant, dispersing local heat and maintaining a satisfactory operating temperature.

## CONTROL SYSTEM

The dynamic behaviour of the test facility is governed by the performance of the control system. An analysis of existing control systems for multi axes test facilities was carried out during the conceptual design phase for the HYDRA facility. It showed clearly that most of these systems have disadvantages that can be avoided by modern control concepts. Most of the conventional control algorithms available on the market are designed for universal applications convenient for various multi-axes environments (e.g. electrodynamic shakers and hydraulic shakers with lower accuracy requirements). They consider the test facility as an abstract object where "n" drive signals produce "m" sensor signals. A mathematical description of these dependencies is assumed by linear mapping given by the so-called "transfer matrix". A desired load to the test item is achieved by iterative signal adaption which consists of two independent steps:

- Automatic identification of the transfer matrix of the loaded facility before the test starts by applying low-level noise.
- Repeated iterations of the test signals including manual correction procedures.

The optimization of the control signals depends on the test item, the reference signals and the acceptable tolerances. It is a complex procedure, which requires engineering knowledge and experience with respect to the facility behaviour as well as the test item. Furthermore, the experimenter might limit the number of iterations to avoid undue exposure of the test item. The new digital control algorithm applied for HYDRA is based on mathematical modelling of the actuators, servo valves, and the overall geometric arrangement. A computational function is implemented to synchronise the actuator controllers in order to avoid warping distortion stresses in the shaker table. Further attention is given to the "dead time" of the facility caused by the hydraulic system, anti aliasing filters, and sensors. To achieve the required accuracy of the test signals, a control loop time of 100 microsec is necessary. This requires a powerful computer system. Furthermore, resonance frequencies of the test item can be determined on line to reduce the input level automatically (notching).

The goals of the modern control techniques as used by the HYDRA control algorithm are:

- Accurate control by non linear actuator control algorithms.
- Control signal generation for optimized use of the special geometric arrangement of the HYDRA actuators.
- Minimized stress at the table, caused by the over determination arising from eight actuators at the table and six degrees of geometrical freedom.
- Granted convergence of the control procedure.
- Minimized manual intervention by the use of self adapting kinematic closed loop controllers.
- High security by a distributed control system.

A customized computer system is employed to support the software of the control algorithm. The treelike structured controller network is shown in Figure 16. It is based on parallel processing with highly distributed computing power, permitting:

- on-line modelling of the actuators;
- on-line, adaptive modelling of the kinematic situation;
- highly accurate data acquisition;
- well structured to identify and react to critical situations.

This leads to the following advantages for the user:

- no special knowledge of operators is required;
- item independent control structure;
- automatic emergency shut down;
- preventive maintenance by an expert system;
- secure shut down procedures;
- automatic notching;
- expandability of number of notching channels.

The overall supervisor and control concept is subdivided into several parts (Figure 17) for data acquisition and emergence control on different levels, the kinematic controller, the pilot sequence controller and the so called supervisor system. Each subdivision can operate as stand alone system as well, allowing different levels of emergency shut down procedures, if one of the components or interface lines fails. In parallel to the specialized closed loop control processing units, a three-processor system (based on the UNIX operation system) allows the comfortable and mostly standardized handling with external ETHERNET access. External data can be used as reference signals. Integrated data analysis can be applied in connection with the item data analysis system. Common data base structures with extensive backup options are used to prevent loss of data even if one of the storage media or power supply fails. As a conclusion, the distributed supervisor and control concept allows redundant operations with high reliability and as a consequence with a maximum security for the test item. The operations are well controlled without requirements for specialized knowledge of the facility operators.

### **FACILITY IMPLEMENTATION**

The implementation of the HYDRA facility is scheduled in two phases:

Phase I        "Design and Engineering"  
Phase II       "Procurement, Installation and Acceptance"

Phase I has started on February 1st, 1992 and will be terminated in May 1993. This phase is subdivided into 4 subphases, each being completed with a formal review:

- Concept Design Review                      (May 1992)
- Preliminary Design Review                  (September 1992)
- Critical Design Review                        (January 1993)
- Final Design Review                            (April 1993)

Phase II will be started by the end of 1993 and the facility will be operational for spacecraft testing by the middle of 1996. According to the present schedule of ESA the first test will be performed on the Polar Platform (PPF), which will be launched with ARIANE V in 1998.

### **CONCLUSION**

The concept design of a 6-degree-of-freedom hydraulic shaker for spacecraft testing has been successfully completed. The design work has resulted in a baseline, which provides confidence that the final facility design and its subsequent implementation will meet the demanding specifications. After successful implementation, it will provide ESA with a very efficient tool for dynamic testing of large structures.

## REFERENCES

1. TRANSIENT VIBRATION TESTING OF SATELLITES  
O. Brunner, C. Stavrinidis & M. Klein  
ESA/ESTEC, Noordwijk, The Netherlands  
(Proceedings of the International Symposium on Environmental Testing for Space Programmes - Test Facilities & Methods, held at ESTEC, Noordwijk, The Netherlands, 26-29 June 1990 (ESA SP-304, September 1990)).
2. MULTI-AXIS VIBRATION SIMULATION IN SPACE STRUCTURES - EXPERIMENTS WITH DFS/STM\*  
G. Lachenmayr, W. Raasch & W. Saad  
Industrieanlagen-Betriebsgesellschaft, Ottobrunn, Germany  
(Proceedings of the International Symposium on Environmental Testing for Space Programmes - Test Facilities & Methods, held at ESTEC, Noordwijk, The Netherlands, 26-29 June 1990 (ESA SP-304, September 1990)).
3. MULTI-AXES TRANSIENT TESTING: EXPERIMENTAL INVESTIGATIONS  
K. Eckhardt (1) and G. Schmidt (2)  
(1) MBB/ERNO Raumfahrttechnik, Bremen, Germany  
(2) Hochtemperatur Reaktorbau GmbH, Jülich, Germany  
(Proc. International Conference: "Spacecraft Structures and Mechanical Testing", Noordwijk, The Netherlands, 19-21 October 1988 (ESA SP-289, January 1989)).

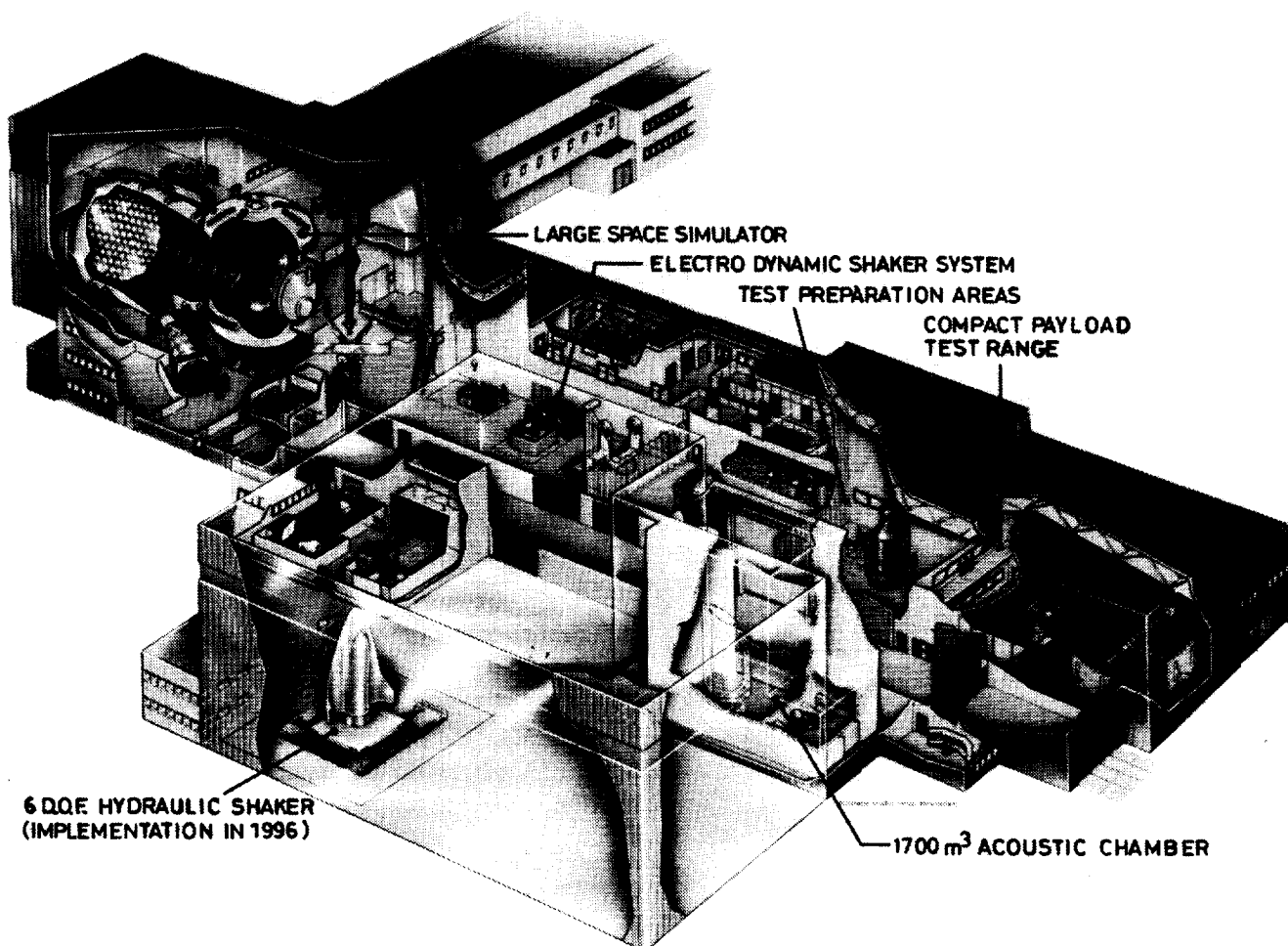


Fig 1 ILLUSTRATION OF THE ESA TEST CENTRE AT THE EUROPEAN SPACE TECHNOLOGY CENTRE(ESTEC)

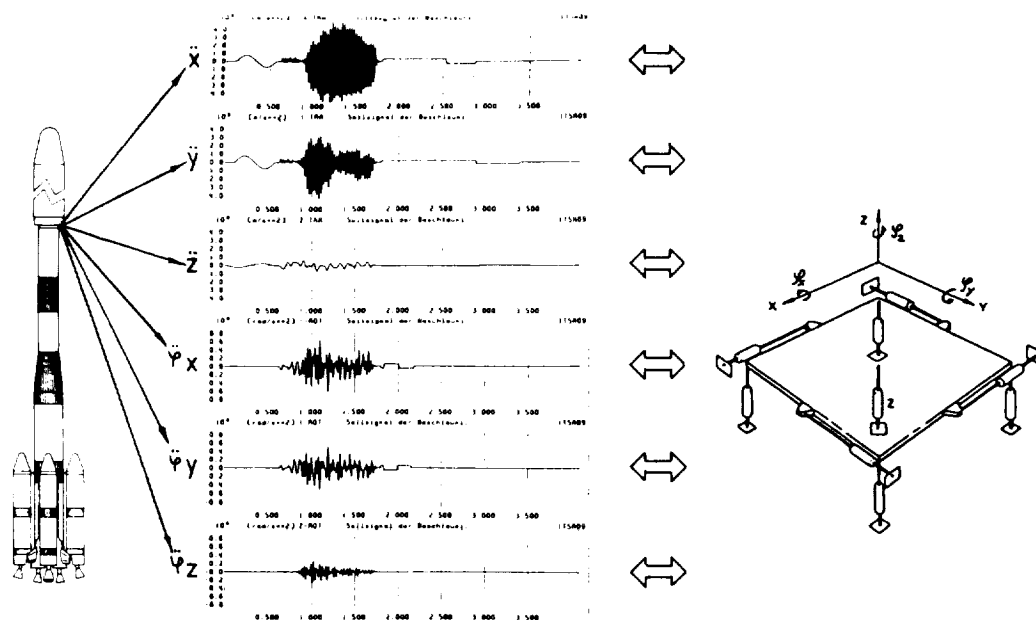


Fig 2 TYPICAL TRANSIENT AT THE PAYLOAD INTERFACE OF ARIANE IV IN 6 DEGREES-OF-FREEDOM

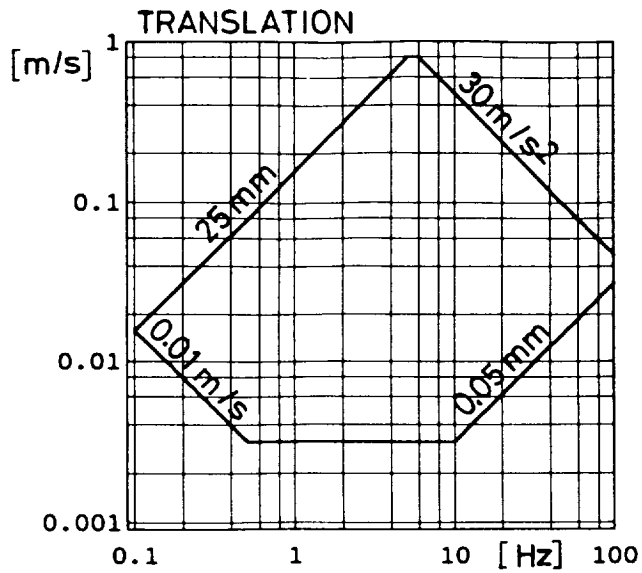


Fig.3 PERFORMANCE DIAGRAM FOR X/Y AND Z TRANSLATION WITH TEST TABLE LOADINGS.

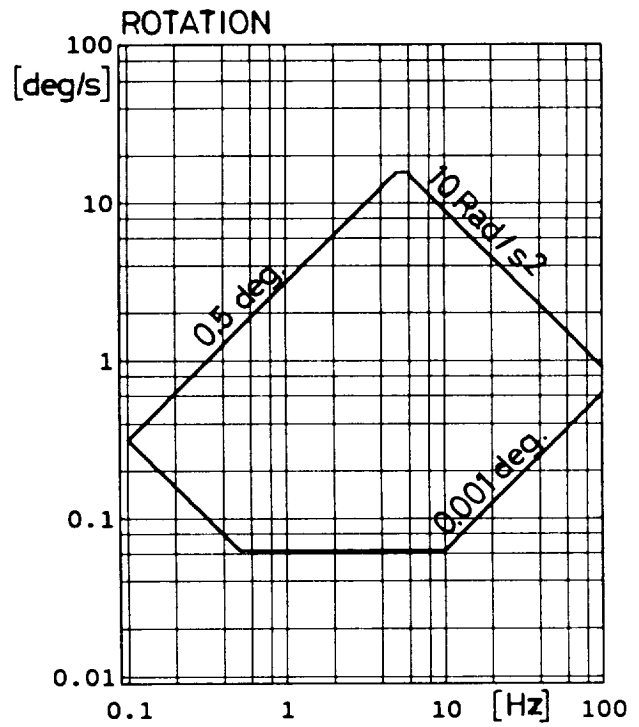


Fig.4 PERFORMANCE DIAGRAM FOR ROTATION ABOUT THE X/Y AND Z AXIS WITH TEST TABLE LOADINGS.

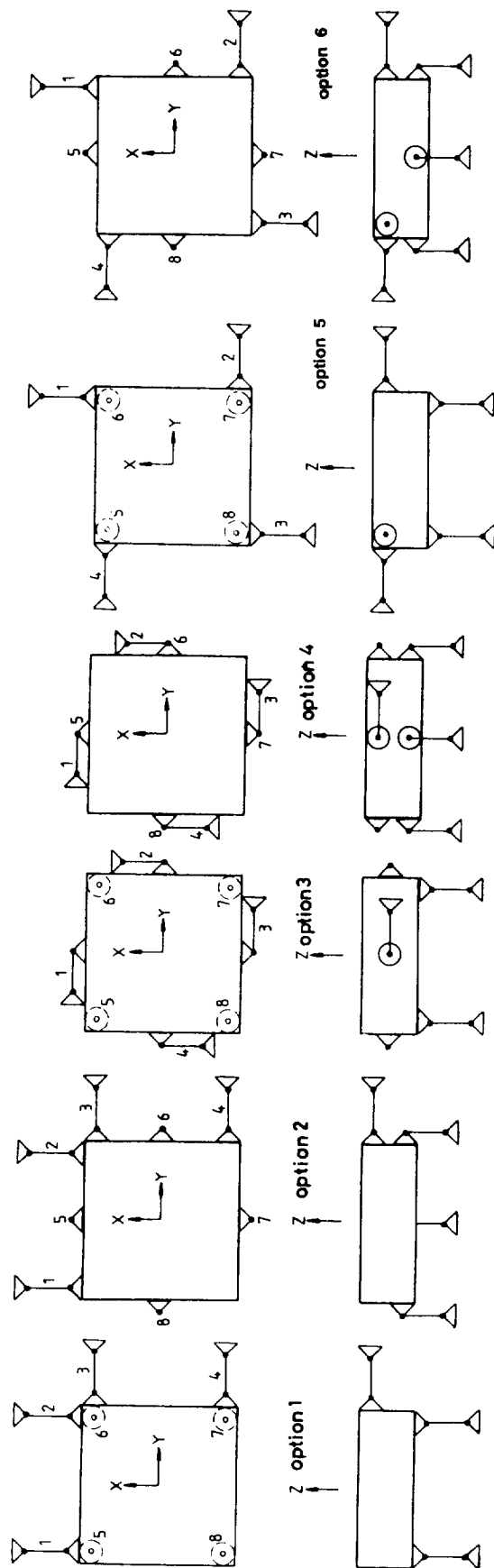


Fig.5 CONFIGURATIONS FOR SYSTEM GEOMETRY TRADE-OFFS



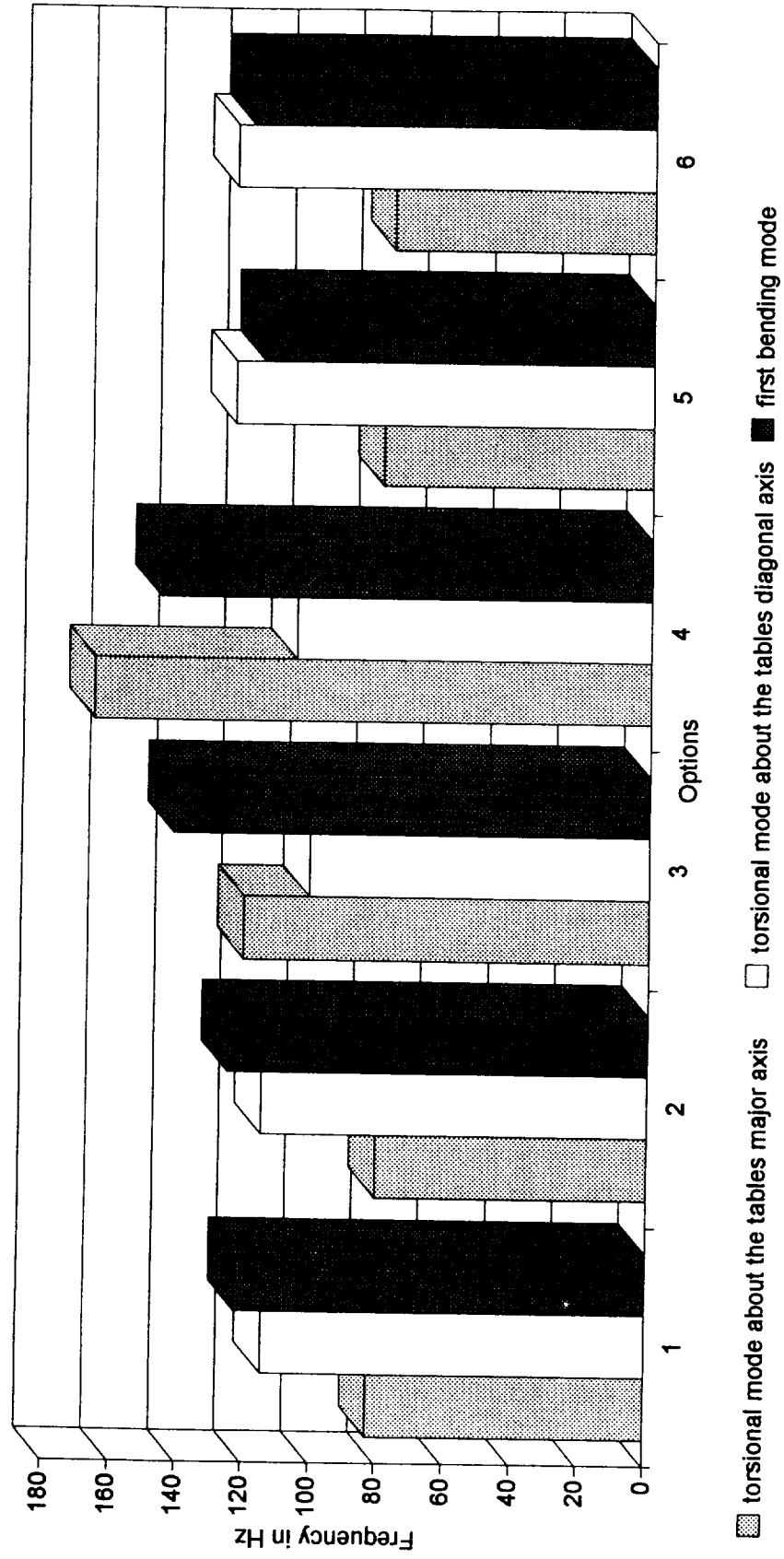
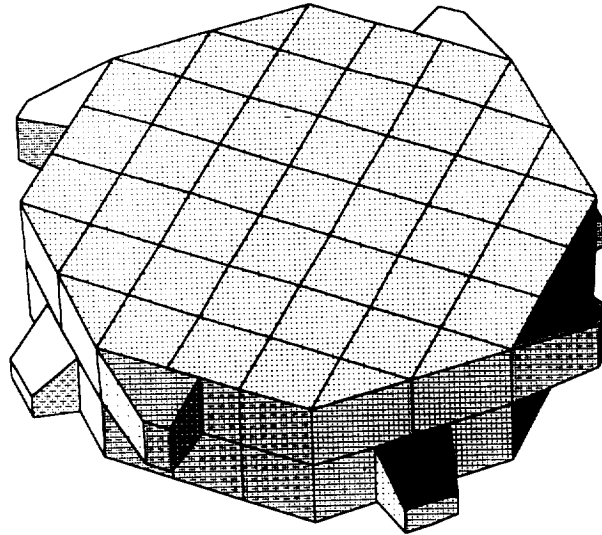
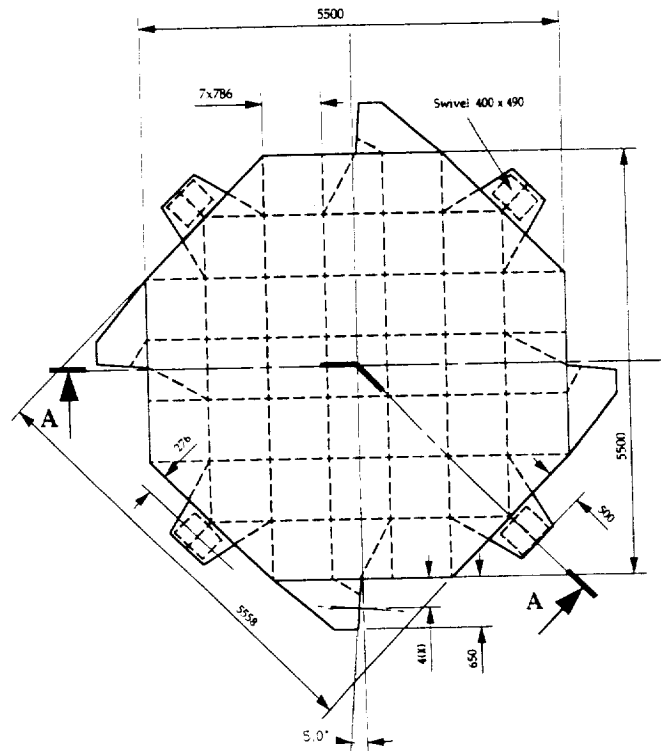


Fig.6 MODES OF DEFORMATION OF THE TEST TABLE



PANORAMIC VIEW



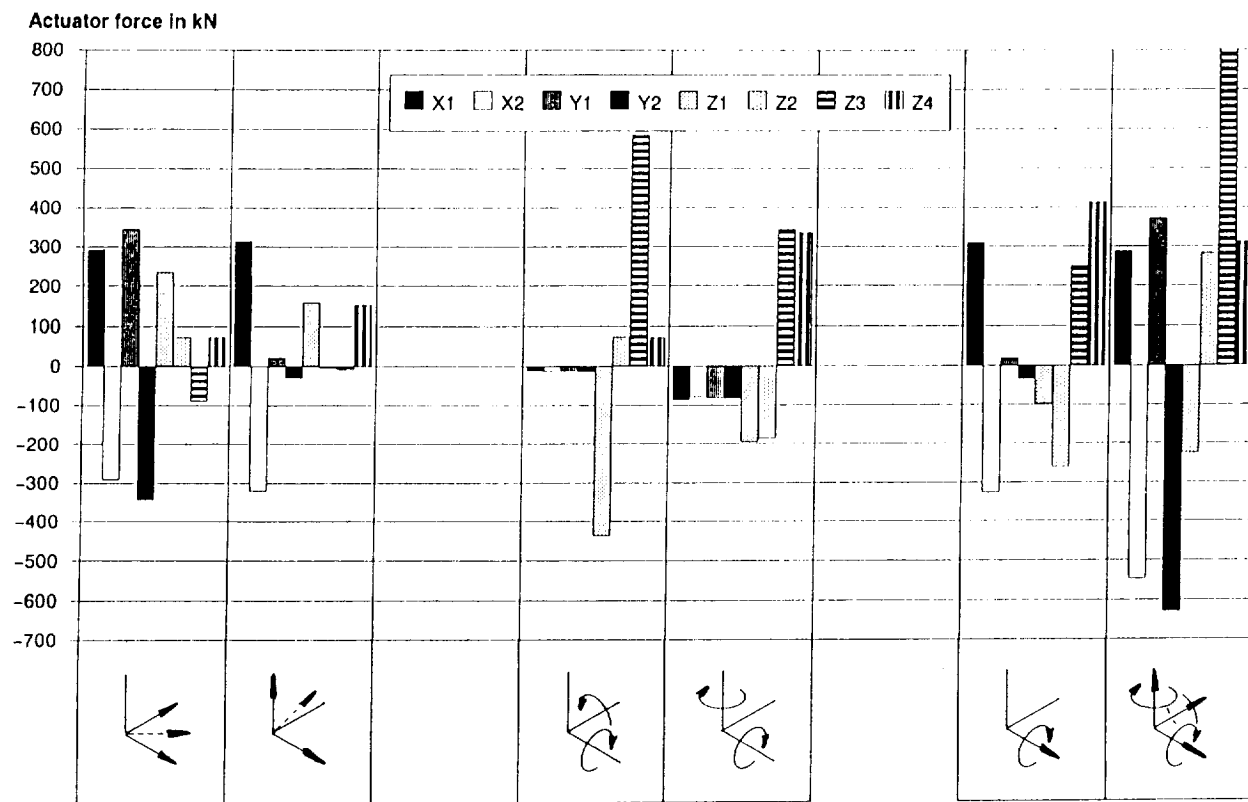
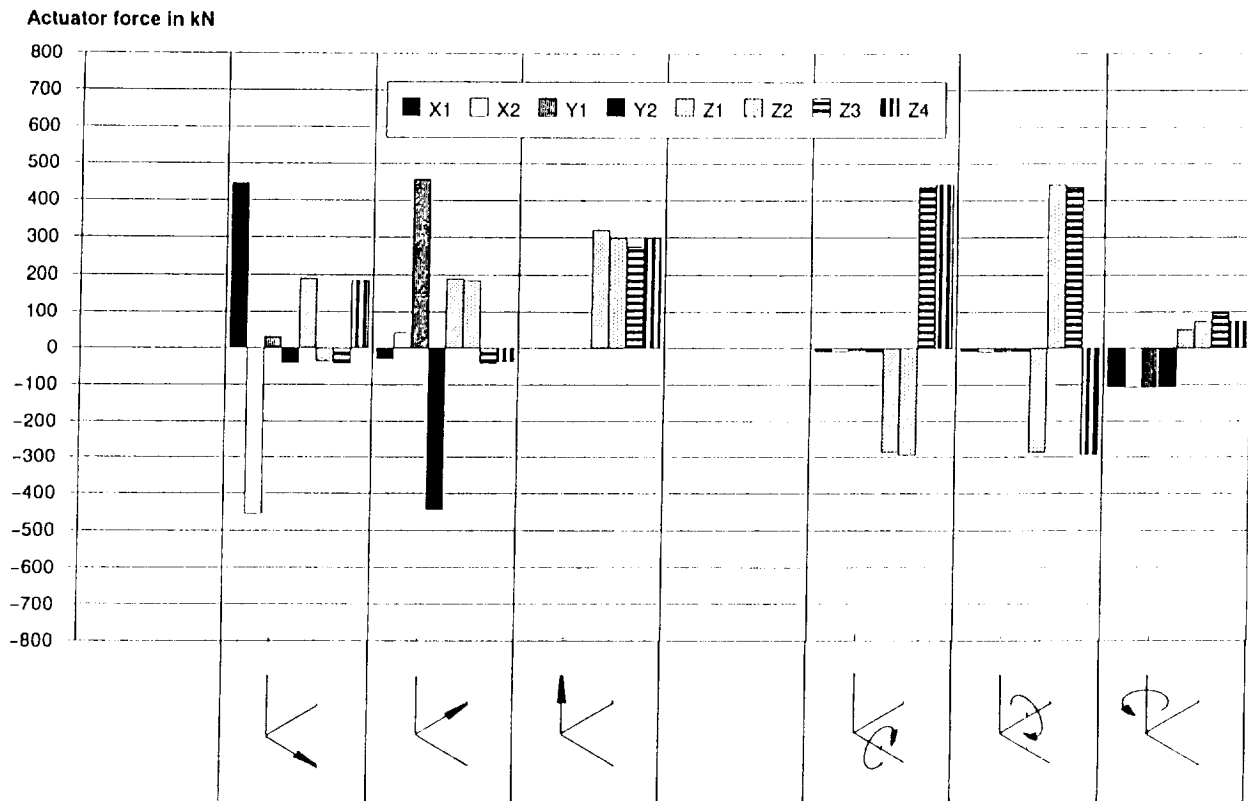
PLAN VIEW

Fig.7 OCTAGONAL TEST TABLE



MAP	Actuator	Foundation			Table			Actuator		
		x	y	z	x	y	z	stroke	start position	piston $\varnothing$
1	X1	-1610	3324	-450	-70	3200	-450	170	85	233
2	X2	1610	-3324	-450	70	-3200	-450	170	85	233
3	Y1	-3324	-1610	-450	-3200	-70	-450	170	85	233
4	Y2	3324	1610	-450	3200	70	-450	170	85	233
5	Z1	-2175	-2175	-3290	-2175	-2175	-1750	170	85	233
6	Z2	2175	-2175	-3290	2175	-2175	-1750	170	85	233
7	Z3	2175	2175	-3290	2175	2175	-1750	170	85	233
8	Z4	-2175	2175	-3290	-2175	2175	-1750	170	85	233
Moving mass		weight	width		length	depth	C of G		moment of inertia	
		23000	kg	5500	5500	1600	x	y	ix	iy
				(8 sided)			0	0	93000	93000
									120000	120000
										kg m <sup>2</sup>
Test article		weight	width		length	depth	C of G		moment of inertia	
		7000	kg	-355	-355	5000	x	y	ix	iy
									40000	40000
									15000	15000
										kg m <sup>2</sup>

Fig.9 SYSTEM MODEL FOR ACTUATOR SELECTION



**Fig.10 ACTUATOR FORCE REQUIREMENTS (AT MAXIMUM ACCELERATION )**

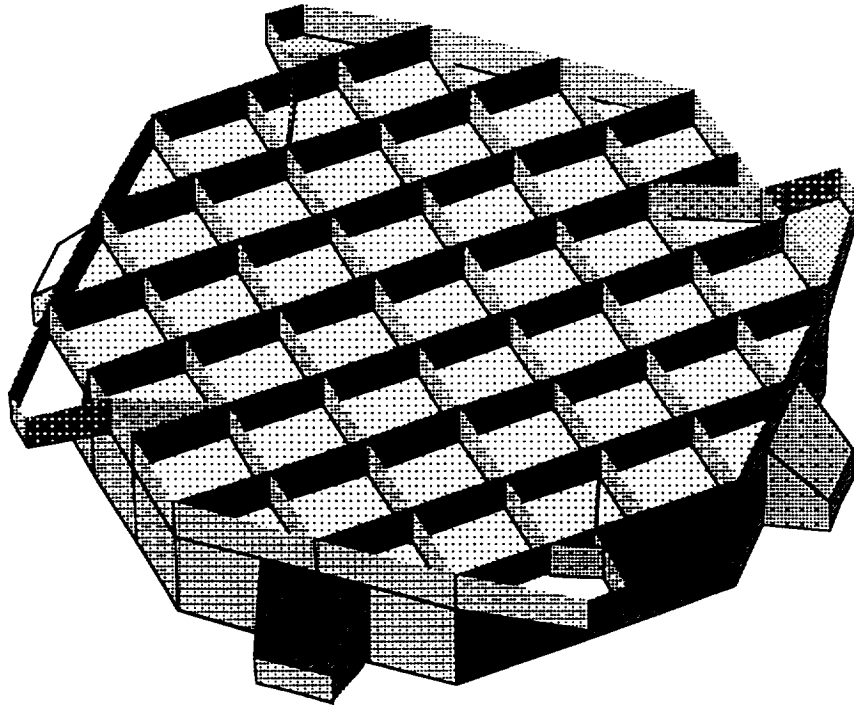


Fig.11 SECTION THROUGH HORIZONTAL ACTUATOR ANCHOR SYSTEM

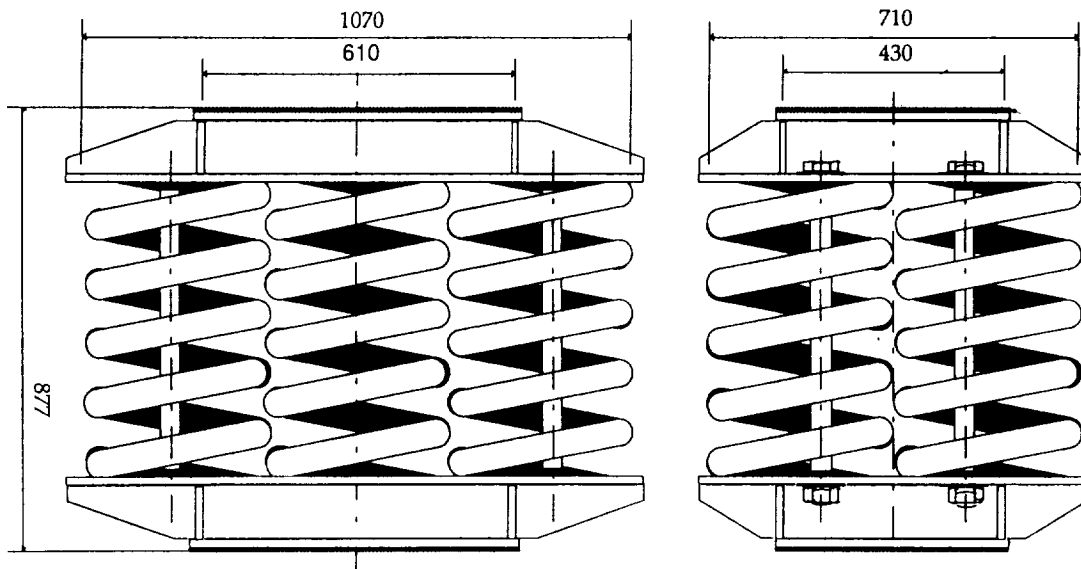


Fig.12 STEEL SPRING BOXES



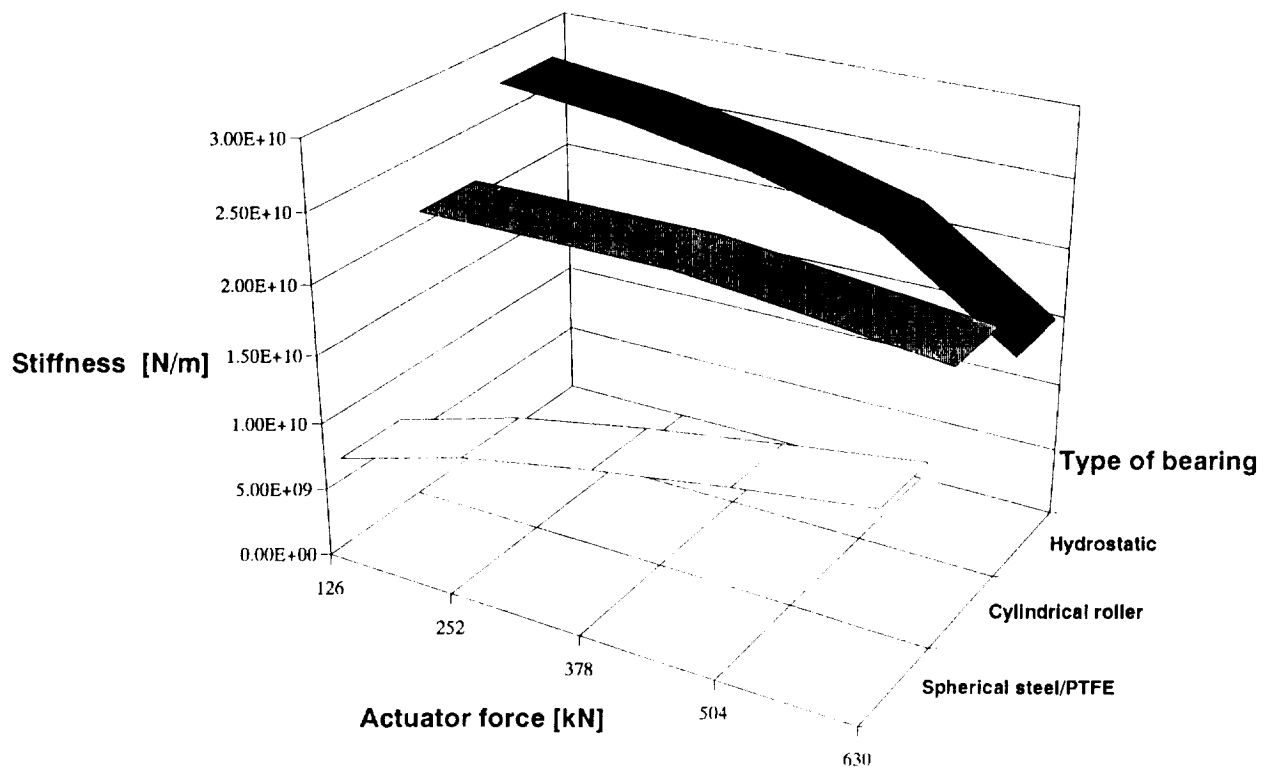


Fig.14 BEARING STIFFNESS COMPARISON



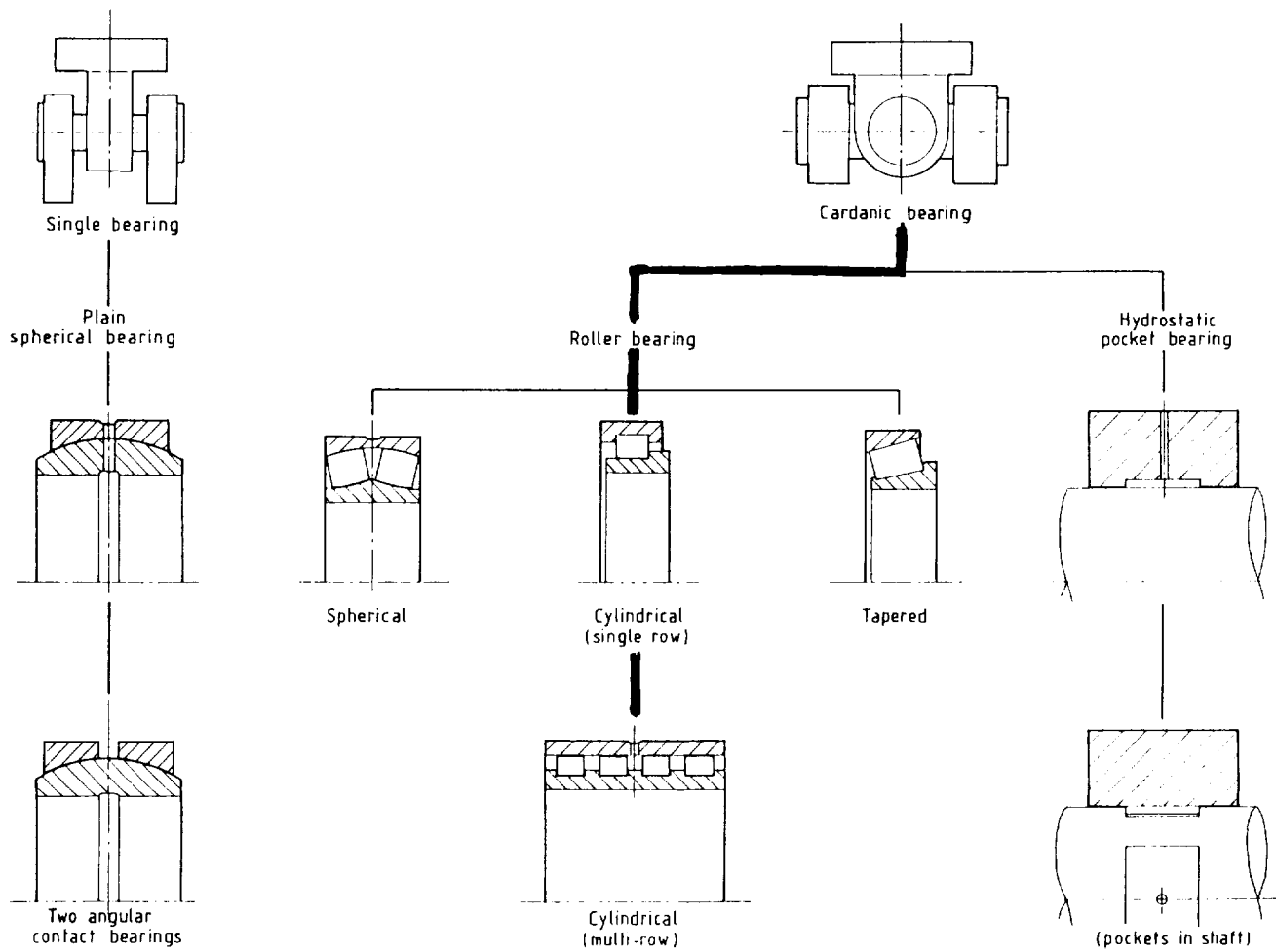


Fig.15 BEARING TRADE-OFF STUDY

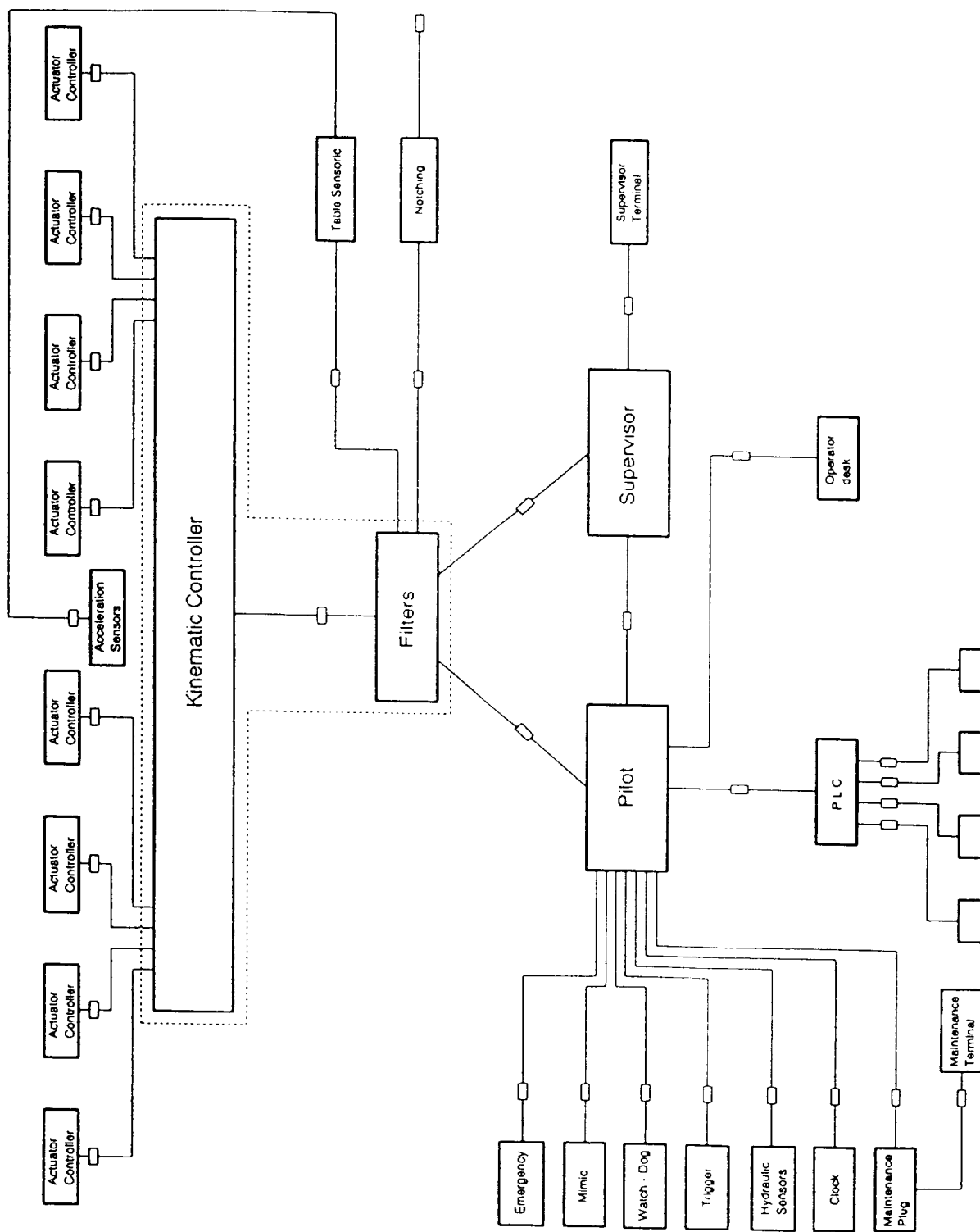


Fig.16 HYDRA CONTROL DISTRIBUTION AND STRUCTURE

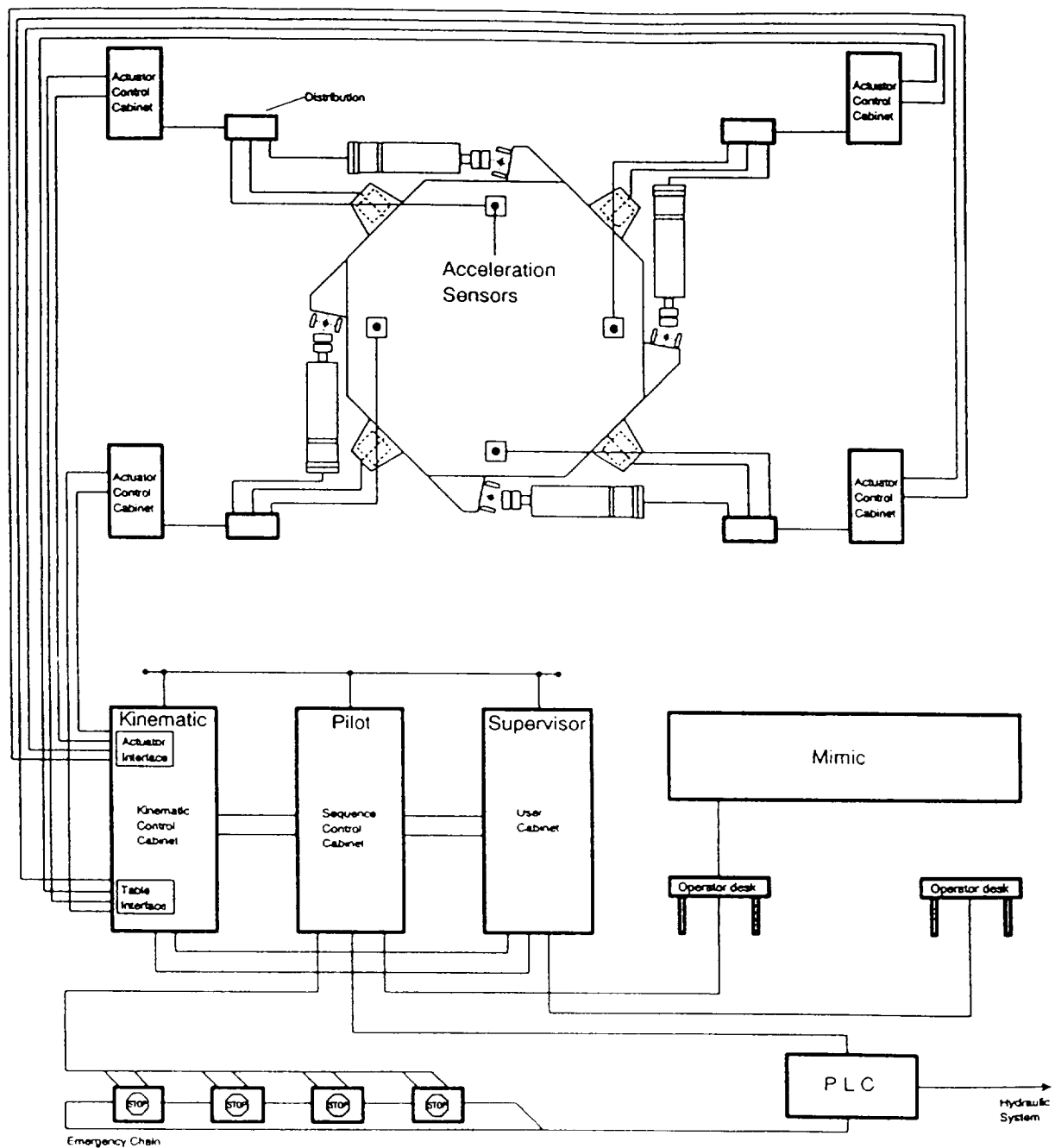


Fig.17 HYDRA CONTROL COMPONENT ARRANGEMENT



**An Environmental Testing Facility for Space Station Freedom  
Power Management and Distribution Hardware**

Arthur S. Jackola, Gary L. Hartjen  
*Rockwell International*  
Rocketdyne Division

This paper addresses the plans for a new test facility, including new environmental test systems, which are presently under construction, and the major environmental Test Support Equipment (TSE) used therein. This all-new Rocketdyne facility will perform space simulation environmental tests on Power Management and Distribution (PMAD) hardware for Space Station Freedom (SSF) at the Engineering Model, Qualification Model, and Flight Model levels of fidelity. Testing will include Random Vibration in three axes - Thermal Vacuum, Thermal Cycling and Thermal Burn-in - as well as numerous electrical functional tests. The facility is designed to support a relatively high throughput of hardware under test, while maintaining the high standards required for a man-rated space program.

The facility, which includes a large Class 100,000 clean room, is arranged in a unique two-level structure that locates each set of Electrical TSE directly overhead of its designated Unit Under Test (UUT). The centerpiece of the facility is a set of two Thermal Vacuum and Cycling Systems (TVACS), which consists of 12 independently controllable stations performing either Thermal Vacuum, Thermal Cycling or Thermal Burn-in testing. The two TVACS provide cost and space effective testing, utilizing four and eight chambers, with each arranged around a central high-vacuum, hub-mounted cryopump. System operation is fully computerized. A control room with operator interfaces is provided for control of operations and system status indication. In addition, two vibration systems will perform random vibration testing on hardware ranging in weight from 15 pounds to over 225 pounds. The shaker systems will be equipped with controllers capable of providing active response limiting by notching at resonant frequencies to prevent overstress of UUT components.



**Manned Testing in a Simulated Space Environment**

Donna L. Fender  
Manned Test Director, EC4  
NASA, Johnson Space Center  
Houston, Texas 77511

Manned thermal vacuum testing is an integral part of reliable certification of flight hardware. Even though the capability of thermal modeling exists, nothing can compare to the actual experience and knowledge gained by operating the hardware in a simulated space environment. This paper presents a view of the facility and operational requirements involved in performing a manned thermal vacuum test. The requirements fall into two major categories. The first category deals with placing the suited crewmen in a hazardous environment and assuring their safety. The second category deals with the constraints and special requirements involved with a suited crewman operating flight hardware in a 1-G environment.

The author discusses design areas that deal with man rating a chamber, including fire suppression, emergency repress, emergency power, backups, reliable instrumentation and data systems, communications, television monitoring, biomedical monitoring, material compatibilities, and equipment supporting the Extravehicular Mobility Unit (EMU). The author also discusses the operational issues that are peculiar to manned testing such as test rules, test procedures, test protocol, emergency drills, availability of hyperbaric facilities, test team training and certification, engineering concerns for a safe mechanical and instrumentation buildup, hazard analysis, and Failure Modes and Effects Analysis.

The author addresses the constraints and special requirements involved with a suited crewman operating flight hardware in a 1-G environment. Facility systems, such as monorails to support the EMU, test article weight relief and translational aids, and calibrated metabolic simulators are discussed. Additionally, operational considerations such as chamber layout evaluations to assess crewman reach envelope and ambient functional, with suited crewman to validate procedures and evaluate the overall test team orchestration are addressed.

To demonstrate the significance and complexity of the facility and operational requirements, the author discusses the EVA Development Flight Experiment (EDFE) Thermal Vacuum Test Program performed in the Johnson Space Center's Chamber A facility. This test program certified the EVA flight hardware utilized on STS-45.





**N 9 3 - 1 5 6 0 3**

**ON-ORBIT DEPLOYMENT ANAMOLIES:  
WHAT CAN BE DONE?**

Michael Freeman  
**Electromagnetic Sciences, Inc.**  
Norcross, Georgia, USA

## ABSTRACT

Modern communications satellites rely heavily upon deployable appendage (i.e. solar arrays, communications antennas, etc.) to perform vital functions that enable the spacecraft to effectively conduct mission objectives. Communications and telemetry antennas provide the radio-frequency link between the spacecraft and the earth ground station, permitting data to be transmitted and received from the satellite. Solar arrays serve as the principle source of electrical energy to the satellite, and re-charge internal batteries during operation. However, since satellites cannot carry back-up systems, if a solar array fails to deploy, the mission is lost.

This article examines the subject of on-orbit anomalies related to the deployment of spacecraft appendage, and possible causes of such failures. Topics discussed shall include mechanical launch loading, on-orbit thermal and solar concerns, reliability of spacecraft pyrotechnics, and practical limitations of ground-based deployment testing. Of particular significance, the article will feature an in-depth look at the lessons learned from the successful recovery of the Telesat Canada Anik-E2 satellite in 1991.

## INTRODUCTION

Although spacecraft failures occur in many different ways, the majority of satellite anomalies in recent years have occurred during the early launch stages. Launch vehicles have exploded several seconds after liftoff; others have been destroyed remotely after going awry by safety engineers; and still some have never even left the launch pad. The unfortunate consequence of this destructive process is that the payload, usually one or more multi-million dollar communication satellites, is also lost.

In a similar respect, the spacecraft that have managed to safely make it into orbit amide the severity of vehicle launch, have themselves found unique ways to fail. The Japanese Superbird A satellite became useless in space after expelling critical oxidizing propellant in late December 1990, resulting in a \$170 million insurance claim by owner Space Communications Corporation, Tokyo (ref. 1); electrical problems crippled the European Space Agency's (ESA) Olympus satellite in 1991 for two months, before ground engineers were able to regain control of the spacecraft (ref. 2); and propulsion problems caused the ESA Hipparcos satellite to be placed in the wrong orbit in 1989, forcing officials to resort to a "revised mission" in order for the spacecraft to achieve its objectives (ref. 3).

However, the most puzzling and subsequently the most unpredictable flight anomalies have generally involved malfunctions related to spacecraft appendage deployment (i.e. solar arrays, communication antennas, booms, etc.). Table 1 shows a partial list of spacecraft failures of late

(1980-present) which were attributed to their inability to deploy appendage on orbit. The table is based upon a previous database compiled by Thomas W. Trafton of the Aerospace Corporation (ref. 4). Of significance, the West German TVSat 1 satellite failed to deploy one of its two outer, four-segment solar array panels after orbital insertion by an Ariane 2 vehicle on November 20, 1987. This catastrophic event, which also prevented the satellite's receive antenna from being deployed, eventually forced the spacecraft's owners, the Eurosatellite European consortium, to abandon the satellite in space several months later. The satellite, valued at \$230 million, was eventually claimed as a \$51 million in-orbit insurance loss (ref. 5).

In April 1991, two well-publicized spacecraft deployment problems occurred which involved the Telesat Canada Anik-E2 satellite and the NASA Galileo Jupiter spacecraft. The Anik-E2 experienced difficulties deploying both of its K-band and C-band antennas, while ground controllers at the Jet Propulsion Laboratory (JPL) were unable to properly unfurl the high gain antenna of the Galileo spacecraft. Circumstances and events surrounding these failures have been well documented in public literature, and it would be redundant to re-examine them here. Also, the author feels that individuals within these two organizations are the best sources for such detailed information and mission status. However, several important lessons learned from the successful Anik-E2 recovery shall be discussed in a later section of this paper.

There have also been several less announced instances of spacecraft experiencing problems deploying appendage, most of these payloads were launched from the U.S. Space Transportation System (STS) or Space Shuttle. Due to the advent of the Space Shuttle in the early 1980s, numerous on-orbit catastrophes have been auspiciously avoided. Various satellites failed to deploy solar arrays, antennas, etc., when commanded, despite futile maneuvers by ground controllers. The Shuttle's Remote Manipulator Arm or "Canadarm", designed and built by Spar Aerospace of Canada, was a major contributor to the successful operation of these problem satellites. As demonstrated in 1984 by Space Shuttle Challenger astronaut, Sally Ride, the manipulator arm was used to shake free one of the 21-ft solar arrays of NASA's 2.5 ton Earth Radiation Budget Satellite (ERBS) (ref. 6).

Extra-vehicular activity (EVA) has also rescued several doomed spacecraft, when salvage attempts using the Shuttle manipulator arm were unfruitful. As an instance, in April 1991, U.S. Space Shuttle Atlantis astronauts, Jerome Apt and Jerry Ross, were forced to perform EVA to manually free the stuck high-gain antenna of the \$617 million NASA Gamma Ray Observatory, after orbiter maneuvers utilizing the Shuttle's manipulator arm did not shake it free (ref. 7). To NASA officials and owners of satellites launched from the U.S. Space Shuttle, the STS has definitely proved its utility. Without the benefit of the Shuttle's

EVA and manipulator arm capabilities, the mission success of several NASA launched payloads would have obviously been left in doubt. Many valuable lessons have been learned from these experiences and they will become key tools in the design of future reusable space orbiters, including the ESA's Hermes and Japanese HOPE spaceplanes.

In light of this string of on-orbit difficulties, there is a growing concern throughout the space community as to the source of such problems. But due to the random nature of such aberrations, there is not presently a trend for which one can find a common cause. The best that one can hope to do is concentrate on a particular type of spacecraft failure, in this case, deployment failures.

In accordance with this agenda, the author has chosen to limit the following discussion to appendage failures only. Since it has not been possible while preparing this paper for the author to review the literature fully in this field, the present review cannot claim to be exhaustive. It is intended only to examine probable causes and events surrounding the series of space anomalies, and suggest feasible solutions to preclude such disasters from occurring in the future.

## THE PROBLEM WITH DEPLOYABLES

Deployable spacecraft appendage such as antennas, solar arrays and booms perform many functions essential to mission success. Remote satellite operation is achieved through the use of RF communication and telemetry antennas to earth ground stations. In general, they provide the only communication link between Earth and the satellite. Booms are used to deploy scientific experiments, probes, sensors, antennas, etc.. Solar arrays are the primary electrical power source for the majority of spacecraft. They also charge the spacecraft's batteries, so that they can provide the energy necessary for a similar level of payload operation during eclipse periods. The importance of proper solar array deployment cannot be overemphasized in that, failure to deploy an array on-orbit ordinarily results in inability to accomplish mission objectives.

Although appendage devices are extremely critical to spacecraft orbital operation, they suffer from several inherent drawbacks. The most obvious is their increased mechanical complexity. Beginning in the early 1960s, spacecraft designs were initially very conservative. They were low-power, low-weight, mechanically simple and had on-orbit lifetimes of only 6 to 8 months. As launch vehicle maximum payload capabilities increased, so did the size and complexity of satellites. Today, solar array and antenna designers have continued to become more intricate and daring in their designs, despite the problems manufacturers are currently facing in deploying such devices on-orbit. In relation to scientific satellites, and to some extent communication satellites, the trend has been to achieve more objec-

tives with single missions, while attaining longer lifetimes in the harsh space environment, with extreme reliability.

Figure 1 shows an artist's impression of NASA's proposed Space Station Freedom, an ambitious joint venture between the U.S., Japan, Europe and Canada. The \$30 billion station will possess six solar arrays, each spanning 39 ft. W X 112 ft L, and an assortment of booms and antennas. In this scaled-down version of the newly proposed space structure (original configuration utilized 8 solar arrays), the solar arrays are the prime electrical source for the 56 Kilowatt power plant. Critics are concerned that if spacecraft manufacturers are currently having trouble coping with the relatively simple deployment problems they have recently faced, how can they realistically attempt to design and build such a complex structure as the Space Station?

Deployable components are also very fragile devices. They generally cannot support their own weight while in Earth's gravity. To prevent mechanical damage during vehicle launch, they must be kept in a stowed configuration, immobilized by various locking apparatuses (cables, pins, locking mechanisms, etc.). Once in space, these devices are released from their latched position through a series of carefully planned explosive charges (pyrotechnics). Deployment motors are designed to exert low forces on deployment mechanisms; usually only a few pounds. Centrifugal forces and speeds used to aid in the transition from the stowed transfer orbit configuration to full deployment are also kept low. Shock and vibration dampers are used to attenuate the mechanical loads experienced by the spacecraft as appendage reach their "end of travel". The appendage itself must exhibit low contact resistance and electrical noise during electrical transfer, and impose low torques on the spacecraft.

The sequence of appendage deployment is additionally important. During orbital transfer, a spacecraft must rely entirely on its batteries for power. Thus, deployment sequences must be performed within short time schedules. Also, the firing of pyrotechnics to deploy booms, antennas and solar arrays introduce small dynamic loads on the spacecraft. However, these firings must not adversely effect the operation of nearby structures, or interfere with the deployment of other appendage. The basis on which these sequence of events is planned is commonly the result of extensive computer analyses and deployment tests conducted on engineering and qualification models.

Figure 2 shows the ESA's European Remote-Sensing Satellite, ERS-1, deployment sequence during the "Launch and Early-Orbit Phase", or "LEOP". The sequence of deployments is driven primarily by the results of a pyrotechnic shock analysis, which showed that the Synthetic Aperture Radar (SAR) antenna could be deployed with the solar array already out, but the array drive mechanisms had to be locked. The ground deployment testing of the SAR is shown in figure 3. Other important factors include critical timing, satellite space visibility

to one (located in Santiago de Chile) of seven different ground stations, battery-powered deployment, and thermal stability. The four antenna and solar array deployments were activated by pyrotechnics and spring forces (ref. 8).

In addition to the forementioned difficulties, appendage deployment mechanisms are also sensitive to the thermal environment conditions imposed during space operation. Thermal gradients, high and low temperature extremes, and the high vacuum of space can cause mechanical elements to lock or stall, or metal surfaces to weld together. To preclude such catastrophes, exhaustive thermal balance and thermal vacuum testing are done at system level prior to launch, to ensure proper operation once in space.

## PROBLEM SOURCES

The 1986 U.S. Space Shuttle Challenger accident left a vivid impression in the minds of many that space operations are not free from catastrophic failures. This incident, along with failures of several expendable launch vehicles which included the European Ariane Rocket, U.S. Atlas/Centaur and Titan rockets compelled launch vehicle manufacturers world-wide to make internal assessments of their own quality, safety and reliability programs.

Following the two year hiatus imposed by the Challenger accident, the number of launch vehicle failures decreased significantly during the latter half of the 1980s. While this trend has continued into the 1990s, a new series of problems have recently emerged — spacecraft failures. The successful launches of the late 80's seemingly gave manufacturers a false sense of confidence concerning the orbital performance of spacecraft. The latest chain of failures has forced a shift in directives for those involved in satellite operations, and the question of space anomalies has now become a major issue.

As previously mentioned, the discussion in this paper is restricted to only those failures resulting from the spacecraft's failure to deploy appendage. Even with such a narrow span of spacecraft failures, the realm of conceivable reasons for satellite deployment problems are far too extensive for discussion here. For the sake of simplification, we shall examine several known factors that can be directly attributed, or highly suspected to be, possible causes of on-orbit spacecraft appendage failures:

- a) mechanical launch loads
- b) on-orbit thermal and solar effects
- c) inadequate ground-based testing
- d) onboard spacecraft pyrotechnics
- e) spacecraft outgassing.

## MECHANICAL LAUNCH LOADS

In general, spacecraft are subjected to the most damaging mechanical loads during the launch period. Due to their

delicate nature, satellite appendage is particularly susceptible to dynamic launch loading. However, since very few spacecraft are ever returned to Earth, and satellite repair and rescue missions such as demonstrated by the U.S. Space Shuttle are far and few between, the extent of launch loading damage to these devices is not a factor easily determined. But, past experience has shown that launch conditions have produced profound effects on spacecraft. For example, the first cluster of the U.S. Skylab, launched in 1973, suffered extensive physical damage as a result of the severe vibroacoustic environment experienced by the structure during launch from a two-stage Saturn 5 rocket. The launch vibrations caused the workshop's meteoroid/thermal shield to be torn away, which in turn ripped away one of the pair of solar array wings and caused the other to be jammed in a partially open position by debris. Two astronauts later conducted EVA to free the jammed solar panel (ref. 9).

In terms of causes of some of the current appendage deployment problems, only one is considered suspect to the effects of mechanical loading. The NASA Galileo Jupiter spacecraft is presently speeding towards Earth for a December 1992 gravitational-boost flyby, without the use of its high gain antenna (HGA), stuck in a partially unfurled position. Figure 4 shows a photograph of the flight antenna fully unfurled at JPL, Pasadena, California. Lateral vibrations induced to the HGA structure during the four cross-country truck trips the spacecraft made between California and Florida, have presumably worn away the dry lubricant (molydisulfide) that allows the HGA rib support pins to freely disengage from the central mast during deployment (ref. 10).

It should be noted that the majority of the deployment problems previously outlined in table 1 were discovered during the first few hours on orbit, during the transfer orbit sequence. This has led many to believe that the cause of the events occurred prior to orbital placement. In this respect, the launch environment is deemed a logical problem source. But again, no conclusive data is presently available to confirm this theory.

The high-intensity noise pressure due to engine thrust or aerodynamic forces are the primary sources of spacecraft structural vibration. But, generally speaking, the vibroacoustic launch environments and corresponding design precautions are regarded as being reasonably well understood by the modern engineering community. Each have been heavily documented in literature over the past two decades, many valuable lessons learned have been applied, and a high level of confidence is now believed to exist in this area. Also, aside from the previously mentioned Galileo situation, the present failures in question are not considered to be vibration-induced. Thus, an analysis in terms of vibration and acoustic related effects will be precluded from this discussion.

One dynamics area that is of concern, and where consid-

erable research has been devoted over the past few years is pyrotechnic shock. Pyrotechnic shocks or "pyro" shocks, are very short-duration, high-frequency shocks produced by certain flight events such as engine ignition, explosive separation of booster stages and the release and deployment of satellites and appendage. Typically, primary attention is given to the shock transients experienced by the spacecraft during the vehicle launch stage, whereas on-orbit loads are considered to be of lower-level and less of a threat to the structure.

Charles Moening of the Aerospace Corporation, El Segundo, California, completed a study in 1984 on the cause of failure of eighty-eight (88) U.S. Air Force (USAF) spacecraft and launch vehicles, under USAF Contract No. F04701-C-0084 (ref. 11). One of the most astounding discoveries of Moening's investigation was that 85 of the 88 anomalies (96.5%) were found to be related to pyrotechnic events, or occurred shortly after shock events when the thermal and the vibration environments were relatively benign. The conclusions of Moening's findings, and the results of several meaningful dynamic investigations pursued by the Aerospace Corporation as a whole, have become key parts of MIL-STD-1540 (USAF), "Test Requirements For Space Vehicles", USAF environmental test tailoring and design handbooks, and MIL-A-83577 (USAF), "Test Requirements for Moving Mechanical Assemblies For Space". The overall effect of the suggested design and test guidelines detailed in these documents, and as implemented by suppliers of equipment to the Air Force, are suggested to have at least partially contributed to the launch vehicle success the USAF space program is presently enjoying.

## THERMAL AND SOLAR EFFECTS

### The Space Environment

Once on orbit, spacecraft must face an array of dissimilar and hostile environments, most of which are foreign to the Earth's atmosphere. Among the varied elements satellites must encounter during their orbital life are high and low temperature extremes, severe electromagnetic (solar) radiation, atomic particle radiation, low vapor pressure (high vacuum), and the absence of gravity. In relation to spacecraft appendage, the large temperature fluctuations that can occur when the satellite moves into the shadow of the Earth during an eclipse are of primary importance.

During an orbital eclipse or as a consequence of the satellite's orientation in space, one side of the satellite, exposed to sunlight, may be at about +150°C whereas the opposite side, in the shadow and facing the blackness of space, may be at -120°C (ref.12). Such large changes of thermal gradients between stationary and rotating components (solar array and antenna drive shafts), have been known to cause unpredictable behavior that includes increased loads, bear-

ing friction and resistance torque on moving surfaces. Also, since deployables extend from the body of the spacecraft they, in general, have low thermal capacities and rely mainly on passive thermal control. Thus, the proper choice of materials and space lubricants are vital keys to appendage on-orbit operation.

### Tribology\*

The important and critical spacecraft functions provided by deployable appendage involve the relative movement of surfaces in contact. In orbit unlubricated metal surfaces can rapidly weld together or exhibit high friction and wear. Tribology is the science and technology of touching surfaces in relative motion, the main topics being friction, lubrication and wear. A knowledge of tribology is therefore vital to successful spacecraft design and operation. Since 1972, researchers at the European Space Tribology Laboratory (ESTL), England, have done extensive R&D and thermal vacuum testing involving the behavior of spacecraft mechanisms and lubricants. As noted by Dr. Rob Rowntree of ESTL, "tribology has an essential role in the modern spacecraft industry and is, or should be, an integral part of the design process. It is not a process to be added when the design is complete" (ref.13).

It is beyond the scope of this article to assess all the prevalent aspects of tribology, thus for this discussion, only two major areas of tribology shall be considered: space mechanisms and lubricants.

Spacecraft mechanisms are generally made to be non-reversible. This is due to the fact that satellites are primarily not designed to be recoverable, thus their appendage is intended to remain in a locked position for the duration of their orbital life. Early spacecraft had few moving parts and very short lives. Mechanisms were relatively simple and conventional terrestrial vacuum lubricants were initially adequate. Today, the mechanical complexity of satellites have increased dramatically. Since redundancy of large satellite appendage such as solar arrays is not possible, parallel or serial duplication of their associated drive and deployment mechanisms is employed to provide a higher level of reliability. Sound tribological practices and testing conducted prior to spacecraft design completion have contributed significantly to the improved operation of spacecraft mechanisms in the low temperature, thermal vacuum of space.

The reliable rotation of solar arrays, gimbals, scanning mechanisms and momentum wheels in the extreme coldness of space is highly dependent upon the lubricant used on bearing or mating mechanical interfaces. The two major classes of space lubricants are dry/solid film and liquid/fluid lubricants. The primary space solid lubricants presently used in industry are MoS<sub>2</sub>, PTFE and Pb (Lead). Major types of liquid lubricants include refined mineral oils, synthetic oils (silicones), esters and perfluorinated

polyethers.

Table 2 outlines the pros and cons of dry/solid and liquid/fluid lubricants. As noted, only solid lubrication is practical for spacecraft mechanisms used at cryogenic temperatures. Another substantial advantage dry lubricating films is that when applied to bearings, the resulting torques are independent of temperature and rotational speed. Also, for certain types of cleanliness requirements, dry lubricants are preferred. However, dry lubricants perform poorly in air, and care in handling must therefore be exercised during the ground test phase where, in addition, much greater loads than in orbit can be encountered. Some of the pros of liquid lubricants are they that allow good radial thermal conductance, produce low torque noise in rotating bearings, and can be used in air. On the down side, the viscosity of fluids varies considerably with temperature which is unacceptable in some applications. Also, liquid lubricants have a small operational temperature range.

**\*Note:** Section based on tribology research, testing and published literature issued by the European Space Tribology Laboratory, UK.

## LIMITATIONS OF LABORATORY TESTING

Ground-based testing accounts for roughly 25-30% of the total cost of a spacecraft, with the average price of a modern communications satellite being in excess of \$60 million. Thus, the cost-effectiveness of exhaustive environmental testing such as vehicle level vibration, acoustic and thermal vacuum testing is easily demonstrated in relation to the satellite's high price tag, and possible financial repercussions of an on-orbit insurance loss.

The key to the effectiveness of any laboratory test is that it be representative of the intended operating environment of the test article. The size and complexity of satellite appendage often requires unique simulation techniques to achieve this objective. While the quality and confidence in space simulation test methods have progressed dramatically since the early 1960s, limitations still remain.

### Vibration Testing

Vehicle-level vibration testing is suggested to provide the most accurate simulation of launch conditions. Due to the increasing size and weight of today's satellites (3-5 tons), multi-shaker vibration test systems have become the norm. But, true launch vibrations occur simultaneously in multiple spacecraft axes, thus requiring the use of a multi-axis vibration test facility for comparable laboratory reproduction.

Until recently, spacecraft manufacturers have been without the capability to excite an entire space satellite concurrently in all three orthogonal directions. Figure 6 shows a photo of the Japanese National Aeronautics and Space

Development Agency's (NASDA) Vibration Test Facility at the Tsukuba Space Center, Japan. The system, which became operational during the summer of 1991, is capable of testing satellites weighing up to 4.5 tons in all three axes (X,Y,Z), without having to reposition the test article. The NASDA installation, designed by the team of Ling Dynamic Systems, UK and Akashi Seisakusho, Japan, employs ten (10) - 48,000 lbf electrodynamic shakers coupled to a cubic vibration table offering a test area of 9 m<sup>2</sup> (96 ft<sup>2</sup>). Presently, it is the largest multi-shaker system in the world (ref.14).

The European Space and Research Technology Centre (ESTEC), the Netherlands, the environmental testing arm of the ESA, is currently pursuing many of the same unique benefits demonstrated by the NASDA system in their proposed Hydraulic-Shaker Test Facility for testing the large Ariane payloads, such as the Hermes Spaceplane. Once complete, the ESTEC vibration system will utilize several long-stroke, high force hydraulic exciters to simulate spacecraft launch conditions.

Another shortcoming of vibration testing is one that does not involve the application of vibration, but instead the decision of whether to apply electrical power to the satellite during test. Moening's forementioned study on Air Force spacecraft notes that powering-up satellites systems during vibration testing, while complicating the tests, has made it possible to detect 'mission-catastrophic' anomalies such as electrical shorts which would have occurred in the high acoustic and vibration environment of a launch (under normal circumstances, power is not applied to satellite appendage or electrical systems during launch). The objective of continuous monitoring of perceptive parameters is to detect intermittent failures that may appear normal during the initial on-orbit checkout. Thus, it is to be used as a diagnostic tool to reveal failures that would otherwise occur and go undetected during launch, only to surface later while the spacecraft is on orbit.

This change in directives is further spelled out in MIL-STD-1540B, of which personnel at the Aerospace Corporation were key contributors. As stated in the specification, for space vehicle qualification testing: "during the test, electrical and electronic components, even if not operating during launch, shall be electrically energized and sequenced through operational modes." However, the document also advises the non-application of power to those components or systems that might suffer damage during testing, due to energization.

### Pyroshock Testing

Pyrotechnic shock testing deficiencies have been outlined by several practitioners, including Moening (ref. 11), Chalmers (ref.15), Czjakowski and Rehard (ref.16). Moening's USAF spacecraft study revealed that inadequacies existed in the use of pyroshock for component, piece

part, qualification, and system level testing and screening. Chalmers conducted a review of pyroshock test techniques in 1990, which showed major limitations in terms of instrumentation measurement capabilities and methods presently being undertaken to increase the confidence of testing. Czajkowski and Rehard also observed several instrumentation problems which involved use of anti-aliasing filters and analog/digital analyzers. It was suggested that very high-frequency sampling rates preclude the use of the filters. The underlying consequence of these testing methodology and equipment limitations is that a possible undertest of the test article results, which does not adequately prepare the spacecraft for the shock levels experienced during launch.

In addition, engineers have also cited that certain pyroshock test specifications were too stringent, and not practical. As an example, the + 3 dB tolerance stipulated in USAF MIL-STD-1540A was widened to + 6 dB in Rev. B, because the previous specification was not realistic, extremely difficult for contractors to adhere to, and was not compatible with industry equipment and test repeatability.

### Deployment Testing

Various methods are used for deployment testing which include neutral-buoyancy testing, air-bearing support systems, and "zero-g" gravity compensation fixtures. There are drawbacks to each technique. Neutral-buoyancy tests have shown to be well-suited for astronaut extra-vehicular activity (EVA) training and space suit testing, but generally are not practical or feasible for most conventional space programs. They require large water reserves and are expensive to maintain. Air-bearing support systems (see figure 6) offer relative ease of operation and much lower system costs as compared to neutral-buoyancy cells. However, such setups are often large, bulky and complex. In addition, such intricate fixturing has been suspected of introducing added resistance loads to the device under test.

It has been concluded by the engineering community that it is virtually impossible to simulate the zero gravity ("zero-g") environment of outer-space in a laboratory test. As long as the test system is within the bounds of the Earth's atmosphere, there will always be some level of gravitational forces acting upon it. Thus, the objective of "zero-g" deployment testing is not so much to provide a true replication of the weightlessness of space, but to suspend the deployable device in a very low-gravity state by which forces acting upon it are considered negligible (this is generally achieved using 1-g off-loading, typically in the deployment mechanisms vertical plane). Although the test may not be representative of the environment (due to air drag, etc.), it does allow spacecraft designers to verify friction margins and appendage functionality.

The use of "zero-g" test rigs and fixtures have proven to be very efficient provided the test set-up is simple and there

is no variation of the potential energy of the item under test (i.e. center of gravity of the test item moves in the vertical plane). Figure 7 shows the "zero-g" test rig used for deployment testing of the ESA's OLYMPUS satellite, at the David Florida Laboratory in Ottawa, Canada. The test rig, designed and built by Spar Aerospace, Toronto, Canada, utilizes a series of constant load springs which were carefully balanced to allow the satellite's solar wings to take their on-orbit "zero-g" shape with little error (ref.17).

"Zero-g" test under ambient condition have been very fruitful, but there is doubt on the value of such test conducted under thermal vacuum conditions. The most important concern is the influence of the test rig on the test data. Since both the deployable and test rig will see virtually the same thermal conditions inside the chamber, the thermal influences of the test rig must be accounted for in order for the test to be considered valid. Also, when deployment tests are done in a thermal vacuum chamber, a certain thermal environment is generally chosen (usually, a cold or hot soak) which will deviate significantly from the real circumstances. Thus, it is often very difficult to create representative temperature gradients.

### Thermal Vacuum Testing

Rigorous thermal vacuum (T/V) testing has proved to be of great value in assessing the reliability of mechanisms under conditions which simulate the space environment. The major limitation of T/V testing has been the internal space capacities of modern chambers. Figure 8 shows the Galileo Jupiter spacecraft undergoing T/V testing in the Space Simulator Chamber at JPL. The 25-ft Space Simulator, built in 1961, has a test volume of 20-ft D X 25-ft H. Throughout its many years of operation, the facility has been sufficient for most spacecraft designs. However, the increasingly wide span of modern solar arrays and size of large deployable structures such as Synthetic Aperture Radar (SAR) antennas makes practical testing of these devices in a T/V chamber, even the size of the JPL installation, unfeasible. Partial solar array deployments are generally performed under vacuum conditions, with RF antennas being the only assemblies able to be fully deployed.

T/V chambers capable of handling extremely lengthy deployables are still a long ways from practical development. However, progress has been made by various testing organizations in an effort to overcome this deficiency. For example, in 1987, the ESTEC made operational the Large Space Simulator (LSS). The LSS, shown in figure 9, is the largest facility of its kind in Europe, with internal chamber dimensions of 33-ft D X 50-ft H. Uniquely different from most T/V chambers presently in existence, the LSS utilizes an advanced motion simulator to provide realistic solar and thermal profiles, and to simulate the relative spinning motion of satellites in space. Due to the volume of the LSS,

the ESA Hippacros satellite was able to be T/V tested in 1989, with its solar panels and telescope baffles fully deployed under simulated space conditions (see figure 10).

## SPACECRAFT PYROTECHNICS\*

For single-function mechanical operations, the efficiency, reliability and speed of pyrotechnic actuators ("pyros") are without parallel. The role of pyros is to aid in the release of long booms, large antenna dishes and solar arrays; open/close valves; push/pull loads; and sever wires and bolts used as launch restraints, etc. However, onboard explosive firings have themselves been seen as a source of appendage problems. Self-induced shocks occur principally when pyrotechnic and pneumatic devices are actuated to initiate the forementioned events. But, spacecraft dynamic analysis utilizing computer models and results of ground testing, have shown that these acceleration levels are much lower those induced during launch, and exhibit little damage potential to the structure. Additionally, shock and vibration dampers are commonly employed to limit the effects of pyrotechnic discharges.

The reliability of spacecraft pyrotechnics has also been suspect to some observers. The fundamental requirement of a pyrotechnic device is that it detonate reliably when commanded and not under any other circumstance (inadvertent firing). Although very few cases of non-firing of pyrotechnics on-orbit have ever been reported, the predominate question generally asked by ground controllers during the early moments of any deployment problem is, "Did the pyros fire correctly?". This is because many times the only indication controllers have as to whether a pyrotechnic explosive actually detonated as commanded, comes from the mechanical linkage of the appendage in question. Electrical signals fed back from the closing of micro-switches as the deployable moves into its operational position, signifies pyrotechnic release as well as appendage deployment. However, other, more indicative methods of verifying pyro firings, are presently being pursued by several spacecraft manufacturers.

Unlike all other hardware onboard a spacecraft, explosive-based components are only usable once. That is to say, the pyrotechnic to be used for flight can never be fully tested before it is required to operate in space. Confidence can only be generated by the performance of like items fired for that purpose. Generally, a large number of samples must be fired in the test program to build any significant level of confidence. The test program must be comprehensive and complete; merely firing a few items under given conditions will not suffice. Also, the number of test items must be large enough to allow firings under all the various chosen conditions. But, even after such extensive testing, there is still no guarantee that the actual units used in the spacecraft will function correctly in orbit. Thus, for reasons of safety and reliability, pyrotechnics are also duplicated in series or

in parallel, according to defined requirements of failure tolerance.

**\*Note:** Section based on reference 18

## SPACECRAFT OUTGASSING

Spacecraft outgassing, or "ballooning" as is sometimes referred, is a phenomenon that occurs as a spacecraft transitions from one atmospheric pressure level to another. The most common form of outgassing generally happens during vehicle launch. Under the normal air pressure conditions of Earth, components such as insulation thermal blankets fit loosely over the body of the spacecraft, and are sealed. The only openings in the blanket are located around rotating shafts, etc. It is known that large areas of material with high outgassing rates are only pumped through such small orifices in space. During ascent into space, the air pressure surrounding the satellite decreases, causing a pressure imbalance between the interior and exterior of the spacecraft. This forces the air trapped beneath the blanket to be pushed outward, thus the ballooning effect is created. While it is understood that some outgassing will always occur, obviously the looser the fit of the thermal blanket to the spacecraft, the more pronounced will be the ballooning. The importance of this scenario is that the blanket will generally stay in this inflated state as long as it remains in space. The danger to appendage is that when instructed to deploy, there is a much greater chance of it snagging on a piece of the blanket, possibly creating an incurable deployment problem.

Another problem with outgassing is that the condition is very difficult to detect during ground testing. Because of the high pumping rates required (the pumping speed of space is essentially infinite), the event is extremely difficult to simulate with a thermal vacuum chamber. The problem becomes more of a challenge as the size of the chamber increases, which is necessary for vehicle-level testing.

A great deal more research needs to be done in this area (Scialdone (ref. 19) and other researchers have done significant studies in this area), which has potentially catastrophic effects on future satellites. Keeping in mind that the outgassing rate varies with each spacecraft, and is influenced by the size and complexity of the design.

## LESSONS LEARNED FROM ANIK-E2

On April 12, 1991 Telesat Canada developed difficulties with the K-band and C-band antennas of its Anik E2 satellite not being able to deploy either after the initial command sequence was sent to the satellite. An anomaly team comprised of engineers from the spacecraft design team, Spar Aerospace Ltd., Canada and GE Astro Space, New Jersey, was quickly formed. The K-band antenna unexpectedly freed itself on April 19, while the C-band antenna



remained stuck. The GE/Spar team later utilized a series of thermal and dynamic maneuvers to finally free the antenna on July 3, 1991. The extensive series of measures, which included a 'dual spin turn' reversal of the satellite, were previously unprecedented for a recovery attempt of a commercial satellite (ref.19).

Although the satellite was nearly claimed as an \$208 million (\$240 million Canadian dollars) insurance write-off, several valuable lessons were learned from the Anik experience.

**1. Technical ingenuity is the key.** The successful deployment of the Anik's C-band antenna was the result of the quick response, timely decisions and carefully planned recovery maneuvers issued by the 12-man team of Spar Aerospace and GE Astro Space engineers. The GE/Spar team, whose activities were coordinated by Doug Jung of Spar, made several critical decisions during the early moments of the Anik experience, including the recommendation to Telesat Canada officials not to deploy the satellite's solar arrays. The extension of the spacecraft's solar panels would have prevented any viable use of dynamic spin maneuvers to free the stuck antenna. In addition, meticulous calculations were also performed by the team used to estimate the rate of spin necessary to overcome the resistance of the presumed thermal blanket holding the appendage, without damaging the antenna during the deployment attempt.

What can be learned by other spacecraft manufacturers is that their most valuable asset is indeed their employees. The best resources available to help remedy an appendage problem usually comes from within the organization(s) responsible for the design and test of the spacecraft. Thus, in general, the same technical staff that is responsible for the satellite's construction, should be utilized in the recovery effort.

**2. Satellite maneuvers are effective salvage tools.** The Anik E2 recovery experience was not the first instance of dynamic and thermal maneuvers being used to free appendage. However, the exercise was unprecedented for the use of exhaustive procedures. The immediate lesson learned is that, although the satellite may be sufficiently insured for a loss, the owner should pursue every conceivable exercise (within the design limitations of the spacecraft and with concurrence of insurance underwriters) to achieve recovery. Secondly, since such maneuvers have been met with success, they should continue to be used to the extent possible.

**3. Innovative spacecraft designs are necessary.** The Satcom 5000 satellite platform, designed and manufactured by GE Astro Space, was clearly a well thought-out design that contributed greatly to the success of the Anik. Had the

solar arrays not been designed to be operational in a stowed position, the owners would have been forced to deploy the solar panels before the batteries were depleted. As a consequence, maneuvers to free the stuck antennas would have been virtually impossible to accomplish with the solar arrays extended.

As previously mentioned, spacecraft appendage designs are generally non-reversible and very unforgiving. As an example, the NASA Galileo spacecraft design does not allow for the remote deployment reversal of its high gain antenna. Had such a capability been employed in its design, the present status of the antenna might have easily been corrected. In light of such instances, spacecraft designers should make detailed evaluations of present and future designs, and employ creative techniques to allow potential appendage problems in space to be recoverable.

**4. Satellite spares and ground simulation are of vital importance.** Remote failure analysis of a satellite is a task often difficult to visualize without some frame of reference. This is mainly due to the fact that telemetry data read back from the satellite is often non-conclusive. The Anik-E1, which was to be launched several months following the Anik-E2, was effectively used to pinpoint the cause of the Anik-E2 failure. Also, numerous environmental tests utilizing the Anik-E1 were conducted at the David Florida Laboratory, Ottawa, Canada. These tests ascertained the antenna could be deployed under various failure scenarios; quantified the forces required and the forces it could withstand; and verified any improvements that would be made on Anik-E1.

It should be noted that engineers at JPL are currently utilizing the flight spare of the Galileo spacecraft antenna to create an accurate picture of the antenna deployment situation. The spare is also being used to plan the course of feasible deployment events during the spacecraft's second Earth flyby in December 1992 (ref. 10).

Thus, the importance of functional flight spares available on the ground cannot be over emphasized. The ability to identify the source of an deployment problem, and undertake recovery maneuvers in the laboratory without consequence to the in-orbit spacecraft, make them invaluable tools.

## WHAT CAN BE DONE?

Spacecraft failures are perceived as technical risks of being in the satellite business. But, there are still steps that can be taken by owners and manufacturers to help reduce these risks.

**1. Continuation of spacecraft technical meetings, symposiums and workshops.** Space symposiums and conferences such as the one today are definitely an outgrowth of the tough times experienced in the 1980s, and are a vital

part of a plan for industry as a whole to learn and grow together. Spacecraft safety and reliability should continue to be the main focus, with increased participation by other related technical societies. In particular, those organizations specializing in areas such as space tribology and structural mechanics.

**2. Public disclosures should be made by manufacturers that have experienced failures, to help preclude future anomalies.** The consensus is, when it comes to matters of this nature, it is in the interest of all industry to have an open discourse concerning spacecraft failures. Despite the competitiveness of the space market and the nature of the business, there are no true winners or losers when one speaks in terms of a loss of a satellite. In the end, worldwide insurance premiums will increase, making it difficult for all manufacturers to obtain spacecraft insurance, and the overall confidence level in space travel will be again be left in doubt.

**3. Increased test effectiveness.** Testing builds a higher level of confidence, validates designs, and increases spacecraft reliability. System and vehicle level testing have shown the most promise in evaluating the performance of appendage. As noted by Trafton (ref.4), many of the recent deployment failures could have been uncovered only by testing at the vehicle level, i.e., after the deployable was fitted to the spacecraft.

Although there is certainly a level of testing that a spacecraft manufacturer cannot go to because it is too cost prohibitive, efforts should also be taken to provide a closer simulation of the launch and space environments. Test stages should follow closely the sequence of events that the spacecraft experiences from launch to the end of its orbital life. For example, vibration, acoustic and pyroshock testing should be performed in the manner they will most likely occur during launch. In general, a satellite is subjected to a combination of dynamic environments. However, to simplify testing, they are usually simulated separately.

**4. Plan for failure.** There is generally a very narrow "window of opportunity" during the early stages of an event such as a solar array deployment anomaly (typically less than 24 hours), before spacecraft batteries are depleted. This does not give manufacturers much time to assembly an anomaly team or come up with an effective plan of recovery, if salvage attempts are to be successful. Thus, many of the owners of spacecraft that have experienced appendage-related problems have been caught totally off-guard.

In the future, it is foreseen that spacecraft anomaly teams will become as common an occurrence as design teams. They will be formed prior to vehicle launch, and possibly wait in a "standby" mode until needed. Once called into action, the probability of their success will rely heavily on

such factors as real-time data analysis, thermal and dynamic maneuvers (if necessary), and knowing the safety/design limits of the spacecraft.

## FINAL REMARKS

The intent of this article was to raise the general level of awareness concerning on-orbit appendage deployment problems. It was the author's hope to spark sufficient interest in the area such that spacecraft manufacturers would realize the seriousness of these aberrations, and the possible repercussions of dismissing them as mere random occurrences. Also, it is hoped that the lessons learned from these situations will help preclude future appendage problems, or at least provide owners and manufacturers with a better idea of how to deal with them.

## REFERENCES

1. Marcus, D.J., "Two Satellite Failures Expected To Spur Rise In In-Orbit Insurance Rates", Space News, February 4-10, 1991, p. 4,20.
2. Jampol, J., "Almost Lost In Space", Space Magazine, November- December 1991, pp. 21-24.
3. Van der Ha, J., "Implementation Of The Revised Hipparcos Mission At ESOC", ESA Bulletin No. 69, February 1992, p.9.
4. Trafton, T.W., "Moving Mechanical Assemblies For Space Vehicles: MIL-A-83577B Test Requirements", Paper delivered as part of presentation given to support the use of MIL-A-83577B in USAF space programs, 1991.
5. Lenorovitz, J.M., Mordoff, K.M., "Failure To Free Stuck Solar Panel Forces Germans To Abandon TVSat 1", Aviation Week & Space Technology, March 7, 1988, p. 57.
6. Turnhill, R., Jane's Spaceflight Directory 1987, 3rd Edition, 1987, p.57.
7. Asker, J.R., "U.S. EVAs Resume As Astronauts Help Deploy Satellite", Aviation Week & Space Technology, May.6, 1991, pp. 42-45.
8. Francis, R., et al., The ERS-1 Spacecraft and Its Payload", ESA Bulletin Number 65, February 1991, pp. 27-48.
9. Turnhill, R., Jane's Spaceflight Directory 1987, 3rd Edition, 1987, p.100.
10. O'Neil, W.J., "Project Galileo Mission Status", paper presented at the 42nd Congress Of The International

Astronautical Federation, October 1991 (IAF Document No. IAF-91-468).

11. Moening, C.J., "Pyrotechnic Shock Flight Failures", proceedings of 1984 IES Aerospace Testing Seminar. Study supported by the USAF Space Division under Contract No. F04701-83-C-0084.

12. Parker, T., "Some Experience Of Thermal Vacuum Testing Of Spacecraft Mechanisms", Vacuum, Volume 37, Numbers 3,4, 1987, pp. 303-307.

13. Rowntree, R.A., Roberts, E.W., and Todd, M.J., "Tribological Design - The Spacecraft Industry", 15th Leeds-Lyon Symposium, September 1988.

14. Freeman, M., "Unique 3-D Vibration Test System At NASDA, Japan", TEST Engineering & Management, August/September 1992.

15. Chalmers, R., "Measuring Pyrotechnic Shock: Why Is It So Difficult?", TEST Engineering & Management, August/September 1990, pp. 17,26.

16. Czajkowski, J., Rehard, J., "Pyrotechnic Shock Testing Equipment Limitations", TEST Engineering & Management, June/July 1989, pp. 20-23.

17. Marks, G., Anders, C., Draisey, S., Elzeki, M., "The Olympus Solar Array Development And Test Program", Proceedings of the 4th European Symposium, 'Photovoltaic Generators In Space', Cannes, September 1984 (ESA SP-210, Nov. 1984).

18. Cable, N., "The Use Of Pyrotechnics On Spacecraft", ESA Bulletin No. 54, May 1988, pp. 66-71.

19. Scialdone, J. and Kruger, R., Seventh Space Conference On Space Simulation, Los Angeles, 1974, NASA SP-336.

20. Gray A.M., "Recovering Anik E", Space Magazine, February-March 1992, pp. 18-21.

## ACKNOWLEDGMENTS

The author would like to express his deepest appreciation to the following individuals for their support and assistance in this project: Allan Piersol, Richard Chalmers, Harry Himelblau, Bruce Batrick, Doug Jung, Carol A. Schmidt, Dr. Rob Rowntree, William J. O'Neil, John W. Harrell, Duncan G. Adams, William F. Bangs, Bill Elsen, Charles Moening, D. Richard, R. Zwanenburg, John H. Paul, Dianne Chenevert, Dan Van Ert, Thomas W. Trafton, Michael Carroll and Vanessa A. Curry.

# TABLE 1

## SUMMARY OF SIGNIFICANT SPACECRAFT APPENDAGE DEPLOYMENT ANOMALIES

SPACECRAFT/ YEAR LAUNCHED	PROBLEM	CAUSE
APPLE (1981) #	Jammed Solar Array	Solar Array Latch Stuck
INSAT 1A (1982)#	Solar Sail Failed To Deploy	Inoperative Mechanical Latch
INSAT 1B (1983)*	Unable To Position Solar Array	Thermal Binding Of Deployment Mechanism
ARABSAT 1A (1985)*	Failure To Deploy Solar Array, C-band Antenna	Mechanical Interference
TVSAT 1 (1987)^	Failure To Deploy Solar Array	Deployment Latching Mechanism Failed to Unlock
OLYMPUS 1 (1989)*	Total Power Loss In One Solar Array	Electrical Short In Cable Harness
GALILEO (1989)#	High Gain Antenna Failed To Deploy	Cold Welding In Ball And Socket Joint
MAGELLAN (1990)#	Solar Array Failed To Latch	Microswitch Misadjusted
ANIK-E2 (1991)*	K and C-band Antenna Deployment Problems	Thermal Blanket Interference
JERS-1 (1992)*	Radar Antenna Failed To Deploy	Wrong Software Command Sequence

**Note:** Based on failure summary generated by T.W. Trafton of the Aerospace Company, 1991.

\* Problem resolved or full recovery of spacecraft achieved

# Spacecraft usable without functioning of deployable

^ Spacecraft claimed as loss

## TABLE 2

### RELATIVE MERITS OF SOLID & LIQUID SPACE LUBRICANTS

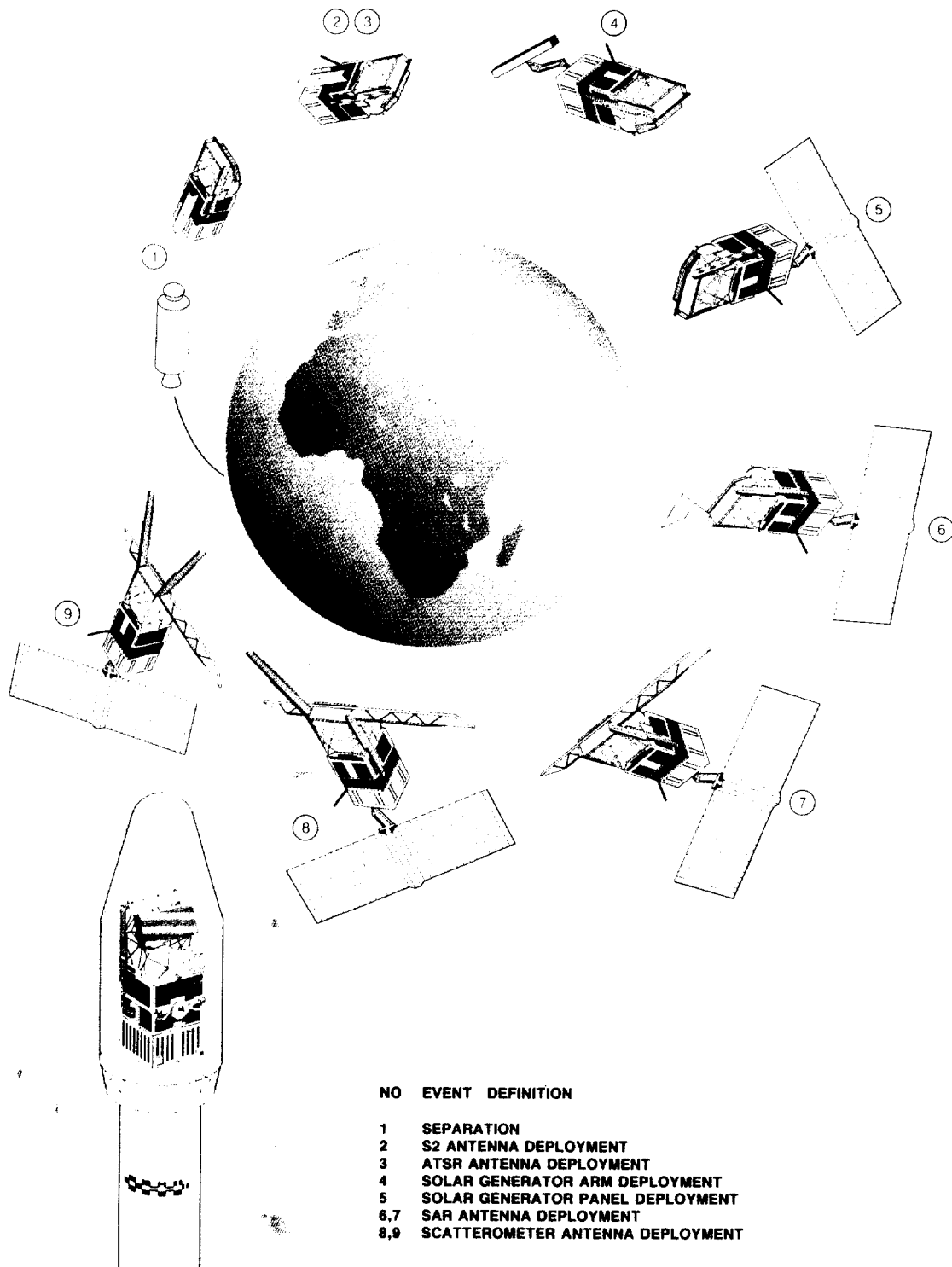
DRY LUBRICANTS	WET LUBRICANTS
NEGLECTIBLE VAPOUR PRESSURE	FINITE VAPOUR PRESSURE
WIDE OPERATING TEMPERATURE	VISCOSITY, CREEP & VP ALL TEMPERATURE DEPENDENT
NEGLECTIBLE SURFACE MIGRATION (DEBRIS CAN FLOAT FREE)	SEALS REQUIRED
VALID ACCELERATED TESTING	INVALID ACCELERATED TESTING
SHORT LIFE IN LABORATORY AIR	INSENSITIVE TO AIR OR VACUUM
DEBRIS CAUSES FRICTIONAL NOISE	LOW FRICTIONAL NOISE
FRICTION SPEED INDEPENDENT	FRICTION SPEED DEPENDENT
LIFE DETERMINED BY LUBRICANT WEAR	LIFE DETERMINED BY LUBRICANT DEGRADATION
POOR THERMAL CHARACTERISTICS	'HIGH' THERMAL CONDUCTANCE
ELECTRICALLY CONDUCTIVE	ELECTRICALLY INSULATING

NOTE: COURTESY OF THE EUROPEAN SPACE TRIBOLOGY LABORATORY.



FIGURE 1. ARTIST'S CONCEPTION OF SPACE STATION FREEDOM. (ARTIST-TOM BUZBEE)

Nominal operations sequence for the Launch and Early-Orbit Phase (LEOP)



**FIGURE 2. THE EUROPEAN REMOTE-SENSING SATELLITE, ERS-1, ON-ORBIT DEPLOYMENT SEQUENCE. (COURTESY OF THE EUROPEAN SPACE AGENCY AND ESA BULLETIN)**

ORIGINAL PAGE  
BLACK AND WHITE PHOTOGRAPH

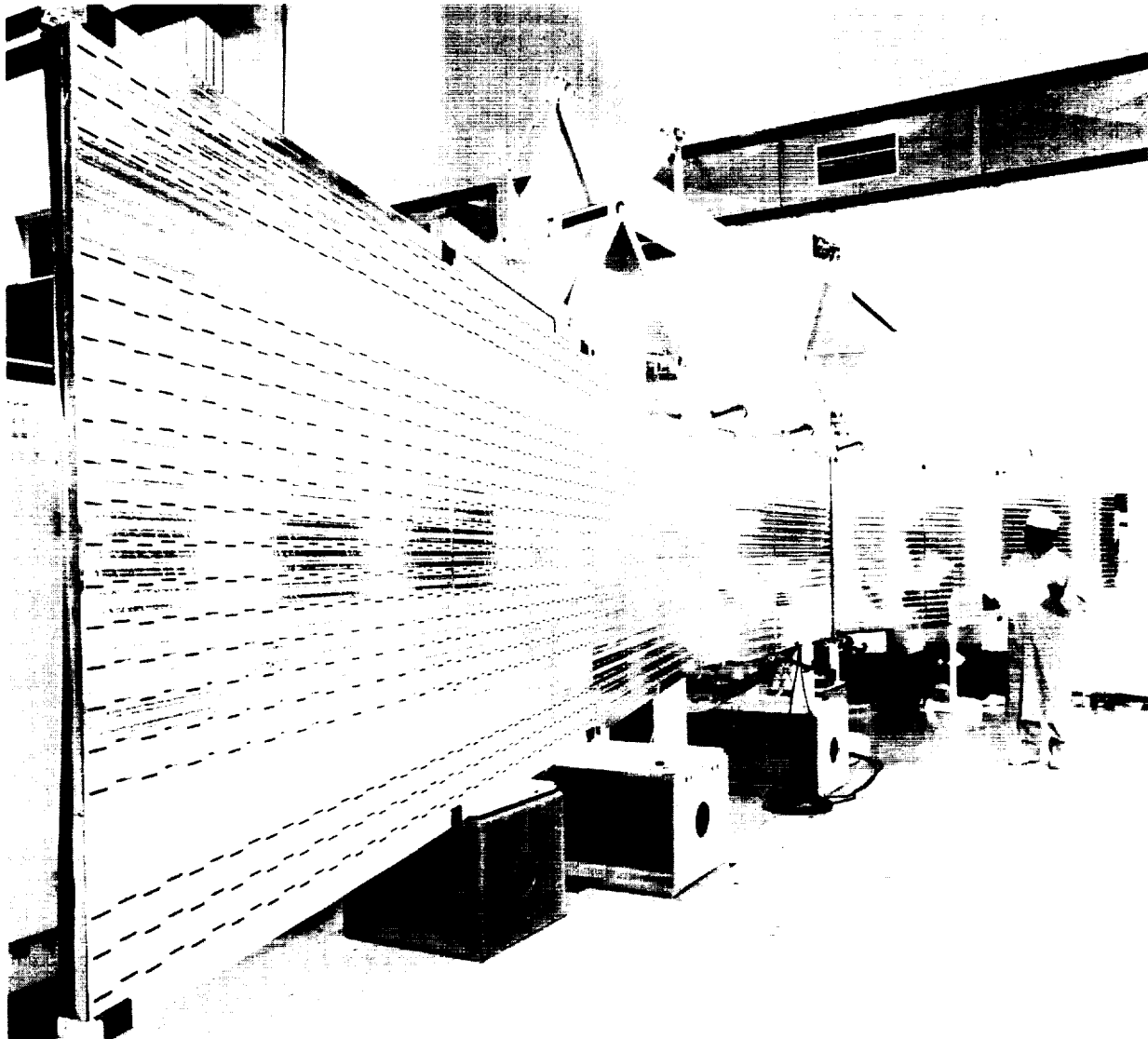
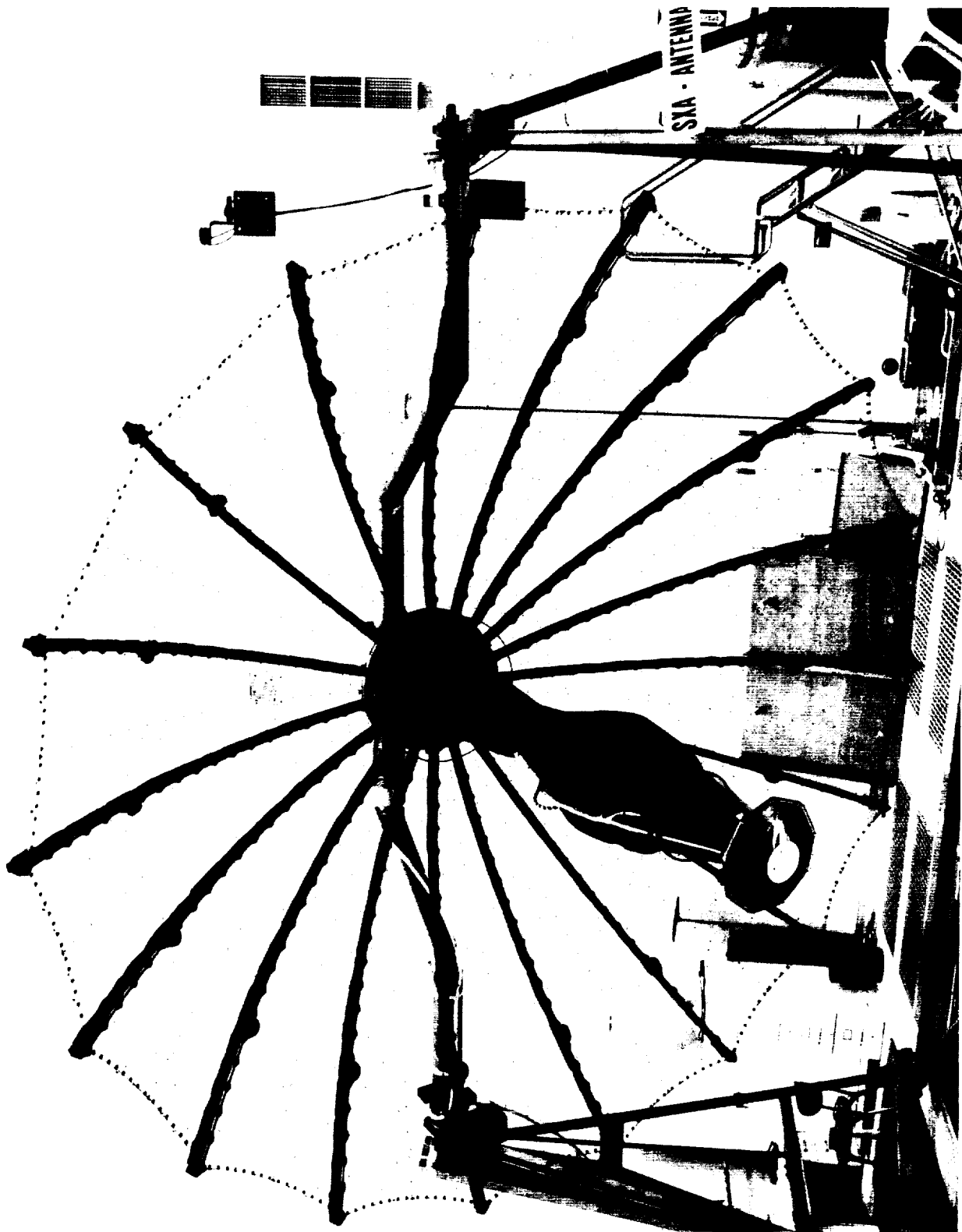


FIGURE 3. SYNTHETIC APERTURE RADAR (SAR) ANTENNA OF ERS-1  
UNDERGOING GROUND DEPLOYMENT TESTING. (COURTESY OF THE EUROPEAN  
SPACE AGENCY AND ESA BULLETIN)



ORIGINAL PAGE  
BLACK AND WHITE PHOTOGRAPH



**FIGURE 4.** FULL DEPLOYMENT OF GALILEO FLIGHT MODEL, HIGH GAIN ANTENNA (HGA) AT JPL. (COURTESY OF THE JET PROPULSION LABORATORY)

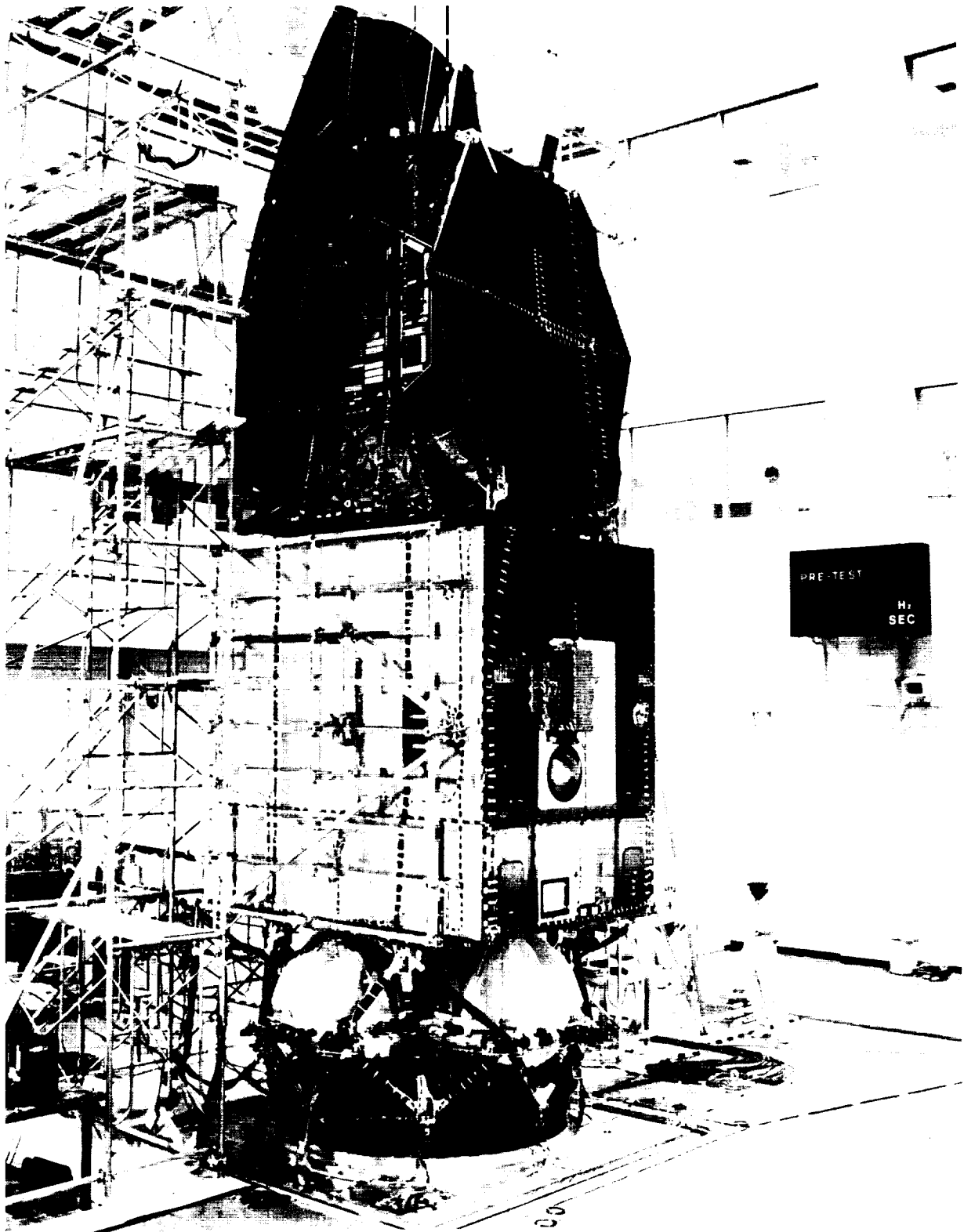


FIGURE 5. ENGINEERING TEST SATELLITE, ETS-1, UNDERGOING VIBRATION TESTING AT NASDA'S TSUKUBA SPACE CENTER, JAPAN. THE VIBRATION SYSTEM IS PRESENTLY THE LARGEST MULTI-SHAKER TEST FACILITY IN THE WORLD. (COURTESY OF THE NATIONAL SPACE DEVELOPMENT AGENCY, JAPAN)

ORIGINAL PAGE  
BLACK AND WHITE PHOTOGRAPH

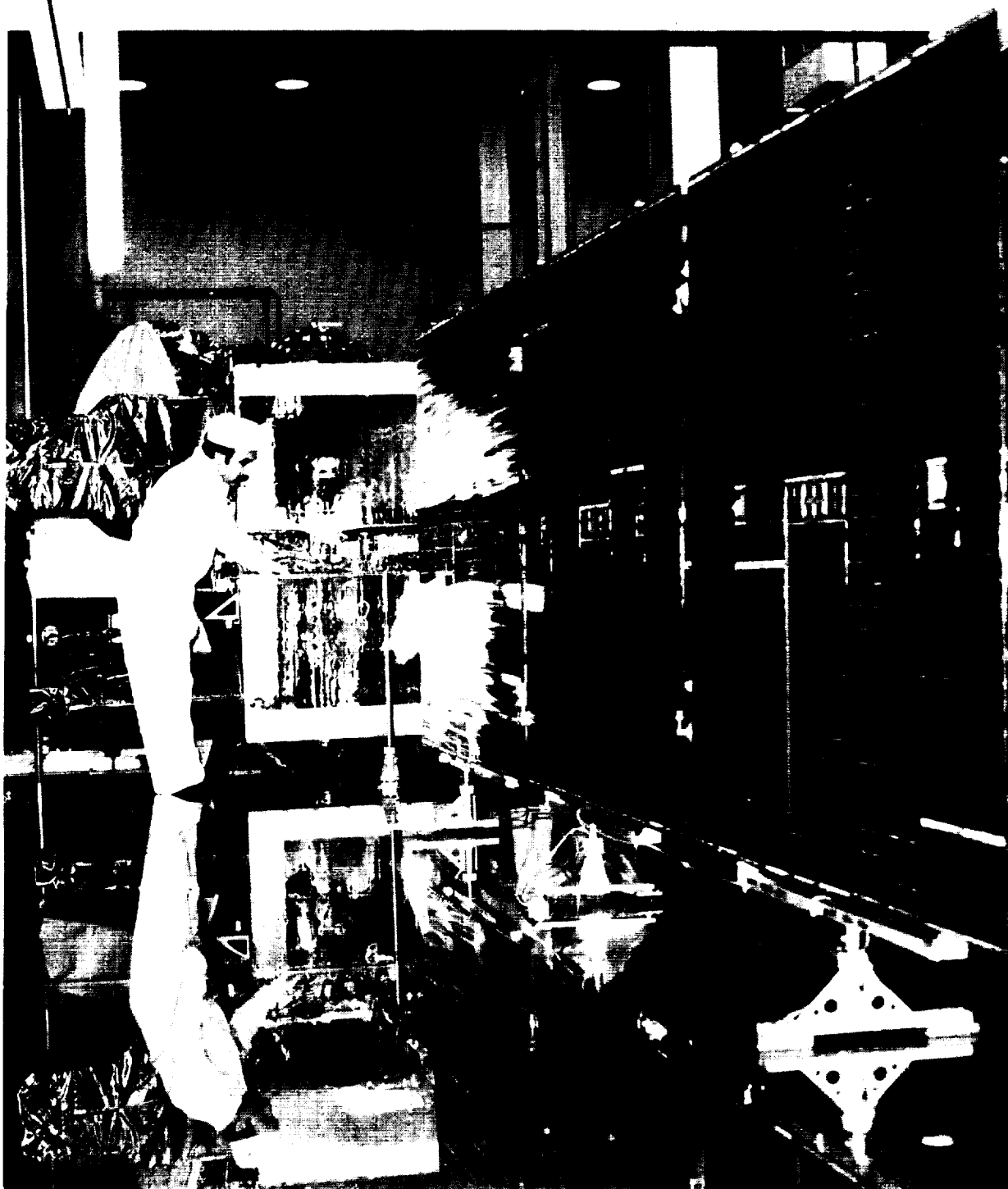


FIGURE 6. SOLAR ARRAY DEPLOYMENT TESTING USING AN AIR-BEARING SUPPORT SYSTEM AT GE ASTRO SPACE, NJ. (COURTESY OF GE ASTRO SPACE)

ORIGINAL PAGE  
BLACK AND WHITE PHOTOGRAPH

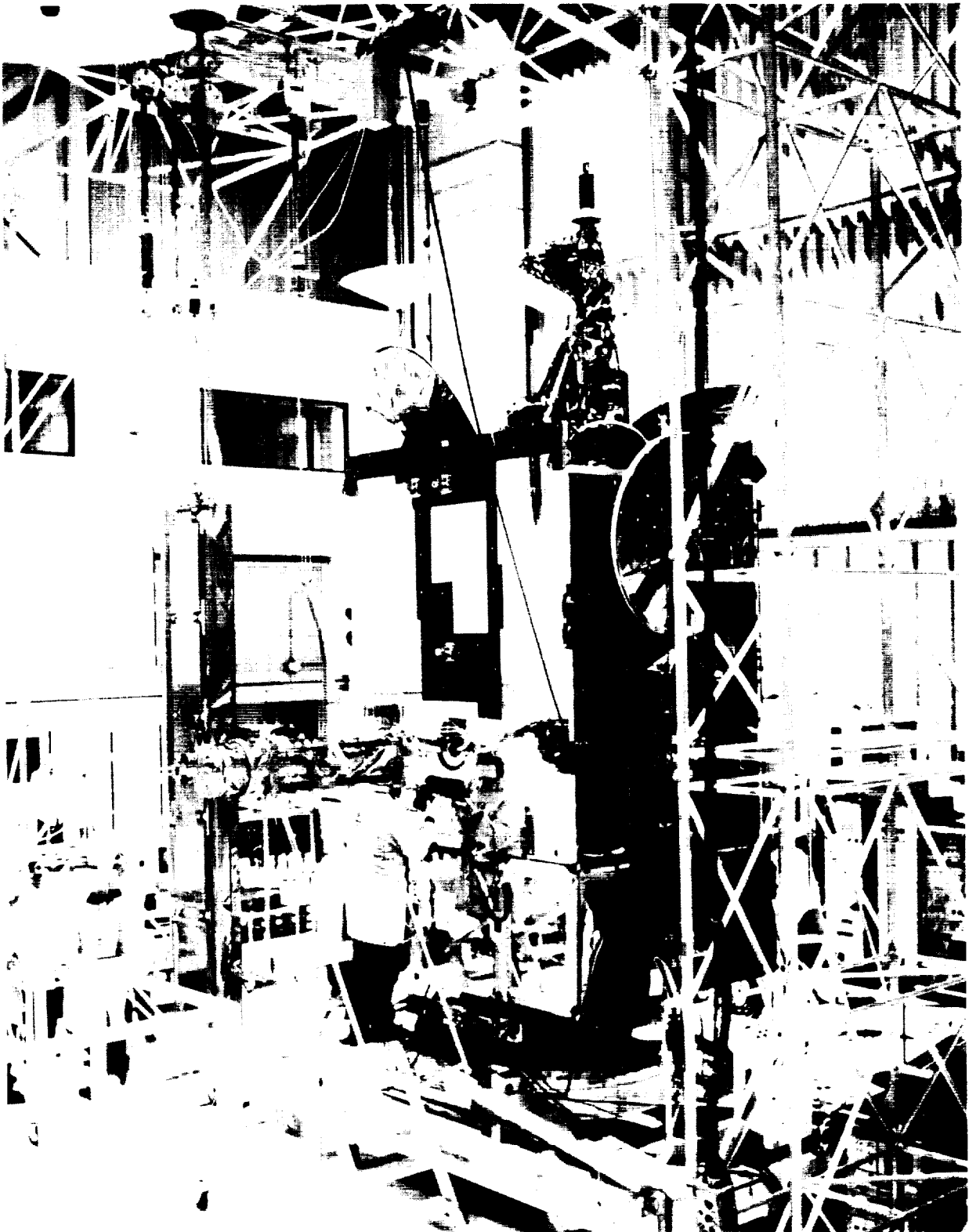


FIGURE 7. SPECIAL "ZERO-GRAVITY" DEPLOYMENT TEST RIG USED TO TEST OLYMPUS SATELLITE AT THE DAVID FLORIDA LABORATORY, CANADA. (COURTESY OF CANADIAN CROWN)

CENTRAL PAGE  
BLACK AND WHITE PHOTOGRAPH

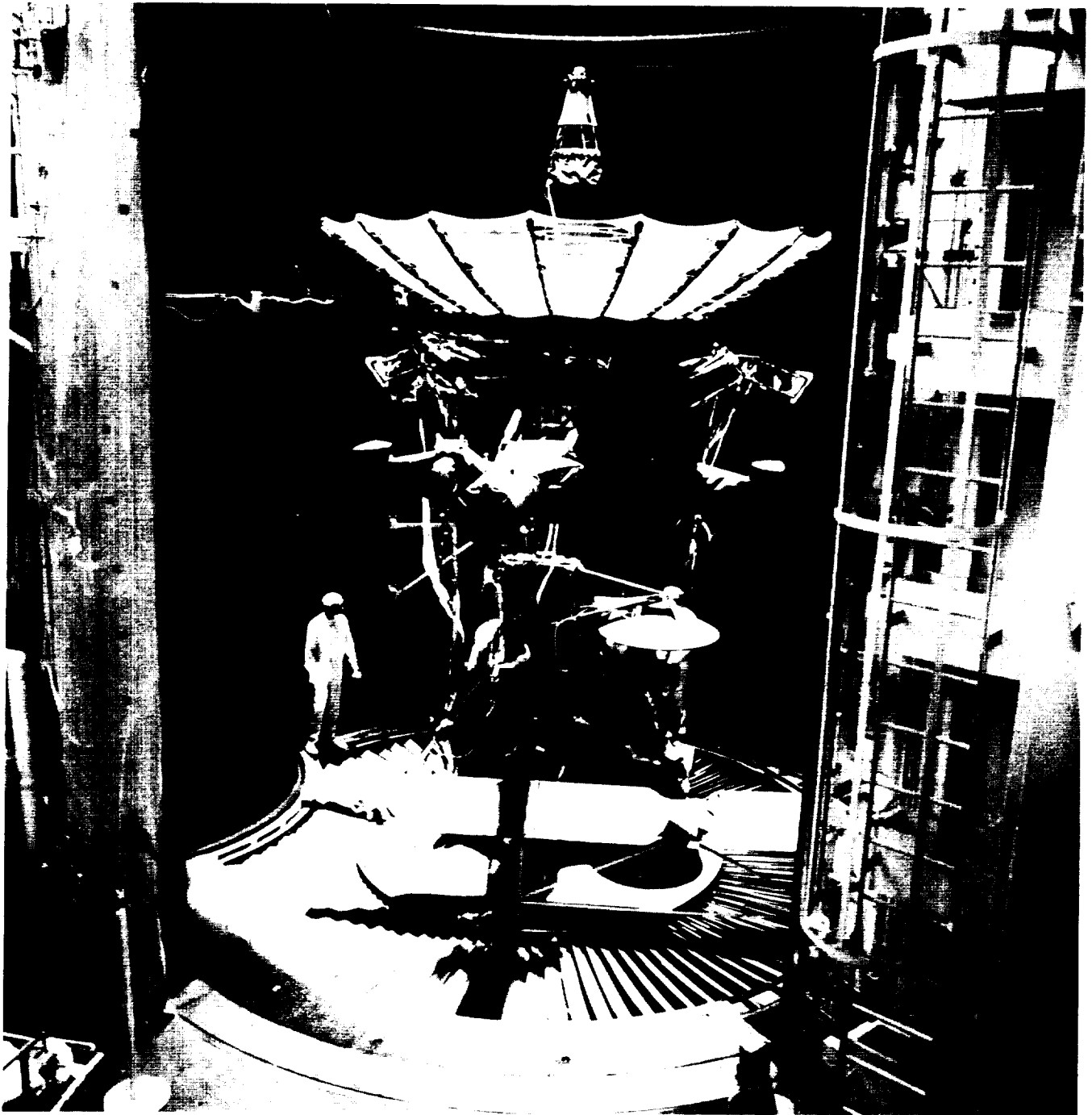


FIGURE 8. NASA GALILEO SPACECRAFT IN 25-FT SPACE SIMULATOR CHAMBER AT JPL. (COURTESY OF THE JET PROPULSION LABORATORY)

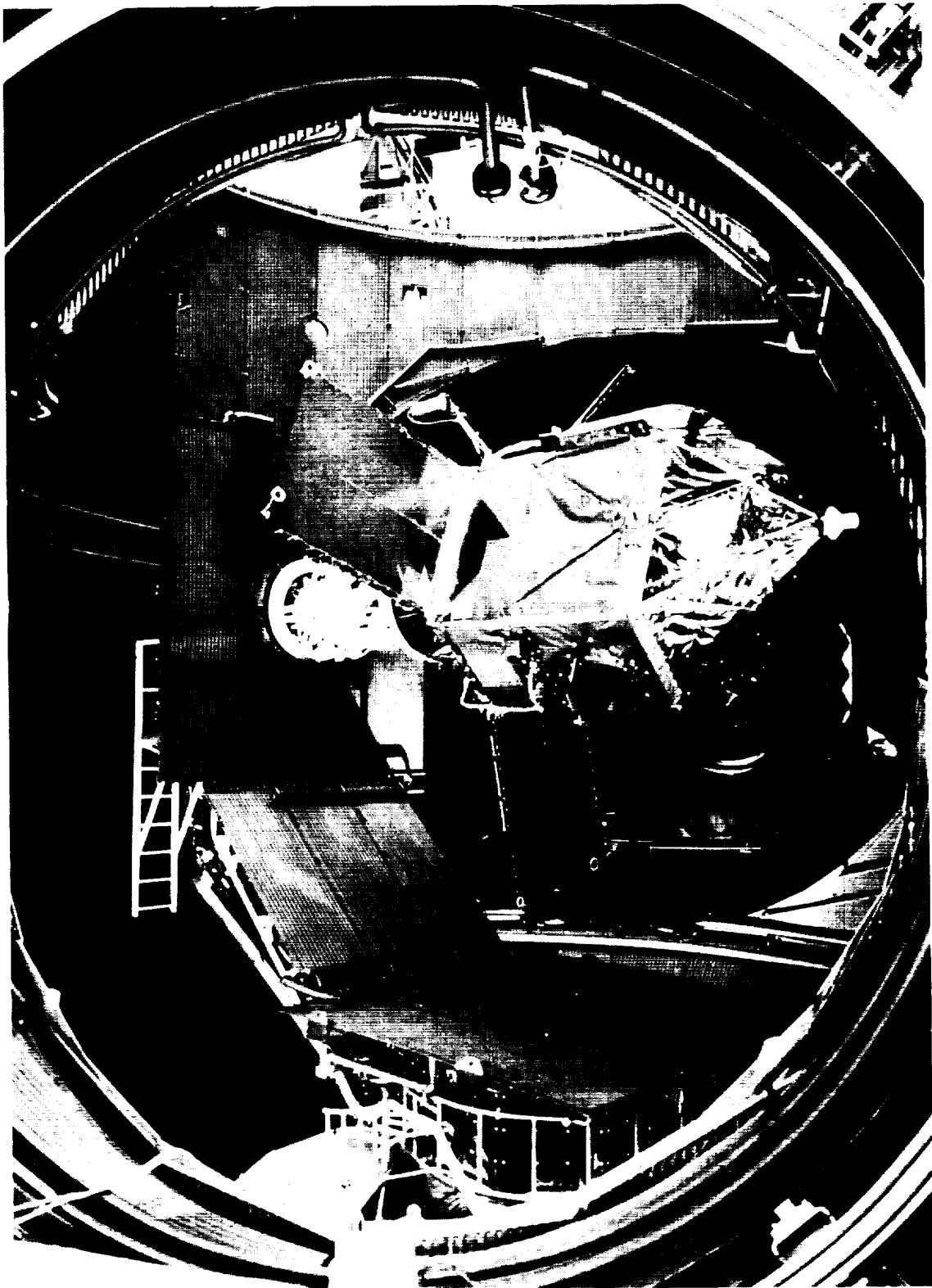


FIGURE 9. EUROPEAN SPACE AGENCY'S (ESA) HIPPARCOS SATELLITE UNDERGOING THERMAL VACUUM TESTING IN THE LARGE SPACE SIMULATOR (LSS) FACILITY AT ESTEC, THE NETHERLANDS. (COURTESY OF THE EUROPEAN SPACE AGENCY AND ESA BULLETIN)

ORIGINAL PAGE  
BLACK AND WHITE PHOTOGRAPH



FIGURE 10. ESA'S HIPPARCOS SATELLITE BEING ROTATED ABOUT ITS SPIN AXIS WITH SOLAR PANELS FULLY DEPLOYED, AT THE LARGE SPACE SIMULATOR (LSS) FACILITY AT ESTEC, THE NETHERLANDS. (COURTESY OF THE EUROPEAN SPACE AGENCY AND ESA BULLETIN)

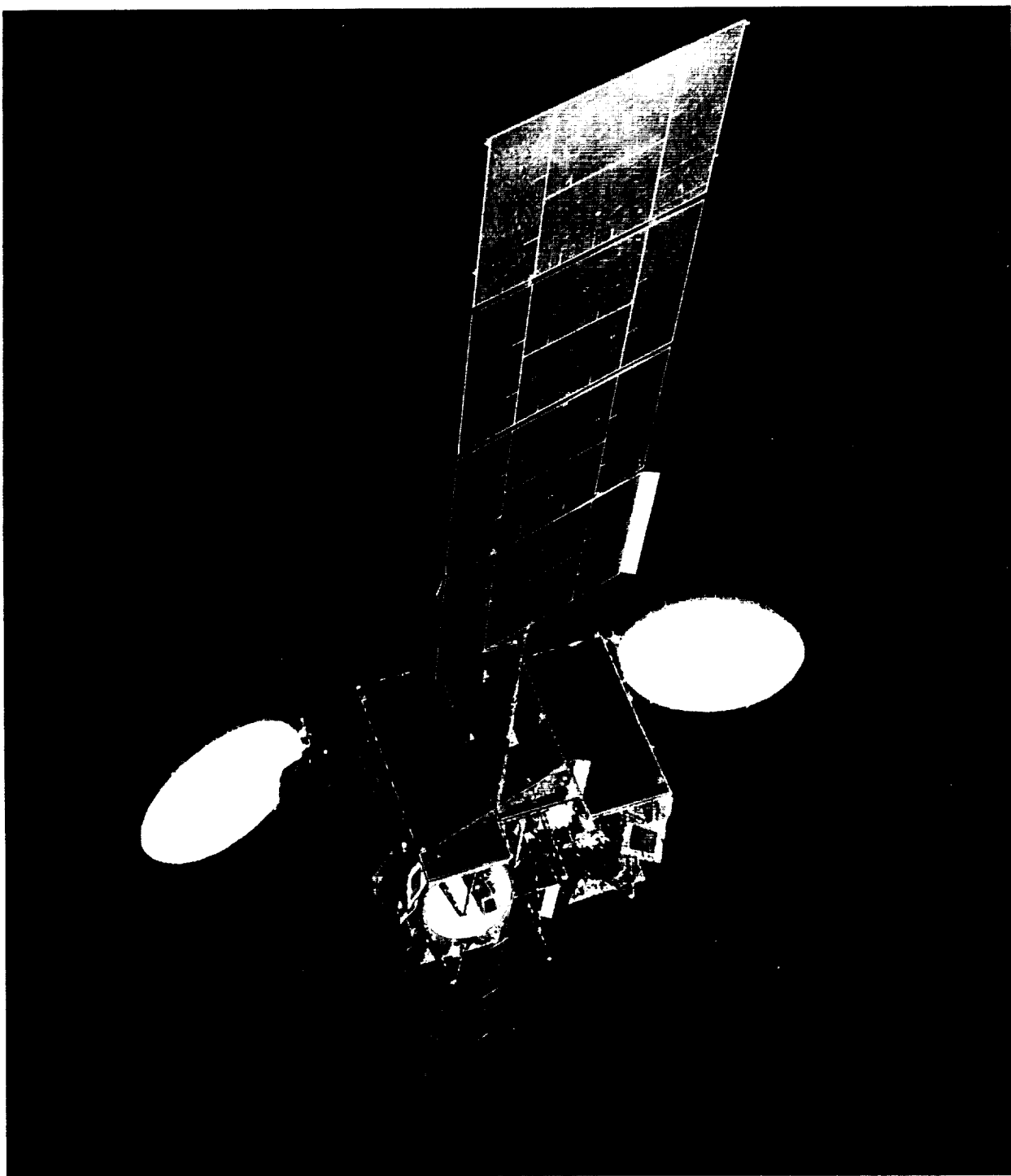


FIGURE 11. TELESAT CANADA'S ANIK-E2 SATELLITE. (COURTESY OF SPAR AEROSPACE, LTD.)



## HYPERVELOCITY IMPACT SIMULATIONS OF WHIPPLE SHIELDS

Dr. Steven B. Segletes and Dr. Jonas A. Zukas

Computational Mechanics Consultants, Inc.  
Towson, Maryland, U.S.A. 21204

## ABSTRACT

The problem associated with protecting space vehicles from space debris impact is described. Numerical simulation is espoused as a useful complement to experimentation: as a means to help understand and describe the hypervelocity impact phenomena. The capabilities of a PC-based hydrocode, **Zeus**, are described, for application to the problem of hypervelocity impact. Finally, results of **Zeus** simulations, as applied to the problem of bumper shield impact, are presented and compared with experimental results.

## INTRODUCTION

The effects of hypervelocity impact have been a topic of interest for as long as satellites have orbited the earth. The continued need to protect orbiting vehicles from impact by low mass, high velocity, particulate debris serves as the driving force for much of the ongoing study.

Space debris originates primarily from two sources. First, there is cometary meteoroid material, consisting mostly of loosely packed ice with a density of approximately  $0.5 \text{ g/cm}^3$ .<sup>1</sup> Though not dense, such debris may impact with velocities of tens of kilometers per second. The second prevalent source of space debris consists of orbital debris fragments originating from man-made devices such as satellites and rockets. Such debris, typically aluminum, may range in size from sub-centimeter to satellite size. Smaller fragments are, by far, the most prevalent in number and, in this regard, pose the greatest threat of impact to orbiting bodies.

The desire to protect space vehicles from such debris spurred the invention of the bumper shield by Whipple.<sup>2</sup> The Whipple shield is a sacrificial plate, whose purpose it is to cause disintegration of the impacting fragment, and in so doing, to distribute the energy of hypervelocity impact over an area large enough to be absorbed by the space vehicle structure, without perforation. Whipple shields continue to serve as a primary means of protection and, as such, a great deal of effort continues to be directed to their study. A sample of studies, presented at the recent AIAA Space Programs and Technologies Conference (24-27 March, 1992/Huntsville, Alabama), may be examined to reveal the focus of current efforts in bumper shield technology. At this conference, experimental bumper shield work focused on novel materials<sup>3,4,5,6</sup>, measurement techniques<sup>7</sup> and parametric variations of

experimental parameters like impact velocity<sup>8</sup> and bumper thickness<sup>9</sup>. Analytical efforts covered the spectrum of empirical<sup>10,11</sup>, semi-empirical<sup>12</sup>, probabilistic<sup>13,14</sup>, system vulnerability modeling<sup>15,16</sup> and numerical simulation<sup>17</sup>.

## NUMERICAL MODELING TOOLS

The paucity of numerical simulation work on the subject speaks to the inherent difficulty in simulating bumper shield effects with computational tools. The extremely harsh pressure and failure environments of hypervelocity impact dictate the need for specialized computational tools, in order to effectively address the problem. The more commonly familiar structural analysis codes, which are geared for computing a global structural response to a distributed or point load, are simply not suitable for handling hypervelocity deformation, where inertia and stress induced failure are primary governing principles. Specially formulated hydrocodes (a.k.a. wave propagation codes) are designed to model high strain, large strain rate deformations and are thus better suited to address the hypervelocity impact problem.

However, the hypervelocity bumper shield problem, specifically, puts added burdens upon hydrocodes. In particular, the bumper shield problem differs from many other high strain rate problems in that physical material separation occurs violently, in tension, and it is the post-failure behavior of the materials which is of the the greatest interest to the bumper shield researcher.

Eulerian hydrocodes, which function by tracking the flow of materials through a mesh that is fixed in space, often perform poorly at resolving the low density, expanding, debris cloud which results from a bumper impact. The natural tendency of Eulerian material transport algorithms to numerically diffuse material through the grid, in an unrealistic manner, especially when material volume fractions are small, can inhibit effective modeling of debris clouds. More accurate (second order) Eulerian techniques have been introduced in recent years which greatly improve the ability of these codes to track material transport like that found in debris clouds. However, only through the use of computationally expensive, very finely resolved, grids have Eulerian codes begun to approach qualitative agreement on the bumper shield problem.<sup>18,19</sup>

In addition to the challenges faced by many Eulerian codes in modeling diffusive transport, the algorithms employed by Eulerian codes, which are used to converge the equations of state, when multiple materials coexist within a single computational cell, may also experience difficulties, when the mass fraction of single material constituent becomes very small. Unfortunately, the debris cloud problem is one which virtually guarantees the existence of small mass fractions within so-called "mixed" cells. In some codes like HULL<sup>20</sup>, difficulties in equation of state convergence are addressed by essentially sweeping away materials with small volume fractions (and replacing them with air) when equation of state convergence becomes a problem. This technique has been rather appropriately, though unofficially, dubbed Alchemy.

Though Alchemy has the beneficial effect of promoting rapid equation of state convergence, it may, in the case of a debris cloud problem, have the net result of dissipating a debris cloud to the point of non-existence.

Lagrangian hydrocodes, which function by having the numerical grid fixed, not to the laboratory, but to the deforming material, may also experience difficulties in modeling a bumper shield debris cloud. Without advanced techniques like rezoning or erosion, a Lagrangian code is unable to handle even the simpler problem of perforation. Even with rezoning capabilities, the physical material separation, which characterizes bumper impacts, can not be modeled. Lagrangian mesh erosion techniques, on the other hand, can provide a tool which offers the potential of describing, more accurately, the formation and expansion of a hypervelocity debris cloud.

The **Zeus** code is a PC-based, 2-D, explicit integration, Lagrangian hydrocode which has been employed in the present study, to model the effects of hypervelocity impact of aluminum spheres upon thin aluminum Whipple shields. Designed to simulate impact over a wide range of velocities<sup>21</sup>, **Zeus** has also had success at simulating hypervelocity events<sup>22,23</sup>. The code makes use of the PC's extended memory so that it may, on a computer having 8MB of extended memory, simulate a problem with 28000 nodes and 56000 elements. Interactive pre- and post-processing modules are a standard part of the **Zeus** package.

**Zeus** employs constant strain triangular elements, in either axisymmetric or plane strain modes of computation. The Mie-Grüneisen is the standard equation of state provided, though a user definable material option exists, which allows the user to program any desired material model, using the FORTRAN computer language.

A sophisticated contact/erosion processor is employed by **Zeus**, which allows the computational meshes of many objects to interact simultaneously, by way of contact. Additionally, the contact/erosion processor permits the erosion of computational elements. Lagrangian mesh "erosion" serves two purposes in the calculation. First, it is a numerical technique designed to permit Lagrangian simulations to proceed when excessive mesh distortion would otherwise make the simulation uneconomical and eventually inaccurate. Secondly, erosion may be used to simulate physical material separation in problems where such phenomena occur.

When some suitable set of erosion criteria are satisfied by a Lagrangian computational cell, that particular cell is removed from the intact grid by the erosion processor. The new mesh topology of the remaining grid must be recomputed. The material in the eroded cell is ideally converted into a free-flying mass point, which is then capable of interacting with remaining Lagrangian grids, by way of the contact processor, and in more sophisticated treatments, with other free flying mass points.

The criterion on which to base mesh erosion is generally related

to some measure of material deformation. **Zeus** employs several erosion criteria. One such metric is equivalent plastic strain, which is a measure of distortional deformation. Another is the volumetric strain, given by

$$\epsilon_v = \frac{V - V_o}{V_o}$$

where  $V$  is the cell volume and  $V_o$  is the cell's original volume. The volumetric strain provides a measure of dilatational deformation, and is the primary operative erosion criterion when simulating the formation of a bumper shield debris cloud. These numerical erosion criteria are roughly based upon the mechanical properties governing physical material separation. Generally, a fairly wide range of values may be successfully employed for these criteria. Solution convergence and/or stability problems may arise however, if these parameters are set either excessively small or large.

On one hand, if material erosion is premature, fundamental flow patterns in the intact, deforming, Lagrangian mesh may not have had the chance to adequately establish themselves. This condition does not usually affect the numerical stability of the simulation; however the accuracy may suffer severely, with the likely result being an unrealistic simulation of deformation.

The other extreme occurs when the material erosion criteria are set to excessively large values, or disabled altogether. In this case, the imposed topology of the connected, Lagrangian grid becomes an obstacle to any large strain fields seeking to establish themselves. A section of the Lagrangian grid, in the region of large strain, will likely produce elements with large aspect ratios, in an attempt to conform to the developing strain field, while simultaneously obeying the constraints of the connected mesh topology. These high aspect-ratio elements become increasingly "stiff", in that their ability to deform fluidly becomes severely curtailed. As a result, their motive degrees of freedom become effectively reduced. Furthermore, the fixed mesh topology "encourages" other cells, in the vicinity of these high aspect-ratio elements, to also acquire the unrealistic aspects and associated stiffnesses. When this hyperdistortional condition occurs, the Lagrangian mesh is said to have "locked up", because the condition, once established, is unlikely to rectify itself. Locked-up grids will certainly produce inaccurate results, but also run the risk of becoming numerically unstable. Fortunately, the judicious use of Lagrangian mesh erosion can usually preclude the onset of grid lockup. It is in this sense that Lagrangian mesh erosion is also a "numerical" technique, in addition to its use as a "physical" technique for simulating the material separation phenomenon.

Prior to the time that erosion of a computational cell might occur, **Zeus** permits the activation of material property degradation, in the form of shear/tensile failure. Such degradation of properties is intended to address the possibility of material fracture and

rubblization. When such conditions occur, the materials effectively become fluid-like, in that only compressive forces may be resisted; shear and tensile resistance become negligible.

## SIMULATIONS

For this paper, a series of experiments by Piekutowski<sup>9</sup> are computationally examined with the **Zeus** code. In his experiments, Piekutowski examines the effect of aluminum bumper thickness upon the debris cloud formed by the nominal 6.7 km/s impact of a 1.275-g, 9.53-mm diameter, aluminum sphere. The ratios of target thickness to projectile diameter ( $t/D$ ) ranged from 0.026 to 0.424. Over this range of bumper thicknesses, Piekutowski notes<sup>9</sup>

an orderly change in debris cloud morphology... For cases where the bumper was overmatched, i.e., the projectile did not breakup completely, a large single fragment of projectile remained at the center of the debris cloud. When the projectile was overmatched, numerous large bumper fragments were distributed throughout the bubble of bumper debris.

In support of his thesis, Piekutowski presents an excellent collection of radiographic records of bumper perforation events. Of particular interest in the current study, in addition to the computed debris cloud geometries, are the residual debris cloud velocity, the radial expansion velocity of the projectile portion of the debris cloud, and the debris particle size, for which Piekutowski provides experimental data points.

Both the projectile and the bumper were modeled with a maximum tensile pressure of 10 kbar. The volumetric strain,  $\epsilon_v$ , over which this tensile pressure may exert itself, was 0.21, beyond which, material separation was permitted to occur. For those computational cells which did not fail as a result of volumetric expansion, an equivalent plastic strain erosion criterion of 150% strain was also retained. However, degradation in the flow stress began at an equivalent plastic strain of 60%, and continued up to the erosion strain. All of the simulations to be discussed employed a modest number of elements, ranging from 2328 to 4064 elements.

Though thirteen experiments are reported by Piekutowski, a subset of those were chosen for simulation. Two simulations were performed in the lower ranges of  $t/D$  (bumper thickness to projectile diameter ratios), namely 0.026 and 0.049 and two at higher  $t/D$  values: 0.163 and 0.234. The progressions of these simulations are shown in Figs. 1 through 4. The computational results are tabulated in Table 1, along with their experimental counterparts. For each case studied, the normalized residual velocity ( $V_f/V_c$ ) and radial expansion velocity of the projectile debris cloud ( $V_r/V_o$ ) are given. Furthermore, the equivalent diameter,  $d_f$ , of the largest residual debris fragment is noted ( $d_f$  is the cube root of the product of the three fragment dimensions,  $(HLT)^{1/3}$ ). The actual impact velocity for each case is specifically noted and the computational (CPU) time required to bring the simulations to 18 microseconds is given as well. The CPU times increased substantially

for the thicker bumpers, because of the increased cost associated with computing the interaction between free flying masses, the task of which reduces to an N-body problem (with  $N(N-1)/2$  pairs of interacting free-flying nodes).

TABLE 1. SUMMARY OF COMPUTATIONAL RESULTS

t/D	V <sub>0</sub> km/s	Experiment			Computation			
		V <sub>f</sub> /V <sub>0</sub>	V <sub>r</sub> /V <sub>0</sub> *	d <sub>f</sub> mm	V <sub>f</sub> /V <sub>0</sub>	V <sub>r</sub> /V <sub>0</sub>	d <sub>f</sub> mm	CPU** hr
0.026	6.70	0.986	0.058	5.49	0.979	0.034 <sup>†</sup>	8.78	2.48
0.049	6.62	0.977	0.104	2.95	0.970	0.104	8.20	3.44
0.163	6.71	0.928	0.284	1.09	0.915	0.292	1.88	9.00
0.234	6.64	0.894	0.259	0.64	0.891	0.316	1.59	9.56
<p>*As measured from graph of Piekutowski<sup>9</sup>  **Running on a 25 MHz 80486 PC.  <sup>†</sup>Varied widely with location; ranged from 0.016 to 0.055.</p>								

The behavior of these debris clouds follows that described by Piekutowski in several important ways. For the thin bumper problem, a fragment shell is spalled off from the rear of the impacting sphere. Also, both experiment and simulation indicate that a large single fragment remains intact (Fig. 1). For thicker bumpers (Figs. 3 and 4), the projectile debris cloud becomes more evenly dispersed, since more of the projectile is fragmented as a result of the longer-duration, initial tensile rarefaction.

Fig. 2 also shows a direct comparison between a **Zeus** simulation for t/D of 0.049 and a Piekutowski radiograph. A qualitative similarity exists in the projectile debris cloud shape and position. The simulation however, does indicate a leading target debris cloud which is more dispersed in space, when compared with the radiograph. Additionally, the leading edge of the computed projectile debris appears less like a homogenous cloud, as indicated by the experiment, but instead, more akin to a large fragment. This discrepancy in the debris particle size may be confirmed by comparing the computed equivalent particle diameter with the experimental data, in Table 1. The reasons for this discrepancy are twofold: first, there is not enough resolution in the computational grid to adequately resolve smaller fragment sizes; secondly, the material failure models available to a code like **Zeus** are likely insufficient to capture the fine details of the fragmentation process. It is probably for this latter reason that the largest computed central fragments are larger than those measured by Piekutowski.

For larger bumper thicknesses (Figs. 3 and 4), the front of the debris cloud becomes more rounded in shape. The debris is expanding radially with a larger velocity. Also, more of the mass is concentrated along the leading edge of the debris cloud. These simulations did not seem to suffer from the dispersion noted for thinner bumpers.

## SUMMARY

The feasibility of using a Lagrangian wave propagation code as an analysis tool in Whipple shield design studies was investigated. Specifically, the morphology of debris cloud formation was studied with the PC based, **Zeus** hydrocode. The numerical simulations indicate a qualitative similarity to the images portrayed in radiographs of experiments by Piekutowski<sup>9</sup>. Because of inadequate resolution and simplistic failure models, however, debris is less homogenous and debris particle size is predicted to be larger than the experiments suggest. Nonetheless, the debris cloud residual velocity, as well as the radial expansion velocity of the fragmenting projectile compared favorably with the cited study.

## REFERENCES

1. Rajendran, A.M. and N. Elfer, "Debris-Impact Protection of Space Structures", in J. Wierzbicki (ed.), Structural Failure, John Wiley & Sons: New York, 1989.
2. Whipple, F.L., "Meteorites and Space Travel," *Astronomical J.*, **1161**, p. 131, 1947.
3. Elfer, N. and F. Baillif, J. Robinson, "External Tank Space Debris Considerations," AIAA 92-1411, AIAA Space Programs and Technologies Conference, Huntsville, Alabama, 24-27 March 1992.
4. McGill, P. and A. Mount, "Effectiveness of Metal Matrix and Ceramic Matrix Composites as Orbital Debris Shield Materials," AIAA 92-1461, AIAA Space Programs and Technologies Conference, Huntsville, Alabama, 24-27 March 1992.
5. Zwiener, J. and A. Mount, K. Herren, A. Nettles, "An Enhanced Whipple Bumper System: Impact Resistance of Composite Materials," AIAA 92-1589, AIAA Space Programs and Technologies Conference, Huntsville, Alabama, 24-27 March 1992.
6. Robinson, J.H., "The Effectiveness of Multi-Layer Insulation as Meteoroid and Orbital Debris Shielding," AIAA 92-1460, AIAA Space Programs and Technologies Conference, Huntsville, Alabama, 24-27 March 1992.
7. Wilbeck, J.S., "Experience with Techniques for Characterizing Debris Generated During Hypervelocity Impact Testing," AIAA 92-1586, AIAA Space Programs and Technologies Conference, Huntsville, Alabama, 24-27 March 1992.

8. Ang, J.A. and L.C. Chhabildas, B.G. Cour-Palais, E.L. Christiansen, J.L. Crews, "Evaluation of Whipple Bumper Shields at 7 and 10 km/s," AIAA 92-1590, AIAA Space Programs and Technologies Conference, Huntsville, Alabama, 24-27 March 1992.
9. Piekutowski, "Properties of Largest Fragment Produced by Hypervelocity Impact of Aluminum Spheres with Thin Aluminum Sheets," AIAA 92-1588, AIAA Space Programs and Technologies Conference, Huntsville, Alabama, 24-27 March 1992.
10. Jolly, W.H. and J.E. Williamsen, "Ballistic Limit Curve Regression for Freedom Station Orbital Debris Shields," AIAA 92-1463, AIAA Space Programs and Technologies Conference, Huntsville, Alabama, 24-27 March 1992.
11. Christiansen, E.L., "Performance Equations for Advanced Orbital Debris Shields," AIAA 92-1462, AIAA Space Programs and Technologies Conference, Huntsville, Alabama, 24-27 March 1992.
12. Lawrence, R.J., "A Simple Approach for the Design and Optimization of Stand-off Hypervelocity Particle Shields," AIAA 92-1465, AIAA Space Programs and Technologies Conference, Huntsville, Alabama, 24-27 March 1992.
13. Williamsen, J.E., "Orbital Debris Risk Analysis and Survivability Enhancement for Freedom Station Manned Modules," AIAA 92-1410, AIAA Space Programs and Technologies Conference, Huntsville, Alabama, 24-27 March 1992.
14. Robinson, J., "Preliminary Design of a Meteoroid/Orbital Debris Shield System for a Mars Mission Spacecraft," AIAA 92-1406, AIAA Space Programs and Technologies Conference, Huntsville, Alabama, 24-27 March 1992.
15. Elfer, N. and R. Meibaum, G. Olson, "Space Debris Surfaces (Computer Code): Probability of No Penetration versus Impact Velocity and Obliquity," AIAA 92-1407, AIAA Space Programs and Technologies Conference, Huntsville, Alabama, 24-27 March 1992.
16. Christiansen, E.L. and J.L. Hyde, G. Snell, "Spacecraft Survivability in the Meteoroid and Debris Environment," AIAA 92-1409, AIAA Space Programs and Technologies Conference, Huntsville, Alabama, 24-27 March 1992.
17. Schonberg, W.P. and J.A. Peck, "A Comparative Study Between Experimental Results and Numerical Predictions of Multi-Wall Structural Response to Hypervelocity Impact," AIAA 92-1591, AIAA Space Programs and Technologies Conference, Huntsville, Alabama, 24-27 March 1992.
18. Holian, K.S. and W.S. Burkett, "Sensitivity of Hypervelocity Impact Simulations to Equation of State," Int. J. Impact Engng., 5(1-4), 1987.



19. Holian, K.S. and B.L. Holian, "Hydrodynamic Simulations of Hypervelocity Impacts," Int. J. Impact Engng., **8**, 1989.
20. Matuska, D.A. and J.J. Osborn, "**HULL** Documentation," Orlando Technology, Inc. Report, Rev. May 1987.
21. Segletes, S.B. and J.A. Zukas, "Simulation of High Strain Rate Effects with Microcomputers," Proc. Int. Conf. Mech. Prop. Materials at High Rates of Strain, Inst. Phys. Conf. Ser. No 102, Oxford, 1989.
22. Zukas, J.A. and S.B. Segletes, "Hypervelocity Impact on Space Structures," ASME Pub. PVP-Vol. 225, Dynamic Response of Structures to High-Energy Excitations, ed. T.L. Geers and Y.S Shin, Book No. H00717, pp. 65-71, 1991.
23. Zukas, J.A. and J.R. Furlong, S.B. Segletes, "Hydrocodes Support Visualization of Shock-Wave Phenomena," Computers in Physics, pp. 146-154, Mar/Apr 1992.

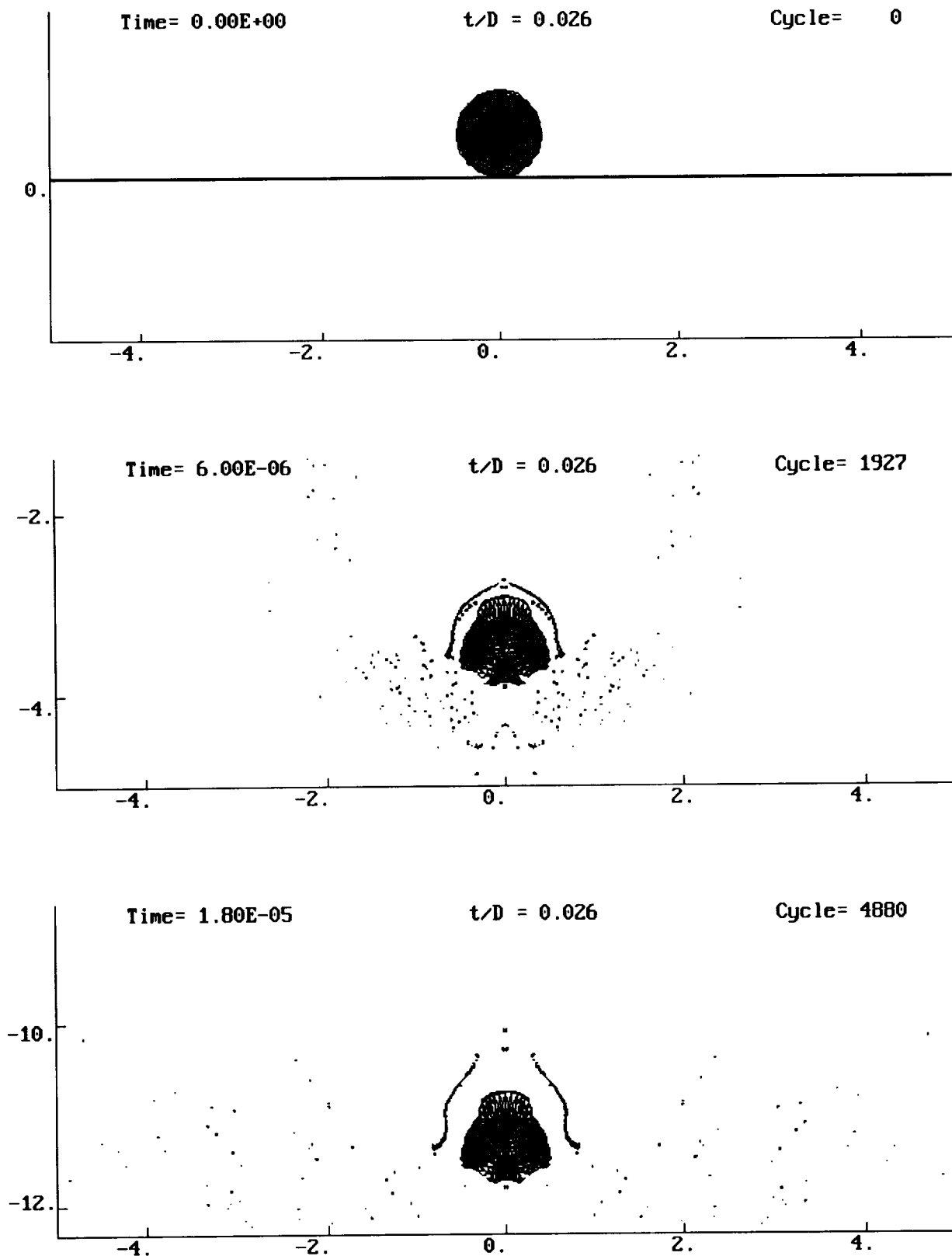


Fig. 1. Simulation of 1.275-g, 9.53-mm diameter aluminum sphere, impacting at 6.70 km/s upon aluminum bumper,  $t/D = 0.026$ .

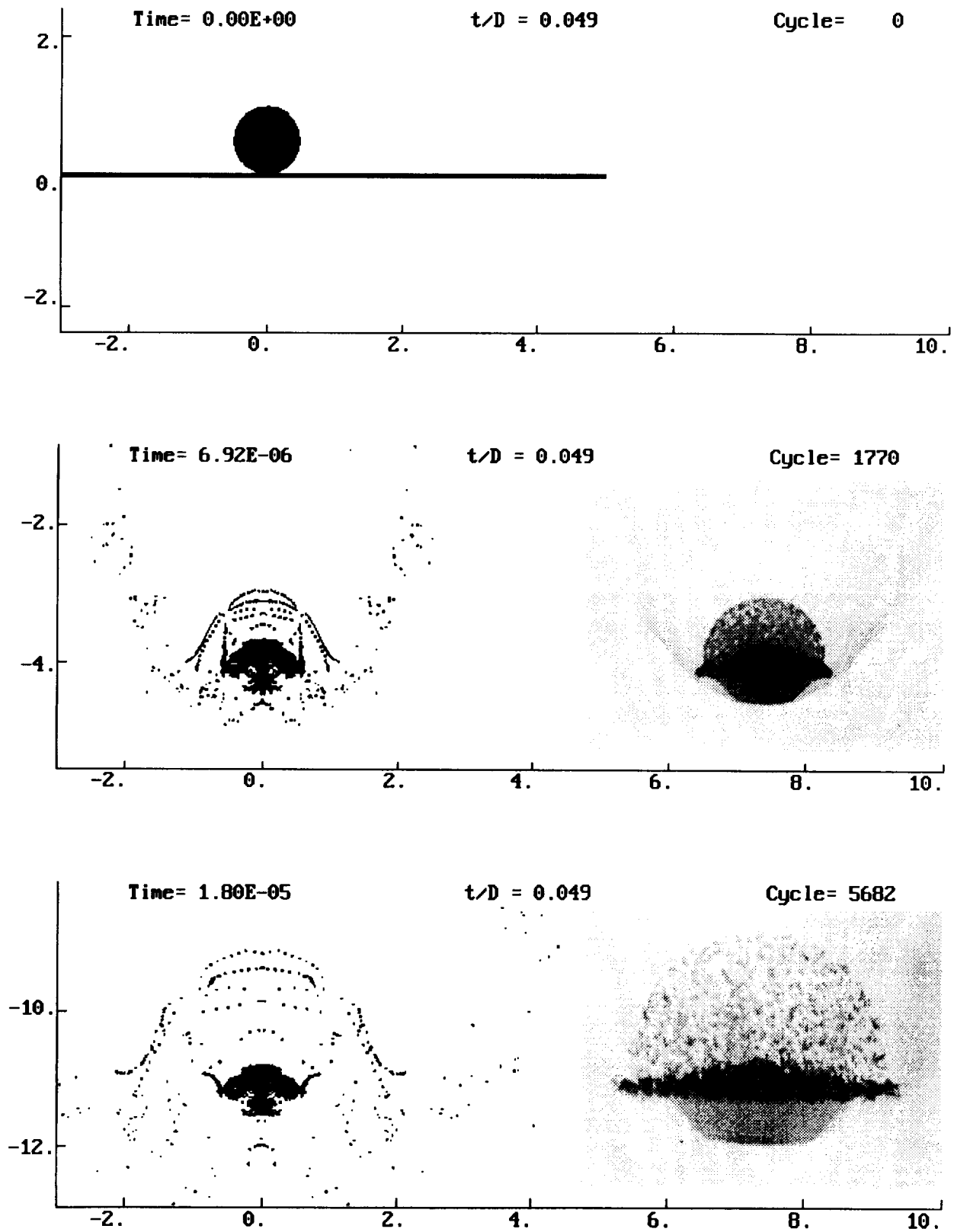


Fig. 2. Simulation and experiment of aluminum sphere impacting aluminum bumper,  $t/D = 0.049$  (Photos courtesy of A.J. Piekutowski).

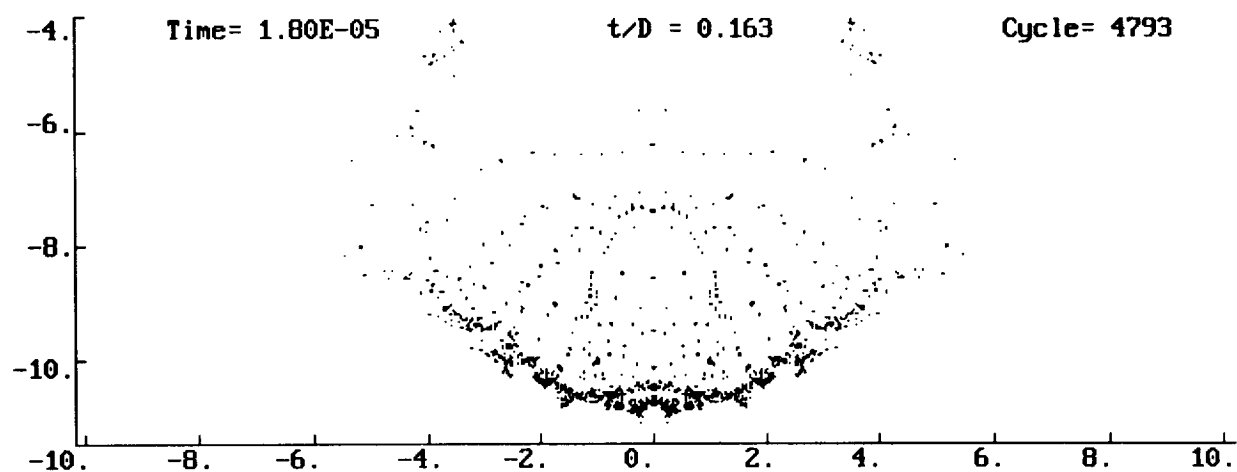
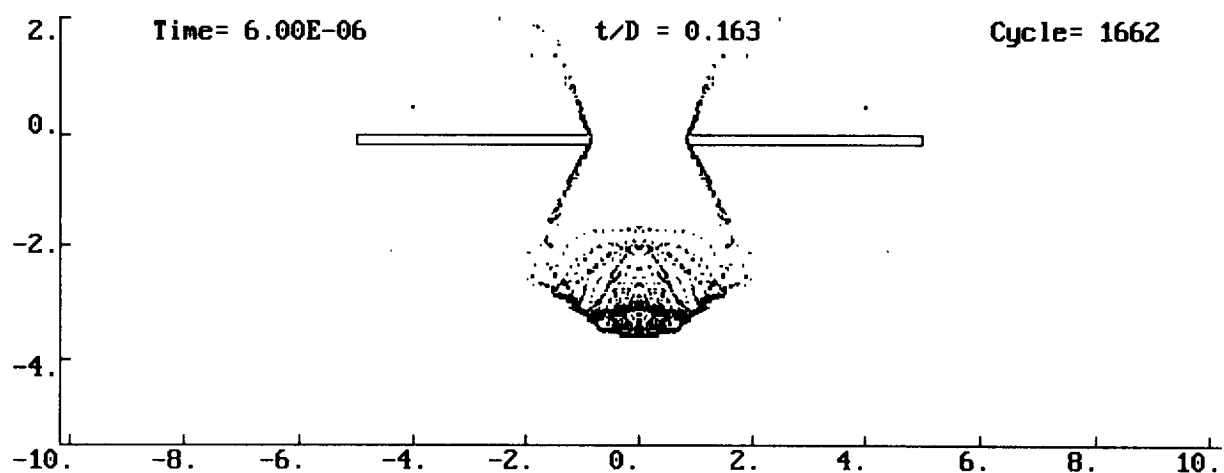
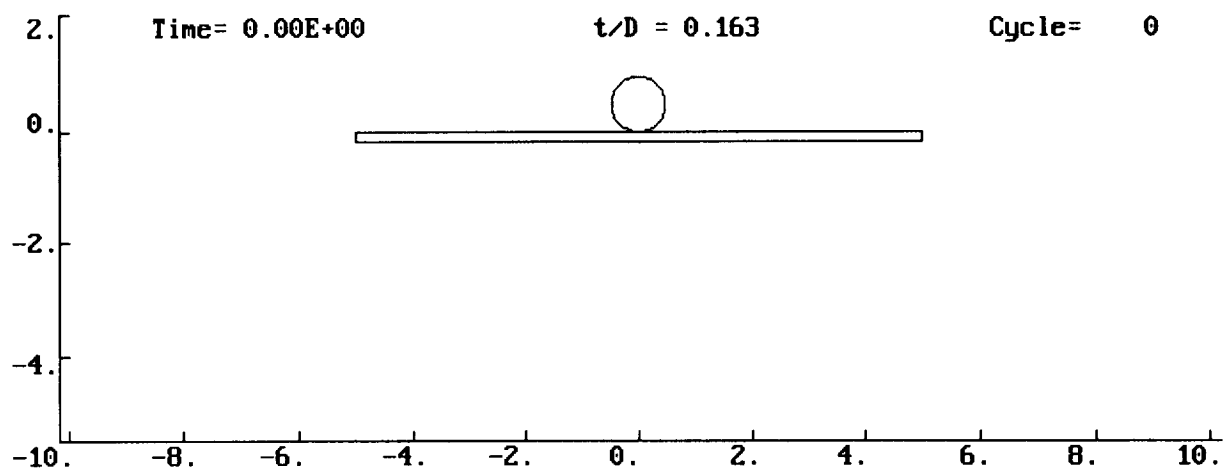


Fig. 3. Simulation of 1.275-g, 9.53-mm diameter aluminum sphere, impacting at 6.71 km/s upon aluminum bumper,  $t/D = 0.163$ .

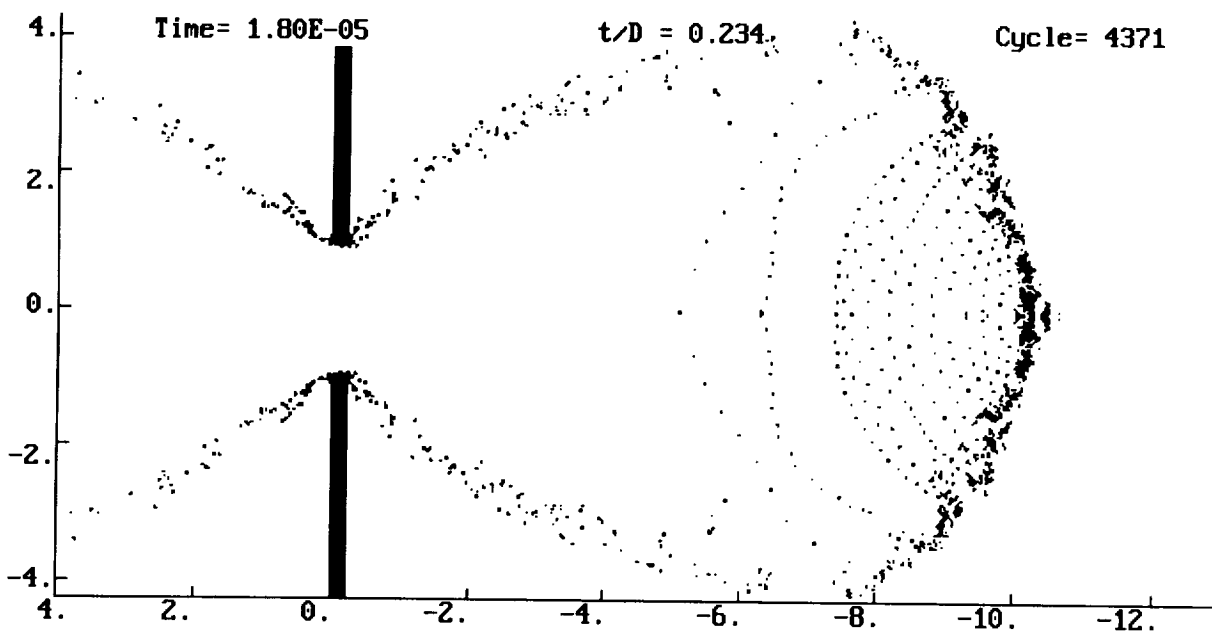
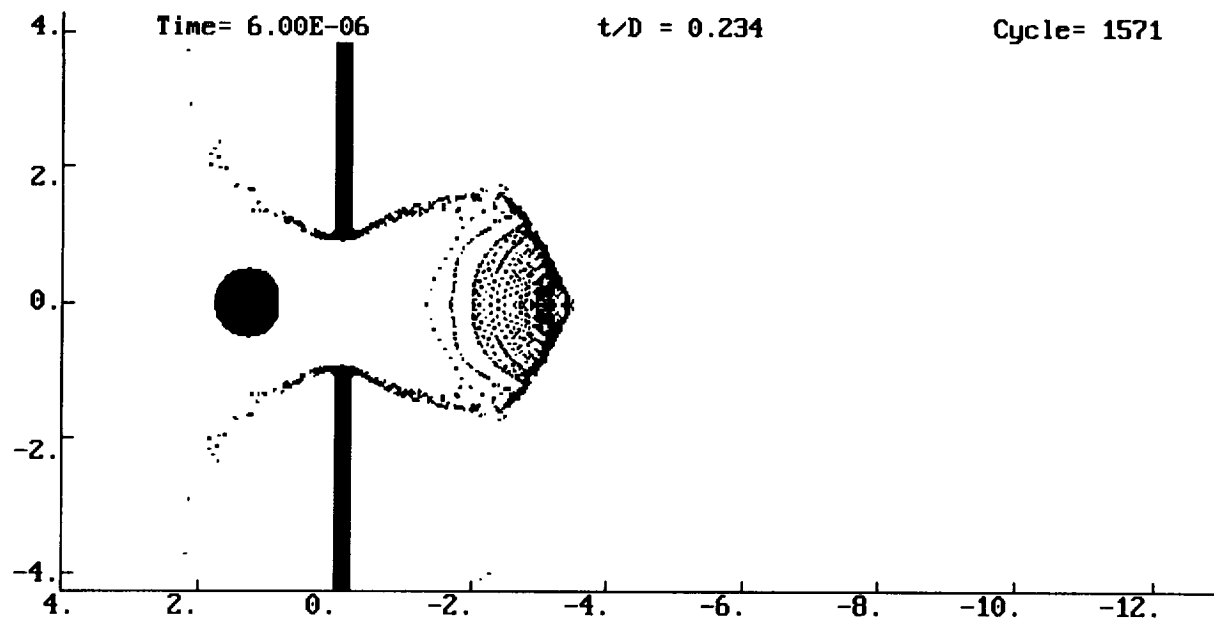


Fig. 4. Simulation of 1.275-g, 9.53-mm diameter aluminum sphere, impacting at 6.64 km/s upon aluminum bumper,  $t/D = 0.234$ .



**Offloading Techniques  
for Large Deployable Space Structures**

Levino Caravaggio, Alex Golob  
*Spar Aerospace Limited*  
Satellite & Communications Systems Division/DFL  
Ottawa, Canada

The validation and verification of large deployable space structures are continual challenges which face the integration and test engineer today. Spar Aerospace Limited has worked on various programs in which such structure validation was required and faces similar tasks in the future. This paper reports on this testing and describes the different offloading and deployment methods which were used, as well as the proposed methods which will be used on future programs.

Past programs to be discussed will be the Olympus solar array ambient and thermal vacuum deployments, and the Anik-E array and reflector deployments. The proposed MSAT reflector and boom ambient deployment tests, as well as the proposed RADARSAT Synthetic Aperture Radar (SAR) ambient and thermal vacuum deployment tests will also be presented. A series of tests relating to various component parts of the offloading equipment systems was required. These tests included the characterization and understanding of linear bearings and large (180 in-lbf) constant force spring motors in a thermal vacuum environment, and the results from these tests will be presented.





**A NEW APPROACH FOR DATA ACQUISITION AT THE JPL SPACE SIMULATORS\***

Terry C. Fisher  
*California Institute of Technology*  
*Jet Propulsion Laboratory*  
*Pasadena, California 91109*

**ABSTRACT**

In 1990, a personal computer based data acquisition system was put into service for the Space Simulators and Environmental Test Laboratory at the Jet Propulsion Laboratory (JPL) in Pasadena, California. The new system replaced an outdated minicomputer system which had been in use since 1980.

This new data acquisition system was designed and built by JPL for the specific task of acquiring thermal test data in support of space simulation and thermal vacuum testing at JPL. The data acquisition system was designed using powerful personal computers and local-area-network (LAN) technology. Reliability, expandability and maintainability were some of the most important criteria in the design of the data system and in the selection of hardware and software components.

The data acquisition system is used to record both test chamber operational data and thermal data from the unit under test. Tests are conducted in numerous small thermal vacuum chambers and in the large solar simulator and range in size from individual components using only 2 or 3 thermocouples to entire planetary spacecraft requiring in excess of 1200 channels of test data. The system supports several of these tests running concurrently.

This paper describes the previous data system and reasons for its replacement, the types of data we acquire, the new data system hardware and software, the criteria used to design the new system, and the benefits obtained from the new system including information on tests performed to date.

---

\* The research described in this paper was carried out by the Jet Propulsion Laboratory, California Institute of Technology, under a contract with the National Aeronautics and Space Administration.

## **INTRODUCTION**

The Jet Propulsion Laboratory (JPL) in Pasadena, California is responsible for the management of unmanned planetary spacecraft for the National Aeronautics and Space Administration (NASA). As part of this task JPL has extensive laboratory facilities (The Environmental Test Laboratory and Space Simulators) for performing thermal vacuum and space simulation tests on components, assemblies and complete spacecraft for design verification and flight qualification.

An integral part of these facilities is the data acquisition system which is used to acquire thermal test data from several tests running concurrently, process the data, perform computations on the data, check limits, control test item heaters, archive the data and present the test data in various formats; all in real time.

A new data acquisition system which can perform the above functions was put into service in August, 1990 to replace a minicomputer based data system which had been in use since 1980. This new system uses personal computers and database management software operating on a network across three buildings. The new data acquisition system utilizes state-of-the-art computer and networking technology with increased reliability and provides a graphic user interface which increases productivity and decreases operator training time.

## **DATA ACQUISITION REQUIREMENTS**

The solar/thermal/vacuum testing activities at the JPL Environmental Test Lab and Space Simulators require many different types of data to be acquired, processed and stored in one data system. Data is acquired for both facility operations and test article monitoring. The data is used for real time decision making and for post test analysis.

The types of data that are recorded for facility operations include chamber cold wall temperatures, vacuum gage outputs, solar radiation intensity and temperature controlled quartz crystal microbalance (TQCM) frequency and temperature signals for contamination monitoring. The amount of facility data to be acquired depends on the chamber being used. The small (.7 by 1.3 meter) thermal vacuum chambers may require only 5 or 6 channels of data while the large (8 by 26 meter) solar/thermal/vacuum chamber requires over 170 channels of data to be recorded just for facility operations.

The principal types of data that are acquired from test articles include temperature from thermocouples and Platinum Resistance Thermometers (PRT), and power supply voltage and current outputs. A typical flight spacecraft test can require over 900 temperature and voltage measurement channels while a small component test may only need a few thermocouple channels.

Most of the thermal vacuum tests performed at JPL also require the use of numerous channels of computed data such as averages, deltas, rate of change, power calculations and conversion of vacuum gage voltage output to exponential torr values.

## **THE OLD SYSTEM**

The previous data system was based on a minicomputer that utilized mid 1970s hardware technology and operated with a 1966 version of FORTRAN IV. This was a fine system in its day; however, as the size of spacecraft grew, so did the required amount of data that had to be recorded during space simulation testing.

During testing of the *Galileo* flight spacecraft in 1988, the system was so overloaded, (1200 channels of data were required) the processing was anything but real time, and the 50 megabyte disk drive was filled to capacity before the end of the test.

Other factors that led to the decision to retire the old system were that replacement parts were becoming difficult to obtain, and software maintenance was complicated by the lack of original source code for some parts of the system. Also the user interface was anything but "friendly" and new users required considerable training on the system before performing simple tasks.

## **REQUIREMENTS FOR THE NEW SYSTEM**

When it was decided to retire the minicomputer system, the first task was to set down a list of requirements for the replacement data acquisition system. The major requirements for the new system were reliability, maintainability, expandability, flexibility, large data storage capacity and a graphical user interface.

Reliability of the system is extremely important since chambers run 24 hours a day, seven days a week, and the loss of test data is unacceptable. Reliability is important for both hardware and software, so only products of proven reliability would be considered for implementation into the new system design.

Maintainability is also very important as downtime during a test can be very costly to the project in terms of both dollars and schedule. To provide for ease of maintenance, the new system would use equipment from the same manufacturer for interchangeability and commercial off-the-shelf software wherever possible.

Expandability is necessary to provide for meeting the future data acquisition requirements of larger, more complex spacecraft. This would be provided by using an open architecture which would allow for the addition of more input and output equipment. Also, the software should not limit growth but have a platform on which to expand.

Flexibility is required to allow several tests to run concurrently at different locations. Since tests are both large and small, and start and stop at different times, it is necessary for the system to be able to manage all this activity transparently to the data acquisition and processing tasks.

The data storage capacity must be large enough to accommodate large tests which can run as long as 30 days, around the clock and require 1200 data channels. The data storage system must also have adequate redundancy to ensure no loss of test data.

The final major requirement is a graphical user interface. Since the data acquisition system is used by personnel of varying degrees of computer expertise, the design of the user interface has to be compatible with the lowest level user and not be cumbersome to higher level users.

## **THE NEW SYSTEM**

The replacement data acquisition system, S<sup>3</sup> (Space Simulator System), was designed and integrated at JPL, using third-party hardware and software and custom software which was written by JPL software and systems engineers. The design makes use of a fault tolerant Client/Server Architecture to distribute the data processing among several personal computers (PCs) and a local area network (LAN) was implemented across the three buildings which comprise the Environmental Test Laboratory and Space Simulators. By using the client/server technology, the data acquisition and processing tasks are distributed to multiple personal computers, and no one computer is ever overloaded and processing speed is always at maximum.

The S<sup>3</sup> design makes use of proven commercial off-the-shelf hardware and software to provide for interchangeability, expandability and maintainability.

The major hardware elements of the data acquisition system are the analog input device, the PC controlling the analog input device, the workstation PC, the output peripherals, the file sever and the local-area-network which ties all the equipment together. See Figure 1.

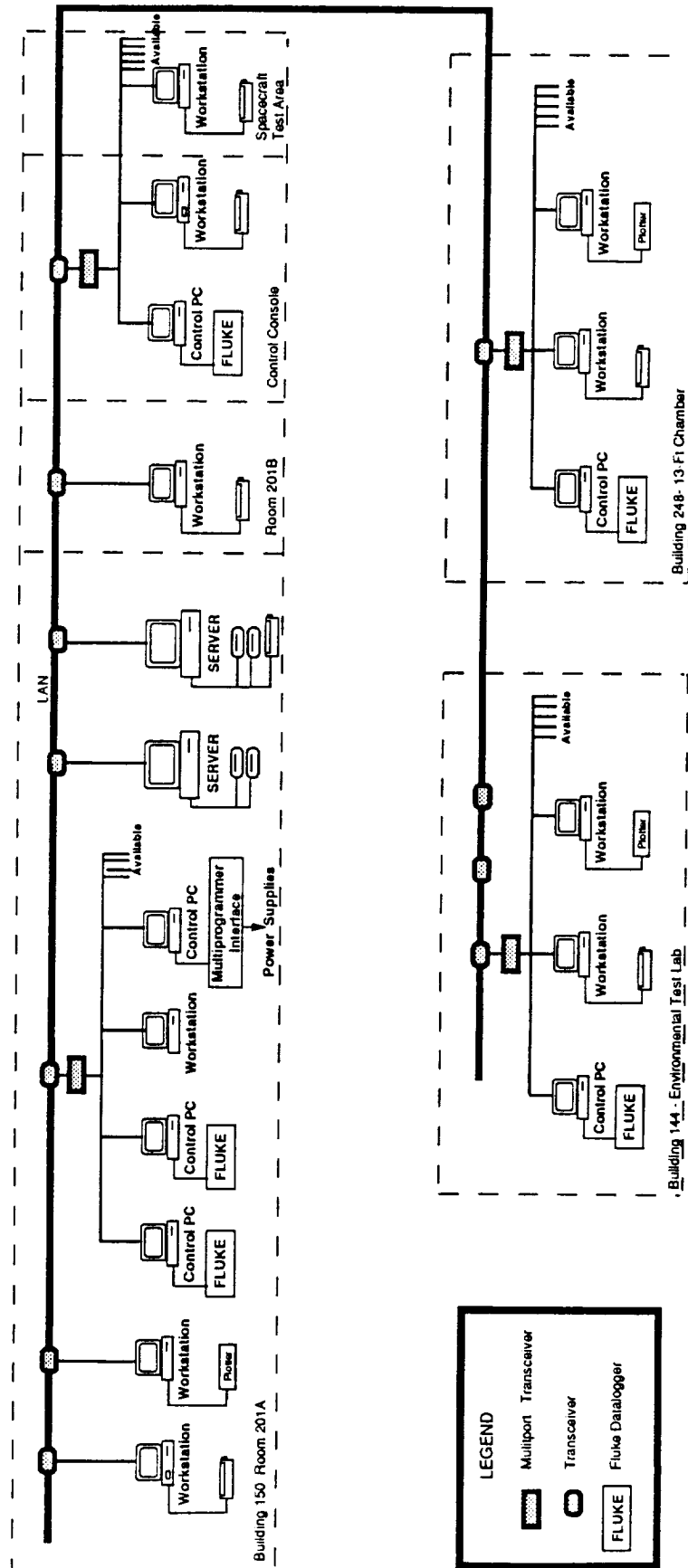
The major software components of S<sup>3</sup> are the networking, database management, communications, graphics and memory management software packages from various software publishers and the custom software that was written at JPL to integrate the total system.

### **Major Hardware Components**

#### **Computers**

All computers in the system are *Compaq 386 DeskPro* machines, manufactured by the *Compaq Computer Corporation*. The PCs are divided into three categories: file servers, controllers and workstations. By using computers of one type and from the same manufacturer, interchangeability throughout the system is maintained.

## Space Simulator System Network Configuration



This is a typical configuration for operations in the 25 Ft Space Simulator, Building 150, and for tests running in smaller chambers in other facilities.

Figure 1.

## File Server

The two file server PCs are the heart of the networked data acquisition system. The file server stores all the application software, controls all network activity, provides storage for all test data and manages all of the printed and graphical output of the system.

In the S<sup>3</sup> configuration, the file servers are 386, 33-MegaHertz (MHz) computers with 10 MegaBytes (MB) of random access memory (RAM) and 1.3 GigaBytes (GB) of hard disk storage. The hard drives are actually two 650-MB units which can be configured to operate as one 1.3 GB unit or two 650-MB units per file server, depending on the amount of redundancy desired.

## Control PCs

There is one PC to control every data-acquiring device (typically a data logger) on the system. The control PC is connected to its data logger by either an IEEE-488, or a RS-232 interface. The control PC is used to program the data logger, initiate scanning, check limits of the data and perform some of the computations on the data. The control PC also stores the test data on its internal hard drive, providing an additional copy of the data that is also saved on the file servers. During operations, the keyboard of the control PC is locked to prevent accidental interference with the acquisition process and the computer's monitor provides a continuously updated display of test status and limits exceeded.

The control PCs are 33 MHz machines with 4 MB of RAM and a 330-MB hard drive. The computer's standard serial port is used for RS-232 communications, and for IEEE-488 communications a General Purpose Interface Bus board is installed in the control PC expansion slot.

## Workstations

As its name denotes, the workstation is the PC that is used for most of the human interface work on the system. The workstation is where the system operators and test personnel set up tests, start acquisition, look at different data reports and perform system maintenance. The workstation is also used for transferring data to floppy disk and magnetic tape for off-line data reduction and data storage. The number of workstations that are used to support a test is dependent on the size of the test. Smaller tests require only a single workstation for the thermal engineer to look at data displays but a large test in the solar/thermal/vacuum chamber might require as many as 7 workstations to allow all of the test team and facility operators to view data, produce plots and perform the tasks associated with a large test.

In the S<sup>3</sup> system configuration, the workstations are 20 MHz computers equipped with 5 MB of RAM and a 110-MB hard drive. Two of the workstations are fitted with 135-MB magnetic tape units for archiving test data and backing up system software files.

## Analog Input Equipment

The system uses model 2286A data loggers from the *John Fluke Manufacturing Co.* as the primary analog data input device. These data loggers scan transducers, perform engineering unit conversions and transmit the data to the control PC.

The *Fluke* model 2286A data logger has the ability to measure a full range of analog inputs, including 11 different types of thermocouples, DC voltages up to 64 volts without conditioning, PRT resistance, and frequencies from 2 Hz to 400 KHz. A single 2286A can scan up to 1500 channels.

*Fluke* 2240B data loggers are also used with the system; however, they are somewhat limited in the types of input signals they will accept.

The 2286A was chosen over other types of input devices because of its ability to act as a stand-alone data logging unit. Equipment that is designed to be operated strictly as a computer "front end" lacks the ability to be used to collect data independently of the host computer, should the host be out of service. Also in our test labs, some small tests do not always need the capabilities of the full data system, so operating with only a data logger can be more cost effective.

Because of the system design and modularity of the software that controls the input devices, just about any type of data logger or data scanning unit could be added to the system with only a minimum amount of reprogramming. The only programming required would be the addition of a new software module to support the new device.

## Output Peripherals

There are numerous types of data output formats available with S<sup>3</sup>. There are various data display screens for the workstation monitors and several formats of hard copy reports and plots from printers and multi-color plotters.

The system uses laser printers, equipped with extended font cartridges for all hard copy reports. The laser printers are connected to the system via the parallel output port of a workstation but are accessible from any workstation on the network.

The plotted output is produced by multi-pen graphics plotters which are connected to the system through the workstation serial output port. These plotters have eight different color pens and provide good quality plots on either paper or transparency film.

## Network Hardware

The Local Area Network (LAN) connects all the PCs of the data acquisition system together. The network is a thick ethernet consisting of a single coaxial cable which interconnects the three buildings of the Environmental Test Laboratory and Space Simulators. Attached to the coax cable are network transceiver units which act as part of the interface between a PC and the network cable.

Each PC has a network interface card installed in an expansion slot which completes the connection to the network. The network interface cards are either a NE2000 from *Novell Inc.* or a PCNIU card from *Ungerman-Bass Inc.* The two cards are essentially the same and can be used interchangeably with minor software modifications.

Also used in the system are eight-channel multi-port adapters which allow the connection of up to eight PCs to a single network cable transceiver.

In its present configuration, (see Figure 1) the LAN can support up to 38 PCs, however it would be possible to support up to 250 PCs by adding more transceivers. Conversely, a minimum system of only three PCs could be operated on a network to support one test.

## **Major Software Components**

### Network Management Software

All of the system hardware is networked under *Netware/386* from *Novell Inc.* The network management software controls the communications between all of the computers on the network. When a workstation or control PC needs information or requires data to update a display, the file server handles the request under the direction of *Netware*. This software functions similarly to an air traffic controller who is directing airliners on a very busy route, preventing collisions between all the airplanes on that route, and making sure every plane gets to its assigned destination. Another major function of the network software is its fault tolerant feature which automatically routes incoming test data to each of the file server hard disks. By this process, called "mirroring", duplicate copies of test data is saved on both 1300 MB disks, and should one drive fail, there would be no loss of data.

Other features of the *Novell Netware* are the print queue and tape backup utilities. The print queue manages all of the printed output of the system. Whenever a hard copy printout is called for or a graph is to be plotted, the job is spooled by the print queue and routed to the proper printer or plotter. The tape backup utility is used to backup system programs and to archive test data to tape for permanent storage.



## Database Management Software

The database management software is the power behind the S<sup>3</sup> data acquisition system. The total system is built around *FoxPro/LAN, 1.02*, *Fox Software Company's* dBase-compatible network database management software. *FoxPro*, a multiuser, relational database development environment, was used to develop all of the application programs used by the system. It was chosen primarily for its speed and advanced features for data storage, manipulation and presentation. The application programs to perform most of the system tasks are written in the *FoxPro* language.

Databases are used for everything from keeping track of test setups to storing test data. The system uses 34 different databases for test setup, and 6 databases for test data for each active test on the system. The system also creates numerous temporary databases each time a test is run for things such as plot files and limit reports.

## Operating System

The operating system used by the PCs of S<sup>3</sup> is *MS-DOS, version 3.31*. This was the latest version available when the system development began and the only operating system supported by both *FoxPro* and *Novell* at that time.

## Communications Software

The software that is used to communicate between the datalogger and its control PC is *SilverComm* from *SilverWare, Inc.* This software package is a database compatible communications program that takes full advantage of the speed of *FoxPro* and the high baud rates of data transfer available with the *Fluke 2286A*. Through *SilverComm*, the system downloads channel programming to the datalogger and provides a path for data transfer from the datalogger to the control PC.

## Graphics Software

The graphics and plotting software within the data acquisition system is *dGE*, produced by *Pinnacle Publishing Company*. This software package is specifically designed to create graphics from within a database program. The software provides for automatic scaling of both the X and Y axis, and produces high resolution plots of test data which can be sent from the workstation to both plotters and printers.

## Memory Management Software

The memory utilization in the workstations and control PCs is managed by *Quarterdeck Extended Memory Management (QEMM 386 5.0)* software from *Quarterdeck Office Systems*. This software package is used to access high-memory addresses and to optimize the computer memory resources for *FoxPro*.

.

## Custom Software

Over 45,000 lines of custom software code were written by the Software and Systems Engineers from the Institutional Data Systems section at JPL. This software code integrates the third-party software packages into a functioning system. Most of this code was written in the *FoxPro* language; however, some was written in assembly language. Over 260 individual program modules were written during the development of S<sup>3</sup>. The modularity of the custom software makes system enhancements and maintenance a relatively easy task for the software maintenance personnel.

Included in this custom software are 98 individual display screens and user interface screens that were designed for the system. These screens are used for data presentation, test setup, system operations and system maintenance. The system operates on a menu-driven format and makes use of numerous pop-up, choice-box and pull-down menus. Each screen has an associated help screen for user assistance.

The custom software development also made provisions for the numerous types of computed channel calculations required for the data system. Software for averaging data channels, computing deltas, determining maximum/minimum values from a group of channels and the conversion of ion gage output voltage to exponential Torr values required a considerable amount of programming effort.

## PERFORMANCE RESULTS OF THE NEW SYSTEM

The new system has met or exceeded all of our initial design requirements and has proven to be an excellent choice for a data acquisition system. Once the capabilities of personal computers, database management and networking was fully understood by our instrumentation personnel, it became apparent that the applications were limitless. The cost savings in maintenance, reduced user training time and reduced test setup times have partially offset the cost for the system development.

The hardware has proven to be very reliable with only a few infant mortality-type failures during the first months of operation. The software has had some "bugs", as is expected with a new system, but because of its modularity and the advanced engineering put into the software design prior to actual coding, repairs have been made quickly with no test down time and no loss of data.

The criteria of flexibility and expandability have been met by the design of the hardware and software. We have recently added three PCs to the network to supplement the original 14 computers and have supported more tests running concurrently than we had ever anticipated. The software modularity has proven to be very beneficial as we have been requested to add several functions to the data processing and mathematical computations that were not part of the original design.

Operationally, the new system has proven to be a vast improvement over the old system. Because of the careful design of the graphic user interface, it takes only 2 or 3 hours to completely train an entry-level technician on basic system operations. A test setup which took 3 or 4 days to perform on the old system can now be completed in less than 8 hours with S<sup>3</sup>. Small tests of approximately 20 channels need less than 30 minutes for complete test setup and checkout.

Other major benefits obtained from the new system are the data processing speed which is considerably faster than with the old system and data is now displayed in "real time", not 2 or 3 minutes after the data scan. System security is a major improvement in S<sup>3</sup> with various levels of entry permission granted to users based on their need to access system features. Without proper permission, it is almost impossible to access the DOS operating system or to operate the floppy disk drive; thereby almost completely eliminating the possibility of a virus entering the system. All system databases are protected to eliminate the inadvertent deletion or corruption of test data.

Another important feature is that the system maintains a continuous history of test events in an event log database as part of the permanent test data. This event log lets the system operators and test users log significant events manually and the system automatically logs all limit changes, limits exceeded and other test related information. This feature has already proven to be useful in reviewing historical events after test completion.

### **TESTS COMPLETED WITH S<sup>3</sup> TO DATE**

To date over 180 tests have been completed using S<sup>3</sup> for data acquisition. These tests have ranged in size from small tests with only 4 thermocouples to large spacecraft subsystem tests with more than 200 channels of data. Numerous tests have been performed on *Wide Field/Planetary Camera II* hardware in preparation for the replacement of the original camera in the *Hubble Space Telescope*. Other space flight programs which have been supported with data acquisition during thermal vacuum tests are: *Mars Observer*, *Topex*, *Lambda Point Experiment*, *MSTI*, *NSCAT*, *Galileo* and the *CRAF/Cassini* projects.

### **PLANS FOR THE FUTURE**

Because of the success of the S<sup>3</sup> data acquisition system and the fact that the system is meeting and/or exceeding all of our operational requirements, no plans exist at present, for any major changes to the software or hardware.

Upgrades and new releases to the various software components will be installed only when it can be shown that the upgrade will significantly improve the performance of the system. Both *Fox Software* and *Novell* plan to release major software updates in the near future and these updates will be evaluated prior to installation into the system.

## **CONCLUSION**

The personal computer based data acquisition system which was designed and built by JPL has met or exceeded all of the requirements for the intended application of acquiring, recording and processing thermal-vacuum test data.

The success of the system design can be attributed to careful up-front planning, development of specific detailed requirements, the implementation of design ideas from a broad range of users, developers and system operators and the attention to detail by the software development engineering staff during both the system design phase and the software coding phase.

The hardware has proven to be very reliable and the use of commercial off-the-shelf software packages and a fault tolerant networking system has also contributed to system reliability.

Finally, the simplicity of operations and the easy to comprehend graphic user interface has provided a significant cost savings in both user training and test setup times.

A  
NEW  
THERMAL VACUUM FACILITY  
at the  
MARTIN MARIETTA  
WATERTON PLANT

Robert N. Watson  
Pitt-Des Moines Inc.

John W. Bonn  
CVI Inc.

---

ABSTRACT

A new Thermal-Vacuum facility has been recently completed at the Martin Marietta Waterton plant near Denver, Colorado. The facility was designed, fabricated, installed and tested as a turn-key project by Pitt-Des Moines Inc. and CVI Inc. The chamber has a 5.49 M by 6.10 M (18' by 20') flat floor and a half-cylindrical roof with a diameter of 5.49 M (18'). Both ends of the chamber have full cross section doors, with one equipped with translating motors for horizontal motion. The chamber is provided with four 0.91 M (36") cryopumps to obtain an ultimate pressure of  $9 \times 10^{-8}$  Torr (Clean-Dry-Empty). The thermal shroud is designed to operate at a maximum of  $-179^{\circ}\text{C}$  ( $-290^{\circ}\text{F}$ ) with an internal heat input of 316 MJ/Hr (300,000 BTU/Hr) using liquid nitrogen. The shroud is also designed to operate at any temperature between  $-156^{\circ}\text{C}$  ( $-250^{\circ}\text{F}$ ) and  $121^{\circ}\text{C}$  ( $+250^{\circ}\text{F}$ ) using gaseous nitrogen, and heat or cool at a rate of  $1.1^{\circ}\text{C}$  ( $2^{\circ}\text{F}$ ) per minute.

INTRODUCTION

In September of 1991, Pitt-Des Moines Inc. and CVI, Inc. completed work on a new Thermal-Vacuum facility for Martin Marietta. The vacuum chamber and associated equipment were installed in an addition to an existing building at Martin Marietta's plant located near Waterton, Colorado. The chamber was designed as a general purpose facility for thermal-vacuum testing of components or systems for satellites and space vehicles, and complements existing capabilities at the plant. While the new chamber shares rough vacuum pumping equipment and bulk  $\text{LN}_2$  storage with the existing chambers, it is otherwise functionally independent of the other chambers. The chamber and support equipment is controlled from a central console mounted on a mezzanine adjacent to the chamber.

The facility consists of three main systems: the chamber system, the vacuum system and the thermal system. The chamber system incorporates the vacuum boundary elements, including penetrations and doors, the personnel and equipment access bridges and the internal hardpoints for mounting test articles and support equipment. The vacuum system comprises the external equipment required to evacuate the chamber, repressurize it, and purge for personnel entry. The thermal system includes the shroud and  $\text{LN}_2$  and  $\text{GN}_2$  equipment necessary for establishing the desired temperature environment in the chamber. Support systems include utility  $\text{LN}_2$  and  $\text{GN}_2$  supplies, instrumentation and control, and primary and backup power distribution.

This paper will provide an overview of each of these systems, including each system's operational features and performance requirements.

## CHAMBER SYSTEM

### Vacuum Chamber

As shown in Figure 1, the vacuum chamber for the facility is in the shape of a mailbox, with a flat operating shroud floor, vertical sidewalls to the midheight, and a cylindrical roof. The chamber floor is 5.49 M (18') wide by 6.10 M (20') long and is flush with the elevation of the surrounding laboratory. In order to match these floor elevations, the chamber is mounted on supports in a pit formed into the foundation for the building addition. The chamber is rigidly attached to a large concrete seismic mass to provide a stable vibration isolated platform for test operations.

This vacuum chamber shape provides several operational and construction advantages. The flat floor minimizes wasted internal volume and allows simple shroud and chamber supports. It also provides a minimum distance between the item under test and the external support equipment. The flat vertical side walls also minimize penetration complexity and difficult interfaces with the surrounding building partitions.

### Chamber Doors

Access to the chamber is provided through o-ring sealed doors located on the east and west ends of the chamber. The PDM FLEX-SEAL door flange system was used on both doors, since it accommodated the square lower corners and door size without costly field machining. The east door is motorized and mounted on rails that permit it to translate outward and then south. The door system consists of three motor driven screw jacks that provide east-west door motion and a motor driven rail drive to move the door in a north-south direction. Limit switches on the system provide door position information to an local programmable logic controller (PLC), which automatically sequences the door motion. The local PLC is also linked to the main console PLC to prohibit door removal if a safe oxygen atmosphere is not present in the chamber. When fully open, the east door provides complete access to the full chamber cross-section. The west door is not currently motorized, with removal requiring the use of temporary rigging equipment. It can be outfitted with the same handling equipment as the east door.

### Access Bridges

At each end of the chamber are bridges [Figure 2] which span the door handling trench and provide access for personnel and equipment to the chamber from the laboratory floor. Each bridge is raised and lowered by a hydraulic system connected to the local control panel used for the door removal system. Limit switches on the system provide door position information to the local PLC which automatically sequences the bridge motion. The bridges have machined rails to allow the use of air casters to move equipment across the bridges and into the chamber.

### Internal Rails

Two full length internal rail hardpoints [Figure 3] are provided along the chamber floor for the support of test articles. These rails are aligned with the bridge rails and are also machined to permit the use of air casters. The rails may be removed for cleaning or maintenance and are not actively thermally controlled.

### Internal Hardpoints

Overhead, 12 pin hardpoints [Figure 4] projecting through the shroud plane provide lifting points for internal rigging. The hardpoints are threaded into sockets so that they may be removed for cleaning, modification or for shroud removal. The hard points can each be loaded vertically to 3340 N (750 pounds).

### Penetrations

The chamber is provided with over 80 penetrations, located predominantly on the vertical north and south walls [Figure 5]. Those on the south wall support the instrumentation, power, and control of the test article, and range in size from 914 mm (36") to 25 mm (1"). These penetrations communicate with a secure control room one floor below the main control room. Those on the north wall are primarily related to systems required for chamber and shroud operation. The largest of these is 406 mm (16") in diameter. Several penetrations are located in the cylindrical top of the chamber, the largest of these being the four 914 mm (36") cryopump penetrations. Five 304 mm (12") viewports are also provided, with four located in a horizontal plane approximately 2 meters above the laboratory floor and the fifth on top of the chamber. The viewports are equipped with lockable metal security covers.

## VACUUM SYSTEM

The vacuum system provides the equipment to evacuate the chamber to the design conditions of  $9.0 \times 10^{-8}$  Torr (clean/dry/empty),  $9.0 \times 10^{-6}$  Torr (hot shroud) and  $6.0 \times 10^{-6}$  Torr (ambient shroud, passive gas load of 0.15 Torr-liter/sec of Nitrogen), and then return it to a safe condition for personnel entry at atmospheric pressure.

### Rough Vacuum Pumping

The roughing segment of this system utilizes the existing Martin Marietta rough vacuum pumping system. The existing system consists of two parallel blowers and one backing pump. The line connecting the chamber to the pump contains a cold trap to stop oil migration from the roughing pumps. A high vacuum gate valve is installed at the chamber for isolation of the roughing system during high vacuum pumping of the chamber. A spectacle blind flange is installed between the cold trap and pumping system to allow blinding of the roughing line if service is required. The cold trap is supplied with a refrigerant compressor for closed loop operation. A warm gaseous nitrogen line can introduce gas to the roughing line at the cold trap to assist in the warm up of the trap.

## High Vacuum Pumping

The high vacuum system consists of four 914 mm (36") CVI Inc. cryopumps, each with a high vacuum gate-type isolation valve, mounted on the upper cylindrical part of the chamber. Connected to the cryopumps are the following support systems:

- LN<sub>2</sub> supply to the internal shrouds
- roughing lines
- high pressure helium supply to the expanders
- Heated GN<sub>2</sub> supply for regeneration
- Heated GN<sub>2</sub> supply for removal of LN<sub>2</sub> from the internal shroud
- auxiliary port for general use, with hand valves

The passive LN<sub>2</sub> supply for the internal shrouds is drawn from a run tank (secondary LN<sub>2</sub> storage) and forced through vacuum jacketed lines to the cryopumps by the vapor-space pressure in the run tank. Liquid level control is performed by vent valves on the exhaust side of the internal shroud system. Boiloff gas is piped to the central vent system and transmitted to the run tank area for venting outside the building. The roughing system for the cryopumps consists of a single rotary pump located in the mechanical room, and valves to connect the pump to one cryopump at a time. Helium gas for cryopump expander operation is supplied by flex hoses run from the compressors mounted on the elevated south platform. The regeneration system GN<sub>2</sub> is piped from the receiver in the mechanical room to the chamber area where it is heated and distributed to each cryopump.

To warmup the cryopump for regeneration or shutdown, warm GN<sub>2</sub> is supplied to the inlet side of the internal shroud system. By addition of GN<sub>2</sub> at this point, all LN<sub>2</sub> in the shroud is forced out into the central vent system.

## Repressurization System

The chamber repressurization system provides a connection from the vacuum chamber to the ambient temperature nitrogen receiver or to the room air. The nitrogen and room air piping combine into a common inlet pipe to the chamber. The system elements include: a flow control valve to control the rate of repressurization, an in-line filter to insure cleanliness of the incoming air or nitrogen, a flexible hose to stop piping vibrations from reaching the chamber, a high vacuum gate valve to isolate the chamber from the repressurization system during vacuum pumping, and a relief valve to prevent excessive pressure to build up against the vacuum gate valve. Within the chamber, the common inlet pipe branches into two pipes with a silencer at the end of each pipe to lessen the noise during repressurization and to break up the incoming flow so that it will not impinge on the shrouds or test articles. The nitrogen branch of the repressurization system contains a restricting orifice. The restricting orifice provides pressure drop during repressurization and limits the amount of flow possible to the vessel in the event of a control valve failure. The room air branch of the repressurization system contains an isolation valve and has a filter/silencer at its inlet to reduce the noise during repressurization. A safety interlock will limit GN<sub>2</sub> repressurization to a value less than one atmosphere and switch to room air for final equalization.



## Purge System

The chamber purge system consists of a HVAC-type blower which draws room air through the chamber to replenish the oxygen content. The blower is connected to the vacuum chamber with duct work which is vibration isolated with a flexible rubber section. A high vacuum gate valve is at the chamber connection to isolate the blower from the chamber during vacuum pumping. A high vacuum gate valve is mounted on the nozzle for isolation of the air inlet during vacuum pumping. A HEPA filter is mounted on the inlet vacuum gate valve to insure cleanliness of the incoming air to the chamber. The chamber oxygen monitoring system consists of two oxygen analyzers independently drawing samples from the chamber. The samples are drawn by a diaphragm pump which draws air from the chamber through a tube for each analyzer. A high vacuum valve isolates each oxygen monitoring system from the chamber during chamber vacuum pumping. A solenoid operated calibration valve is located in the line to each analyzer. It is a three way valve which allows either room air or chamber air to flow to the oxygen analyzer. A flow switch in the line checks to be sure that there is flow to the analyzer. The controls to open the chamber door remain deactivated until both oxygen sensors indicate a safe environment inside the chamber.

## SUPPORT SYSTEMS

### Liquid Nitrogen Supply System

LN<sub>2</sub> is supplied to the chamber Run Tank from the existing Martin Marietta storage sphere using a transfer pump [Figure 6]. The Run Tank is designed to provide buffer storage of LN<sub>2</sub> for use on the 18x20 Thermal-Vacuum Chamber, instead of drawing all needed LN<sub>2</sub> directly from the main LN<sub>2</sub> sphere. With this arrangement, a test in the 18x20 chamber can be continued for up to 5 hours while maintenance is performed on the main storage sphere or LN<sub>2</sub> transfer pump. The secondary function of the Run Tank is to serve as the ultimate heat sink for the shrouds and program loads by way of the subcooling coil. Finally, the run tank serves as a recovery system in the event that LN<sub>2</sub> is to be removed and stored from the shrouds, program loads or water vapor pump.

The LN<sub>2</sub> transfer system consists of the pump, associated inlet and outlet isolation valves, a cooldown valve, and piping from the LN<sub>2</sub> sphere to the run tank. A temperature element in the cooldown line determines if the cooldown valve is needed to be open. If all the valves around the pump are closed, a pressure relief valve will protect the system from overpressure. The PLC will automatically maintain the tank at a preset level and interlocks will also prevent closure of all valves and trapping of LN<sub>2</sub>.

The run tank is a 22.7 M<sup>3</sup> (6000 gallon) double wall LN<sub>2</sub> storage tank located on the exterior pad on the south side of the building. Inside the inner tank is the subcooler coil connected to the Shroud and Auxiliary LN<sub>2</sub> systems. The run tank is equipped with a level sensor (based upon differential pressure) that controls the operation of the LN<sub>2</sub> transfer pump at the main LN<sub>2</sub> sphere. The vent system from the inner tank is provided with a pressure control valve which is used to vent excess gas to maintain a nominal 103 KPa to 138 KPa (15 to 20 PSIG) pressure in the vapor space. To provide makeup GN<sub>2</sub> during top fill operations, a supply from the receiver with a pressure regulator has been provided. The tank is also equipped with provisions for filling from a tank truck and pressurization

using a pressure building coil.

### Gaseous Nitrogen Supply System

Gaseous nitrogen is supplied to the facility by use of an electric vaporizer. Nitrogen leaves the vaporizer and is piped to a receiver inside the building at 21 °C (70 F) plus/minus 2.8 °C (5 F) by a SCR controlled electrical power supply. The SCR output is based on the temperature measured at the vaporizer outlet. A high temperature limit will shut down the power to the unit if the heater temperature reaches 149 °C (300 F). The temperature of the GN<sub>2</sub> leaving the vaporizer is continuously indicated at the main control console.

### Instrumentation and Control System

The chamber and support systems are controlled from a central console located one floor above the chamber operating floor. The console [Figure 7] houses the main system Programmable Logic Controller (PLC), all instrumentation displays, all valve and equipment controls, and the central data logging system. The front panel provides a graphic depiction of all chamber systems.

Interlocks for operation of valves and equipment are provided by a Programmable Logic Control system. The system consists of an Allen-Bradley PLC-5 unit mounted in the main rack inside the control console and two remote Input/Output racks, one mounted above the vacuum chamber and another on the south exterior pad. The three racks contain removable input, output, power supply, communications and processor cards. A plug has been provided in the front right face of the control console for connection of a supplied Allen-Bradley T-50 programming terminal.

The data logging system is designed to acquire and record the shroud temperatures, chamber pressure and roughing line pressure during a test. The shroud temperatures are sensed by Type E thermocouples distributed throughout the shroud zones. Temperatures in the auxiliary LN<sub>2</sub> circuits are monitored by Type E thermocouples.

## THERMAL SYSTEM

### Shroud System

The shroud system consists of subassemblies fabricated from aluminum extrusions (that include passage ways for the thermal conditioning fluids) welded onto aluminum sheet materials. End shrouds are attached to the chamber's end doors and move with those doors. Floor sections of the shroud system are fabricated from aluminum plate with channel shaped aluminum extrusions that also include passage ways for thermal conditioning fluids. The sidewalls, ceiling panels and floor panels are removable from the chamber, using a tailored handling fixture.

This shroud system is divided into seven thermal control zones. All floor sections of the shroud are designed to support the loads incurred from test technicians walking on the shroud. A complete schematic of the shroud LN<sub>2</sub>/GN<sub>2</sub> piping and distribution system is presented in Figure 8.

The test function of these shrouds is to provide an adequate thermal simulation of the specified test conditions. Using LN<sub>2</sub> as the thermal conditioning fluid, they will simulate the thermal sink conditions of the satellite environment and using GN<sub>2</sub> as the thermal conditioning fluid, a wide range of thermal simulations can be produced (both steady-state and thermal ramps). In the steady-state LN<sub>2</sub> mode, subcooled liquid nitrogen (e.g., liquid at temperatures well below the boiling point associated with the elevated pressures within the closed loop system) is circulated through the shroud system and absorbs the heat loads originating from the test article and from the warmer, outside chamber walls. All seven shroud thermal control zones are connected in series with each other, in this mode. With LN<sub>2</sub> circulating through the shrouds at 0.3 M<sup>3</sup>/Min (80 gpm) and a heat load of 3.72 W/M<sup>2</sup> (40 watts/ft<sup>2</sup>) applied to the shrouds, the fluid temperature rise through the shroud will be approximately 7.2 °C (13 F).

In GN<sub>2</sub> operating modes (steady-state and transient), the seven shroud zones are connected in parallel with each other. Flow control valves at the exit of each zone are automatically modulated by temperature controlled valves in a feedback control loop to maintain uniform thermal control over the shroud zone temperatures. As in the LN<sub>2</sub> operating mode, the fluid absorbs the combined heat loads from the test article and the chamber walls. The shroud system and its' GN<sub>2</sub> Thermal Control System are designed to support steady-state operations with the shroud temperature ranging from -179 to 121 °C (-250 F to +250 F). They will also support transient thermal ramp tests over this temperature range, at rates up to ± 1.1 °C/Min ( ±2.0 F/minute). Depending on the test conditions and the test article, the GN<sub>2</sub> controlled shroud may serve as either heat sink or heat source.

### LN<sub>2</sub> Supply System

Liquid nitrogen for the thermal system is drawn from the Run Tank and fed to the Main Pump Skid. The LN<sub>2</sub> Main Pump Skid includes two parallel LN<sub>2</sub> pumps. The Shroud LN<sub>2</sub> Pump supplies LN<sub>2</sub> to the chamber shroud system and the Auxiliary LN<sub>2</sub> Pump supplies LN<sub>2</sub> for the GN<sub>2</sub> Thermal Unit, the Program Loads (auxiliary LN<sub>2</sub> zones) and the LN<sub>2</sub> Vaporizer. At elevated pressures (above one atmosphere) LN<sub>2</sub> will have elevated boiling temperatures (above the 77.4 K at one atmosphere). By maintaining sufficiently elevated pressures throughout the complete LN<sub>2</sub> circuit, the fluid can absorb heat from the thermal loads and still remain in the liquid state. In this system, a low pressure point is created at the throat of the venturi that's located just upstream of the LN<sub>2</sub> pump inlets. In steady state operating modes, these pumps draw LN<sub>2</sub> from the subcooling heat exchanger, in the Run Tank, through a venturi, where any necessary make-up LN<sub>2</sub> is introduced. Either or both of these pumps can be operated in an off-line, closed loop mode or feed the liquid through the respective loads. A schematic of this pump skid subsystem is presented in Figure 9.

## GN<sub>2</sub> Thermal Unit

The GN<sub>2</sub> Thermal Control Unit manufactured by CVI Inc. is a stand-alone skid mounted system supplying thermally controlled GN<sub>2</sub> to the shroud system using a 75 HP turbine as the circulating device and a combination of electric heater and LN<sub>2</sub> mixer/injector for thermal modulation. A schematic of this skid subsystem is presented in Figure 10. This closed loop, GN<sub>2</sub> system is designed to provide steady-state shroud operations at any selected temperature between -179 and 121 °C (-250 F and +250 F). It will also support shroud thermal transients within the range of 1.1 °C/Min (2.0 F/minute). Maximum flow rate is required from this system to accomplish the maximum warm-up and cooldown rates; much lower flow rates are required at the design steady-state operating conditions. The rotational speed of the hermetically sealed turbine unit is automatically modulated by a variable frequency drive. This speed is modulated by a controller using turbine load feedback. A 100 KW, in-line electric heater adds heat to the circulating stream, when heat is being added to the GN<sub>2</sub>. When heat is being extracted from the GN<sub>2</sub>, the supply temperature is maintained by injecting a spray of LN<sub>2</sub> into the circulating fluid. Both power to the heater and LN<sub>2</sub> to the mixer are controlled by a temperature controller. Excess or make-up GN<sub>2</sub> is accommodated by pressure regulating valves on a vent line and on a GN<sub>2</sub> supply line from the GN<sub>2</sub> Receiver Tank.

For steady-state operation at -179 °C (-250 F), with an internal heat load of 65.4 MJ/Hr (62,000 Btu/hr), the turbine operates at about 3,000 rpm, supplying about 7390 Kg/Hr (16,300 lb/hr) of GN<sub>2</sub> and maintaining the maximum shroud temperature differential within ±11.1 °C (±20 F). For steady-state operation at 121 °C (+250 F), with an internal heat extraction of 22.2 MJ/Hr (21,000 Btu/hr), the turbine operates at about 6,000 rpm, supplying about 4310 Kg/Hr (9,500 lb/hr) of GN<sub>2</sub> and maintaining the maximum shroud temperature differential within ±11.1 °C (±20 F). During 1.1 °C/Min (2.0 F/min) transients between -179 and 121 °C (+250 F and -250 F), flow rate and rpm will vary from 23100 Kg/Hr (51,000 lb/hr) and 8,600 rpm at -179 °C (-250 F) to 9980 Kg/Hr (22,000 lb/hr) and 13,000 rpm at 121 °C (+250 F).

## CONCLUSIONS

The new Thermal Vacuum facility completed by PDM and CVI for Martin Marietta verified the utility and value of several of its novel features. The mailbox shape of the vacuum vessel proved to be a convenient, space-saving arrangement for test operations. The shape also met the required vacuum level and leak tightness requirements in an economical manner. In the GN<sub>2</sub> Thermal Unit, the use of the cold turbine circulator appears to be a reliable solution for shroud operations between -179 and +121 °C (-250 and +250 °F). It also permitted much smaller line sizes and skid size over that required using a warm blower with a heat exchanger.

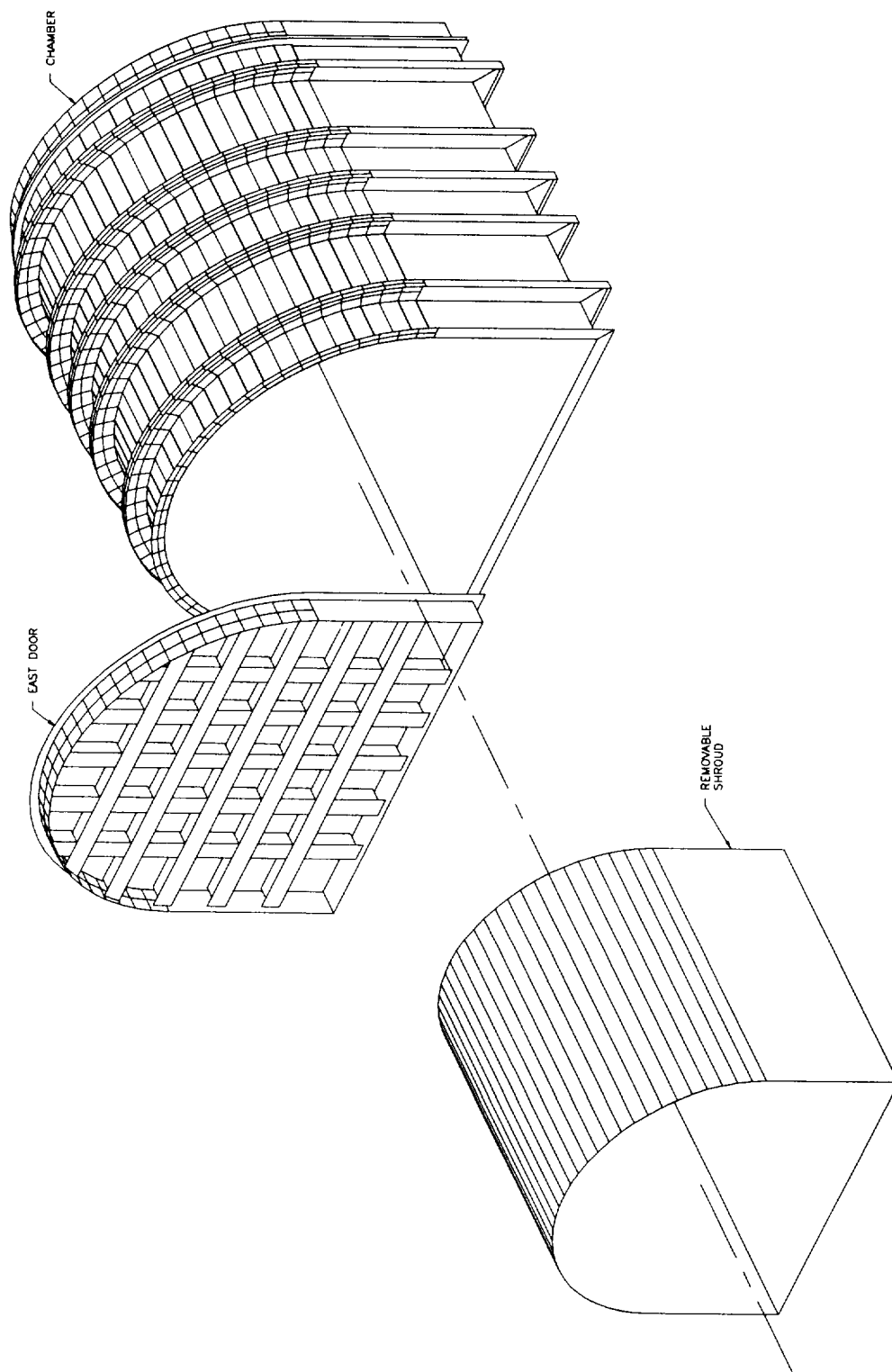
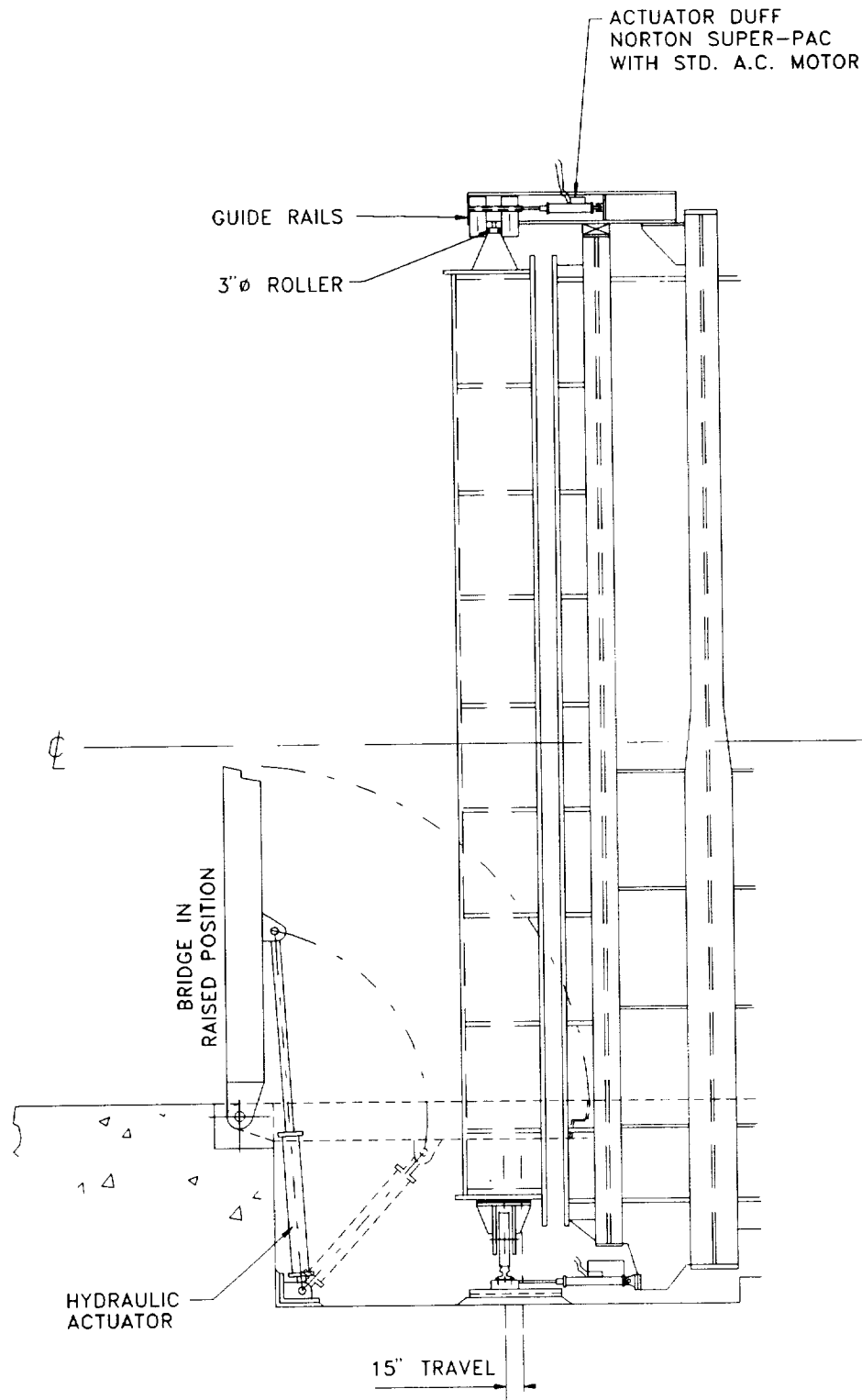
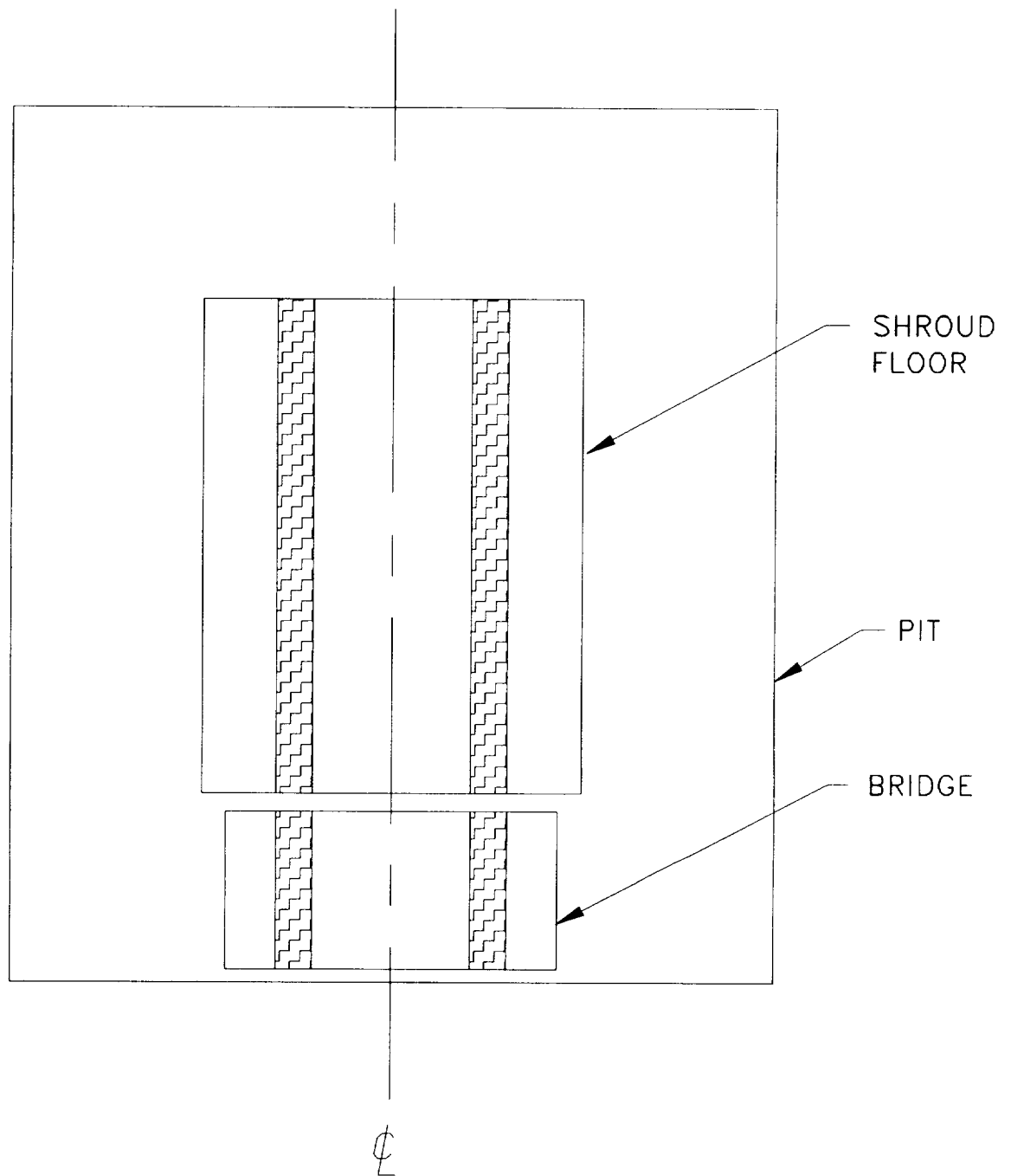


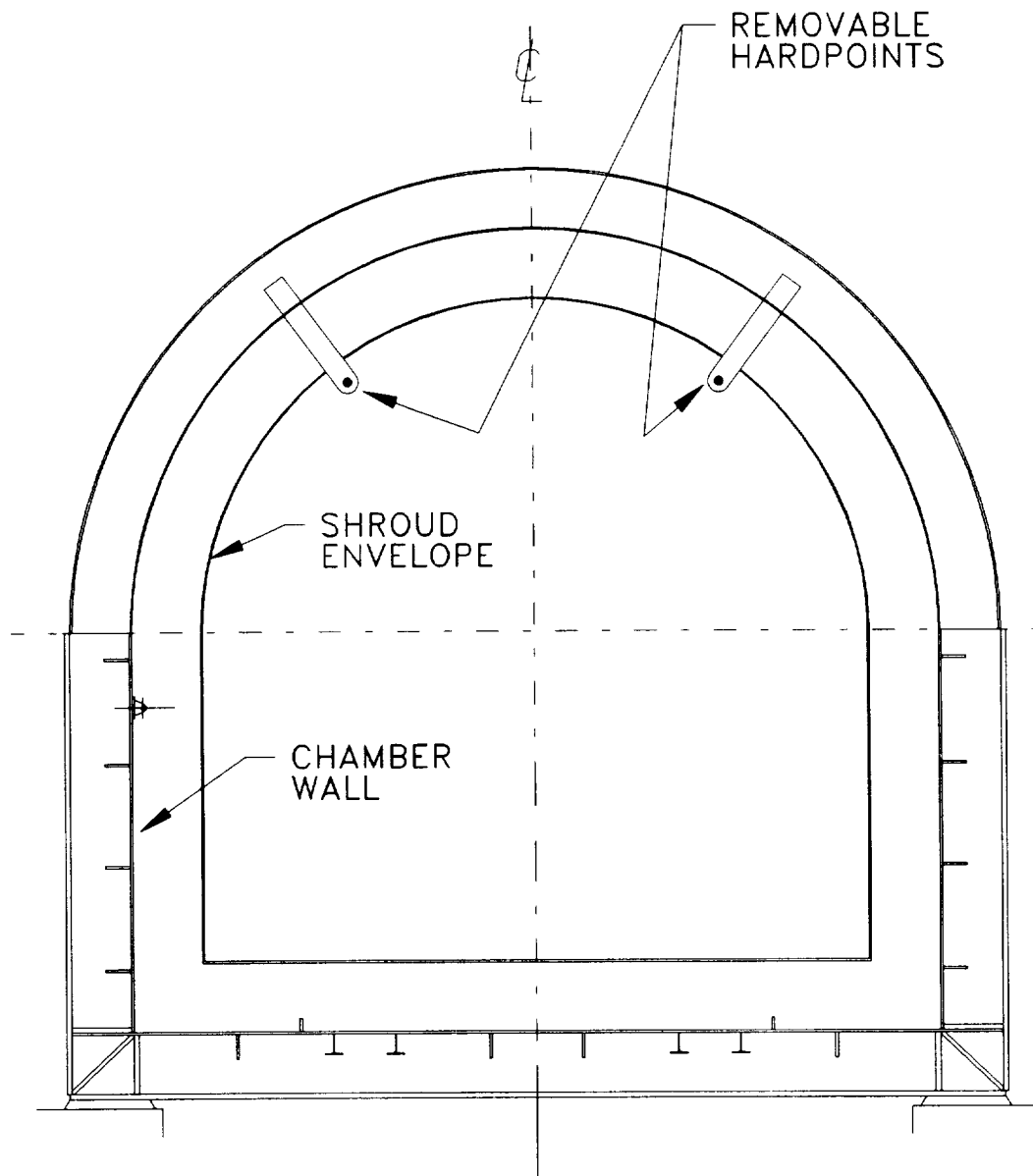
FIGURE 1  
GENERAL ARRANGEMENT



**FIGURE 2**  
EAST DOOR ELEVATION

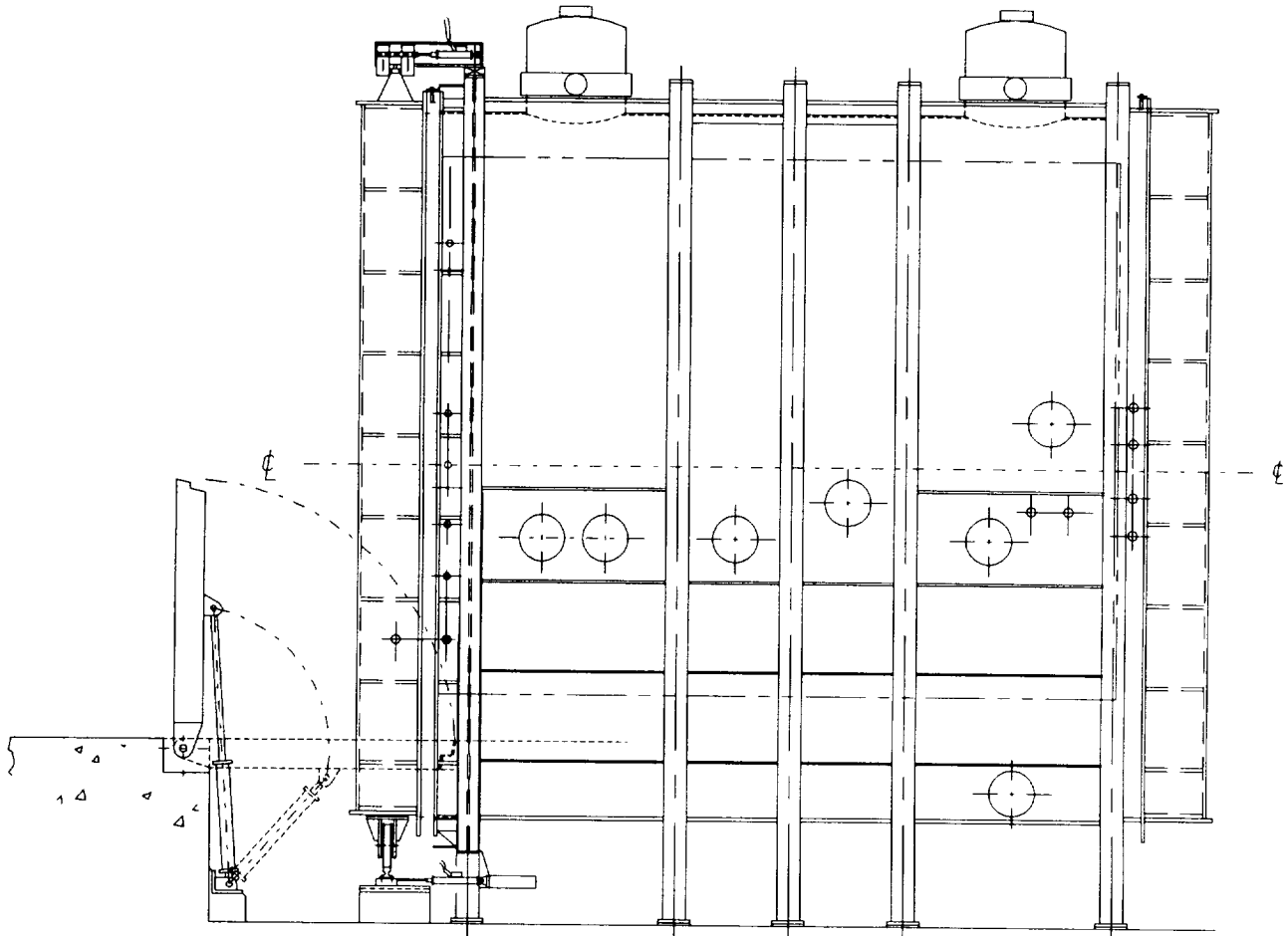


**FIGURE 3**  
RAIL HARDPOINTS – PLAN VIEW

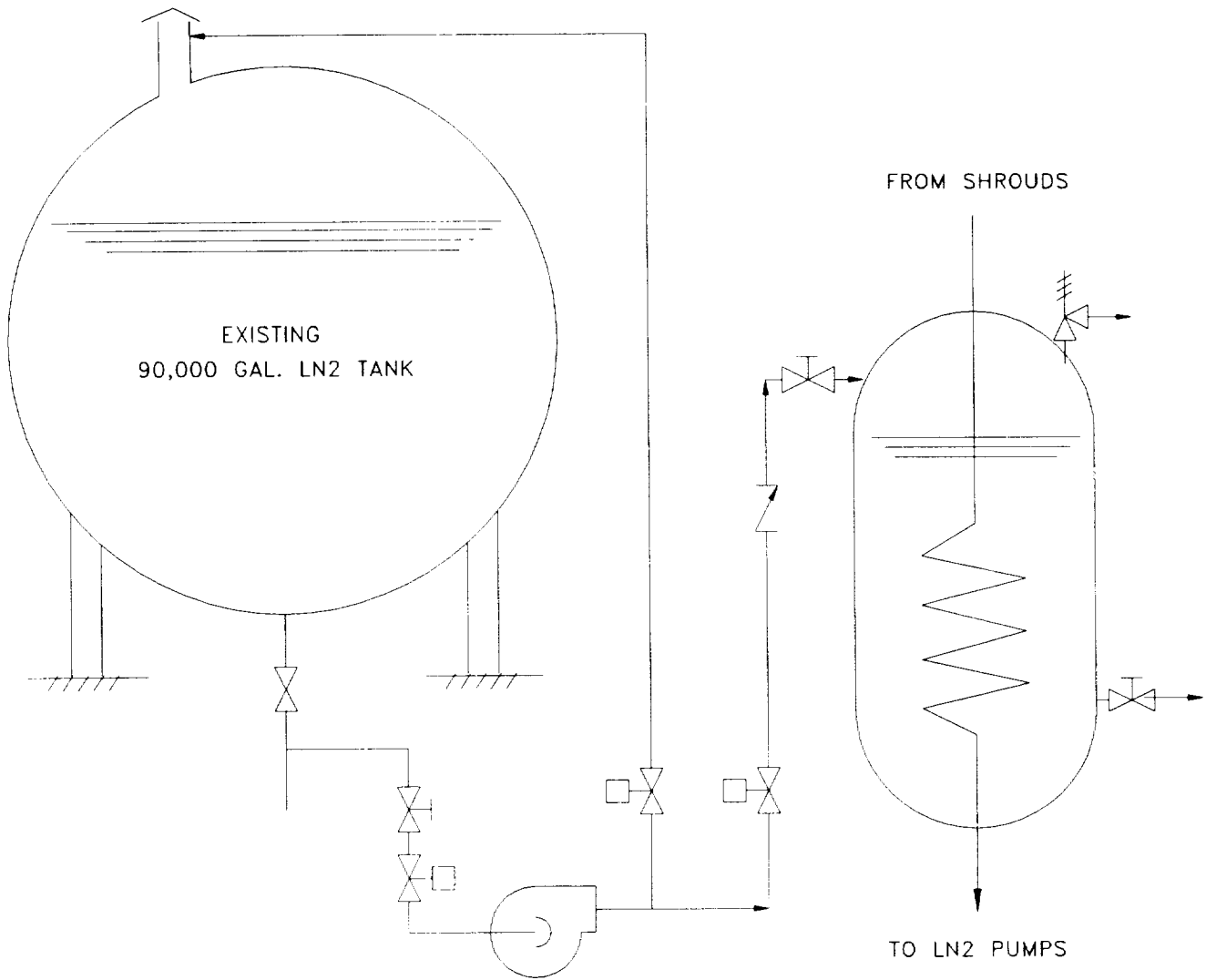


**FIGURE 4**  
PIN HARDPOINTS





**FIGURE 5**  
NORTH PENETRATIONS



**FIGURE 6**  
**LN2 SUPPLY SYSTEM**

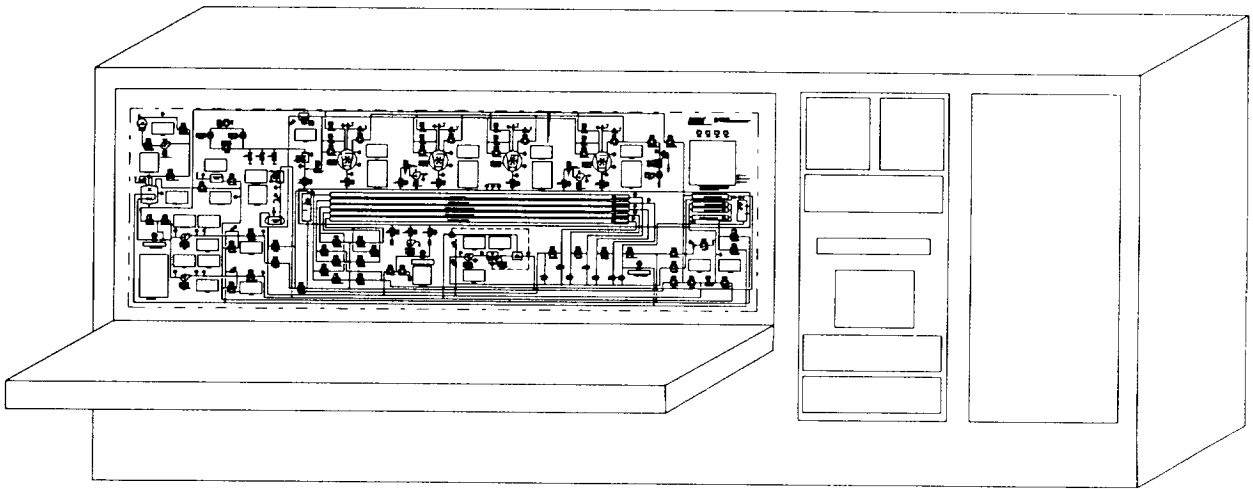
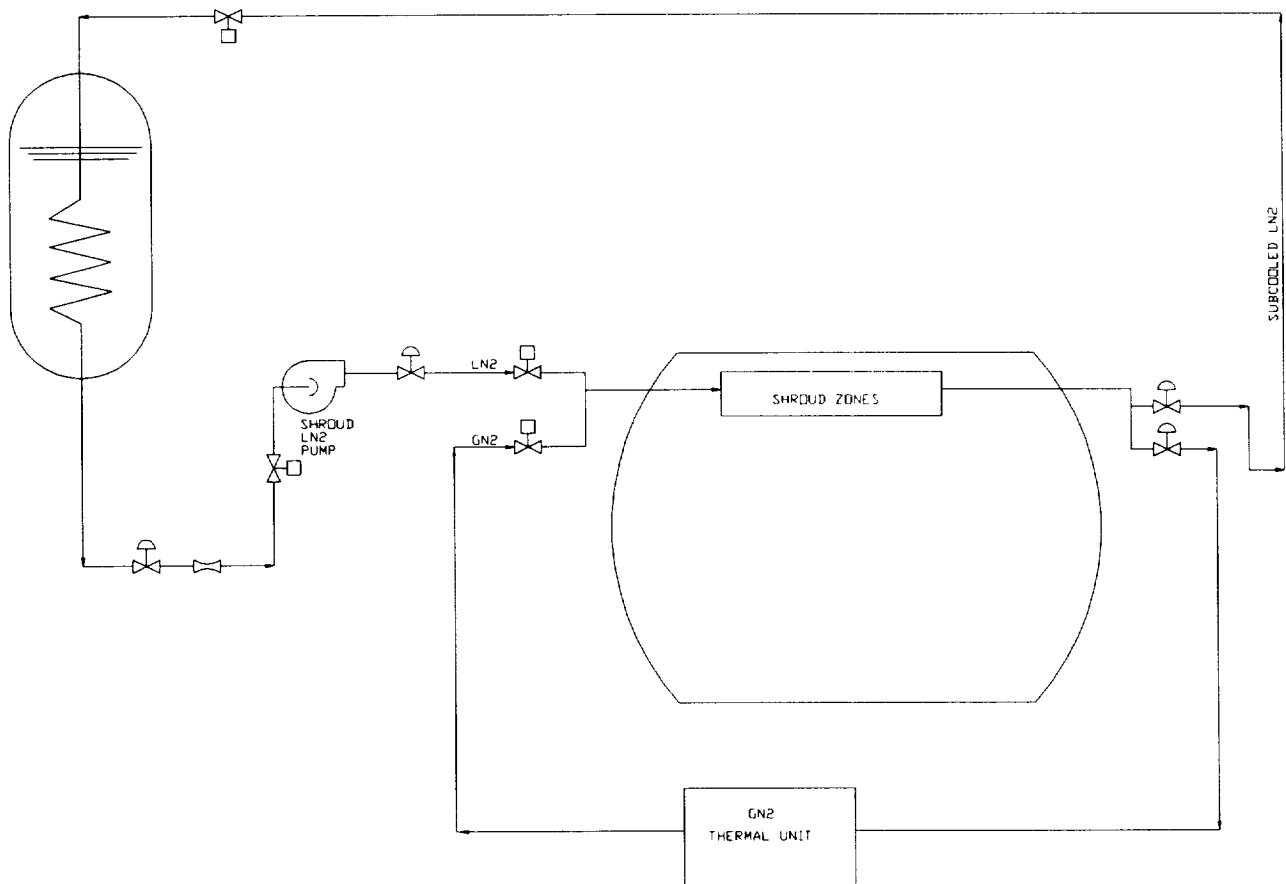
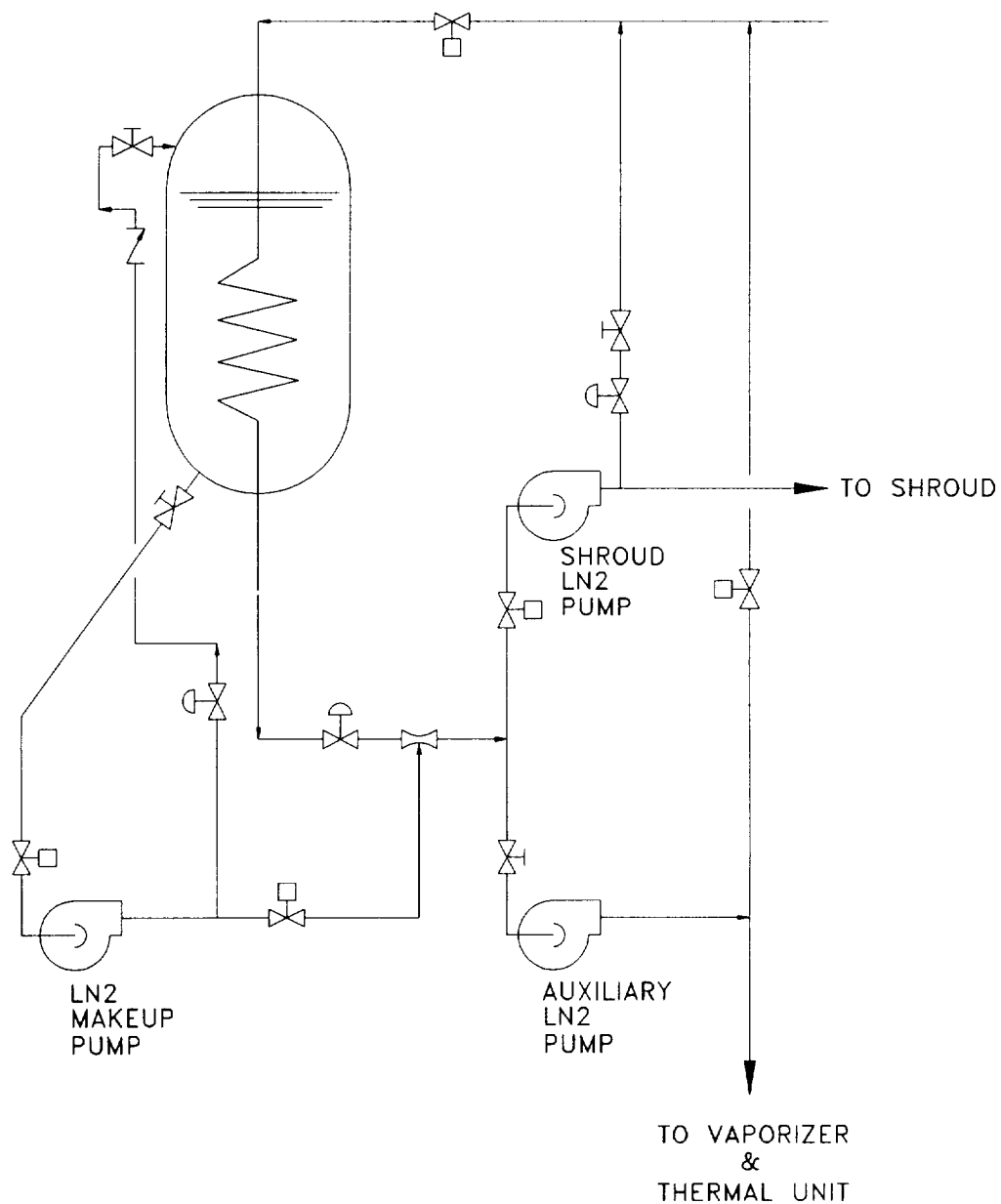


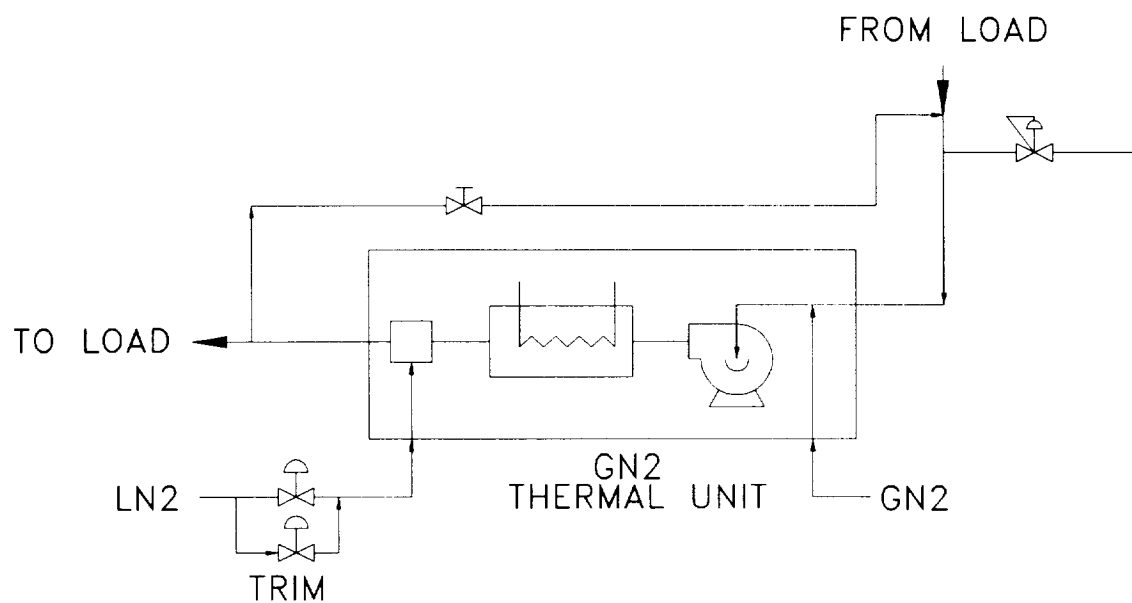
FIGURE 7  
CONTROL CONSOLE



**FIGURE 8**  
**SHROUD LN2/GN2 SYSTEM**



**FIGURE 9**  
**LN2 PUMP SKID**



**FIGURE 10**  
THERMAL UNIT

## APPLICATION OF PROGRAMMABLE LOGIC CONTROLLERS TO SPACE SIMULATION

Janet Sushon  
NSI Technology Services Corp.

### PART I

#### MODERNIZATION OF SPACE ENVIRONMENT SIMULATOR AT THE GODDARD SPACE FLIGHT CENTER

As a contractor at GSFC, NSI Technology Services Corporation is involved in operating the Center's Test and Integration facilities, and in planning and implementing modernization projects.

The Space Environment Simulator located at the Goddard Space Flight Center in Greenbelt, Md., is a large chamber designed for system level thermal vacuum testing of spacecraft. It was built in the early 1960's and at that time represented a the state-of-the-art vacuum pumping and control system. It was supported by the following subsystems:

Vacuum pumping system - consisting of 17 large LN<sub>2</sub> trapped, oil diffusion pumps.

Thermal system: LN<sub>2</sub>, GN<sub>2</sub> and Helium skids

Solar simulator - capable of projecting one solar constant filtered to a close spectral match of the Sun.

Data acquisition system.

CCTV system.

Voice and data communication.

The vacuum system upgrade included: replacement of seventeen diffusion pumps with eight cryogenic pumps and one turbomolecular pump, replacing a relay based control system, replacing vacuum instrumentation, and upgrading the data acquisition system.

This paper discusses incorporating a state-of-the-art process control and instrumentation system into this complex system for thermal vacuum testing.

The challenge was to connect several independent control systems provided by various vendors to a supervisory computer. This combination will sequentially control and monitor the process, collect the data and transmit it to color a graphic system for subsequent manipulation.

Even though most manufacturers claim to have some sort of computer interface, there is no standard computer interface. Among several types of interfaces were: Binary Coded Decimal (BCD) both at TTL level and low true 30V open collector; analog (5 volts pressure signal, linear on a logarithmic scale, and 0-10 volts linear signal); and RS-232C, RS-422. Equipment was scattered over a large area, and the floor space for the control console was limited.

To accommodate all these essential considerations and to reduce development time, it was decided to select off-the-shelf hardware and software packages. After review and demonstration of several methods, we selected a system compatible with the requirements.

A control device called a Programmable Logic Controller (PLC) was chosen to perform numerous control functions, and to serve as a gateway between multiple control and measurement subprocesses.

Initially developed to replace the use of the electro-mechanical relay, PLCs have gone far past that requirement. Modern PLCs are powerful industrial computers with a broad assortment of highly sophisticated input and output devices and advanced instruction sets.

Among many advantages offered by the PLC are the following:

- PLC-based systems can be easily altered through a programming device to handle changes in the process control requirements without having to rewire relays.
- PLC-based systems are easy to maintain and repair because of plug-in assemblies, and are more reliable in an industrial environment - thus reducing downtime.
- PLCs are also smaller than relay control panels, saving expensive floor space.

Several functions executed by PLC's that cannot be performed by relays are: supplying data to computer-based monitoring and data acquisition systems. Personal computers, loaded with appropriate software and linked to PLCs on the data highway can provide a full graphical operating environment for operators, as well as a programming and applications development capabilities for engineers.

Placing the programmable controller's main processor in the control console and a using a remote input/output (I/O) interface to equipment minimized wire runs and simplified start-up and maintenance.

Proper grouping of remote I/O's allows minimization of single point failure impact on other systems. The grouping of the I/O's allows signal and power lines to be routed properly through the wiring ducts, so that crosstalk interference is substantially reduced.

PLC system architecture for this project was mapped in the following manner:

- Two Central Processing Units (CPU) arranged in redundant configuration to assure a high level of reliability;
- Fourteen remote I/O drops on a single coaxial communication link;



- Two 386-33MHz colorgraphic systems, communicating to both PLC's on the data highway.

Intelligent devices exchange data on the following independent levels:

1. Primary CPU to secondary CPU
2. Primary CPU to remote I/O drops
3. Primary CPU to colorgraphic systems
4. Intelligent field transducers to PLC input modules.

All the communication nodes on the system are distributed among the following physical sites:

Vacuum Console  
Field Interface Cabinets  
Facility Monitoring Console  
Mimic Panel.

ORIGINAL PAGE  
BLACK AND WHITE PHOTOGRAPH



Figure 1: Vacuum Console

### Communication Between Primary and Secondary CPU's

In the relay-based control system, a relay failure can take the whole system out of operation. By configuring the PLC system for hot backup communications, shutdowns caused by processor faults are virtually eliminated.

However, a PLC hot backup communication scheme will not guard against shutdowns

caused by faults in equipment other than the programmable controller, s.a. power losses, instrumentation faults, etc.

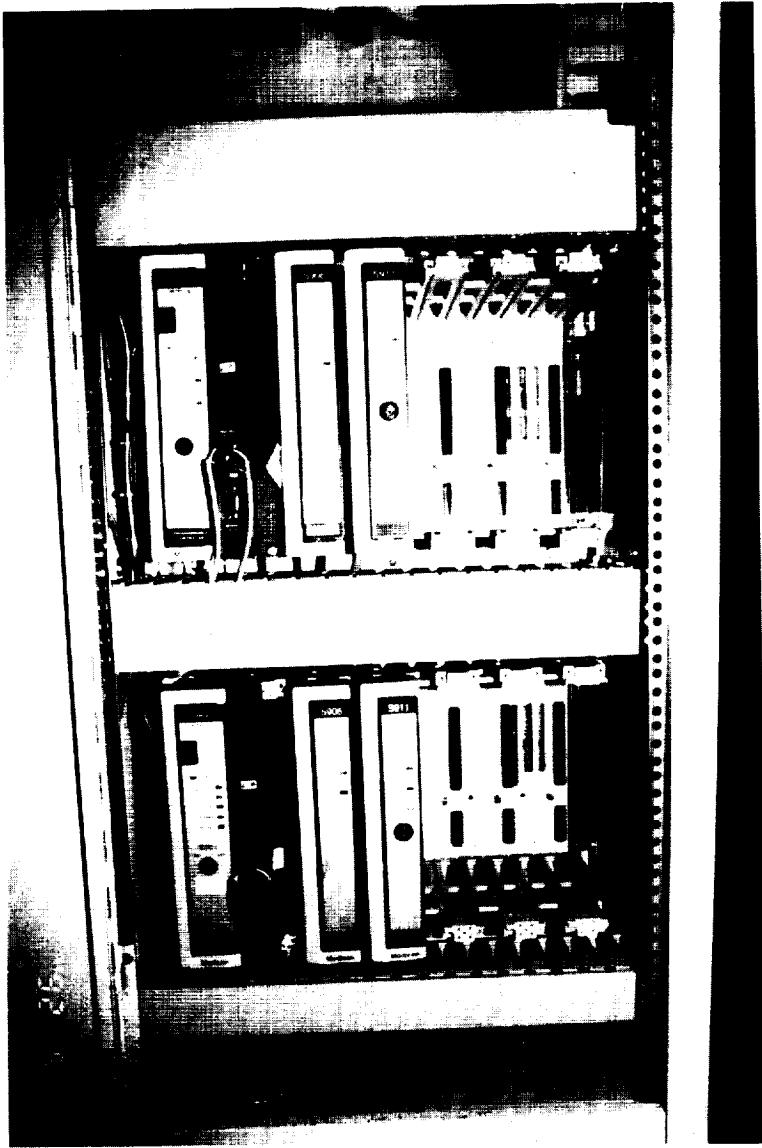


Figure 2: Two CPU's arranged in redundant configuration

The hot backup scheme works as follows: both the primary and backup processors monitor the same inputs; the backup processor takes control quickly (within 40msec) when the primary processor shuts down.

Peer to peer communication between the primary PLC and other equipment on the communication link is set up in the same manner as with a PLC without backup. Both processors have the same station number.

Every PLC switchover is detected and properly reported on the annunciator panel.

The program scans are not synchronized and the switchover, although fast (conservatively estimated, 50 msec) is not instantaneous. Therefore, it is possible that the processors could see different input conditions during a given program scan and the outputs may be assigned different states in the two processors. This can cause a sudden change in operation when switchover occurs.

Possible consequences of such an event are:

- An output controlling pump can switch to the OFF state.
- Any input pulse with a short duration (less than 40 ms) can be missed by the processor.

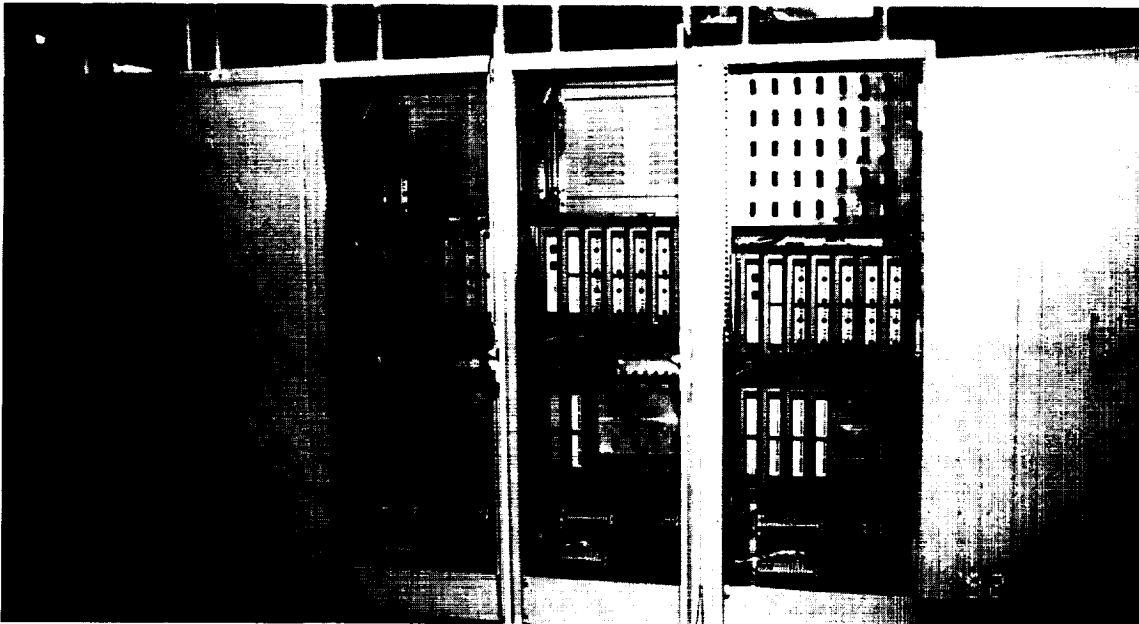
The probability of such pulses occurring is not great but it has to be considered.

The situation is handled as follows:

Should a pump pause briefly, it will not restart automatically; all vital inputs (such as Emergency Shutdown) are hardwired to interrupt power.

#### **Primary CPU to remote I/O drops**

Due to the fact that equipment is widely spread over a large area and pulling a lot of cables to one central location would not be practical, the PLC's inputs/outputs were distributed throughout the lab. A group of cabinets housing I/O modules was strategically placed to collect all the data associated with the process, as well as to control its machinery and equipment. Sequencing of the equipment and coordination of the independent control systems requires the system to communicate with the I/O's.



**Figure 3: Field Interface Cabinets**

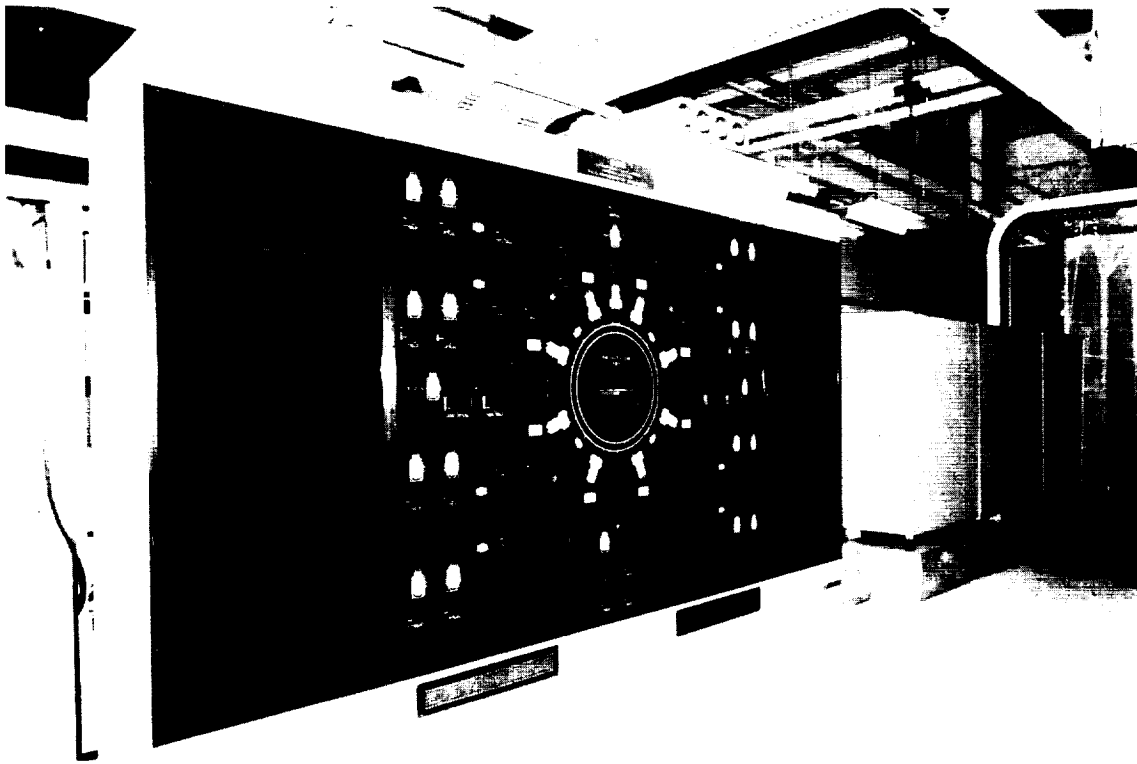


Figure 4: Mimic Board

The mimic board provides a graphical representation of the process as well as information on process status, s.a. pump status, valve position. Digital readouts provide the process variables (pressure & temperature) information.

#### **Primary CPU to colorgraphic systems**

One of the desired system features included an effective operator interface with high quality graphics and multiple screen capabilities. To provide this feature two identical colorgraphic systems were utilized for the operator interface. Both monitors display a facility mimic screen for any of several standard configurations selected by the operator. Each display provides a graphical representation of the valves, piping and equipment used for this particular subsystem. The status of the valves (Open/Closed), pumps (On/Off), process variables are dynamically updated. Screen selections in the system are made with a mouse. This simplifies operator learning and eliminates the possibility of pressing the wrong key on a keyboard.

System development was based on a total quality management approach in which the users - that is both operating and maintenance technicians viewed animated sequences and display screens at various stages of development. This approach promoted operator acceptance of the system, while enabling numerous changes to be implemented to improve the facility operations.



Figure 5: Colorgraphic System

### Intelligent field transducers to PLC intelligent input modules

The PLC gathers information from vacuum instrumentation in the following manner:

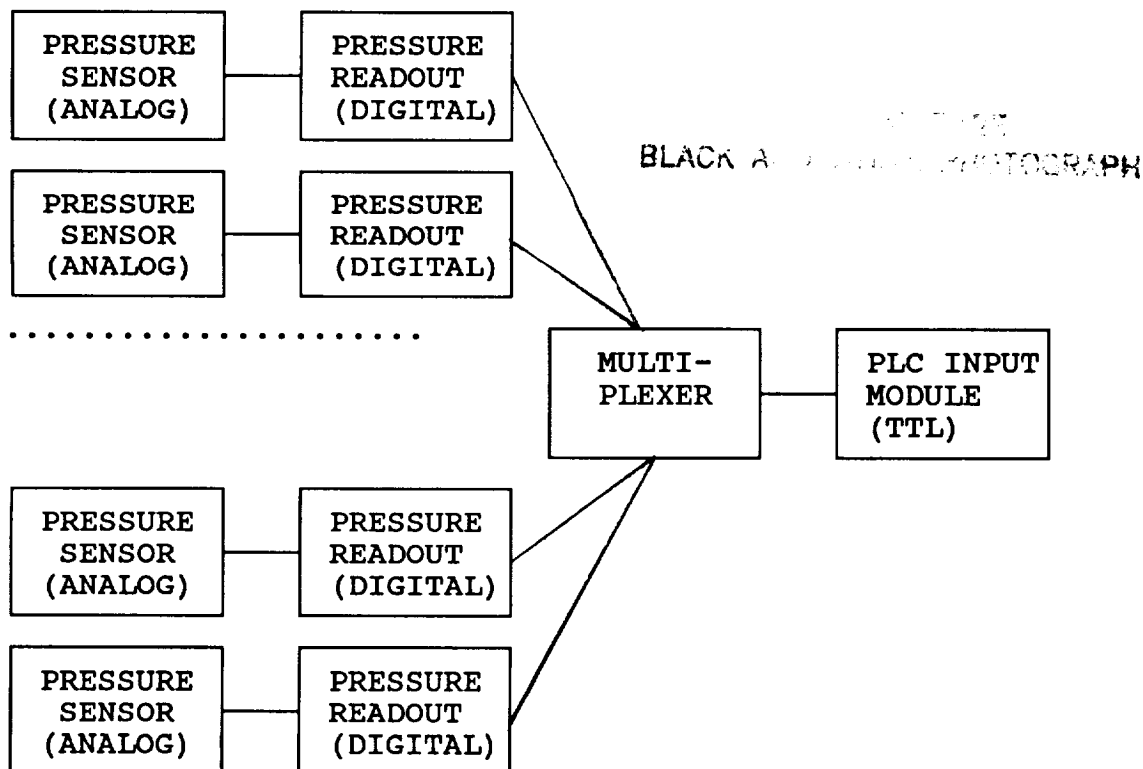


Figure 6: Gathering of Pressure Data

It then gets distributed to a number of key locations, where this information is important: operators, experimenters, engineers.

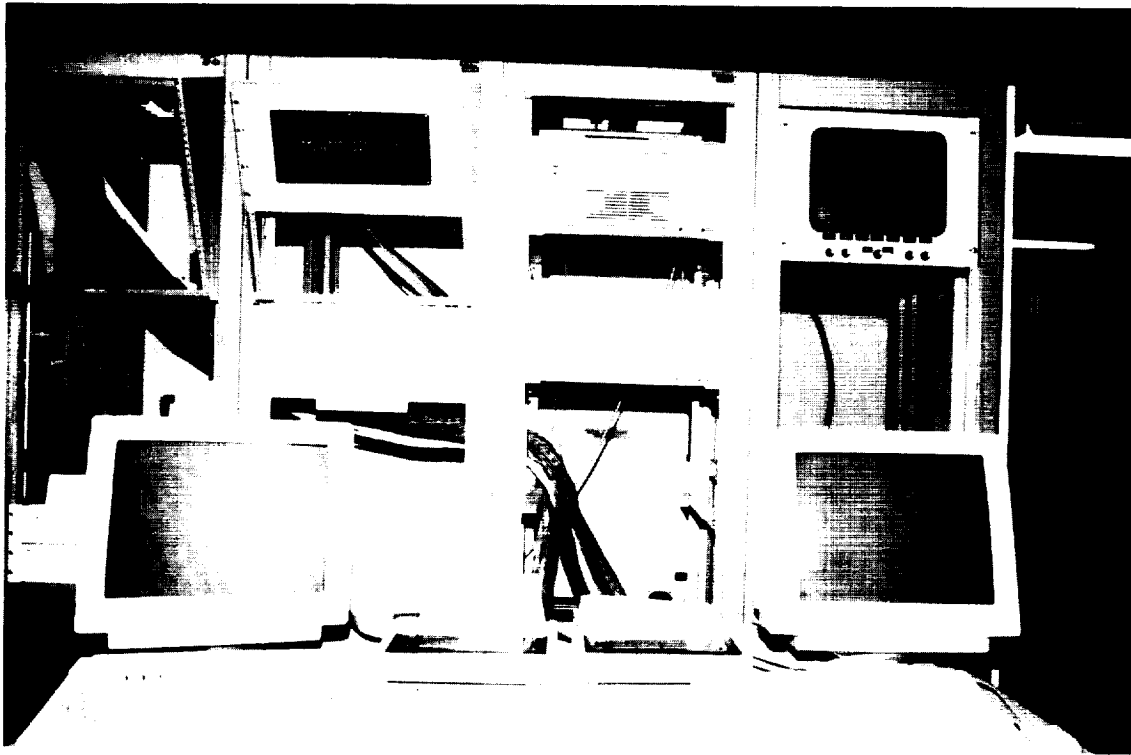


Figure 7: Chamber Pressure Display at the Experimenter's Station

### PROCESS OF REDUCING CHAMBER PRESSURE

The system is initially evacuated using mechanical pumps, backed by blowers. When the pressure reaches a designated level, the cryogenic compressors are turned on, which evacuate the chamber to pressures  $10^{-4}$  Torr or below. The turbomolecular pump is then used to pump on helium and other inert gases. When the pumps are turned on, sequential manipulation of the process valves is performed to stage the pumpdown process.

**Results** The upgraded chamber has performed successfully during a 45-day spacecraft test without a single failure. The greatest achievements of the project were:

- Reliability
- Color graphics interface
- Networking data highways
- Advanced I/O interface
- Capability of unlimited future expansion.

## PART II

### IF YOUR NEXT UPGRADE PROJECT INCLUDES UPGRADING A CONTROL SYSTEM

Consider the following:

If the requirements of the project are:

Improved control,  
Better operator interface,  
Higher reliability,  
Less maintenance - then a PLC is your best solution.

If the types of controls required are: interlock logic and sequencing, continuous control (PID), custom optimization - then a PLC is your best solution.

If flexibility - the ability to modify control strategies, displays, etc., expandability - extension to other process units, addition of I/O or consoles, interconnectability - present or future communication with other systems or devices are important - then a PLC is your best solution.

Process interface and control functions must be clearly defined and documented. Additional drawings and specifications, addressing specific design areas of the PLC based system, must be issued and transmitted to the vendor and affected design disciplines. This stage of the project represents a period of information gathering, decision making and communication with the vendor and client.

■ **Point count.** An accurate point count must be developed to determine the total number of analog and digital inputs/outputs serviced by the system. This information is taken from the latest mechanical Piping and Instrument Diagram. A percentage of spare I/O's based on number of points controlled and monitored by the system should be calculated and a total point count established.

■ **Types of I/O's:** High level analog (-10 to +10 VDC), low level analog (mV, T/C), discrete I/O, power outputs for large inductive loads, interface to other devices (Data Acquisition System, printer).

■ **System Architecture and Rack Layout.** Once the point count has been established, the type and quantity of input/output modules, switches, pushbuttons, pilot lights, enclosures and other supportive hardware can be identified. From this equipment list, the system racks can be identified and laid out.

■ **Field Terminal Assignments.** After the rack layout has been finalized and termination panels located, field terminal numbers are assigned. These assignments should be structured in a logical and functional manner.

■ **Control Panel Interface.** The control panel interface with a large distributed I/O system must be designed carefully. To minimize installation costs, the digital equipment racks and control panels can be wired with receptacles, and multi-conductor cable assemblies used to make the final connection. Coordination between different vendors on matters of signal grounding, fusing, shielding and pin assignments can be very cumbersome. Errors discovered once the computer racks and control panel fabrication is underway can be very costly to correct.

■ **Grounding and Shielding.** A single ground reference should be provided for all logic, instrument and shield grounds. All vendor recommended grounding practices should be followed. Clear guidelines for grounding and shielding are not always available, especially for large customized systems. Grounding practices are further complicated when the digital system must interface to an analog control panel. In such cases an integrated approach to grounding must be followed for both the digital system and analog instrumentation. A single common ground reference must be established for both the analog and digital systems. All signal interfaces between the two systems must be analyzed to ensure that ground loops are not inadvertently introduced into shields and signal returns. Analog and digital input cards should be selected with adequate input filtering, isolation and common mode noise rejection characteristics.

■ **The Field Wiring Interface** should be accomplished in such a manner that the I/O cards and field equipment can be removed without disconnecting the field wiring.

■ **Signal power and interconnection requirements.** Power supplies are usually required to provide the necessary power for energizing transmitters and sensing contact inputs. Digital outputs may be dry contacts (passive), or may provide necessary power to drive certain loads (active). When configuring digital inputs and outputs it is advisable to avoid connecting two common points together and run two wires for each contact input and output. This method is more labor consuming but it provides a clean interface and avoids wiring problems when connecting to other control systems.

■ **Data Highway Communications.** Communication requirements must be established for remotely located color graphic man-machine interfaces. Our system communicates over a twisted pair, which functions as a data highway. The data highway links the remote units together in a daisy chain. Typically, total cable length varies from 5,000 to 10,000 feet. In general, these maximum lengths are for the total length of cable on the data highway, including branches and loops. The most popular communication protocols are: master/slave access (CSMA/CD carrier sense multiple access with collision detection), and masterless access (token passing). Both protocols utilize bus topology rather than star topology.

■ **Operator Console Design.** The operator's console consists of an interactive CRT station with operator keyboard. Additionally, pushbutton stations, pilot lights indicating status of equipment, and a hardwired annunciator are mounted on the



operator console. A separate control console as installed next to the CRT station to house the hardwired instrumentation. In general, CRT console provides a much more efficient and cost effective operator interface with the process than dedicated instruments.

■ **Communication with Data Acquisition System.** Process information can be communicated on a timely basis utilizing either IEEE-488 or RS-232C communication links.

■ **Software Configuration.** The PLC system must be programmed with the process information, control algorithms, safety interlocks, and operator interface instructions necessary for proper operation. Without the configuration data, the control system is incapable of performing its intended functions. System performance and payoff is ultimately determined by the software that is implemented. Normally, point addresses and hardware assignments need to be defined early, as this information is required for racks and equipment layouts, wiring lists and field terminal assignments. Sufficient time must be allowed for loading and debugging the configuration data prior to acceptance testing.

■ **Color Graphic System Data Base Generation.** Most software packages come with standard, fill-in-the-blanks software for data acquisition, process control, alarming and operator displays. Data base generation requires identification of necessary process and control information for each point. Information for the data base is gathered from many sources, such as piping and instrument drawings, instrument loop drawings, and instrument user manuals. Process and instrument information must be organized for each point in the system. Decisions must be made as to what input processing, control algorithms, alarm types and other software functions are required for each point.

Data base forms must be filled out, reviewed and updated. The data base is then loaded and errors are diagnosed by the system and corrected. Normally, the data base is in a constant state of revision, which continues through acceptance testing, start-up and system operation.

■ **Displays.** Process indication and control are provided through a variety of displays. In general, the displays include a plant overview, group and detailed formats. In the process of data base generation the user assigns points to various groups to perform indication, alarm and control functions. Once points are assigned to a particular display, other information pertaining to that point can be assigned (such as controller modes, limits, scaling factors, etc.) After that plant flow diagrams, schematics, one-line diagrams and other customized displays can be built. Chambers, heaters, pumps, valves and other equipment are drawn with interconnecting process lines. Process data indication areas are defined for the display. Color, intensity, blink action and character size are assigned for each shape and process data readouts. Tabs can be set on the display, allowing convenient paging to another display. This feature can be used on an overview display to provide a zooming effect. More information can be presented on the screen by positioning the cursor in the area of interest and using

the tab function, which addresses a detailed display of the selected area.

■ **Reports.** Facility operations require the capability to format and print out process data, alarm, software configuration and system diagnostics. A printer interface provides hard copy of alphanumeric information displayed on the CRT. The computer is capable of storing historical data on selected points, and of generating reports on both a periodic and a demand basis. Historical data points must be identified in the data base, as well as sample periods, process averaging and data storage requirements.

■ **Maintenance and Spare Parts.** These requirements should be addressed during the bid evaluation stage of the project instructing the vendors to list and price their recommended spare parts for start up and one year of operation.

■ **System Start-up and Check-out.** Every component in the system should be exercised during the acceptance test. Each input and output should be tested to check wiring and point addressing. Analog inputs are simulated with a potentiometer and power supply. Analog outputs are checked with the milliammeter. Digital inputs and outputs can be simulated in several ways. Contact inputs can be shorted with test leads and alligator clips. An ohmmeter (or a voltmeter) can be used to test output operation.

Backup systems should be tested by failing the primary components and observing the system response. System diagnostics are tested by simulating failures, observing what alarms are initiated, and verifying the diagnostic information presented on the CRT. The data highway card for each highway should be removed to test the system's response to failures in the data highway electronics.

Once the system is on-line and the data base is operating properly, additional functions, such as operation logs, system reports, and custom programs can be added. Process can be further optimized and automated. As new applications and future expansions are implemented, the system's hardware and software configurations can be in a constant state of change throughout equipment useful life.

## **REFERENCES**

1. Liptak, Bela, Editor-In-Chief: INSTRUMENT ENGINEERS' HANDBOOK. REVISED EDITION. Chilton Book Company, 1985.
2. DISTRIBUTED CONTROL SYSTEMS MANUAL. Applied Digital Research, Inc., Houston, TX.
3. T. Bisby, K. Sipe: OPERATOR INTERFACE... Industrial Computing, An ISA Publication, March/April 1992.
4. A. Laduzinsky: STANDARDS AND INTERFACES... Control Engineering, March 1992.
5. T.G. Fisher, P.E.: ALARM AND INTERLOCK SYSTEMS. ISA publication, 1988.



## AN ALTERNATE METHOD FOR ACHIEVING TEMPERATURE CONTROL IN THE -130°C to 75°C RANGE <sup>1</sup>

Kenneth R. Johnson, Mark R. Anderson,  
Robert W. Lane, Maximo G. Cortez  
*California Institute of Technology  
Jet Propulsion Laboratory  
Pasadena, California 91109-8099*

### ABSTRACT

Thermal vacuum testing often requires temperature control of chamber shrouds and heat exchangers within the -130°C to 75°C range. There are two conventional methods which are normally employed to achieve control through this intermediate temperature range: 1) single-pass flow where control is achieved by alternately pulsing hot gaseous nitrogen (GN2) and cold LN2 into the feed line to yield the setpoint temperature; and, 2) closed-loop circulation where control is achieved by either electrically heating or LN2 cooling the circulating GN2 to yield the setpoint temperature. A third method, using a mass flow ratio controller along with modulating control valves on GN2 and LN2 lines, provides excellent control but equipment for this method is expensive and cost-prohibitive for all but long-term continuous processes. The single-pass method provides marginal control and can result in unexpected overcooling of the test article from even a short pulse of LN2. The closed-loop circulation method provides excellent control but requires an expensive blower capable of operating at elevated pressures and cryogenic temperatures. Where precise control is needed ( $\pm 2^\circ\text{C}$ ), single-pass flow systems typically have not provided the precision required, primarily because of overcooling temperature excursions. Where several individual circuits are to be controlled at different temperatures, the use of expensive cryogenic blowers for each circuit is also cost-prohibitive, especially for short duration or one-of-a-kind tests.

At JPL, a variant of the single-pass method has been developed that has been shown to provide precise temperature control in the -130°C to 75°C range while exhibiting minimal setpoint overshoot during temperature transitions. This alternate method uses a commercially available temperature controller along with a GN2/LN2 mixer to dampen the amplitude of cold temperature spikes caused by LN2 pulsing. This paper describes the design of the GN2/LN2 mixer, the overall control system configuration, the operational procedure, and the prototype system test results .

---

1] The research described in this paper was carried out by the Jet Propulsion Laboratory, California Institute of Technology, under a contract with the National Aeronautics and Space Administration

## **INTRODUCTION**

Preparation for the thermal vacuum testing of the Wide Field/Planetary Camera II (WF/PC II) required the review of existing temperature control methods to determine which method could best accommodate the WF/PC II special test needs. Since the instrument will be inserted into the instrument bay of the Hubble Space Telescope (HST) body and, when in place, its curved surface will face cold space while all other surfaces will be enclosed within the warmer HST body, there was a need to create a test fixture that would simulate multiple temperature environments. At JPL, a test fixture consisting of eight individually controllable shroud circuits has been built which can simulate these multiple temperature environments.

Because the WF/PC II thermal vacuum test is of relatively short duration, closed-loop temperature control of each circuit was deemed cost-prohibitive. Also, since the single-pass temperature control method that had been used to test WF/PC I had not provided the desired precision, a different technique was requested. In response, an alternate temperature control method was developed to provide precision temperature control in the -130°C to 75°C range with minimal overshoot during temperature transitions. This method includes a custom designed in-line GN2/LN2 mixer used to dampen the amplitude of cold temperature spikes from LN2 pulsing. The flow schematic and instrumentation layout of this system is illustrated in Figure 1. Details of the GN2/LN2 mixer design are shown in Figure 2.

## **GN2/LN2 MIXER CONFIGURATION**

The GN2/LN2 mixer consists of a high-conductivity mass acting as a thermal shock-absorber at the point of GN2 and LN2 mixing. The GN2/LN2 mixer design criteria were: 1) provide enough in-line mass to yield the desired thermal shock-absorber effect but not so much as to make the system temperature control feedback response sluggish; 2) configure the mass in a way that provides high heat transfer rates to the flowing GN2; 3) minimize the pressure drop in the mixer; and, 4) make the design as simple and low-cost as possible. Based on these criteria, the configuration described below was developed.

The GN2 feed line to the GN2/LN2 mixer is a 3/4" copper tube located at the center of the mixer assembly. The LN2 feed line is a 1/2" copper tube which is plumbed concentrically inside the 3/4" GN2 feed line and extends downward about half the distance of the GN2 feed line. The 3/4" GN2 feed line passes through the center of and is attached to seven 1/4" thick copper discs. The copper discs have two configurations: the first has twelve evenly spaced 3/8" holes drilled near the outer diameter of the disc, and the second has eight evenly spaced 3/8" holes drilled near the inner diameter of the center hole in the disc. The copper discs are silver soldered to the GN2 feed line at 2.25" spacing, the two disc configurations mounted alternately. This internal structure, consisting of the GN2 feed line and copper discs, penetrates at and is silver soldered to the top center of a 150# brass blind flange. An off-center 3/4" exit port tube penetrates and is soldered to this flange. The internal

structure is enclosed by a 3" copper pipe (Type K) which has a slip-joint pipe cap silver soldered at the bottom end and a 3" 150# brass flange silver soldered at the top end. The two flanges, sealed with a durable gasket, bolt together to complete the assembly. The assembly is insulated with foam, about 3" thick, and is encased within a 10" diameter section of sonotube. A thermocouple is installed on the outside surface of the 3" copper pipe near the bottom to provide a means for monitoring the mix-point temperature. The thermal mass in the system is about 15-lbs.

## OPERATIONAL PROCEDURE

A constant flow rate GN2 stream is fed into the control circuit at the GN2 manifold, first through a hand controlled shut-off valve, and then through an open/close solenoid valve (which opens when the master temperature controller is powered). Next, the GN2 passes through a flow element (a rotameter equipped with a small throttle valve to provide manual GN2 flow control adjustment) and then through an in-line electric heater (controlled by a triac power unit with zero crossover firing), installed just upstream of the mixer. A mixer by-pass line allows heated GN2 to flow directly to the shrouds for bakeout tests when cooling is not needed. Power to the heater is automatically shut off if the shroud overheats beyond the limit setpoint of the failsafe temperature controller. Heater power is also turned off whenever the setpoint temperature is below ambient (~20°C). The LN2 is fed into the control circuit at the LN2 manifold, first through a failsafe open/close solenoid valve, then through a master control open/ close solenoid valve (operated by a solid state relay) and a hand-controlled throttle valve. The failsafe solenoid is automatically de-energized (closed) if the shroud overcools beyond the limit set-points of the failsafe temperature controller. The master control solenoid cycles open and closed as the master controller calls for cooling. The throttle valve is manually adjusted to limit the amount of LN2 delivered per cycle or pulse. The pressure in the circuit is manually adjusted with a backpressure hand control valve located downstream of the shroud and just upstream of the vent manifold.

During cooling periods, GN2 is fed down the 3/4" copper tube at the mixer at constant temperature (unheated, ambient) and flow rate. When the master temperature controller calls for cooling, LN2 is pulsed into the mixer through the 1/2" copper tube. The pulsed slug of LN2 mixes with the continuous GN2 stream and the mixture impinges on a bed of copper wool to provide turbulent mixing. The flow then changes direction 180 degrees and is directed upward through the holes in the 1/4" thick copper discs in a weaving flow path (which prevents flow channeling and enhances heat transfer to the copper discs and the pipe wall). The tempered GN2 then leaves the mixer through the exit port and continues to the shroud.

Two types of master temperature controllers were used to test the prototype circuit, and are referred to here as type-one and type-two. These two types of controllers were chosen because each type was available and we wanted to determine if one provided better control than the other in this control system configuration. Type-one used average shroud temperature as the control variable (measured by connecting

together two thermocouples: the shroud inlet (TE-2) and the shroud outlet (TE-3)). This type of control configuration is illustrated in Figure 1. Type-two used a cascade-like control technique where the test article temperature (measured by TE-4) is the primary control variable and the temperature at the top of the mixer is the secondary control variable. In both cases, the test article temperature (thermocouple TE-4) was used as the input to the failsafe temperature controller.

## **PROTOTYPE SYSTEM TEST RESULTS**

Two sets of tests were run to study the response of the prototype control system. The temperature control variable for the first set of tests was a 30-lb copper plate heat exchanger, and, for the second set of tests, the control variable was a small (3 to 4-lb) stainless steel heat exchanger (used for cooling a thermoelectric quartz crystal microbalance (TQCM)). Both types of commercial temperature controllers were used in each set of tests to provide a functional comparison between the two types. The purpose of this comparison was to determine which type to install in the control circuits for the WF/PC II thermal vacuum tests.

The type-two controller was tested first. At the beginning of testing, the prototype mixer was filled with about 10-lbs of small steel balls (BBs) to provide mass. The BBs filled the spaces between the copper discs. Very sluggish feedback response from the first test revealed that there was too much mass in the mixer. The BBs were removed and the test was started again with copper wool at the bottom of the mixer and nothing between the discs. This arrangement yielded a more rapid feedback response, but showed that temperature control was quite sensitive to the GN2 and LN2 throttle valve settings. Several trials were required to establish optimum settings for the valves and the temperature controller (programmable settings for proportional, integral, and differential control). However, within three test days, optimum settings had been determined and stable temperature control had been established. Figures 3 through 8 illustrate the results of subsequent temperature control testing.

Figure 3 illustrates results from a test using a type-one controller to provide temperature control of the 30-lb copper plate heat exchanger. The test begins with the copper plate at ambient temperature, then the plate is cooled in steps to setpoints at -25°C, -50°C, -75°C, -100°C, and -130°C,. After holding at -130°C, the plate is reheated in steps to setpoints at -25°C and 20°C. At each step, the temperature was held at setpoint for only ten minutes so that several setpoint levels could be demonstrated within a short time period. It is evident in Figure 3 that no overshooting occurred at the setpoint temperatures. Figure 4 shows results from a test using a type-one controller to provide temperature control of the TQCM heat exchanger. This test was conducted to demonstrate the ability of the control system to hold precise setpoint temperatures (in this case -80°C and -110°C) for long durations.

Figure 5 illustrates results from a test using a type-two controller to provide temperature control of the TQCM heat exchanger. This was a comparison test at the same



conditions as the test shown in Figure 4, and, as can be seen in Figure 5, similarly favorable control precision results were demonstrated. Figure 6 shows detail of the control precision in the -110°C region ( $\pm 2^\circ\text{C}$ ) demonstrated by this test.

Figure 7 illustrates results from a test using a type-two controller to provide temperature control of the TQCM heat exchanger during a rapid temperature transition from 75°C to -80°C which occurred within 20 minutes. Even here, when the temperature of the TQCM heat exchanger was changing at over 7°C per minute, there was no significant overshoot of the setpoint temperature as evidenced by the detail shown in Figure 8. Even in this case the control precision at setpoint was  $\pm 1^\circ\text{C}$ .

## CONCLUSIONS

An alternate method for providing economical and precise temperature control in the -130°C to 75°C range has been developed and demonstrated. There are no apparent reasons why this method cannot be used effectively for controlling test articles below -130°C but temperature control below this level has not yet been demonstrated. Use of this method requires close attention to the establishment of optimum valve and temperature controller settings prior to testing. Also, it is important to understand that, during test periods when the control setpoint is below ambient temperature, the GN2 flow rate and temperature must remain constant and the LN2 feed pressure must remain stable so that the LN2 delivery rate is the only variable affecting the outcome of the controlled temperature. Therefore, the heater should not be powered during periods when the control setpoint is below ambient temperature.

Based on the favorable results presented here, ten separate temperature control circuits containing GN2/LN2 mixers of the design detailed in Figure 2, and having the configuration as illustrated by Figure 1, were installed at JPL's 10-FT Space Simulator facility in preparation for WF/PC II thermal vacuum testing. The type-one controller was chosen for installation because it had demonstrated its ability to deliver precise temperature control and we already had enough of these controllers onhand to provide ten master controllers and ten failsafe controllers. Test results using these installed circuits were not yet available at the time of this writing.

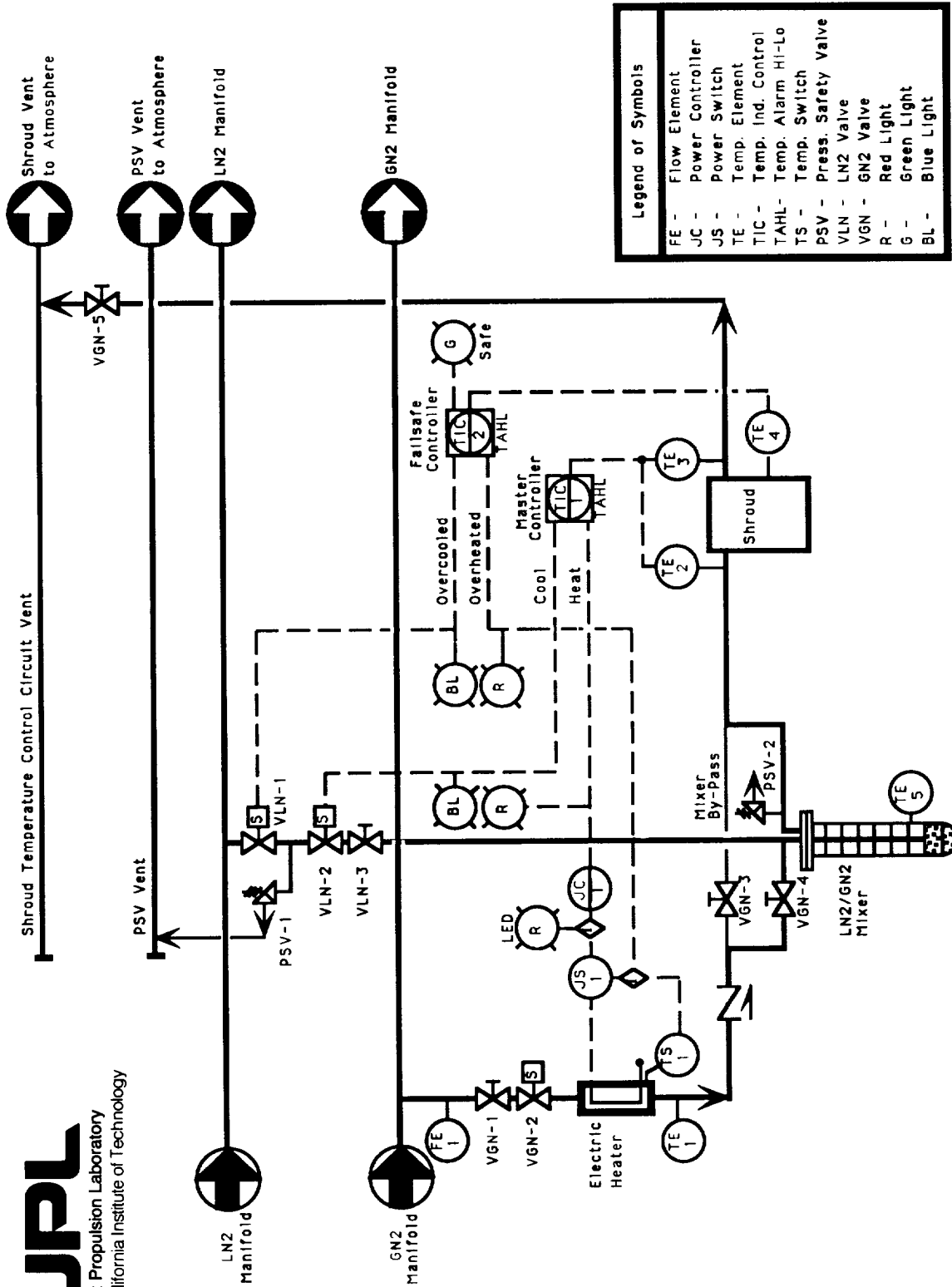
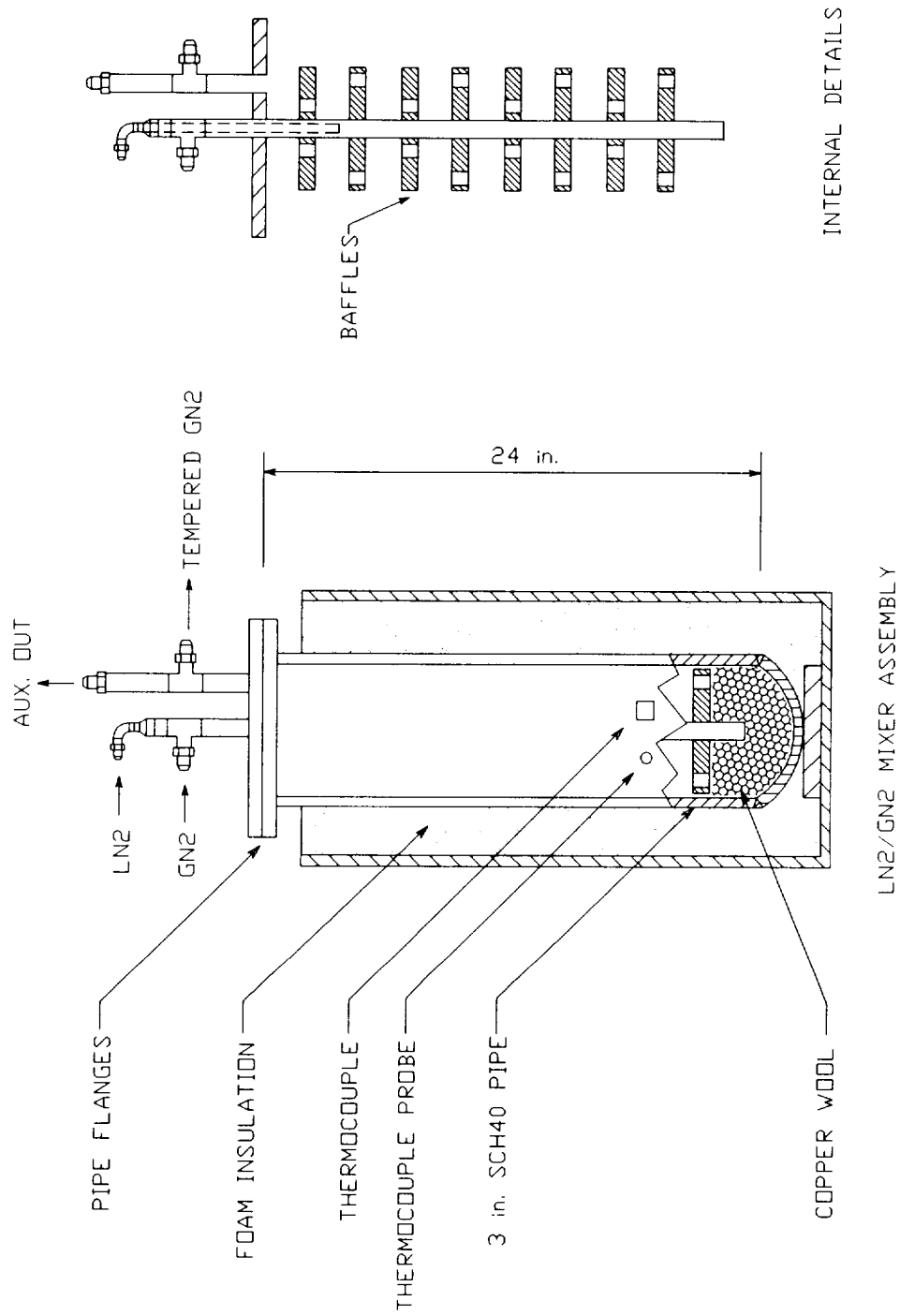


Figure 1. Prototype Control System Flow Schematic and Instrumentation Diagram



**Figure 2. GN2/LN2 Mixer Detail**

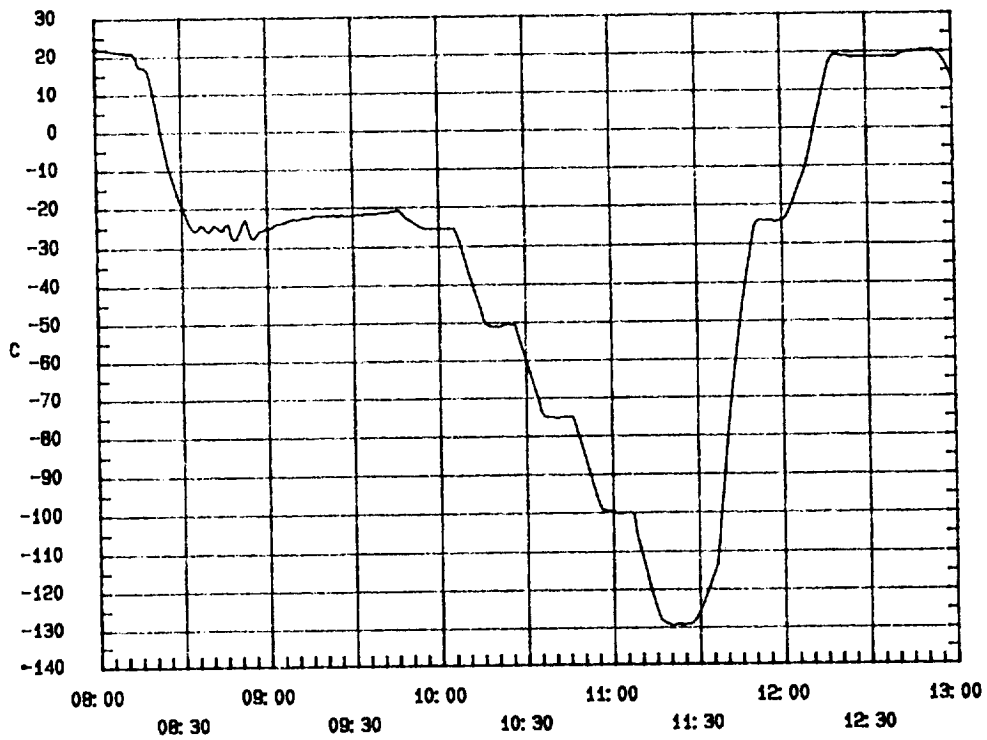


Figure 3. Copper Plate Heat Exchanger Temperature Control Profile Using Type-One Controller

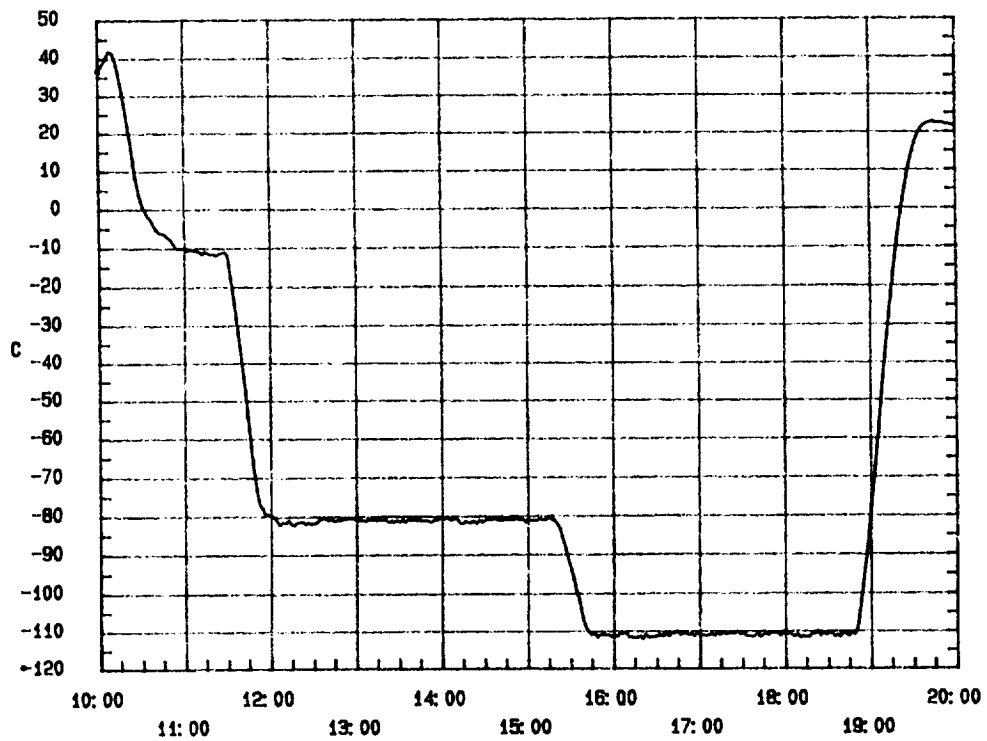


Figure 4. TQCM Heat Exchanger Temperature Control Profile Using Type-One Controller

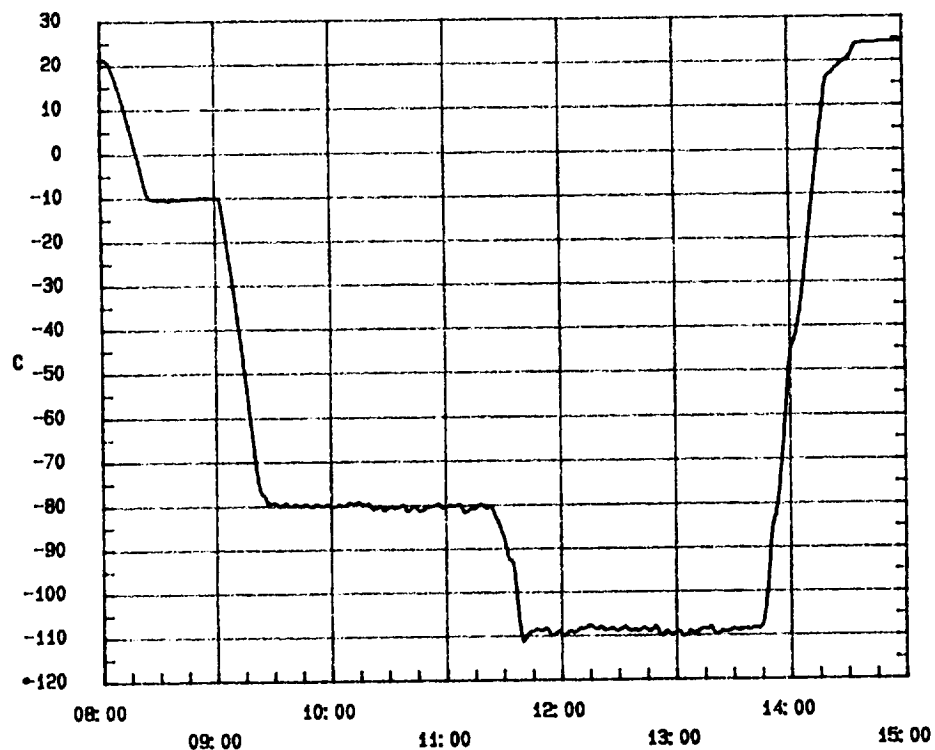


Figure 5. TQCM Heat Exchanger Temperature Control Precision Profile Using Type-Two Controller

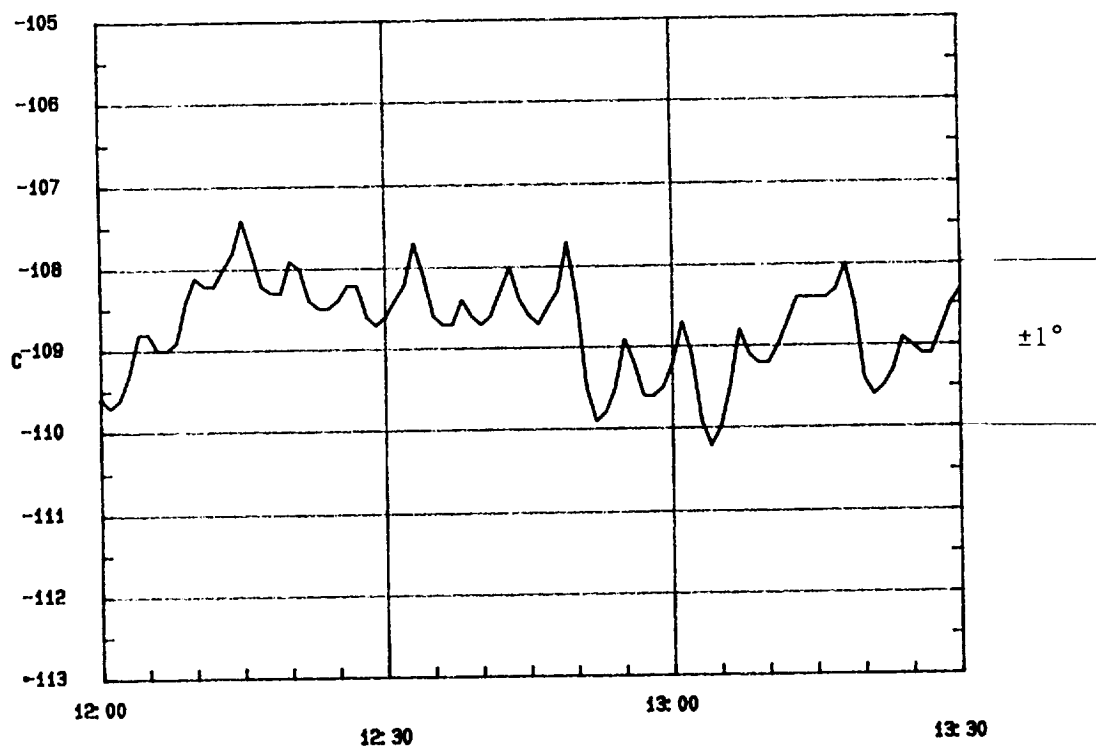


Figure 6. TQCM Heat Exchanger Temperature Control Precision Profile at -110°C Using Type-Two Controller

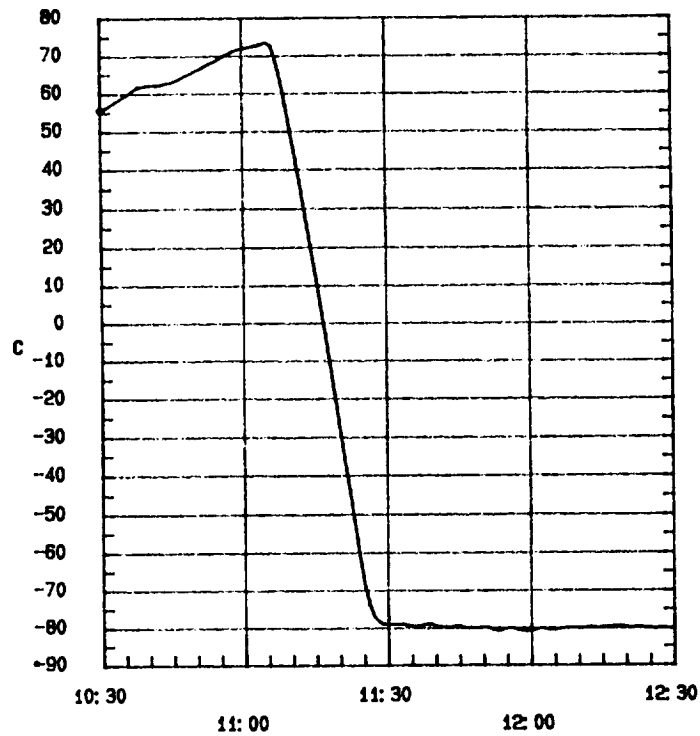


Figure 7. TQCM Heat Exchanger Temperature Control Precision Profile for Rapid Cooling Test Using Type-Two Controller

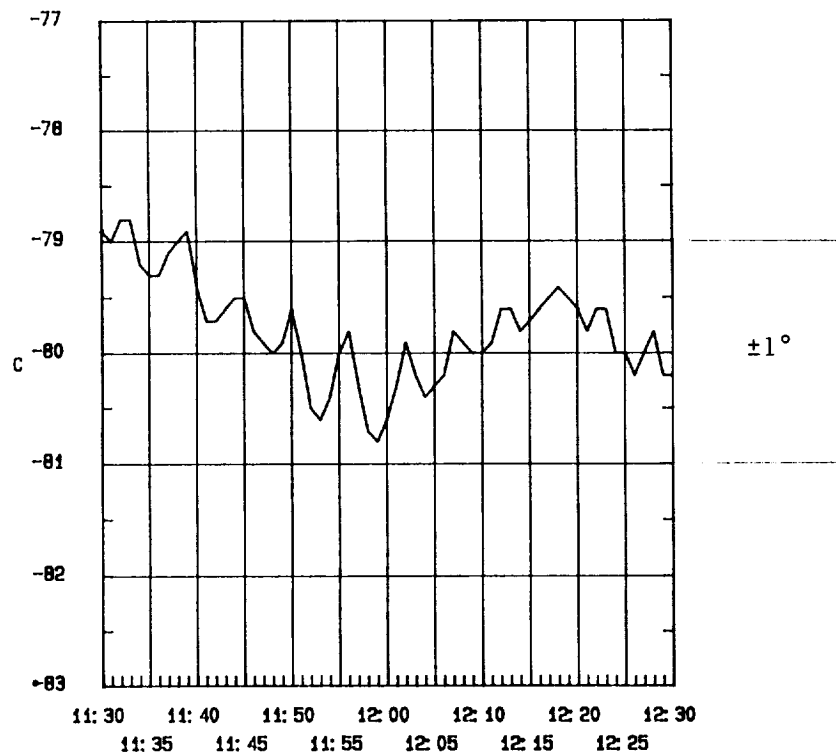


Figure 8. TQCM Heat Exchanger Temperature Control Precision Profile at  $-80^{\circ}\text{C}$  Following Rapid Cooling Test Using Type-Two Controller

## THE EVOLUTION OF SPACE SIMULATION

Arthur A. Edwards  
Space Systems/Loral  
Palo Alto, California

### ABSTRACT

Thirty years have passed since the first large (more than 15' diameter.) thermal vacuum space simulation chambers were built in this country. Many changes have been made since then, and the industry has learned a great deal as the designs have evolved in that time. I was fortunate to have been part of that beginning, and have participated in many of the changes that have occurred since. While talking with vacuum friends recently, I realized that many of the engineers working in the industry today may not be aware of the evolution of space simulation because they did not experience the changes that brought us to today's technology. With that in mind, It seems to be appropriate to take a moment and review some of the events that were a big part of the past thirty years in the thermal vacuum business. Perhaps this review will help to understand a little of the "why" as well as the "how" of building and operating large thermal vacuum chambers.

### INTRODUCTION

This paper will not attempt to present a catalogue of all of the early chambers, nor will it include pictures, sizes, pump down curves, pumping speeds and test specimen characteristics of each. I have neither the time nor the data to provide such a compilation. Rather, I will present a brief overview of the operating characteristics of chambers with which I am familiar, the mistakes that were made along the way and the evolution that brought us to today's technology. Naturally, I was not every where at once during those years, so this paper will not cover all situations or changes that occurred along the way. I can only speak from my own experience and about those with which I am familiar. Also, because of my experiences during those years, I have developed beliefs and expectations about specific vacuum equipment which will be covered here. As this paper frankly deals with these issues, I hope no one will take offense with any thing said or any conclusions reached. We all know that every one was doing his best along the way to provide the industry with the equipment it needed to be successful. The facts are that some equipment succeeded better than others.

In the industry today, we feel confident that chambers will operate effectively to provide the environment required for satellite testing. There were times during the early years however, when reaching high vacuum with a satellite inside the chamber was problematic at best. The confidence we have today was not easily attained, but is the result of years of trial and error, theory that proved to be unworkable, experience slowly acquired and considerable work that went on simultaneously in this country and around the world.

## **CHARACTERISTICS MATRIX**

In an attempt to organize the past thirty years into a logical sequence, I have developed a characteristics matrix that arbitrarily breaks the period into three phases. Included in the matrix is a summary of the dominant technology and some of the problems experienced by the industry during each phase. As in most attempts to condense complex issues, this one results in some over simplifications. Many of the characteristics overlap, and no attempt is made to list the relative importance of each. But perhaps it will provide a reference to consider to as we progress through the years.

### **PHASE ONE**

The first large thermal vacuum chambers were completed in 1962 and included those built at General Electric, Valley Forge, Pa; Lockheed Missiles and Space Co. Sunnyvale, Ca; NASA Goddard, Greenbelt, Md; and Jet Propulsion Labs, Pasadena, Ca. Shortly after, chambers were built at NASA, Houston, Tx; McDonnell Douglas, St. Louis, Mo; TRW, Los Angeles, Ca; RCA, Princeton, NJ; Hughes Aircraft, Los Angeles, Ca; and McDonnell Douglas, Huntington Beach, Ca. The creation of these chambers was the result of industry's need to test full sized satellites in the environment of outer space. Since this was the pioneer group, the technology applied on these new chambers was based on what was being practiced at the time. Vacuum technology in the early 1960's consisted mostly of what had previously been used in the building of small and medium sized chambers. At that time, we all wondered if the technology that had worked for small chamber could be applied to the design of large chambers.

### **CONTRACTORS**

The two prime contractors for the first chambers, excluding the two at NASA, Houston, were F. J. Stokes Corporation in Philadelphia, Pa. and Consolidated Vacuum Corporation in Rochester, N. Y. It is interesting to note that neither of these two companies is in the business of building large space chambers today. Both companies had dropped out of the prime business by the mid 1960's. From those pioneers and their experiences, we all learned valuable lessons and their designs contributed to the industry for some years afterward. I have always had a great respect for those two companies and their subcontractors who were willing to strike out into a new and previously untried technology.

### **CONFIGURATION**

What did those first chambers look like? To begin with, their prime mode of high vacuum pumping consisted of a cluster of large diffusion pumps (in excess of thirty in some cases) coupled in some chambers with 20° K helium cryogenic pumps. The chambers were either vertical cylinders or spheres, and most were either top or bottom loaders. The spheres were generally 39' and the cylinders were over 18 feet in diameter. On one of the chambers, the owner believed it to be necessary to bake the chamber to 400° F before each test. This belief was based on years of testing bell



jar systems at high vacuum. That particular chamber is still operating and has never been baked out since its acceptance test in May, 1962. The oil sealed roughing pumps used in those days were similar in design to those used today. Some were quite large however, and looked like something out of a Jules Verne submarine. The intermediate range pumps were either diffusion ejector pumps or roots type mechanical blowers.

Although diffusion pumps were the prime mode of high vacuum pumping, a helium cryogenic pump had recently been developed by CVI Incorporated in Columbus, Oh. Unfortunately, the aerospace companies did not generally know in those early days how much pumping speed would be needed to maintain the chamber and specimen at high vacuum ( $10^{-6}$  Torr or better). In any case, the number of diffusion pumps could be reduced by adding 20° K cryogenic pumps as a supplement. These pumps had massive speeds (in excess of 1,000,000 liters / Sec) and were intended to provide enough speed to cover the unknown gas loads in satellite testing. A typical 39 ft spherical chamber could attain a vacuum of  $2 \times 10^{-10}$  Torr empty with all diffusion pumps and cryogenic pumps operating simultaneously. The pumps were certainly effective and the chambers were definitely vacuum tight.

## LESSONS LEARNED

During this first phase , the industry learned several important facts:

- 1) Gas loads, and consequently, pumping speed requirements, were not as high as had been assumed.
- 2) Diffusion pumps could, and would at the worst possible times, back stream oil into the chamber and onto the specimen.
- 3) It was not necessary to bake out a chamber to reach high vacuum.
- 4) Cryogenic pumps could not, by themselves, attain high vacuum.

Because of item #2, the industry decided that it was time to abandon diffusion pumps and move into the second generation of vacuum chambers. The chambers of phase two were called "selectively pumped" because their high vacuum pumps were each selected to pump certain gases. But before we proceed into the next chamber phase, let's talk for a moment about the characteristics of high vacuum pumps.

## HIGH VACUUM PUMPS

As you know, cryopumps that operate at 20° K are able to pump all gases except hydrogen, helium and neon. The vapor pressures of these three gasses are too high at that temperature to allow the chamber to reach high vacuum. Although neon is not usually an issue in vacuum chambers, both hydrogen and helium can be severe problems. Outgassing is the main source of hydrogen and can often be the limiting factor in high vacuum work. Helium levels can also be significant when leak checking has been or is being done in the chamber. Consequently, if the diffusion pumps were to be eliminated in future designs in favor of cryogenic pumps, additional pumps would have to be found to handle these two gases.

## **PHASE TWO**

This now brings us to the second phase in the evolution of large thermal vacuum chambers. This period began around the mid 1960's and was characterized by the elimination of diffusion pumps from large chambers. In the place of diffusion pumps, cryogenic pumps were added and were supplemented with two new pumps. These two were the ion and titanium sublimation pumps and were included to remove helium and hydrogen. Aerospace companies that built chambers during the second phase included Boeing, Seattle, Wa; Ford Aerospace, Palo Alto, Ca; Lockheed, Sunnyvale, Ca; Martin-Marietta, Denver, Co; TRW Los Angeles, Ca; Hughes, Redondo Beach, Ca; and Perkin-Elmer, Danbury, Cn. A new set of prime contractors were now in the business to build chambers; PDM Steel Co in Pittsburgh, Pa, CBI Corp. in Chicago, Il, and CVI Corp. in Columbus Oh.

The industry soon discovered that, although these chambers no longer had diffusion pumps to backstream, they presented a different set of problems that turned out to be characteristic of the new pumping systems. Titanium sublimation pumps had been used previously in smaller chambers in lieu of diffusion pumps. But their purpose in large chambers was to supplement the cryo pumps and handle hydrogen. The purpose of the ion pump was to handle helium and neon. Together the three "selective" pumps would pump all the gases and bring the chamber to high vacuum. Unfortunately, it often did not work that way.

## **TITANIUM SUBLIMATION PUMPS**

Titanium sublimation pumps work on the principle that a layer of deposited titanium captures hydrogen through chemical reaction and thereby "pumps" it from the chamber. Titanium must be evaporated and deposited (sublimated) on the wall of the chamber for the coating to pump successfully. We soon discovered that getting the rod of titanium to reach the correct evaporation temperature could be tiresome, frustrating, and sometimes impossible. I can remember spending hours trying to achieve evaporation temperatures on the rod while the hydrogen partial pressure overwhelmed the chamber. But the worst part of these pumps was their tendency to coat the back end of chambers with a dusty, dirty layer of a titanium compound that defied efforts to remove it. Something needed to be done to successfully pump hydrogen or the industry would be back with diffusion pumps. Titanium sublimation pumps were not the answer.

## **ION PUMPS**

Ion pumps were another source of discontent during the late 1960's and were included in selectively pumped systems to handle helium. This statement may seem to be contradictory since ion pumps are not inherently capable of pumping helium. However, they will pump a small amount of helium if a layer of getter material (titanium I believe) is coated on the inside of the pump. So industry was assured that our helium pumping problems were over; the titanium coated ion

pumps would handle it. Again we found a technology that sounded good in theory but did not work in practice.

The problems we faced with ion pumps were first of all based on the fact that most satellites had more helium in them than had been predicted when the chambers were designed. Secondly, although ion pumps could theoretically pump helium, in fact, any significant helium gas load soon saturated the gettering surface and reduced its net speed to zero. Ion pumps could be regenerated when saturated, but only at a high cost and significant loss of time. They were so susceptible to helium contamination that we were removing and regenerating our pumps after only two tests, a situation that was intolerable. I would have been happy to give our ion pumps to anyone who wanted them.

### **HELIUM GAS LOADS**

Of particular interest to those of us in the aerospace industry at that time was the question of the source of the helium gas load. After much searching, I asked one of the satellite engineer to describe every test that the satellite had been through before it was delivered to the thermal vacuum facility. We discovered that just before it arrived, its fuel tanks had been subjected to a helium leak check. But the engineer assured us that all of the helium had been vented after the leak test and should therefore not cause us a problem. What he failed to consider was the fact that when the satellite was placed in a vacuum environment, the fuel tank pressure was then 15 psi greater than that of its surroundings. This pressure difference caused the helium to flow into the chamber at what ever leak rate was characteristic of the tanks. The leak resulted in a higher than expected helium partial pressure and a corresponding need for an effective helium pump. Ion pumps could not handle so much helium on a long term basis.

Let me qualify the previous conclusion by saying that I am sure that both ion and titanium sublimation pumps have their use in vacuum testing and are very effective in some applications. There are industries in which they are used continuously and effectively. We reached the conclusion early in phase two however, that they are not effective for use on large chambers to pump helium and hydrogen. Consequently, in about 1970, we had reached a point of serious concern. Diffusion pumps had been exchanged for selectively pumped systems, and other than the cryo pumps, selective pumping did not work. We could not guarantee that our chambers would pump down to high vacuum under any given set of circumstances. A breakthrough was needed.

### **TURBOMOLECULAR PUMPS**

A break through presented itself around 1971. One day a vacuum equipment salesman came by to show me his line of pumps. I remember being only marginally awake during the interview having just returned from lunch, when he turned the page of his brochure to what he described as his company's new line of turbomolecular pumps. As I scanned the page, I noticed that its pumping speed curve was displayed and showed that it was capable of pumping both helium and

hydrogen. This capability was not available on earlier models. I awoke with a start and remember asking him if the graph was accurate, could his T. M. pump actually pump these two illusive gases. He was a bit cautious and replied that he did know for sure, but felt that if his company had said so, it must be true. Not wanting to show too much excitement, I asked him if he would loan me a 6 inch pump that I could install on our chamber for a trial. He brought me one that I installed and tested to exhaustion. Needless to say it worked and the rest is history. Probably no one today would build a large chamber without including a turbo molecular pump in its vacuum system. The hydrogen-helium pumping problem had been solved.

## MID RANGE VACUUM PROBLEMS

The industry experienced other problems during that period. One that gave us particular trouble was the inability to pump through the mid vacuum range in a timely manner. A slow transition through the  $10^{-2}$ ,  $10^{-3}$ ,  $10^{-4}$  Torr ranges was never a problem with diffusion pumps because it was not necessary to flood the LN<sub>2</sub> shroud to make these pumps operate. Typically, the chamber would be pumped into the  $10^{-5}$  Torr vacuum range, the shroud flooded and the heat flux heaters energized to counteract the cold shroud. With early cryogenic pumping however, the process was not so simple. Cryogenic panels, which typically operate at 20 ° K, were shielded with an LN<sub>2</sub> cooled surface to reduce the panels' radiant heat loss. Consequently, with a selectively pumped system, the pump down sequence typically went as follows: the roughing pumps brought the chamber down to  $10^{-2}$  or  $10^{-3}$  Torr range, the LN<sub>2</sub> shroud was flooded and cooled to 77 ° K, and, as the LN<sub>2</sub> panels reached operating temperature, the cryopanel would be energized and cooled. This worked fine when the chamber was empty, but with a satellite inside, bad things happened. Since it takes several hours for the shroud and cryopanel to reach their operating temperatures, and since the satellite is sitting in a pressure range that permits some convective and conductive as well as radiated heat transfer, the satellite became cold. And the longer it remained in that environment and waited for the panels to become operational, the colder it became. In fact it became so cold that the satellite manager demanded that the heat flux system be energized to prevent the satellite temperature from dropping below its lower damaged-beyond-repair limit. So we did, but only for a split second, only long enough for the heat flux breakers to open or the fuses to blow (if we were lucky) or, worst of all, for the heat flux system to melt into a pile of metal. And so, we were introduced to two previously unknown phenomena, corona discharge and arcing.

## ARCING

The problem with arcing, other than the fact that it can damage whatever is in the chamber, is that it has many causes most of which were mainly unknown to us at that time. As we searched through the literature to learn about the phenomenon, we found that several things influenced the probability of its occurrence. The literature claims that it is caused by just the right combination of circumstances. These circumstances include the voltage difference, the local pressure, the distance between electrodes, the shape of the electrodes and the type of

gas around the electrodes. The right combination of these variables would cause first of all, a corona discharge and then a sudden arcing between the two surfaces. The arcing inevitably resulted in a big surge of electrical current and a potential meltdown of either or both electrode surfaces or of the wires and feedthroughs in between. The variable that concerned us most, and over which we had some control was the chamber vacuum. Unfortunately, arcing occurs in the  $10^{-1}$  to  $10^{-3}$  Torr vacuum ranges, and this is the region in which the vacuum systems were having the most trouble pumping through.

## SOLUTIONS

This paper is not long enough to cover all the attempts that were made to successfully and unsuccessfully solve the arcing problem. I will, however, mention the effort that was directed at the design of the cryo pumping system. Changes were made in the cryopumps to allow them to pump the chamber through the mid vacuum range without having to flood the main LN<sub>2</sub> shroud. This meant that it was not necessary to cool the shroud until the vacuum was in the low  $10^{-4}$  Torr range and out of the corona region. The result was that the satellite was not prematurely subjected to a cryogenic environment. Consequently, the heat flux did not have to be energized until the chamber pressure was below the corona region. This was accomplished by building at least part of the cryopanel at the end of the chamber out of sight of the satellite where its LN<sub>2</sub> shield would have no effect on the satellite's temperature. In addition, a pod cryopanel had been recently invented that could be isolated and valved off from the main body of the chamber. Other changes were made in the design of heat flux systems to reduce arcing and I have not heard of any problems experienced recently. It is a problem that should not, however, be ignored or taken lightly. All design efforts that are made to avoid arcing are worth the expense.

## LIQUID NITROGEN PUMPS

From the beginning, the industry had problems with LN<sub>2</sub> transfer pumps. A reliable LN<sub>2</sub> pump is essential for successful and continued operation of the vacuum chamber over a typical thirty day test. Centrifugal pumps had been used for many years in other industries. The petroleum industry is a good example of an industry that has had success with centrifugal transfer pumps. Unfortunately, the application of these pumps to LN<sub>2</sub> service was not at first successful. Centrifugal pumps are a natural for providing high flow of liquid over a large pressure range, and pumping water or fuel with them was easy. However, pumping a cryogenic fluid introduces a more serious set of problem.

Liquid nitrogen is typically stored at or near the saturated temperature that corresponds to its storage pressure. As the stored LN<sub>2</sub> flows into the suction side of the pump, the liquid pressure suddenly drops at the "eye" or suction impeller. This sudden pressure drop results in the liquid changing to gas if the LN<sub>2</sub> is not subcooled. This gas or "vapor lock" causes the pump to "cavitate" and prevents the pump from obtaining "prime." Consequently, the impeller spins in the gas pocket and no liquid moves through the system.

All centrifugal pumps require a certain net positive suction head (NPSH) in their liquid supply before they can obtain prime and pump effectively. A typical LN<sub>2</sub> pump requires approximately fifteen feet of head (net) for the pump to operate successfully. The word "net" means that this head (storage tank height) has to be available after all losses and heat gain into the liquid are considered. Early mistakes were made in the design and placement of pumps and of the supply headers between the storage tanks and the pumps. These mistakes often compromised the available NPSH and made it impossible to start the pumps.

There is a way to artificially subcool the stored LN<sub>2</sub>. To do this, the storage tank's pressure should be vented to atmospheric, and then increased to a value that provides the proper NPSH. Unfortunately, this is a very expensive (in boiled off LN<sub>2</sub>) and time consuming process. There have been times, however, when it was necessary to do this to get the test started. It is important to be very careful in the design and placement of LN<sub>2</sub> storage tanks and transfer systems. The main consideration is the storage tank height, the supply line size and pressure drop and supply line insulation. Nothing is more frustrating than a transfer pump that can not be primed.

The industry had other problems with LN<sub>2</sub> pumps, casing temperature, shaft seal alignment and shaft seal leakage to name a few. But the designs changed and we now have reliable pumps that can operate successfully through a long test.

Other lessons were learned, and phase two closed with the space simulation industry emerging on a much sounder technical footing. This point was finally reached because the critical nature of the business demanded that we attain a high level of reliability and effectiveness in the operation of space chambers. Necessity was certainly the mother of invention in this business.

### **PHASE THREE**

Phase three saw several changes in the design of thermal vacuum facilities. First of all, chambers tended to be in the shape of horizontal cylinders or spheres with horizontal doors. Gone for the most part was the building of top and bottom loaders. Top loaders are easy to load but require a building and crane system that are very expensive. Either the chamber must be set down in the ground a considerable distance, or the crane hook and consequently the building must be quite high. Both of these alternatives result in very high facility costs, particularly in California where earthquake loads can be significant. Bottom loaders also tend to be expensive and a bit more difficult to deal with under some conditions. Horizontal cylinders are more economical overall, especially in the larger size chambers.

Chambers built during phase three included those at RCA, Hightstown, NJ; Lockheed Missiles and Space Co, Sunnyvale, Ca; Rockwell, Seal Beach, Ca; Ball Aerospace, Boulder, Co; and CRC, Ottawa, Canada. Also during this period, Process

Systems International of Westborough, Ma. joined the ranks of prime contractors through the purchase of High Vacuum Equipment Corporation.

### **MECHANICAL PUMPS**

Although the design of mechanical pumps has not radically changed in the past thirty years, both oil sealed pumps and roots blowers have been improved. Reduced internal clearances, canned motors and staged intercooled blower systems have resulted in lowered blank-off pressures for mechanical systems and higher pumping speeds in the mid vacuum ranges. These new mechanical systems have helped to reduce the pump down time through the corona region and lower the pressure at which the cryopumps can be brought on line.

### **APPENDAGE CRYOPUMPS**

Another big help in the pumpdown process has been the development of appendage cryopumps. Since these pumps can now be valved off from the chamber, they can be cooled down in advance of need and opened to the chamber without waiting for the shroud and internal cryopanel to cool down. Because of a more accurate understanding of satellite gas loads, several (four to six) appendage 48 inch cryopumps can now do the job of the multi hundred thousand liter per second cryopumps that were once thought to be necessary. In addition, these cryopumps now come equipped with a charcoal gettering material inside the casing that allows them to pump helium, hydrogen and neon. The original compressor/expander systems designed thirty years ago served their purpose, but anyone who has operated one knows the true meaning of the question "will the reciprocating expander and Swiss compressor make it through another test?" Dependability has certainly been improved.

### **LIQUID NITROGEN SHROUD**

The one area that is still of concern in large thermal vacuum chambers is the liquid nitrogen system. In 1984, I presented a paper at this meeting in Orlando, Florida (ref. 1) on the subject of newly discovered endurance failures of aluminum LN<sub>2</sub> shrouds. At that time, many of the field welded jumper tubes in our chamber at what was then Ford Aerospace had cracked and were preventing the chamber's use for thermal vacuum testing. We did an extensive evaluation of the problem and discovered that the heat affected zones in LN<sub>2</sub> tubing are very susceptible to endurance failures. We concluded among other things that an aluminum shroud probably has a finite life span caused by repeated thermal cycling. Unfortunately, the time to failure is unknown for any given chamber, but is dependent on the shroud's design and the welding techniques used in its construction. Since the second of these two variables is generally unknown for most chambers, it is impossible to predict accurately if and when a given shroud will fail. Other LN<sub>2</sub> shrouds that were designed and built during that period have been replaced or are under consideration for replacement because of cracking tubes. One must remember that shrouds do not fail at ambient, they fail when a satellite is inside the chamber and it is trying to reach high vacuum. Shroud failure has a large potential for causing great financial and schedule related havoc.

## **LIQUID NITROGEN SYSTEM**

The last subject that I want to address has also to do with liquid nitrogen systems. I firmly believe that when this business started, less was known about LN<sub>2</sub> systems than about any other component of thermal vacuum chambers. In the beginning, we had very little idea of how much heat would be applied to satellites during test. Consequently, as with vacuum pumping speeds, the capacity of LN<sub>2</sub> systems was generally over designed and was sufficient to provide considerable safety factor. The typical system of thirty years ago was capable of handling a 300 KW heat load. In fact, this number has often been used in chambers designed recently. However, over the years most satellite testing has used no more than 50 to 70 KW for normal earth orbit heat flux levels. One's response might be to wonder why this over design would be a problem since it provides plenty of safety factor. The answer and our concern lies in the fact that an over designed LN<sub>2</sub> system can result in a large consumption of liquid nitrogen. This is true even when the system is operating at low heat loads.

## **LN<sub>2</sub> CONSUMPTION**

When discussing LN<sub>2</sub> consumption, we must first consider the thermodynamic cycle by which the LN<sub>2</sub> removes heat from the chamber. Some of the first chambers kept their shrouds cold by using liquid level sensors that operated zone supply valves. When the sensor detected that the liquid had changed to gas in the exhaust header of that zone, it opened the valve and the zone was filled with liquid. In this cycle, the satellite heat load was absorbed as latent heat of vaporization as all the liquid in the shroud eventually changed to gas. This boiling system had worked well on smaller chambers and is probably still in use in some vacuum chambers today. However, it was often found to be inadequate to provide the high flow rates required to meet most chamber heat loads. Its big advantage was that it probably consumed the least amount of LN<sub>2</sub> for any given heat load as long as the flow requirement was not too great. Since the flow of LN<sub>2</sub> was energized by a pressurized storage tank, its main inefficiency was caused by the vaporized LN<sub>2</sub> that was required to maintain the proper tank pressure.

## **SUBCOOLED LN<sub>2</sub> SYSTEMS**

The main alternative to the boiling system is known as the pressurized or subcooled system. It was actually developed in the early 1960's by CVI Corporation and was designed to counter the disadvantage of the boiling system. It has been very successful over the years and is presently in use in most of the chambers around the country today. It works on the principle that as the liquid is pressurized and circulated through the shroud, it picks up thermal energy as sensible heat, but is prevented from boiling by its high pressure. The liquid, after it is discharged from the shroud, is then pumped through a heat exchanger where it gives up its sensible heat to the latent heat of an atmospheric pool of LN<sub>2</sub>. The LN<sub>2</sub> that leaves this "subcooler" is now subcooled and returns to the pump where its pressure is



increased and it starts its round trip again. This closed loop pressurized system maintains a very stable temperature distribution through a large range of heat loads without vaporizing or vapor locking. This characteristic has significant advantages when high localized heat loads are a problem. However, this system also has one major disadvantage.

The high pressure and flow rates required to keep the subcooled liquid from boiling require large centrifugal pumps with correspondingly high horsepower motors to drive them. In cryogenic systems, all of the horsepower that goes into the pump shows up as boiled or consumed LN<sub>2</sub>. In one typical subcooled system of a 39 foot spherical chamber with which I have been recently associated, the LN<sub>2</sub> pumps are 25 Horsepower, and all of this power goes into consumed LN<sub>2</sub>. In a typical 30 day thermal vacuum test, the heat flux simulator would radiate approximately 50 KW of thermal energy onto the satellite. This thermal load itself consumes approximately 300 gallons of LN<sub>2</sub> per hour. However, under these conditions, the chamber boils off around 600 gallons per hour. This means that the pump and miscellaneous system heat gains in the chamber run about 300 gallons per hour. At the present cost of LN<sub>2</sub>, that company is spending over \$2000 per day on wasted LN<sub>2</sub>, or almost \$65,000 per thirty day test. Since this company is now running about four tests per year, their yearly cost of thermal inefficiency is almost a quarter of a million dollars. Not all of this loss is caused by the pumps, and not all of the pump loss can be eliminated, but there is room for improvement. When space simulation testing started, no one was concerned about the cost of running a thermal vacuum test. Today, the industry has changed. Contracts are awarded on price, and our customers and the taxpayers are rightly concerned about the cost of satellite testing.

Because of these high LN<sub>2</sub> consumption costs, work has been done in the industry to design a better, more efficient thermodynamic cycle to maintain the cold black body temperature of outer space. There are designs for saturated and boiling systems which will remove the sun's heat load at lower LN<sub>2</sub> consumptions. Without going into details, a saturated system could save significantly in operating costs and still provide low enough shroud temperatures. I believe that this is the area in thermal vacuum testing in which the optimum design has not been reached.

## GN<sub>2</sub> SYSTEMS

Several companies have developed a new approach to the thermal balance process in lieu of the traditional heat flux/LN<sub>2</sub> shroud technique. Shroud temperatures can be controlled with a gaseous nitrogen system between LN<sub>2</sub> temperature and +150° F. Heat exchangers establish the pre set temperature and the gas is circulated through the shroud by a blower at the shroud's operating pressure. This technique can provide the required thermal balance on the satellite with a very minimum in LN<sub>2</sub> consumption. This process is not exactly new: the first GN<sub>2</sub> thermal system was designed by High Vacuum Equipment Corporation and installed at the Honeywell facility in St. Petersburg, Florida in 1961.

## **A NEW CHAMBER**

At Space Systems/Loral in Palo Alto, the most recent large space simulation chamber has been designed using the lessons that have been learned over the last thirty years. This chamber will be a horizontal cylinder, 30'x30' and will incorporate the latest in vacuum equipment and system controls that has been discussed in this paper. It will have a flat floor at the same elevation as the building floor to permit access with an air bearing cart. It will have four 48" appendage cryopumps with isolation valves, a turbomolecular pump and the latest data and heat flux control systems. As I considered the technique of system control in its design however, I deliberately avoided the use of computer control of the vacuum process. Some chambers built recently have included in them a vacuum pump down and control system that is computer controlled. Without criticizing what others have done, I believe that manual control and human decision making in the vacuum process is essential to a sound operation of the system. Computers have a important responsibility in providing data in a timely and efficient manner. However, decisions need to be made by people. Well-trained operators learn from making decisions, not from watching a computer.

## **CONCLUSION**

In conclusion, the design of thermal vacuum chambers and the testing done in them have come a long way since their inception only thirty years ago. It seems that everything that was learned, was learned the hard way. As they say in the Navy, safety instructions are written in blood. None of our experiences cost any one any blood, at least as far as I know, but they usually cost us a great deal of sweat and tears, lost time and much frustration. Perhaps this short review of vacuum history will remind the old timers of some of the challenging times we once had and will hopefully prevent the industry from having to relive them again.

# **THERMAL VACUUM CHAMBER CHARACTERISTICS MATRIX**

<b>COMPONENT</b>	<b>PHASE ONE 1960-1965</b>	<b>PHASE TWO 1965-1972</b>	<b>PHASE THREE 1972-</b>
CHAMBER SHAPE	VERTICAL CYLINDER SPHERE	HORIZONTAL CYLINDER SPHERE	HORIZONTAL CYLINDER
CHAMBER LOADING	TOP BOTTOM	TOP SIDE	SIDE
ROUGH PUMPING	BELT DRIVE MECH PUMPS	DIRECT DRIVE M. P.s	DIRECT DRIVE M. P.s
INTERMEDIATE PUMPS	EJECTOR PUMPS ROOTS BLOWERS	ROOTS BLOWERS STAGED ROOTS BLOWERS	STAGED ROOTS BLOWERS CRYO PUMPS
HIGH VACUUM PUMPS	OIL DIFFUSION PUMPS LARGE HE CRYO PUMPS WITH RECIP. EXPANDERS	LARGE HE CRYO PUMPS MODULAR CRYO PUMPS APPENDAGE CRYOPUMPS ION PUMPS TI. SUBLIMATION PUMPS	APPENDAGE CRYOPUMPS TURBOMOLECULAR PUMPS CRYOPUMPS WITH CHARCOAL LARGE HELIUM CRYOPUMPS WITH TURBO EXPANDERS
LIQUID NITROGEN SHROUD	ALUMINUM PIN WHEEL SOLID	ALUMINUM SOLID	ALUMINUM SOLID
LIQUID NITROGEN SYSTEM	BOILING SUBCOOLED SATURATED	SUBCOOLED	SUBCOOLED SATURATED
HEAT FLUX CONTROLS	POWERED VARIACS PROPORTIONAL CONTROL	ZERO CROSS OVER POWERED VARIACS PROPORTIONAL CONTROLS	DIRECT CURRENT POWERED VARIACS
POWER PENETRATIONS	MULTI PIN	INDIVIDUAL CONNECTOR	INDIVIDUAL POTTED
PROBLEMS	D. P. BACK STREAMING LN2 PUMP RELIABILITY SHROUD WARM SPOTS	PUMPING HELIUM PUMPING HYDROGEN PUMP THROUGH MIDDLE VACUUM RANGE ARCING/CORONA ELETRICAL NOISE HELIUM COMPRESSORS RECIPROCATING EXPANDERS PLASTIC CONTAMINATION	SHROUDS BEGINNING TO FAIL HIGH LN2 CONSUMPTION

## REFERENCES

1. Edwards, A. A.: Fatigue Induced Cracking in Aluminum LN<sub>2</sub> Shroud of 39 Foot Vacuum Chamber. NASA CP-2340, 1984. 13th Space Simulation Conference

**FROM DIFFUSION PUMPS TO CRYOPUMPS: THE CONVERSION OF  
GSFC'S SPACE ENVIRONMENT SIMULATOR**

**Ron Cary  
NSI Technology Services Corporation  
A Subsidiary of ManTech International Corporation**

**ABSTRACT**

The SES (Space Environment Simulator), largest of the Thermal Vacuum Facilities at The Goddard Space Flight Center, recently was converted from an oil diffusion pumped chamber to a Cryopumped chamber. This modification was driven by requirements of flight projects.

The basic requirement was to retain or enhance the operational parameters of the chamber such as pumping speed, ultimate vacuum, pumpdown time, and thermal system performance. To accomplish this task, seventeen diffusion pumps were removed and replaced with eight 1.2 meter (48 inch) diameter cryopumps and one 0.5 meter (20 inch) turbomolecular pump.

The conversion was accomplished with a combination of subcontracting and in-house efforts to maximize the efficiency of implementation.

**INTRODUCTION**

The SES (Space Environment Simulator) is a vertical, cylindrical, 8.2 meter (27 foot) diameter by 12.2 meter (40 foot) high working volume thermal vacuum test chamber. It is located in Building 10 at the GSFC (Goddard Space Flight Center) in Greenbelt, Maryland. Constructed in the early 60's the chamber used 17 oil diffusion pumps, without isolation valves, to create the high vacuum environment. The high vacuum system had worked quite well for almost thirty years, but driven by ever increasing cleanliness requirements of flight projects it was decided that the facility must be upgraded. The upgraded facility would allow NASA to support advanced payload development with continued strong in-house capability.

This upgrade was the seventh in a series of upgrades to thermal vacuum facilities at the Goddard Space Flight Center. Using lessons from the previous upgrades, this task was accomplished by a combination of in-house efforts and subcontracting to maximize the efficiency of implementation, meet flight project schedule requirements, and to stay within

budget constraints. A three phased approach that spanned four years was used to accomplish this task.

## **IMPLEMENTATION**

### **Phase 1 - Preliminary Engineering Report**

In July of 1987 a PER (Preliminary Engineering Report) was undertaken to determine the scope of modifications necessary to convert the SES into a state of the art Thermal Vacuum Facility on par with the industry. The basic task requirement was to maintain or enhance the operational characteristics of the chamber, while eliminating the possibility of contaminating payloads with oil. These operational characteristics included rough down time, high vacuum pumpdown time, high vacuum pumping speed, and ultimate pressure. Also to avoid disruption to Flight test schedules, the chamber down time must be kept to a minimum. A timeline of the Project is shown in Figure 1.

To meet the task requirements for cleanliness, it was decided that the high vacuum system would have to be replaced. Cryopumps were chosen to replace the oil diffusion pumps because of their "innate cleanliness" and the net decrease in operational and maintenance costs. The 17 oil diffusion pumps and cold wall elbows would be removed and replaced with eight 1.2 meter (48 inch) diameter cryopumps with chamber isolation valves. The eight cryopumps provided a net pumping speed of approximately 238,000 L/S, which was 20% more capacity than the seventeen diffusion pumps. To reduce cost and ease installation, the diffusion pump chamber penetrations were utilized to mount the cryopumps.

Because some of the future payloads would be evolving a large amount of noncondensable gases, a .5 meter (20 inch) diameter Turbomolecular pump was added to assist the cryopumps which have a finite capacity for pumping these gases. Another benefit of this pump is that it would aid in leak checking the chamber. The turbomolecular pump is capable of pumping approximately 5,000 L/S of non-condensable gases. To again reduce cost and ease installation, a diffusion pump chamber penetration was utilized to mount the turbomolecular pump.

To improve roughing system performance, the facility roughing piping would be enlarged and rerouted for better conductance and reduced pumpdown times. Chamber isolation valves and cold traps were added to reduce the possibility of backstreaming roughing pump oil. To increase the reliability of the roughing system, each roughing pump was rebuilt. Rebuilding the system was more cost efficient than an outright replacement.

To increase system reliability, reduce maintenance, and make the system more "user friendly" a new vacuum system control console was developed along with a new PLC (Programmable Logic Controller) based control system. The vacuum console featured a full graphic representation of the vacuum process and a PC (Personal Computer) based color graphic system that will link the operators in near real time to the vacuum process. The

specification provided for the selected contractor to be responsible for removing the old diffusion pumps, cutting the diffusion pump elbows, and modifying the roughing system. As well as procuring the new cryopumps, chamber isolation valves, VJ (vacuum jacketed) LN2 piping and installing these components on the chamber. The contractors were asked to bid a firm fixed price for the work. The contractor proposals were evaluated and a contractor was selected and a letter of intent was issued contingent on project funding.

Realizing that the .5 meter (20 inch) turbomolecular pump was a unique and possibly long lead time item, a specification was generated and this pump was also competitively bid during this Phase.

Another aspect considered during this phase was the preparation of demolition plans for the facility. Because the chamber is located in an operational lab area, contamination of the lab with dust, dirt, vapors, and other debris was of a major concern. Another concern was the safety of flight hardware and personnel in the immediate vicinity of the construction work. Working with the mechanical subcontractor, a demolition plan was developed that would minimize contamination to the lab and provide safety for personnel and equipment.

The plan revolved around enclosing the facility in a large fire proof canvas "tent" This tent would contain dust and debris and prevent personnel from entering the construction area. In addition, to keep particle contamination to a minimum all of the small piping would be sheared off rather than sawed. The mechanical subcontractor also devised a method of actually milling the stainless steel diffusion pump elbow off the chamber. This cutting method generated large chips of steel that were easy to clean up. Plasma cutting, which would have generated a large amount of contamination was not necessary.

### **Phase 3 - Construction**

In March of 1990 funding for the project was received and work immediately began on implementing the task. The first step in our plan was to release the prime mechanical subcontractor. It would be about 7 months before the mechanical subcontractor was ready to move on site to install the vacuum system. During this seven month period, the project team concentrated on our in-house efforts and reviewing the efforts of the mechanical subcontractor.

In-house work began on the design of the PLC control system, the Mimic Panel (A large graphic panel), and fabrication of numerous shop drawings. Procurement specifications were developed, RFP's requested, and contracts awarded for the PLC, the color graphics system, the vacuum console, and the mimic panel.

In June of 1990 in-house demolition of the Facility began. Demolition began with the utility systems such as air, water, and nitrogen piping and electrical wiring. Removing these items cleared the way for the mechanical subcontractor to remove the diffusion pumps and elbows.

PLC based control system is covered in an "Application of Programmable Logic Controllers to Space Simulation", 17th Space Simulation Conference NASA CP-\_\_\_\_, 19\_\_\_. (Paper \_\_\_\_ of this compilation).

Cleanliness of the vacuum was a prime concern. So it was decided the entire interior of the chamber would be cleaned to remove residual traces of diffusion pump oil.

## **MODIFICATION OF THE SPACE ENVIRONMENT SIMULATOR PROJECT TIME LINE**

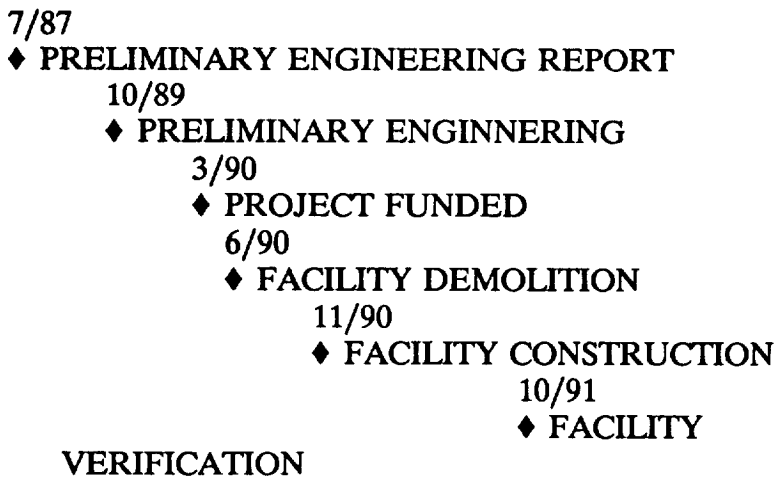


Figure 1: Project time line for SES showing major milestones.

### **Phase 2 - Preliminary Engineering**

Prior to project funding, preliminary engineering work began in October of 1989. Driven by flight test schedules for the HST (Hubble Space Telescope) project, a 19 month construction schedule was decided. To meet this tight schedule it was decided that a combination of both in-house personnel and subcontractors would be necessary.

Four contractors that expressed an interest in this project were contacted. Each of the contractors visited GSFC to review and comment on the task. To utilize the expertise and construction capabilities of these subcontractors, a performance specification was generated that covered the procurement and installation of the new vacuum system. The



The mechanical subcontractor began on site work in November of 1990 and completed the task of installing the vacuum system in about three months. In March of 1991 the in-house mechanical construction crew took over and began the task of connecting all of the utilities to the new vacuum system (air, water and nitrogen), see Figure 2, and rebuilding the roughing system. The in house electrical construction crew installed the new vacuum console (see Figure 3), mimic, re-built the motor control center, and began point to point wiring of the facility. Construction of the Facility was completed in September of 1991.

ORIGINAL PAGE  
BLACK AND WHITE PHOTOGRAPH

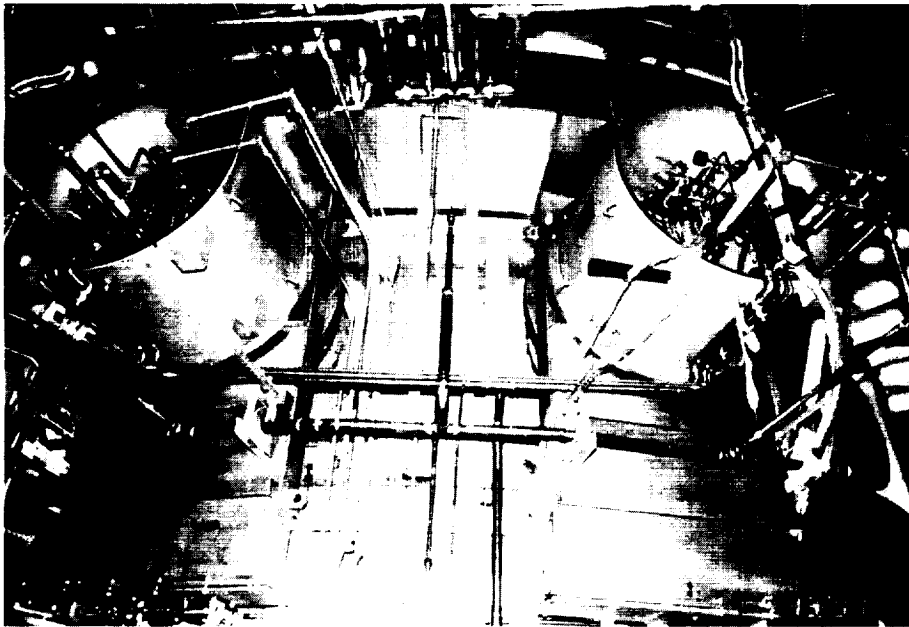


Figure 2: Installation of utility piping to 48 inch diameter cryopumps.

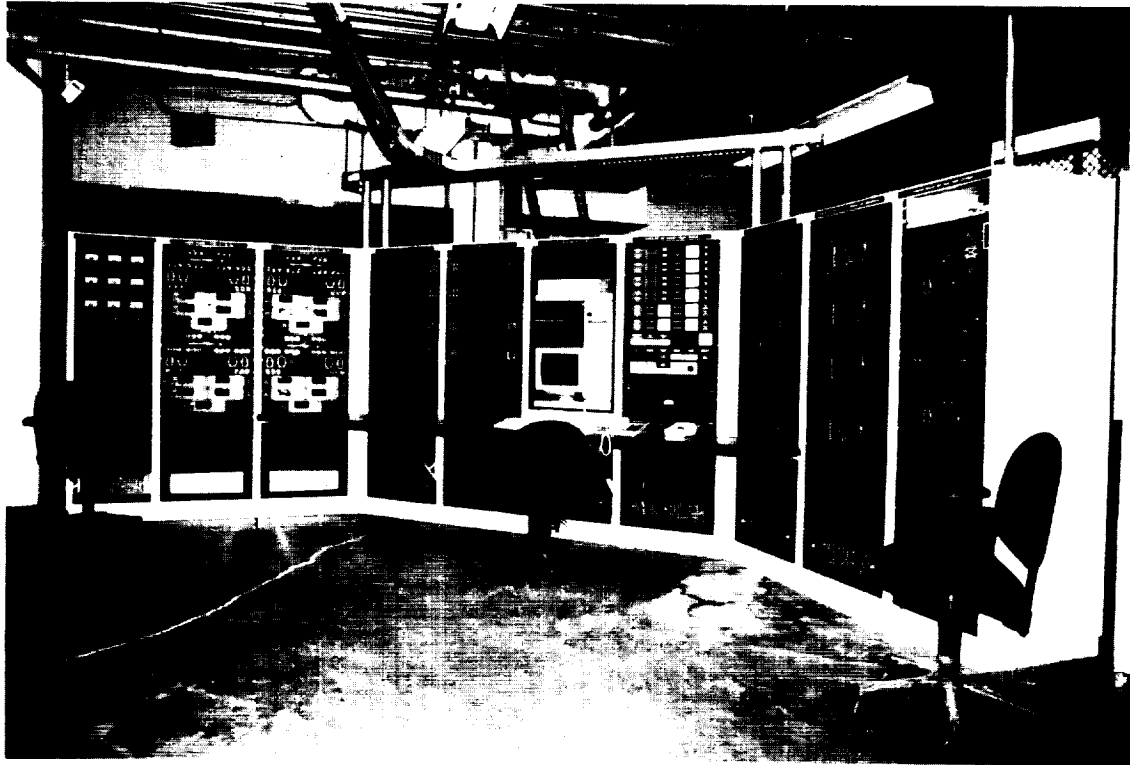


Figure 3: New vacuum control console during construction phase.

### Verification And Performance Testing

During the month of September 1991, the chamber shrouds and shell were extensively cleaned to remove traces of diffusion pump oil. This task was subcontracted so that in-house efforts could be channeled at checkout of the facility. Prior to cleaning of the facility, wipe samples were taken at selected areas on the shell and shrouds. The samples were evaluated by the NASA materials branch and a base line cleanliness of the facility determined. The cleaning subcontractor then used a three stage cleaning process. In the first phase the chamber was completely vacuumed from top to bottom using HEPA filtered vacuum cleaners. This removed the large contamination from the chamber, while preventing the generation of more dust. The second stage was to completely wash the chamber shell and shrouds with an emulsifying detergent, followed by a DI (deionized) water rinse. The detergent wash was applied by a combination of high pressure washers and hand scrubbing with sponges. In the final cleaning stage, the chamber shell and shrouds

were completely rinsed and wiped down with reagent grade alcohol. Wipe samples were again taken and showed that all surface traces of diffusion pump oil had been removed. A baking of the chamber would provide the final cleaning of the chamber.

During the month of October 1991, the facility was certified and performance verified. The goal of the verification was to prove that each of the new sub-systems, the PLC, and system interlocks operated as designed and that systems not upgraded during the task still functioned as designed. During the facility verification every component of the facility was exercised by procedure. Each electrical circuit was tested and the system tested by simulating failures and observing that alarms were initiated and systems shutdown as designed.

## **CONCLUSION**

System performance met or exceeded all goals established in the PER. The chamber is capable of roughing down to 100 microns, our crossover pressure, in 2.5 hours. With six cryopumps operating the chamber was able to reach a pressure of  $2 \times 10^{-7}$  Torr in less than 4 hours. Regeneration of the pumps can be accomplished in less than six hours. To complete the cleaning process, the chamber was baked and certified at +75 deg C with two QCM's (Quartz Crystal Microbalances) at -20 deg C with a delta frequency of less than 300 HZ for 3 consecutive hours. The chamber is now qualified for most all NASA projects.

The task however was not completed without learning a few new lessons. The number one lesson learned on this task was to require complete performance testing of key equipment and then to witness the vendor tests. In spite of witnessing many performance tests of equipment, in more than one instance equipment that was not tested and witnessed at the vendors shop failed during facility verification. A second lesson learned concerned the use of prime subcontractors. The use of a prime contractor was a great benefit. Not only were we able to bring to bear additional resources, the task was completed for a fixed cost. This allowed us to coordinate a large amount of work through a single subcontractor.



**CLEANING OF A THERMAL VACUUM CHAMBER  
WITH SHROUDS IN PLACE**

William R. Bond  
NSI Technology Services Corporation

**ABSTRACT**

In February, 1991, a failure of a rotary booster pump caused the diffusion pumps to backstream into a 10' x 15' thermal vacuum chamber. Concerns existed about the difficulty of removing and reinstalling the shrouds without causing leaks. The time required for the shroud removal was also of concern. These concerns prompted us to attempt to clean the chamber without removing the shrouds.

**INTRODUCTION**

Facility 225, a 10' x 15' thermal vacuum chamber, was built and installed at Goddard Space Flight Center in 1962. The chamber was first located at Building 4 where it remained until 1987. For the majority of this period the chamber was used as a solar simulator. During the normal solar simulator test the shrouds were flooded with liquid nitrogen at 30 psi. At the conclusion of the test the liquid was dumped. The thermal system was then operated in a gaseous mode to return the system to ambient temperatures. Heating was achieved by the frictional effects resulting from the circulation of nitrogen, and by the heat generated by the 150 horsepower blower motor. Occasional chamber bake out procedures raised the shroud temperature to 100 °C. Towards the end of the Building 4 period a new project changed the operation from that of a solar simulator to a pure thermal vacuum system. Operating temperatures for this project ranged from ambient to 50°C.

During the end of 1987, and the beginning of 1988, the chamber was disassembled, moved approximately ¼ of a mile, and reassembled in the main Space Simulation Laboratory in Building 7. The original design had welded connections between the shrouds and the external thermal system piping. The removal of the shrouds for the relocation required cutting the connection and bending the shroud to allow the connection stub to clear the chamber wall. This was an approximate 6" deflection of the 111" diameter shroud. In Building 7 the shrouds were fitted with flanges and connected to the thermal header through a bellows assembly. Although the welded connections were gone, the ends of each shroud were now held in a fixed position by support clamps.

The recommissioning of the chamber occurred in August of 1989. Because of cost considerations, with the exception of the shroud connections and piping, the thermal system was unchanged. The

major vacuum components were also substantially unchanged. The rotary piston pump and rotary lobe booster pump did not come with the chamber but were of similar age to the originals. Inside the chamber the thermal system consisted of front and rear shrouds and four pairs of side shrouds. (Figure 1) Shrouds 3 and 5 have cutouts to allow an opening for the old solar simulator source.

Besides the previously mentioned piston and booster pumps, the vacuum system consists of three diffusion pumps and a small rotary piston pump. All of the mechanical pumps are located in a machine room in the basement. (Figure 2) The three diffusion pumps are located at the back of the chamber behind the rear shroud. No valves exist between the diffusion pumps and the chamber. The diffusion pumps use an oil described as 100% mixed isomers of pentaphenyl ether. Based upon the MSDS provided with the oil, the boiling point is 476°C and the flash point is 288°C.

#### **SYSTEM FAILURE**

On the evening of Tuesday, February 5, 1991, Facility 225 was performing a "bake out" of a test fixture. At 22:50 an event occurred that was documented by the following "Error Malfunction Report." "All 3 DPs went off line, GN<sub>2</sub> blower off, cold traps stop filling, chamber pressure at 6 Torr. Informed mechanical and electrical maintenance." Inspections of the chamber and vacuum equipment on the morning of the 6th revealed that the booster pump input shaft had fractured. This fracture allowed air to enter the foreline causing the three diffusion pumps to backstream coating the chamber walls with diffusion pump oil.

#### **Initial Response**

An emergency response team was established to return the chamber to service as quickly as possible. The initial meeting was held after members of the team had an opportunity to view the chamber and its mechanical components. Technicians, facility and test operations engineers, and the Maintenance and Operations Supervisors were members of the team. At the first meeting the team outlined possible approaches to the cleaning task. The two basic approaches were: 1 Remove the shrouds to allow a thorough cleaning of all surfaces; 2 Clean the chamber without removing the shrouds. At the end of this meeting the team had identified most of the benefits and probable difficulties associated with each approach. The team leader made assignments to determine the availability of personnel and materials for the cleanup project. A second meeting was held in the early afternoon to discuss scheduling for the two basic approaches and to form the recommendations for presentation to NASA.

While it seems obvious that the suggestion of one of these approaches suggests the other, the idea that this chamber could be cleaned without removing the shrouds seemed optimistic at best. The chamber is 25 feet long with a six inch gap between the shrouds

and the outside wall. The rear shroud covers, and is close to, the lower half of the back wall of the chamber. Cleaning the chamber without removing the shrouds would probably require a spray of liquid which was complicated by the fact that another facility is operating with people only ten feet from the door of Facility 225. How do we determine that the areas that are hard to reach are actually clean? While the questions about the possibility of leaving the shrouds in place seemed to present serious concerns, so did the alternative.

Removal and reinstallation of the shrouds required that the shroud ends be pulled together at least one and probably two times. (The shrouds would have to be held in the deflected position during the cleaning process to allow only one stress cycle.) Leak checking the shrouds while they were out of the chamber made sense since any leak found could easily be repaired. The shrouds still would have to be leak checked after they were reinstalled in the chamber. Leak checking the back side would be hard. Repairing the back side could well require the removal of the shroud for a second time. Even the flange connections between the headers and the shrouds would be difficult to assemble.

### **Proposal**

The afternoon meeting helped to clarify the proposal that we would be making to NASA. If we could find a chemical that would remove the diffusion pump oil, that would not damage the chamber and whose use was without risk to people, the lab and the environment, we would perform the cleaning with the shrouds in place. The task could be accomplished quicker, for less money and less risk if that chemical could be found. Unfortunately the manufacturer of the diffusion pump oil was recommending the use of freon based solvents or acetone. Both of these materials were unacceptable for spray application in an area where recovery would be very difficult.

### **Decision**

NASA officials approved a parallel effort at the beginning of the cleanup task. This effort would allow the initial work for both cleaning approaches to proceed. If our investigation found a chemical that could satisfy our requirements for a cleaner or solvent, and a satisfactory method of application, we would proceed with the shrouds in place. While the investigation into chemicals was going on, the assembly and improvement of the shroud removal fixture would be undertaken.

### **CLEANING EFFORT**

#### **Parallel Tasks**

On Saturday, February 9th, the recovery effort officially began. The work effort was to continue 24 hours a day until the chamber was recertified. Work began by removing the test cart and payload fixture. The auxiliary test equipment and the cart rails were

removed next. By the end of Monday all three of the diffusion pumps had been removed from the chamber and transported to an available work area. Once the diffusion pumps were in the work area the process of removing the oil began. Because of the viscous nature of the oil, removing the oil required the application of heat and two days to complete. Most of the old shroud removal fixture had been located and the disassembly of the failed blower had begun. The blower disassembly was completed the next morning.

Because the large Space Environmental Simulation Chamber (SES) had eight identical booster pumps, the cause of failure of the blower had additional significance. We completed the disassembly of the pump on Tuesday. Our evaluation of the failure was that fracture was due to fatigue. Because of the importance of the answer to the other facility we contacted the Materials Branch of the Office of Flight Assurance to conduct an analysis of the failure. The final report of the failure concluded that the failure was "a result of combined torsion and bending fatigue." As the result of this investigation engineering specified the use of new booster pumps for the SES.

#### Chemical Investigation

The investigation into possible cleaning solutions ran through many paths. Numerous telephone calls were made to firms that supply vacuum equipment and others that use or install diffusion pumps. We found two chemicals that seemed to be worth testing. Both were identified as glycol ethers. One was identified as a mixture of 1-Methoxy-2-propanol (97%) and 1-Methoxy-1-propanol (3%). The second chemical was Dipropylene glycol monomethyl ether (99%). The chamber door was used to test these chemicals. Since a spray system had not yet been developed, each chemical was tested by pouring it over a contaminated area. A second area was subjected to a wipe using the chemical. We then asked the Polymers Section of the Materials Branch to test the four areas. They reported that the Dipropylene glycol monomethyl ether appeared to be the best choice. We had checked the four test areas using a black light and had come to the same conclusion.

#### Application Method

While the chemical evaluation was taking place, other technicians and engineers were busy with the application and removal problem. The design of the chamber has eight bellows assemblies along the bottom centerline. Any liquid in the chamber will fill these assemblies with approximately three gallons of the solution per assembly. We concluded that both the spray and the removal of the solution could be accomplished with an air operated polypropylene diaphragm pump. A wand was made using 0.5" OD stainless steel tubing. A nozzle was made locating six 0.060" holes spaced evenly around the diameter. Operating the pump at 40 psig produced a flow of one gpm. A series of 0.25" OD flexible copper tubing wands was made to remove the liquid from the bellows assemblies. The end of the removal tube was inserted in the bellows assembly through a



small gap that existed between the left and right shroud halves. The insertion was difficult. The wand was inserted as far as it could be reasonably inserted. This left varying amounts of liquid in each bellows assembly.

### **Decision Made**

The decision to proceed with the attempt to spray clean the chamber occurred on Monday the 18th. The effort to revise the shroud removal system was also complete at this point. This provided a fall back position if it turned out that the spray wash did not work. The cleaning effort for roughing and other lines and the reassembly of valves that had been serviced and leak checked took until the 19th.

### **Preparations**

A cleaning procedure was written and signed by company and NASA representatives. The procedure was more of a safety document than a true cleaning procedure. The first line of the section that discussed the actual cleaning procedure stated: "The operation will not begin until all safety measures have been taken." It included information taken from the MSDS as well as the MSDS itself. Personnel directly involved in the cleaning were required to use breathing apparatus and face shields.

Final preparations for the cleaning effort took place on the 19th and the early morning hours of the 20th. Loose mylar and other bits of testing debris were vacuumed out of the chamber. The rear anchor beam and pedestal for the shroud removal fixture were removed. Ports that had been opened during the first stages of the project had to be blanked off. The cleaning chemical's full drum weight was recorded as were the empty drum weights of the containers that would collect the used chemical. Hose connections were made to drain the solution to the collection drums in the basement. A rubber sheet and plywood dam was installed at the front of the chamber.

Fume and mist control was established using curtains and an exhaust fan. 20 foot long plastic curtains were hung around the entrance to the chamber. A flexible exhaust duct attached to an exhaust fan was inserted through one of the diffusion pump ports at the back of the chamber. The roof exhaust fans as well as fans that exhaust air from the basement were also operated. This combination of containment and exhaust maintained good air quality in both the lab and the basement.

### **Cleaning**

The actual spray cleaning of the chamber started at 0600 hours on the 20th and was completed at 0800 hours on the 21st. The chamber had been sprayed with chemical twice. Since the chemical is classified as being infinitely soluble in water we followed these applications with two clean water rinses. The last step of this

phase of the project was to pump as much of the liquid as possible out of the bellows assemblies. The Polymers Section took five test samples. Three of the samples were rated excellent. One sample taken next to the chamber lip at the top showed a trace of diffusion pump oil. Since a second sample also taken from the top but further into the chamber showed no sign of the oil, we treated this area by hand wipe. The last wipe sample showed no diffusion pump oil but had trace materials "from earlier bake outs." Black light examination showed the chamber walls to be in excellent condition. We did find that over spray had contaminated parts of the black inside shroud surface. We wiped the black surfaces with alcohol. This successfully removed the contamination.

The time from the 22nd until the 28th was spent reassembling the chamber and leak checking. This included installing the new booster pump that we had purchased on an emergency basis. (In spite of the emergency the blower procurement was still done on a competitive bid basis.)

On Thursday, February 28th, at 0645 hours we began the pump down of the chamber. By noon we had to change the oil in the piston pump because of the accumulation of moisture. This procedure was repeated six times during the first 30 hours. As we pulled a vacuum on the chamber the liquid in the bellows cooled, eventually producing frost on the outside of the bellows. Based upon the frost lines, and the approximate 3 gallon capacity of the bellows, we had between 5 and 8 gallons of liquid trapped in the bellows. We started the thermal system at approximately 0830 hours on March 1st. The initial setting was 25°C. The temperature was set to 30°C at 0900 and raised to 40°C at 0930. At 1000 we set the temperature to 50°C with plans that this would be the final increase until the moisture was driven off. The last of the frost disappeared at 1045 hours and the final piston pump oil change was performed. The operations technicians started the diffusion pumps at 1300 hours on the 1ST. They decided to maintain the temperature at 50°C. until 1900 hours. At 1900 hours the technicians began to increase the set point in 25°C steps to 100°C with a final increase to 120°C. At 2200 hours the chamber temperature was 120.8°C and the pressure was  $1.3 \times 10^{-5}$  Torr. Technicians held the chamber at the 120°C set point for 48 hours. At 1300 hours on March 2nd the pressure reached  $3.7 \times 10^{-6}$  Torr. The chamber was shut down on March 3rd. Personnel took test samples to be evaluated by the Polymers Section were taken at 2240 hours.

## Results

The test samples taken after the initial chamber bake out showed the presence of both the dipropylene glycol monomethyl ether and the diffusion pump oil. The total residue on the cold finger was 28.8 mg. A sample was also taken from the scavenger plate. (Table 1) The bake out had been resumed before the test results were back from the Polymers Section. On March 7th a sample was taken from the cold finger. A second set of samples was taken on March 11th. By this time the total residue on the cold finger was

reduced to 1.3 mg. Although both chemicals were still present the lab report concluded, "The smaller amounts of residue seem to indicate that a satisfactory level for testing flight hardware is being approached."

The need to resume work in this chamber was made easier by the fact that the first jobs that were scheduled were fixture and tool box bakeouts. Based upon the March 11th results, NASA proceeded with the fixture bakeout. Neither dipropylene glycol monomethyl ether nor diffusion pump oil were listed in the test reports of cold finger samples taken at the conclusion of the bakeout on March 15th. The diffusion pump oil was still present on the scavenger plate. The next bakeout was the tool box. Samples from March 20 from both the cold finger and scavenger plate were clear of both chemicals.

### **Time and Costs**

Not including the bakeout time, the cleaning of Facility 225 had required 1770 hours of technician effort. Estimates for the removal of the shrouds were between 2220 and 2780 hours. Since the normal level of effort was 96 hours per day even the lowest estimate would require an additional 4.5 days. Beyond that, however, we would have had to depend upon outside services for insulation and possibly certified welding as well.

The material cost, not including the replacement booster pump and diffusion pump oil, totaled less than \$2500. We estimated that insulation work would add \$6000 and, if required, welding work would have added another \$4000.

### **CONCLUSION**

When faced with a requirement to clean a thermal vacuum chamber, the possibility of a clean up without removing the shrouds should always be considered. Where shroud removal would be the normal, although difficult, approach to cleaning time can be gained by testing. Test coupons coated with diffusion pump oils, or other potential contaminants, should be treated with cleaning chemicals to determine the agents effectiveness.

A regular Preventive Maintenance program including nondestructive examination of all rotating, or otherwise high stress level, equipment should be considered for all components that are a part of the vacuum boundary. Although this will not eliminate the need to clean a chamber, it will minimize the unexpected failure.

Table 1  
Residual Contamination After Completion  
of Each Bakeout

Sample Date	Sample Source	Residue	Contamination
3/4/91	Cold Finger	28.8mg	1. Dipropylene glycol monomethyl ether.
	Scavenger Plate	1066mg	1. Dipropylene glycol monomethyl ether. 2. Diffusion pump oil.
3/7/91	Cold Finger	2.3mg	1. Aliphatic hydrocarbons 2. Diffusion pump oil. 3. Esters 4. Dipropylene glycol monomethyl ether. 5. Organic acids.
	Scavenger Plate	N/A	N/A
3/11/92	Cold Finger	1.3mg	1. Diffusion pump oil. 2. Aliphatic hydrocarbons 3. Small amounts of esters 4. Small amounts of Dipropylene glycol monomethyl ether.
	Scavenger Plate	48.6mg	1. Aliphatic hydrocarbons 2. Diffusion pump oil. 3. Esters 4. Traces of Dipropylene glycol monomethyl ether.
3/15/92	Cold Finger	0.1mg	1. Aliphatic hydrocarbons 2. Traces of butoxy compound
	Scavenger Plate	17.4mg	1. Aliphatic hydrocarbons 2. Dibutyl phthalate 3. A butoxy compound 4. Lauric acid 5. Diffusion pump oil.

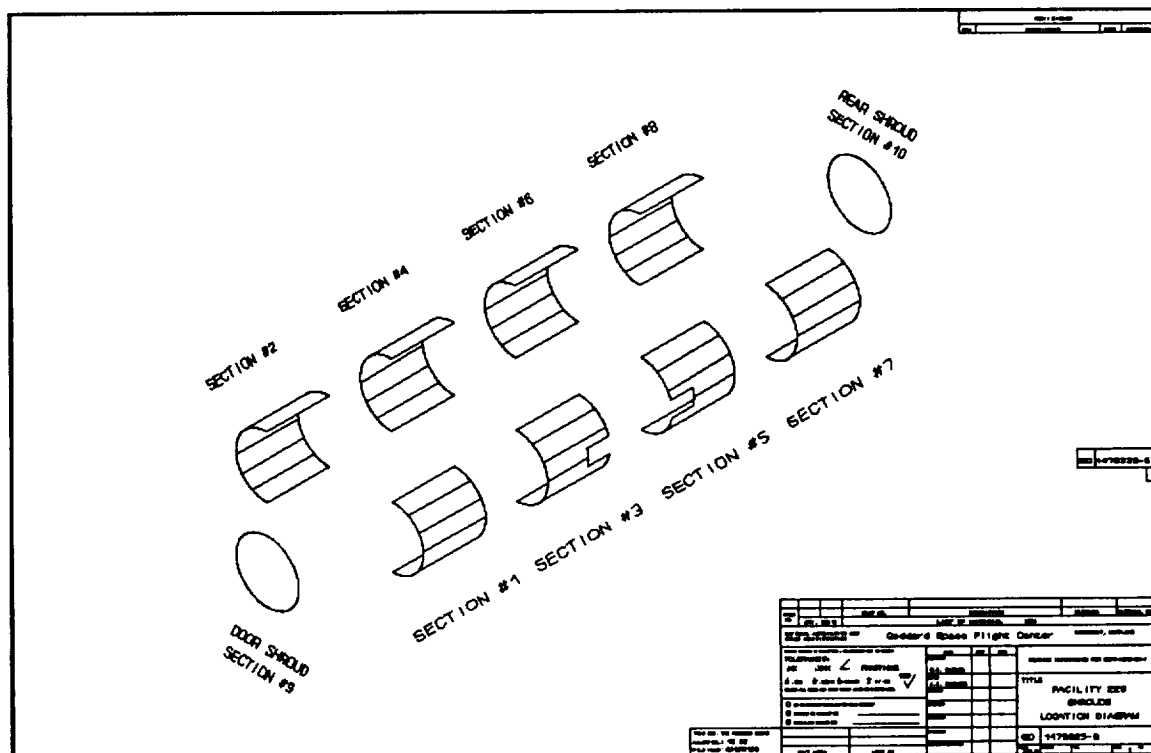
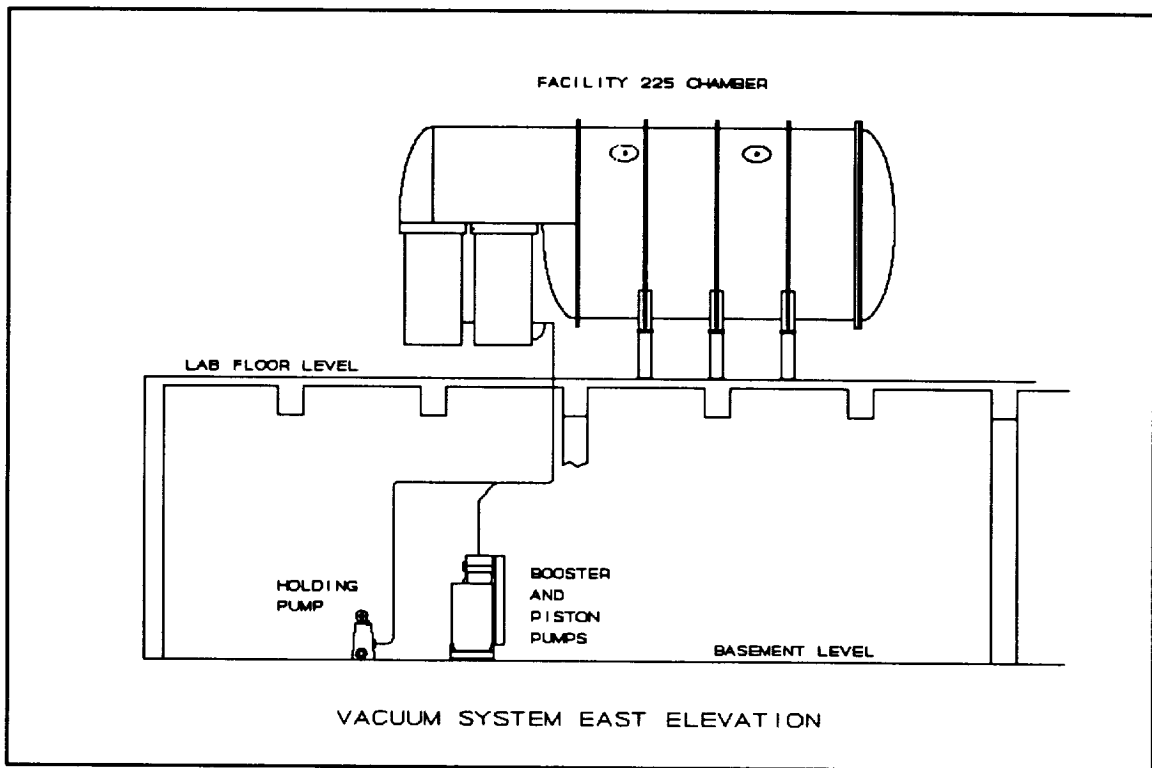


Figure 1 - Facility 225 Shroud Arrangement



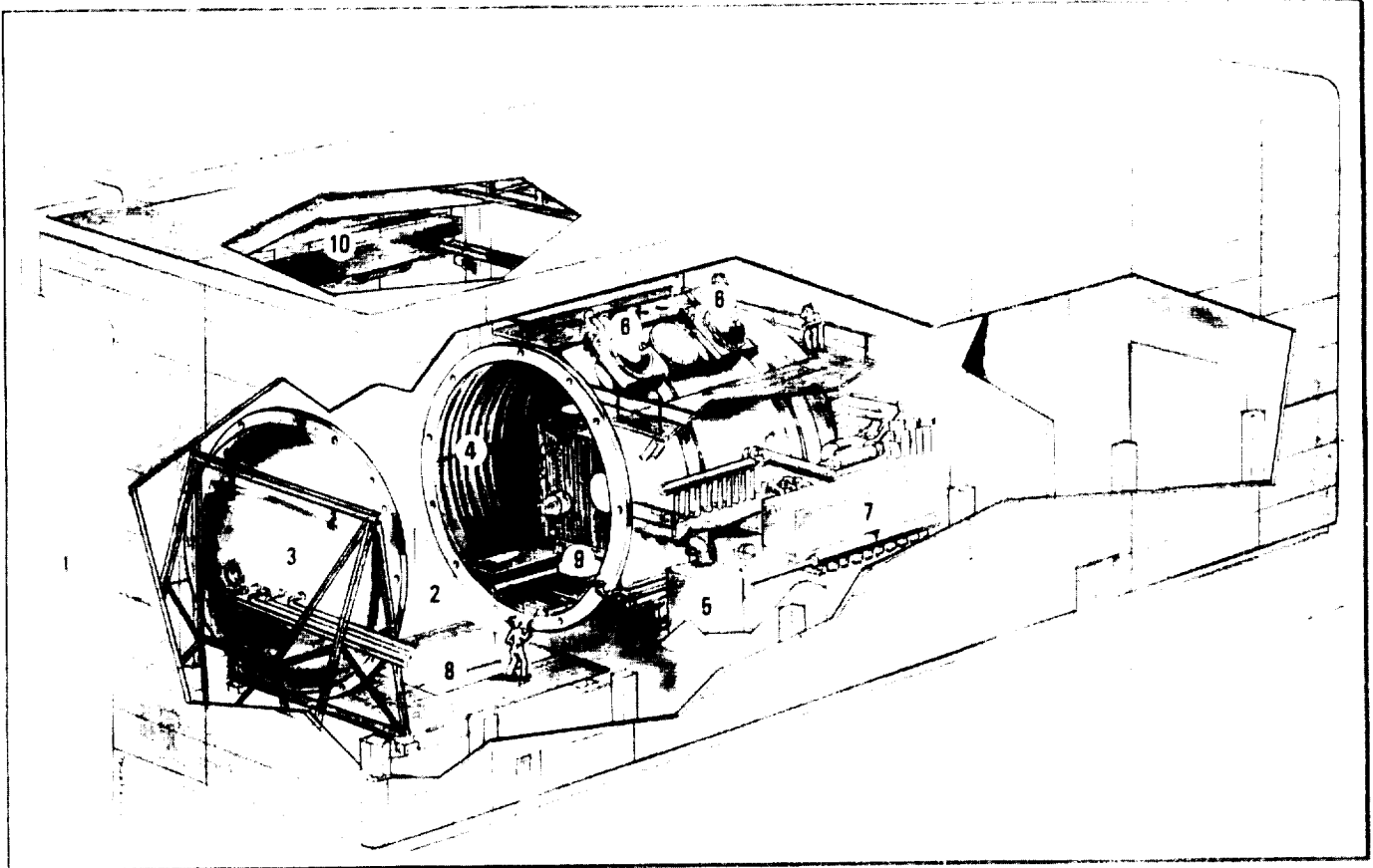
**Figure 2 - Facility 225 Vacuum Pump Locations**

# INTESPACE's NEW THERMAL-VACUUM TEST FACILITY : SIMMER

Raymond DUPRAT, André MOUTON

INTESPACE

N 93 - 15613



- 1- Entrance Airlock
- 2- Preparation Area Class 100.00
- 3- Vacuum Chamber
- 4- Radiating screens

- 5- Primary Pumps
- 6- Cryogenic Pumps  
Turbomolecular Pumps
- 7- Thermal Generator

- 8- Lifting Device
- 9- Platform
- 10- Travelling Crane

## ABSTRACT

The development of an European satellite market over the last 10 years, the industrialization of space applications and the new requirements from satellite prime contractors have led INTESPACE to increasing the test center's environmental testing capacities and notably through the addition of a new thermal-vacuum test facility of impressive dimensions referred to as the SIMMER.

The SIMMER is a simulator specifically created for the purpose of conducting acceptance tests of satellites and of large structures of the double launching ARIANE IV or half ARIANE V classes.

The chamber is 8.3 meters long with a diameter of 10 meters.

The conceptual design of a chamber in the horizontal plane and at floor level is in a view to simplify test preparation and to permit final electrical checks of the spacecraft in its actual test configuration prior to the closing of the chamber.

The characteristics of the SIMMER complies with the requirements being currently defined in terms of thermal-vacuum tests :

- thermal regulation (temperatures cycling between 100 K and 360 K),
- clean vacuum ( $10^{-6}$  mbar),
- 600 measurement channels,
- 100 000 cleanliness class.

The SIMMER is located in INTESPACE's space vehicle test complex in which a large variety of environmental test facilities are made available for having a whole test program completed under one and a same roof.

## 1 - INTRODUCTION

Set up in Toulouse in 1969, INTESPACE has developed a wide range of facilities to fully match the test requirements as defined for launch vehicles.

The effective use of the modular Ariane IV launcher put into service in 1988 plus the ever-increasing competition on the global marketplace have led INTESPACE to developing new resources for the testing of satellites in view of qualification and acceptance. At the same period of time INTESPACE had to get involved in the testing of payloads as will be carried by the next-generation, heavy-lift ARIANE V launch vehicles.

The new test facility SIMMER for thermal vacuum testing was designed and manufactured as per the following criteria :

- Optimization of the chamber to conduct thermal vacuum acceptance tests for new families and/or recurrent models of satellites.
- Test configuration capabilities for Ariane IV- and Ariane V-launched satellites.
- Optimization of the test campaign durations and notably of the preparation, handling and test phases.

- Integration in the test configuration of a satellite of previously-defined functional connections.
- Verification of the proper functioning of a satellite under extreme environmental conditions (low and high temperatures) and this at different stages of its lifetime.
- Accommodation of the operations and integration staff members, installation of the equipment, facilities and determination of the areas needed for satellite testing and the series of operational checks.
- Extension capabilities for future enhancements of the chamber.

The simulator is housed in a building equipped with all the equipment and areas necessary to carry out testing operations (i.e. offices, OCOE and SCOE areas, preparation area in a clean room of class 100 000, storage area, and the like).

The simulator is linked via a specific airlock to the other facilities being available under one and a same roof for the purpose of performing qualification and acceptance tests.

INTESPACE Space Test Center	
Qualification	Acceptance
<b>Integration and Test Preparation Area</b> Experimenters' area Spacecraft checkout area High bay clean room  <b>Tests :</b> Vibrations : 300 kN multi shaker Acoustics : 1100 m <sup>3</sup> chamber Thermal balance : 7m Ø x 9 m chamber plus 3,8 m Ø solar simulator EMI/EMC : 16 x 10 x 11 m shielded anechoic chamber Mass properties : 4 tons combined facility	<b>Integration and Test Preparation Area</b> Experimenters' area Spacecraft checkout area High bay clean room  <b>Tests :</b> Acoustics : 1100 m <sup>3</sup> chamber <b>Thermal vacuum : 10 m Ø x 8.3 m thermal vacuum chamber</b> Mass properties : 4 tons combined facility



## 2 - MARKETING CONSIDERATIONS

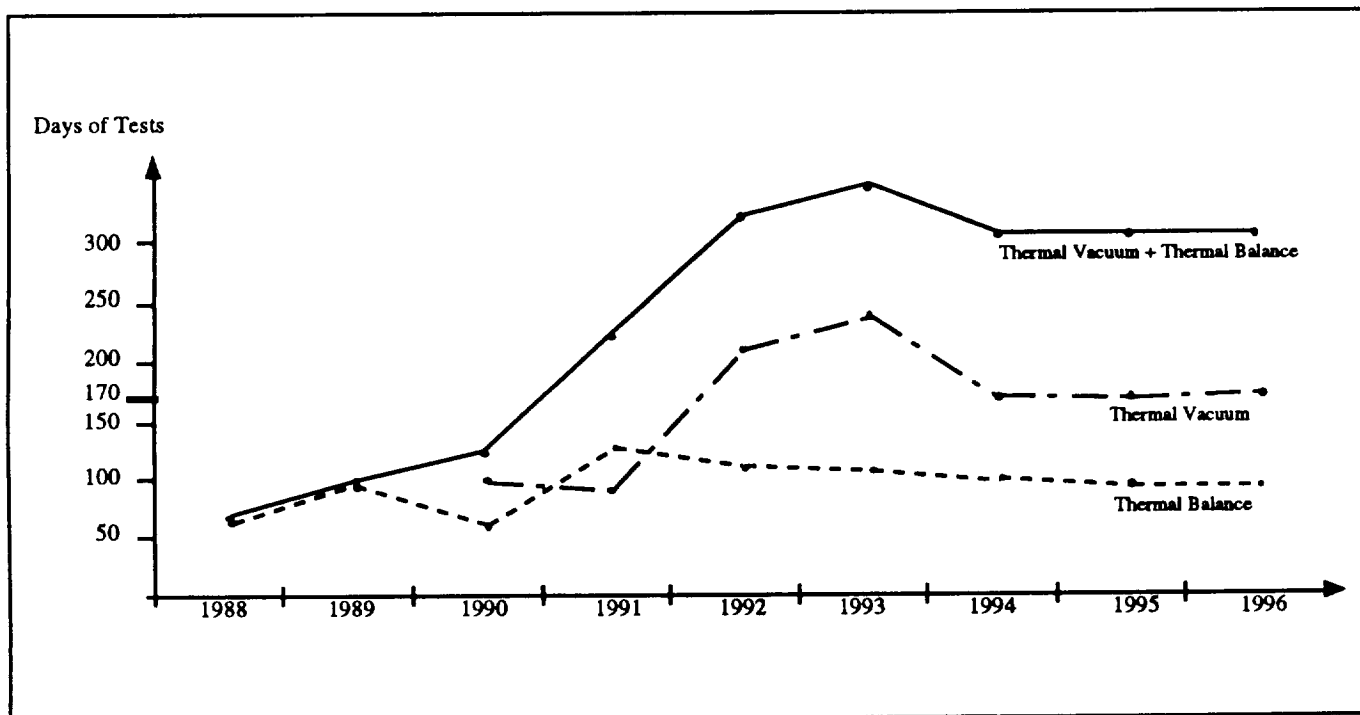
The curve presented below gives a clear indication of the market niches INTESPACE is in a position to gain and of the major industrial partners for which the company works today.

This curve evidences a growing demand for tests of the thermal vacuum type and a relative stability of the need for thermal balance tests.

The forecasts predicted from 1994 onwards are based on the market growth that the studies conducted by Arianespace and Euroconsult and by other industrials lead to expect, as well as on the ascertained loyalty of INTESPACE's major European customers.

All these indications converge towards predicting a substantially boosted demand.

It is to be noted that an optimized test facility with an operational capability of 200 days (preparation, test, removal) in terms of thermal vacuum tests shows a most satisfactory workload. In contrast, a simulator used for its maximized thermal balance performance (with solar simulation) lets from 40 to 60% of its capability unused each year, that is 70 to 100 days.



### **3 - FACILITY's MAIN CHARACTERISTICS**

#### **3.1. Preparation Area**

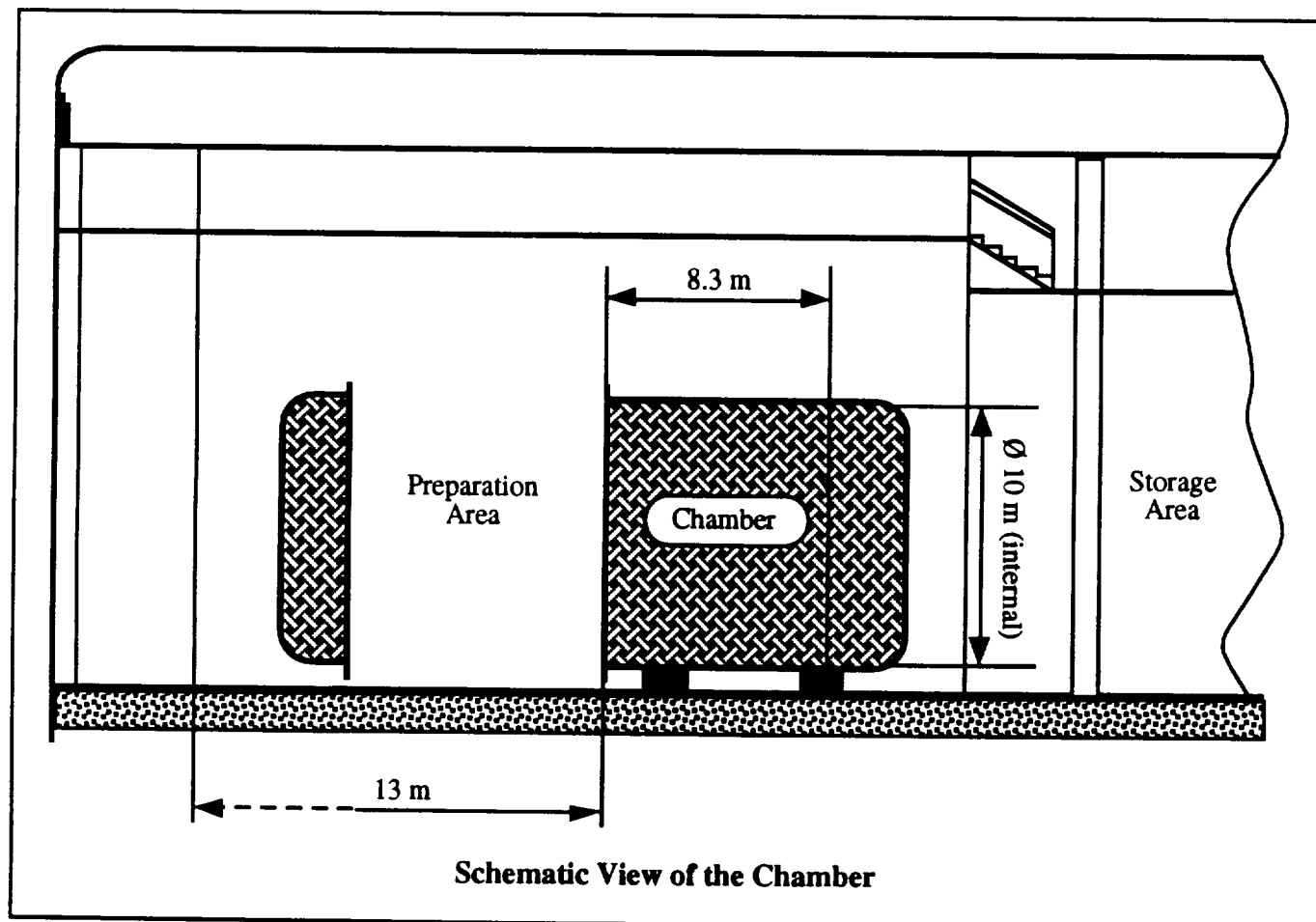
The preparation area is used to conduct the following operations :

- Preparation and servicing of the specimen prior to the test.
- Transfer of the specimen to the integration trolley.
- Insertion of the specimen into the test facility.
- Displacement and storage of the chamber's front door.
- Storage of the means of access to the specimen during the tests.

This area shall be maintained as a clean room of class 100 000. An overhead traveling crane of 7t is kept in this area.

Surface : 374 m<sup>2</sup> - Effective height : 13 m under the overhead traveling crane's hook.

#### **3.2 Chamber**



The chamber consists of a cylinder in the horizontal plane closed by two spherical bulkheads, that is :

- The front bulkhead, in the clean area, is used as an access door to enter the chamber and is moved away on an automotive trolley.
- The aft bulkhead, in the grey area, is permanently attached and provides capabilities for additional cylindrical rings to be fixed, permitting thereby later extensions of the simulator.

Overall dimensions :

- diameter : 10 meters
- length : 8.30 meters

A number of removable feedthroughs are distributed over the simulator so as to have the data from the specimen (electrical feedthroughs, thermocouples, ...) and/or from the simulator itself to be properly transmitted (vacuum gauges, temperature measurements). A series of windows are evenly distributed over the chamber to permit visual monitoring of the specimen when being tested.

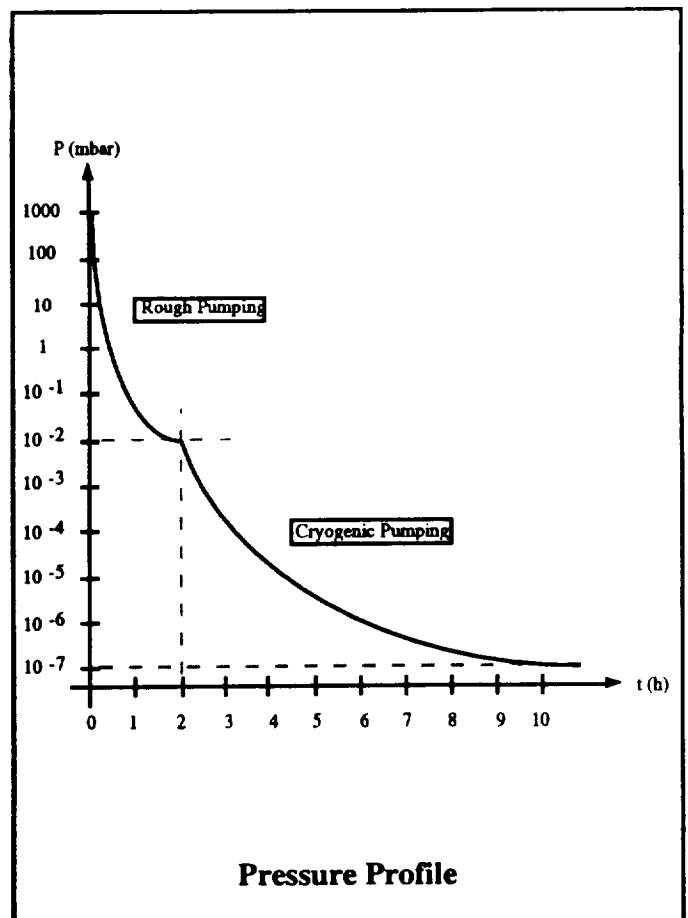
Two rails are mounted on both sides of the lower part of the simulator for the trolley carrying the specimen to be rolled inside.

A fixed beam is secured to the upper part of the simulator along the vertical axis. This beam is capable of sustaining a load of up to 7 tons.

In addition, the chamber is equipped with an inner lighting system, a ventilation system and with a number of servicing platforms to access the satellites and the electrical feedthroughs.

### 3.3 Pumping System

- Rough pumping : two parallel pumping chains with a total flow rate of  $12000 \text{ m}^3 \cdot \text{h}^{-1}$ .
- Cryogenic pumping : two 15 K pumps including shut-off valves and delivering a flow rate of  $100\,000 \text{ l} \cdot \text{s}^{-1}$  at  $10^{-6} \text{ mbar}$ .
- Turbomolecular pumping : one pump including shut-off valves and with a flow rate of  $5000 \text{ l} \cdot \text{s}^{-1}$  at  $10^{-6} \text{ mbar}$ .  
The turbomolecular pump is also used for leak detection with Helium .
- Cryogenic shroud : one cryogenic shroud of  $16 \text{ m}^2$  filled with LN2 being used for the pumping of outgassing flows.
- Operating pressure :  $P < 4 \cdot 10^{-6} \text{ mbar}$ .
- Elapsed time from atmospheric pressure to operating pressure : 6 hours.
- Recovery time from operating pressure to atmospheric pressure : 1h 30 (min.) or 8 hours (nominal).



### 3.4 Thermal Shrouds

The shrouds are made of stainless steel and have an inner diameter of 9 meters.

- Emissivity > 0.85 (at ambient temperature).
- Absorptivity > 0.95 (at ambient temperature).

Under the gaseous nitrogen configuration, the system offers the following performance capabilities :

- Temperature range : 100 K to 360 K (temperatures regulated with gaseous nitrogen).
- Regulation drift : 1 K/h.
- Regulation accuracy :  $\pm 3$  K over the whole range.
- Temperature uniformity for the thermal shrouds : 10 K (stabilized temperature).

With a view to achieve temperature uniformity, the shrouds are partitioned into 17 zones, each having its own flow control loop.

- Variation speed (up or down) : 60 K/h.
- Power capacity : 25 kW.

Liquid nitrogen(optional) :

When filled with pressurized liquid nitrogen, the system's power capacity is 150 kW.

### 3.5 Platform

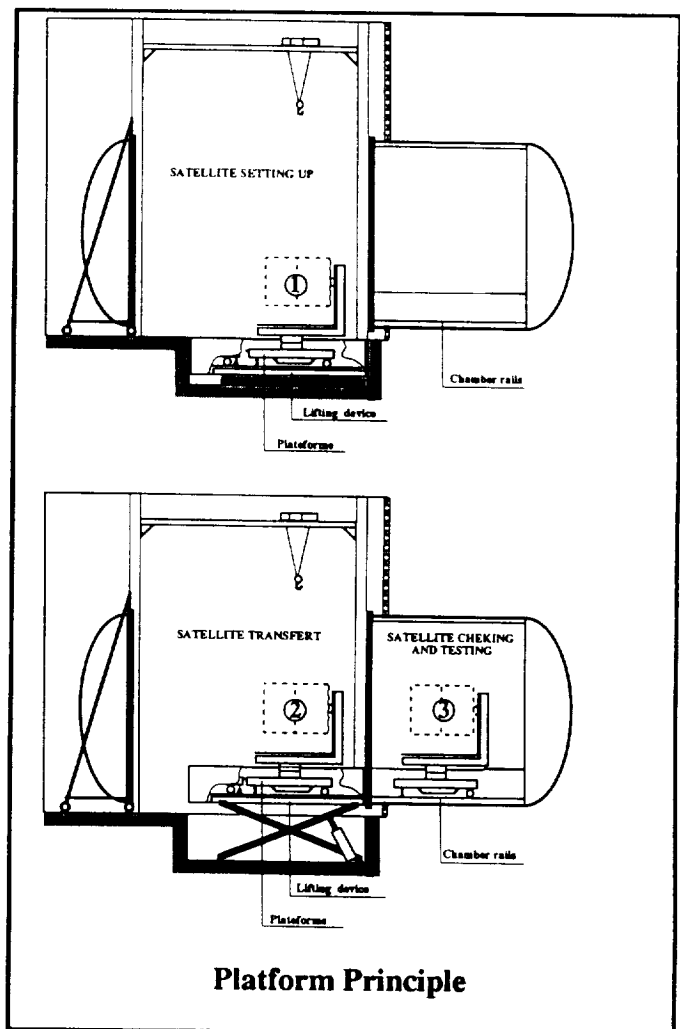
In the process of being tested, the specimen is placed inside the simulator on a platform (see schematic diagram) possibly equipped with a horizontality table and a specific leveling arm. In order to have the specimen placed inside the simulator, the platform is first installed on a lifting device and the specimen mounted on the platform. The lifting device raises the platform rails at the same level that the rails integral with the chamber so as to have the platform rolled inside the chamber.

The principal characteristics of the platform are as follows :

Specimen mass :

- vertical axis : 4000 kg
- horizontal axis : 2500 kg
- cog : 2 m above the interface plane
- interface plane horizontality (to be adjusted during the test) :
  - . accuracy : 0.5 mm/m
  - . range :  $\pm 30$  mm/m.

The platform is covered with thermal shrouds so as to ensure temperature homogeneity inside the chamber.

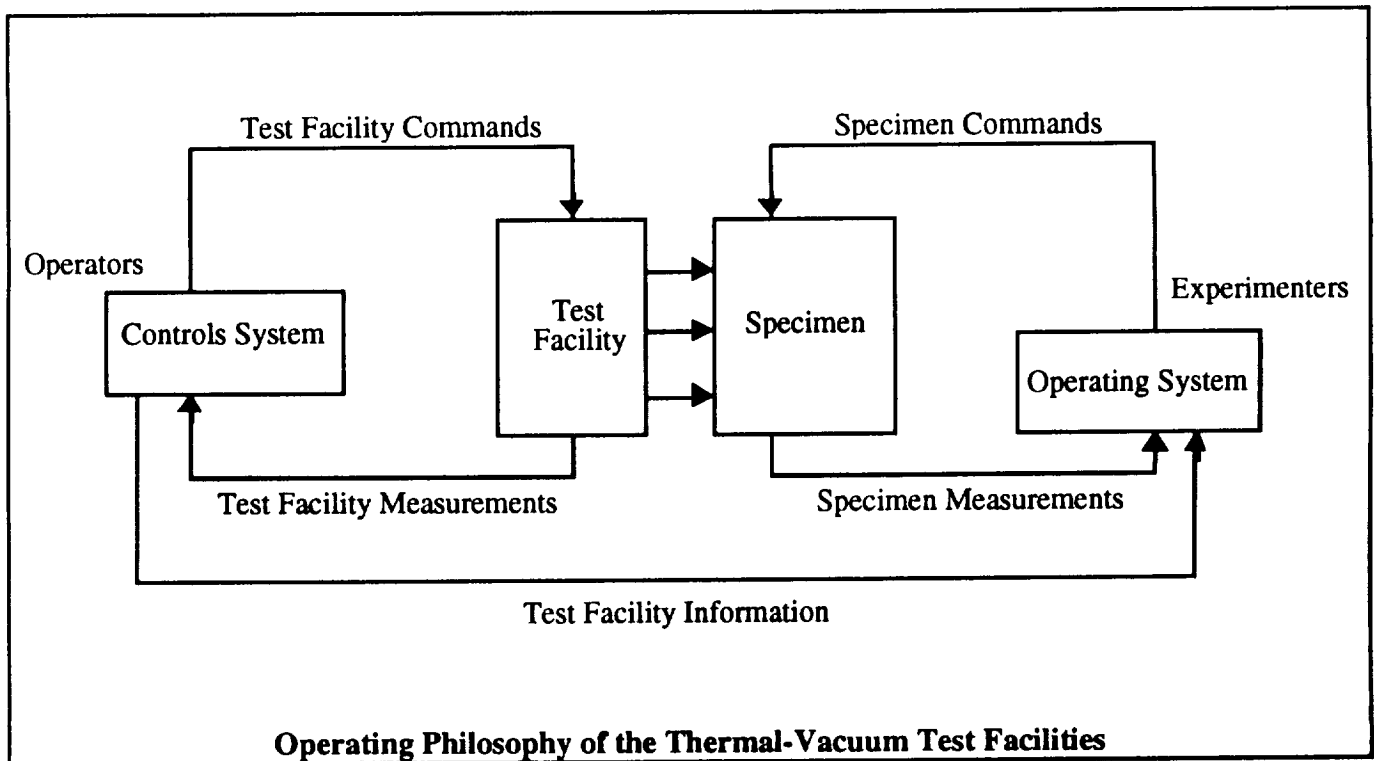


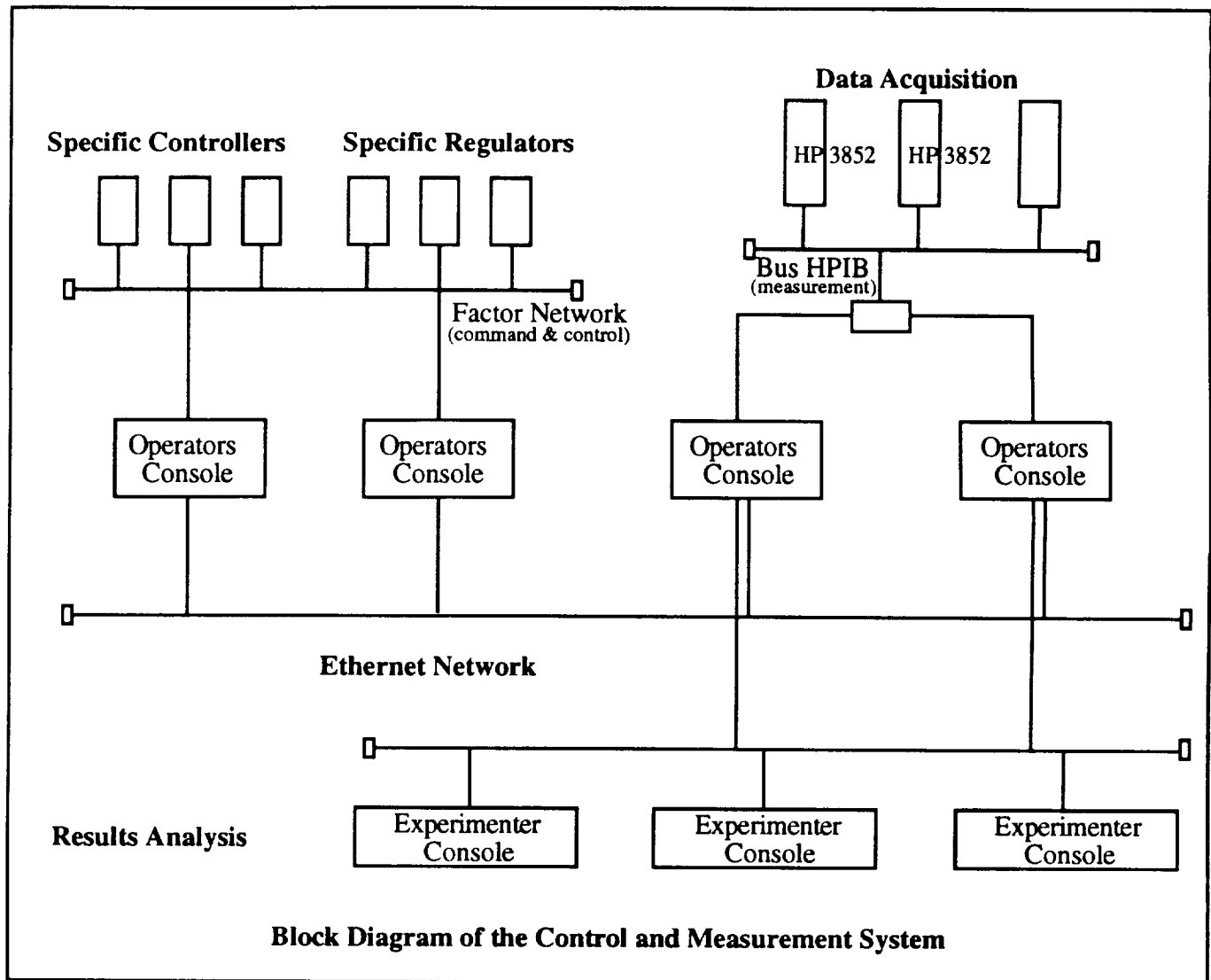
### 3.6 Integrated Control and Measurements System

In conjunction with this new simulator, the necessity for improvement of the thermal measurements systems has been appearing with the following objectives :

- Use of modular acquisition means so as to satisfy the need for adapting the measurements capacities to customers' requests.
- Use of new generation computing means to meet various needs such as :
  - improved performance capabilities,
  - improved reliability,
  - reduced maintenance costs,
  - maximized test facilities /equipment park.
- Use of standards as an operational system and man-machine interface so as to minimize software maintenance and to reduce training.
- Having the computing means made available to the customers for test preparation so as to reduce the duration of this phase, to verify the data inputs, and to reduce the test costs.
- Having the software for management and analysis of the test results made available for real-time operation. This, in order to improve the test effectiveness and thus, to reduce its overall cost.

All the technological choices retained as associated with the defined requirements has led to considering a new concept for an integrated test facility based upon the observed operating philosophy of the thermal vacuum test facility.





At data acquisition level are present either programmable automatic systems or regulators or else, acquisition systems HP 3852. Also note the two dedicated buses, one for command and control -i.e. Factor network- and the other being specific to measurements -i.e. bus HP-IB. At monitoring level, there are the operator consoles. These consoles are linked one to another via the monitoring Ethernet network. Thanks to this network, the consoles are standardized and thus provide for redundancy among themselves. Finally, at operations level, there are the experimenter consoles linked to the measurements operator consoles and also one to another via the Ethernet network for results analysis.

## **4 - CONCEPTUAL DESIGN**

The new test facility has been designed in response to the basic objective of limiting operation costs. To this end, the overall conceptual design to be satisfied has been defined as follows :

- Restriction of the mission assigned to the simulator to thermal-vacuum tests of satellites for the purpose of acceptance only.
- Connection of the simulator to other test facilities under one and a same roof.
- Choice of proven technical solutions.
- Ensuring mechanical and electrical compatibility with the other existing thermal vacuum facilities.
- Ensuring operations flexibility and, more specifically, for pre-test setup operations of the specimen to be tested.
- Reduction of the time required for the pumping down process.

The following is a detailed description of the technical choices which have been prevailing at the time of the construction of the SIMMER facility.

### **4.1 The Chamber**

- The concept of a chamber in the horizontal position permits accessibility to the satellite by the experimenters as per the determined test configuration for the purpose of functional checks prior to and following the test.
- The minimization of the section of the simulator in the clean area means a reduced surface of the clean area and is thus reflected through investments and operations savings made in terms of air-conditioning and required power.
- The clean area is connected to the other areas of the integration and test complex. For this reason, the satellite secured on the integration trolley can be easily transferred from one test facility to another.
- The initial location of the upper beam and of the horizontal rails for rolling the trolley permit simple solutions to be considered for setting up the mechanical installations needed for the tests (i.e. mounting of anechoic loads, unloading devices, ...).
- The overall layout of the building plus its manufacturing specificity permit possible extensions of the simulator from its rear section to be considered.
- The "experimenters" room located in the first floor of the building contains the control stations of the satellite. The windows placed on the partition between the experimenters room and the test facility area open onto the feedthrough plates placed on the chamber and are one meter distant from the feedthroughs. The cablings are thus reduced to a minimum.

## 4.2 The Pumping System

The solutions retained are the result of considerations on the operation costs and ease-of-use of the facility.

- The solution consisting of two parallel primary pumping systems of smaller dimensions has been preferred to the installation of a single larger primary pumping system. In case of a failure, the test is not interrupted during the time needed for repairing.
- The turbomolecular pump has been dimensioned so as to pump light gas. This pump is however also used during two basic phases of the life of the test facility :
  - . For decontamination of the simulator, for which two auxiliary pumping means only are used, that is the turbomolecular pump and the LN2-filled cryogenic shroud.
  - . For leak detection on the simulator, the pumping speed of the turbomolecular pump generates a brief response time from the moment of the virtual detection of a leak and the moment of its recording on the leak detector.
- The cryogenic shroud consists of a non-expensive and yet highly effective pump for the outgassing products from the specimens being tested. For satellites of the SPOT dimensions for example, a significant amount of outgassing flows are released at the beginning of the test. The later are water vapors but also outgassing products such as paintings (e.g. toluene), pottings, cablings, honeycombed structures-induced leakages, wave guide, and the like. The cryogenic shroud pumps these flows and thereby prevents contamination of the cryogenic pumps.

## 4.3 The Thermal System

- *Gaseous nitrogen circulating in the radiative shrouds :*

The gaseous nitrogen option has been retained versus the liquid nitrogen circulation on account of the advantage in terms adaptability to meet specific test requirements. Note that the essential role assigned to the simulator is to perform acceptance tests for satellites, that is, to reproduce on the equipment the extreme temperatures as encountered in flight and not to verify the thermal subsystem of the satellite.

- *Extensibility :*

The specified power of 25 kW is largely overdimensioned. The energy dissipated by a satellite is approximately 3 kW. A noticeable margin is thus available permitting thereby to take into account dissipative test devices (internal anechoic loads, temperature-maintained wave guides) and additional simulators (stimulus, IR grids, etc. ...).

The simulator shrouds, the input and output collectors, the regulation valves are so dimensioned as to supply the simulator with circulating liquid nitrogen through the addition of a specific generator. In this case, a power of 150 kW can be absorbed, thus allowing a new type of simulation process.

## 4.4 The Platform

A specific trolley provides the interface between the specimen and the simulator. The lifting platform on which is installed the specimen facilitates the loading of the satellite and its positioning inside the simulator.

During the preparation or the post-test phase, the platform is used to position the satellite at floor level in the preparation hall and to facilitate experimenters access to the specimen.



#### **4.5 The Control and Measurement System**

To control and monitor this facility a new concept has been developed : an integrated measuring-control and monitoring system.

This new concept is based on :

- A computer network using UNIX operating system and X-WINDOWS as operator interface.
- A process supervisor software which controls the test facility, the process measurements and test article measurements.
- A dedicated software for test data analysis connected with a data base feeded on-line by the supervisor. This software has the capability for the operator to have access to whatever measurement channel to do visualization, computations or comparisons. All these actions are updated as long as the acquisition is activated and can be made with previous measurements saved in the data base (i.e. measurement on other test articles).

This new concept allows :

- An improvement of the characteristics of the control and monitoring system by a clear division of the various functions.
- A standard operator interface for the softwares, so a reduced training and a least specialization of operator.
- A feasibility of delocalization of control room, due to the computer network therefore a possible cost reduction.
- An improvement of reliability due to standard software and hardware.
- A new capability for test team : on-line visualization and data analysis of measurement.

## **5 - CONCLUSION**

The SIMMER embodies the voluntarist strategic choice made by INTESPACE to position the company on the commercial market of application satellites.

The simulator represents a long-term investment viewed to be operated over a period of more than 30 years and as a complement to INTESPACE's integrated test center.

Availability- and operation costs-related considerations have guided all the technological choices.

The SIMMER offers to INTESPACE's European and worldwide customers a highly effective and competitive solution as regards thermal tests for acceptance of medium and large satellites.

## **Operational Strategies for Contamination Control of Composite Materials**

Patricia A. Hansen  
*Science Applications International Corporation*  
2605 East Foothill Boulevard, Suite A  
Glendora, California 91740

Composite materials, used on many instruments, are a potential contamination source for sensitive sensors, especially for sensors or detectors cooled below  $-80^{\circ}\text{C}$ . It is a well known fact that composite materials absorb water during fabrication, integration, test and launch activities and desorb this water under vacuum conditions. Water absorption can be divided into two types: shallow water and deep water. Shallow water is generally about  $500\text{\AA}$  thick on a clean material surface and is easily desorbed under vacuum conditions. Deep water is a function of the material and is absorbed into the bulk of the material. Deep water can outgas for weeks, months or years, depending on the vent path, the amount of absorbed water, and the temperature of the material.

Several operational strategies have been successfully employed on the Wide Field Planetary Camera. The operational strategies include ultradry gaseous nitrogen purge, dew point of less than  $-80^{\circ}\text{C}$ , and vacuum bake-out with verification of outgassing rates. The nitrogen purge is instituted during the fabrication phase and is continued through launch activities. Great care is taken to avoid extended periods of time that the material is exposed to the ambient environment (50% relative humidity). On-orbit operational strategies include heat-up and cool-down scenarios which allow the deep water to be sufficiently outgassed before cooling the sensors or detectors.



**ACCELERATED SIMULATION OF  
NEAR-EARTH-ORBIT POLYMER DEGRADATION\***

**Eric Laue  
Jet Propulsion Laboratory**

**ABSTRACT**

There is a need to simulate the near-Earth-orbit environmental conditions, and it is useful to be able to monitor the changes in physical properties of spacecraft materials. This document presents two different methods for simulating the vacuum-ultraviolet (VUV) and soft X-ray near-Earth-orbit flux. Also, methods for monitoring the changes in optical ultraviolet transmission and mass loss are presented. The results of exposures to VUV photons and charged particles on these materials are discussed.

**INTRODUCTION**

The electromagnetic environment for near-Earth-orbit spacecraft is probably the most difficult to characterize since it ranges from the Earth's magnetic field through the radio-frequency, infrared, visible, ultraviolet (UV), X-ray, vacuum-ultraviolet (VUV), and extreme-ultraviolet (EUV) parts of the electromagnetic spectrum and out as far as high-energy cosmic rays. The 22-year solar cycle accounts for the wide variation in the EUV, X-ray, and particle environment. These fluxes can vary by orders of magnitude. Reference 1 contains a review of the trapped-radiation environment.

The recent return to Earth of the Long-Duration Exposure Facility (LDEF) has provided the opportunity to observe the effects of a 5-year exposure. Damage to spacecraft organic thermal blankets and to metallic surfaces has been observed. Simulation of these effects has been attempted by many different laboratories throughout the world.

This document reports on recent work at JPL that has resulted in two methods of exposure and two methods of in situ monitoring of changes in the sample undergoing exposure.

---

\* The research described in this paper was carried out by the Jet Propulsion Laboratory, California Institute of Technology, under a contract with the National Aeronautics and Space Administration.

Reference herein to any specific commercial product, process, or service by trade name, trademark, manufacturer, or otherwise, does not constitute or imply its endorsement by the United States Government or the Jet Propulsion Laboratory, California Institute of Technology.

## SIMULATION METHODS

The VUV photon source in the present work is provided by the Cathodeon<sup>1</sup> deuterium model VO1 lamp. Its spectrum and long-term performance have been studied by Hindsberg and Kanazawa (Ref. 2) of the British National Laboratory.

Reference 2 covers a study by the British National Laboratory of the spectrum and long-term performance of the Cathodeon deuterium model VO1 lamp. Figure 1 is a plot of the solar spectral irradiance between 100 to 300 nm; Figure 2 is a comparison of the VO1 lamp radiance to other available reference vacuum ultraviolet sources. The 124-nm line from the deuterium gas simulates the solar Lyman alpha line. The system shown in Figure 3 has been in use during a recent 9-month period. Figure 3 is a section view and block diagram of the 124-nm irradiation source. The system has been used to expose various polymers. A 20-day cycle has been found to be useful in that changes in weight and UV transmission can be measured. The changes in the characteristics of the sample undergoing 124-nm irradiation can be monitored by the change in transmission versus time for partially transparent samples or by the use of a quartz crystal macrobalance (QCM) for opaque materials.

During the Grand Tour work, a 2-ft diameter aluminum disc was installed in a 1.8-m vacuum chamber and charged up to 1 kV. This isolated disc retained its charge for 18 hours with only a 200-volt drop. When the 254-nm (low-pressure mercury vapor) source was used to illuminate the disc through a quartz window, the charge was dissipated in less than 1 hour. Based upon this effect, a second type of near-Earth-orbit simulator was developed. A sample of the material under test was installed in a 0.61-m-diameter vacuum chamber. A 4-watt, ozone-producing, mercury lamp was used to illuminate the sample. At the same time, a brush corona, at approximately 2 kV, was generated, which also illuminated the sample. The roughing pump's base pressure to approximately  $1.4 \cdot 10^{-2}$  Pa. A small gas leak sets the nominal chamber pressure during exposure to approximately  $3.4 \cdot 10^{-2}$  Pa. This combined irradiance (254-nm and corona) has been used to irradiate several samples. Figure 4 is a plot of the approximate corona current at the sample location versus chamber pressure. Figure 5 is a block diagram of the system.

Figure 6 is a photograph of the open tank showing the QCM and 10-cm-by-10-cm corona reference plate, while Figure 7 is a photograph showing the source details.

## IN SITU MONITORING

Concurrent with the development of the sources, two different techniques to monitor changes in the material under test were developed. For the 124-nm source, a Hamamatsu<sup>2</sup> model R1132 phototube (spectral sensitivity from 115 to 160 nm) was found to be effective. Since the specified bias is 15 volts, a battery bias supply is not a source noise and can be used without special precautions to avoid Paschen breakdown. A downward "drift" in sensitivity of the R1132 detector has been reported by Hamamatsu. Their source is a Krypton capillary discharge, and it

---

<sup>1</sup> Cathodeon Ltd., Nuffield Rd., Cambridge, England.

<sup>2</sup> Hamamatsu Corp., San Jose, CA

develops a 6-nA current in the diode. In the system at JPL, the diode current is 0.05 nA. Monitoring the 254-nm irradiation is accomplished using either a 7–54 nickel-cobalt glass filter or a 260-nm filter in conjunction with a Hamamatsu GaAsP model G1126-02 photovoltaic cell.

Recently, the IBM New Almaden Research Center<sup>3</sup> has developed a technique for driving quartz crystals whose mechanical load has degraded the Q of the crystal several orders of magnitude (Ref. 3). The conversion from frequency change to mass loss involves many assumptions. In reporting such conversions, a careful listing of these assumptions will avoid false interpretation of the data. References 4 and 5 discuss some facets of these assumptions. A test using Dykem, a cellulose-acetate-based dye, has revealed the effects of irradiation by the 254-nm source on mass loss, the corona's mass loss characteristics, and the mass loss resulting from the combined sources. Figure 8 is a plot of frequency versus time and Figure 9 is a computed frequency-change-per-hour for the three different conditions of exposure. Figure 10 shows the loss in weight and change in transmission of an FEP sample exposed in the 254-nm and corona system, while Figure 11 shows the change in frequency of a QCM for a white dot of the paint such as is used for spacecraft at JPL. This represents the loss in mass of the paint.

During the development of these irradiation sources and monitoring techniques, certain procedures were found to be valuable. Measurement without the samples before and after the sample test will, 1), verify source and detector stability during the sample exposure and, 2), provide a baseline to quantify sample transmission. Secondly, an 18- to 24-hour conditioning period before starting irradiation allows the effects of evacuation or moisture loss to settle down.

## SAMPLE EVALUATION TECHNIQUES

The major advantage to laboratory simulation rests in the fact that it is possible at any time to interrupt the exposure and perform a variety of analytical measurements on the samples. The following is a brief discussion of sample evaluation techniques, with some comments as to their limitations and approximate resolution.

1. The film samples are clamped between two aluminum rings whose dimensions are 2.54 cm for inside diameter and 3 cm for outside diameter. The films are nominally 0.0051 cm (0.002 in.) thick. The initial mass of the films is 0.1 gm and the weighing resolution 0.0001 gm. The change in mass after an exposure can be measured.
2. The change in UV and visible transmission can be measured. Measurement in the VUV would be more useful, but is much more difficult to accomplish.
3. Infrared transmission (FTIR) was used to monitor any changes in the existing absorption bands or the appearance of new absorption bands and to provide information on changes in the molecular structure of the sample.

---

<sup>3</sup> IBM New Almedan Research Lab., San Jose, CA

4. Comparison of an unexposed sample with the exposed sample using a scanning electron microscope can provide insight into the nature of the surface after exposure; however, the application of the required conducting surface on the samples would prevent additional exposures.
5. Because of the ability to measure the 4-MHz basic frequency to 1 Hz and, under ideal conditions, to 0.1 Hz, the QCM technique is used to measure sample changes during exposure. Using the information from Ref. 2, the "K" for 4 MHz is 1.13 angstroms/Hz. Assuming that the sample has a density of 1, the resolution is  $10 \text{ E-}8$  gms. Since, on occasion, the load is a small dot in the center of the crystal, the results indicated in Ref. 5 should be considered. Thus, any quantitative calculations have an uncertainty of  $\pm 30$  percent. Figure 12 is a comparison of the spectral transmission of a reference versus a 40-day exposure of demetallized 0.5-mil Mylar. Figure 13 is the spectral transmission of 2-mil FEP after a 40-day exposure. This was a repeat of the exposure used for Figure 10.
6. The Atomic Force Microscope (AFM) allows the measurement of the surface of materials on an atomic scale. Figure 14 shows the AFM scan of an FEP sample from the LDEF spacecraft and a similar sample which had been exposed for 40 days in the 254-nm and corona irradiation source. While the laboratory-exposed sample does not exhibit a depth of erosion as great as the LDEF sample, the similarity is obvious. The LDEF sample was exposed for approximately 5000 hours. The 254-nm and corona exposure was 960 hours, an acceleration of approximately five times the near-Earth-orbit environment.

## CORONA CHARACTERIZATION

The corona voltage source is a 13.5-kV power supply with a 15-M $\Omega$  series resistor to control the current. It is possible to reverse the polarity of the corona electrode voltage with respect to the chamber and sample ground. When the corona electrode is negative, its potential is -4.4 kV. The voltage drop across the 15 M $\Omega$  is 9.1 kV. The corona electrode current is 0.6 mA. With a positive electrode, the potential is only 2.3 kV and the current is 0.75 mA.

A description of the nature of the corona in terms of the energy distribution and particles generated in the bleed air would be desirable. In the present system this is not feasible. Instead, a 2-cm-by-2-cm CRES electrode was installed in place of the normal samples and used as a Langmuir probe by monitoring the current as the probe was biased between a plus and a minus voltage (with respect to the chamber ground).

Figure 15 is a plot of electrode current versus bias voltage with the corona source at a negative potential with respect to the chamber ground. This appears to be a normal diode curve, except that if a bias voltage greater than 120 V is applied, the observed current exhibits instability and appears to "run away". Figure 16 is a plot of the  $\mu\text{A} \cdot \text{cm}^{-2}$  with a positive voltage on the corona electrode. While this appears to be a "diode type" curve, it requires a bias potential greater than 100 V before the current changes polarity. One plausible explanation for the nature



of the positive-biased source could be that the collisions between the ionized gas and the neutral molecules are producing electrons and gamma-ray particles. With the positive potential on the corona source, a blue glow is present on the corona electrode and there is a 10-percent increase in the current from a GaAsP diode +7–54 filter monitor. The percentage distribution in 20-V bins is shown in Figure 17. This data was generated by weighing the total curve and the weight of the 20-V segments. Apparently, an observable percentage of the current between 0 and +100 V still are positively charged particles.

## CONCLUSIONS

There is no claim that this system accurately reproduces the fields and particles in the air mass zero environment. Nevertheless, the ability to remove and evaluate samples from the system, then continue the exposure has been useful. Changes in sample characteristics have been observed for all of the materials except metallized Mylar.

The system is reasonably simple to set up and, when stabilized after the first 24 hours, can function unattended except for a daily monitoring of the system parameters.

## REFERENCES

- [1] E.G. Stassinopoulos and J.P. Raymond, Proceedings of the IEEE, vol. 76, no. 11, p. 1423, Nov. 1988.
- [2] W.D. Hindsberg and K.K. Kanazawa, Rev. Sci. Instru., vol. 60, no. 3, p. 489, Mar. 1989.
- [3] P.J. Key and R.C. Preston, J. Physics E: Sci. Instru., vol. 13, p. 866, Great Britain, 1980.
- [4] C.E. Reed., K.K. Kanazawa, and H. Kaufman, J. Appl. Phys., vol. 68, no. 5, p. 1993, Sept. 1990.
- [5] P.J. Cumpson and M.P. Seah, Meas. Sci. Technol., vol. 1, p. 544, 1990.

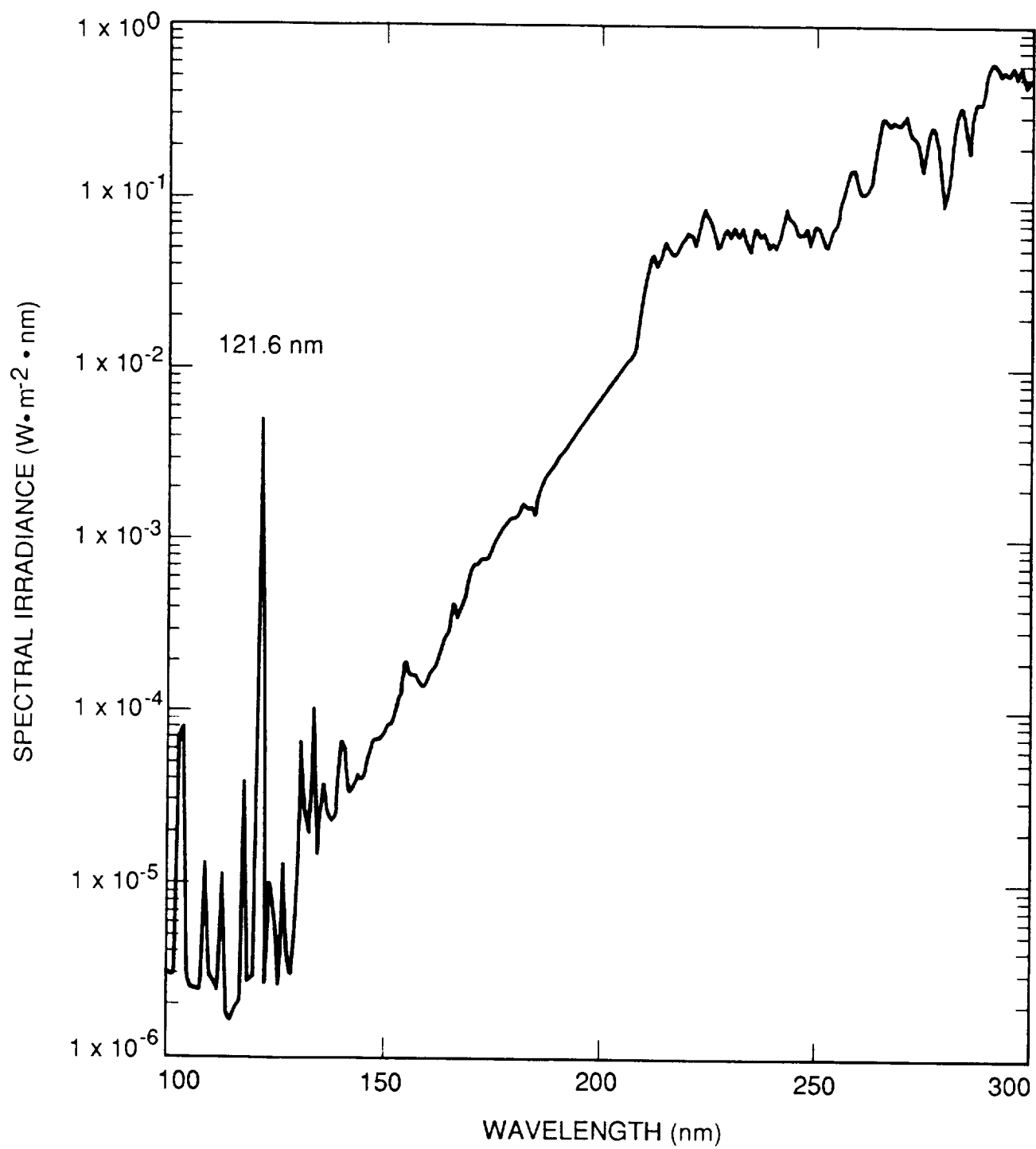


Figure 1. Air Mass Zero Solar Spectrum

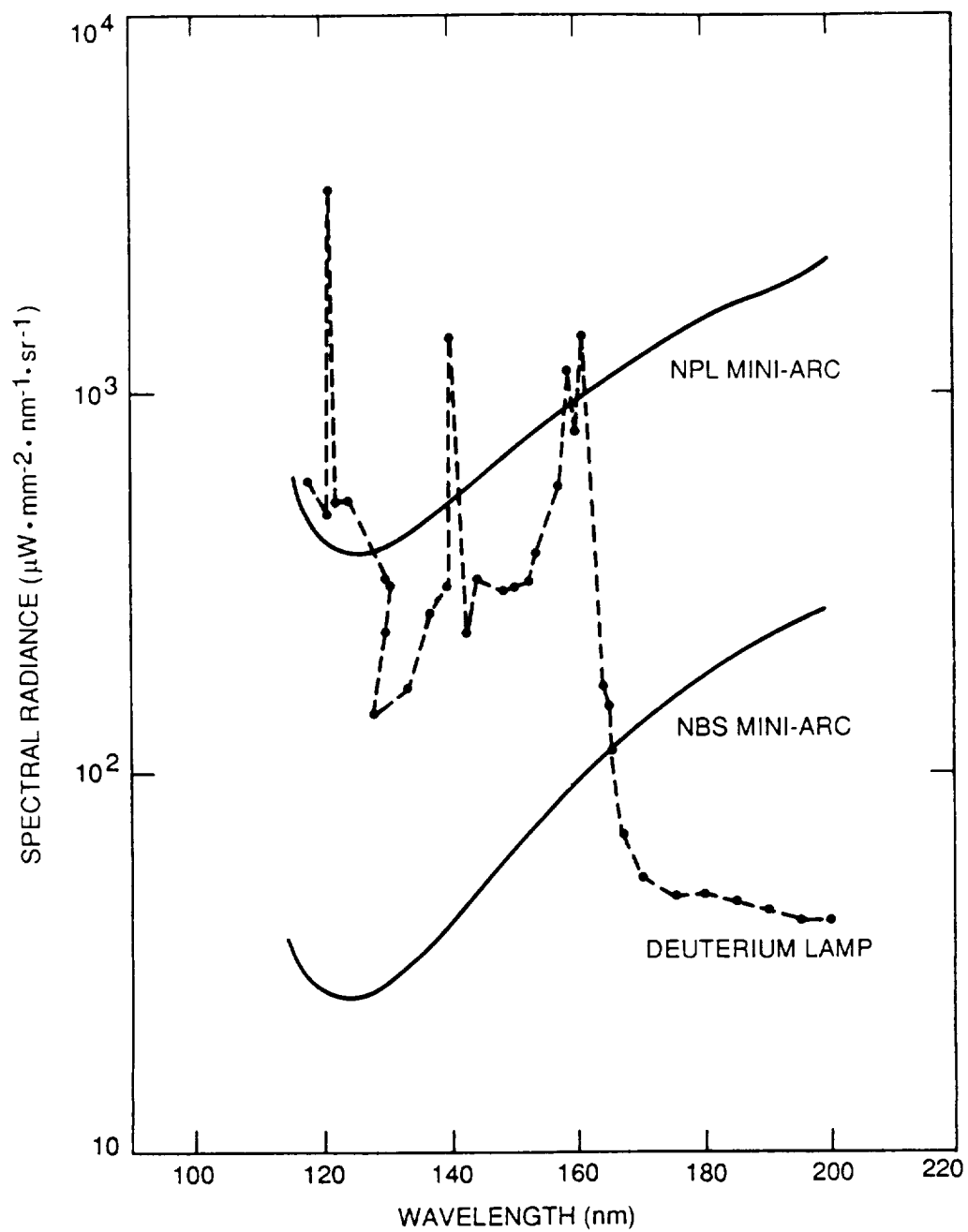


Figure 2. Radiance Levels of Cathodeon V01 Lamp



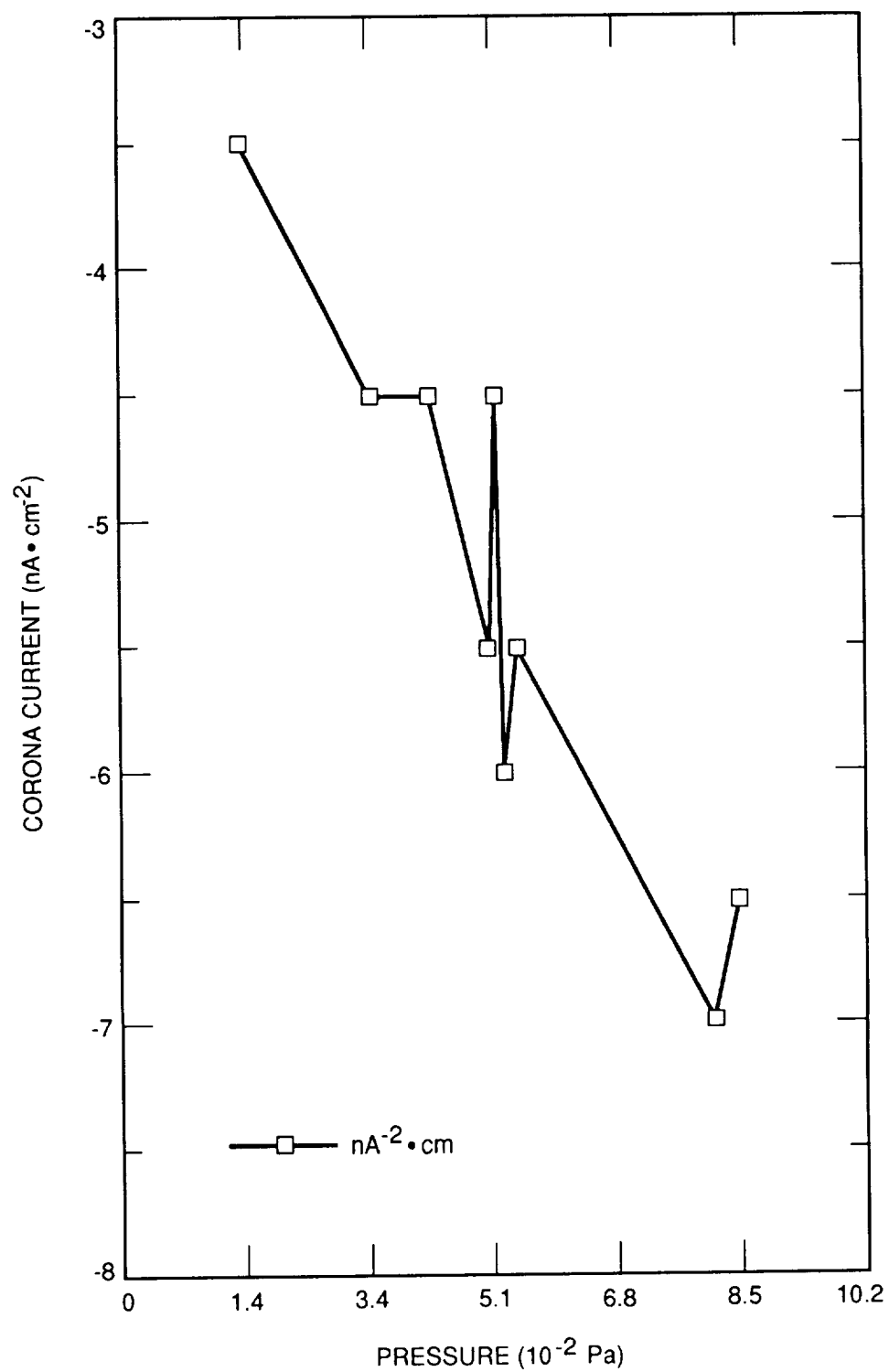


Figure 4. Corona Current Versus Chamber Pressure



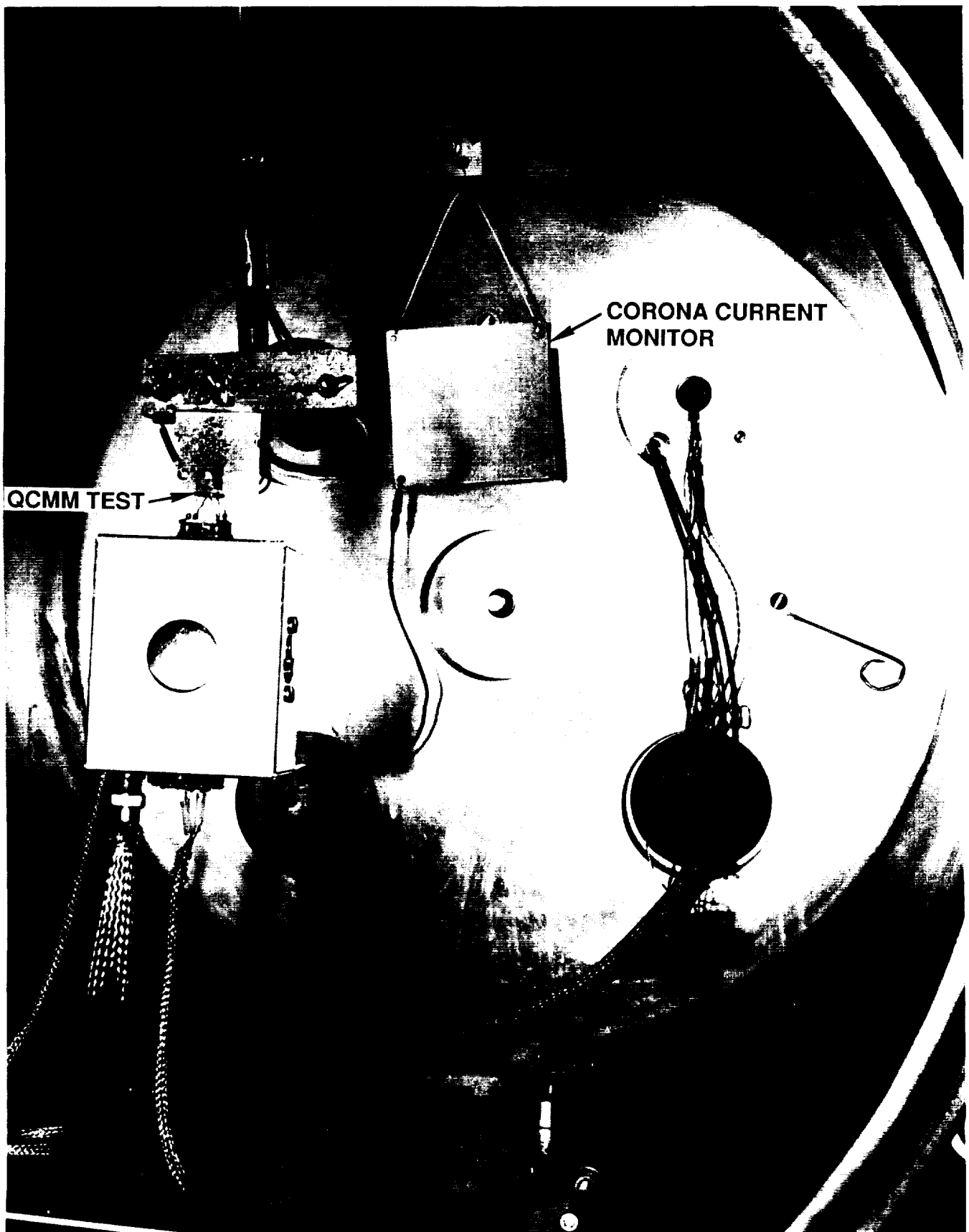


Figure 6. Photograph of 254-nm and Corona Irradiation Tank (JPL-15329B)



Figure 7. Photograph of 254-nm and Corona Irradiation Source (JPL-15329A)



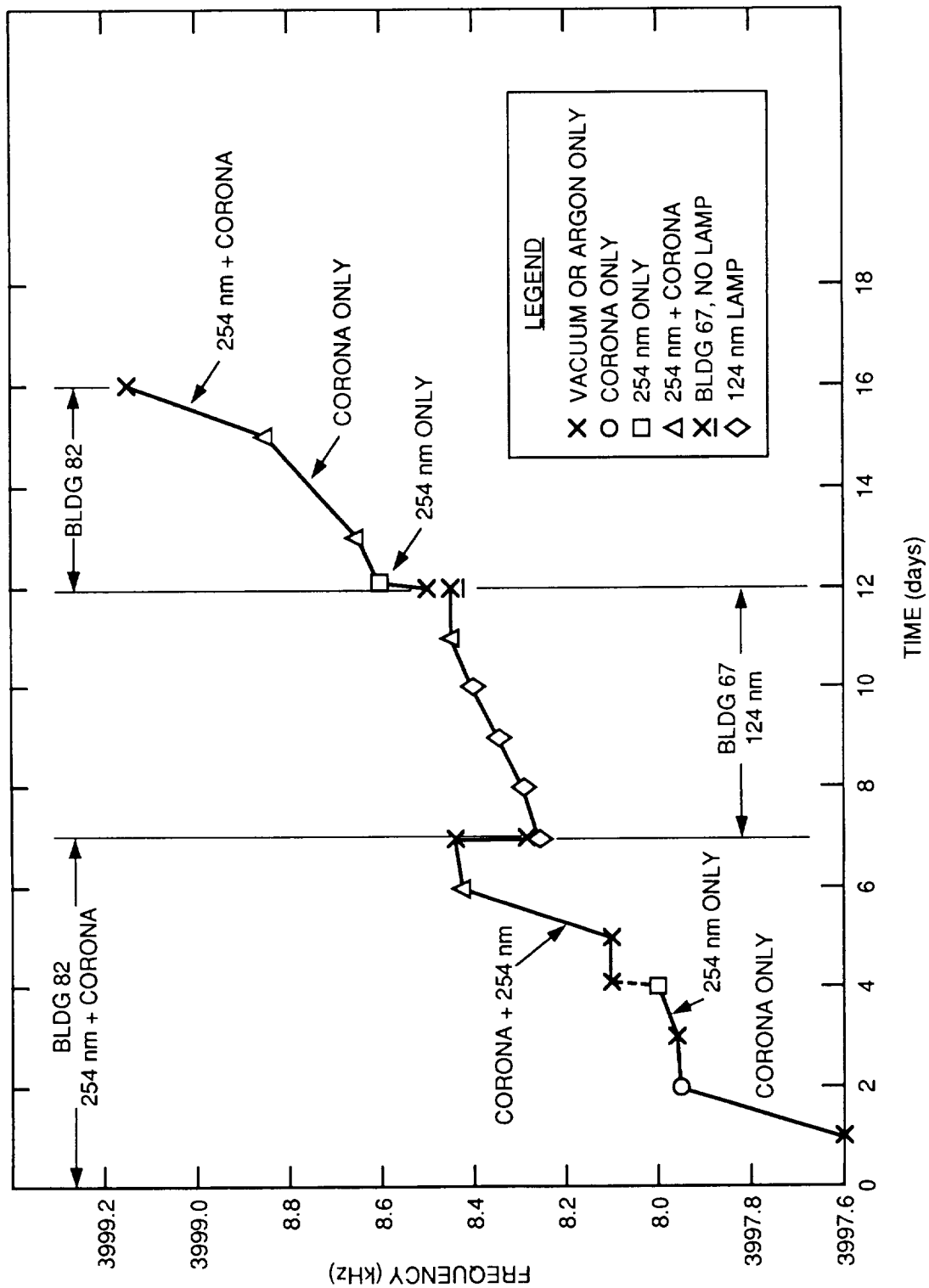


Figure 8. Plot of Dykem Sample Crystal Frequency Versus Time

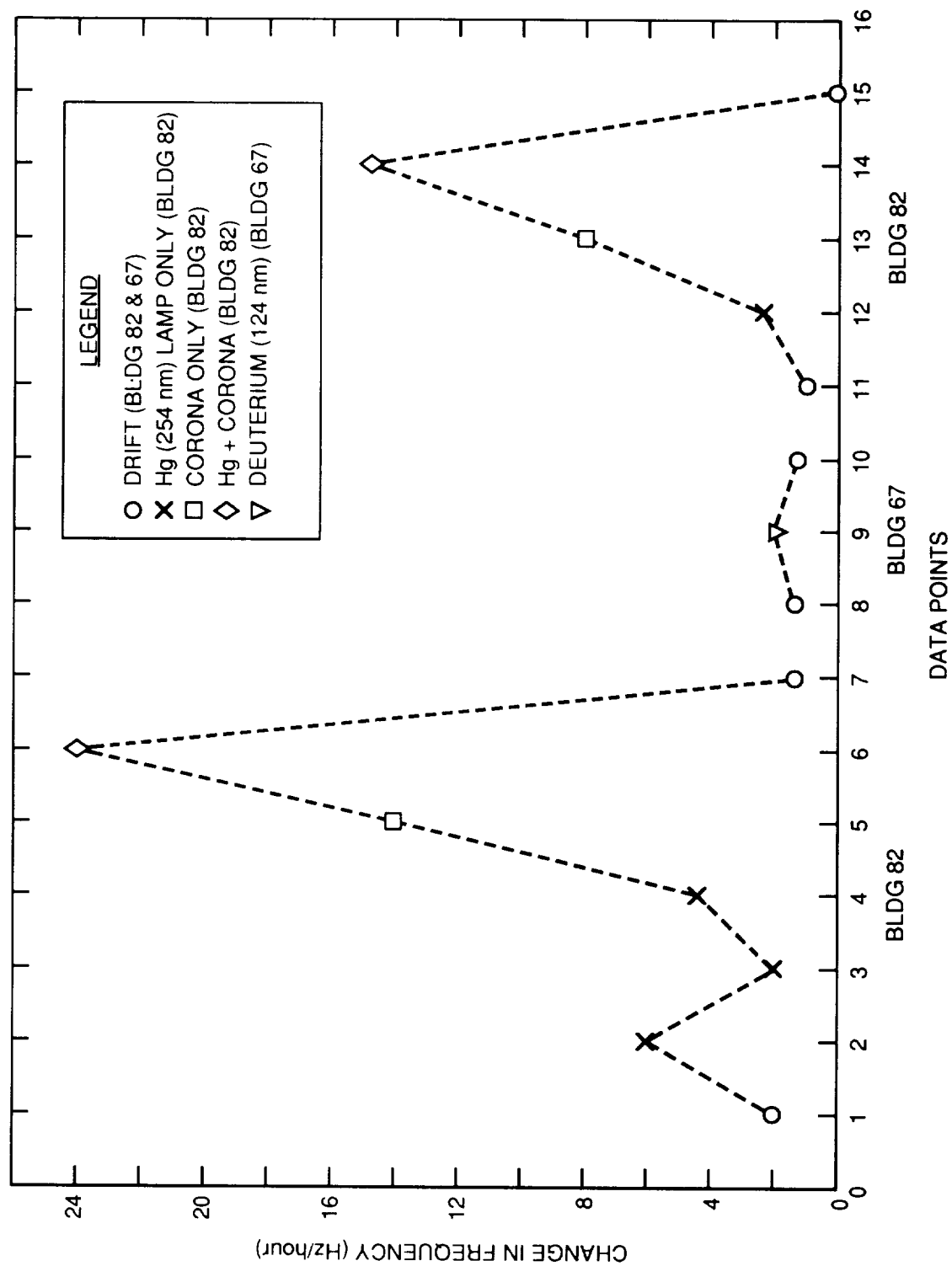
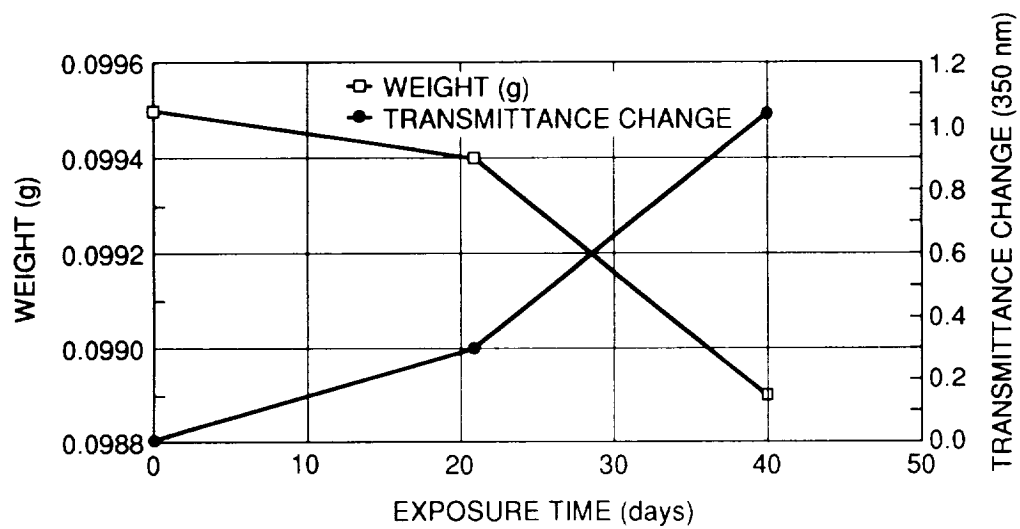


Figure 9. Dykem Sample Frequency Rate of Change



FEP-VUV EXPOSURE

	<u>124 nm EXPOSURE</u>	<u>WEIGHT (g)</u>	<u>TRANSMITTANCE CHANGE</u>
1)	0	0.0995	0
2)	21	0.0994	0.3
3)	40	0.0989	1

Figure 10. FEP Mass Loss and Spectral Transmission

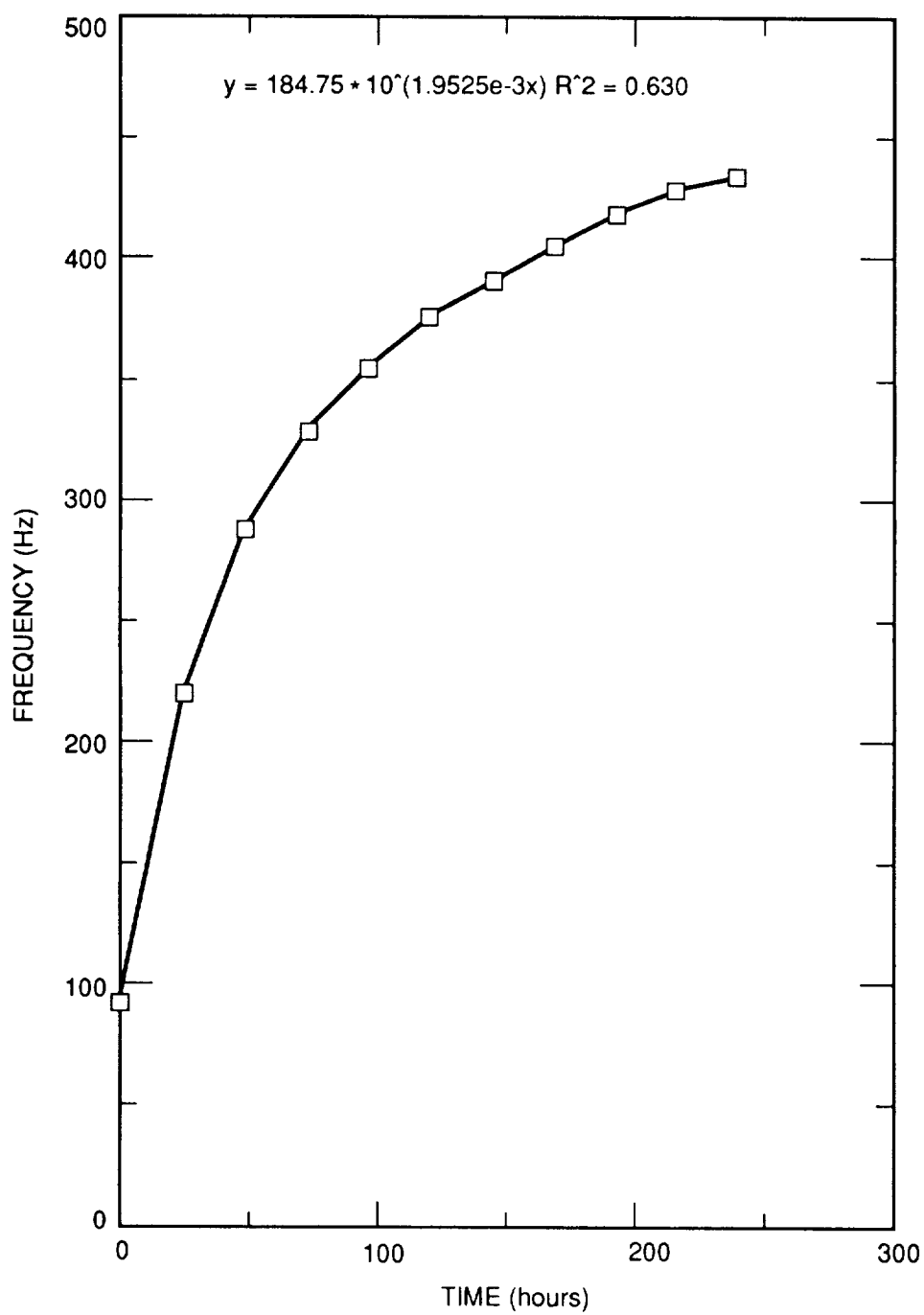


Figure 11. Plot of Frequency Versus Time, White Epoxy Sample, 254-nm and Corona Irradiation Source

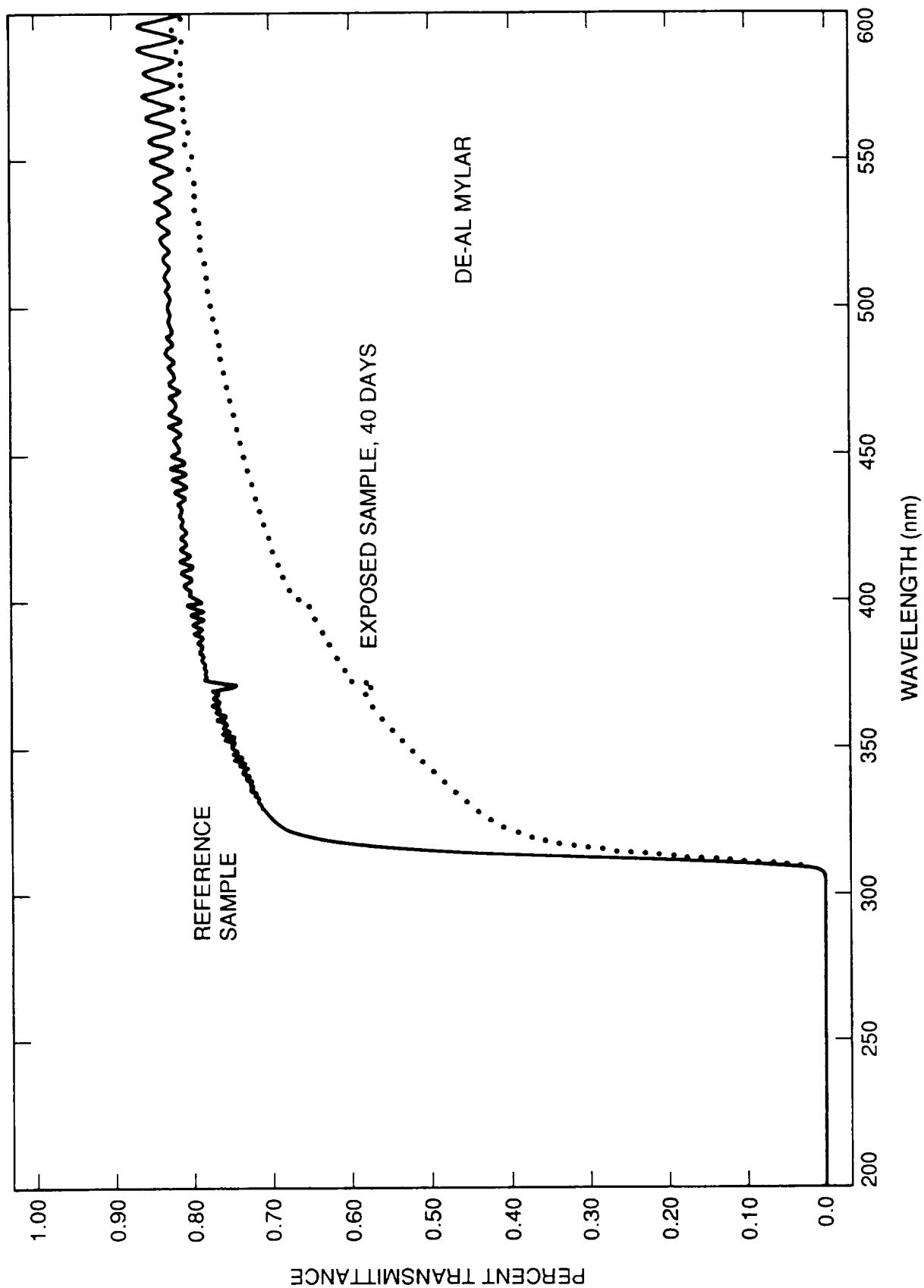


Figure 12. DE-AL Mylar Spectral Transmission

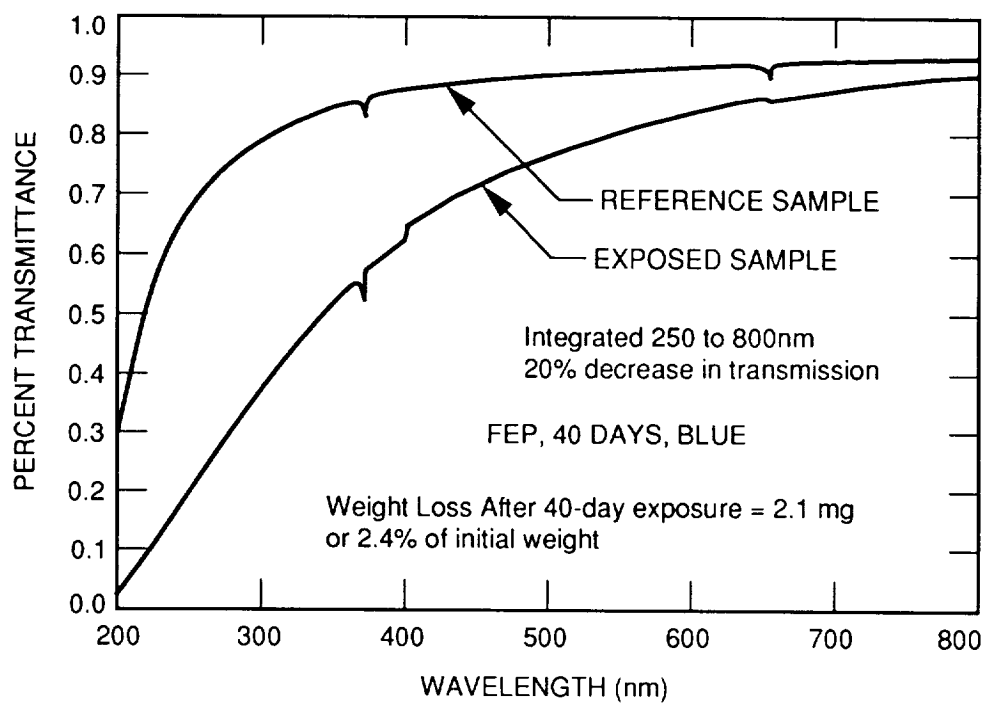
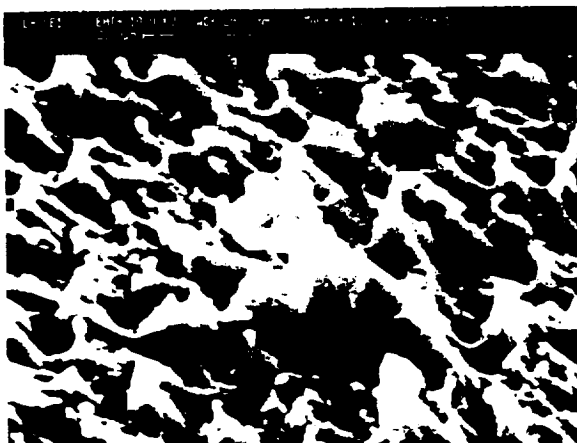
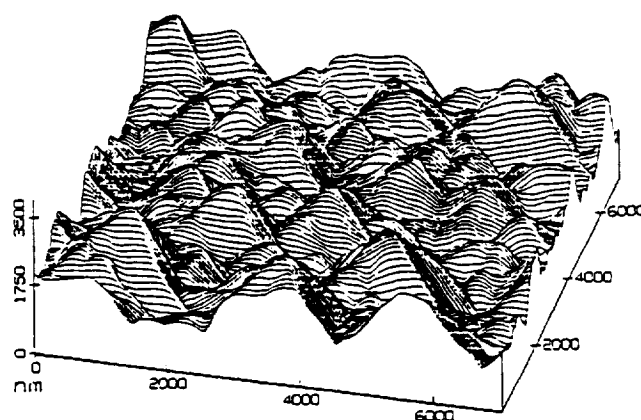


Figure 13. Spectral Transmission of 0.002-mil FEP After 40-Day Exposure

- a. LDEF Sample  
SEM Scan



- b. LDEF Sample  
AFM Scan



- c. 40-Day-Exposure Sample,  
254-nm and Corona  
Irradiation Source

AFM Scan

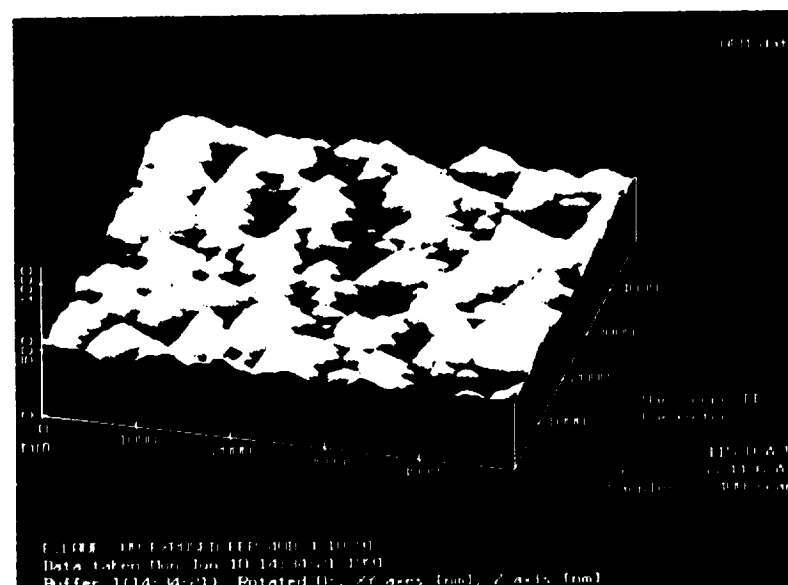


Figure 14. Scans of LDEF FEP Sample (a. and b.) Versus FEP 40-Day-Exposure Sample (c.), 254-nm and Corona Irradiation Source

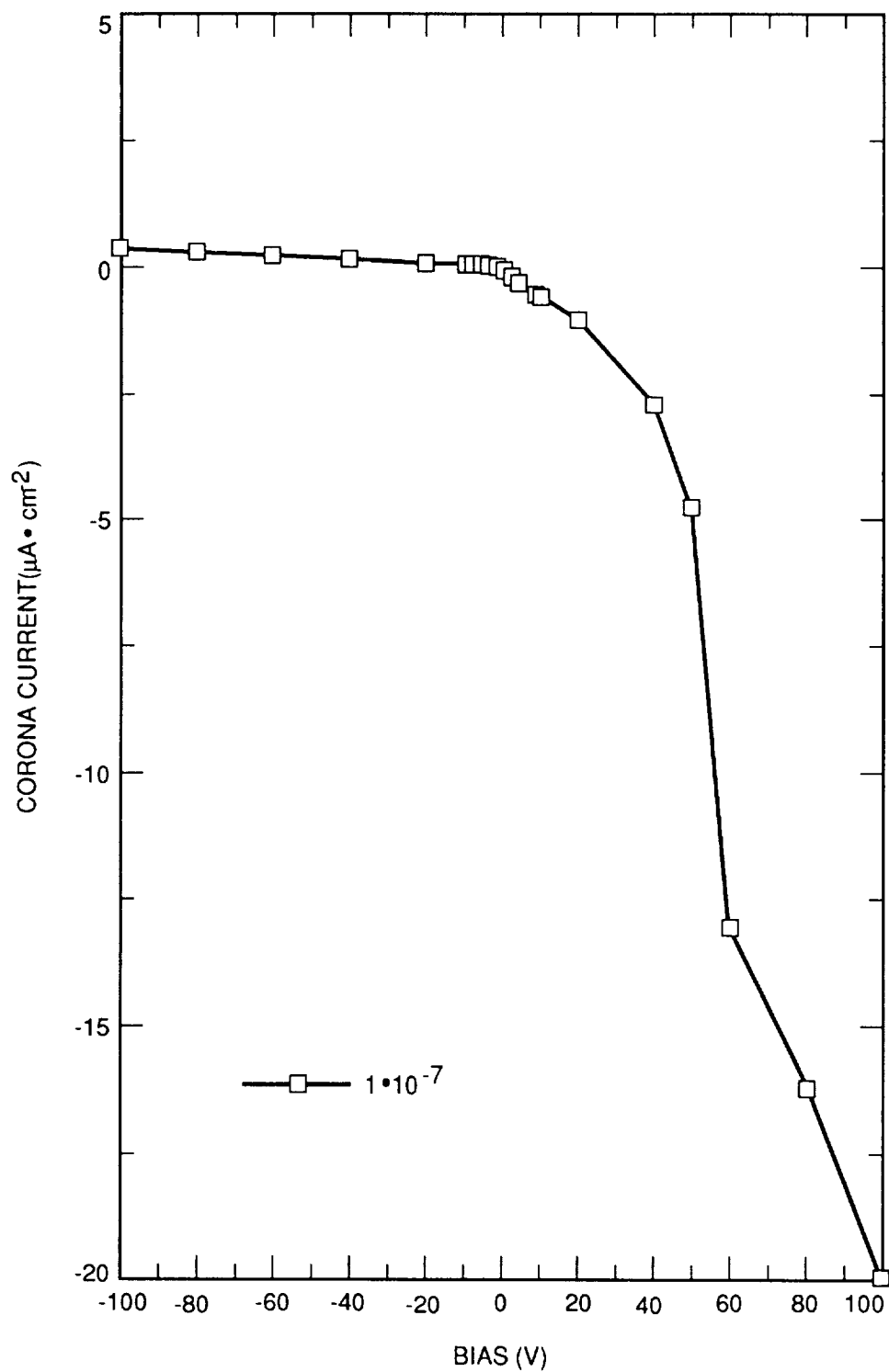


Figure 15. Plot of Current Versus Bias Voltage, -4.4-kV Corona



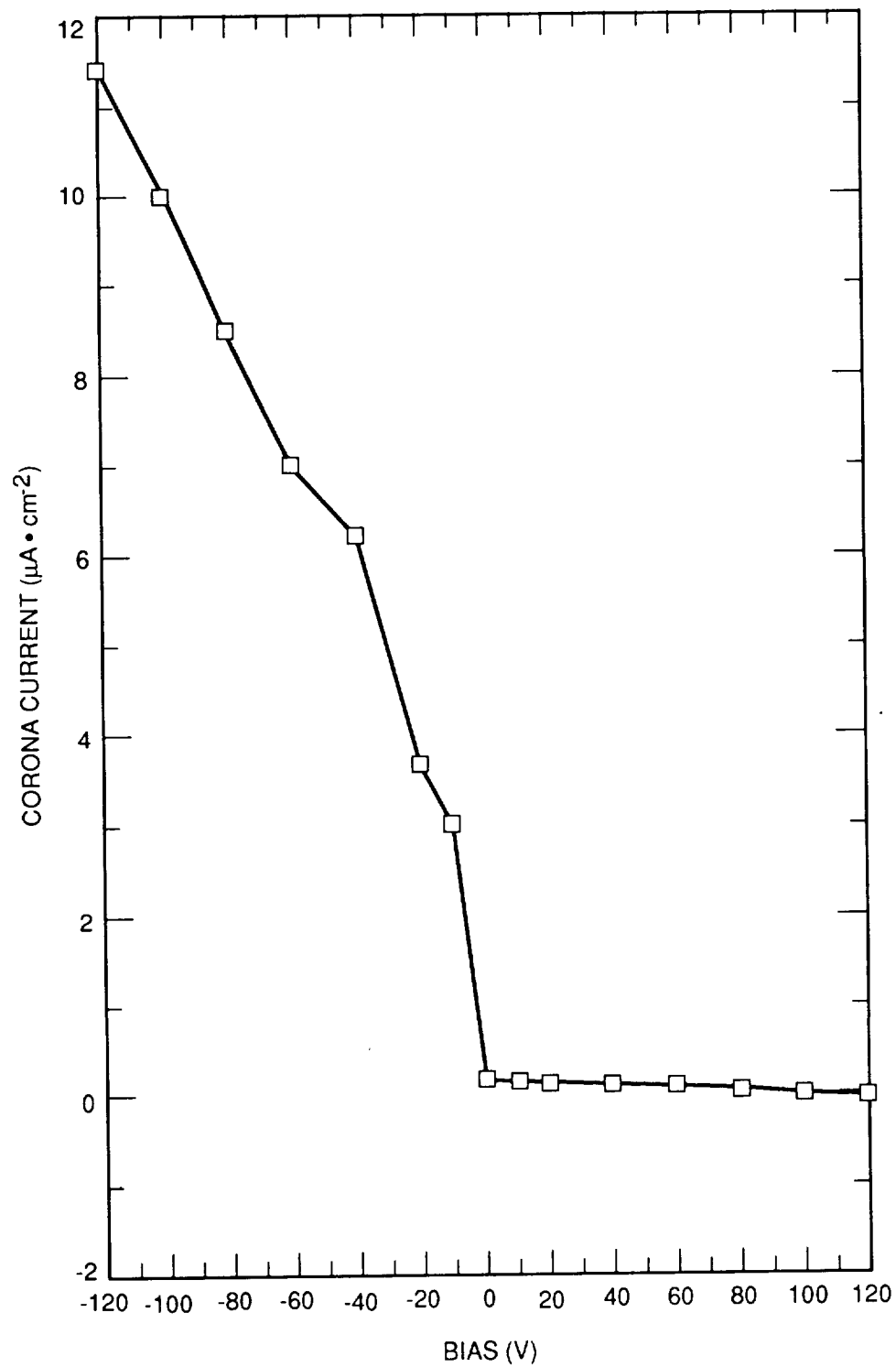


Figure 16. Plot of Current Versus Bias, +2.3-kV Corona

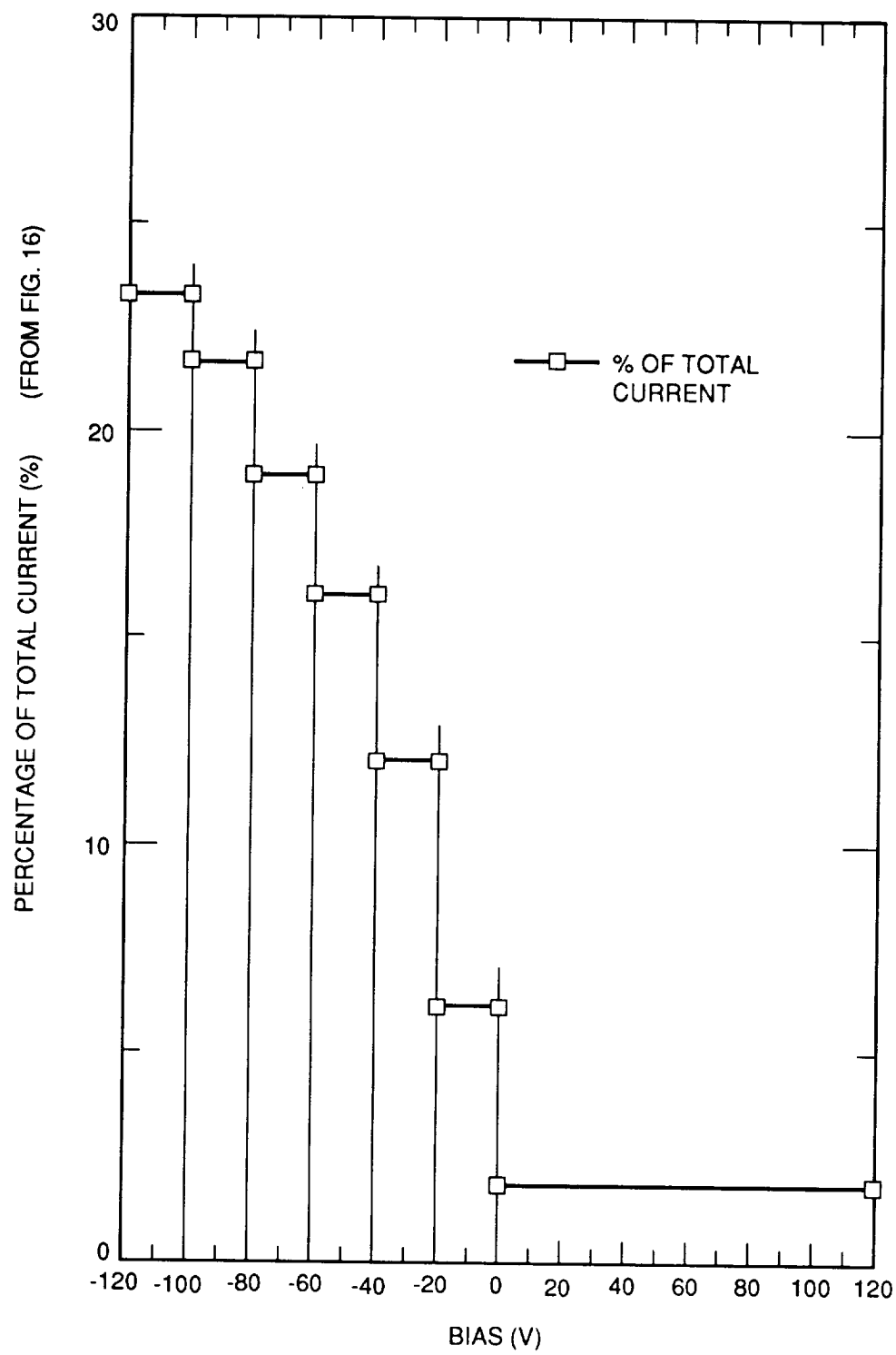


Figure 17. Percentage of Total Current Versus Bias

**DEGRADATION OF RADIATOR PERFORMANCE ON MARS DUE TO DUST**

James R. Gaier, Marla E. Perez-Davis, Sharon K. Rutledge  
National Aeronautics and Space Administration  
Lewis Research Center  
Cleveland, Ohio 44135

Mark Forkapa  
Cleveland State University  
Cleveland, Ohio 44115

**ABSTRACT**

An artificial mineral of the approximate elemental composition of Martian soil was manufactured, crushed, and sorted into four different size ranges. Dust particles from three of these size ranges were applied to arc-textured Nb-1%Zr and Cu radiator surfaces to assess their effect on radiator performance. Particles larger than 75  $\mu\text{m}$  did not have sufficient adhesive forces to adhere to the samples at angles greater than about 27°. Pre-deposited dust layers were largely removed by clear wind velocities greater than 40 m/s, or by dust-laden wind velocities as low as 25 m/s. Smaller dust grains were more difficult to remove. Abrasion was found to be significant only in high velocity winds (89 m/s or greater). Dust-laden winds were found to be more abrasive than clear wind. Initially dusted samples abraded less than initially clear samples in dust laden wind. Smaller dust particles of the simulant proved to be more abrasive than large. This probably indicates that the larger particles were in fact agglomerates.

**INTRODUCTION**

NASA is doing the preliminary planning to send a manned expedition to Mars sometime in the early twenty-first century. One of the roles that the Lewis Research Center will play is that of designing the power system which will operate on the planet's surface. During these early planning phases it is critical to consider the Martian surface environment and how it might affect the power system.

There are several factors in the Martian environment which could put vulnerable power system components at risk. These include a carbon dioxide atmosphere which may react with surfaces that maintain high temperatures, such as radiators. The atmospheric pressure fluctuates from 700 to 1200 Pa, which is a region where the dielectric breakdown strength of the atmosphere will be low. Water and carbon dioxide ice may form, altering the surface characteristics. Mars lacks a substantial ionosphere, and that, coupled with the low atmospheric pressure means a significant number of energetic particles from the solar wind may impact the surface. The low pressure atmosphere will also enable high levels of ultraviolet light to penetrate to the surface. Results of the experiments aboard the Viking landers suggest that highly oxidizing species, such as peroxides or superoxides, may be present in the soil which could attack organic compounds (ref. 1).

The factor which has drawn the most concern, however, is that of Martian dust storms. Local dust storms arise in a wide variety of locations about the planet (ref. 2). Occasionally, about once per Martian year, these storms grow into large regional dust storms which cover large areas of the planet, sometimes engulfing the entire surface. During these storms the opacity of the

atmosphere increases from about 0.5 to greater than 4 (ref. 3). Aeolian features seen in the Viking Lander photographs imply that the sand and dust velocities must occasionally rise to well over 45 m/s (100 miles/hour) (ref. 3). This could result in significant abrasion of spacecraft surfaces. In addition, after the storm, dust which has been suspended in the atmosphere will settle out, depositing a thin coating of dust on everything. This study was concerned with the effects of particle size of such dust on the degradation of high temperature radiator surfaces placed on the Martian surface.

## **METHODS AND MATERIALS**

The technique of arc-texturing has shown promise as a way to make durable high-performance high temperature radiators (ref. 4). As a carbon arc is drawn across a metal surface the surface is microscopically roughened by a combination of melting, vaporization, and condensation of both the metal and carbon. The emittance of the roughened surface is enhanced by as much as a factor of 14. The radiator materials tested in this study were arc-textured niobium with one percent zirconium (Nb-1%Zr) and arc-textured copper (Cu).

Circular disks with a diameter of 2.4 cm and a thickness of 0.08 cm of both materials were fabricated and arc-textured. Their hemispherical reflectivity ( $\rho$ ) was measured over the wavelengths of 0.4 to 2.5  $\mu\text{m}$  using a Perkin-Elmer Lambda-9 spectrophotometer with an integrating sphere. A Perkin-Elmer Hohlraum reflectometer was used to measure the reflectivity over the wavelengths from 1.5 to 15  $\mu\text{m}$ . The spectral emissivity ( $\epsilon_{(\lambda)}$ ) was calculated from

$$\epsilon_{(\lambda)} = (1 - \rho_{(\lambda)})$$

where  $\lambda$  is the wavelength. The spectral emissivity was then convoluted with the black body spectral emissive power ( $\phi_{b(\lambda)}$ ) to approximate the total hemispherical emittance using (ref. 5):

$$\rho_{(\lambda)} = \frac{\int \rho_{(\lambda)} \phi_{b(\lambda)} d\lambda}{\int \phi_{b(\lambda)} d\lambda}.$$

This technique yields the emittance of the surface, but it is important to realize that this may not be the emittance of the radiator. If there is a layer of highly insulating dust on the surface (as is probably the case with Martian dust), the temperature of the bulk of the radiator may be higher than that of its surface, resulting in lower radiator efficiencies.

The dust used to coat the samples was a synthetic mineral manufactured by Ferro Corporation (Independence, OH) to have a chemical composition similar to Martian soil. It was not the purpose of these experiments to accurately simulate the Martian soil, but to generate several different dust samples with the same chemical composition, relevant to Martian dust, varying only in size. Table I compares the composition of this material to the soil composition found at the Viking Lander sites. The dust was dry sieved into four different ranges with nominal diameters of

10, 30, 60, and  $> 75 \mu\text{m}$ . There was not a sufficient amount of the  $60 \mu\text{m}$  material to include it in our tests.

An initial layer of dust with a nominal diameter of  $10 \mu\text{m}$  was deposited on half of the samples by placing them in a dusting chamber where the dust was elevated using dry air and allowed to settle out onto the samples. Details about the method of dusting are described elsewhere (ref. 6). The uniformity and extent of the dust deposition was monitored optically. The transmittance of cover-glasses placed next to the samples was used as a probe of the extent of the amount of dust deposited on the samples.

The winds on Mars were simulated using the Martian Surface Wind Tunnel (MARSWIT) at NASA Ames Research Center. The MARSWIT is a low pressure ( $\approx 10^2 \text{ Pa}$ ) wind tunnel 14 m in length with a 1 m by 1.1 m by 1.1 m test section located 5 m from the tunnel's entrance. This flow-through wind tunnel is located within a  $4,000 \text{ m}^3$  vacuum chamber. The characteristics of the MARSWIT are described in detail elsewhere (ref. 7). The samples were placed in the MARSWIT at an attack angle  $45^\circ$  to the wind because this angle has been shown in previous tests to be the angle where dust was blown off of the samples most easily (ref. 8). The samples were tested under the conditions listed in table II.

The method used to simulate a Martian dust storm is illustrated in figure 1. The test dust was fed through a hopper into the top of the MARSWIT, near the entrance. First the wind was generated in the MARSWIT at a velocity below that which would clear dust off of the pre-dusted samples. Then the hopper feed was started, dropping the dust into the air stream. Immediately thereafter the wind velocity was increased to the test conditions. The time reported in table II is the time spent at the maximum speed. The finer particles were carried along the wind stream and struck the samples, much as would happen during a dust storm on Mars. The MARSWIT was shut down before the hopper was turned off, consequently there was no time when high velocity clear air hit the samples. Both initially clean and initially dusted samples were included in these tests.

The emittance of the samples was remeasured after the exposure tests and compared with the initial measurements. The transmittance of the accompanying cover-glasses was used as a probe of the extent of dust occlusion of the samples after the tests.

## **RESULTS AND DISCUSSION**

### **LARGE PARTICLE SIZES**

The largest particle sizes used in this study, being larger than  $75 \mu\text{m}$ , might be better classified as sand. The smaller particles, having high adhesion to the sample plates, could be tipped to  $90^\circ$  or even inverted with no significant loss of particles. Particles larger than  $75 \mu\text{m}$  however, would slide off of the plates when tipped to a high angle. Our measurements indicate that the angle of repose for these particles was about  $27^\circ$  (figure 2). However, these measurement were done in a gravity field of  $1.0 \text{ g}$ . On Mars, with a gravity of  $0.377 \text{ g}$ , a sliding force this strong could not be developed at any angle, so this material would be expected to behave like dust in the Martian environment. In fact, any particles with an angle of repose greater than about  $22^\circ$  would be expected to exhibit dust-like behavior. Therefore, particles larger than  $75 \mu\text{m}$  were not used to dust

sample plates, but were used in the wind stream to examine the effects of particle size on clearing, deposition, and abrasion.

## INITIALLY DUSTED SAMPLES IN CLEAR WIND

Pre-dusted arc-textured samples were subjected to clear martian winds of 32 and 96 m/s. These velocities were chosen because previous studies indicated that these values would be below and above the threshold dust clearing velocities respectively at the 45° attack angle (ref. 9). Figure 3a shows that in the case of arc-textured Nb-1%Zr there are no significant changes in the total emittance of the surface over a 300 - 3000 K temperature range (the error of the instrument is estimated to be  $\pm 5$  percent). Figure 3b shows that in the case of arc-textured copper, the emittance of the sample subjected to low velocity winds shows no change, but that subjected to the high velocity wind decreased by 10 to 15 percent.

Visual inspection of these two samples subjected to the 32 m/s wind reveals a patchy pattern of dust clearing. There appeared to be miniature landslides of dust. In-situ inspection of the developing pattern revealed that the landslides did not occur during the wind test, but rather after the test when the chamber which contains the sample was being brought up to atmospheric pressure. The effect could not be reproduced by evacuating and then repressurizing samples in an 18 inch bell jar. Even attempts to create vibrations within the bell jar during repressurization did not reproduce the effect. The amount of material lost in this way from the Nb-1%Zr sample was small, but the patch cleared near the center of Cu disk is of significant size. The fact that the sample emittance is unchanged indicates that the emittance of the dust is similar to that of the sample.

Visual inspection of the samples subjected to the 96 m/s wind revealed that nearly all of the dust was removed. Regions developed where a significant amount of the arc texture was removed from the copper sample, but not from the Nb-1%Zr. This no doubt is the reason for the lower emittance of the copper sample. The comparison of the two materials thus reveals that the arc-textured Nb-1%Zr is more durable to abrasion. This may be due to the formation of a niobium carbide layer which enhances the bonding of the carbon to the metal. Copper does not form such a carbide layer.

## INITIALLY CLEAR SAMPLES IN DUST-LADEN WIND

Small particles (30  $\mu\text{m}$ ) entrained in a low velocity (23 m/s) Martian wind tended to accumulate on surfaces. Figures 4a and 4b show that the low temperature emittance degrades slightly less for the arc-textured Nb-1%Zr sample than the Cu sample. Since the emittance is dominated by that of the dust, this may be an artifact of higher initial emittance of the Nb-1%Zr sample. The absolute final emittances for the two samples are nearly identical, which supports the notion that the emittance is dominated by the dust deposited on the samples.

When this same experiment is repeated but with large particles (75  $\mu\text{m}$ ), the results are quite different. Samples subjected to 24 and 40 m/s winds had very little dust remaining on their surfaces. Either the larger grains do not stick as well to the arc-textured surfaces or they slide off

of the surface, which is inclined to an angle greater than the angle of repose. There is no significant change in the emittance of the Nb-1%Zr sample subjected to the 24 m/s wind-blown dust. There was a 5 - 15 percent drop in the emittance of the Nb-1%Zr sample subjected to the 40 m/s wind-blown dust, and perhaps a small drop in the Cu sample as well (fig. 4). From the color photographs a tinge of copper-color could be seen through the arc-textured layer which was not visible before the tests, so a slight amount of abrasion is suspected, at least in the case of the Cu sample.

These abrasion affects were clearly evident with both the smaller and larger wind-blown particles when the velocity was high (89 and 116 m/s respectively) (fig. 5). In the case of the arc-textured copper (89 m/s) it can be seen that nearly all of the carbon has been removed. The effects are also obvious from the change in the emittance (fig. 4) which dropped to below 40 percent of its original value in the low temperature region when the smaller particles were suspended, and below 60 percent with larger particles.

Both the photographs and the emittance measurements bear out that the smaller particles were somewhat more abrasive on the Nb-1%Zr samples (fig. 5). This can be most easily explained if the larger particles are in fact agglomerates of small particles. A larger particle at similar velocity will have greater kinetic energy than a smaller one. Thus, some of that energy must be dissipated by breaking the particle apart rather than by abrading the surface.

## INITIALLY DUSTED SAMPLES IN DUST-LADEN WIND

When initially dusted samples were subjected to dust-laden wind, the result was always a net clearing of dust from the surface over the velocity range of 23 - 116 m/s. Thus, particles suspended in the wind substantially lowers the threshold velocity above which dust is removed from the surface (from 40 m/s to less than 23 m/s). At low velocity the smaller particles were not cleared from the surface as effectively as the larger, but at high velocity virtually all of the dust was cleared regardless of particle size.

The incomplete clearing of the small particles from the low velocity (23 m/s) wind resulted in an emitting surface which had a substantial fraction made up of the dust. The resulting emittance was only slightly lower than the pristine value for the Nb-1%Zr, but for the Cu samples the emittance dropped to about 80 percent of its pristine value (fig. 6). With larger particles (24 m/s) there was little dust on the sample and the emittance was essentially unchanged. At slightly higher velocities (40 m/s) and large particles there was no change in the Cu samples, but perhaps a slight degradation of the Nb-1%Zr. There was little evidence of abrasion of the samples.

Once again there was significant abrasion for both the small and large particle sizes at high velocity (fig. 5). Unlike the initially clear samples subjected to dust-laden wind, the large particles seemed to abrade the Nb-1%Zr slightly more than the small. This may be due to the fact that the velocity (and thus kinetic energy) was somewhat higher. It may also be that whether the particle is an agglomerate or not is not as important in the case where the particle hits a pre-dusted surfaces. In both cases the primary collisions are between dust particles. This is born out in that when the large particles impact the dust covered Nb-1%Zr, the emittance drop was about 10 percent less than when they impact an initially clear sample. The presence of dust on the radiator

surfaces appears to retard the abrasion rate, probably by the dissipation of energy via the dust-dust collisions.

## **CONCLUSIONS**

In order to determine the effects of Martian dust storms on arc-textured Nb-1%Zr and arc-textured Cu radiator surfaces, an artificial mineral of the approximate elemental composition of Martian soil was manufactured, crushed, and sorted into four different size ranges. Particles larger than 75  $\mu\text{m}$  did not have sufficient adhesive forces to adhere to the samples when tilted to angles greater than about 27°. However, in the reduced gravity of the Martian surface, they would behave as dust, so the effects of blowing this size particle was studied. Pre-deposited dust layers (nominal 10  $\mu\text{m}$  particle size) were largely removed by clear wind velocities greater than 40 m/s, or by dust-laden wind velocities as low as 25 m/s. Smaller dust grains were more difficult to remove. Abrasion of the arc-textured radiator surfaces was found to be significant only in high velocity winds (89 m/s or greater). Dust-laden winds were found to be more abrasive than clear wind. Initially dusted samples abraded less than initially clear samples in dust laden wind. Smaller dust particles proved to be more abrasive than large. This probably indicates that the larger particles in the artificial mineral were in fact agglomerates.

## **REFERENCES**

1. H.P. Klein, *"Viking Biological Experiments on Mars"*, Icarus **34** (1978) 666-74; also R.L. Huguenin, K.J. Miller, and W.S. Harwood, *"Frost-Weathering on Mars: Experimental Evidence for Peroxide Formation"*, J. Molecular Evolution **14** (1979) 103-32.
2. A.R. Peterfreund, *"Contemporary Aeolian Processes on Mars: Local Dust Storms"*, Ph.D. Dissertation, Arizona State University (1985).
3. J.B. Pollack, et al., *"Properties and Effects of Dust Particles Suspended in the Martian Atmosphere"*, J. Geophys. Res. **84** (1979) 2929-45.
4. B.A. Banks, et al., *"Arc-Textured Metal Surfaces for High Thermal Emittance Space Radiators"*, NASA TM-100894 (1988).
5. M. Kussmaul, M.J. Mirtich, and A. Curren, *"Ion Beam Treatment of Potential Space Power Materials at the NASA Lewis Research Center"*, Surface and Coatings Technology **51** (1992) 299.
6. M.E. Perez-Davis, J.R. Gaier, R. Kress, and J. Grimalda, *"Simulation of Martian Dust Accumulation on Surfaces"*, NASA Conference Publication 3096, 16th Space Simulation Conference (1990) 447.
7. R. Greeley, et al., *"Dust Storms on Mars: Considerations and Simulations"*, NASA Technical Memorandum 78423 (1977).



8. James R. Gaier, Marla E. Perez-Davis, and Mark Marabito, "*Aeolian Removal of Dust Types From Photovoltaic Surfaces on Mars*", 16th Space Simulation Conference, NASA Conference Publication 3096 (1990) 379.
9. James R. Gaier and Marla E. Perez-Davis, "*Effect of Particle Size of Martian Dust on the Degradation of Photovoltaic Cell Performance*", NASA TM-105232 (1991). Also: Solar Engineering 1992, (Ed. W. Stine, J. Kreider, and K. Watanabe, ASME, NY, 1992) 867-73.

**Table I – Composition of Dust Used in MARSWIT Test**

Mineral	Viking Landser	Test Dust
SiO <sub>2</sub>	44.7 %	53.5 %
Fe <sub>2</sub> O <sub>3</sub>	18.1	21.7
MgO	8.3	9.9
Al <sub>2</sub> O <sub>3</sub>	5.7	6.8
CaO	5.6	0.0
TiO <sub>2</sub>	0.9	1.1
Na <sub>2</sub> O	?	6.7
K <sub>2</sub> O	0.0	0.3
CO <sub>2</sub>	?	0.0
TOTAL	83.3 %	100.0 %

"?" indicate species not detectable by Viking Landers

**Table II – Test Conditions for MARSWIT Tests**

Test	Initial Dust Size μm	Wind Dust Size μm	Velocity m/s
1	10	none	32
2	10	none	96
3	10	30	23
4	10	30	89
5	10	> 75	40
6	10	> 75	24
7	10	> 75	116

Test sequence

1. Chamber pumped down to 1 kPa
2. Dust dropped past MARSWIT mouth
3. Flow initiated in MARSWIT
4. Dust laden wind strikes samples

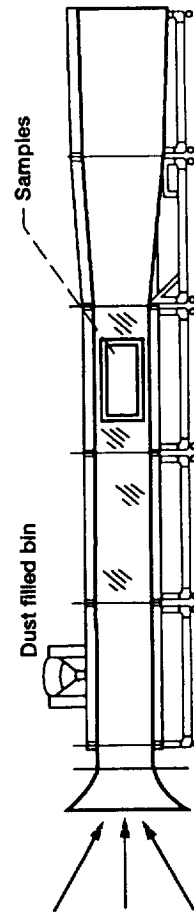
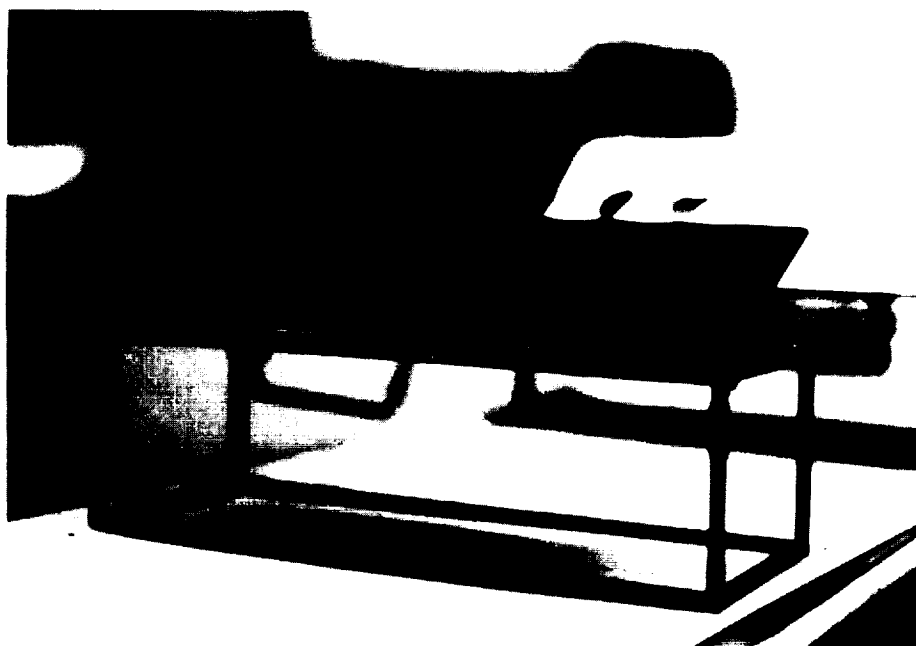
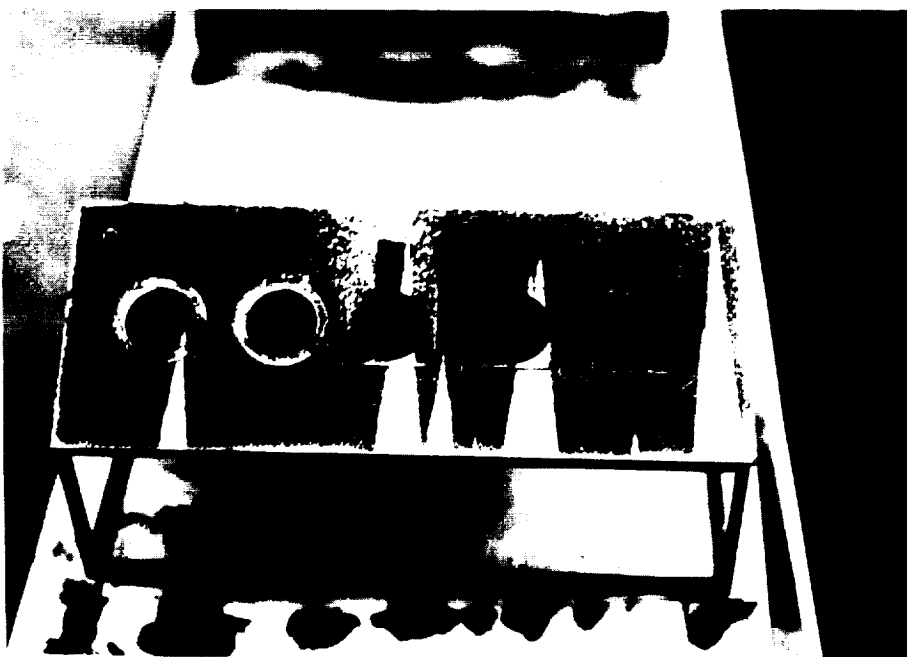


Figure 1.—Experimental set-up to simulate a Martian dust storm.

ORIGINAL PAGE  
BLACK AND WHITE PHOTOGRAPH



(a) 22.5°.



(b) 27°.

Figure 2.—Effect of tilting a plate covered with simulated Martian dust with nominal particle size greater than 75  $\mu\text{m}$ .

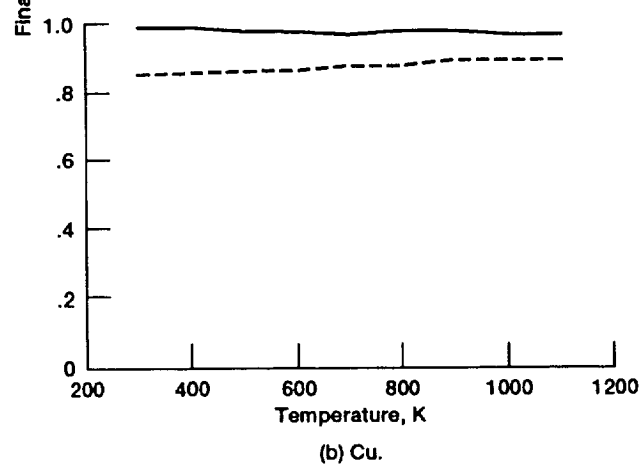
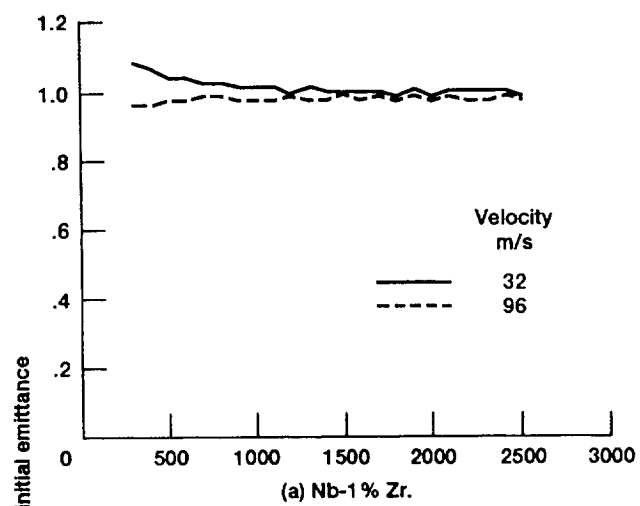


Figure 3.—Emittance values for initially dusted arc-textured samples exposed to clear wind.

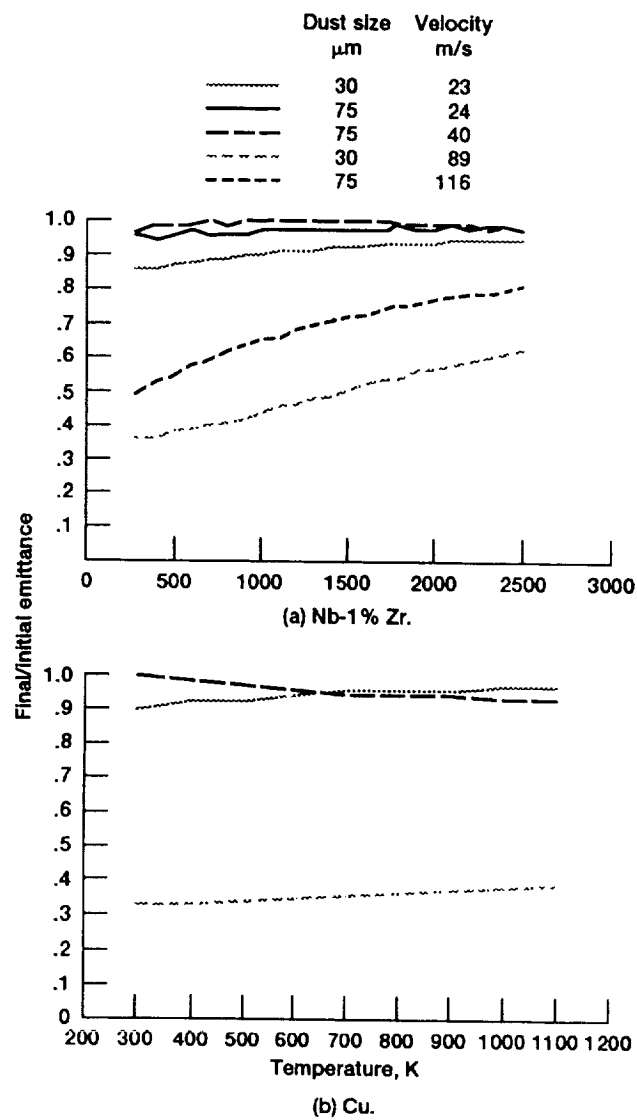
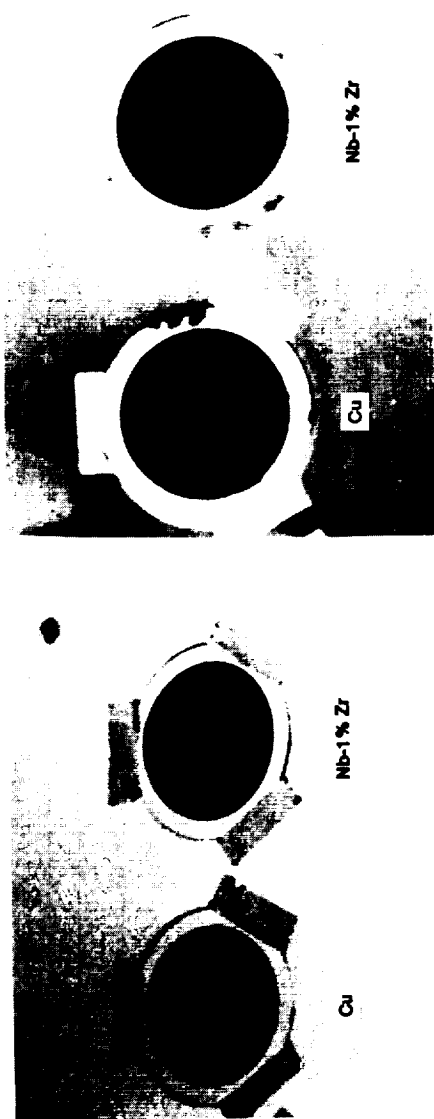
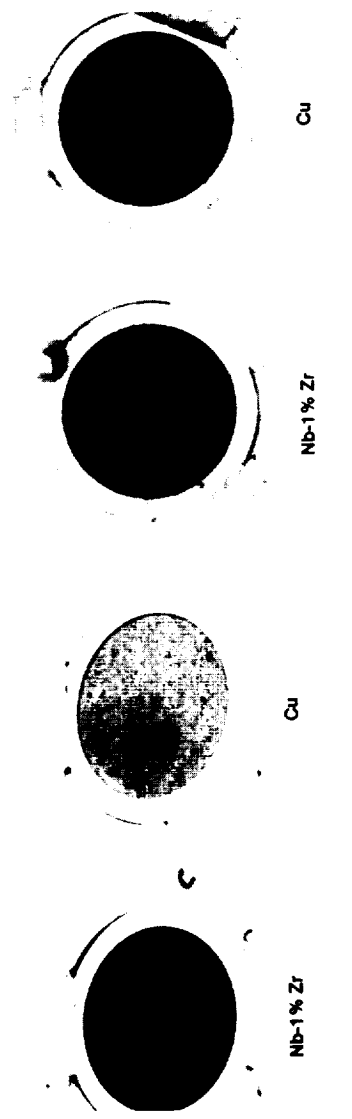


Figure 4.—Emittance values for arc-textured samples exposed to dust-laden wind.

ORIGINAL PAGE  
BLACK AND WHITE PHOTOGRAPH



(a) Initially clear-small particles-89 m/s.



(b) Initially dusty-small particles-89 m/s.

(c) Initially clear-large particles-116 m/s.

(d) Initially dusty-large particles-116 m/s.

Figure 5.—Abrasion is apparent in these arc-textured metal samples subjected to high velocity winds.

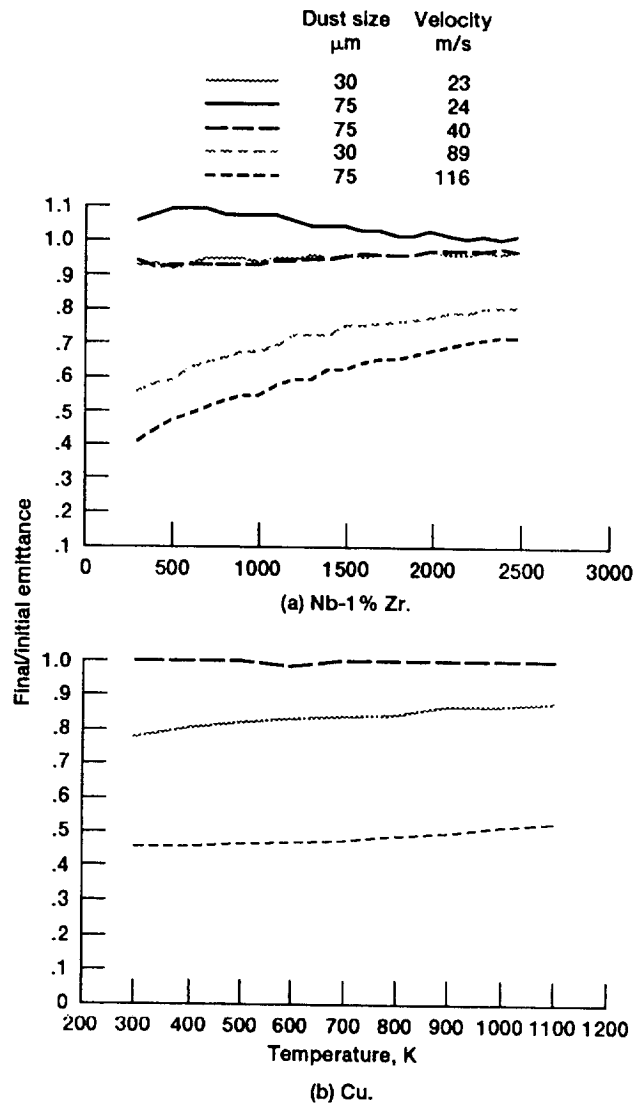


Figure 6.—Emittance values for initially dusted arc-textured samples exposed to dust-laden wind.



**CONTROL of ON-ORBIT CONTAMINATION for the ARGOS (P91-1) SATELLITE**

Joseph G. Kelley  
Rockwell International

**ABSTRACT**

The ARGOS (P91-1) satellite presents a challenging combination of on-orbit contamination concerns while mandating a low-cost approach. Several experiment payloads contain contamination sensitive optics, another contains large quantities of CO<sub>2</sub> and Xe for release in orbit, and one contains an NH<sub>3</sub> fueled arc jet thruster. The latter includes a suite of sensors to measure contamination; so prelaunch calculations will be tested. Planned contamination control techniques include: physical separation of sensitive surfaces from contamination sources; flight covers to protect sensitive surfaces during early outgassing on-orbit; gas release and thruster operation early in the flight, before flight covers are opened; and careful control of plumes and venting through a detailed analysis of each.

**INTRODUCTION**

The Air Force, Space Test Program, satellite ARGOS (Advanced Research and Global Observation Satellite), otherwise known as P91-1, will carry a number of experiments in an 833 km (450 nmi) polar orbit (98° inclination) in 1995. One year of experiment operation is planned, but the vehicle is designed for a three year on-orbit life. The diversity of the experiments presents a number of contamination control concerns; while the nature of the program mandates a low cost approach. This paper presents the contamination requirements and concerns, describes the contamination control approach, and provides an estimate of launch and post launch accumulations.

The current vehicle concept is shown in figure 1. A brief summary of the experiments is provided in table I.

**CONTAMINATION CONCERNS and ACTIONS****Contamination Impact**

Contamination is of concern primarily for its impact on experiment and vehicle End of Life (EOL) capabilities. For optical instruments, including optical attitude sensors, contamination attenuates the signal by absorbing and scattering the incoming signal, and may increase noise by scattering unwanted radiation into the sensor. Contamination on thermal control surfaces causes an increase in solar absorptivity proportional to the area ob-

scured by particles and the molecular film thickness. The change in emissivity can usually be neglected (ref 1). The radiators will not be sufficiently colder than the rest of the space vehicle that condensation of contaminants is a concern. Molecules will attach to a surface only if polymerized, by solar UV, to form a compound with a much lower vapor pressure (ref 2). Thus, shadowed thermal surfaces are of less concern than sunlit ones. Molecular contamination on solar arrays decreases power (ref 3) as shown in figure 2. The power loss for the expected particle obscuration (~1%) will be negligible (ref 4).

The major contamination sensitivities and EOL requirements, for both the experiments and the space vehicle (SV), are summarized in table II together with the intended precautions. As described below, the ESEX and CIV experiments have much shorter mission lives than the other experiments.

### **Precautions**

On-orbit contamination control, for ARGOS, is achieved by four methods: materials selection, geometry control, flight covers, and time phasing of operations.

All outgassing materials must meet the usual criteria: Total mass loss less than 1% when heated to 125 °C for 24 hours, and collected volatile material on a 25 °C witness plate less than 0.1%. It has been assumed that: 1. the outgassing so measured represents the total loss over mission life; 2. the collected material consists of heavy (~150 amu), polymerizable molecules; 3. the uncollected material is light (~18 amu), non-polymerizable molecules. These assumptions are crude, but are the best values available until the actual materials are defined and measured.

The geometry is shown in figure 3. Emissions, both internal outgas products and thruster plumes, are restricted, in so far as possible, to one end of the vehicle. USA was mounted on the rear to minimize meteor and debris impacts; this required that CIV and ESEX be mounted on the front. The mean free path in the ambient atmosphere is 1600 km; so there are no ram effects. The attitude control thrusters, which share the CIV gas supply, are not shown. In an emergency they will be used to orient the vehicle in a sun-safe mode pending ground intervention. If used, they will emit small CO<sub>2</sub> plumes to the sides; the contamination effects will be negligible. USA has a small leakage of argon with a trace of methane, and the emitting face can be rotated 90° up and down. However, these gasses are noncontaminating, the amount is small, and they do not impinge on the vehicle: they are not a contamination problem.

The optical surfaces of the experiments require a much greater cleanliness than can be economically achieved for rest of the space vehicle. These will be provided with flight covers and controlled internal environ-

ments by the experimenters. The covers will remain closed from delivery for integration until favorable conditions are achieved on-orbit, as discussed below. If they must be opened before launch, e.g. for testing, it will be under the direction of the experimenter, who will be responsible for maintaining experiment cleanliness. After opening, the optical elements will not be permitted to view outgassing surfaces, e.g. solar arrays; exceptions will be at the experimenter's risk.

Finally the on-orbit operations have been time phased to limit cross contamination. During phase 1 (two days to two weeks) all experiments will be off, flight covers will remain closed, and no high voltage surfaces will be exposed while the vehicle is checked out and tested. Phase 2 (4-6 weeks) will be devoted to ESEX and CIV operations. The other experiments will remain off, with flight covers closed, and no high voltages will be exposed, except for ESEX operation. Phase 3 will start with a brief (one week) delay to allow any residual thruster effects to disperse. At this point (~ week 8 on orbit) over half of the total outgassing will have occurred and the outgassing rate will be about a tenth of its value at the end of the first day on orbit. Flight covers will now be opened and the operation of the rest of the experiments initiated.

## **CONTAMINATION SOURCES AND ACCUMULATION**

### **Prelaunch**

All exposed surfaces (thermal control surfaces, experiment exteriors, etc) will be cleaned immediately before packing for shipment to the launch site. This cleaning will be to Visibly Clean Level I, which corresponds to an obscuration of 0.5% by particles and less than one microgram/cm<sup>2</sup> (100 Angstrom (A)) molecular film. Thereafter the space vehicle will be protected in a 100,000, or better, cleanroom until launch (122 days); most of this time will be in a class 10,000, or better, environment. This exposure will add 2% obscuration to upward facing surfaces and 0.1% particle obscuration to other surfaces. It will also add 100 A of molecular film to all exposed surfaces. The satellite will be maintained in a vertical position with USA uppermost. There will be some redistribution of large particles by transportation and handling shocks, but these are not expected to significantly increase the particle density on any critical surface.

Ground covers (solar arrays, attitude sensors, ESEX diagnostics) will be removed at payload fairing closure. These surfaces will be visibly clean level I, except for the ESEX diagnostics which will be level II (for definition see below). The prelaunch exposure time for these surfaces will be only five days, which will increase the obscuration of non-upward facing surfaces by 0.004% (no sensitive surface faces upward in this orientation of the satellite). These surfaces will acquire a total of 12 A additional molecular film while covered and during the five days exposure.

## Launch/Venting

The payload fairing will be cleaned to Visibly Clean Level II, which corresponds to 0.1% particle obscuration and less than one microgram/cm<sup>2</sup> molecular film. During launch most particles larger than 5 microns will be shaken free and, unless swept out by the vented gas, will redeposit, primarily on the upward facing surfaces. Assuming a two to one area ratio due to the curvature of the fairing, one finds an obscuration increase of less than 0.3% on upward facing surfaces and 0.02% on other surfaces. Molecular film addition will be less than 20 Angstroms due to fairing emissions and and thruster splash. Since there are no cold surfaces to condense molecules and no sunlight to polymerize them, it is assumed that the vented gasses have no contamination effect.

## Plumes

ESEX emits 0.25 gm/sec of ammonia (NH<sub>3</sub>), nitrogen (N<sub>2</sub>, N), and hydrogen (H<sub>2</sub>, H). It may also emit trace amounts of contaminants and trace amounts of metallic dust (from the electrodes). There will be ten firings of fifteen minutes each. The experimenter has provided a Monte Carlo analysis showing that most of the emission is confined to a cone centered on the arc axis. Self interaction produces a small amount of backscatter, mostly hydrogen with small amounts of ammonia and nitrogen. This conforms to the expectation that conservation of momentum will cause preferential backscattering of the lightest components. These emissions are not expected to present a contamination problem to the rest of the vehicle.

CIV will release twenty bursts each of carbon dioxide (CO<sub>2</sub>) and Xenon (Xe); ten seconds per burst, 100 gm/sec. The gasses will expand, and cool, supersonically (See table III for parameters). It is expected that 75% of the gas will remain within 45° of the vent axis and 95% within 75° (ref 5). The CIV emissions will be very clean, contaminants of concern will be less than one part per million. However, outgas products may be entrained and scattered by the heavy Xe atoms. Also, the CIV plume can produce pressures up to 0.03 Torr or more at points a meter forward of the nozzle. High voltages must not be exposed to these pressures. Pressures at points behind CIV and within enclosures must be calculated on a case by case basis.

## Outgassing

The material list is not yet available; so one must make some assumptions to calculate the outgassing. The Tribble and Haffner (ref 3) assumption that the mass of outgassing material interior to the vehicle is equal to one-third the mass of the boxes and wiring, was valid for GPS and appears reasonable for use here for internal emissions. One must also consider external emissions from the Thermal Control Surfaces (TCS) and the solar arrays (adhesives and substrate). Estimates are provided in table

IV. It is expected that outgassing will be completed in less than three years at the temperatures expected.

The outgas effluents of concern, those capable of being polymerized by solar UV, are very heavy molecules,  $> 150$  amu, and their mean free path is long, on the order of meters or more. They will be emitted, with a Lambertian cosine distribution, in straight lines; a threat only to surfaces in line of sight (LOS) of the vent: the shaded side of ESEX and panels two and three of the solar array on that side.

There is one exception to the line of sight rule: the Xenon atoms from CIV may entrain the heavy contaminants and carry them to the ESEX diagnostics. The  $\text{CO}_2$  molecules are not heavy enough (44 amu) to significantly divert the heavy contaminants ( $>150$  amu), but Xenon (131 amu) may have some effect. CIV operation may begin as early as the second day ( $t=8.6 \times 10^4$  sec) on orbit. Space vehicle temperature will be about 300 K. The outgas rate formula used by Tribble and Haffner,

$$dm/dt = 3100 \times M_0 \times \exp(-5032/T) / t^{1/2}, \quad (1)$$

gives a total deposit of about 20 nanograms/cm<sup>2</sup> on the ESEX diagnostics, after 200 seconds exposure (120 exposures, 10 seconds each) if 2% of the incident flux is polymerized.

Each solar array consists of three panels, each 144 cm long. The panels are angled  $60^\circ$  to their rotation axis at a point 17 cm from the vehicle. The first panel is mounted 74 cm from the pivot (figure 4). Panels two and three of the solar array on the vent side are exposed to the effluent when they extend beyond the plane of the vent. For simplicity, the distance and angle to the midpoint of each panel, at its point of closest approach to the vent, was used for the entire area of the panel. Exposure is modified by the cosine effect of the Lambertian emission, the cosine of the angle between the incident flux and the panel normal, and the fractional exposure time. Tribble and Haffner's maximum polymerization factor of 0.008 was used. The calculated deposit is less than 100 nanograms per square centimeter on each panel; this has negligible effect on the power generation when averaged over all six panels.

All solar panels see emissions from the vehicle surface materials. Allowing a  $\cos 60^\circ$  modification of panel area and allowing 0.8% polymerization as before, the total deposit is less than 1000 nanograms/cm<sup>2</sup> for panel 1, 390 nanograms/cm<sup>2</sup> for panel 2, and 210 nanograms/cm<sup>2</sup> for panel 3. Combining this with the deposit from the vented material gives no more than a microgram/cm<sup>2</sup> for any panel and little impact on the total power output.

The vehicle thermal control surfaces, and the radiator on the sunlit side of ESEX will be exposed to outgas products from the solar arrays.

Totaling the emissions from the three panels (with proper distances for each), including a  $60^\circ$  factor for Lambertian emission, and using a polymerization factor of 2%, one finds deposits up to 1.6 micrograms/cm<sup>2</sup>. This corresponds to an absorptivity increase of 0.008. Note that minimum distances were used and the receiving surfaces were assumed to be perpendicular to the line of sight; both cause overestimation of the effect.

## **SUMMARY**

The objective is to provide low cost contamination control for a satellite with diverse experiments. This is done by controlling materials, controlling the locations and fields of view of the experiments, using flight covers over the optical surfaces, and time phasing the on-orbit operations. The results are summarized in table V. All requirements are satisfied with adequate margins. Given the added consideration of the conservative nature of the approximations, the margins become very comfortable.

## REFERENCES

1. Hamberg, O.; Tomlinson, F.D.; Sensitivity of Thermal Surface Solar Absorptance to Particulate Contamination; AIAA 6<sup>th</sup> Thermophysics Conference; p 137-151; April 1971
2. Stewart, T.B.; Arnold, G.S.; Hall, D.F.; Marten, H.D.; Absolute Rates of Vacuum-Ultraviolet Photochemical Deposition of Organic Films; J Phys Chem, 93; pp 2393-2400, 1989
3. Tribble, A.C.; Haffner, J.W.; Estimates of Photochemically Deposited Contamination on the GPS Satellites; J Space & Rockets; 28; pp 222-228; 1991
4. Raab, J.H.; Particulate Contamination Effects on Solar Cell Performance; Final Report, MCR-86-2015, Rev A, Contract FO4701-83C-0045, Jan 1987
5. Scialdone, J.J.; Flow Fields of Low Pressure Vent Exhausts; 16th Space Simulation Conference, pp 75-83, Nov 1990

Table I ARGOS EXPERIMENTS		
EXPERIMENT	SOURCE	INSTRUMENT/TECHNIQUE
CIV	USAF/Phillips Lab	Critical Ionization Velocity; CO2 and Xe Release Arcjet Propulsion; NH3 Propellant
ESEX	USAF/Phillips Lab	
EUVIP	Army	EUV Imager
GIMI	NRL	Far UV Cameras Extreme and Far UV Spectroradiometer Stellar X-Ray Observation
HIRAAS	NRL	
USA	NRL	
ADCNS	DARPA	Attitude & Navigation; Celestial Star Tracking
SPADUS	ONR	Space Dust Measurement

Table II CONTAMINATION CONCERNS AND PRECAUTIONS			
ELEMENT	CONCERN	PRECAUTION	EOL REQUIREMENT
CIV	Orifice Blockage, Gas Cleanliness	Use Hydrazine Spec for Components	* <20 ppm Emitted Contamination
ESEX -Diagnostics -Radiator	Sensor Background Absorptivity	Ground Cover, Clean Before Launch	* $\Delta m < 5 \mu \text{ gm/cm}^2$ * $\Delta \alpha < 0.08$
EUVIP GIMI HIRAAS ADCNS	Throughput Loss	Flight Covers, No LOS to SV	Experimenter Determined & Controlled
USA SPADUS Shaded TCS	None	Not Applicable	Not Applicable
Sunlit TCS Solar Arrays Attitude Sensors	Absorptivity ** Loss of Illumination Loss of Throughput	Limit Venting, Clean before Launch  Ground Cover	$\Delta \alpha < 0.08$ $\Delta P/P < 0.02$  Throughput Loss < 20%
* EOL = End of Phase 2; ** Contamination Driver			



Table III CIV EXPANSION PARAMETERS						
SPECIES	MASS	VELOCITY	TEMP	<--1 m from release -->		
	amu	cm/sec	K	DENS #/cc	PRESS Torr	MFP cm
CO2	44	6.9x104	137	1x10 <sup>17</sup>	1.5	1x10 <sup>-3</sup>
Xe	131	3.1x104	118	8x10 <sup>16</sup>	1.0	2x10 <sup>-3</sup>

Table IV OUTGASSING ESTIMATES			
SOURCE	MASS	OUTGAS	
	grams	TYPE amu	MASS grams
Internal	2.4x10 <sup>5</sup>	18 150	2100 240
TCS	3.4x10 <sup>4</sup>	18 150	310 34**
SA	4.2x10 <sup>4</sup>	18 150	380 42**
** TCS and solar array are expected to emit much less than 0.1% of their mass as polymerizable material			

Table V ADDED CONTAMINATION (obscure/film) AND IMPACT						
SURFACE	PRE-LAUNCH	LAUNCH	POST-LAUNCH	TOTAL	IMPACT	MARGIN
ESEX	4x10 <sup>-5</sup> 3 Ang	2x10 <sup>-3</sup> 100 Ang	0.3 Ang	2x10 <sup>-3</sup> 100 Ang	$\Delta m = 2.1 \mu\text{g/cm}^2$ $\Delta \alpha = 0.021$	1.4 2.8
Sunlit TCS	1x10 <sup>-3</sup> 80 Ang	2x10 <sup>-3</sup> 100 Ang	500 Ang	3x10 <sup>-3</sup> 680 Ang	$\Delta \alpha = 0.025$	2.2
Solar Arrays	4x10 <sup>-5</sup> 3 Ang	2x10 <sup>-3</sup> 100 Ang	150 Ang	2x10 <sup>-3</sup> 250 Ang	$\Delta P/P = 0.009 - 0.012$	0.7 - 1.2
Attitude Sensors	4x10 <sup>-5</sup> 3 Ang	2x10 <sup>-3</sup> 100 Ang	---	2x10 <sup>-3</sup> 100 Ang	1.7% Loss	11

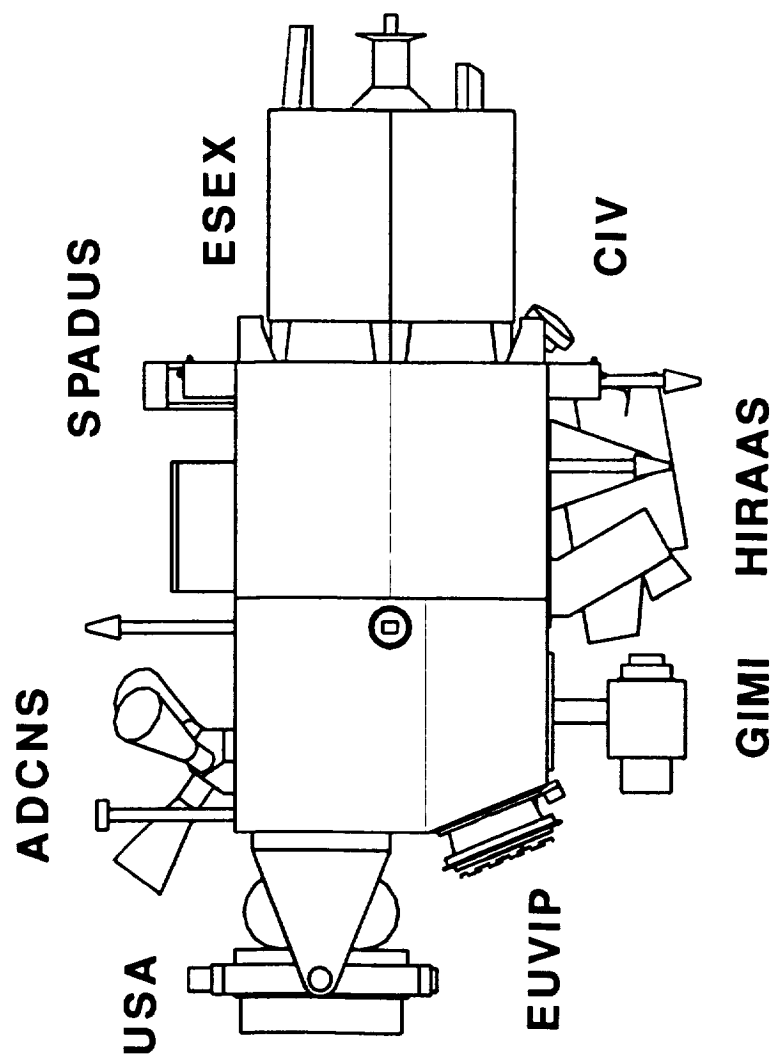


Figure 1 ARGOS vehicle with experiment locations.  
Solar arrays have been omitted for clarity.

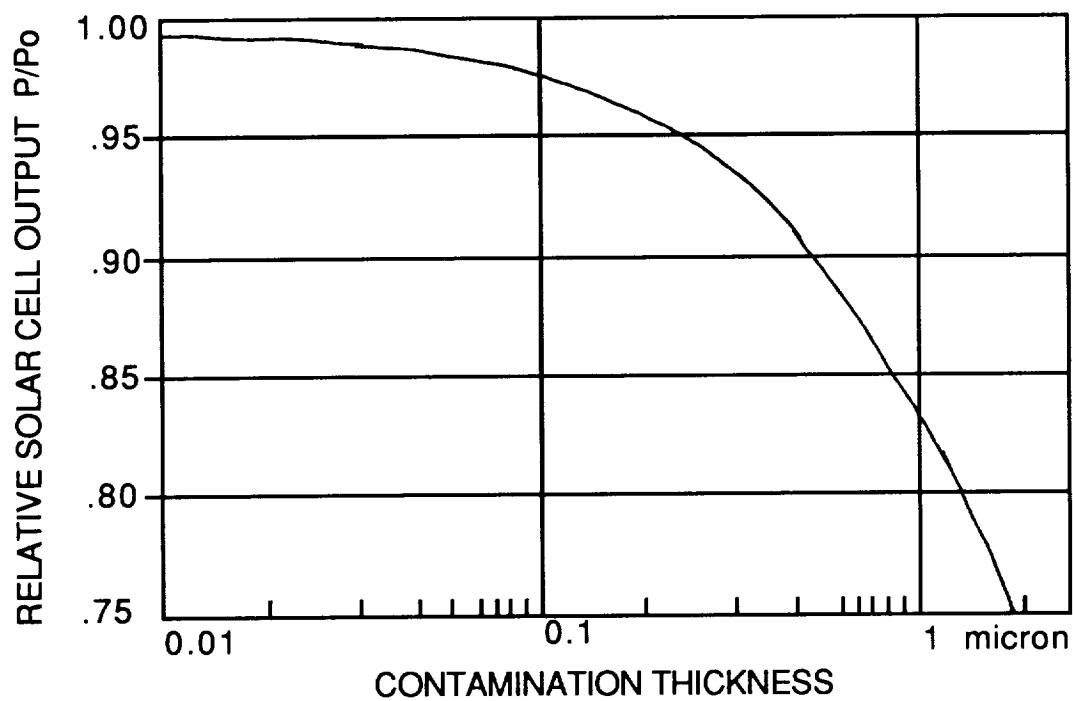


Figure 2 Solar Array Power is a function of molecular film thickness (It was assumed that 0.01 microns is equivalent to one microgram per square centimeter).

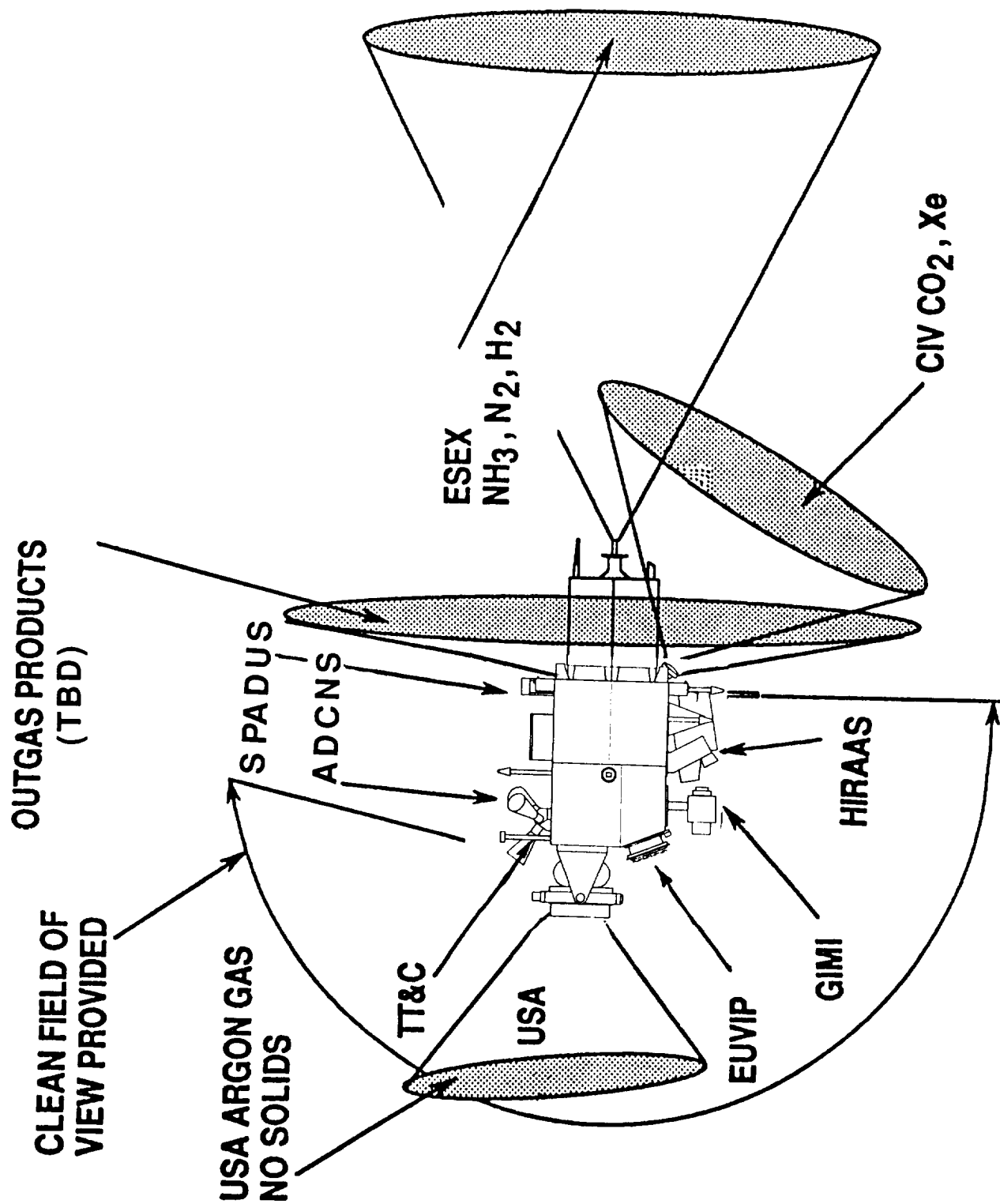


Figure 3 Sensitive surfaces are located as far as possible from contamination sources and do not view them.

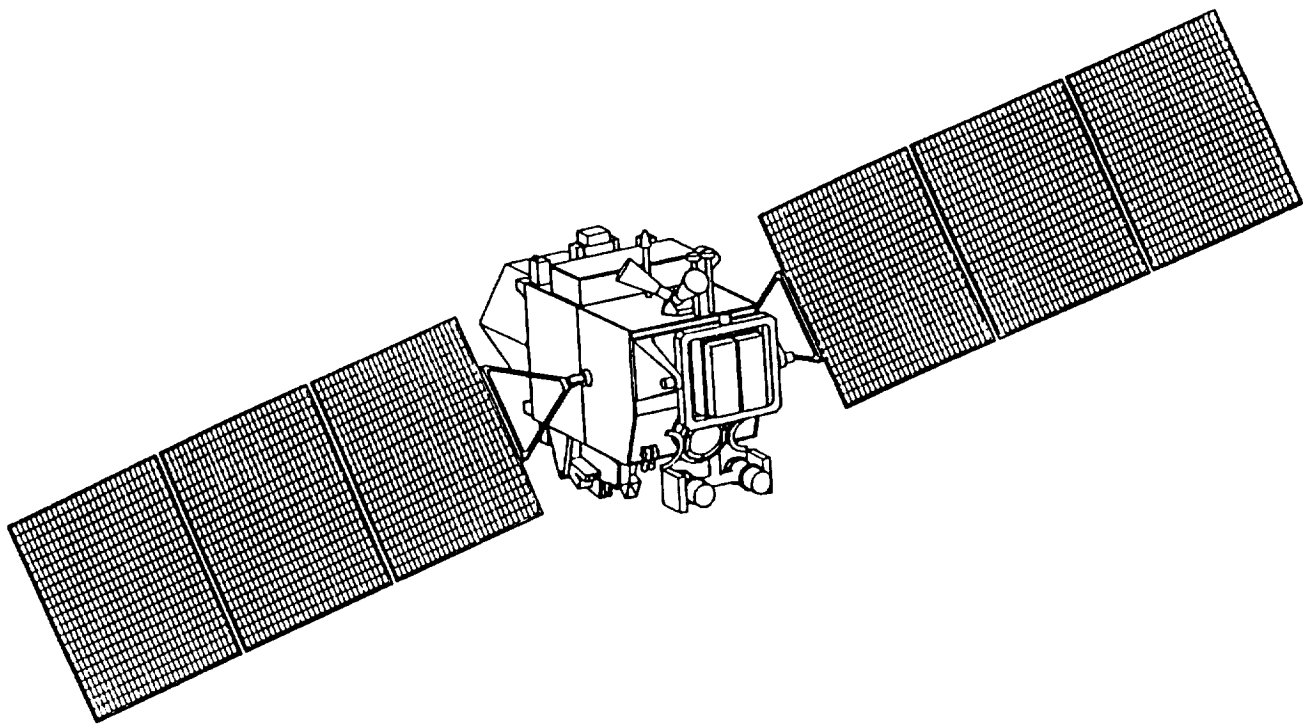


Figure 4     Each solar array is angled  $60^{\circ}$  to the rotation axis for the array.



## A NEW APPROACH FOR PERFORMING CONTAMINATION CONTROL BAKEOUTS IN JPL THERMAL VACUUM TEST CHAMBERS <sup>1</sup>

Kenneth R. Johnson, Dr. Daniel M. Taylor,  
Robert W. Lane, Maximo G. Cortez, Mark R. Anderson  
*California Institute of Technology*  
*Jet Propulsion Laboratory*  
*Pasadena, California 91109-8099*

### ABSTRACT

Contamination control requirements for the Wide Field/Planetary Camera II (WF/PC II) are necessarily stringent to protect against post-launch contamination of the sensitive optical surfaces, particularly the cold charge coupled device (CCD) imaging surfaces. Typically, thermal vacuum test chambers have employed a liquid nitrogen (LN2) cold trap to collect outgassed contaminants. This approach has the disadvantage of risking recontamination of the test article from shroud offgassing during post-test warmup of the chamber or from any shroud warming of even a few degrees during the bakeout process. By using an enclave, essentially a chamber within a chamber, configured concentrically and internally within an LN2 shroud, a method has been developed, based on a design concept by Taylor (Ref. 1), for preventing recontamination of test articles during bakeouts and subsequent post-test warmup of the vacuum chamber. Enclaves for testing WF/PC II components were designed and fabricated, then installed in three of JPL's Environmental Test Lab chambers. This paper discusses the design concepts, operating procedures and test results of this development.

### INTRODUCTION

The WF/PC II has been designed as an on-orbit replacement of WF/PC I to enhance the performance of the Hubble Space Telescope by providing a view of the far-ultraviolet spectral region using improved CCD sensors which operate below a temperature of -60°C. The far-ultraviolet performance of WF/PC II is extremely sensitive to molecular contamination of the optics and the CCDs. Thus, very stringent contamination control requirements have been mandated to minimize the molecular emission rate of all subsystems within the instrument's structural housing. Molecular emission rates are to be minimized by baking all flight hardware at elevated temperatures under vacuum conditions ( $<1 \times 10^{-5}$  Torr).

---

1] The research described in this paper was carried out by the Jet Propulsion Laboratory, California Institute of Technology, under a contract with the National Aeronautics and Space Administration

In 1989, JPL determined that conventional vacuum chambers could not be used to bake hardware to the stringent WF/PC II requirements. In fact, one conventional vacuum chamber that was baked at 125°C for several weeks did not even yield contaminant background levels low enough to permit direct measurement of the cleanliness level of most WF/PC II hardware. Consequently, a new approach for performing contamination sensitive bakeouts was devised based on three criteria set forth by Taylor<sup>2</sup>: (1) the test article hardware must not be recontaminated by outgassed volatiles at any time during the bakeout, contamination level testing, or post-test warmup of the chamber; (2) the background emission rate of the chamber hardware must be negligible as compared to that of the test article hardware; and (3) the contamination measurement method must positively verify that the required cleanliness results have been met.

By June 1990, one chamber (ETL Chamber 13) had been reconfigured and by June 1991, two additional chambers had been reconfigured (ETL Chambers 15 and 10). Subsequently, an effective bakeout operating procedure was developed after several operational trials which yielded background cleanliness level results acceptable for WF/PC II hardware. Figure 1 presents a side view of the overall enclave and LN2 shroud configuration as installed in the JPL ETL Chamber 10. Figure 2 is a flow schematic illustrating Chamber 10 shroud and enclave temperature control systems. The labels VGN and VLN signify valves on GN2 and LN2 lines, respectively.

### **CHAMBER RECONFIGURATION DESIGN CONCEPTS**

The test article containment system was designed to prevent recontamination of the test article hardware. By enclosing the test article inside an enclave, and by always maintaining the temperature of the enclave walls higher than that of the test article throughout the duration of the bakeout, the outgassed volatile contaminants are prevented from condensing on the inner walls of the enclave. Instead, the contaminants exit through strategically placed orifices in the enclave and are removed from the chamber either by the vacuum pumping system or by condensing on the LN2-cooled shroud. Before conducting the post-bakeout final cleanliness testing of the test article, the enclave temperature is lowered slowly to prevent condensation on the enclave wall of volatiles still emitting from the test article (whose temperature lags that of the enclave). After post-bakeout testing is done, the shrouds are warmed slowly while the enclave is purged with high purity GN2 to minimize the possibility of contaminants backstreaming into the enclave.

Enclaves were fabricated from stainless steel in two main parts: a can and a cover. After fabrication, both the cans and covers were electro-polished to remove surface embedded contamination. The enclaves were installed in the chambers and were thermally isolated from the LN2 shrouds by multilayer insulating blankets.

---

2] New Technology Report: Hardware Containment System for Vacuum Bakeout, August 1992



The background contaminant emission rate of the chamber hardware is minimized first by sufficiently baking the enclave at a temperature higher than the maximum expected operating temperature of the test article, then by lowering the enclave to a nominal operating temperature of the test article. It was assumed that sufficient baking had been completed when the measured contamination rate did not change more than 5 % over a 24 hour period.

The contamination measurement method is a multistep process and involves the use of several instruments. Before any contamination measurements are made, the chamber pressure must be well below  $1 \times 10^{-5}$  Torr. Chamber pressures are measured using convectron gauges to  $1 \times 10^{-3}$  Torr and ion gauges below that pressure. Below pressures of  $1 \times 10^{-5}$  Torr, high level contamination rates are measured using a Residual Gas Analyzer (RGA), a quadrupole mass spectrometer with an electron multiplier that senses molecules in the range of 0 to 200 atomic mass units (AMU). The RGA enables real time monitoring and interpretation of gas composition and chamber pressure. Low level contamination rates are measured using two types of quartz crystal microbalances (QCM) using 15 MHz crystals with a sensitivity of  $1.56 \times 10^{-9}$  g/cm<sup>2</sup>Hz: (1) a thermoelectric QCM, or TQCM, which has thermoelectric devices that can control the crystal's temperature between 80°C and -55°C; and, (2) a cryogenic QCM, or CQCM, which has only a heating capability. CQCM crystals must be cooled conductively using a heat sink (attached to a heat exchanger whose temperature is controlled by a LN<sub>2</sub>/GN<sub>2</sub> temperature control system), then warmed to the desired test temperature with the CQCM instrument heater. This system can effectively control the crystal temperature between -170°C and 80°C. The RGA, TQCM, and CQCM were all mounted and aligned such that they have a significant view factor only of their respective enclave orifices in order to minimize the possibility of measuring back scattering contaminants from the chamber door.

Although all three reconfigured chambers used an RGA, a TQCM and a CQCM for contamination measurements, the instruments were mounted differently in Chamber 10 (10' diameter x 10' long) than they were in Chambers 13 and 15 (3' diameter x 5' long). For Chamber 10, a stainless steel shutter was developed that could be operated from outside the chamber which, when in the up position would provide a large opening for contaminant flow at high outgassing rates as well as a flow path to the RGA, and when in the down position would close the opening entirely. The TQCM and the CQCM were mounted on the enclave cover and fitted directly in-line with enclave orifices. The TQCM and CQCM orifices are always open and are unaffected by the shutter position. During bakeout operations, the crystals are kept hot until the chamber vacuum level and the RGA readings indicate that measurements of cold crystal frequency rate change can be made without excess contaminant accumulation. Figure 3 gives a detailed view of the shutter assembly and the TQCM and CQCM mounts on the enclave cover in Chamber 10.

For Chambers 13 and 15, a stainless steel shutter was developed (designed for use in the smaller chambers) that could be operated from outside the chamber which would open the orifice flow paths to the CQCM, the TQCM and RGA for high level

contamination measurements (Position 1), and would leave open only the CQCM orifice for low level contamination measurements (Position 2). Figure 4 shows detail of the Chamber 13 and 15 assemblies.

### **BAKEOUT PROCEDURES**

The following procedure for performing bakeouts to yield high level cleanliness test articles has been developed over the past two years through analysis of test data.

1. Rough pump to about  $5 \times 10^{-2}$  Torr and turbopump to  $1 \times 10^{-5}$  Torr. Heat the TQCM and/or CQCM to 75°C and maintain that temperature throughout the pump-down. Also, keep the enclave and the LN2 shroud at ambient temperature during pumpdown. Open the shutter to allow unhindered gas flow from the enclave.
2. When at the  $10^{-5}$  Torr range, begin heating the enclave to the maximum bakeout temperature while allowing the temperature of the shroud to drift slowly upward. This heating is often done in steps to avoid excessive pressure buildup in the chamber due to high outgassing rates.
3. As the temperature of the enclave rises and the bakeout proceeds, the chamber pressure fall to an asymptotic value indicating a steady state condition where the pumping system rate equals the bakeout outgassing rate. When the maximum bakeout temperature has been attained and the chamber pressure has leveled off, maintain this condition (soak) for about 12 to 24 hours.
4. Flood the shrouds with LN2. Flooding the shrouds usually has the effect of lowering the chamber pressure by a factor of ten. Open the cryopump hi-vac valve.
5. When the the chamber pressure has stabilized, lower the temperature of the TQCM to 0°C and make a measurement of the TQCM frequency change rate. Close the shutter while making this measurement so that the outgassing contaminants flow from the enclave only through the TQCM orifice. To avoid TQCM damage, if the frequency change rate is greater than 8000 Hz/hr, do not operate the TQCM for more than ten minutes before beginning TQCM desorption. Other guidelines are:
  - a. for a rate change > 1000 Hz/hr - collect data for 30 minutes;
  - b. for a rate change between 500 and 1000 Hz/hr - collect data for 1 hour;
  - c. for a rate change between 15 and 500 Hz/hr - collect data for 2 hours;
  - d. for a rate change < 15 Hz/hr - collect data for 4 hours.
6. After collecting frequency rate data, reopen the shutter and reheat the TQCM to the maximum desorption temperature,  $T_{Max}$ , to desorb accumulated contaminants. Normally, the TQCM is heated in 20°C increments (holding for 5 to 10 minutes between increments) to avoid thermally stressing the crystals. However, in cases where the contamination control engineer needs data to characterize the identity of the desorbed contaminants, the TQCM is reheated in steps. At each step TQCM

frequency data is gathered to indicate the degree of offgassing that occurs at each increment. These steps are: (1) heat from 0°C to 5°C over a half hour period; (2) heat from 5°C to 15°C over a half hour period; (3) heat from 15°C to 35°C over a half hour period; (4), heat from 35°C to  $T_{Max}$  over a half hour period and hold at  $T_{Max}$ .

7. Gather TQCM frequency change rate data on a daily basis at 24 hour intervals. Monitor the change rate deltas from day to day. Reheat the TQCM to  $T_{Max}$  after each data collection period. When the 24 hour change rate delta is less than 5 to 10%, proceed to the final cleanliness verification test.

8. The final cleanliness verification test is performed with the test article at 20°C. During cooling, the test article radiates heat to a cooler enclave. To prevent recontamination on the enclave from the cooling test article, the enclave temperature is lowered in steps as follows. Lower the TQCM temperature by 10°C (say to 65°C) and begin lowering the test article temperature slowly. When the TQCM frequency change rate due to desorption has leveled off at this lower temperature (65°C), lower the TQCM temperature by 15°C (say to 50°C). Continue lowering the TQCM temperature in steps (to 30°C then to 0°C), until the TQCM frequency stabilizes at 0°C and the test article stabilizes at 20°C. Maintain a test article temperature of at least 15°C higher than the TQCM and 5°C higher than the enclave.

9. When the test article has reached 20°C, the CQCM temperature is lowered directly from 0°C to -70°C. A typical goal for test article cleanliness certification is a TQCM frequency change rate which does not exceed 1-10 Hz/hr at -70°C..

10. When the cleanliness certification goal has been met, the CQCM is reheated to 75°C. Because the thermal lag between the CQCM and its heat exchanger thermal lag protects the crystal from thermal stress, heating in 20°C increments is not required. However, in cases where the contamination control engineer needs data to characterize the identity of the desorbed contaminants, the TQCM is reheated in steps as described in Step 6 above.

11. Close the cryopump hi-vac valve, begin purging the the enclave with high purity GN2, and begin warming the LN2 shrouds slowly. Continue the GN2 purge while the LN2 shrouds are warmed to ambient temperature. Ensure that the LN2 shroud temperature stays at least 20°C below the temperature of both the enclave and test article during the warmup process. When the LN2 shrouds have been warmed to ambient temperature, turn off the vacuum system and continue the backfill of the chamber with high purity GN2 to ambient pressure.

## **WF/PC II OPTICAL BENCH BAKEOUT RESULTS**

Table 1 represents typical results of CQCM measurements taken during a bakeout run of the WF/PC II Optical Bench in Chamber 10.

## CONCLUSION

Sensitive optical instruments intended for service in space require a high level of cleanliness to minimize the potential for contamination of optical surfaces. A new approach for performing bakeouts of this sensitive hardware has been developed and demonstrated at JPL. The use of a heated enclave which is mounted concentrically inside of and thermally isolated from the LN2 shrouds inside a thermal vacuum test chamber has been shown to provide acceptably clean bakeout results. This enclave configuration minimizes the possibility of recontamination of test hardware during the post-test chamber warmup.

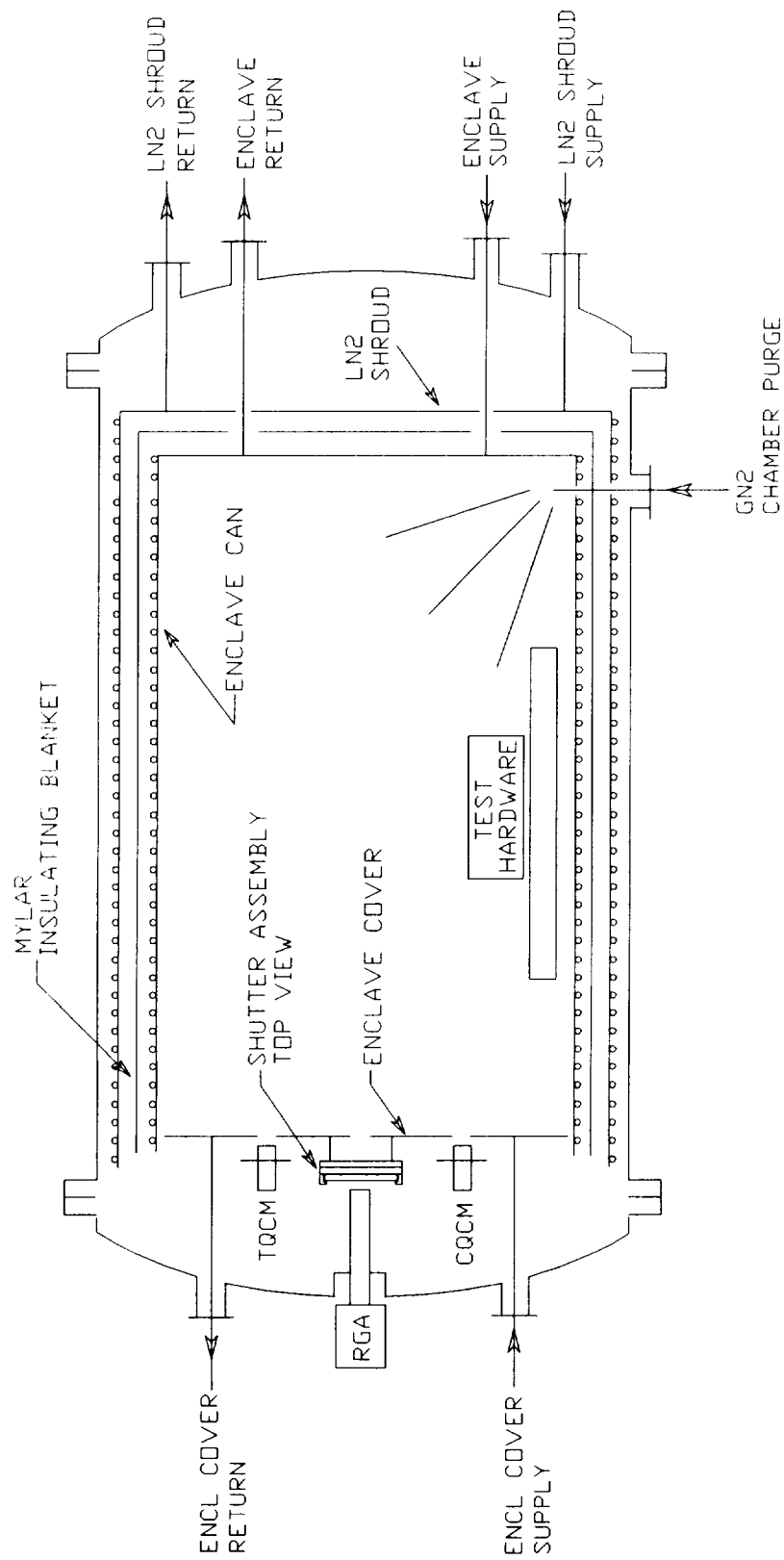
Effective bakeout procedures have been optimized through operational testing and have been shown to provide an effective method for maintaining test article cleanliness during and after sensitive hardware bakeouts.

## REFERENCES

1. Taylor, D.M., Soules, D., and Osborn, D.: The JPL Molecular Contamination Investigation Facility, SPIE vol. 1329, Optical Systems Contamination Effects Measurement Control - 1990, pg. 233-244.

**Table 1. CQCM Results of a WF/PC II Optical Bench Bakeout Run**

<u>Date</u>	<u>Time</u>	<u>Test Article Temp</u>	<u>CQCM Crystal Temp</u>	<u>CQCM Freq. Rate Change</u>
09/29/91	0800	62°C	0°C	115
09/30/91	0900	62°C	0°C	69
10/01/91	0800	62°C	0°C	55
10/02/91	0800	62°C	0°C	52
10/03/91	1100	62°C	0°C	62
10/04/91	1100	62°C	0°C	24
10/05/91	1100	62°C	0°C	25
10/06/91	1100	62°C	0°C	24
10/07/91	1100	62°C	0°C	23
10/08/91	2000	20°C	-70°C	6
10/09/91	0100	20°C	-100°C	19
10/09/91	0600	20°C	-100°C	17.5



*Figure 1. Chamber 10 Enclave Configuration*

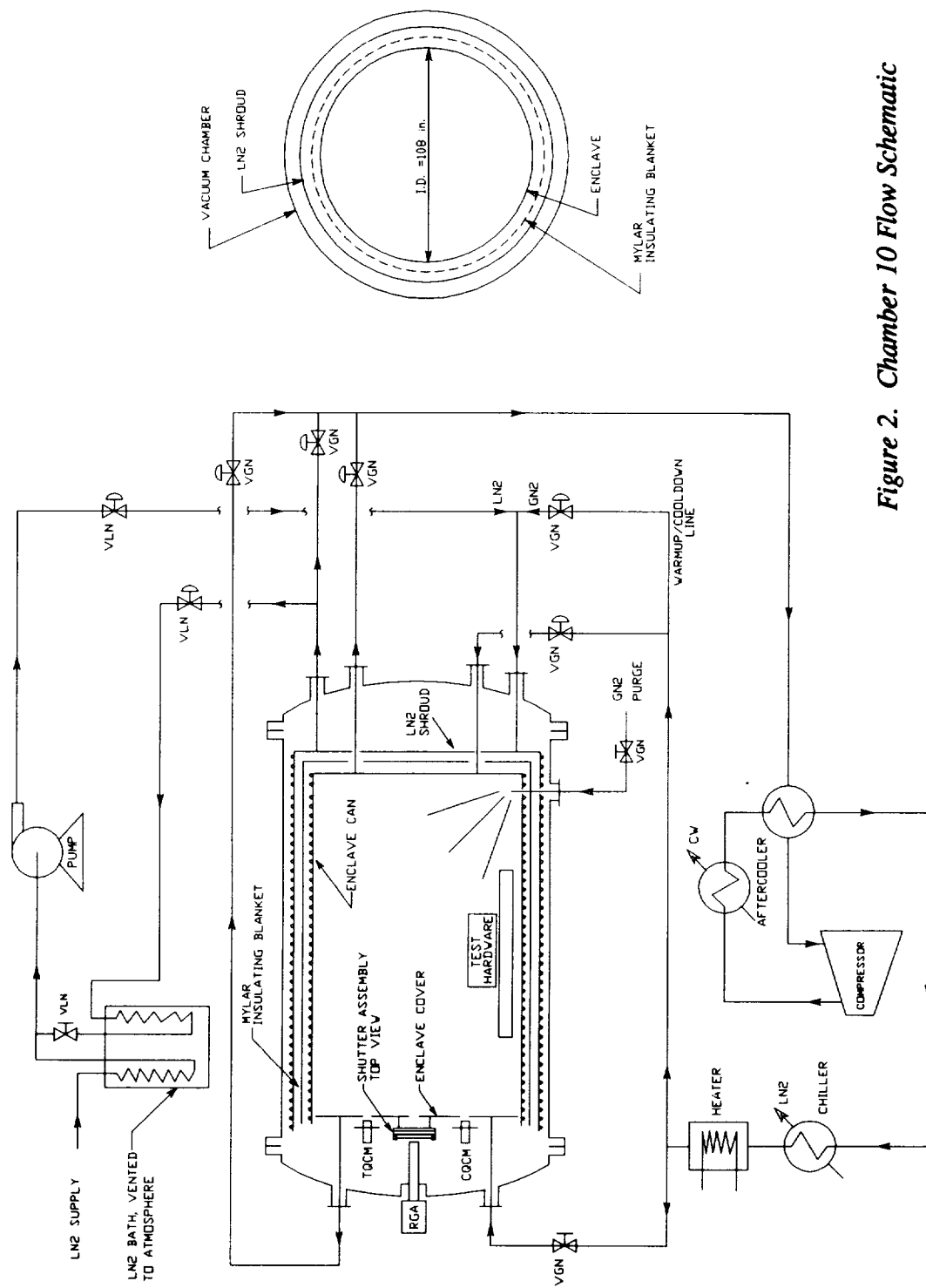
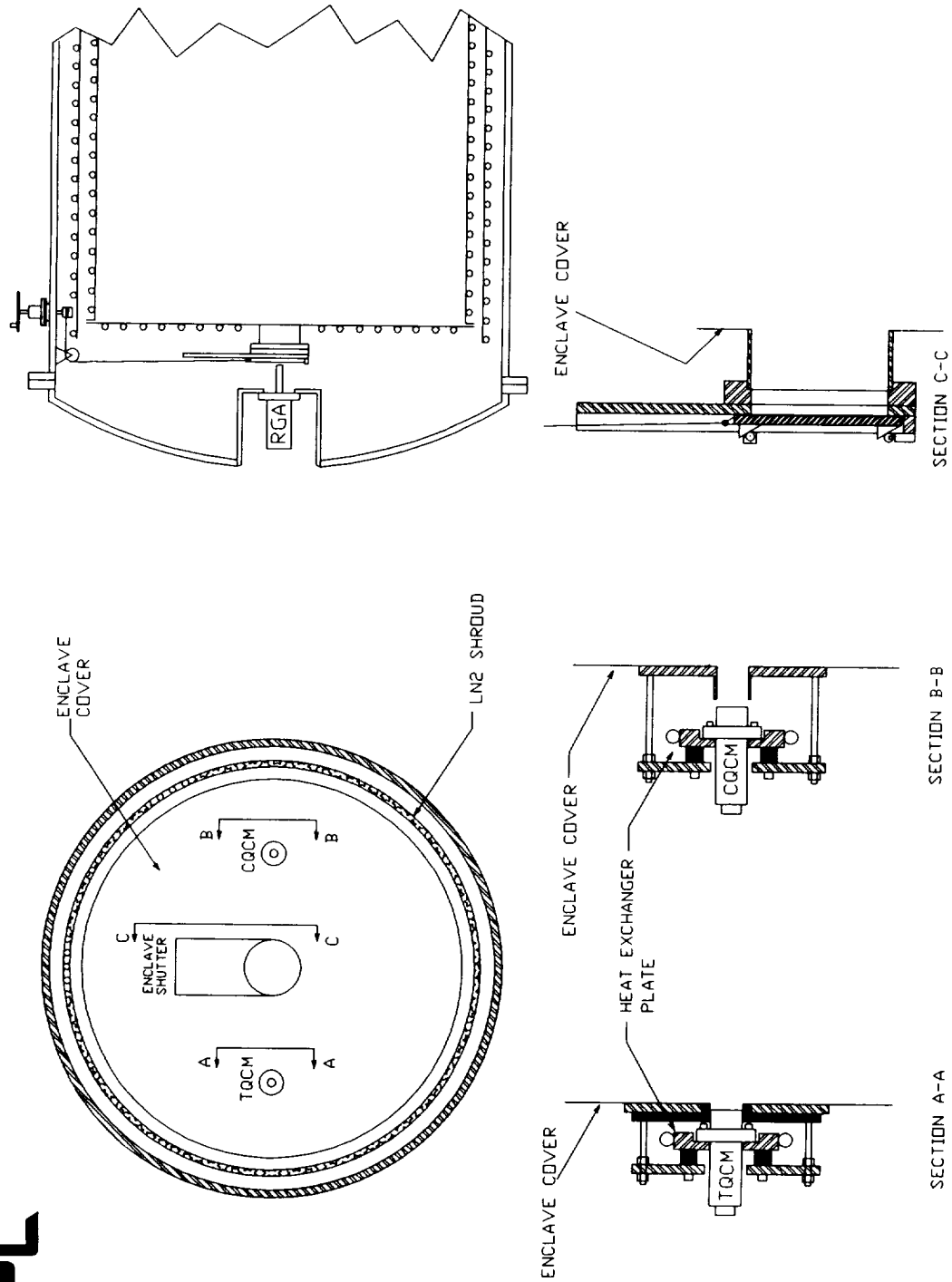
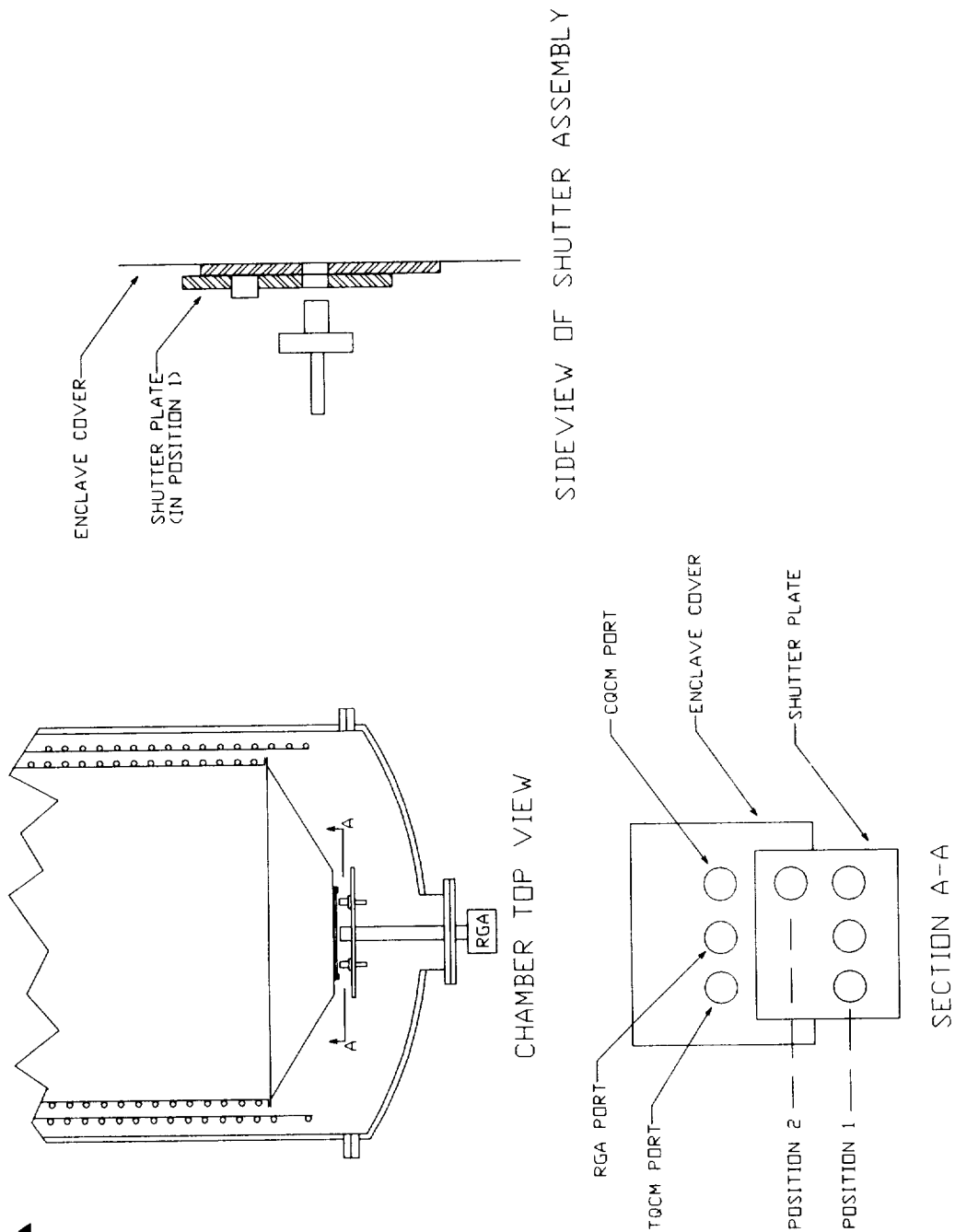


Figure 2. Chamber 10 Flow Schematic

**JPL**



*Figure 3. Chamber 10 Detail of Shutter and Mounts for RGA, TQCM and CQCM*



**Figure 4. Chamber 13 Detail of Shutter and Mounts for RGA, TOCM and CQCM**



**MASS SPECTROMETER USE IN A LARGE CHAMBER**

Tom Chuvala  
*GE Astro Space Division*  
Princeton, New Jersey 08543

The early satellites were somewhat insensitive to contamination produced during the construction and testing phases. The On-Orbit lifetime was such that contamination effects went either unnoticed or unrecognized. With today's On-Orbit lifetimes approaching 10+ years, contamination has become a paramount concern. The scientific payloads have increased in complexity and sensitivity. The ability to clean a contaminated sensor has greatly diminished. This requires better pumping systems and methods for improved monitoring.

The conversion from diffusion pumped thermal vacuum chambers to cryo pumped chambers with the use of Misner traps and selective cold traps have reduced contamination. Witness samples supply a record of the condensates that remain after a testing cycle, but impart no knowledge of the contaminant migration during the cycle that may be a month in duration.

Due to a customer's request that mass spectrometry be used during the testing of their spacecraft, a consultant was contracted to install a mass spectrometer to determine the feasibility of the instrument. The equipment and methodology described in this paper will start with the original system and its evolution to GE's present system.



## TQM IN A TEST ENVIRONMENT

Gary D. Chambers, Elizabeth A. King, and Keith Oleson  
Martin Marietta Astronautics Group  
Denver, Colorado

ABSTRACT

In response to the changing aerospace economic climate, Martin Marietta Astronautics Group (MMAG) has adopted a Total Quality Management (TQM) philosophy to maintain a competitive edge. TQM emphasizes continuous improvement of processes, motivation to improve from within, cross-functional involvement, people empowerment, customer satisfaction, and modern process control techniques. The four major initiatives of TQM are Product Excellence, Manufacturing Resource Planning (MRP II), People Empowerment, and Subcontract Management. This paper focuses on the Defense Space and Communications (DS&C) Test Lab's definition and implementation of the MRP II and people empowerment initiatives within TQM.

The application of MRP II to environmental test planning and operations processes required a new and innovative approach. In an 18 month span, the test labs implemented MRP II and people empowerment and achieved a Class "A" operational status. This resulted in numerous benefits, both tangible and intangible, including significant cost savings and improved quality of life. The following is a detailed description of the implementation process and results.

INTRODUCTION

In recent years, MMAG recognized that there was a real threat of losing their competitive business base in the aerospace industry. This was the result of a number of factors including a shrinking defense budget and a changing world climate. In 1987, MMAG began to implement various initiatives in order to improve productivity with reduced cost. The Department of Defense (DOD) was also investigating TQM. In early 1989, the DOD released guidelines for the implementation of TQM. In response to the guidelines, MMAG published a TQM implementation plan in October, 1991. This paper describes how TQM was implemented into testing functions versus the traditional manufacturing process and the current operations of test laboratories within the TQM environment. It also includes lessons learned during the implementation and discusses the benefits of incorporating TQM philosophies into a test environment. This paper emphasizes implementation in the Space Simulation Lab (SSL) due to the authors' SSL background and the unique problems created by 24 hour per day, seven day per week operations in the lab.

DS&C TEST LABORATORIES

MMAG's Environmental Test Laboratories have a 25 year history of testing in state of the art facilities, performed by well educated, trained and empowered personnel. Laboratory employees are experienced in spacecraft testing at all levels, component to systems. Some examples are: Magellan Venus Radar Mapper, Tethered Satellite, Transfer Orbit Stage, Viking, Several Skylab Subsystems, and extensive support of our Titan Launch family. They are experts in numerous environmental disciplines including: Acoustics Testing, Antenna Design/Test, Data Acquisition/Digital Processing, EMI/EMC Testing, Modal Survey Testing, Pyro Shock Testing, Test Tooling Design/Build, Thermal Vacuum/Balance/Solar/Cycle Testing, and Vibration Testing.

## TQM/MRP II

TQM emphasizes continuous improvement of processes, motivation for personal improvement, crossfunctional involvement, people empowerment and modern process control techniques. TQM is comprised of four primary initiatives: Product Excellence, People Empowerment, Subcontract Management, and Manufacturing Resource Planning (MRP II), Figure 1. The primary focus for the Defense Space and Communications (DS&C) Test Labs was people empowerment and MRPII.

MRP II was the lead initiative in the TQM implementation for MMAG. The following definition of Manufacturing Resource Planning (MRP II) is from Thomas E. Wallace's "MRP II: Making It Happen" (ref . 1)

A method for the effective planning of all resources of a manufacturing company. Ideally, it addresses operational planning in units, financial planning in dollars, and has a simulation capability to answer "what if" questions. It is made up of a variety of functions, each linked together: business planning, production planning, master production scheduling, material requirements planning, capacity requirements planning, and the execution support systems for capacity and material. Output from these systems would be integrated with financial reports such as the business plan, purchase commitment reports, shipping budget, inventory projections in dollars, etc. Manufacturing Resource Planning is a direct outgrowth and extension of closed loop MRP. MRP II has also been defined, validly, as a management system based on network scheduling. Also, and perhaps best, as organized common sense.

This definition specifically mentions a manufacturing company, but the theories apply to any company producing a product for a customer. MRP II philosophies are directly applicable to the aerospace industry. As shown in Figure 2, the DS&C Test Labs were able to take the manufacturing processes and apply them to a test environment. The only difference between the processes is that a manufacturing application produces hardware, where a test application produces a tested product.

## HISTORY

MRP II began in the 1960's as Material Requirements Planning (ref. 1). Material Requirements planning used what Oliver Wight, hereafter referred to as the consultant, called the Universal Manufacturing Equation. This equation answers the questions "What are we going to make", "What does it take to make it", "What do we have" and "What do we need" (ref. 1). The equation then becomes:

$$\text{MPS+BOM+IR=FR} \quad (1)$$

where:

MPS = Master Production Schedule

BOM = Bill of Material

IR = Inventory Record

FR = Future Requirements

The original users of this tool soon found that its possibilities far exceeded what was originally intended. It not only was usable as a procurement tool in fabrication and assembly, but could also be used to schedule (ref. 2). MRP was then adapted to include capacity planning and converted to a closed loop process. This adaptation, with the additions of finance and simulation, resulted in MRP II as it is known today (ref. 1). MRP II is used to plan and control, two of the basic functions of management of any organization (ref. 3).

## THE PROCESS

The current model for MRP II is illustrated in Figure 2 (ref. 4). This figure includes all aspects of the business and the ability for simulation. It is a feedback process with communication being essential. The process consists of eight steps. The first step is **Business Planning**. The Business Plan is the financial statement of projected business in terms of an income projection (ref. 3). This plan is used to develop and communicate the financial plans of the company. This plan should directly support the companies strategic plans (ref. 5). The

next step, **Sales & Operations Planning**, is defined as "the function of setting the overall level of manufacturing output (production plan) and other activities to best satisfy the current planned levels of sales (sales plans and/or forecasts), while meeting general business objectives of profitability, productivity, competitive customer lead times, etc., as expressed in the overall business plan" (ref. 4). The Sales & Operations plan is essentially the tactical plans of the company and is developed concurrently with the Business Plan.

The next step in the process is **Master Production Scheduling**. The Master Production Schedule is essentially the build schedule (ref. 3). This plan drives material requirements planning and the capacity planning functions. **Material Requirements Planning** is used to determine the requirements for items. This step is the basis for closed loop MRP and is now thought of as a scheduling technique (ref. 3). This stage then leads into the **Capacity Requirements Planning**. This is defined as "the process of determining how much labor and/or machine resources are required to accomplish the tasks of production, and making plans to provide these resources" (ref. 3). This stage is obviously dependent on the Material Requirements Schedule.

The next stage of MRP II is the **Comparison Stage**. It forces the user to validate his plans. If the plans are not realistic, the user should go back to the Material Requirements Planning stage and repeat the process. If the plans are realistic, the user should begin executing the capacity and material plans. This is not the end of the process, it is the beginning. **Execution of the plans** needs to be graded on accepted performance measures and must be flexible enough to resolve problems, it is a separate process of feedback and control in itself. MRP II is an ongoing and adaptable process.

MRP II has four grades to determine how the organization is operating, Classes "A" through "D". At Class "D", MRP II is simply a scheduling system. At Class "A", MRP II becomes an overall business management system. DS&C Test Labs were given the goal of achieving Class "A" status within the recommended 18 month span. The Test Labs were the only true non-manufacturing area within MMAG to implement MRP II.

## IMPLEMENTATION

Oliver Wight was selected as the professional guidance to be used by MMAG. The implementation process defined by the consultant is called the Proven Path (ref. 1). This process followed eleven steps required to achieve MRP II Class "A" status. The eleven steps of the proven path are as follows (ref. 1):

1. First cut education
2. Cost justification and commitment
3. User controlled project team
4. Assign full time project leader
5. Establish an Executive Steering Committee
6. Obtain professional guidance
7. Education of critical mass
8. Pilot approach to MPS/MRP
9. Close the loop
10. Include finance and simulation processes
11. Dedication to continuing improvement

The first step in the plan, first cut education, was completed by the executive staff and management of MMAG. They then completed a cost justification analysis that determined the implementation should continue. This resulted in a high level of commitment from top management to implement MRP II. The next step in the implementation was to form implementation teams for each of the areas, with full time project leaders. Space Systems company created six implementation teams, Figure 3, with an Executive Steering Committee in place to ensure success. As stated previously, professional guidance was provided by the Consultant.

The Test Laboratories MRP II Implementation team, Figure 3, was comprised of personnel from each functional area, supported by management leadership. The participants were engineers and planners who would use MRP II on a daily basis. Each team member was assigned a specific MRP II function and was challenged to become the team expert for that function. Functions were integrated planning, capacity planning,

master test schedules, test readiness, systems/architecture, inventory/BOM, and design engineering.

The next step in the implementation was to educate all of the users in the labs. The Consultant recommended education of at least 80% of all affected personnel to ensure successful implementation. Implementation Team Members were extensively trained via consultant sponsored seminars and video tape sessions. They in turn, became the instructors for the weekly laboratory personnel training sessions. Leaders were tasked with tailoring the sessions to the lab environment and providing a question and answer period. All employees of the labs were required to complete the full video training over a four month period. This was approximately 40 hours of training per person. In addition to education, training on the computer system that was to be used was given to a limited number of personnel who were expected to use the system. The software tool chosen by MMAG was Mac-Pac/D by Arthur Andersen. This tool was integrated with current shop floor control, finance and purchasing systems. After the education had been completed, a pilot program was created to validate the MRP II process. MMAG first tested the software they had chosen using an Integrated Test Bed. A company wide team was formed which validated software performance and application across MMAG. After the 12 week validation process was completed, team members had gained the expertise required to train users in their respective areas. Pilot teams in each area then tested the software for functionality. At the completion of the pilot, the Test Lab's schedules were loaded onto Mac-Pac/D and a cutover to the new formal planning system was accomplished. This completed the close the loop step of the implementation.

The finance and simulation steps of the implementation integrated the financial and operational systems and initiated use of "what-if" capability. These steps were accomplished at the MMAG level with the Test Labs following the direction given. The final step of the implementation was a dedication to continuous improvement. Continuous improvement had been addressed by identifying problems caused by poor interface and communications between intercompany departments. High performance work teams (HPWT) were formed and challenged to work chronic problems not addressed through formal measurement systems. One team focused on the coordination of the DS&C Test Labs and the MMAG Facilities Department in regards to maintenance and repair of the labs, capital projects and utility outages. The Product Protection HPWT focused on protection of hardware during transportation, handling, and test activities. Test Planning teams were formed to ensure facility and customer readiness and to share lessons learned from similar testing experiences.

The Space Simulation Laboratory High Performance Work Team (HPWT) initiated two other important programs in 1990-1991 which reflect the continuous improvement and employee empowerment concepts which are the cornerstone of TQM. The first of these programs was targeted at improving the level of service provided by SSL. One means of measuring the level of quality provided is the number of testing incidents and anomalies resulting from lab operations. An incident is defined as a condition or event which resulted in injury to personnel or damage to test support or flight hardware. An anomaly is defined as a out-of-tolerance condition or event which did not involve hardware damage or personnel injury and was caused by a deviation from the controlling SSL environmental test procedure or a deviation from an accepted laboratory practice. The program began by analyzing contributory causes to incidents/anomalies caused by the laboratory. Contributory causes were grouped in the following categories: Follow-through, Laboratory Practices, Training, Procedures, Engineering, Supervision, Failure Modes Effects Analysis, Capital, Staffing, and Maintenance. Each incident/anomaly was analyzed to determine if a deficiency in one of these categories was responsible for the occurrence. Each category was also assigned a number from one to five to show its relative contribution to the incident/anomaly, a one being a minor contributor and a five being a major contributor. The incident/anomalies from 1990 were analyzed in this manner and overall leading causes for the year were determined by forming a matrix and adding individual scores. The two leading deficiencies, follow-through and laboratory practices, were targeted for improvement programs. A formal management program was established to achieve a reduction in incidents/anomalies caused by poor follow-through. Laboratory practices for test engineering, design and fabrication engineering, and operations engineering were developed and issued to all personnel. A metric was established to measure the rate of incidents/anomalies monthly.

The HPWT set two goals for 1991; reduce the number of incidents to zero and reduce the anomaly rate by 10% under the 1990 rate. Due to the implementation of these continuous improvement programs and an increased awareness of the impact of incidents/anomalies on test costs the goal of zero incidents was reached and the anomaly rate was reduced by 14% (one anomaly every 4,500 test "touch" hours). A goal of another 10%

reduction in the anomaly rate for 1992 was set. Through July of 1992, the anomaly rate has been reduced by 32%.

The second program developed by the HPWT was an innovative alternative work week for the Operations Group to solve some of the unique problems encountered by SSL. This idea was conceived by an operations supervisor, brought to fruition by the HPWT, and enthusiastically endorsed by laboratory management. Top management not only approved the plan but contributed as part of the HPWT to ensure its success. Several MMAG programs use the lab at any one time. The level of testing for each of these programs varies weekly, consequently, the laboratory's required capacity also varies. Laboratory capacity planning for manpower projection purposes strives to reach a compromise between limiting overtime during high capacity periods and staying within overhead budget limitations during low capacity periods. Thermal vacuum testing is inherently lengthy in practice. Component tests can run three to four weeks while systems tests can run up to two months. Stopping tests to allow personnel weekends off is not schedule or cost effective. Consequently, test personnel often work extensive overtime. In 1990, the average overtime for an SSL operations test technician was 920 man-hours. The average overtime for operations supervisors was 1320 man-hours.

The HPWT developed a work week system that changed this traditional approach, Figure 4. The objective of the work week was to provide 24 hours/day, 7 days/week test operations support while reducing overtime, test cost, and overhead spending during low capacity periods. The operations group was divided into four crews, designated as D1, D2, N1 and N2. Each crew works three 12 hour days and one six hour day, followed by three and one half days off. This equates to a 42 hour work week (40 during low capacity periods) resulting in two hours of paid overtime per week. The D1 crew schedule is Monday through Wednesday, 7 AM to 7 PM, and Thursday, 7 AM to 1 PM; the N1 crew schedule is Monday through Wednesday, 7 PM to 7 AM, and Thursday, 7 PM to 1 AM; the D2 crew schedule is Thursday, 1 PM to 7 PM, and Friday through Sunday, 7 AM to 7 PM; the N2 crew schedule is Friday, 1 AM to 7 AM, and Friday through Sunday, 7 PM to 7 AM. The crew rotation is set up such that each crew rotates to a different shift every four weeks. Each crew receives seven days off to make the adjustment from days to nights or from nights to days. This change occurs every eight weeks and has improved operator morale. Several metrics were devised to measure system performance. Employee days off doubled from one day off per week to two. Overtime was reduced by 60% and an estimated savings of \$100,000 was realized from the conversion of overtime hours (paid at one and a half and double salary) to straight time hours. Employees also worked an average of 45 hours per week as opposed to the 1990 average of 57 hours per week. Periodic employee surveys rating the new system indicated a significant quality of work life improvement over the traditional system. Additional benefits realized were improved personnel scheduling flexibility and more efficient operations due to fewer shift turnovers.

## VALIDATION/QUALIFICATION

In order to validate the path the labs were taking for implementation, several design reviews were held. The reviews allowed the Executive Steering Committee and the consultant to evaluate adherence to the plan and review actions taken to attain Class "A" status. These reviews were held at approximately three month intervals during implementation.

The consultant graded the test labs using the ABCD checklist. This checklist is comprised of 35 overview/audit questions which allow the user and the consultant to measure the effectiveness of their MRP II operations. The checklist is comprised of four major areas, with four subsections for each area. The first area is Planning and Control. This section is comprised of Management, Demand, Supply and Product Development. It focuses on the planning and control processes of the business and the management of the continuous improvement process. This area requires strategic planning, business planning, sales and operations planning, financial planning, "what if" simulations, demand management, master production scheduling, supplier planning and control, material planning and control, shop floor control, capacity planning, and new product development processes to be established and maintained. These processes are the heart of MRP II. The second area is Data Management. This area is subdivided into Bills of Material, Routings, Inventory Records, and Change Control. This section verifies that processes are in place and ensures the data being used is correct. The third section is the Continuous Improvement process. It's divided into the areas of Education, Employee Involvement, One-Less-At-A-Time, and Partnerships. This section is aimed towards ensuring that the MRP II process is being continuously evaluated and improved. The final section is Performance Measurement. The

subsections are Planning and Control, Management, Quality, Service and Cost, and Velocity. This is a verification that measurements of performance are in place for all critical processes and a correction plan is established where necessary. A company which can answer yes to all 35 questions is considered Class "A" and operating in a closed loop MRP II mode, and uses the formal process to develop the plans which the company lives to. The DS&C Test Labs were able to answer yes to all 35 questions over an 18 month period and were awarded Class "A" status in July, 1991.

## CURRENT OPERATIONS

The Test Labs are currently operating as a Class "A" organization. The planning processes in place include Sales and Operations Planning (S&OP), Material Requirements Planning, and Capacity Planning/Shop Floor Control. Sales and Operations planning is defined as our ability to acquire and analyze the necessary data to accurately forecast manpower requirements. A current, accurate plan is crucial for effective resource allocation. The master production schedule provides forecasted contract work, referred to as direct charges, and in house projections for overhead expenditures, called indirect charges. All Independent Research and Development (IRADS), Capital funded facility modifications/upgrades and company funded engineering studies are considered direct charges. To convert schedules into manpower projections, the labs have been divided into work centers. A nominal charging rate is then assigned to each work center in man hour units. Summing work center man hours with planned overhead expenditures provides a comprehensive database for resource forecasting. The S&OP is updated monthly and spans five years. The first twelve months of the forecast are analyzed extensively. It is measured monthly with a goal of 80% -110% actual to plan.

Material Requirements Planning is being accomplished using Mac-Pac/D as the primary planning tool and various PC applications for detailed planning. The Master Schedule of all tests is maintained on Mac-Pac/D. This schedule is then broken into further detail depending on the complexity of the test. The ultimate goal is to perform all detailed planning on Mac-Pac/D. Due to software limitations, this is not currently feasible, and detailed planning is accomplished using PC packages such as MacProject II. The master schedule is updated on a weekly basis to reflect any changes or resolve any resource conflicts. Another area of material planning in the Test Labs is procurement of hardware. Mac-Pac/D is used to procure parts required for a specific test. Parts which are procured using overhead funds are processed using the manual system due to the inability of Mac-Pac/D to process overhead charge numbers.

Capacity planning, putting manpower and machine requirements against a task, is done using the master schedule from Mac-Pac/D, capacity reports from Mac-Pac/D, and assigning manpower requirements to the machine hours shown in the capacity reports. The coding in Mac-Pac/D has been arranged to output machine hours required to fulfill the master schedule. These hours are then converted to manhours by determining the number of people required and available for the test. There is a bi-weekly capacity meeting held between the operations lead, the master scheduler, and the individual test engineers to determine which tests will be running, capacity required for each test, and resolve capacity problems.

The actual execution phase of the process is recorded using a combination of systems. The technician will record the hours spent on a task using a timecard which is then input into an accounting database at the end of each week. This database allows the engineer to track budgets and maintain costs. When a test is completed, the responsible engineer closes out the order on Mac-Pac/D, produces a test summary, completes a budget analysis, and compiles all the pertinent information in a test folder.

Material control and inventory accuracy are critical to effective test planning. The laboratory inventory has been grouped into three general categories, test equipment, materiel required to fabricate test fixtures and test controls, and overhead supplies and spares. Test equipment is currently controlled with the company's Equipment Accountability System (EAS). This system schedules all equipment calibration and repair. The Test Engineer uses this automated system to ensure timely calibration and equipment availability. Materiel used to build test fixtures and controls (customer owned) is controlled using laboratory satellite stockrooms. These stockrooms are rigidly controlled, inventoried monthly, and must meet 95% accuracy standards. After fixtures have been fabricated, they are assigned a part number and controlled using the EAS system described above. Overhead supplies and spares are controlled with an in-house inventory system. Each test engineer utilizes



these systems to ensure timely delivery and availability of test tools, fixtures and equipment.

The DS&C Test Labs currently take 28 performance measurements called metrics. These measurements range from schedule accuracy, fixture design accuracy, test bill of material accuracy, inventory accuracy and requirements received on time. These measures are used to identify problem areas. The Labs then meet with their customers and suppliers each month to work a resolution plan for problem areas. This allows open communication and encourages ownership of each process. Metrics are also reviewed on a regular basis to determine whether they are still measuring the right thing, and if not, to re-define the metric so that it is a valid measurement. It is critical that the metrics be changeable and valid.

## CONCLUSION

In today's defense environment, a TQM philosophy is required to win contracts. The DS&C Test Labs have embraced the TQM philosophy and become Class "A" in MRP II. They have also formed numerous HPWTs and continue to investigate continuous improvement in all processes. Lessons learned for other test organizations who wish to implement a TQM philosophy focusing on MRP II and HPWTs include the following. Implementation team members must be laboratory experts, otherwise valuable time will be lost to educating unfamiliar participants. It is also important to ensure that all levels of the organization are committed. A key concept of people empowerment states that individuals must own their process and be involved in the decisions affecting their process.

Without integration of all customers and suppliers, islands of TQM are created. This results in each organization having different philosophies, tools, and language. When each organization's formal process is different, the company as a whole will suffer. The implementation should emphasize the importance of selecting software and tools which are compatible to all users.

The keys to success of TQM are integration, participation and empowerment. The organization must make a commitment to the success from the start and be open to the changes that are required. There is nothing harder than change, yet nothing is more critical in today's environment.

## REFERENCES

1. Wallace, Thomas F. MRP II: Making It Happen. Essex Junction, Vermont: Oliver Wight Limited Publications, Inc., 1985.
2. Wight, Oliver W., Speaker The Applications of MRP - 9.2., Videocassette, Oliver Wight Video Publications, Inc., 1989. color sd., VHS, 30 min.
3. Wight, Oliver W. Manufacturing Resource Planning: The Five Day Class for Aerospace and Defense Companies. Essex Junction, Vermont: Oliver Wight Limited Publications, Inc., 1990.
4. Wight, Oliver W. Manufacturing Resource Planning: MRP II Unlocking America's Productivity Potential. Essex Junction, Vermont: Oliver Wight Limited Publications, Inc., 1981.
5. Goodard, Walter, et. al. The ABCD Checklist. Essex Junction, Vermont: Oliver Wight Limited Publications, Inc., 1988.

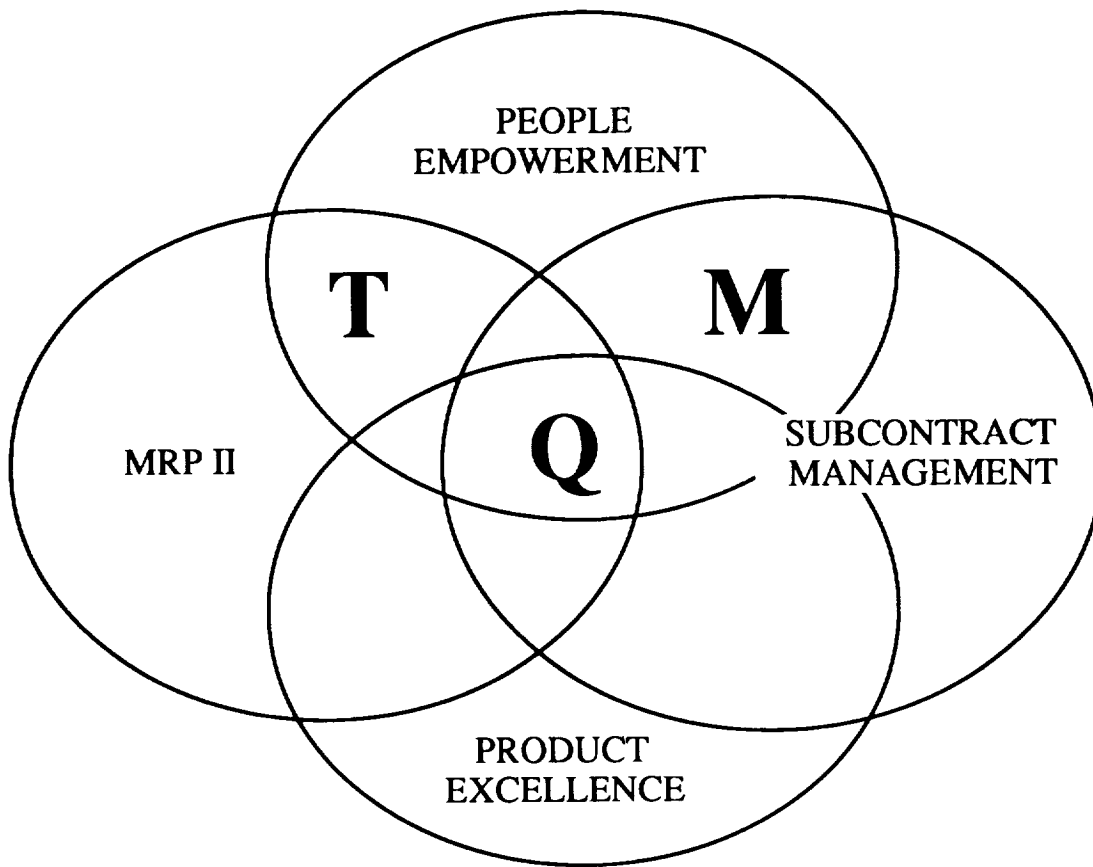


Figure 1 - TQM Primary Initiatives

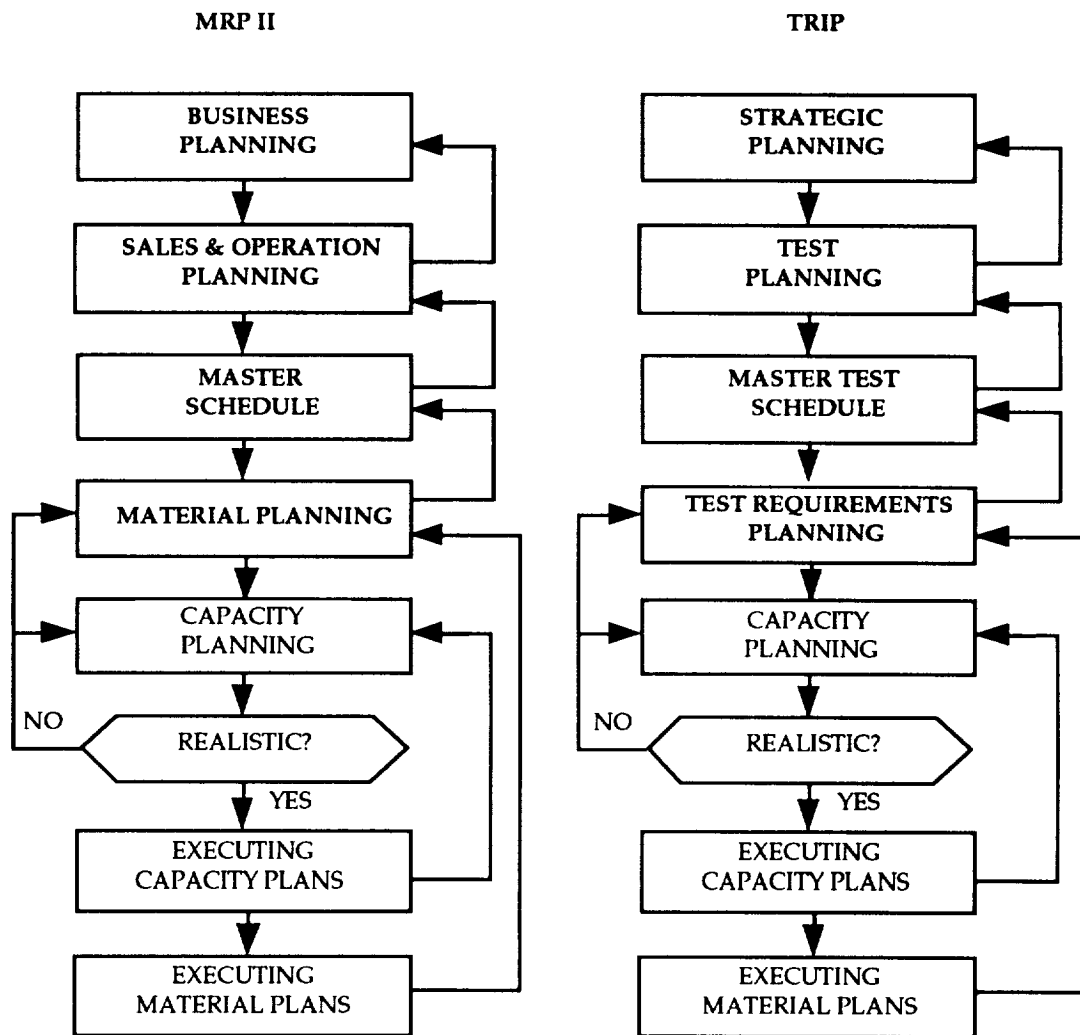


FIGURE 2 - MRPII VS. TEST RESOURCE INTEGRATED PLANNING (TRIP)

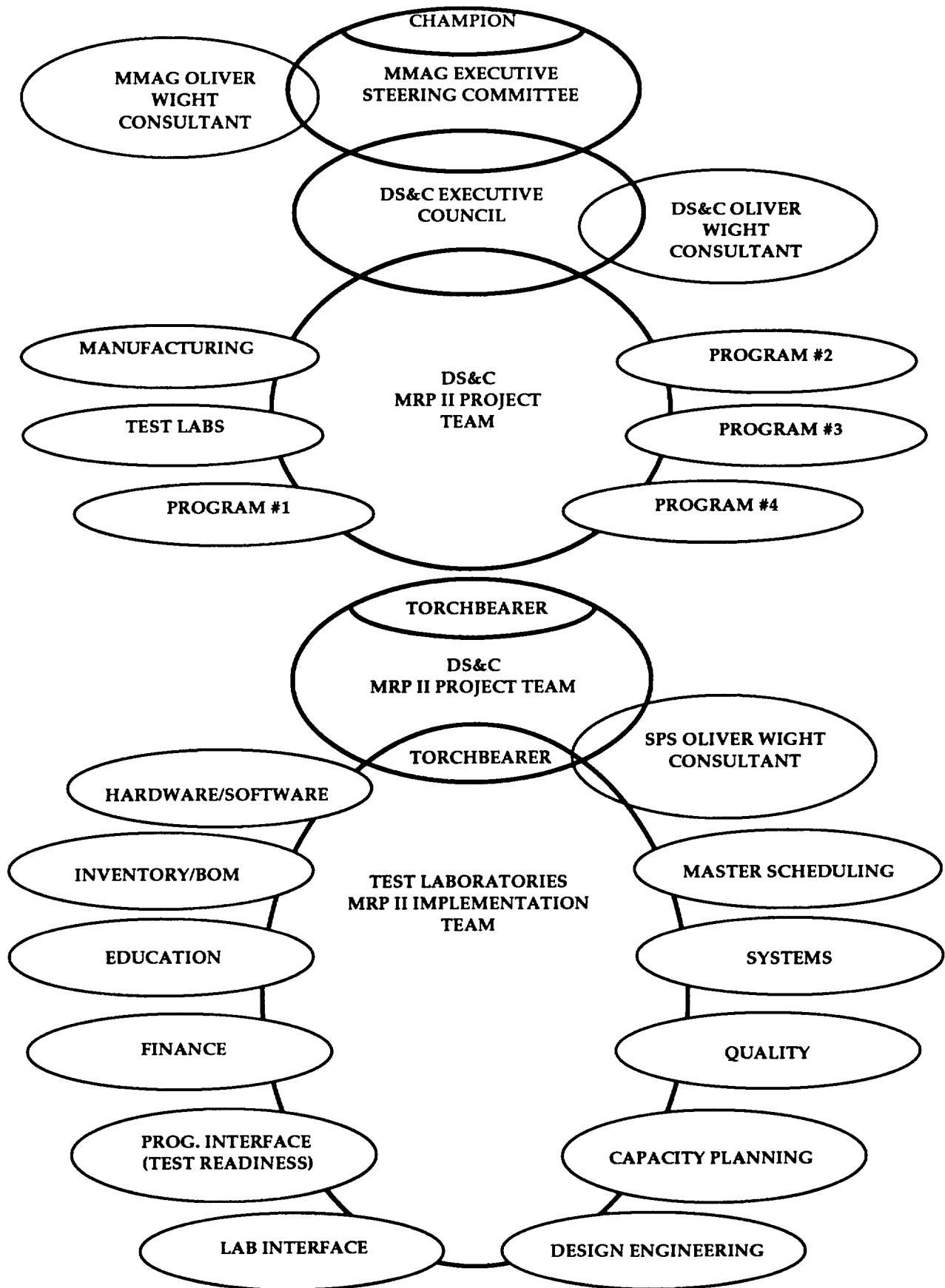


FIGURE 3 - SPACE SYSTEMS AND DS&C TEST LAB IMPLEMENTATION TEAMS

EACH SHIFT HAS 2 CREWS, 5 PERSONS PER CREW

DAY SHIFT (7AM - 7PM)



= CREW D1



= CREW D2

NIGHT SHIFT (7PM - 7AM)



= CREW N1



= CREW N2

CHART BELOW IS AN EXAMPLE OF A TWO WEEK WORK PERIOD

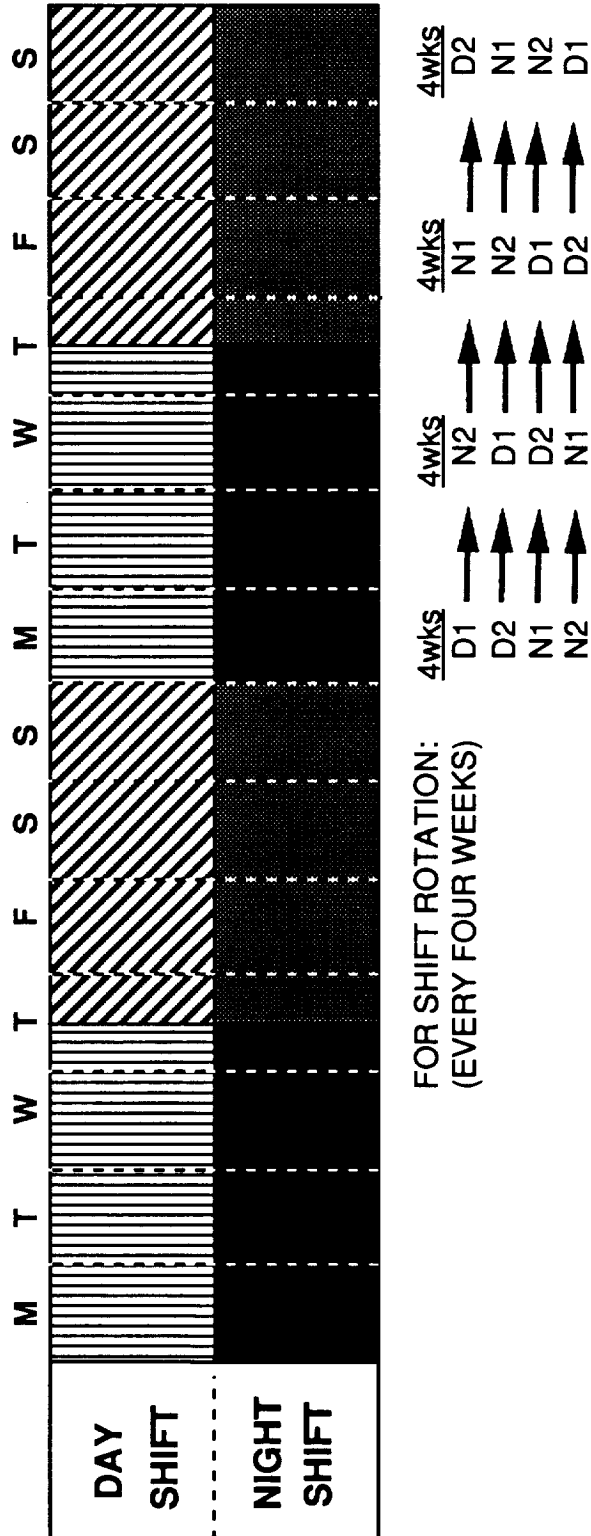


Figure 4 - 3.5 Day Workweek

**Acoustic and Thermal Testing of the  
Titan/Centaur Upper Stage**

**Mark Gehringer, Chris Gibson, Ron Janes**  
*General Dynamics Space Systems Division*

A new version of the Centaur high-energy upper stage is being produced by General Dynamics for the USAF/Martin Marietta Titan launch vehicle. The Titan/Centaur upper stage is subjected to consecutive acoustic and thermal testing in General Dynamics' Acoustic and Thermal Test Facility (ATTF). All data is acquired and processed digitally using the high-speed data acquisition system located in the ATTF. Processed data from over 250 sensors measuring acceleration, temperature, and sound pressure level is made available to the test team in minutes for use in making real-time test decisions. These tests represent the first consecutive large-scale environmental tests conducted on a complete, pressure stabilized, cryogenically tanked space launch vehicle. This paper describes some of the unique challenges involved in testing the Titan/Centaur and how these challenges were met using the ATTF.





## SYSTEM TEST APPROACH FOR THE SAX SATELLITE

*Pietro GIORDANO, Giacomo RAIMONDO, Piero MESSIDORO*

**Alenia Spazio S.p.A.**  
Turin - Italy

### ABSTRACT

SAX satellite verification is based on a protoflight approach, in which only one system model is realized at flight standard level, taking into account the utilization of hardware already qualified for other space programs and the necessity to respect the schedule constraints for a scientific objective. In any case, this approach was tailored with some deviations in order to reduce risks inherent such a choice.

The protoflight approach was also pursued at subsystem/unit level in particular for those subsystems and units considered critical from the schedule point of view. Payload Instruments followed the same approach but complete spare units were developed to reduce the risks associated with such an approach.

The paper will deal first with the description of the model philosophy and then, at satellite level, it will present the testing approach and rationale for each model. Finally, a brief description of each test will be given, highlighting objectives, methodologies and test configurations. Moreover, for the major tests, problems encountered and solutions applied in establishing a correct approach are described.

### INTRODUCTION

SAX is a satellite for X-Ray Astronomy. It is a major element of the overall basic Science Program of the Italian Space Agency (ASI) and is being developed with the contribution of the Netherlands Agency for Aerospace Programs (NIVR).

The scientific objectives of SAX, see Ref. 1, are to carry out systematic and comprehensive observations of celestial X-Ray sources over the 0.1 + 300 KeV energy range with special emphasis on spectral and timing measurements.

The satellite will also monitor the X-Ray sky to investigate long-term source variability and to permit the localization and study of X-Ray transients.

Alenia Spazio is developing the satellite that is intended for launch at the end of 1993 (December) into a low (600 Km), near-equatorial orbit (inclination lower than 5 degrees) and with a lifetime of 24 months.

SAX, shown in Figure 1, is a three axis stabilized satellite with a total mass of 1400 kg and about 3.5 m high for 2.7 m of diameter. Power sources are two Ni-Cd batteries (30 Ah) during eclipse and two non sun-tracking deployable solar arrays and one body mounted solar panel during sun viewing. The maximum Telemetry bit rate is 917 KBPS on the stored data channel.

SAX uses on-board magnetometers for the AOCS that is utilized to align the Satellite with the Earth's magnetic field. The error allowed in the pointing accuracy due to the equipment magnetostatic emissions is of 5 deg.

The satellite can be subdivided into two main modules (Figure 2):

- Spacecraft (S/C) Module
- Payload (P/L) Module

The S/C Module is composed of a Service Module which accommodates the service subsystems like Power, Data Handling, Attitude Control, Reaction Control Subsystem and Telemetry & Telecommand and the Science Instrument electronic units. The Service Module is an aluminum sandwich panel structure with an inside corrugated cone interfacing with the Launch Vehicle (Atlas Centaur). Shear sandwich panels connecting the internal cone and the external panels complete the configuration giving the suitable stiffness to the Service Module.

The Payload Module is composed of a Payload support structure and a shade structure. The P/L support structure that accommodates the five Science Instruments consists of a carbon fiber optical bench and concentrator tubes. The shade structure is the Science Instrument enclosure and ensures the required fields of view for Instruments and AOCS sensors.

## MODEL PHILOSOPHY

The overall Model philosophy is shown in Figure 3. At system level the model philosophy is basically a two model approach: Structural/Thermal Model and Protoflight Model.

The **Structural/Thermal Model** consists of a flight standard structure equipped with dummy units having representative mass and thermal power loading. Some units, like RCS valves and tank, are also built up in such a way as to permit the passage of a tracing gas for leakage testing the satellite. Harness subsystem mass is represented only in areas where the unit density is low and where its mass is meaningful. Thermal hardware will be flight standard as well but it will be partially integrated, mainly for blankets and heaters.

With the above configuration the Model will be subjected to a structural qualification test campaign. Then the Model will be refurbished into a Thermal configuration with the integration of the remaining thermal hardware and shadowing panels and will undergo Thermal Testing. This model will be used to attain the maximum confidence in the mechanical and thermal behaviour of the satellite.

Furthermore, the STM Model will be used to verify the validity of mechanical integration procedures, Mechanical Ground Support Equipment (MGSE), and for personnel training.

The **S/C Engineering Model** consists of a mock-up structure equipped with Engineering (EM) or Engineering/Qualification (EQM) Models of service subsystems. It will be used for a partial mechanical and electrical integration procedure validation, Units/Subsystems interface compatibility and performance (where possible) and Electrical Ground Support Equipment (EGSE) interface and performance validation. Before the above activities, the mock-up is used also to develop the harness subsystem routing.

The **Protoflight Model**, built to flight standard level, will undergo a complete acceptance test campaign (thermal/structural/electrical). A launcher adaptor interface test will be performed very early in the Protoflight Model activities at the end of the flight structure manufacturing. Moreover the Protoflight Model will be connected to the Ground Station in order to perform a data and frequency Compatibility Test. Such test, in a preliminary way, will also be performed as off line activity with S/C EM using a satellite Suitcase.

Even if this paper deals basically with the System test approach, it is worth giving information about testing at lower level in order to understand the choice made at system level better.

Spacecraft units following the EQM/FM approach are subjected to a complete qualification on EQM in terms of environmental, EMC, functional and performance tests while FM models are only tested for workmanship evaluation.

Some units following the EM/PFM approach are subjected to a pre-qualification test campaign which includes vibration, thermal testing in ambient, conducted EMC and functional testing. This in order to get as much confidence as possible on the performances of the units decreasing the risk of finding problems at PFM level, which are subjected to full qualification including environmental, EMC, performance testing. Duration of environmental testing is reduced in order not to overstress electronic units. Partial or complete development models are used, case by case, in order to increase confidence in the design.

P/L experiments follow a pure protoflight approach where only a model is built up to be qualified, accepted and flown.

Risks associated with this approach are reduced firstly by using a structural/thermal model of high representativeness, as Science Instruments are constituted by non-standard material and new processes, and secondly by having a complete spare Instrument to be used in case of PFM failure at any time.

Structural/thermal models are subjected to full vibration tests and in some cases also to thermal tests. Spares are subjected to full acceptance tests for workmanship investigation. Also development models for the most critical components and subassemblies are manufactured and tested.

PFM models, as per S/C PFM units, are subjected to protoflight testing including environmental, with limited duration, functional/performance, EMC testing and scientific calibration. Details on lower level test approach can be found in Ref. 2 and 3.

## SYSTEM TEST APPROACH

As summarized in the model philosophy, two models at system level are used to accomplish qualification and flight readiness. Moreover, other partial models are used including a partial EM model, limited to the S/C and with a mock-up structure, a suitcase and a Software Validation Facility (SVF). Each model has a well-defined aim whose rationale is herebelow described.

The **Structural/Thermal Model** is used for the following purposes:

- \* to qualify the structure subsystem and the thermal control subsystem
- \* to qualify the RCS subsystem, not testable at subsystem level, and verify leakage
- \* to validate the mathematical models of structure and thermal control subsystems
- \* to provide confirmation of unit environments and check amplification factors
- \* to verify alignment stability of the items of interest
- \* to verify functionality of mechanisms at system level
- \* to develop and amend procedures
- \* to check interfaces and performances of MGSE.

The **S/C Electrical Model**, with a mock-up structure, equipped with S/C electronic units, has the goal to:

- \* verify the S/C electrical design
- \* verify the electrical interfaces including the ones toward the P/L
- \* validate the on-board software
- \* develop and commission the test SW
- \* verify the conducted EMC performances
- \* verify the interfaces and the performances of the EGSE
- \* develop and amend the procedures
- \* familiarize and train the personnel.

In the process of increasing confidence in satellite performances, two other development tools are used:

- \* a **Suitcase** which performs a preliminary data and frequency compatibility test with the Ground Station
- \* a **Software Validation Facility** which performs compatibility tests among the on-board processors to check communication protocols, timing and signal interfaces.

For this last scope, a **FUnctional MOdel (FUMO)** of each processor was requested to subcontractors. The Suitcase is constituted by a Transponder, a Telecommand Decoding module, a Telemetry generation and coding module and a power supply module. The above models and tools led to a Protoflight Model with a minimum risk.

The **Protoflight Model** has the goal:

- \* to demonstrate the workmanship of the satellite and to gather the data required to ensure flight worthiness
- \* to demonstrate that no functional degradation will affect the required performance during its life
- \* to show that all performances are compliant with the contractual requirements
- \* to demonstrate the flight readiness.

## TEST PROGRAM

The System Test program for SAX was accomplished by performing the tests outlined in the preceeding paragraphs and in compliance with the aim of each model. All major tests, except the centrifuge, will be performed at the ESA/ESTEC (European Space Technology Center) facility. The following test program will be performed, see Figure 4:

- \* Mass Properties Measurement and Balance Test (STM & PFM)
- \* Modal Survey Test (STM)
- \* Centrifuge Test (STM)
- \* Acoustic Test (STM & PFM)
- \* Sine and Random Vibration Tests (STM)
- \* Thermal Balance Test (STM)
- \* Alignment measurement (STM & PFM)
- \* Leak Test (STM & PFM)
- \* Deployment/Release Tests (STM & PFM)
- \* Electromagnetic Compatibility (PFM)
- \* DC Magnetic Field Measurement (PFM)
- \* System Validation Test (PFM)

Major test activities involving critical methodologies are described herein.

- **Mass Property Measurements** will be carried out with the objective to measure the physical characteristics (mass, center of gravity and moments of inertia) and balance the system statically and dynamically. Details are contained in Ref. 4.
- **Modal Survey** will be performed at Alenia Spazio premises, connecting the satellite STM through an interface flange to a seismic mass in a fixed-free boundary condition. The Modal Survey test will yield the definition of Eigenfrequencies, Eigenvectors, Modal Damping Factors and Generalized Masses in order to correlate the Finite Element Model (FEM) and refine it if necessary. First of all, a Mode Identification Process will start applying random forces with different input levels at each foreseen location/orientation to check which one adequately excites primary modes up to 100 Hz. Levels will be varied until a satisfactory level to collect data is established. Moreover linearity checks at the above locations, using random excitations, and reciprocity checks will be performed. Then, with the multipoint random excitation technique, the mode characteristic measurement will be performed. Finally, the analysis of the acquired data will be performed and the individual modal parameters will be extracted by using the Polyreference Modal Parameter Estimation Method. This will permit the test data validation/correlation. Details are contained in Ref. 5.
- **The Acceleration Test (Centrifuge)** will be performed at Cesta premises in Bordeaux. This shall demonstrate the structure's capability to survive the quasi-static loads deriving from the launcher. The satellite will be installed into a centrifuge nacelle by means of an inclined adaptor to simulate the resulting load direction from axial and lateral dimensioning flight loads, acting simultaneously. The Nacelle is a cylindrical module attached to an arm rotating around an axis perpendicular to the ground. The choice of the centrifuge method for the static test was dictated by the necessity to minimize time consumption and optimize both the quality of the results and the hardware's integrity. In order to ensure a good coverage of the qualification load distribution, two test cases, which correspond to two different configurations (see Figure 5), will be tested, anyway saving time with respect to a traditional whiffle tree method. One configuration is with the complete satellite and the other without the shade structure to get a greater inclination inside the nacelle. Because of the limited tilting angle, the correct lateral loads could not be reached on each structural part. They will be compensated by increasing the axial loads and introducing dedicated compensation masses. In the centrifuge test, the static loads simulating the design ones can be applied continuously to the whole structure, reproducing the exact values in the areas of interest (Interface Ring and Optical Bench Interface) and allowing an "average loading" of the other parts (not exactly corresponding to the real situation). On the contrary, with the traditional static test it is possible to apply the exact load only to a limited number of points, without loading the whole structure. Ref. 6 contains the test requirements while the rationale on the establishing the correct configurations is given in Ref. 7.
- **The Acoustic Test** will be performed to demonstrate the capability of the satellite to withstand acoustic noise environment during launch phase. The satellite will be installed onto a suitable jig supported by elastic devices in order to avoid coupling with the ground. Adequate instrumentation will be placed internally and all around the satellite to measure the sound pressure field level. Before starting with the satellite testing, a reverberant chamber equalization will be performed, both at low level and at high level. Equalization performed without the satellite will allow to set up the acoustic test spectrum and to confirm the ability of the facility to meet the requirements. Details are contained in Ref. 8.
- **The Vibration Tests** consist of sine and random excitations at low and high frequencies respectively of the satellite STM (Ref. 9). They will verify the capability of structural hardware to withstand dynamic loads due to lift-off. They will not be repeated on the Protoflight Model because random are covered quite enough by the acoustic test and sine due to the particular approach given at unit level. In fact most of the flight units are already subjected to sine vibration and the interfaces between units and structure are verified at STM level with the dummy interfaces being equal to the ones of the flight units. Details on this rationale are given in Ref. 10.
- **The Thermal Balance test** is performed on the STM model to demonstrate the validity of Thermal Control S/S design and to validate the Thermal Mathematical Model, which, after correlation with test results, will be used for flight predictions. Analysis has shown the worst case conditions to be the operative ones. So transfer phase will not be tested at all. The satellite will be placed on the Attitude Simulator of the Large Space Simulator (LSS) of ESTEC, via the Thermal Test Support Rig. As SAX is a low orbit satellite, influence of albedo and infrared Earth emission will be simulated through dedicated radiative plates installed all around the S/L. They shall be supported by a removable frame fixed to the Thermal Test Support Rig in order to follow the S/L in all the foreseen test configurations. Cases tested are the Winter Solstice (+30° Sun Aspect Angle (SAA)) which is the worst hot case for P/L, -30° SAA Winter Solstice as the worst hot case for Service Module, -45° SAA Summer Solstice as worst cold case for all the satellite, Summer Solstice Eclipse (transient), and a calibration case (see Figure 6). During the test, power supplies will be used to feed the Thermal Control S/S, the dummy units and the guard heaters. Details are contained in Ref. 11.

- The **Thermal Vacuum** test will be performed at Protoflight level, again in LSS. Its objective is to demonstrate the ability of the satellite to meet operation requirements in the space environment and also to detect any material, process and workmanship defects that could occur under thermal vacuum and thermal stress conditions. The test will consist of a cycle of 12 hrs at hot and cold temperature extremes in order to detect failures that become evident early in the test before the more time-consuming soaks. Then 72hr hot/cold soaks will be performed to find out weaknesses that become evident only during prolonged periods of temperature and vacuum conditions. Another 12hr hot/cold cycle, in order to find out degradation that may have occurred in the preceding soaks, will be performed. At the end a final hot/cold exposure will be performed and used to correlate again and refine if necessary the TMM. Stabilization will normally be reached when temperatures of all thermocouples do not vary more than 3°/hr, but during of the last exposure, a stabilization of 1°/8 hrs will be considered because of the correlation purpose with TMM. Temperature transient will be adjusted to the performance of the most sensitive components which are the P/L instruments. In fact, a strong constraint is their thermal gradient which can not override the value of 1°/hr.
- The **Electromagnetic Compatibility** test performed at Protoflight level will be conducted to verify the EMC margin of the system and the compatibility with the Launcher. Verification of the satellite will investigate integrated System EMC aspects, support any System EMC analysis, and provide final closure to any deviations.  
The EMC test concerns the conducted and radiated tests in E and H fields. At system level the ESD test will not be performed due to the low orbit of SAX.  
The conducted tests - conducted emission common mode (CECM) and the conducted susceptibility common mode (CSCM) - will be performed at Alenia Spazio premises because it is not necessary to perform the tests in an anechoic room.

The CECM will measure the current emission appearing on signal lines to provide a baseline threshold to be used for margin susceptibility verification.

The CSCM will be performed by injecting interference, 6 dB higher than emission levels, in the wire bundles, in the same position of the conducted tests. The radiated tests - radiated emission E-field (RE-E), radiated susceptibility E-field (RS-E) and radiated susceptibility H-field (RS-H) - will be performed at the ESA/ESTEC anechoic facility.

The Satellite will be installed in the shielded anechoic chamber minimizing as much as possible hardline connections towards EGSE in order to ensure satellite simulation and monitoring.

The RE-E field will be performed to verify that the emission levels are under the required levels in order to assess the compatibility with the launcher.

The RS-E field will be performed by radiating electrical fields into the satellite to demonstrate both the internal compatibility and the Launcher compatibility. During the susceptibility tests it will be verified that the satellite will not exhibit malfunctions.

RS-H-field will be carried out to verify that no malfunction occurs in the satellite when exposed to the radiated magnetic fields.

The satellite will operate in the relevant operation modes and linked to the EGSE via the RF anechoic cap or umbilical hardline during all the above tests. Details are contained in Ref. 12.

- The **Magnetic Cleanliness** of the SAX satellite has been defined with the objective to minimize the magnetic contamination of the Satellite and to minimize the residual magnetic field, in particular in close proximity to the AOCs magnetometer sensor. The DC H-field radiated emission of the SAX S/L measured at the magnetometer location shall not exceed 125 dBpT.

The verification of the requirement will be carried out both with a test at PFM level and with a dedicated analysis of the Solar array's contribution to the overall magnetic vector. The test will be performed at Alenia Spazio's facility, that does not permit to have magnetic cleanliness; i.e., Earth magnetic field compensation. For this reason, the test at System level will be performed with a subtraction technique in two steps. First, the magnetostatic field will be measured at S/L magnetometer location, with a test magnetometer that will have a resolution at least an order better than the measurement value.

The Satellite will be completely integrated except for the Solar Array and in "on" condition. In this case, the measured B (tot) includes the effects of: the Earth's magnetic field, the stray and remnant fields generated by the Satellite and the environmental field. Second, the magnetostatic field due to the Earth's magnetic field only will be measured, with the same test magnetometer and in the same location as in the first step. In this case we get the Earth's magnetic field and the environmental field. Subtracting the value measured in the two steps above we get the actual field value to be verified.

The above approach is based on the following assumptions.

The Earth's magnetostatic field is identical during steps a. and b. of the test. From an engineering point of view, this is equivalent to having the same position of the test magnetometer in the two steps a. and b.. In order to reach this, an alignment activity will be performed. Moreover this is equivalent to having possible local fluctuations of the Earth's magnetic field that are negligible with respect to the requirement to test.

The above measurements imply the linearity of the test magnetometer in the range of interest.

In order to avoid an effect of the Integration Dolly on the magnetic ambient emissions, because the structural elements are build up of magnetic materials, a dedicated non-magnetic dolly will be utilized.

- The **System Validation Test (SVT)** between SAX and the Space and Ground Segments will be performed with the main objectives of:
  - confirming the Operative Control Center's (OCC) capability to support all functions necessary for conducting the Mission Operations;
  - validating of the complete communication chain between the OCC and the Satellite.

This activity will be carried out through real telecommand from OCC to Satellite and by processing the actual Satellite telemetry at the OCC. The SVT will be performed in two different phases called SVT1 and SVT2, this both to reach a validation with a Ground Station as soon as possible and to verify after the environmental tests that the compatibility is still valid. The SVT1 will be performed at ALENIA premises after the functional tests on SAX: ISST and IST and the SVT2 will be performed at ESA/ESTEC premises as the last activity, before transporting SAX to the Launch pad.

To perform the SVT1, part of the Ground Segment will be moved, with dedicated shelter, in Alenia, and in particular this will be the TT&C Section and the Station Computer Section (STC).

During the test the S/L will be under the control of the EGSE through hardwired umbilical connection and the Ground Station communication to/from the Satellite will be performed through the RF S-Band link. The SVT2 will be carried out with the same configuration as for the SVT1. Moreover, a back-up test configuration will be carried out in case of the unavailability of the Ground Station at ESTEC due to schedule problems. This back-up foresees a simplified test set-up with only a few modules to allow communication with the Ground Station via RF.

This test is previously performed using the Suitcase linked to the S-Band station and to the OCC computer. The Suitcase will simulate the telemetry generation from the satellite and is capable of reacting to any command sent by the OCC computer.

## CONCLUSIONS

The SAX satellite development and qualification approach was conceived with the objective of minimizing the schedule and the total project costs while maintaining program performances. It was established first by investigating the mission, in order to define the present or induced environments, and then by defining the project requirements to be verified.

From the above investigation, and considering the constraints imposed by the Customer, a Protoflight approach, with some tailored deviations, was derived. An accurate balance between project risks and costs is reflected in the chosen protoflight model philosophy.

At system level, two full models are used:

- a **Structural-Thermal model (STM)** in order to qualify the structure and thermal control design and
- a **Protoflight model (PFM)** to confirm requirement performances and to give evidence of the flight readiness.

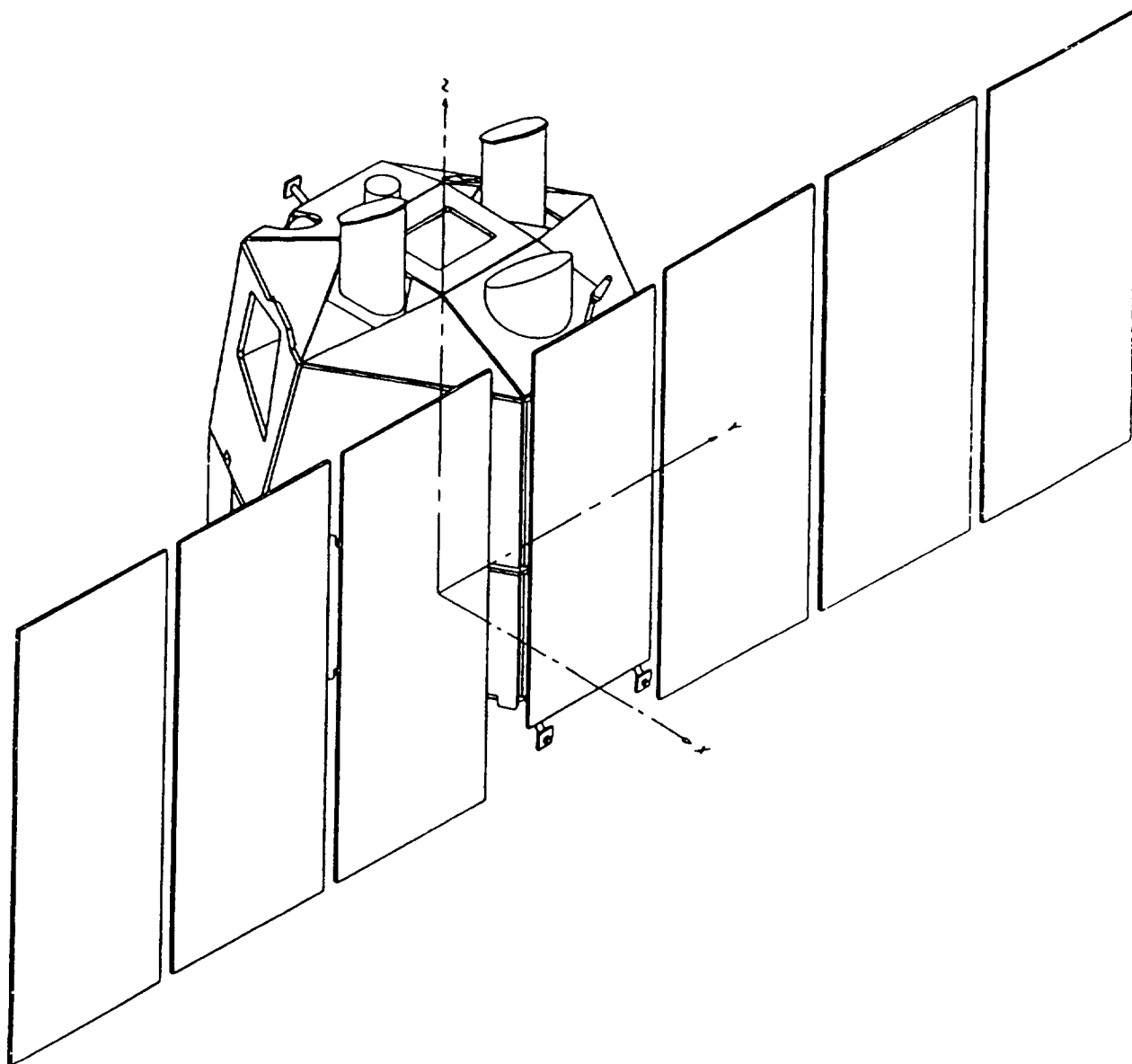
Moreover, a partial mock-up, limited to the Spacecraft part, was used to verify electrical interfaces and performances and to validate EGSE interfaces before its use at PFM level.

At subsystem/unit level, only critical schedule-wise units were developed with protoflight approach.

Payload instruments used a pure Protoflight approach, that is, only a PFM unit was developed, tested and delivered for actual flight. The risk deriving from the above approach was considered and complete spare units were developed.

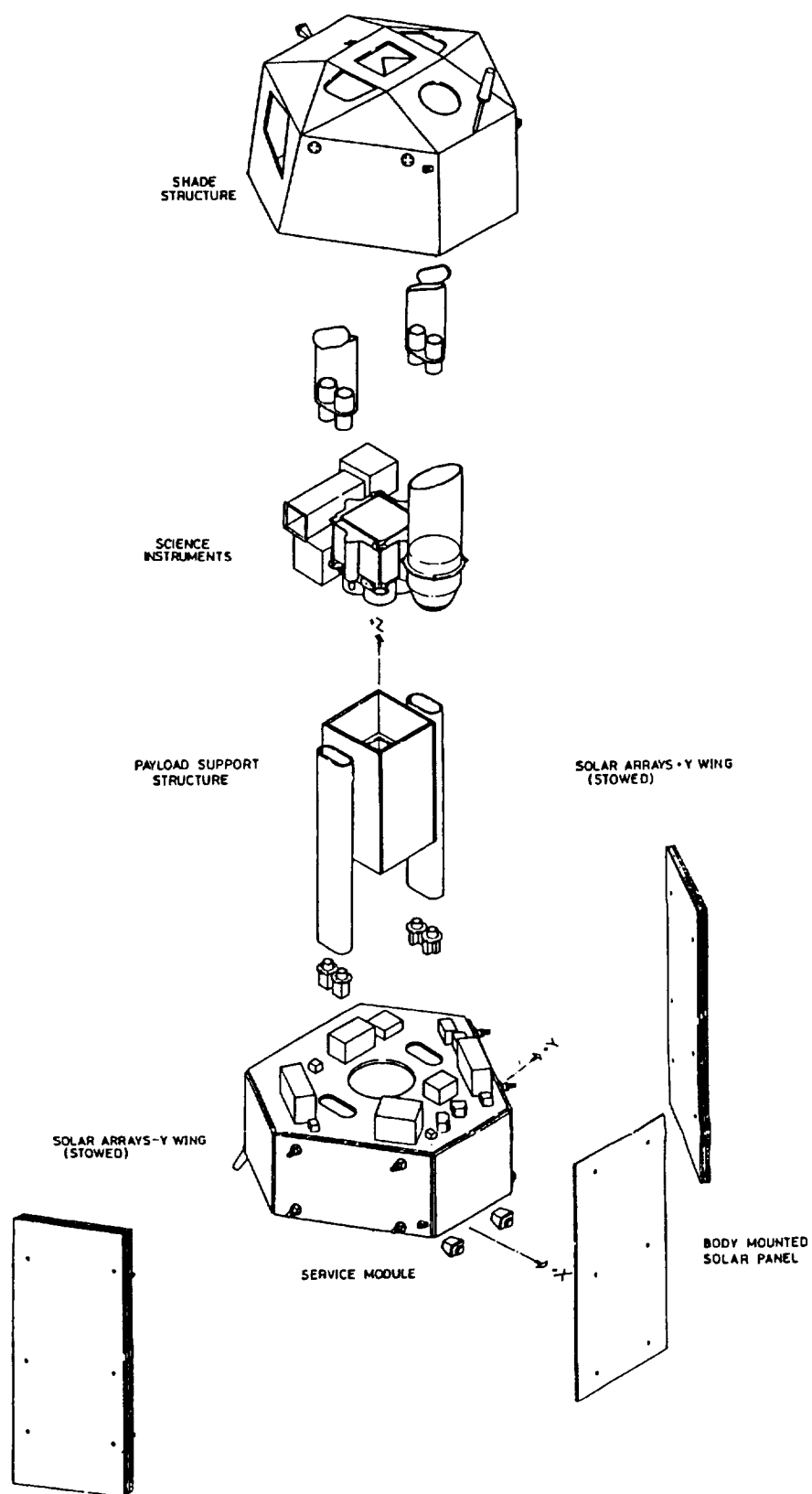
## REFERENCES

1. **P. Attinà** - *Satellite for X-Ray Astronomy (SAX)*, Brighton, 31st IAF
2. **P. Giordano** - *Test requirement specification*, Alenia Spazio Document, SX-SR-AI-001
3. **P. Giordano** - *Protoflight testing approach for SAX Science Instruments*, Alenia Spazio Document, SX-TN-AI-202
4. **G. Raimondo, P. Giordano** - *Mass Properties and Balance Test Specification*, Alenia Spazio Document, SX-SP-AI-015
5. **G. Raimondo, P. Giordano** - *Modal Survey Test Specification*, Alenia Spazio Document, SX-SP-AI-011
6. **G. Raimondo, P. Giordano** - *STM Centrifuge Test Specification*, Alenia Spazio Document, SX-SP-AI-012
7. **G. Raimondo, P. Giordano** - *First Assessment of potential STM Centrifuge Test Cases*, Alenia Spazio Document, SX-TN-AI-218
8. **G. Raimondo, P. Giordano** - *Acoustic Test Specification*, Alenia Spazio Document, SX-SP-AI-014
9. **G. Raimondo, P. Giordano** - *Vibration Test Specification*, Alenia Spazio Document, SX-SP-AI-013
10. **G. Raimondo, P. Giordano** - *Technical Rationale for deletion of the Sine Vibration Test on S/L PFM*, Alenia Spazio Document, SX-TN-AI-203
11. **G. Raimondo, P. Giordano** - *STM Thermal Balance Test Specification*, Alenia Spazio Document, SX-SP-AI-016
- 12.. **V. Ancona, P. Giordano** - *EMC Test Specification*, Alenia Spazio Document, SX-SP-AI-019



**Fig. 1 - Satellite Overview**





**Fig. 2 - SAX Satellite Configuration**

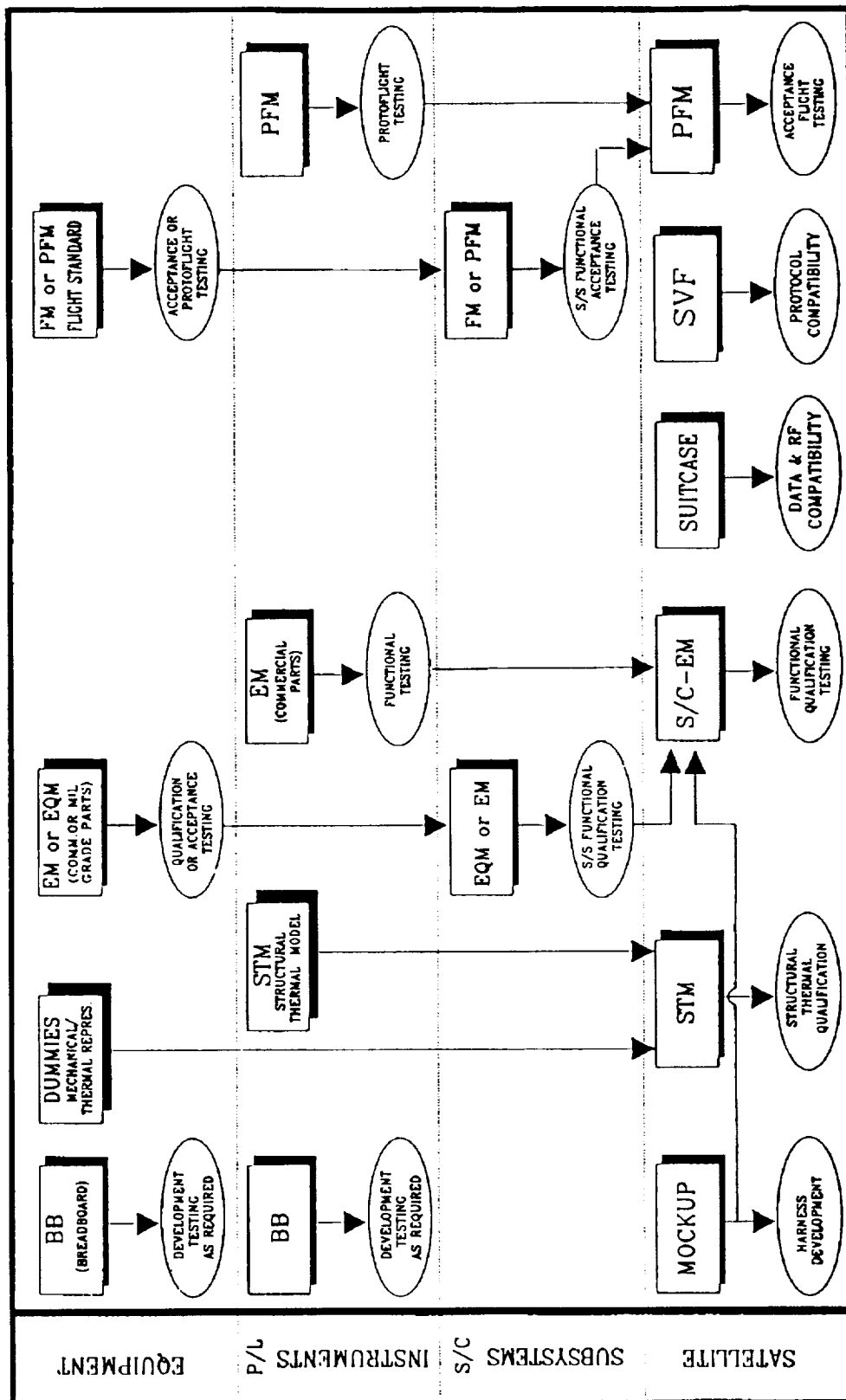


Fig. 3 - Model Philosophy

TYPE OF TEST	TEST DESCRIPTION	SAX SATELLITE MODELS		
		STM	EM (S/C)	PFM
PHYSICAL PROPERTIES	Mass Mol/CoG Balancing	X	--	X
		X	--	X
		X	--	X
STRUCTURAL TESTS	Modal Survey Acceleration Vibration Acoustic	X	--	--
		X	--	--
		X	--	--
		X	--	X
THERMAL TESTS	Thermal Balance Thermal Vacuum	X	--	--
		--	--	X
ALIGNMENTS		X	--	X
COMPATIBILITY	EMC/EMI	--	--	X
LEAK TESTS		X	--	X
FUNCTIONAL PERFORMANCE TESTS	ISST IST/ISC	--	X	X
		--	--	X
DEPLOYMENT/RELEASE	Solar Array C/S Shutter	X	--	X
		X	--	X
SPECIAL TESTS	P/L Calibration Ground Segment Comp. Match Mate Test Magnetic Field Measurement	--	--	X
		--	--	X
		--	--	X
		--	--	X

Fig. 4 - Test Program

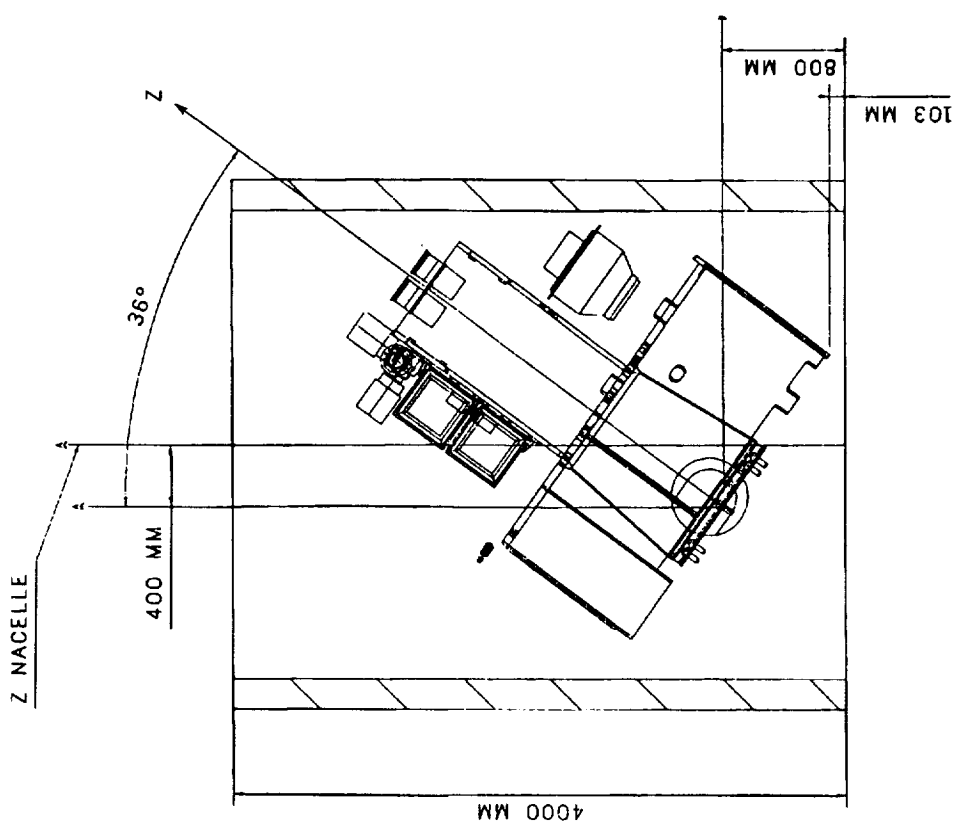
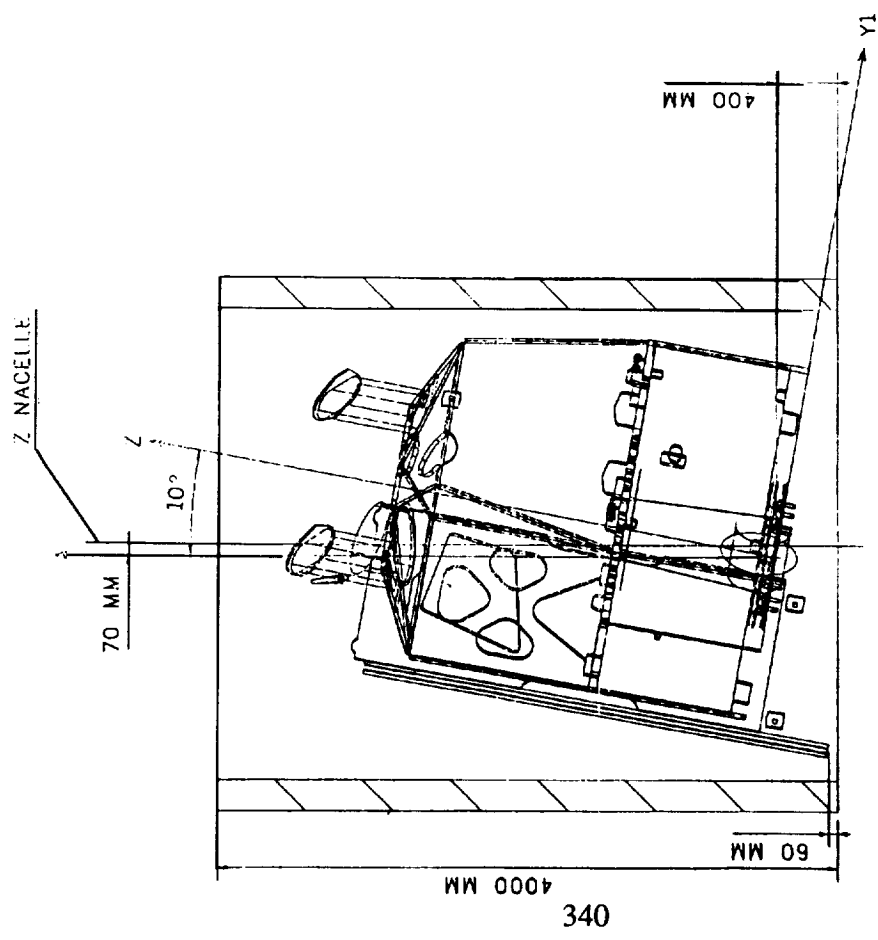


Fig. 5 - Centrifuge Test Configurations


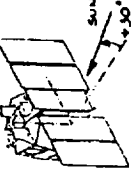
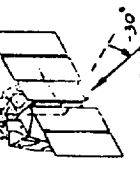

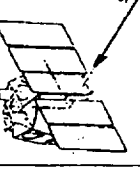

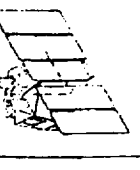
Task No	1	2	3	4	5	6	7
Phase Description	Pump Down & Cooling Down	+ 30° SAA Winter Solstice	- 30° SAA Winter Solstice	+/- 45° SAA Summer Solstice	Summer Solstice Eclipse	Calibration Case	Chamber Recovery
Test Case	Reaching Test Cond.	Steady State	Steady States	Steady State	Transient	Steady State	Reaching Ambient C
Duration	12 Hrs	24 Hrs	24 Hrs	24 Hrs	5 Hrs	24 Hrs	12 Hrs
Spacecraft Orientation and Attitude							
Spin Rate	Fixed						
Solar Intensity	from 0 to 950 W/m <sup>2</sup>	950 W/m <sup>2</sup>	950 W/m <sup>2</sup>	880 W/m <sup>2</sup>	0 - 1320 W/m <sup>2</sup>	0 W/m <sup>2</sup>	0 W/m <sup>2</sup>
Radiative Plates Power Dissipation	TBD	TBD	TBD	TBD	TBD	"	"
Chamber Vacuum	from ambient to 10 <sup>-5</sup> mbar	10 <sup>-5</sup> mbar or better					from 10 <sup>-5</sup> Torr to ambient
Shrouds Temp.	from ambient to 100° K	100° K					from 100° K to ambient
Comments		Hot Case for P/L	Hot Case for S/M	Cold Case for S/L	Verification of Transient Eclipse Performance		

Fig. 6 - Thermal Balance Test Cases



## OVERVIEW OF ENVIRONMENTAL TEST PLANS FOR SPACE STATION FREEDOM WORK PACKAGE 4

Tom J. Peterson  
Manager, Test Operations  
Rocketdyne Division, Rockwell International  
Electric Power System  
Space Station Freedom

### ABSTRACT

The generation and distribution of electric power for Space Station Freedom (SSF) is critical to the station's success. Work Package 4 (WP-04) has the responsibility for the design, development, test, and delivery of the Electric Power System (EPS) for the SSF. During launch, assembly, and operation, the EPS will be subjected to various environments. A test and verification approach has been developed to assure that the EPS will function in these environments. An overview of that test program is presented with emphasis on environmental testing of hardware.

Two key areas of the test program are highlighted in the overview. One area is the verification of the Solar Power Module (SPM) and associated cargo element hardware. This area includes detailing the plans for development and qualification testing of the SPM hardware. One series of tests, including modal and acoustic, has been completed on a development cargo element.

Another area highlighted is the acceptance testing of high-power Orbital Replacement Units (ORU). The environmental test equipment plans are presented and reviewed in light of an aggressive production rate, which delivers ORUs to the WP-04 and other Space Station Work Packages.

Through implementing the test program as outlined, the EPS hardware will be certified for flight and operation on the Space Station Freedom.

### INTRODUCTION

The detailed verification plans for testing the SSF EPS were developed during the initial proposal effort in 1987. Refinement of the plans has continued from that time and has been subjected to several architectural and configuration changes since. Through these modifications, hardware designs for every item has changed along with the functional requirements and schedules.

The latest change, called Restructure, initiated a major redesign of SSF to comply with congressional requirements. A Restructure Design Review (RDR) was held in

August 1991, which outlined all major requirement changes and gave approval to implement the Restructure changes.

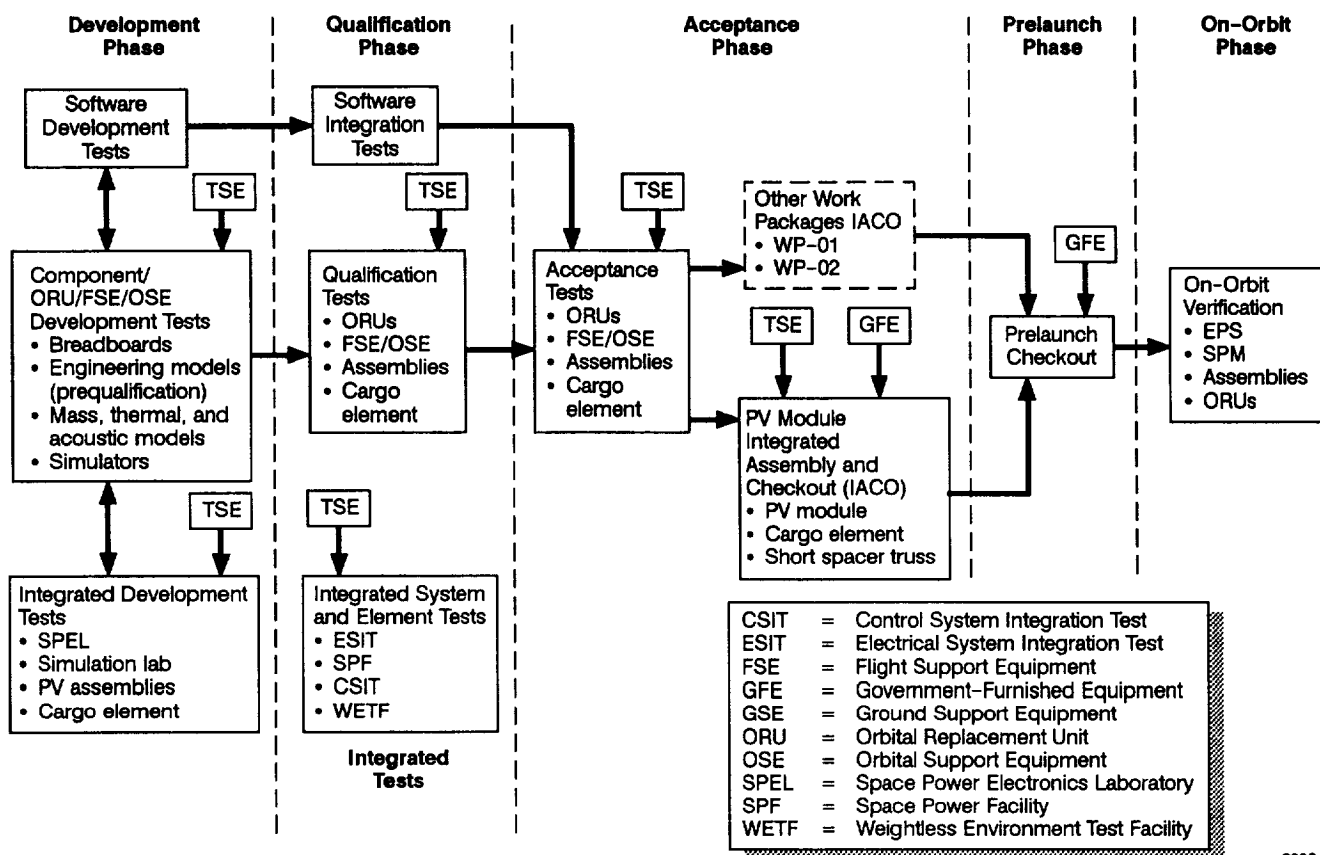
The intent of this paper is to present an overview of the WP-04 test and verification plans with emphasis on environmental testing. The particular environmental requirements invoked on WP-04 are specified in the WP-04 Technical Requirements Document, LeRC-SS-0001. This document includes a section on test requirements (Appendix C) and invokes compliance with MIL-STD-1540B, Test Requirements for Space Vehicles; SSP 30467, Master Verification Requirements Documents, Volumes 1 and 2; and NSTS 07700J, Space Shuttle System Payload Accommodations Handbook, Volume 14.

### BASIC PHILOSOPHY FOR TESTING

The basic building block of the EPS is the ORU. Due to the Station's anticipated 30-year life, the current design philosophy is to provide a configuration that could be built, serviced, and repaired easily and inexpensively. The concept of ORUs comes from the aircraft industry where Line Replaceable Units (LRU) are commonly used. The EPS utilizes the ORU for items such as electronics, batteries, pumps, radiators, solar arrays, cables, and gimbals.

The WP-04 verification planning utilizes the ORU as the basic element for the conduct of qualification and acceptance testing. The ORU is qualified so it can be replaced in a system or assembly meeting a set of common requirements and not modified as a one-of-a-kind item for a unique configuration. Where a configuration or assembly of ORUs are necessary to meet a higher level of operating requirements, an assembly test at the higher level for qualification and acceptance has been identified.

The WP-04 has developed a test program, incorporating development, qualification, and acceptance phases of hardware development (Figure 1). Progressively higher fidelities of hardware are used in the test phases and complement the iteration of the design development process. The fidelities are Breadboard, Mass Thermal/Acoustic Model (MT/AM), Engineering Model (EM), Flight



6382-1

**Figure 1. WP-04 Verification Test Logic**

(qual), and Flight. Table I identifies the qualities of each fidelity.

## EPS DESCRIPTION

WP-04 is responsible for the EPS and the associated SPM on the SSF (Figure 2). Rocketdyne is under contract to NASA Lewis Research Center (LeRC) for the design, development, test, and delivery of the EPS. Rocketdyne has several team member contractors that support this effort. The EPS is composed of ORUs and assemblies that

control, store, and distribute power from sunlight to the power user. The WP-04 ORUs are housed in the SPMs, pallets attached on the Preintegrated Truss (PIT) and in all the SSF modules.

The SPMs are made up of one (port side) or two (starboard side) Photovoltaic Power Modules (PVP) that are designed to produce 18.75 kW of power each. Major assemblies of the PVP are the Integrated Equipment Assembly (IEA) and Photovoltaic Array/Beta Gimbal Assembly. Inboard PVPs are attached to the SSF Solar Alpha Rotary Joint (SARJ). The outboard starboard side PVP utilizes long and short truss sections to attach to the inboard PVP (Figure 3).

The IEA includes the ORUs that house electrical power, control, and distribution electronics, battery cells, and ammonia coolant distribution hardware. Other hardware on the IEA comprise the Thermal Control Subsystem (TCS) and include a radiator, radiant finned heat exchanger plates, tubing, quick disconnects, and plumbing manifolds.

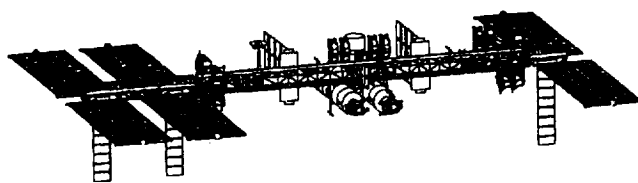
SPM hardware is launched on four National Space Transportation System (NSTS Space Shuttle) flights as pre-integrated sections. Assembly and connection of the

**Table I. Hardware Fidelities**

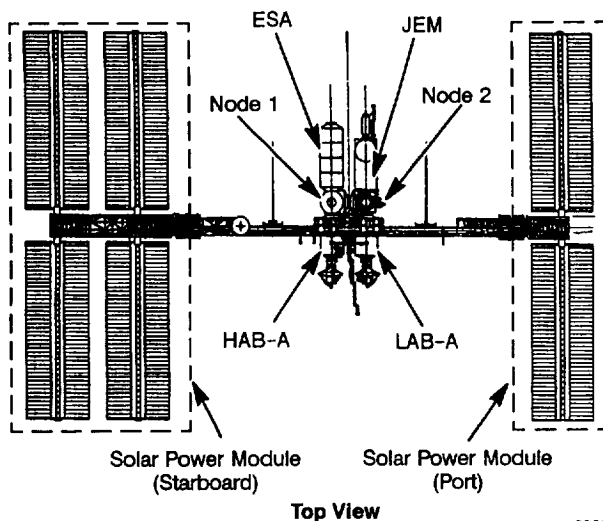
Hardware Fidelity	Functionality
Breadboard (BB)	Function only
Mass Thermal/Acoustic Model (MT/AM)	Physical weight, CG and configuration, nonfunctional
Engineering Model (EM)	Form, fit, and function of the flight hardware, "B" level EEE parts
Flight (Qual)	Flight hardware modified with qual instrumentation
Flight	Deliverable hardware for flight

D663-0005



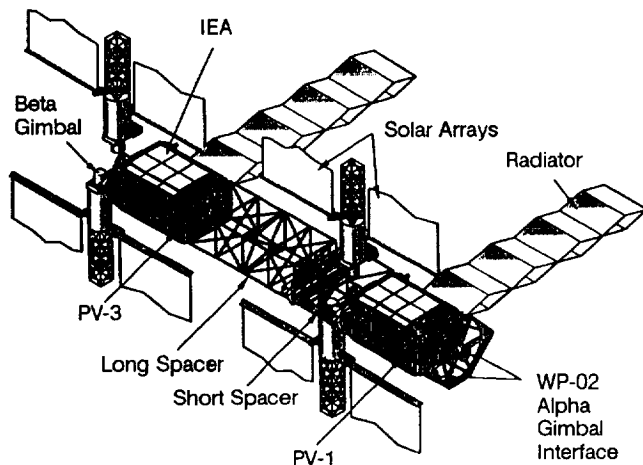


View Looking Aft



**Figure 2. Space Station Freedom  
Permanently Manned Capability  
Configuration**

6382-2



**Figure 3. Solar Power Module**

6382-3

sections are made in orbit. The sections, identified as cargo elements, are identified as Types I through IV. Types I, II, and III include a PVPM. Type IV is the short spacer truss.

Other EPS hardware is distributed throughout the SSF to provide control, power distribution, and system protection. The hardware, as ORUs, is designed and manufactured by WP-04 and provided to WP-01, WP-02, and the international SSF partners [European Space Agency

(ESA) and NASDA (Japan)]. Connection of the ORU hardware to the EPS is on-orbit.

## CARGO ELEMENT VERIFICATION

Each cargo element will be subjected to a series of test activities at each verification phase to assure they meet the launch and on-orbit requirements. Types I and II cargo elements are identified as a combined element with element pieces from WP-04 and WP-02 (Figure 4). The cargo element will be subjected to a series of modal, acoustic, and static structural tests to qualify it for NSTS launch. Modal testing will fulfill the requirements of NSTS 07700J. Mechanical and electrical functional tests will be conducted after hardware is assembled and during the acoustic testing. Functional tests are not necessary during modal and static structural testing.

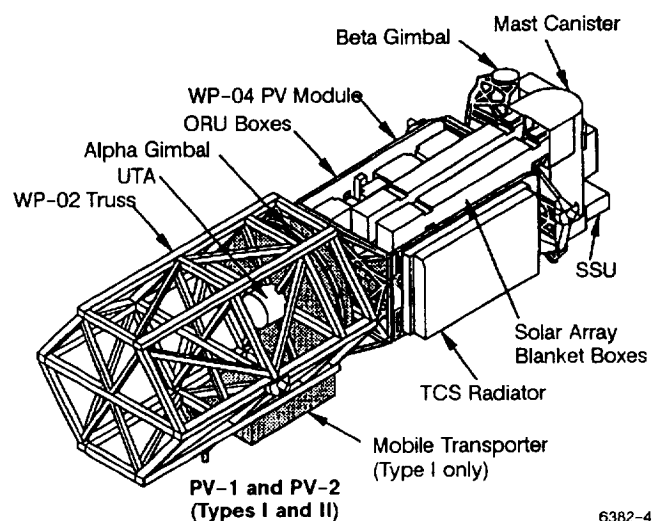
Types III and IV cargo elements will be subjected to a similar series of tests at qualification as Types I and II (Figure 5).

A key part of the verification of the PVPM in the on-orbit condition will be conducted at the LeRC Space Power

**Test Matrix**

Test	Qual	Flight Acceptance
Electrical functional	X	X
Mechanical functional	X	X
Modal	X <sup>1</sup>	
Acoustic	X	
Structural	X <sup>1</sup>	

<sup>1</sup> Qualification test with WP-04 hardware and WP-02 hardware



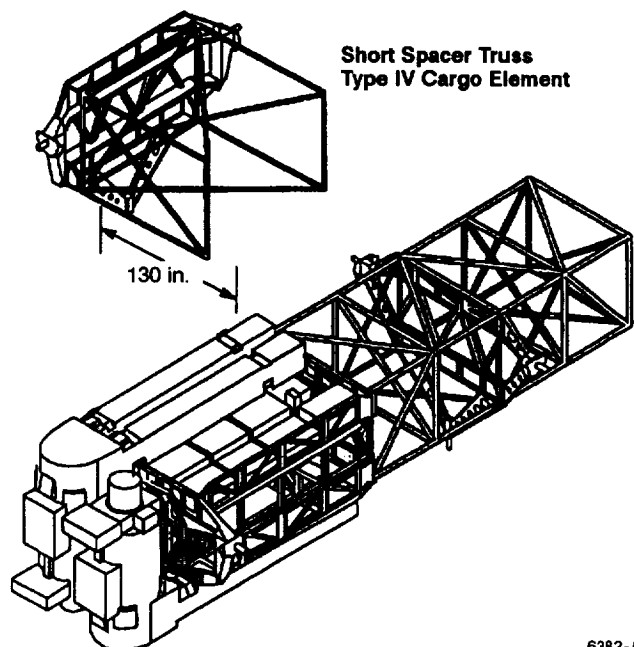
**Figure 4. PV Cargo Elements  
Types I and II**

6382-4

**Test Matrix**

Test	Qual <sup>1</sup>	Accep
Electrical functional	X	X
Mechanical functional	X	X
Modal	X	
Acoustic	X	
Structural	X	

<sup>1</sup> Type III cargo element tests utilize qual PV IEA

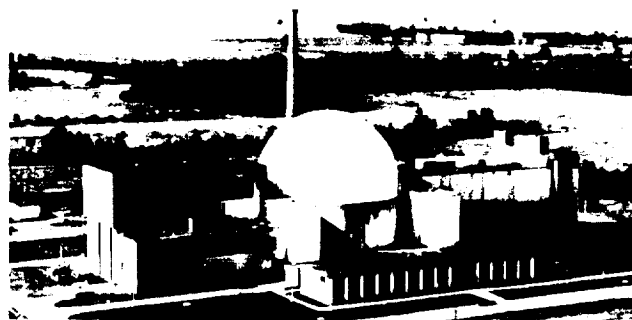


**Figure 5. PV Cargo Elements Types III and IV**

Facility (SPF) located at Plum Brook Station, Ohio (Figure 6). The test configuration will include a deployed Radiator and Beta Gimbal with Solar Array electrical and mechanical simulators attached. The test will be a mission simulation and will demonstrate PVPM start-up, operation, and shutdown in a space thermal and vacuum environment. One objective of the test is to verify the operation of the TCS used on the PV IEA. Functional tests will be conducted at peak, continuous, and contingency power modes.

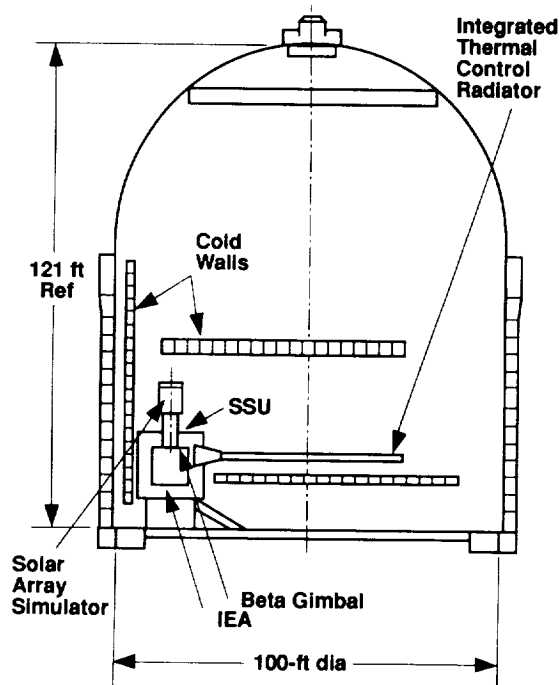
The SPF will have several minor modifications performed on the facility to support PVPM testing. A backup power system will be installed and activation of the LN<sub>2</sub>/GN<sub>2</sub> system is in work. A cryoshroud cold wall is currently being designed and will be installed at the facility in 1994.

Before shipment to Kennedy Space Center (KSC), each cargo element will be processed through an Installation, Assembly, and Checkout (IACO) (Figure 7). IACO



**Space Power Facility  
Plum Brook Station Ohio**

NASA C-71 3066

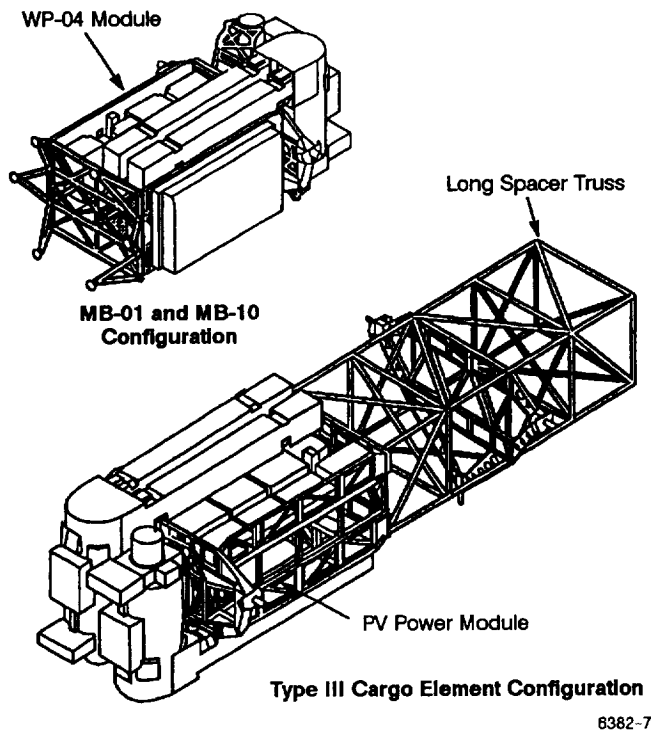


**Figure 6. PV Module SPF Test**

will serve as the final factory acceptance test of the cargo element. The hardware will be configured in the launched configuration with checks of the mechanical and electrical interfaces, including the test of element-to-element interfaces.

The IACO process will involve the installation, alignment, and checkout of the PV Radiator (PVR), the Beta Gimbal/Solar Array Assembly and the installation of lighting and camera mounts to the cargo element. Checkout will verify data and communication interfaces and issue commands to the cargo element simulating SSF communications. These checks will be similar to those performed at KSC upon receipt of the hardware and before launch.

Integration of the WP-02 and WP-04 elements for the Types I and II cargo elements will be performed at KSC.



**Figure 7. PV Module IACO  
MAJOR ASSEMBLY AND  
ORU VERIFICATION**

The IEA, which is the heart of the PVPM and weighs 34,000 lb, conditions and stores the electrical power collected by the PV arrays. It serves as the launch structure and supports the PVPM outboard of the SSF SARJ. The IEA houses the control, storage, and power ORUs for the PVPM. The IEA will be subjected to tests that affect its performance in space. Those tests are thermal vacuum and EMI/EMC (Figure 8). Structural tests, such as acoustic, static structural and modal, will be tested at the cargo element level.

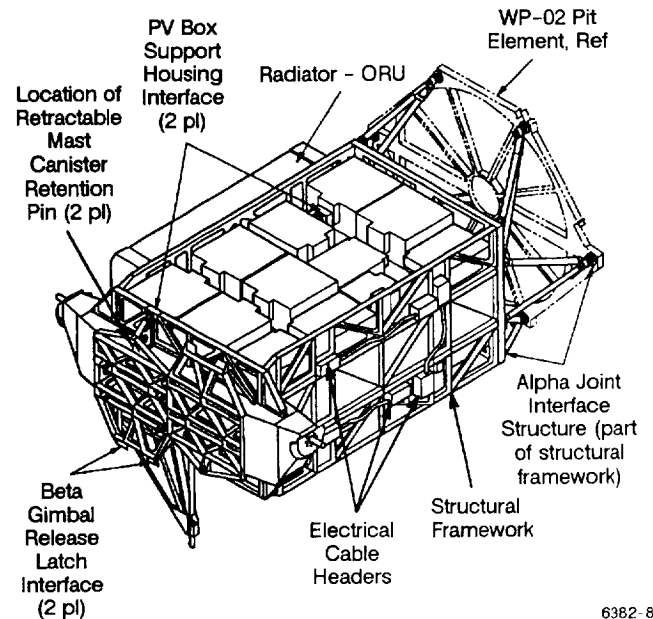
The current test plan is to conduct the cargo element Type I testing and IEA tests for development and qualification at one facility. The planning includes shipment of all the hardware and support equipment for both IEA and cargo element to a single site after IEA assembly. The sequence of tests is shown in Table II.

Due to a tight test schedule (approximately 7 months), detailed plans have been generated to minimize the nontest time. The plan includes the installation of the electrical functional support equipment in a set of trailers. This will allow quick setup and checkout at the test facility.

The Beta Gimbal Assembly (BGA) provides the structural support and positioning for the Solar Array and allows control and power transfer through its rotating joint. The

**Test Matrix**

Test	Qual	Flight Acceptance
Electrical functional	X	X
Mechanical functional	X	X
Thermal vacuum	X	
EMI/EMC	X	



**Figure 8. Integrated Equipment Assembly**

**Table II. PV IEA/Cargo Element  
Type I and II Test Sequence**

Test	Hardware Configuration
EMI/EMC	PV IEA
Thermal Vacuum	PV IEA
Acoustic	Type I Cargo Element
Modal (development only)	Type I Cargo Element
Static Structural (qual only)	Type I Cargo Element

D663-0015

assembly is made up of Beta Gimbal Transition Structure (BGTS), bearing motor and roll ring module, and a platform. The tests planned for the BGA hardware are shown in Figure 9. The current plan is to utilize the test facilities at Rockwell Space Systems Division, Seal Beach, for BGA testing.

Other major PVPM hardware items are the Solar Array Wing and PV Radiator (PVR). The wing is supplied to Rocketdyne by Lockheed Missile and Space Company (LMSC). Two wings are required for each PVPM. The wing

### Beta Gimbal Assembly

Test	EM	Qual
Electrical functional	X	X
Mechanical functional	X	X
Modal		X
EMC/EMI	X	X
Random vibration	X	X
Structural	X	X
Thermal cycle	X	X
Thermal vacuum	X	X

### Angular Contact Bearing

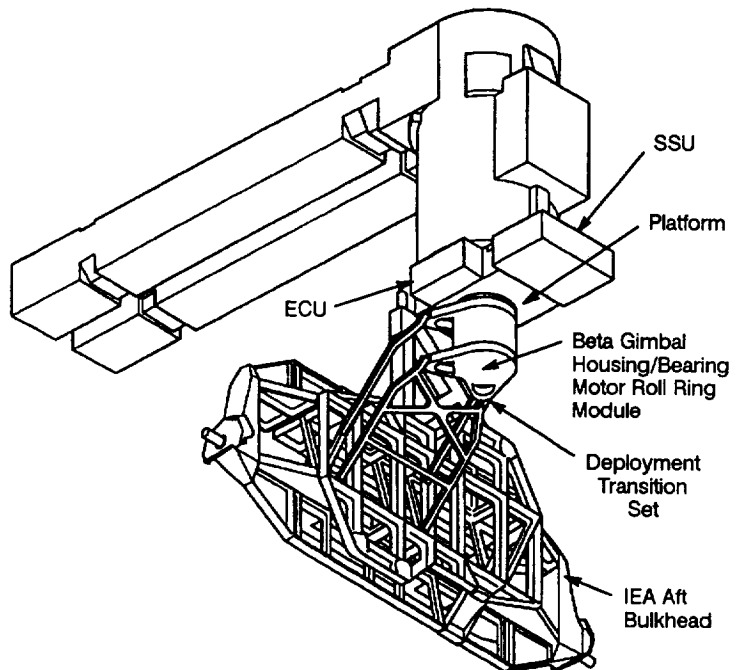
Test	EM	Accep
Life	X	
Mechanical functional	X	
Random vibration	X	
Proofload	X	

### Deployment Transition Set

Test	Qual	Accep
Mechanical functional	X	X
Vibration	X	X
Structural	X	X

### Bearing Motor and Roll Ring Module

Test	EM	Accep
Mechanical functional	X	X
Electrical functional	X	X
Random vibration		X
Thermal vacuum		X



### Platform

Test	EM	Accep
Mechanical functional	X	X
Electrical functional	X	X
Random vibration		X

6382-9

Figure 9. Beta Gimbal Assembly

is made up of a mast ORU and two blanket and box ORUs. One blanket and box ORU, measuring 15.3 ft by 111.6 ft (when deployed) contains 16,400 8-cm square solar cells. The planned tests for the wing hardware are shown in Figure 10.

The PVR is built by LTV Aerospace and Defense Company and includes eight panels 11.7 ft by 6.5 ft. It is deployable in space and contains two thermal loops for radiation of waste heat from the IEA to space. The heat transfer fluid is single-phase ammonia. The test plans to the PVR are shown in Figure 11. A thermal vacuum deployment test of the PVR is currently planned to be conducted at SPF, Plum Brook, Ohio.

### PMAD ORU TESTING

The Power Management and Distribution (PMAD) ORUs and the associated cabling control and manage the EPS power. They are located throughout the SSF to provide power feeds, conversion from 160 Vdc (primary power) to 120 Vdc (secondary power), and remote power con-

trol and distribution to the users. The ORU types are shown in Table III.

The DDCU(I) and DDCU(E) will be located throughout the SSF including attached to truss sections, housed in Nodes, Lab, Hab, Attached Pressurized Module (APM), ESA and Japanese Experiment Model (JEM) Modules and attached to the IEA. The DC Switching Unit (DCSU) is housed on the IEA also. The Electronic Control Unit (ECU) is attached to the Beta Gimbal Platform. Main Bus Switching Units (MBSU) will go on a truss section and Remote Power Controllers (RPC) will be located throughout the SSF.

Each ORU type will be subjected to an environmental development test series and formal qualification testing. The required tests for qualification of the ORUs are identified by LeRC-SS-0001 and MIL-STD-1540B. The ORU is classified as a component in MIL-STD-1540B terms. Table IV shows the tests identified for the PMAD ORUs.

Requirements for development testing of EM ORUs will be very close to the requirements of the qualification test. Tailoring of the test requirements will be specified for

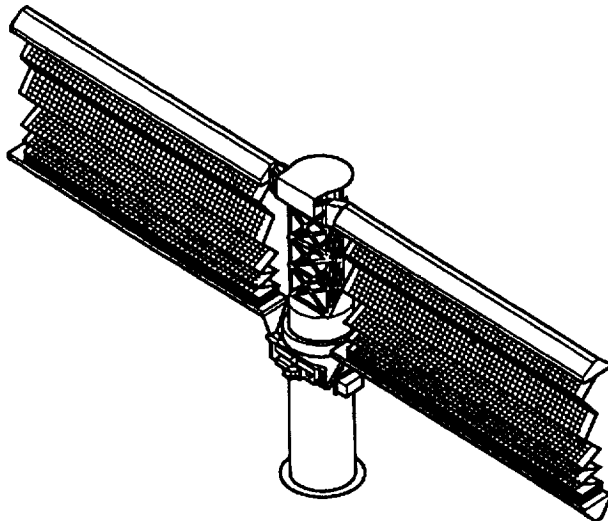
### Solar Array Wing

Test	Test Phase	
	Qual	Accep
Mechanical functional	X	X
Thermal vacuum	X	X
Thermal cycling		
Random vibration		
Acoustic EMC	X*	X

\*Conducted with EM PV IEA test

### Component and Assembly Tests

Test	Test Phase		
	Dev	Qual	Accep
Thermal vacuum		X	X
Thermal cycling	X	X	X
Random vibration		X	X



6382-10

Figure 10. Solar Array Wing

unique environments that the hardware was designed to meet. The development testing will provide design data to support the release of the flight hardware drawings. The test will also be used as a lessons learned experience to assure that qualification testing progresses smoothly.

Qualification of the ORUs will be conducted on flight quality hardware and will utilize a dedicated unit for testing. Tailoring of the test requirements will also occur for the qualification test.

Acceptance testing of the ORUs follow the required tests as identified in requirement documents. Test tailoring includes the deletion of burn-in of ORUs, with the exception of RPCs. Burn-in of hardware items at the sub-ORU level is conducted before ORU assembly. This allows for

### PV Radiator

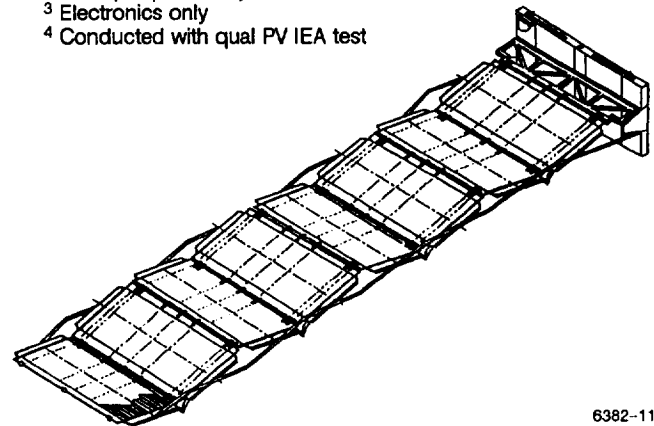
Test	Test Phase		
	Dev	Qual	Accep
Functional	1	X	X
Thermal vacuum			
Panel	1	2	
Assembly		X	X
Acoustic		X <sup>4</sup>	
Leakage		X	X
Pressure		X	X
Flow	1	X	X
Thermal cycling		3	3
EMI/EMC		3	
Burn-in			3

<sup>1</sup> Element testing only

<sup>2</sup> One qual panel only

<sup>3</sup> Electronics only

<sup>4</sup> Conducted with qual PV IEA test



6382-11

Figure 11. PV Radiator

Table III. Rocketdyne PMAD ORU Types

Acronym	Name	EM, F(Q), and F Qty (Units)
DDCU(E)	DC/DC Converter Unit (External)	38
DDCU(I)	DC/DC Converter Unit (Internal)	35
DCSU	DC Switching Unit	14
ECU	Electronic Control Unit	11
MBSU	Main Bus Switching Unit	13
RPC Type I	Remote Power Controller 8 Ch/12A	71
RPC Type II	Remote Power Controller 4 Ch/25A	48
RPC Type III	Remote Power Controller 2 Ch/50A	65
RPC Type IV	Remote Power Controller 1 Ch/65A	53
RPC Type V	Remote Power Controller 3.5A/12A	324
RPC Type VI (noncurrent limiting)	Remote Power Controller 4 Ch/25 A	32

D663-0005

**Table IV. PMAD ORU Tests**

Development and Qualification Tests	Acceptance Tests
Functional	Functional
Random Vibration	Random Vibration
Thermal Cycling	Thermal Cycling
Thermal Vacuum	Thermal Vacuum
Burn-in (RPCs only)	Burn-in (RPCs only)

D663-0005

less test time on the ORU saving manpower and test equipment and reducing failures at the ORU level.

Table III shows the quantity of each hardware type to be produced for ground test and for flight. Based on the quantities and the required tests, the challenge was to develop a method for testing space-rated hardware at rates up to 15 items per month and to keep costs at a minimum. Each item requires a series of acceptance tests. Due to the long duration of the testing and the high production rate, a study was conducted to determine attributes and requirements of a test system that would meet the test requirements and be cost efficient. As part of the study, a test equipment system was reviewed that provided the features of conducting all the thermal tests in one setup and thus utilizing a common vacuum system. The system, known as the Multiple Environments Test System (METS), is utilized by Rockwell Space Systems Division, Seal Beach, for thermal testing of Navstar Global Positioning Satellite (GPS) electronic hardware. The EPS hardware is larger than the GPS items, but the concept proved to be cheaper than a system of separate chambers and vacuum system.

The systems devised, called the Thermal Vacuum and Cycle System (TVACS) and patterned after the METS, uses a configuration of four or eight chambers in a star configuration around a common cryogenic vacuum pump. The system would meet the requirements of thermal cycling, thermal vacuum, and burn-in tests in a single test setup minimizing setup and checkout times.

The TVACS and associated support equipment, along with functional checkout and vibration test areas, will be installed in a newly modified 100,000 class building at Rockwell. The area has been designated for the performance for development, qualification, and acceptance testing of the ORUs. The one exception is electromagnetic interference/electromagnetic compatibility (EMI/EMC) testing. That testing is planned for Rockwell Autonetics Marine & Aircraft Systems Division where EMI/EMC capabilities exist.

## CURRENT PROGRESS

The early development testing of WP-04 hardware is progressing and is supporting the detailed design of the flight hardware. The major tests include efforts on ORU boxes and an acoustic test of an early version of the PVPM.

A series of tests on ORU boxes is continuing. These tests include vibration, thermal cycling, and thermal vacuum. The objectives of the testing are to verify the thermal analysis of the box design and to verify the structural design of the box.

A major development milestone was completed in the fall of 1990 with the successful completion of dynamic testing on the PV IEA MT/AM. The tests were key to the development of the IEA. The tests were also the first major test of a SSF cargo element in a dynamic environment.

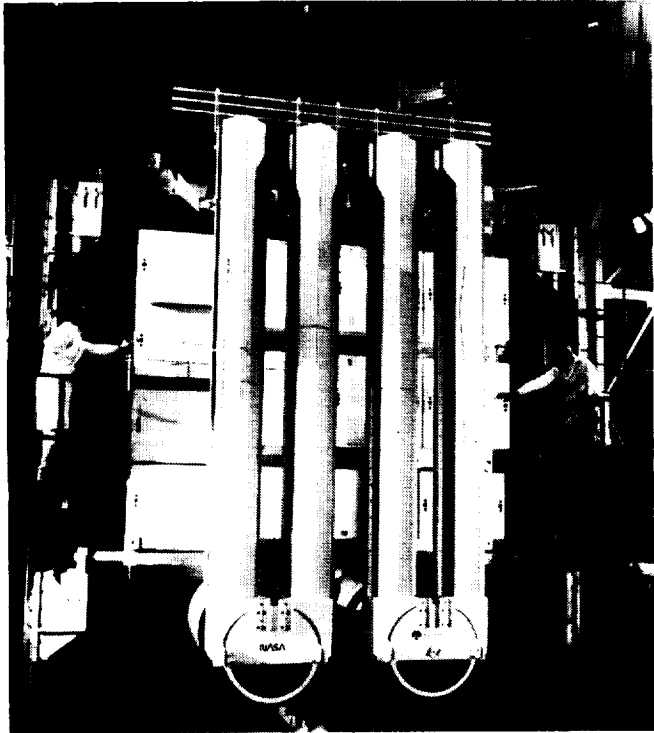
The series of tests provide the detailed data to verify the analysis models generated by Rocketdyne. The analysis is being used to approve future IEAs and cargo element configurations for flight.

The test series include a modal test and an acoustic test of the IEA. The modal test was conducted on the bare IEA structure. The test, using low amplitude vibration excitation, measured the natural frequency and mode shapes of the IEA structure. The test was conducted by Rocketdyne Division at Rockwell North American Aviation Division located in El Segundo. The test involved the acquisition of 300 channels.

The acoustic test simulated the dynamic (noise) environment of a Space Shuttle launch, plus a 6 db design margin, and was used to verify and measure the dynamic environment each ORU would experience during an NSTS launch. This information will be used to assure each design would endure launch and operate during orbit.

The test involved configuring the IEA into a cargo element. This included the installation of ORU boxes simulating electronics, batteries, and other simulators for solar arrays, gimbal joints, and a radiator. The IEA was then instrumented, transported to the Martin Marietta facility in Denver, and placed in a 30 ft by 38 ft by 60 ft acoustic chamber at that facility (Figure 12).

The IEA was subjected to seven different acoustic levels in 3 db increments, including the NSTS launch level, and concluding at 6 db higher than the launch level. The IEA passed all test levels with no problems. Data review of the test indicated that the acquired information was as expected and invaluable to the development and design of the IEA.



**Figure 12. IEA Installed in Acoustic  
Test Facility**

## **SUMMARY**

WP-04 has a wide variety of hardware to test requiring extensive planning and utilization of several test facilities. The applicable requirements documents have been reviewed and a tailored approach to testing has been identified. The approach will meet the unique SSF requirements and will assure that the WP-04 hardware will function nominally when subject to the launch and on-orbit environments. Testing has begun with results being utilized in the flight hardware design.

# REPORT DOCUMENTATION PAGE

Form Approved  
OMB No. 0704-0188

Public reporting burden for this collection of information is estimated to average 1 hour per response, including the time for reviewing instructions, searching existing data sources, gathering and maintaining the data needed, and completing and reviewing the collection of information. Send comments regarding this burden estimate or any other aspect of this collection of information, including suggestions for reducing this burden, to Washington Headquarters Services, Directorate for Information Operations and Reports, 1215 Jefferson Davis Highway, Suite 1204, Arlington, VA 22202-4302, and to the Office of Management and Budget, Paperwork Reduction Project (0704-0188), Washington, DC 20503.

1. AGENCY USE ONLY (Leave blank)		2. REPORT DATE November 1992	3. REPORT TYPE AND DATES COVERED Conference Publication	
4. TITLE AND SUBTITLE Seventeenth Space Simulation Conference Terrestrial Test for Space Success			5. FUNDING NUMBERS  Code 750	
6. AUTHOR(S)  Edited by Joseph L. Stecher, III				
7. PERFORMING ORGANIZATION NAME(S) AND ADDRESS(ES)  Goddard Space Flight Center Greenbelt, Maryland 20771			8. PERFORMING ORGANIZATION REPORT NUMBER  92B00118	
9. SPONSORING/MONITORING AGENCY NAME(S) AND ADDRESS(ES)  National Aeronautics and Space Administration Washington, D.C. 20546-0001			10. SPONSORING/MONITORING AGENCY REPORT NUMBER  CP-3124	
11. SUPPLEMENTARY NOTES				
12a. DISTRIBUTION/AVAILABILITY STATEMENT  Unclassified - Unlimited Subject Category 18			12b. DISTRIBUTION CODE	
13. ABSTRACT (Maximum 200 words)  The Institute of Environmental Sciences' Seventeenth Space Simulation Conference, "Terrestrial Test for Space Success" provided participants with a forum to acquire and exchange information on the state of the art in space simulation, test technology, atomic oxygen, dynamics testing, contamination, and materials. The papers presented at this conference and the resulting discussions carried out the conference theme of "terrestrial test for space success."				
14. SUBJECT TERMS  Space Simulation, Thermal Simulation, Contamination Control, Dynamic Testing, Spacecraft Materials, Total Quality Management (TQM)			15. NUMBER OF PAGES  356	
			16. PRICE CODE	
17. SECURITY CLASSIFICATION OF REPORT  Unclassified	18. SECURITY CLASSIFICATION OF THIS PAGE  Unclassified	19. SECURITY CLASSIFICATION OF ABSTRACT  Unclassified	20. LIMITATION OF ABSTRACT  Unlimited	